Ediacarian Isotope Stratigraphy of Australia

by Clive R. Calver, B. Sc. (Hons.)

A thesis submitted in partial fulfilment of the requirements for the degree of Doctor of Philosophy

School of Earth Sciences

Macquarie University

1995

Except as stated herein, this thesis contains no material which has been accepted for the award of any other degree or diploma in any University, and to the best of my knowledge and belief, this thesis contains no copy or paraphrase of material previously published or written by another person, except where due reference is made in the text of the thesis.

C. R. Calver

September 1995

Contents

List of Tables x
List of Figures x
List of Plates xiv

Abstract **1**

Foreword **5**
Chronostratigraphic nomenclature 6
Layout and Scope of Thesis 8
Terminology 10
Acknowledgments 10

1: Review of Neoproterozoic Isotope Chemostratigraphy **13**
1.1 Introduction 13
1.2 Mechanisms of secular change 14
1.2a Carbon Isotopes 14
Mechanism (i) 14
Mechanism (ii) 16
1.2b Oxygen Isotopes 18
1.2c Sulphur Isotopes 19
1.2d Strontium Isotopes 21
1.3 Neoproterozoic - early Cambrian isotope stratigraphy 22
1.3a $\delta^{13}C$ Stratigraphy 22
Proterozoic-Cambrian boundary studies 28
1.3b $\delta^{18}O$ Stratigraphy 30
1.3c $\delta^{34}S$ Stratigraphy 31
1.3d Strontium Isotopes 34
1.3e Conclusion: 'Global' Neoproterozoic $\delta^{13}C$ and $^{87}Sr/^{86}Sr$ curves 37

2: Methods in Isotope Chemostratigraphy **41**
2.1 Introduction 41
2.2 Carbonate stable isotopes and $^{87}Sr/^{86}Sr$ 41
2.2a Initial Variability 41
2.2b Post-depositional Alteration 43
Carbonate stable isotopes - general observations 43
Organic and meteoric diagenesis 45
Strontium isotopes 46
2.2c Reading the $\delta^{13}C_{carb}$ and $^{87}Sr/^{86}Sr$ signals: Monitoring Alteration 46
2.3 Organic carbon isotopes in chemostratigraphy 49
2.3a Introduction 49
Factors affecting $\delta^{13}C_{org}$ 50
2.3b Benthic Microbial Mats 52
Description 52
Strew slide observations 55
Isotopic composition of mats 56
Discussion 57
2.3c Correcting for $\delta^{13}C_{org}$ - TOC covariance 60
2.3d Monitoring regional variation in thermal maturation 65
Kerogen colour 70
Collation of maturation data 70
High Ediacarian $\Delta\delta$ 70
2.4 Sampling protocols and analytical methods followed in this study 71
2.4a Sampling 71
2.4b Analytical Methods 72
Organic carbon 72

Carbonates 73
Sulphates 74
Sulphides 74

3: Isotope Chemostratigraphy of Ediacarian Successions in the Adelaide Geosyncline and Officer Basin 77
3.1 Introduction 77
3.1a Adelaide Geosyncline - Officer Basin correlation: Previous Work 79
3.2 Geological Setting: Adelaide Geosyncline 82
3.3 Nuccaleena Formation 82
3.3a Lithostratigraphy 82
3.3b Isotope Stratigraphy 86
3.3c Interpretation 87
3.4 Brachina and ABC Range Formations 91
3.4a Lithostratigraphy 91
3.4b Isotope Stratigraphy 95
Maturation data 95
3.4c Interpretation 96
3.5 Bunyeroo Formation 96
3.5a Lithostratigraphy 96
3.5b Isotope Stratigraphy 98
3.5c Interpretation 98
3.6 Wonoka Formation 99
3.6a Lithostratigraphy 99
Sections at Bunyeroo Gorge, Brachina Gorge and SCYW1a 99
Unit 1 99
Unit 2 100
Units 3 - 7 100
Units 8 - 11 and dolostone in Bonney Formation 102
Sections at First Hill and Umberatana Syncline 102
The Wonoka 'canyons' and associated facies 104
3.6b Isotope Stratigraphy 107
3.6c Interpretation: the Dilemma of Low $\delta^{13}C_{carb}$ in the Wonoka Formation 109
Unit 1 111
Units 3 - 7 111
Diagenetic alteration of $\delta^{13}C_{carb}$ 112
Stratification of the water body 114
Some quantitative constraints 118
Other considerations 120
Other possible sources of sulphate and ^{12}C 123
Conclusion 123
Units 8 - 11 and dolostone in Bonney Formation 124
3.7 Geological Setting - Officer Basin 125
3.8 'Giles Mudstone' 126
Lithostratigraphy 126
3.8a Isotope Stratigraphy 126
3.9 Murnaroo Formation 127
3.9a Lithostratigraphy 127
3.9b Isotope Stratigraphy 128
3.10 Rodda beds 128
3.10a Introduction 128
3.10b Unit A: Lithostratigraphy 130
3.10c Unit A: Isotope Stratigraphy 131
3.10d Unit B: Lithostratigraphy 131

3.10e Unit B: Isotope Stratigraphy 136
3.10f Unit C: Lithostratigraphy 139
3.10g Unit C: Isotope Stratigraphy 139
3.11 Adelaide Geosyncline - Officer Basin correlation 140

4: Isotope Chemostratigraphy of Ediacarian Successions in the Amadeus and Georgina Basins 145
4.1 Introduction 145
4.2 Geological Setting: Amadeus Basin 149
4.2a Correlation of the Ediacarian Succession: Previous Work 152
4.3 Olympic and Pioneer Formations, excluding cap dolostone 155
4.3a Introduction 155
4.3b Olympic Formation 155
Isotope Stratigraphy 156
4.3d Pioneer Formation 157
Isotope Stratigraphy 162
4.3e Interpretation 162
$\delta^{18}O$ and palaeoclimate 163
4.4 Cap dolostone 166
4.4a Introduction 166
4.4b Lithostratigraphy 166
Mt Capitor 166
Wallara 1 167
Ellery Creek 167
Hidden Valley 168
4.4c Isotope Stratigraphy 168
4.4d Interpretation 170
$\delta^{18}O$ and palaeoclimate 173
4.5 Pertatataka Formation and correlatives 175
4.5a Introduction 175
Basin Geometry 175
4.5b Lithostratigraphy 178
Ellery Creek 178
Glen Helen 180
Areyonga Creek 180
Wallara 1 182
Mt Conner 184
Hidden Valley - Ross River 184
Ringwood area - Mt Capitor 187
Rodinga 4 188
4.5c Isotope Stratigraphy 190
Carbonate carbon and oxygen 190
Organic carbon 190
Thermal grade 193
Sulphide sulphur isotopes 194
4.5d Interpretation 196
Correlation of the Pertatataka Formation within the Amadeus Basin 196
Scheme A 196
Scheme B 196
Scheme C 197
Chemostratigraphic correlation 197
Stratification of basin waters early in Pertatataka time 203
4.6 Julie Formation 203
4.6a Stratigraphy 203

Ross River 206
Ellery Creek - Glen Helen 207
Katapata Gap 210
Phillipson Pound 210
4.6b Isotope Stratigraphy 212
Carbonate carbon and oxygen 212
Organic carbon 214
$^{87}Sr/^{86}Sr$ 216
4.6c Interpretation 216
Correlation 216
Geochemical and isotopic variation, Ross River section 217
4.7 Boord Formation 218
4.8 Georgina Basin - Geological Setting 220
4.9 Elyuah and Grant Bluff Formations 221
4.9a Lithostratigraphy 221
4.9b Isotope Stratigraphy 222
Thermal maturation 224
4.10 Elkera Formation 225
4.10a Stratigraphy 225
4.10b Isotope Stratigraphy 226
Carbonate carbon and oxygen 226
$^{87}Sr/^{86}Sr$ 227
Organic carbon 228
Sulphur 230
4.11 Central Mt Stuart Formation 230
4.12 Chemostratigraphic correlation within the Georgina Basin 231
4.13 Correlation scheme - Amadeus and Georgina Basins 231
4.14 Correlation with Adelaide Geosyncline and Officer Basin 235

5: Isotope chemostratigraphy of some Tasmanian Neoproterozoic successions 241
5.1 Introduction 241
5.2 Geological framework 242
5.3 Geological setting: Smithton Basin 244
5.4 Black River Dolomite 246
5.4a Stratigraphy 246
5.4b Isotope Geochemistry 251
5.4c Interpretation 252
5.5 Kanunnah Subgroup 254
5.5a Stratigraphy 254
5.5b Isotope Geochemistry 257
5.6 Smithton Dolomite 257
5.6a Stratigraphy 257
Lower member 257
Upper member 258
5.6b Isotope Geochemistry 260
5.6c Interpretation 262
5.7 Age and Correlation of the Togari Group 263
Black River Dolomite 263
Smithton Dolomite 264
5.8 King Island 265
5.9 The Jubilee Region 266
5.9a Geological setting 266
5.9b Clark Group 267
Isotope Geochemistry 267
5.9c Weld River Group 268

Isotope Geochemistry 270
5.9d Correlation between Jubilee Region and Smithton Basin 271

6: The Australian Ediacarian isotope-chemostratigraphic record and its correlation 275
6.1 Introduction 275
6.2 Ediacarian marine stratification - timing and extent 275
Sulphur isotopes and basin stratification 280
6.3 The Isotope-Chemostratigraphic Record of the Australian Ediacarian 281
6.3a Carbon Isotopes 281
6.3b Strontium Isotopes 286
6.3c Sulphur Isotopes 288
6.4 Correlation with overseas sections 288
6.5 Conclusion 294

References 297

Appendix 1.1: Sample locations, descriptions, stable-isotopic analyses and TOC
Appendix 1.2: Carbonate and sulphate trace-element (Mn, Sr, Rb) and $^{87}Sr/^{86}Sr$ analyses
Appendix 1.3: Elemental analyses of kerogen

Appendix 2: Reprint of Walter, M.R., Grey, K., Williams, I.R., & Calver, C., 1994: Stratigraphy of the Neoproterozoic to ealy Palaeozoic Savory Basin, Western Australia, and correlation with the Amadeus and Officer Basins. *Australian Journal of Earth Science,* 41:533-546.

Appendix 3: Reprint of Walter, M.R., Veevers, J.J., Calver, C.R. & Grey, K., (1995): Neoproterozoic Stratigraphy of the Centralian Superbasin, Australia. *Precambrian Research,* 73: 173-196.

List of Tables

Table 0.1: Basins and major stratigraphic units sampled in this study, and outcrop sections and drillholes (in italics).

Table 2.1: Location, megascopic appearance, generalised isotopic data (from Table 2.2), lithological associations, and ages of six black shale occurrences interpreted to be of benthic microbial mat origin.

Table 2.2: Carbon isotopic composition and TOC of black shales of benthic microbial mat origin ($\delta^{13}C_{bs}$, TOC_{bs}); of associated shales ($\delta^{13}C_{bkgd}$, TOC_{bkgd}); calculated isotopic compositions of benthic microbial mats($\delta^{13}C_{bmm}$) and of isotopic difference between 'pelagic' and 'benthic' carbon (Δ_{p-b}).

Table 2.3: H/C ratios and $\Delta\delta_{org}$ (calculated following Des Marais et al., 1992) of samples analysed in this study, together with one analysis from McKirdy (1976). Average results shown for each section/locality; indicated uncertainties are ± one standard deviation.

Table 2.4: Selected same-sample organic and carbon isotopic compositions, and derived $\Delta\delta$ and $\Delta\delta^N$ values. Average results shown for each section/locality; indicated uncertainties are ± one standard deviation.

Table 2.5: Collation of maturation data.

Table 3.1: Trace-element and strontium isotopic data, Nuccaleena Formation.

Table 3.2: Trace-element and strontium isotopic data, Wonoka Formation.

Table 3.3: Trace-element and strontium isotopic data, Rodda beds correlative.

Table 4.1: Trace-element and strontium isotopic data, carbonates of Olympic and Pioneer Formations including cap dolostone from Wallara 1.

Table 4.2: Trace-element and strontium isotopic data, Julie Formation and limestone from upper Pertatataka Formation at Acacia Well.

Table 4.3: Trace-element and strontium and sulphur isotopic data, Elkera Formation.

Table 5.1: Trace-element and strontium isotopic data, Black River Dolomite.

Table 5.2: Trace-element and strontium isotopic data, Smithton Dolomite.

Table 6.1: Selected strontium isotopic and associated analytical data from mainland Australian Ediacarian successions.

List of Figures

Fig. 0.1: The Neoproterozoic Era and constituent periods as recently defined; adapted from Plumb (1991).

Fig. 0.2: Australian Neoproterozoic chronostratigraphic units, with major lithostratrigraphic units of the Adelaide Geosyncline and major glacial units indicated (right-hand column). Adapted from Preiss (1987b).

Fig. 1.1: Major carbon fluxes and typical isotopic compositions into and out of the global ocean. Adapted from Schidlowski et al. (1983) and other sources.

Fig. 1.2: Conceptual model illustrating changes in carbon isotopic composition of average, surface and deep ocean water with , at time A, a change in ocean state from poorly to well-ventilated; at time B, an instantaneous increase in f_{org}.

Fig. 1.3: Coupled organic and carbonate $\delta^{13}C$ stratigraphic variation in Svalbard and East Greenland.

Fig. 1.4: Stratigraphic column, $\delta^{13}C_{carb}$ stratigraphy and distribution of early metazoans in the Witvlei and Nama Groups, Namibia.

Fig. 1.5: Stratigraphic column, $\delta^{13}C_{carb}$ stratigraphy and distribution of early metazoans in the upper Windermere Supergroup, NW Canada.

Fig. 1.6: Stratigraphic column, $\delta^{13}C_{carb}$ stratigraphy and fossil occurrences in the terminal Proterozoic of the Olenek Uplift, NE Siberia.

Fig. 1.7: $\delta^{13}C_{carb}$ data from the Sinian-early Cambrian sequence from the Yangtze Gorge.

Fig. 1.8: Precambrian-Cambrian boundary profiles.

Fig. 1.9: Part of Siberian carbon isotope stratigraphic and magnetostratigraphic data of Kirschvink, Margaritz and co-workers, illustrating extremely well-defined $\delta^{13}C_{carb}$ signals form widespread localities.

Fig. 1.10: Secular change in sulphate evaporite $\delta^{34}S$.

Fig. 1.11: Ranges and mean values for pyrite $\delta^{34}S$ in Proterozoic sedimentary rocks.

Fig. 1.12: Secular variation in $^{87}Sr/^{86}Sr$ of latest Proterozoic and Cambrian seawater estimated from least-altered carbonates.

Fig. 1.13: A recent compilation of secular change in (a) $\delta^{13}C$, and (b) $^{87}Sr/^{86}Sr$ of marine carbonates of Cryogenian to early Cambrian age (850 - 530 Ma).

Fig. 1.14: The depositional model of sequence stratigraphy, shown (a) in relation to depth (with great vertical exaggeration), and (b) in relation to time.

Fig. 2.1: Carbon isotopic composition versus H/C in kerogens with ages of 1.6 Ga or less.

Fig. 2.2: Frequency histogram of log TOC (TOC = total organic carbon content in mg/g); all data of this study.

Fig. 2.3(a): Organic carbon isotopic composition versus log TOC; all data of this study; carbonates and non-carbonates (nearly all shales) plotted separately.

Fig. 2.3(b): As Fig. 2.3(a) but with TOC calculated on a carbonate-free basis (TOC_{insol}).

Fig. 2.4: Organic carbon isotopic composition variation with respect to log TOC_{insol} in 20 samples from widespread Ediacarian marine successions; lines join subsamples from individual samples.

Fig. 2.5: Frequency distribution in Munta-1 (Rodda beds, Officer Basin), of $\Delta\delta$ (above) and $\Delta\delta^N$ (below).

Fig. 3.1: Generalised Ediacarian tectonic elements of South Australia, and locations of Officer Basin drillholes.

Fig. 3.2: Locality map and main tectonic elements, Adelaide Geosyncline and environs.

Fig. 3.3: Stratigraphic nomenclature and proposed correlation between the type Ediacarian (Adelaide Geosyncline) and the southeastern Officer Basin.

Fig. 3.4: Lithologic columns and $\delta^{13}C_{carb}$ profiles of Nuccaleena Formation at six localities.

Fig. 3.5: Two models to explain regional vatiation in $\delta^{13}C_{carb}$ profiles in the Nuccaleena Formation.

Fig. 3.6: Lithologic column and organic $\delta^{13}C$ data, Brachina, ABC Range, Bunyeroo and lowermost Wonoka Formations, SCYW1a drillhole.

Fig. 3.7: Lithologic column and organic $\delta^{13}C$ data, Brachina and Bunyeroo Formations, Bunyeroo Gorge. Asterisk indicates position of Acraman ejecta layer.

Fig. 3.8: Lithologic column and organic $\delta^{13}C$ data, Nuccaleena and Brachina Formations, drillhole BWM1A-1. Calculated $\delta^{13}C_{bmm}$ indicated adjacent to $\delta^{13}C_{bs}$ points.

Fig. 3.9: Lithologic column and organic $\delta^{13}C$ data, Bunyeroo Formation, Brachina Gorge. Asterisk indicates position of Acraman ejecta layer.

Fig. 3.10: Lithologic column, carbonate $\delta^{13}C$ and $\delta^{18}O$, and Mn/Sr data for Wonoka Formation at Bunyeroo Gorge.

Fig. 3.11: Lithologic column, carbonate $\delta^{13}C$ and $\delta^{18}O$, and Mn/Sr data for Wonoka Formation at First Hill.

Fig. 3.12: Lithologic column and carbonate $\delta^{13}C$ data for part of Wonoka Formation at Old Station Creek, Umberatana Syncline.

Fig. 3.13: Lithologic column and organic $\delta^{13}C$ data for the Wonoka Formation at Bunyeroo Gorge.

Fig. 3.14: Lithologic column and organic $\delta^{13}C$ data for the Wonoka Formation at First Hill.

Fig. 3.15: Mn/Sr versus $\delta^{13}C_{carb}$, Wonoka Formation. $^{87}Sr/^{86}Sr$ indicated for least-altered samples (identified on the basis of high $\delta^{18}O$, low Mn/Sr and low $^{87}Sr/^{86}Sr$).

Fig. 3.16: Stratified, evaporative basin model for the deposition of the Wonoka Formation.

Fig. 3.17: Lithologic column, $\Delta\delta$ and $\Delta\delta^N$ data for the Wonoka Formation at Bunyeroo Gorge.

Fig. 3.18: Lithologic column and organic $\delta^{13}C$ data for the 'Giles Mudstone' in drillhole Giles 1. Calculated $\delta^{13}C_{bmm}$ indicated adjacent to $\delta^{13}C_{bs}$ point.

Fig. 3.19: Lithologic columns and locations of major lithologic and sequence boundaries in drillholes Observatory Hill 1, Munta 1 and Ungoolya 1.

Fig. 3.20: Lithologic column and organic $\delta^{13}C$ data for the Rodda beds and uppermost Murnaroo Formation, drillhole Munta 1.

Fig. 3.21: Lithologic column and organic $\delta^{13}C$ data for the Rodda beds, drillhole Ungoolya 1.

Fig. 3.22: Lithologic column and organic $\delta^{13}C$ data for the Rodda beds, drillhole Observatory Hill 1.

Fig. 3.23: % carbonate, $\delta^{13}C_{carb}$, $\Delta\delta$ and $\Delta\delta^{N}$ data for the Rodda beds, drillhole Munta 1.

Fig. 3.24: % carbonate, $\delta^{13}C_{carb}$, $\Delta\delta$ and $\Delta\delta^{N}$ data for the Rodda beds, drillhole Ungoolya 1.

Fig. 3.25: $\delta^{13}C_{carb}$, $\Delta\delta$ and $\Delta\delta^{N}$ data for the Rodda beds, drillhole Observatory Hill 1.

Fig. 3.26: Correlation scheme linking major sections in the Adelaide Geosyncline and Officer Basin.

Fig. 4.1: Stratigraphic nomenclature and proposed correlation between the type Ediacarian (Adelaide Geosyncline), the northern Amadeus Basin and the southwestern Georgina basin; (a) after Preiss et al. (1978) and Walter (1980); (b) after Jenkins (1993b).

Fig. 4.2: Known and inferred extent of Ediacarian sedimentation in Australia; inferred limits of Neoproterozoic Centralian Superbasin; major present structural basins and Lake Acraman bolide impact site.

Fig. 4.3: Tectonic elements of the Amadeus Basin.

Fig. 4.4: Locality map, northeastern Amadeus Basin.

Fig. 4.5: Lithologic column and carbonate $\delta^{13}C$ and $\delta^{18}O$ profiles, dolostone unit within Olympic Formation, Hijinx Syncline.

Fig. 4.6: (a) Lithologic column, eastern face of Mt Capitor; (b) carbonate $\delta^{13}C$ and $\delta^{18}O$ profiles of cap dolostone and 'Halfway Dam Formation'.

Fig. 4.7: Lithologic column and carbonate $\delta^{13}C$ and $\delta^{18}O$ profiles of a dolostone unit (probable Pioneer Formation correlative) at Fenn Gap.

Fig. 4.8: Lithologic column and carbonate $\delta^{13}C$ and $\delta^{18}O$ profiles of a sandstone and dolostone unit (probable Pioneer Formation correlative) and overlying stromatolitic chert bed (probable cap dolostone) at Hidden Valley.

Fig. 4.9: $\delta^{13}C$ - $\delta^{18}O$ crossplot incorporating cap dolostones, (older) Pioneer/Olympic Formation. carbonates and limestones of the Halfway Dam Formation.

Fig. 4.10: $\delta^{18}O$ frequency distributions of cap dolostones, older Pioneer/Olympic dolostones, Julie Formation and Elkera Formation.

Fig. 4.11: Lithologic column, carbonate $\delta^{13}C$ and $\delta^{18}O$ profiles and organic $\delta^{13}C$ data of cap dolostone and lowermost Pertatataka Formation, Wallara 1 drillhole.

Fig. 4.12: Sequence architecture in foreland basin: model of Swift et al. (1987). Compare with passive-margin model shown in Fig. 1.14.

Fig. 4.13: (a) Elements of palaeogeography of the Amadeus Basin in Pertatataka time; (b) Diagrammatic S-N cross-section showing basin geometry for Olympic-Pertatataka-Julie sequence, from Shaw et al. (1991); (c) Proposed cross-section for Pertatataka time with subdued Central Ridge.

Fig. 4.14: Proposed correlation of Winnall beds at Mt Conner and Liddle Hills (from Wells et al., 1970) and Pertatataka Formation at Wallara 1.

Fig. 4.15: Lithologic column and organic $\delta^{13}C$ data, Pertatataka and Julie Formations, Ellery Creek.

Fig. 4.16: Lithologic column and organic $\delta^{13}C$ data, Pertatataka Formation, Pioneer Formation (including cap dolostone), and Aralka Formation, Wallara 1.

Fig. 4.17: Lithologic column and organic $\delta^{13}C$ data, Pertatataka Formation, Hidden Valley.

Fig. 4.18: Lithologic column and organic $\delta^{13}C$ data, lower Pertatataka Formation, Alice Springs 27.

Fig. 4.19: Lithologic column and organic $\delta^{13}C$ data, Pertatataka Formation, Rodinga 4.

Fig. 4.20: Stratigraphic variation in pyrite $\delta^{34}S$ in the Pertatataka Formation (composite section of Wallara 1 and Rodinga 4 correlated as in Fig. 4.36).

Fig. 4.21: Alternative correlation schemes for the Pertatataka Formation and associated units. (a) As proposed in this study, and in part by Preiss et al. (1978); (b) as proposed in part by Jenkins et al. (1992) and Jenkins (pers. comm., 1993); (c) as proposed by Preiss (pers. comm., 1993).

Fig. 4.22: Proposed chronostratigraphic correlation of Wallara 1 and Ellery Creek Pertatataka sections, showing relaltionship of sequence-stratigraphic framework to $\delta^{13}C_{org}{}^{N}$ chemostratigraphic profiles. HST: highstand systems tract; TST: transgressive systems tract. Chemostratigraphic profiles from Figs. 4.15, 4.16.

Fig. 4.23: Typical parasequence of Julie Formation, and lithologic symbols used in Figs. 4.23 - 4.27.

Fig. 4.24: Lithologic column and carbonate $\delta^{13}C$ and $\delta^{18}O$ data, Julie Formation, Ross River (type section).

Fig. 4.25: Lithologic column and carbonate $\delta^{13}C$ and $\delta^{18}O$ data, Julie Formation, Ellery Creek.

Fig. 4.26: Lithologic column and carbonate $\delta^{13}C$ and $\delta^{18}O$ data, Julie Formation, Katapata Gap section.

Fig. 4.27: Lithologic column and carbonate $\delta^{13}C$ and $\delta^{18}O$ data, Julie Formation, Phillipson Pound composite section.

Fig. 4.28: $\delta^{13}C$ - $\delta^{18}O$ crossplot for the Julie Formation at Ross River.

Fig. 4.29: Mn/Sr versus $\delta^{13}C_{carb}$, Julie Formation, differentiated according to locality.

Fig. 4.30: $^{87}Sr/^{86}Sr$ versus $\delta^{13}C$, Julie Formation, differentiated according to locality.

Fig. 4.31: $^{87}Sr/^{86}Sr$ versus $\delta^{18}O$, Julie Formation, differentiated according to locality.

Fig. 4.32: Lithologic column and organic $\delta^{13}C$ data, Elyuah, Grant Bluff and Elkera Formations, DDC 1 drillhole. 'e' indicates presence of anhydrite.

Fig. 4.33: Lithologic column and organic $\delta^{13}C$ data, Elyuah Formation, DDC 2 drillhole.

Fig. 4.34: Lithologic column and carbonate $\delta^{13}C$ and $\delta^{18}O$ profiles, Elkera Formation, DDC 1 drillhole. 'e' indicates presence of anhydrite.

Fig. 4.35: Lithologic column and carbonate $\delta^{13}C$ and $\delta^{18}O$ profiles, Elkera Formation, Huckitta 7 drillhole.

Fig. 4.36: Correlation scheme linking major sections in the Amadeus and Georgina Basin. See text for full explanation.

Fig. 4.37: Correlation scheme for Ediacarian successions in Adelaide Geosyncline, and Officer, Amadeus and Georgina Basins, based on Figs. 4.36 and 3.26.

Fig. 5.1: Simplified geological map of Tasmania with post-Cambrian successions omitted, showing present distribution of major Proterozoic-Cambrian tectonic elements.

Fig. 5.2: Simplified geological map of Smithton Basin showing sections and localities mentioned in text.

Fig. 5.3: Lithologic column of Black River Dolomite, eastern Arthur River section, and carbonate isotopic data.

Fig. 5.4: Lithologic column of upper Black River Dolomite and lower Kanunnah Subgroup, Forest 1 drillhole; with organic carbon and carbonate isotopic data.

Fig. 5.5: Plot of $^{87}Sr/^{86}Sr$ vs. Mn/Sr, Black River Dolomite.

Fig. 5.6: Lithostratigraphy of the Kanunnah Subgroup at western Arthur River section, eastern Arthur River section and Forest 1 drillhole.

Fig. 5.7: Lithologic column and carbonate isotopic data, Smithton Dolomite, Montagu River and Redpa sections.

Fig. 5.8: Simplified geological map of the northern part of the Jubilee region.

Fig. 5.9: $\delta^{13}C$-$\delta^{18}O$ crossplot of carbonates from the Jubilee region.

Fig. 5.10: Generalised lithologic column and stratigraphic plot of $\delta^{13}C_{carb}$ for the Weld River Group. Vertical error bars indicate uncertainty of stratigraphic placement.

Fig. 6.1: Generalised stratigraphic columns (not to scale, but with timelines roughly horizontal) from the Adelaide Geosyncline, Officer Basin and Amadeus Basin showing distribution of features relating to stratification of the water column.

Fig. 6.2: Generalised $\delta^{13}C$ signals, Australian Ediacarian basins.

List of Plates

Plate 2.1: Thin section, mudstone with anastamosing organic-rich thin layers interpreted to be remnant benthic microbial mats. Kanunnah Subgroup, sample ABS51, 235 m depth, Forest-1 drillhole, Smithton Basin.

Plate 2.2: Thin section, mudstone with thin, anastamosing, organic-rich laminae (benthic microbial mats) (TOC 4.4 mg/g) overlain by organic-poor mudstone (TOC 1.3 mg/g) with planar-parallel lamination. Pertatataka Formation, sample 28.112, 1206.5 m depth, Wallara-1 drillhole, Amadeus Basin.

Plate 2.3: Thin section, siltstone with wispy intraclasts of organic-rich mudstone (reworked benthic microbial mat fragments). Kanunnah Subgroup, sample ABS53, 281.3 m depth, Forest-1 drillhole, Smithton Basin.

Plate 2.4: Palynological strew slide showing large corroded fragment of amorphous kerogen, probably of benthic microbial mat origin. Pertatataka Formation, sample 28.116, 1225.5 m depth, Wallara 1 drillhole, Amadeus Basin.

Plate 2.5: Palynological strew slide showing fragment of coccoid sheet.

Plate 2.6: Palynological strew slide showing mass of filaments. Rodda beds correlative, sample 26.10, Ungoolya 1 drillhole, Officer Basin.

Plate 3.1: Outcrop photograph of Nuccaleena Formation showing irregular, erosive tops to some of the paler, dolostone layers. Uppermost dolostone at Hallett Cove section (located at 70 m on Fig. 3.4).

Plate 3.2: Nodular bedding in micritic limestone. 'Karlaya Limestone' unit of Rodda beds correlative, 1661 m depth, Munta 1 drillhole, Officer Basin.

Plate 3.3: Very fine-grained sandstone and siltstone with erosional surfaces and low-angle cross-lamination, Rodda beds correlative, 1233.0 m, 1234.7 m depths, Munta 1 drillhole, Officer Basin.

Plate 3.4: Lenticular gypsum crystals in calcareous mudstone, sample 5.43, Unit 5, Wonoka Formation, Bunyeroo Gorge.

Plate 3.5: Pseudomorphs of calcite after ?gypsum, sample 5.36, Unit 4, Wonoka Formation, Bunyeroo Gorge.

Plate 4.1: Thin section of silty dolostone from 0.5 m above base of 'cap dolostone' at Mt Capitor, showing clearly detrital nature of most carbonate. Sample 22.03.

Plate 4.2: Thin section of 'cap dolostone' showing dolomicrosparite with microfenestrae, filled with dolospar and barite. Sample 22.09, 17.4 m above base of cap dolostone at Mt Capitor.

Plate 4.3: Thin section showing small-scale erosional scour in the top of a dolostone bed in 'cap dolostone', sample 28.126, 1272.4 m depth, Wallara 1 drillhole, Amadeus Basin.

Plate 4.4: Drillcore showing upward gradation from pale buff-coloured, laminated 'cap dolostone' into massive red mudstone of the basal Pertatataka Formation. Note diffuse nodules and layers of dolostone in basal part of red mudstone. Wallara 1 drillhole.

Plate 4.5: Drillcore showing interbedded black shale (benthic microbial mat facies) and grey-green shale in lower part of Pertatataka Formation, 1236-1241 m depth, Wallara 1 drillhole.

Plate 4.6: Thin laminae and starved ripples of quartz siltstone in red and green shale, Pertatataka Formation. 943 m depth, Wallara 1 drillhole.

Plate 4.7: Lenticular bedding in fine-grained sandstone and shale, upper Pertatataka Formation, 734 m depth, Wallara 1 drillhole.

Plate 4.8: Part of two parasequences, Julie Formation, Ross River section. Lower part of outcrop, showing massive, then laminated fine-grained dolostone, is the upper part of earlier parasequence; upper part of outcrop - massive, brown, sandy, recrystrallised dolomite oolite - is lower part of the next parasequence.

Plate 4.9: Low-angle and swaley cross-stratification in sandy limestone, lower Julie Formation, Phillipson Pound section.

Plate 4.10: Thin section of dolomicrite with calcite-after-anhydrite pseudomorphs with geopetal floors. Sample 6.42, 47 m above base of Julie Formation, Ellery Creek section.

Plate 4.11: Thin section showing texturally well-preserved micritic ooids, deformed by compaction so that cement is negligible apart from a very thin isopachous early (marine?) phase. Sample 24.21, upper Julie Formation, Phillipson Pound section.

Plate 4.12: Thin section of anhydrite-cemented oolitic dolostone, Elkera Formation, Georgina Basin. Ooid cores are detrital quartz. Sample 31.26, 468.8 m depth, DDC 1 drillhole.

Plate 4.13: Thin section of 'half-moon' ooids, uppermost Elkera Formation. Pore space is mostly void. Sample 31.12, 381.3 m depth, DDC 1 drillhole.

Plate 5.1: Thin section of clear dolomicrospar replacing dolomicrite matrix of oolitic dolostone, Black River Dolomite, Smithton Basin. Sample ABS88, 990 m depth, Forest 1 drillhole.

Plate 5.2: Thin section of dolostone clast in diamictite within Black River Dolomite, showing truncation of cement phases at surface of clast. Sample ABS84, 890 m depth, Forest 1 drillhole.

Plate 5.3: Thin section showing texturally well-preserved oolitic dolograinstone, lower member of Smithon Dolomite, Montagu River area. Sample 001661.

Plate 5.4: Thin section showing turbid, fabric-destructive coarse dolomitization characteristic of upper member of Smithton Dolomite; clear late calcite fills void. Sample 11.14, 1295 m, Montagu River section.

Plate 5.5: Thin section of oolitic limestone from the upper member of the Smithton Dolomite. The well-preserved radial-fibrous ooids are ca. 1mm in diameter. Replacive granular ferroan dolomite at lower left. Sample 17.18, 890 m, Redpa section.

Abstract

This study establishes a precise isotope-chemostratigraphic framework for the Australian terminal Proterozoic (Ediacarian), a framework that contributes to the emerging global chronostratigraphic synthesis of a period that saw momentous changes in the Earth's surface environment.

A dearth of carbonates in Australian Ediacarian marine successions has necessitated a focus on isotopic composition of total organic carbon for chemostratigraphy. The $\delta^{13}C_{org}$ record reveals a surprising richness of information and, together with more limited shallow-marine $\delta^{13}C_{carb}$ and $^{87}Sr/^{86}Sr$ data, shows excellent utility in correlation within and between the Adelaide Geosyncline and Officer, Amadeus and Georgina Basins.

$\delta^{13}C_{org}$ displays, even within individual hand-specimens, an inverse relationship to total organic carbon (TOC). The resolution of the organic $\delta^{13}C$ signal is improved if a correction factor is applied to filter out this effect, which may be related to changes in the degree of heterotrophic reworking before or soon after burial. The utility of the signal is further improved by quantifying the shifts in $\delta^{13}C_{org}$ that are caused by regional variation in thermal maturation, using kerogen H/C and $\Delta\delta$ ($= \delta^{13}C_{carb} - \delta^{13}C_{org}$).

In several units of at least three distinct ages, carbonaceous laminae in black shales show petrographic features indicating an origin as fossil benthic microbial mats. These tend to be strongly ^{13}C-depleted, being up to 14 ‰ lighter than organic carbon in associated shales that is probably dominantly of pelagic origin.

Six cycles or positive excursions in ^{13}C content of organic carbon are seen in the pre-Pound Subgroup Ediacarian of the mainland Australian basins, cycles IV and VI also being evidenced by congruent ^{13}C variation in shallow-water carbonates. Carbon and strontium isotope stratigraphy support earlier correlation schemes based on lithostratigraphy. The Brachina-ABC Range-Bunyeroo succession of the type Ediacarian is a correlate of the Pertatataka Formation of the Amadeus Basin. The Julie Formation (Amadeus Basin) correlates with the first major limestone unit ('Karlaya Limestone') in the Rodda beds equivalent of the southeast Officer Basin, and is older than the upper part of the Wonoka Formation. There is probably little, if any, overlap in age between the Rodda beds equivalent and the Pound Subgroup. The isotope data support correlation of the Elyuah and Grant Bluff Formations (Georgina Basin) with the lower Pertatataka Formation, and the lower Elkera Formation corresponds to the Julie Formation. Within basins there are

lateral variations in $\delta^{13}C$ profiles that correspond to diachronous patterns of basin fill that can be deduced *a priori* from sequence-stratigraphic principles.

Some sublittoral micritic carbonates of two distinct ages (upper Nuccaleena Formation and correlatives and lower Pertatataka Formation; and lower and middle Wonoka Formation and a correlative part of the Rodda beds) show unusual ^{13}C depletion ($\delta^{13}C_{carb}$ = -3 to -10 ‰) despite evidence for preservation of depositional $\delta^{13}C_{carb}$ (such as good textural preservation, evidence for seafloor lithification, low $^{87}Sr/^{86}Sr$, and low Mn/Sr). Rare subaqueous evaporite, and relatively heavy $\delta^{13}C_{org}$ except for anomalously ^{13}C-depleted organic carbon of benthic microbial mat origin are associated with the depleted carbonates, and a common cause - salinity stratification of the water column - is postulated. The indicated palaeogeographic setting - an evaporative mediterranean basin tenuously connected to the world ocean - is consistent with previous suggestions of one or more Messinian-type desiccation events to explain very deep (1 km) incised valleys or canyons in the Adelaide Geosyncline and Officer Basin, at horizons within the second of the two postulated phases of stratification. Low TOC despite likely anoxia of the lower water mass may be attributed in part to the efficiency of Proterozoic water-column remineralization of organic matter in the absence of fecal pellet production. Positive excursions in $\delta^{13}C_{org}$ during basin stratification (cycles I, V) may simply result from enhanced ^{13}C-enrichment of surface waters where most carbon fixation was occurring.

Isotope data are equivocal on the question of intercontinental synchroniety of terminal Proterozoic glaciations, and more data are required, particularly from pre-Ediacarian successions. There is no evidence in mainland Australia for the major negative $\delta^{13}C$ excursion post-dating glacials in Namibia and Spitzbergen. The excursion may partly precede the Marinoan glaciation suggesting the latter may be younger. However, the proposed semi-isolation of the Australian basins suggests basin waters may have evolved separately in $\delta^{13}C$ from the global ocean. Within the Ediacarian, a positive excursion in the Julie and 'Karlaya' Formations (Cycle IV, maximum $\delta^{13}C_{carb}$ +6 ‰) coincides approximately with the occurrence of distinctive large acanthomorphic acritarchs and near-primary $^{87}Sr/^{86}Sr$ of 0.7079. This excursion is not recognised in overseas sections with the possible exception of the Doushantuo Formation, China. A later excursion (Cycle VI) seen in the uppermost Wonoka Formation and uppermost Rodda beds equivalent, associated with near-primary $^{87}Sr/^{86}Sr$ of 0.70875, probably corresponds to a positive excursion widely recognised on other continents (e.g. Zaris Formation, Namibia; upper Sheepbed Formation, northwest Canada).

The Australian data support previous work suggesting a monotonic rise in Ediacarian marine $^{87}Sr/^{86}Sr$. Sulphate evaporite $\delta^{34}S$ rises gently from 20 ‰ to 25 ‰ in the sections studied. Pyrite $\delta^{34}S$ compositions are variably depleted (-31 to +4 ‰) in accordance with varying degrees of partial closure during early diagenesis.

In the Smithton Basin, northwest Tasmania, the Black River Dolomite is early Cryogenian on $\delta^{13}C$, $^{87}Sr/^{86}Sr$ and stromatolite-biostratigraphic evidence. A diamictite unit, perhaps corresponding to the Sturtian glacials, coincides with a negative $\delta^{13}C$ excursion at the top of the Black River Dolomite. The Smithton Dolomite is, at least in part, Ediacarian on $\delta^{13}C_{carb}$ and $^{87}Sr/^{86}Sr$ evidence but is lithologically and isotopically dissimilar to mainland Australian Ediacarian successions in that it is comprised of a thick succession of mainly ^{13}C-depleted shallow-water carbonates. Crystalline dolostones comprising most of the Smithton Dolomite are a late, burial-diagenetic phenomenon. Reconnaisance $\delta^{13}C_{carb}$ data suggest the Weld River Group of southern Tasmania may be a correlative of the Smithton Dolomite.

Foreword

The Neoproterozoic was a time of profound biological, biogeochemical, climatic and tectonic change (Knoll & Walter, 1992; Brasier, 1992). Stratigraphic correlation in this part of the geologic record has long been hampered by the relatively very poor resolution offered by biostratigraphy, but an array of emerging methodologies offers a prospect of greatly improved correlation. Isotope chemostratigraphy is one such technique (Knoll & Walter, 1992; Narbonne et al., 1994; Kaufman & Knoll, 1995). Acritarch biostratigraphy, improved U - Pb geochronometry and sequence stratigraphy are other methods being applied with renewed impetus in the late Proterozoic (e.g. Zang & Walter, 1992; Bowring et al., 1993; Christie-Blick et al., 1988; 1995). Together with the more traditional methods - stromatolite biostratigraphy, correlation of glaciogenic units and metazoan and trace fossil biostratigraphy - these techniques provide the basis for substantial advances in our understanding of the timing of Neoproterozoic environmental change (see Knoll & Walter, 1992 for a discussion).

The base of the Cambrian has been recently fixed at a global stratotype section and point (GSSP) in Newfoundland (Landing, 1994). Carbon isotope chemostratigraphy played an important role in global correlation of Precambrian-Cambrian boundary sections in the search for the best GSSP (Brasier et al., 1990; 1992; Margaritz et al., 1991). The new chronometric subdivision of the Precambrian (Plumb, 1991; Fig. 0.1) leaves the naming and determination of the base of the terminal Proterozoic System and Period to be considered by an IUGS Working Group. Australia has a particularly rich record of this time interval, and a candidate stratotype section is located in the Adelaide Geosyncline. Ediacarian successions are considered prospective for hydrocarbons in several Australian basins (Jackson et al., 1984a; Brewer et al., 1987; Stainton et al., 1988; Lindsay et al., 1992; Lemon et al., 1992). There are thus cogent economic reasons as well as timely scientific reasons for undertaking systematic chemostratigraphic and biostratigraphic studies of the terminal Proterozoic in Australia.

This chemostratigraphic study is part of a coordinated research effort at Macquarie University into the Ediacarian Earth history of Australia. A companion project on acritarch biostratigraphy, by K. Grey, is being conducted concurrently with this study, from much the same sample set. Results from both these projects are being incorporated into the broader Neoproterozoic palaeogeographic and tectonic framework by M. R. Walter and J. J. Veevers (e.g. Walter et al., 1995).

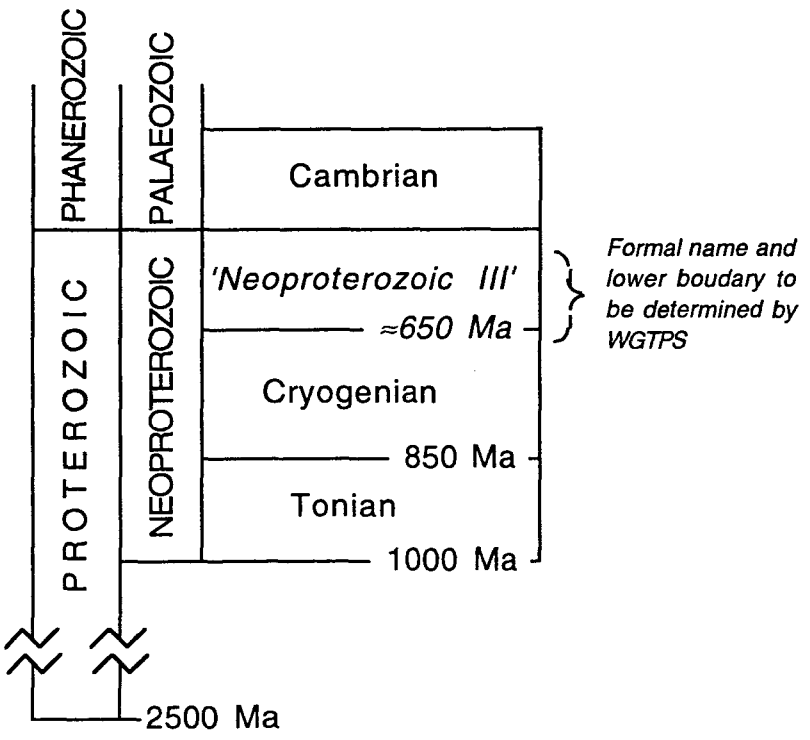

Fig. 0.1: The Neoproterozoic Era and constituent periods as recently defined; adapted from Plumb (1991).

CHRONOSTRATIGRAPHIC NOMENCLATURE

A number of chronostratigraphic and chronometric terms used in this work require brief explanation. In particular, there is potential confusion over the term 'Ediacar(i)an'.

It is anticipated that the lower boundary of the presently un-named final period of the Proterozoic (Fig. 0.1) will be defined with reference to the last widespread Neoproterozoic glaciation (Knoll & Walter, 1992). The widely used term 'Vendian' extends from the base of the Varangian glaciation that is widespread in the northern hemisphere, to the base of the Cambrian (Harland & Herod, 1979; Semikhatov, 1979). Cloud & Glaessner (1982) formalised the *Ediacarian* System and Period, intended to embrace the earliest metazoan assemblages, and with a type section in the Adelaide Geosyncline extending from the top of the Marinoan glacials to the base of the Cambrian. These authors proposed that the Phanerozoic and Palaeozoic be extended downward to include the Ediacarian. The *Ediacaran* Stage/Epoch of Harland & Herod (1975) is roughly equivalent, extending from the top of the glacial Varangian Stage to the base of the Cambrian. Jenkins (1981) formalised an *Ediacaran* System in the Adelaide Geosyncline beginning at the base of the Wonoka Formation, some distance stratigraphically higher than the top of the Marinoan glacials. Like the Ediacarian of Cloud & Glaessner (1982) the main intent was to set up a

system that included occurrences of soft-bodied 'Ediacara fauna'. Preiss (1987b) gave cogent reasons for preferring the greater stratigraphic extent of Cloud & Glaessner's (1982) proposal.

Knoll & Walter (1992) argued that the top of the glacigene interval is more likely to provide a globally correlatable datum suitable for a terminal Proterozoic system, than any lower horizon such as the base of the glacials. Perhaps most importantly, the marine transgression and other environmental changes associated with the end of the Marinoan/Varangian glacial phase should be widely represented in the rock record. Given the rarity and facies-dependence of Ediacara-grade metazoan fossils, it is doubtful whether their first appearance provides a useful chronostratigraphic datum. Hence the Ediacarian System *sensu* Cloud & Glaessner (1982) forms the basis of this study, although following general practice, the Phanerozoic and Palaeozoic are here regarded as commencing at the base of the Cambrian rather than the base of the Ediacarian.

Evidence for low palaeolatitude of the Marinoan glacials in Australia (Embleton & Williams, 1986) and of the Varangian glacials in Europe (Harland & Herod, 1975) suggests that they are the synchronous results of an ice age of global extent (Knoll & Walter, 1992). However, Eyles (1993) proposed that the Marinoan and Varangian glaciations were not synchronous, but related to localised adiabatic ice cover on uplifted crustal blocks associated with two separate episodes of rifting along the 'palaeo-Pacific' and 'palaeo-Atlantic' margins, respectively. Available isotope-chemostratigraphic data are equivocal on the question of synchroneity of the Marinoan and Varangian glacials (see Chapter 6 for a discussion).

The time-rock terms Adelaidean (System), and Willouran, Torrensian, Sturtian and Marinoan (Series) are long-established in Australia (Fig. 0.2; Dunn et al., 1966; Preiss, 1987b and references therein). Boundaries between these Series cannot be located with any precision away from their type localities (Preiss, 1987b), but the terms 'Sturtian' and 'Marinoan' usefully differentiate the two main Adelaidean glacial phases and are widely used for this purpose, even outside Australia. The presence of a System (Ediacarian) within a Series (Marinoan) is an unresolved nomenclatural problem (Preiss, 1987b).

The Ediacarian Period lasted about 50 million years. The Proterozoic-Cambrian boundary is dated at ca. 540-545 Ma and the Varanger ice age at 590-610 Ma (Jenkins, 1984; Conway Morris, 1989; Harland, 1990). Significant recent zircon U-Pb dates include 544 ± 1 Ma for a volcanic breccia within the basal part of the Nemakit-Daldyn succession in the Olenek Uplift, northern Siberia, which must closely approximate the base of the Cambrian (Bowring et al., 1993); 565 ± 3 Ma for volcanic ash in an Ediacara fauna-bearing succession in

Newfoundland (Benus, 1988); and 602 ± 3 Ma and 606 ± 3 Ma for volcanics immediately underlying Varanger tillites in Massachusetts and Newfoundland, respectively (Krough et al., 1989; Kaye & Zartman, 1980). In Australia the only reliable precise isotopic date in the Adelaidean is a U/Pb zircon date of 802 ± 10 Ma from the Willouran Rook Tuff (Fanning et al., 1986; Walter et al., 1995).

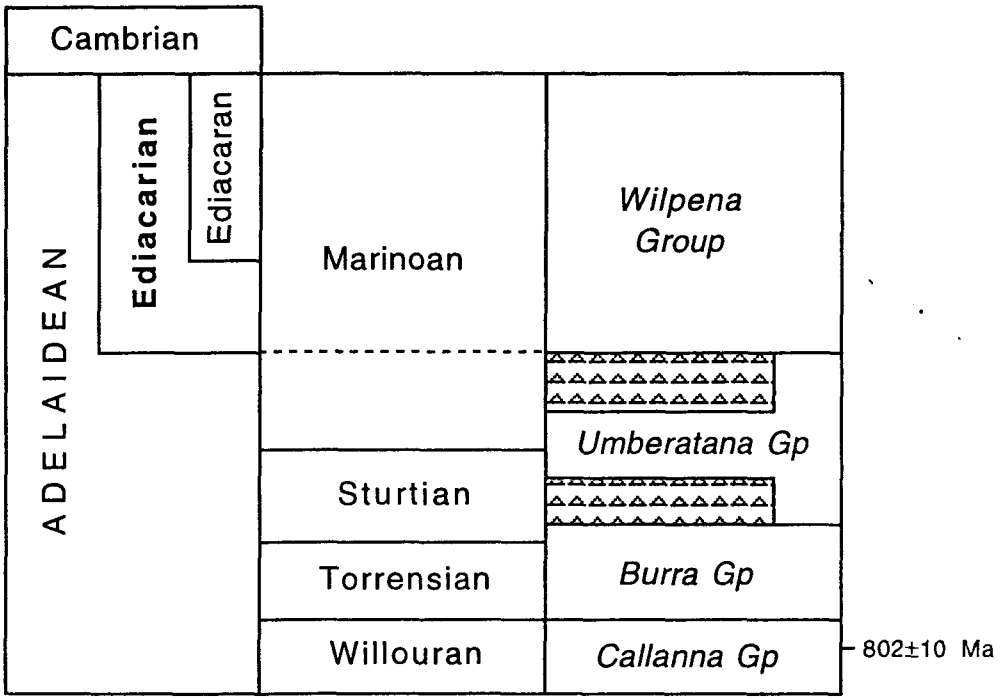

Fig. 0.2: Australian Neoproterozoic chronostratigraphic units, with major lithostratrigraphic units of the Adelaide Geosyncline and major glacial units indicated (right-hand column). Adapted from Preiss (1987b).

Layout and Scope of Thesis

This thesis is divided into chapters most of which are written as somewhat expanded initial versions of papers for publication. Chapters are therefore to some extent self-contained, necessitating some repetition. Chapter 1 is a brief review of the principles underlying isotope chemostratigraphy, and of previous work in the Neoproterozoic. Chapter 2 reviews methods in deriving chemostratigraphic signals from the rock record and develops the approaches used in this investigation. Chapters 3-5 each deal with correlation within closely related sets of basins (Table 0.1). Chapter 6 attempts correlation of Australian sections with those overseas. All analytical data are tabulated in Appendix 1. A reprint of Walter et al. (1994), incorporating reconnaisance isotope chemostratigraphic work on the Savory Basin, is included as Appendix 2. A reprint of Walter et al. (1995), a synthesis of the stratigraphy of

	Basin Stratigraphic Units	Locality/*drillhole*(units sampled)
CHAPTER 3	**Adelaide Geosyncline** Bonney Fm Wonoka Fm Bunyeroo Fm ABC Range Quartzite Brachina Fm Nuccaleena Fm	Brachina Gorge (Bu, W, Bo) Bunyeroo Gorge (N, Br, Bu, W) *BWM1A-1* (N, Br) First Hill (W) Hallett Cove (N) Near Angepena (W) *SCYW1A* (N, Br, A, Bu, W) *UB-17* (N) Umberatana (N) Umberatana (Old Station Ck) (W)
	Officer Basin Rodda Beds Murnaroo Fm 'Giles Mudstone'	*Giles-1* (G) *Munta-1* (M, R) *Observatory Hill-1* (R) *Ungoolya-1* (R)
CHAPTER 4	**Amadeus Basin** Todd River Dolomite Namatjira Fm Julie Fm Pertatataka Fm Olympic/Pioneer Fm Aralka Fm Boord Fm	Acacia Well (P) *Alice Springs-27* (P) Ellery Creek (O, P, J) Fenn Gap (O) Gardiner Range (N) Glen Helen (J) 'Hidden Valley' (O, P) Hijinx Syncline (O) Katapata Gap (J) Mt Capitor (O, P) Mt Conner (O) Mt Greene (B) Phillipson Pound (J) *Rodinga-4* (P) Ross River (P, J, T) *Wallara-1*(A, O, P)
	Georgina Basin Elkera Fm Grant Bluff Fm Elyuah Fm	*DDC (Mt Skinner)-1* (Ely, G, Elk) *DDC (Mt Skinner)-2* (Ely, G) *Huckitta-7* (Elk)
APPENDIX 2	**Savory Basin** Boondawari Fm	Boondawari Creek
CHAPTER 5	**Smithton Basin (Tas)** Smithton Dolomite Keppel Ck Fm Black River Dolomite Dolostone (King I.)	Arthur River (B) *Forest-1* (B, K) King I. (D) Montagu R. (S) Redpa (S)
	Jubilee Region (Tas) Weld River Gp Clark Gp	Jubilee Region (W, C)

Table 0.1: Basins and stratigraphic units sampled in this study, and outcrop sections and drillholes (in italics).

the Centralian Superbasin that includes a preliminary summary of the isotope chemostratigraphic results reported here, is included as Appendix 3.

Seven basins or regions were studied. Table 0.1 lists these, together with all localities and stratigraphic units sampled. A total of about 800 isotopic analyses was undertaken.

TERMINOLOGY

This work follows standard practise (e.g. see Hoefs, 1987) in expressing stable isotope compositions as delta (δ) values representing parts per thousand (‰) difference between the isotopic ratio of the heavier, rarer isotope to the most abundant isotope (i.e. $^{13}C/^{12}C$, $^{18}O/^{16}O$, $^{34}S/^{32}S$), in the sample to the same ratio in an international standard; for instance,

$$\delta^{13}C_{sample} = [(^{13}C/^{12}C_{sample} - {}^{13}C/^{12}C_{PDB\ std.})/{}^{13}C/^{12}C_{PDB\ std}] \times 1000$$

Carbon and oxygen isotopic compositions are given with reference to the Peedee Belemnite (PDB) standard; oxygen isotopic compositions of waters with reference to Standard Mean Ocean Water (SMOW). Sulphur isotopic compositions are relative to the Canyon Diabolo Troilite (CDT) standard.

Fractionation effects are quantified by means of the ε notation:

$$\varepsilon_{A\text{-}B} = [(1000 + \delta_A)/(1000 + \delta_B) - 1] \times 1000$$

Note that units for ε, as for δ, are parts per thousand or ‰; and that for small values of ε and especially when δ values are near 0, differences between $\Delta_{A\text{-}B}$ and $\varepsilon_{A\text{-}B}$ are small:

$$\Delta_{A\text{-}B} = \delta_A - \delta_B \approx \varepsilon_{A\text{-}B}$$

Abundance of ^{87}Sr is measured relative to the stable isotope ^{86}Sr, and is herein quoted as the simple atomic abundance ratio ($^{87}Sr/^{86}Sr$) (Faure, 1986).

In several instances in this study, the sequence-stratigraphic concepts of Vail et al. (1977), van Wagoner et al. (1988) and associated studies are used in evaluating chronostratigraphic patterns in sedimentary successions. Thus the terms *depositional sequence*, *sequence boundary*, *parasequence*, *condensed section*, *maximum flooding surface*, *transgressive systems tract*, and *highstand systems tract* (Fig. 1.14) are used below in the sense of these authors.

ACKNOWLEDGMENTS

I firstly wish to acknowledge the contribution of fellow 'Ediacarian team' members at the School of Earth Sciences, Macquarie University: Malcolm Walter, John Veevers and Kath Grey, who provided encouragement, exchange of ideas, infusions of enthusiasm, and

hospitality on visits to Sydney. The project was funded by an ARC grant to Walter and Veevers. I received financial support from an Australian Postgraduate Research Award and from Mineral Resources Tasmania (formerly Department of Mines), and I thank Rod Hargreaves, formerly Deputy Director, and Tony Brown, State Chief Geologist, for allowing leave of absence and considerable logistical support from MRT.

Most isotope-analytical work was carried out at the Central Science Laboratory, University of Tasmania, where the professionalism of staff, particularly Mike Power, was much appreciated. Strontium and some sulphur isotopic analyses were carried out at the CSIRO laboratories at North Ryde, by Bo Zhou, Geoff Denton and Andrew Todd. Harald Strauss, John Hayes, Anita Andrew, Ric Morante, Roger Summons, Zarko Roksandic, and Dave Whitford provided advice on analytical methods. My ideas have benefitted from discussions at various times with Steve Grant, John Hayes, Prasada Rao, Richard Jenkins, Wolfgang Preiss, John Lindsay, Roger Summons and Ian Percival; and with various participants in the June 1993 Australian field excursion of the Working Group on the Terminal Proterozoic System.

Fieldwork on the mainland was carried out in collaboration with Kath Grey and, at times, Malcolm Walter and John Veevers. In Central Australia the Northern Territory Geological Survey provided a 4WD vehicle, and were generous in provision of corestore facilities. The Conservation Commission of the Northern Territory gave permission for sampling in reserves. Sandy Menpes, of Pacific Oil & Gas, told us of the dolostone outcrop at Mt Conner.

In South Australia, our field program benefited considerably from the local knowledge of Richard Jenkins, Wolfgang Preiss and Chris von der Borch. The South Australian Parks and Wildlife Service gave permission for sampling in the Wilpena Pound area. The South Australian Department of Mines and Energy provided assistance and staff at the SADME Core Library provided a highly efficient service.

In Tasmania, some fieldwork (Arthur River, Huon River traverses) was carried out in collaboration with John Everard. Nic Turner, Tony Brown and Dave Seymour were generous with information and samples. Ritchie Woolley and Les Hay helped in the lab; Les carrying out the AAS analyses; and Ralph Bottrill helped with petrography and the electron probe. Helen Waldron provided samples from King Island.

1

Review of Neoproterozoic Isotope Chemostratigraphy

1.1 Introduction

Stratigraphic patterns of change in stable isotopic composition of marine chemical sediments have been known for some time (e.g. Emiliani, 1955; Keith & Weber, 1964; Holser & Kaplan, 1966; Peterman et al., 1970; Veizer & Hoefs, 1976), but the exploitation of such patterns for chemostratigraphic purposes in Proterozoic successions is relatively new, dating from the seminal paper of Knoll et al. (1986). Isotope stratigraphy, particularly of carbon and strontium, is becoming increasingly useful in Neoproterozoic correlation, aided by an expanding database of results, a better understanding of the mechanisms of secular change, and the establishment of techniques to monitor post-depositional alteration of isotopic compositions (e.g. Knoll et al., 1986; Brasier et al., 1990; Asmerom et al., 1991; Kaufman et al., 1991, 1992; Narbonne et al., 1994; Kaufman & Knoll, 1995). The magnitude of observed $\delta^{13}C$ variations in Neoproterozoic successions makes this interval uniquely well suited to carbon isotope stratigraphy (Kaufman & Knoll, 1995).

The stable isotopes ^{13}C, ^{18}O and ^{34}S, and the radiogenic isotope ^{87}Sr are of most interest in chemostratigraphy firstly because their oceanic residence times are sufficiently long that their instantaneous distribution throughout the global ocean approaches uniformity, secondly because they undergo large natural variations in abundance that lead to secular change in seawater isotopic compositions, and thirdly because preservation of the original marine imprint in the rock record appears to be commonplace and post-depositional alteration is generally recognisable (Fallick & Hamilton, 1989; Kaufman & Knoll, 1995).

This chapter has two parts. Firstly, briefly described below for each element are mechanisms of secular change in seawater isotopic composition and implications for the nature of the isotope signal in the rock record. Secondly there is a brief review of published work on isotope chemostratigraphy in Neoproterozoic to early Cambrian sequences, with emphasis on the Ediacarian, leading to a brief synthesis of chemostratigraphic data for Ediacarian and correlative sequences worldwide. Kaufman & Knoll (1995) review most of these issues in relation to C isotopes.

1.2 Mechanisms of secular change

1.2a Carbon Isotopes

Two mechanisms of secular change must be addressed in ^{13}C chemostratigraphy (e.g. Margaritz et al., 1992): (i) Change in average seawater isotopic composition resulting from changes in the magnitudes, or isotopic compositions, of the fluxes into and out of the oceanic reservoir; (ii) Change in the vertical oceanic ^{13}C gradient, that may strongly affect ^{13}C abundance in surface waters without necessarily altering average seawater isotopic composition.

Mechanism (i)

The *average* carbon isotopic composition of dissolved inorganic carbon in seawater ($\delta^{13}C_{DIC}$) is maintained by isotopic compositions and relative strengths of carbon fluxes into and out of the global ocean, shown schematically in Fig. 1.1 (Broecker, 1970; Schidlowski et al., 1983; Strauss et al., 1992d). Carbon entering the oceanic reservoir from continental weathering or from the mantle has a long-term average isotopic composition of approximately -5 ‰. Carbon leaves the oceans as either carbonate sediment or as organic carbon. The latter flux is limited by nutrient availability to roughly 0.2 of the total outward flux (Broecker & Peng, 1982). Marine HCO_3^- and CO_3^{2-} exchange readily with dissolved CO_2 (the principal substrate for photosynthetic carbon fixation). Autotrophic carbon fixation is accompanied by a large fractionation resulting in depletion of ^{13}C in organic matter by 25-30 ‰ relative to dissolved inorganic carbon (Schidlowski et al., 1983; Schidlowski, 1988). Withdrawal of organic matter thus leaves the oceanic dissolved inorganic carbon reservoir enriched in the heavier isotope relative to the input flux.

Isotopic compositions of primary marine carbonates ($\delta^{13}C_{carb}$), on the other hand, are slightly enriched (by 0 to 2 ‰) relative to dissolved inorganic carbon of ambient seawater, and carbonate sedimentation has little net effect on $\delta^{13}C_{DIC}$. The residence time of carbon in the modern oceans is ca. 10^5 y (e.g. Broecker & Peng, 1982). Long-term (>ca.10^5 y) changes in average $\delta^{13}C_{DIC}$ are therefore considered to result mainly from changes in the fraction of carbon buried as organic matter (Broecker, 1970; Holser et al., 1988; Strauss et al., 1992d).

Shorter-term, non-steady-state changes in oceanic $\delta^{13}C$ may also occur, for example the early Holocene 0.7 ‰ positive shift caused by sequestering of 3% of oceanic DIC into terrestrial biomass (Shackleton, 1977; Adams et al., 1990) or shelf sediments (Broecker &

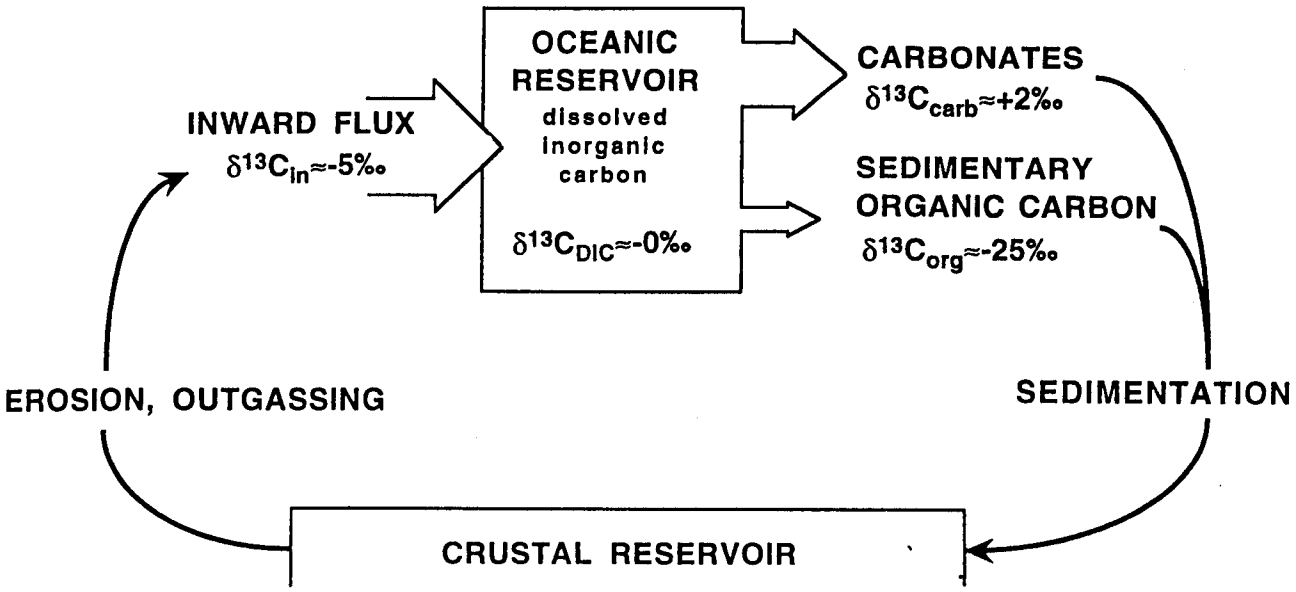

Fig. 1.1: Major carbon fluxes and typical isotopic compositions into and out of the global ocean. Adapted from Schidlowski et al. (1983) and other sources.

Peng, 1982). In the absence of terrestrial biomass, change in the total biomass size is not considered in itself to be a significant cause of $\delta^{13}C_{DIC}$ change in Neoproterozoic oceans (cf. Shackleton, 1977; Margaritz, 1989): total marine biomass carbon is presently only ca. 0.00005 the size of the oceanic dissolved inorganic carbon reservoir (Harte, 1988).

Simple modelling of the global mass balance shows that at steady state (i.e. at timescales of greater than 10^5 years, the residence time of carbon in the oceans) the fraction of carbon buried as organic carbon ('f_{org}') is related to isotopic compositions of the fluxes by the equation

$$f_{org} = (\delta^{13}C_{carb} + 5)/\Delta_B$$

(Strauss et al., 1992d) where Δ_B is the difference in isotopic composition between the global fluxes of organic carbon and carbonate carbon undergoing burial at a particular time ($\Delta_B = \delta^{13}C_{carb} - \delta^{13}C_{org}$). Δ_B is largely a function of ε_P, the fractionation associated with photosynthesis, in turn affected by physiological and ecological parameters that are variable in space and time (Hayes et al., 1983, 1989; Rau et al., 1989; Freeman & Hayes, 1992; Des Marais et al., 1992; and see Chapter 2).

Another possible source of long-term change in average oceanic $\delta^{13}C_{DIC}$ is change in the isotopic composition of the incoming flux (δ_{in}), usually assumed to be close to -5 ‰, the global average isotopic composition of crustal carbon (Holser et al., 1988). At times - such

as just after marine regressions, when large areas of organic-rich sediment might be exposed to erosion - values significantly lower than this might be possible (Berger & Vincent, 1986). However, the possibility of changes in δ_{in} remains largely unevaluated in modelling studies.

The carbon isotope record thus charts the relative strengths of burial fluxes of oxidised and reduced carbon species and is an important monitor of the oxygen cycle. A few studies have used globally integrated isotope chemostratigraphic data to model the release of oxidising potential from the carbon cycle through the Proterozoic (e.g. Knoll et al., 1986; Des Marais et al., 1992; Derry et al., 1992). The ratio f_{org} is not a direct measure of the release of oxidising power; the rate of cycling through the exogenic reservoirs must also be estimated. Two approaches have been used. Des Marais et al. (1992), in a study spanning the whole Proterozoic, assumed that the long-term rate of sedimentary recycling was essentially constant. They found periods of enhanced organic carbon burial at 2.1 - 1.8 Ga and 1.1 - 0.8 Ga, a conclusion that was sufficiently robust to allow for substantial variation in the rate of sedimentary recycling. These times can be correlated with intervals of enhanced global rifting and orogeny rather than with development of new biological sources of O_2 (Des Marais et al, 1992).

Derry et al. (1992), on the other hand, used Sr and Nd isotope data to constrain rates of continental weathering and hence sedimentary recycling. Low marine $^{87}Sr/^{86}Sr$ throughout the Cryogenian implies low rates of sedimentary cycling and hence low rates of release of oxidising power despite high f_{org} (Fig. 1.13). In the early Ediacarian, strongly rising $^{87}Sr/^{86}Sr$ combined with high f_{org} implies a very high rate of release of oxidising power, very likely accompanied by atmospheric O_2 buildup. Significantly, this coincides with the first appearance of diverse assemblages of metazoans (the Ediacara fauna).

Mechanism (ii)

Although present ocean mixing time (ca.10^3 y) is much less than the residence time of carbon in the oceans, $\delta^{13}C_{DIC}$ is not spatially homogeneous in today's oceans (see Kroopnick, 1985). The most significant heterogeneity is ^{13}C enrichment of surface waters (< ca. 50 m) by 1 to 3 ‰ relative to deeper waters by the 'photic pump effect': fixation of carbon in the photic zone, sinking of this depleted carbon into deeper waters and its oxidation and re-entry into the dissolved inorganic carbon reservoir at depth (Berger & Vincent, 1986). Geographic variations in productivity and in the strength of vertical water movements lead to secondary, areal variation in $\delta^{13}C_{DIC}$ (Kroopnick, 1985). Modern oceans are relatively well-mixed mainly because of strong latitudinal temperature gradients associated with the Antarctic icecap (Broecker & Peng, 1982). In the relatively poorly mixed Black Sea,

difference in $\delta^{13}C_{DIC}$ between surface and bottom waters is much greater (ca. 7 ‰: Deuser, 1970). Poorly-mixed (stratified) ocean states may have been commonplace in the past (Goodfellow, 1986). Changes in the oceanic vertical $\delta^{13}C_{DIC}$ gradient are therefore a potential mechanism for generating secular $\delta^{13}C$ change in the sedimentary record. Changes will be particularly marked in the (volumetrically much smaller) upper water layer (Fig. 1.2). Since $\delta^{13}C$ chemostratigraphic studies generally use carbonates precipitated in shallow-marine environments (i.e. in the upper water layer) this mechanism may be more important than generally realised, and remains largely unknown and unevaluated in pre-Cretaceous successions (Hoffman et al., 1991; Margaritz et al., 1992; for an exception see Aharon & Liew, 1992).

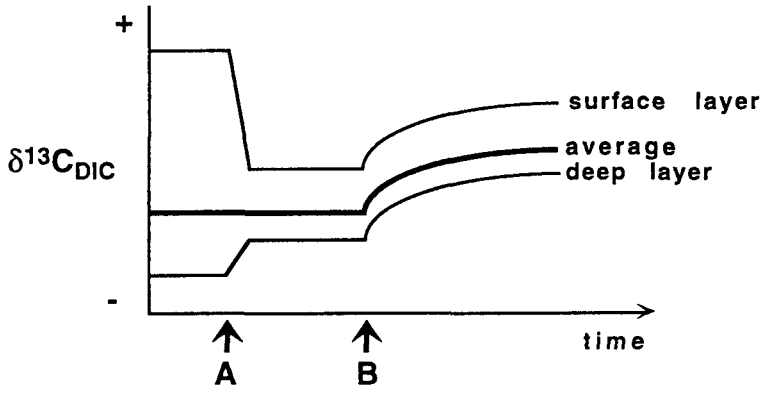

Fig. 1.2: Conceptual model illustrating changes in carbon isotopic composition of average, surface and deep ocean water with , at time A, a change in ocean state from poorly to well-ventilated; at time B, an instantaneous increase in f_{org}.

In broad terms, the vertical oceanic $\delta^{13}C$ gradient may change in two ways: by variations in productivity, and by changes in deep-ocean ventilation. Small (±1 ‰) productivity-linked changes in the oceanic vertical $\delta^{13}C_{DIC}$ gradient are possible on timescales of 10^2 to 10^3 years (Berger & Vincent, 1986). Disappearance of the gradient and a negative shift in surface-water $\delta^{13}C_{DIC}$ of up to 3 ‰, as a result of catastrophic productivity decline, seems to have occurred at the Cretaceous-Tertiary boundary (the 'Strangelove effect': Broecker & Peng, 1982, p. 466; Zachos & Arthur, 1986; Kump, 1991). A similar event proposed for a negative shift near the Proterozoic - Cambrian boundary (Hsü et al., 1985) now seems doubtful (Kirshchvink et al., 1991).

Periods of oceanic stagnation or stratification have been proposed to lead to strong isotopic differentiation of surface and deeper waters, with surface waters relatively enriched in ^{13}C

(also ^{32}S, and ^{87}Sr: Hoffman et al., 1991; Gruszczynski et al., 1992; Goodfellow, 1986). Faster mixing or destratification could then lead to relatively rapid (10^3 y) and potentially large changes in isotopic composition of shallow waters (and hence of sediments deposited on the shelves). Destratification events have been proposed to explain apparently rapid negative shifts in $\delta^{13}C$ in the Neoproterozoic (e.g. Donnelly et al., 1990) and late Permian (Gruszczynski et al., 1992; but see Baud et al., 1989). Periods of faster oceanic overturn may explain the consistent association of negative $\delta^{13}C$ excursions with glacial periods in the Neoproterozoic (Knoll et al., 1986; Kaufman et al., 1991).

Carbonates or organic carbon precipitated or fixed in the lower water layer will carry relatively depleted isotopic signatures. Some ^{13}C-depleted Palaeoproterozoic carbonates associated with iron formation are interpreted to have been deposited under the lower water mass of stratified oceans (Beukes et al., 1990). Some Ediacarian carbonates in the present study are inferred to have a similar origin (see sections 3.3c, 3.6c, 6.2); although Kaufman & Knoll (1995) considered all Neoproterozoic carbonates in their global review to be representative of upper water layer, or well-mixed ocean chemistries. A false impression of secular $\delta^{13}C$ change may be gained if, through sediment aggradation or relative sealevel change, the sediment-water interface in a given succession crosses the pycnocline. For this and other reasons, sedimentary facies analysis is imperative in $\delta^{13}C$ chemostratigraphic studies.

In summary, at steady-state (i.e. for excursions lasting $>10^5$ y) the mean ocean $\delta^{13}C_{DIC}$ is set by the organic fraction of the total carbon burial rate, and Δ_B. Secular change in $\delta^{13}C_{DIC}$ results in parallel changes in both carbonate and organic carbon, although organic carbon is a less reliable signal-carrier because of the inherent variability of ε_p and a kinetic isotope effect associated with thermal maturation (see Chapter 2). Surface waters may at times have had significantly ^{13}C-enriched compositions relative to deep waters and rates of change in the shallow realm are potentially rapid. Longer-term positive isotopic excursions are linked to high f_{org} and thence to enhanced conditions for deposition of hydrocarbon source rocks (e.g. Schlanger et al., 1987); and in the Proterozoic also to increases in atmospheric oxygen (Knoll et al., 1986; Lambert & Donnelly, 1990; Derry et al., 1992; Des Marais et al., 1992).

1.2b Oxygen Isotopes

Carbonates are enriched in ^{18}O by 25 to 30 ‰ compared to water at isotopic equilibrium, and this fractionation is strongly temperature-dependent (Epstein et al., 1953; Craig, 1965): $\delta^{18}O$ of common carbonate minerals decreases by roughly 1 ‰ for every 4°C increase in temperature. The relationship is known with some precision for calcite:

$$t(°C) = 15.7 - 4.36(\delta_c - \delta_w) + 0.12(\delta_c - \delta_w)^2$$

where δ_c is the $\delta^{18}O$ value of calcite and δ_w that of water, relative to SMOW (Anderson & Arthur, 1983). The temperature dependence of oxygen fractionation in carbonates and other minerals is the basis for most surface-environment palaeotemperature work, but the $\delta^{18}O$ of the water must be known unless coprecipitated mineral pairs can be used (Karhu & Epstein, 1986).

$\delta^{18}O$ in carbonates is relatively vulnerable to diagenetic alteration, because of the high concentration of isotopically exchangeable oxygen in diagenetic fluids and because burial cements are generally strongly depleted because of high temperatures of precipitation. The $\delta^{18}O$ of carbonates, cherts and phosphates decrease irregularly with increasing geological age (e.g. Veizer & Hoefs, 1976). Whether this is due to substantially higher average temperatures in the past, secular change in $\delta^{18}O$ of seawater, diagenesis, or sequestering of ^{18}O into deep saline waters, is disputed. There is evidence that oceanic $\delta^{18}O$ is buffered near 0 ‰ by high-temperature seawater-basalt interaction (Muehlenbachs & Clayton, 1976). However, this value gives unreasonably high palaeotemperatures (40°-70°C) for Palaeozoic and Precambrian rocks. Similarity of the $\delta^{18}O$ trend in phosphates, cherts and carbonates argues against a purely diagenetic explanation. Hudson & Anderson (1989) recently reviewed problems associated with the interpretation of the oxygen isotope record.

The huge mass of the oceans precludes rapid secular change in seawater $\delta^{18}O$ except by glaciation (Gregory, 1990). Late Cenozoic fluctuations of 1.5 ‰ are related to volume of continental ice sheets that preferentially withdraw ^{16}O from the oceans (Emiliani, 1955; Broecker & Peng, 1982).

Oxygen isotopes are unlikely to play a significant role in Proterozoic chemostratigraphy, because secular changes in seawater $\delta^{18}O$ are unlikely to have been of sufficient size to be detectable through the 'noise' of temperature variation and diagenetic change. A possible exception is glacial to non-glacial variation in which the combined effect of colder temperatures and loss of oceanic ^{16}O to icecaps during glacial phases may have produced a useful signal.

1.2c Sulphur Isotopes

Like carbon, secular variation in seawater isotopic composition of sulphur can be understood in terms of fluctuations in the operation of the elemental crust-exosphere cycle (Holser et al., 1988). The $\delta^{34}S$ of the averaged weathering flux is close to 0 ‰. The main dissolved sulphur species in the sea - sulphate - is maintained at considerably heavier isotopic

compositions by sequestering of the lighter isotope into the reduced, largely biogenic species (sedimentary sulphides produced by bacterial sulphate reduction). As with carbon, the flux of sulphur into sediments is divided into an isotopically light reduced species and a heavy oxidized species. Precipitation of sulphate as evaporite minerals entails enrichment of just 1 to 2 ‰ over dissolved sulphate. Marine sulphate $\delta^{34}S$ is spatially homogeneous as residence time of sulphur (20 million years) greatly exceeds oceanic mixing time (ca. 10^3y). Thus evaporite sulphate, if exempt from replacement or biological reduction, monitors closely the isotopic composition of dissolved marine sulphate.

The formation of sedimentary sulphide, on the other hand, is subject to a large and variable kinetic isotope effect resulting in depletion of 30 to 50 ‰ relative to the dissolved sulphate precursor. The great bulk of sulphate reduction is carried out by desulfobacteria as an energy-yielding anaerobic metabolic process, coupling reduction of sulphate with oxidation of organic matter. Resultant bacteriogenic H_2S reacts with sedimentary iron, and sulphide isotopic ratios are preserved mainly in pyrite (Berner, 1970; 1984). As desulfobacteria are obligate anaerobes, most sulphate reduction takes place in interstitial porewaters of newly deposited sediment, in microenvironments not subject to free replenishment of marine sulphate. In such closed or semi-closed systems the preferential removal of light sulphur leads to the $\delta^{34}S$ values of both residual sulphate and late-formed sulphide becoming heavier with increasing extent of the reaction. Thus - unfortunately for the utility of sulphide as a chemostratigraphic signal-carrier - a very wide spread of isotopic compositions is possible. Recent bacteriogenic sulphide is typically depleted by 15 to 45 ‰ relative to seawater sulphate.

In the Phanerozoic, there is a broad inverse correlation between $\delta^{13}C_{carb}$ and $\delta^{34}S_{sulphate}$ (Veizer et al., 1980), while on the basis of much sparser data, no such correlation exists in the Precambrian. At the end of the Proterozoic, cycles of carbon and sulphur became linked, apparently by mutual interaction with O_2 (Berner, 1987; Garrels & Lerman, 1984). However, the mechanisms underlying the Phanerozoic linkage of the carbon and sulphur cycles are controversial (e.g. Berner & Raiswell, 1983; Walker, 1986).

The total observed range of secular variation in marine sulphate $\delta^{34}S$ (Fig. 1.10) is much greater than the corresponding isotopic variation seen in marine carbonate, mainly because formation of pyrite is limited only by the amount of organic matter available to the sulphate-reducing bacteria (Berner, 1984) and the proportional size of the flux is consequently much more variable, and generally larger, than f_{org}. The much longer oceanic residence time of sulphate means that potential rates of change of $\delta^{34}S$ are slower than oceanic $\delta^{13}C$ and less

fine structure is apparent in the Phanerozoic $\delta^{34}S$ curve. Rapid rises in oceanic $\delta^{34}S$ in the Triassic, Devonian, and possibly the Neoproterozoic, however, appear to be too fast to be accommodated by geologically reasonable rates of sulphide burial (Claypool et al., 1980). Holser (1977) gave as a possible explanation, isolation of a large stratified hypersaline basin with sulphide precipitation causing enrichment of sulphate in the bottom brine. Tectonic destruction of the basin then released the accumulated heavy sulphate, to mix rapidly with the world ocean and give a worldwide sharp rise in oceanic $\delta^{34}S$. Hoffman et al. (1991) suggest that such rapid rises may be explained by mixing events following prolonged periods of global oceanic stratification.

In conclusion, the chemostratigraphic utility of ^{34}S is enhanced by the potentially large amplitude of seawater secular variation but is severely limited by the relative rarity of evaporites in the Proterozoic rock record and by the partial closure of the diagenetic system in which sulphides are precipitated. Sedimentary sulphides are likely to reflect only the largest secular changes in oceanic $\delta^{34}S_{sulphate}$.

1.2d Strontium Isotopes

Strontium's four natural isotopes include ^{87}Sr, the proportion of which is slowly increasing due to radioactive decay of ^{87}Rb, with a half-life of 48.8 Gyr (Steiger & Jäger, 1977). There is no measurable natural fractionation of Sr isotopes, because of the small relative mass differences. In different geological reservoirs the $^{87}Sr/^{86}Sr$ ratio is proportional to the age and Rb content. Rubidium, a lithophile element, is enriched in continental crust over mantle by a factor of about 10. Hence mantle and oceanic crust have a depleted $^{87}Sr/^{86}Sr$ ratio of approximately 0.703, while the continents are enriched in ^{87}Sr ($^{87}Sr/^{86}Sr > 0.710$). This enrichment is highest in the oldest cratonic regions. Oceanic crust contributes ^{87}Sr-depleted strontium to seawater through hydrothermal interaction at midocean ridges, while ^{87}Sr-enriched ('radiogenic') strontium enters the dissolved load of seawater through continental erosion. Secular variation in the strontium isotopic composition of seawater is essentially a result of changes in the relative strengths of these two fluxes (Veizer, 1989).

The strontium isotopic ratio is spatially uniform throughout the oceans as the residence time of strontium, 2.5 to 4 x 10^6 yr (Hodell et al., 1990; Palmer & Elderfield, 1989) greatly exceeds the oceanic mixing time; and unlike carbon isotopes, there are no inhomogenieties generated by biological fractionation. Even in brackish waters the ratio remains essentially unchanged because of the relatively very low concentrations of strontium in fresh water (Veizer & Compston, 1974). However, Gruszczynski et al. (1992) recently suggested that different $^{87}Sr/^{86}Sr$ ratios may arise in surface and deep waters during times of ocean

stratification, and they proposed that a rapid late Permian drop in $^{87}Sr/^{86}Sr$ was the result of a destratification 'event'.

1.3 Neoproterozoic - early Cambrian isotope stratigraphy

1.3a $\delta^{13}C$ Stratigraphy

Early, exploratory isotopic studies of Precambrian sedimentary rocks used large numbers of isolated samples (e.g. Schidlowski, 1975; Veizer & Hoefs, 1976). Clear evidence of preservation of chemostratigraphic $\delta^{13}C$ signals only emerged with relatively recent, systematic studies of widespread similar-aged sequences (e.g. Knoll et al., 1986; Brasier et al., 1990). Stratigraphic patterns of fluctuating $\delta^{13}C$ have now been documented from a large number of geographically widespread Cryogenian to early Cambrian sequences. Integration of these signals, assisted by $^{87}Sr/^{86}Sr$ chemostratigraphy, biostratigraphy, glaciostratigraphy and radiometric dating, to produce a 'global' signal (Fig. 1.13) must rate as one of the most significant recent developments in Neoproterozoic stratigraphy and biogeochemistry (Knoll & Walter, 1992; Kaufman & Knoll, 1995; Kaufman et al., 1993).

Precise carbon isotope chemostratigraphy was first demonstrated by Scholle & Arthur (1980) who documented essentially identical isotope signals from a number of widely separated Cretaceous sequences, confirming the global consistency of the carbonate $\delta^{13}C$ signal during two 'oceanic anoxic events'.

Knoll et al. (1986) documented the carbon isotope stratigraphy of three thick, coeval Neoproterozoic sections in Svalbard and east Greenland. Parallel variations in $\delta^{13}C$ of organic carbon and carbonate were found, persuasive evidence for the predominantly primary nature of the signal. The patterns in all three sections were broadly consonant with each other and with lithostratigraphic and biostratigraphic data. A markedly enriched ($\delta^{13}C_{carb}$ ca. +5 ‰ or higher) isotopic record was found to characterise Cryogenian strata, with minor negative excursions (Fig. 1.3). Fairchild & Spiro (1987) show that a positive (+4 ‰) marine signal persists in carbonates (Elbobreen Fm) between two Varangian diamictites. The (basal Ediacarian?) 'cap dolostone' immediately overlying the diamictite has a distinctly negative (-3 to -3.5 ‰) signature and sparse organic and carbonate data higher up are likewise relatively depleted at first, then rise to $\delta^{13}C_{carb}$ of +2 ‰. The upper Ediacarian record is missing because of a non-marine incursion and a major unconformity.

Similar-aged successions in Namibia were sampled by Kaufman et al. (1991). They found highly enriched carbonates (+6 to +10‰) in the Cryogenian Otavi Group with a pronounced

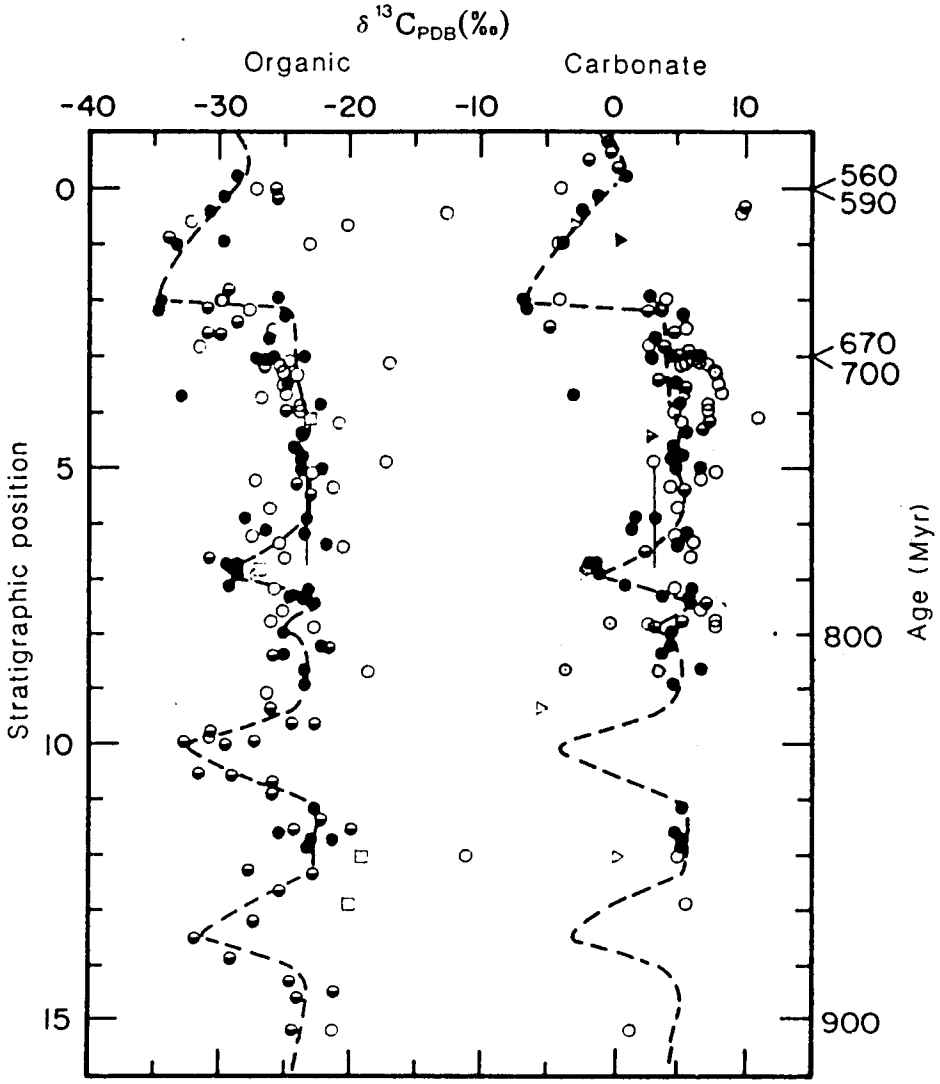

Fig. 1.3: Coupled organic and carbonate $\delta^{13}C$ stratigraphic variation in Svalbard and East Greenland. Analyses from three widely separated sections, each several km. thick, plotted on common depth scale. Numbers at left refer to litho- and biostratigraphic tie points: points 1 and 2 bracket the Varangian glacials. Filled symbols have $\Delta\delta$ within 2‰ of 28.5‰. From Knoll et al. (1986).

negative excursion coinciding with the (probably Sturtian) Chuos Tillite. Unconformably above the ?Marinoan Numees Tillite (Fig. 1.4), there are depleted carbonates (-3 to -6 ‰: Buschmansklippe Fm) succeeded by moderately enriched (+4 ‰) carbonates (uppermost Gariep Group: Fig. 13 of Kaufman et al.). An unconformity separates these units from the overlying Nama Group. The lower Nama Group exhibits an initial rise in $\delta^{13}C_{carb}$ from -2 ‰ up to +6 ‰ in the Zaris Formation. A stratigraphic gap in $\delta^{13}C$ data follows, and is partly coincident with the Vingerbreek Diamictite. Then follows a moderately enriched (ca. +2 ‰) plateau that persists up to a base-Cambrian unconformity. Ediacara-grade metazoan fossils first appear in the Nama Group during the initial rise in $\delta^{13}C$, and range through most of the Nama Group (Fig. 1.4). Kaufman et al. suggest correlation of the positive excursion with

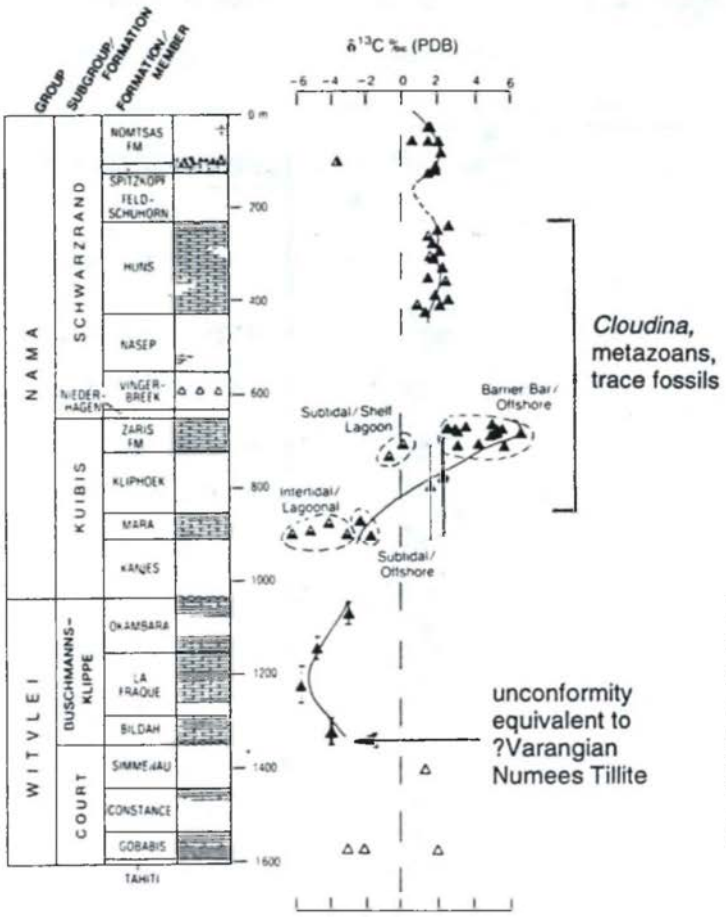

Fig. 1.4: Stratigraphic column, $\delta^{13}C_{carb}$ stratigraphy and distribution of early metazoans in the Witvlei and Nama Groups, Namibia. The Ediacarian here probably extends from the base of the Buschmansklippe Fm. to the base of the Nomtsas Fm. From Kaufman et al. (1991).

that of the Nemakit-Daldynian (see below), but this is clearly in error on biostratigraphic and other grounds (A. J. Kaufman, pers. comm., 1993).

A similar Cryogenian pattern of variation is seen in the Pocatello Formation and Brigham Group of Idaho (Smith et al., in press). A thin dolostone overlying the lower, glacigene part of the Pocatello Formation has a depleted (-3 to -5 ‰) $\delta^{13}C_{carb}$; limestone higher up (in the Caddy Canyon Quartzite) has a highly enriched (up to 8.8 ‰) composition. The rocks have undergone lower greenschist facies metamorphism, and $\delta^{18}O$ and $\delta^{13}C_{org}$ are highly altered. The authors infer a Sturtian (approximately late Cryogenian) age for this succession on the basis of low least-altered $^{87}Sr/^{86}Sr$ and the magnitude of the positive excursion which is not attained in known Varangian or Ediacarian successions. A sequence boundary near the top of the Caddy Canyon Quartzite is stratigraphically equivalent to the ?Varangian Ice Brook Formation (Christie-Blick & Levy, 1989).

Highly enriched (+6 to +12 ‰) $\delta^{13}C_{carb}$ compositions are found in a number of other poorly-dated successions in western North America (Wickham & Peters, 1993, and references therein). At least some of these appear to be pre-Varangian (e.g. Kaufman et al., 1992).

Asmerom et al. (1991) reported lower positive (+3 to +6 ‰) carbonates from the early Cryogenian (850-790 Ma) Shaler Group of northwest Canada.

Narbonne et al. (1994) report $\delta^{13}C$ chemostratigraphic data from the Neoproterozoic Windermere Supergroup of NW Canada (Fig. 1.5). The Keele Formation, immediately underlying the (?Varangian) glacigene Ice Brook Formation, has highly enriched $\delta^{13}C_{carb}$ (+8 to +10 ‰) which, with low $^{87}Sr/^{86}Sr$ (see below) strongly corroborates a pre-Varangian age. Unlike the pre-Varangian record in Spitzbergen (Fairchild & Spiro, 1987), there is a marked negative excursion in the uppermost Keele Formation to -5 to -7 ‰, which is also seen in $\delta^{13}C_{org}$. The (?basal Ediacarian) 'cap dolostone' (here informally known as the 'Tepee dolostone') that immediately overlies the Ice Brook Formation exhibits depleted $\delta^{13}C_{carb}$ (-2 to -5 ‰). There is then a long stratigraphic gap with no $\delta^{13}C$ data, followed by a positive excursion to +7‰ in the uppermost Sheepbed Formation. Higher up, the Blueflower and Risky Formations exhibit a plateau of $\delta^{13}C_{carb}$ values around +1 to +3 ‰. As in the Nama Group, Ediacara-grade metazoan fossils are associated with the positive excursion and plateau (Fig. 1.5). The basal Ingta Formation has a pronounced negative excursion, suggested to be correlative with the Nemakit-Daldynian minimum at approximately the base of the Cambrian (see below).

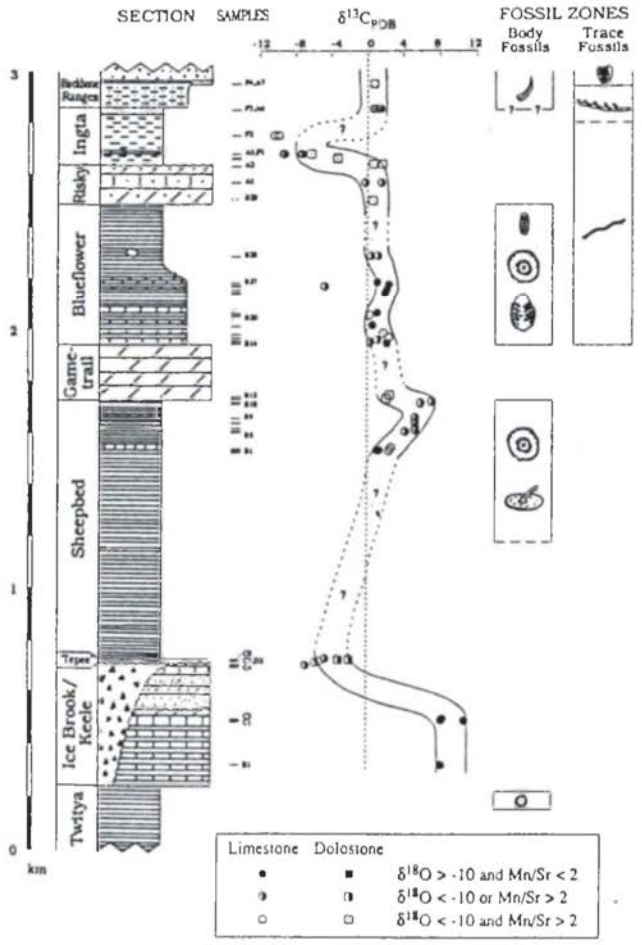

Fig. 1.5: Stratigraphic column, $\delta^{13}C_{carb}$ stratigraphy and distribution of early metazoan fossils in the upper Windermere Supergroup, NW Canada. The Ediacarian probably extends from the base of the 'Tepee Dolostone' to the middle of the Ingta Fm. From Narbonne et al. (1994).

Knoll et al. (1995) document carbon isotope stratigraphy from a late Vendian (Ediacarian) succession on the northern Siberian Platform (Fig. 1.6). The lowest unit, the Mastakh Formation, rests unconformably on Riphean rocks (there is no known record of the Varangian glaciation on this part of the Siberian Platform). The Mastakh Formation is marked by moderately enriched (up to +5.5 ‰) carbonates, and is followed by a thicker succession (Khatyspyt, Turkut Formations) with predominantly lighter (0 to +3 ‰) values. Ediacaran metazoan fossils occur near the top of the Khatyspyt Formation. Shelly fossils of Nemakit-Daldynian aspect appear near the top of the Turkut Formation, and this horizon is followed by the negative, then positive (+4 ‰) excursion in the overlying Kessyusa Formation that appear to mark the Nemakit-Daldynian interval elsewhere (see below). The Proterozoic-Cambrian boundary, marked by the incoming of trace fossils of Cambrian aspect, is situated approximately at the top of the Turkut Formation. A volcanic breccia in the basal Kessyusa Formation is dated at 544 ± 1 Ma (Bowring et al., 1993), an important radiometric constraint on the boundary.

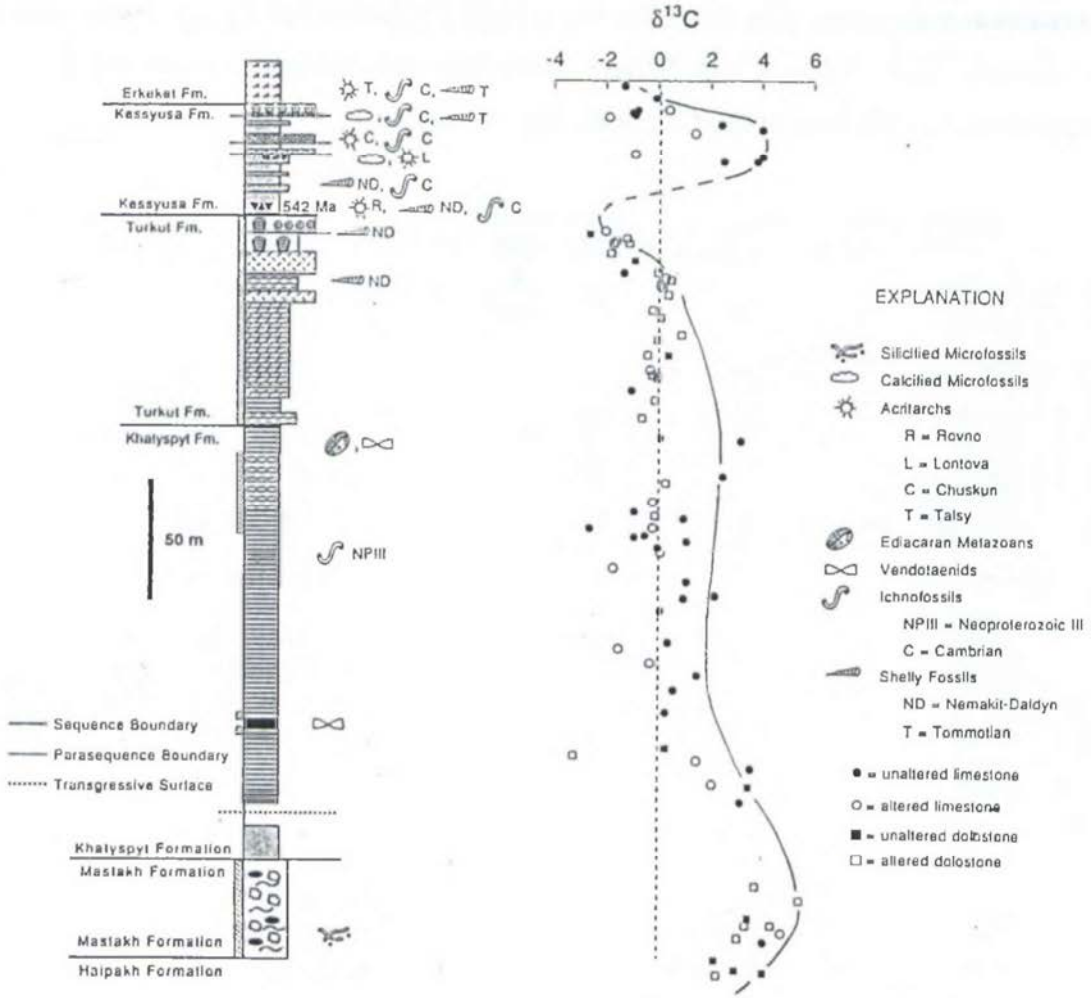

Fig. 1.6: Stratigraphic column, $\delta^{13}C_{carb}$ stratigraphy and fossil occurences in the terminal Proterozoic of the Olenek Uplift, NE Siberia. The Ediacarian probably extends from the unconformable base of the Mastakh Fm. to the top of the Khatyspyt Fm. From Knoll et al. (1994).

A $\delta^{13}C$ profile from the Yangtze Gorge, between ?Varangian tillite and basal Cambrian, was published by Lambert et al. (1987). Values initially range up to +7 ‰ in the Doushantuo Formation, where some organic-rich strata have anomalously depleted, probably altered isotopic compositions. The Doushantuo Formation contains large acanthomorphic acritarchs similar to those of the upper Pertatataka Formation of the Australian Ediacarian (Zang & Walter, 1992; and see Chapter 3). An irregular plateau around +2 to +3 ‰ is seen in the overlying Dengying Formation, which contains an Ediacara-type fauna (Fig. 1.7). A disconformity may be present at the base of the Cambrian here (Brasier et al., 1990).

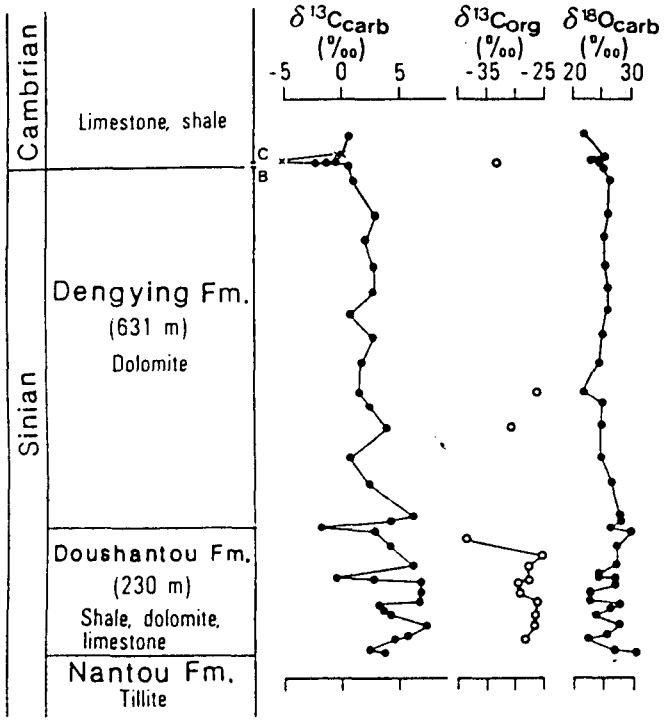

Fig. 1.7: $\delta^{13}C_{carb}$ data from the Sinian-early Cambrian sequence from the Yangtze Gorge. From Lambert et al. (1987).

G. Williams (1979), in a study of Sturtian and Marinoan 'cap dolostones' in Australia, found a predominance of slightly negative values (averaging -1.9 ‰).

Jenkins et al. (1992) and Pell et al. (1993) report carbonate $\delta^{13}C$ chemostratigraphic data for some Ediacarian units in South Australia. Strongly depleted (-6 to -8 ‰) carbonates are found through most of the middle Ediacarian Wonoka Formation in the Adelaide Geosyncline (see also Urlwin et al., 1993). There is a swing to highly enriched (+6 to +7 ‰) values in the topmost Wonoka and overlying Billy Springs Formation. The Ediacara fauna occurs stratigraphically higher, in the middle of the thick siliciclastics of the Pound Subgroup. The upper Rodda beds of the nearby Officer Basin have a $\delta^{13}C_{carb}$ signature of 0 to +3 ‰, and partly because this is a signature characteristic of Ediacara fauna-bearing successions in other parts of the world, these authors correlate the upper Rodda beds with the

Pound Subgroup. However, this correlation is controversial (compare with Sukanta et al., 1991; Walter et al., 1995; and see Chapter 3). In the present study, a different Officer Basin-Adelaide Geosyncline correlation scheme to that of Jenkins et al. (1992) and Pell et al. (1993) is presented on the basis of a synthesis of $\delta^{13}C_{org}$, $\delta^{13}C_{carb}$ and $^{87}Sr/^{86}Sr$ data (see Chapters 3, 6).

Proterozoic-Cambrian boundary studies

Recent interest in the definition of the Precambrian-Cambrian boundary has led to a spate of publications on carbon isotope stratigraphy from boundary localities around the world. Many of these papers were reviewed by Brasier et al. (1990). At widespread localities - most notably China (Meishucun), Iran, Siberia (Margaritz et al., 1986, Knoll et al., 1995), India (Aharon et al., 1987), and Morocco (Tucker, 1986a) - there is a $\delta^{13}C$ maximum, preceded and followed by isotopically negative carbonates (Fig. 1.8). Global correlation of the $\delta^{13}C$ peak (and associated minima) is proposed, and this seems to be commensurate with biostratigraphic evidence (Brasier et al., 1990). In Siberia the base of the Tommotian - long regarded as synonymous with the base of the Cambrian - coincides with the steep decline in $\delta^{13}C$ above this maximum. In many sections, small shelly-fossil assemblages of Nemakit-Daldynian aspect first appear within the $\delta^{13}C$ minimum before the peak.

Kirschvink et al. (1991) and Margaritz et al. (1991) extended the Siberian profile upwards into the Atdabanian, documenting three later, less pronounced $\delta^{13}C$ maxima (Fig. 1.9). With correlations backed up by magnetostratigraphy, they found essentially identical signals at widespread localities across the Siberian Platform, and they refined the $\delta^{13}C$ correlation between Siberia and Morocco. In contrast to Brasier et al. (1990), Kirschvink et al. correlate the Meishucun (China) $\delta^{13}C$ peak (Fig. 1.8g) with the fourth (Atdabanian) $\delta^{13}C$ maximum in Siberia. The steep decline in $\delta^{13}C$ above the Meishucun peak is attributed partly to a sedimentary hiatus.

A section in Newfoundland was recently chosen as the Precambrian-Cambrian boundary stratotype. The horizon selected is older than the base of the Tommotian on biostratigraphic evidence, and lies within a sequence lacking carbonates (Brasier et al., 1992). Strauss et al. (1992a) attempted organic carbon isotope chemostratigraphy but found a large scatter of values, attributed to thermal alteration and low TOC. However, a carbonate $\delta^{13}C$ profile compiled from slightly younger rocks in Newfoundland and England is similar to the Siberian profile, and suggests that the pre-Tommotian (Nemakit - Daldynian) $\delta^{13}C$ rise and maximum lie within the (newly-defined) Cambrian (Brasier et al., 1992).

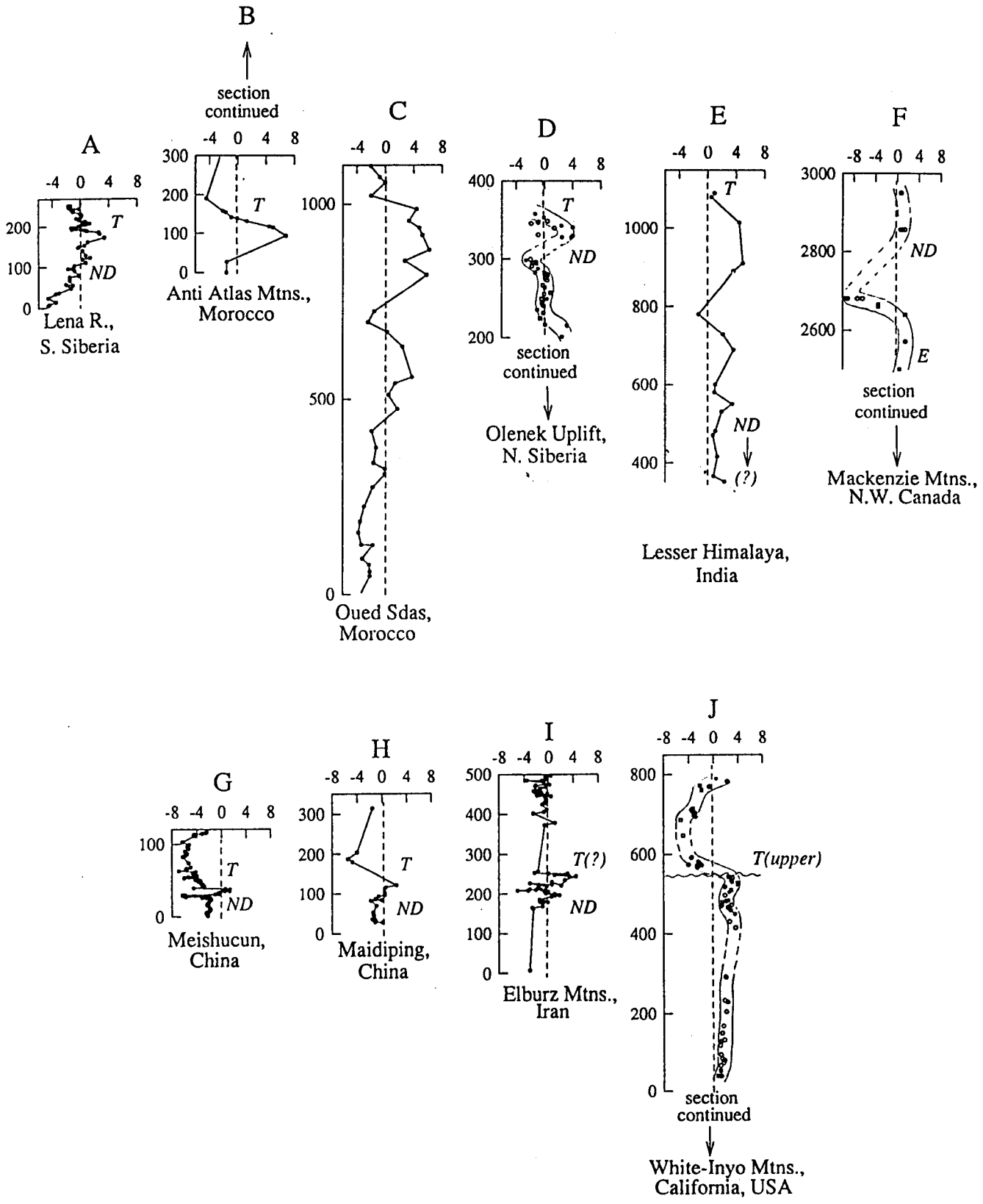

Fig. 1.8: Precambrian-Cambrian boundary profiles. In some profiles, filled symbols are least-altered; open symbols are altered. T = Tommotian small shelly fossils; ND = Nemakit-Daldynian small shelly fossils. A, from Margaritz et al. (1986); B, Tucker (1986); C, Margaritz et al. (1991); D, Knoll et al. (1994); E, Aharon et al. (1987); F, Narbonne et al. (1994); G and H, Brasier et al.(1990); J, Corsetti & Kaufman (in press). From Kaufman & Knoll (1995).

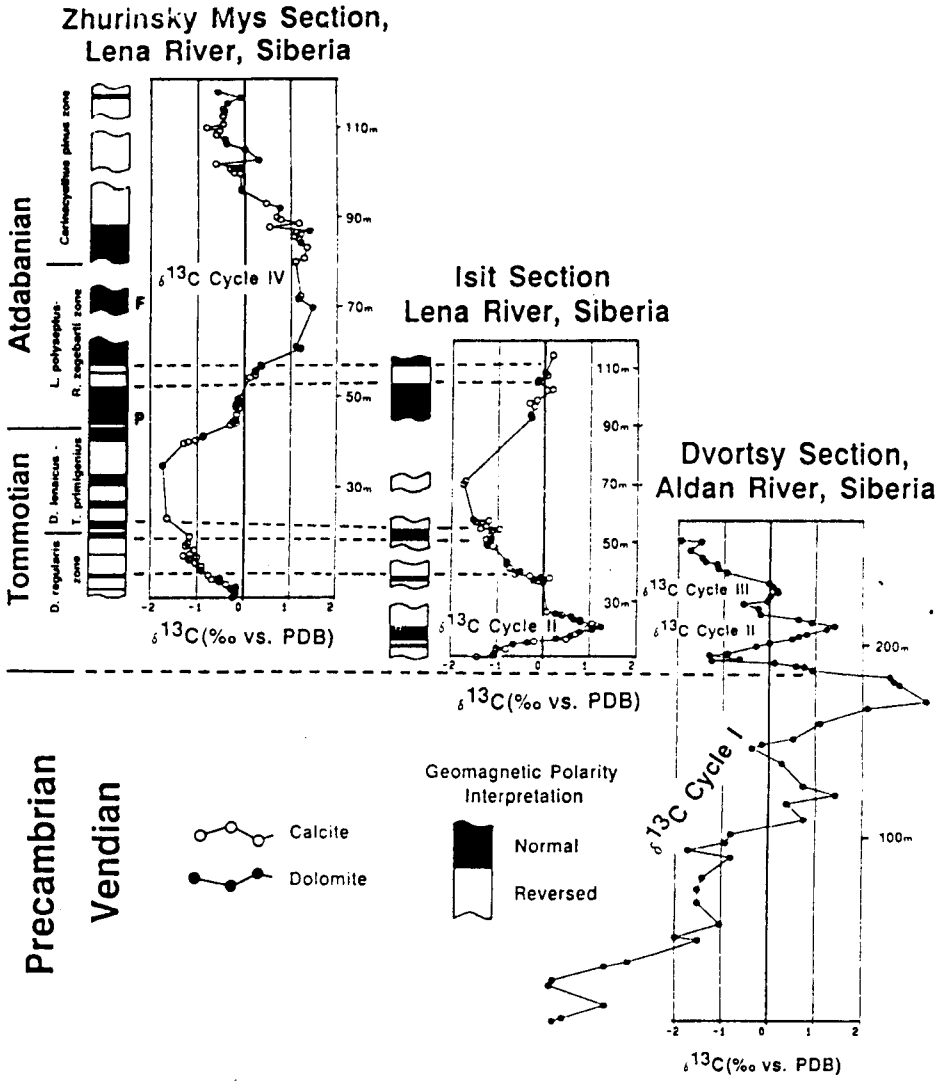

Fig. 1.9: Part of Siberian carbon isotope stratigraphic and magnetostratigraphic data of Kirschvink, Margaritz and co-workers, illustrating extremely well-defined $\delta^{13}C_{carb}$ signals form widespread localities. The base of the Cambrian has since been revised downward to include most of the Dvortsy section. From Kirschvink et al. (1991).

Brasier et al. (1994) have recently extended the Siberian $\delta^{13}C_{carb}$ signal throughout the lower Cambrian, documenting a total of eleven lower Cambrian 'cycles' of $\delta^{13}C_{carb}$.

1.3b $\delta^{18}O$ Stratigraphy

A number of studies have put forward estimates of $\delta^{18}O$ for Proterozoic seawater, based on isotopic compositions of well-preserved ooids and marine cements and assuming a palaeotemperature on the basis of a uniformitarian sedimentological interpretation. Examples are (relative to SMOW): -9.75 ± 1.0 ‰ at 1.9 Ga (Burdett et al. 1990); -0.5 ± 2 ‰ at 1.0 Ga (Zempolitch et al., 1988); -4 ± 2 ‰ at 0.8 Ga (Tucker, 1986b) and -3 ± 1 ‰ at 0.6 Ga (Fairchild & Spiro, 1987). Oxygen isotope ratios of well-preserved brachiopods and marine cements suggest oceans in the mid Palaeozoic were -2 to -3 ‰ in $\delta^{18}O$ (Popp et al.,

1986; Veizer et al., 1986; Carpenter et al., 1991), and on weaker evidence, -7‰ in the Cambrian (Wadleigh & Veizer, 1992).

Glacial to non-glacial variation in carbonate $\delta^{18}O$ may have been sufficiently large and rapid to have left a useful signal. In the present study, probably-marine carbonates coeval with the Marinoan glaciation have $\delta^{18}O$ several ‰ heavier than younger carbonates (see sections 4.3e; 4.4d); amplification of any ice-volume signal by the temperature effect on fractionation is likely. In Spitzbergen, there is no particular ^{18}O-enrichment in marine carbonates thought to be Varangian in age; and lack of strong ^{18}O-depletion in Varangian tillite-associated lacustrine carbonates may be an indication of low palaeolatitude (Fairchild & Spiro, 1987; Fairchild et al., 1989).

1.3c $\delta^{34}S$ Stratigraphy

There was early recognition of large, age-related changes in sulphate evaporite $\delta^{34}S$. The most recent compilation of data, covering Phanerozoic and Neoproterozoic time, is that of Claypool et al. (1980). Some more recent data for the Proterozoic are plotted with the curve of Claypool et al. in Fig. 1.10.

There is a large body of data for the Phanerozoic, and there is a dispersion of ±2 ‰ in isotopic composition about the curve of best fit in this part of the record. The Proterozoic

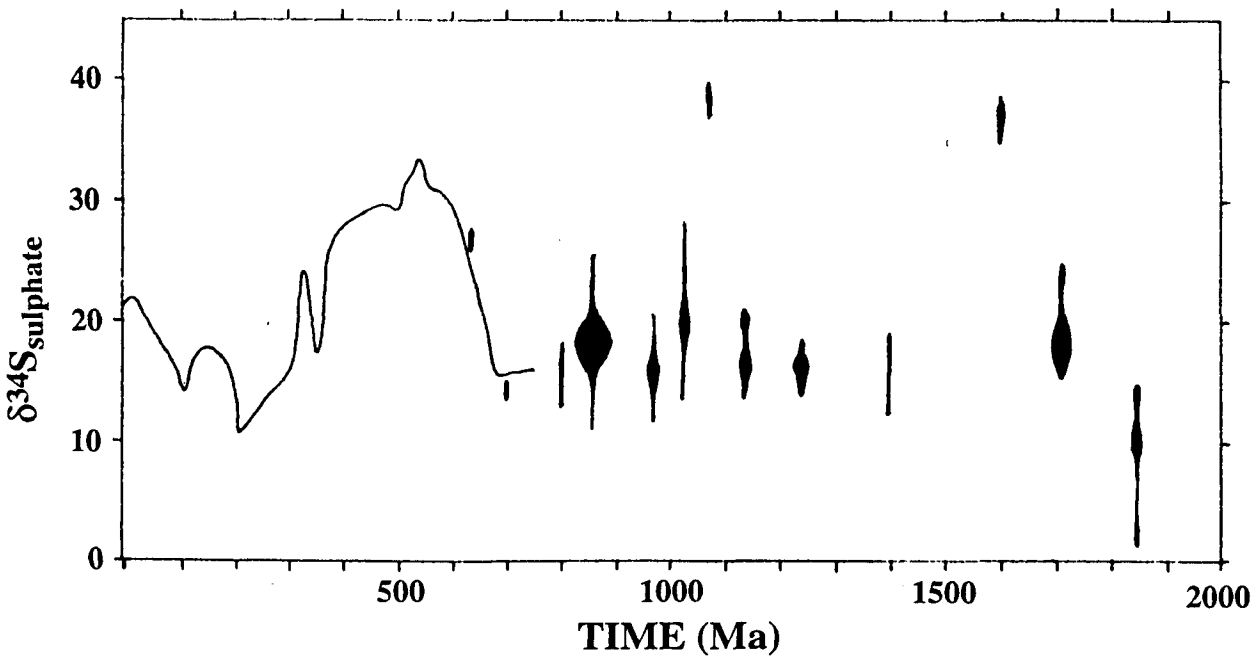

Fig. 1.10: Secular change in sulphate evaporite $\delta^{34}S$ as reported by Claypool et al. (1980), indicated as a curve (0-800Ma), with additional Proterozoic data from Hayes et al. (1992).

data set is much sparser and individual evaporite occurrences such as the Bitter Springs Formation are marked by a much greater dispersion of values, at least partly due to alteration. It would appear, however, that at some (poorly-constrained) time in the Neoproterozoic, seawater sulphate $\delta^{34}S$ values rose from around +15 ‰ to reach very high values (ca. +35 ‰) during the Cambrian.

Time ordering of $\delta^{34}S$ data is problematic in the Precambrian. Superposition of strata is of limited usefulness as the time interval represented by sulphates in a particular basin is typically geologically very short. Oscillations as marked as those of the Phanerozoic may be expected in the Proterozoic but presently available data are insufficient to define them, with the exception of the large rise in $\delta^{34}S_{sulphate}$ in the latest Proterozoic.

Recent compilations of Proterozoic sulphide isotopic data show the broad spread of values characteristic of biological sulphate reduction persisting throughout the Proterozoic, with a range, typically -10 to +20 ‰, that is heavy relative to Phanerozoic marine sulphides (Bottomley et al., 1992; Hayes et al., 1992) (Fig. 1.11). The heavy isotopic compositions can

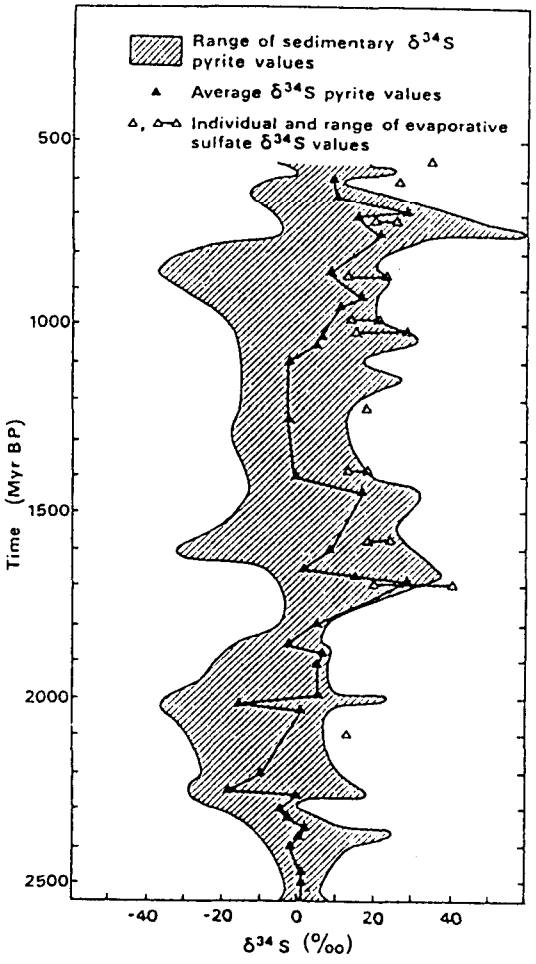

Fig. 1.11: Ranges and mean values for pyrite $\delta^{34}S$ in Proterozoic sedimentary rocks. From Lambert & Donnelly (1992).

be at least partly explained by the likelihood that reduction more readily approached completion and maximum enrichment in Proterozoic sedimentary environments because of lower sulphate concentrations in sea water and lack of bioturbation, or because preserved sediments are predominantly those of restricted intracratonic basins (Lambert & Donnelly, 1990). The mass balance requirement that long-term average isotopic composition of sulphur buried be close to 0 ‰, appears to be violated. Possibly, euxinic deep oceans were the site of maximal fractionation and burial of highly depleted sulphides that are poorly represented in the geologic record (Hayes et al., 1992). Significant in this regard, sulphides in deep-water sediments of the Neoproterozoic Windermere Supergroup are characterised by relatively strong ^{34}S-depletion, reflecting an inferred kinetic isotope effect of about 1.05, similar to the Phanerozoic (Ross et al., 1995).

Paradoxically on present data the latest Proterozoic is marked by decreasing $\delta^{34}S_{sulphide}$ values at the same time as $\delta^{34}S_{sulphate}$ was increasing (Figs 1.10, 1.11). Lambert et al. (1987) document upward-decreasing pyrite $\delta^{34}S$ in a Sinian to Cambrian sequence in China, with values of +11 to +26 ‰ in the Doushantuo Formation falling to -4 to +9 ‰ in the Cambrian. However, Ross et al. (1991, 1995), in a poorly age-constrained (740-570 Ma) part of the Windermere Supergroup, documented upward-increasing $\delta^{34}S_{sulphide}$: from a range of -31 to +19 ‰ in the Kaza Formation to a range of -18 to +35 ‰ in the overlying Isaac Formation. Within each formation, $\delta^{34}S_{sulphide}$ correlates positively with inferred sedimentation rate and hence reflects degree of closure, but the overall stratigraphic shift is attributed to a rise in marine $\delta^{34}S_{sulphate}$ from roughly +15 to +30 ‰, corresponding to the rise seen in the sulphate data of Claypool et al. (1980). A tentative correlation of a horizon in the upper part of the Kaza Formation with the Ice Brook (= Varangian?) glacials (Ross et al., 1995) suggests the rise may have happened relatively rapidly, in the early part of the Ediacarian. Strauss et al. (1992a) report a number of pyrite $\delta^{34}S$ values from the Proterozoic-Cambrian boundary interval in Newfoundland. A very broad range, from -20 to +53 ‰, was found, with a stronger predominance of positive values in the Proterozoic part of the section.

Further progress in $\delta^{34}S_{sulphide}$ chemostratigraphy might be aided by identification of earliest-formed, maximally-fractionated phases (Knoll & Walter, 1992). Strauss & Schieber (1990) used reflected-light petrography to differentiate early diagenetic (-14 ‰) and late diagenetic (up to +14 ‰) phases, the former representing reduction in near-open conditions. On the other hand, Ross et al. (1995), in a succession apparently characterised by isotopically uniform pyrite at any one horizon (i.e. no discernible differentiation of early and late phases) show that the heaviest $\delta^{34}S_{sulphide}$ values approach marine sulphate isotopic composition, as they reflect near-total closure of the diagenetic system.

1.3d Strontium Isotopes

The strontium isotopic composition of seawater was early predicted to show secular change, and Peterman et al. (1970) first demonstrated fluctuations in $^{87}Sr/^{86}Sr$ in primary, biogenic carbonates. Burke et al. (1982) compiled mid-Cambrian to recent data to produce a detailed Phanerozoic curve. The ratio in palaeoseawater is now known to within .00005 in the Tertiary and .0002 in the rest of the Phanerozoic (Veizer, 1989).

Diagenetic alteration of $^{87}Sr/^{86}Sr$ is generally more of a problem than in $\delta^{13}C$ chemostratigraphy, necessitating rigorous selection procedures for minimally-altered samples (see Chapter 2).

Veizer & Compston (1976) obtained a generalised, first-order curve for the Precambrian, showing a sharp increase in the lower Proterozoic followed by a gentler rise to the Cambrian maximum. Veizer et al. (1983) used Sr and Mn contents to evaluate post-depositional alteration in late Proterozoic carbonates from the Adrar sequence (Mauritania), Adelaide an carbonates and the Nama Group (southern Africa). The few acceptably unaltered samples showed a decline to a very low ratio (0.7056) at ca. 900 Ma (ascribed to a 'mantle event'); followed by a rise to very high values at the end of the Proterozoic, encompassing a range exceeding the total Phanerozoic variation.

Strontium isotope ratios from the thick, well-preserved Svalbard and east Greenland sections were documented by Derry et al. (1989). High-strontium (200-2500 ppm), low-rubidium (< 1 ppm) samples were selected, and these have $^{87}Sr/^{86}Sr$ ratios that fall within a narrow (0.0004) band varying slightly about 0.707, in a sequence loosely dated as 800-650 Ma. These and some later authors (Asmerom et al., 1991; Derry et al. 1992) used basin subsidence modelling to interpolate ages, but absolute age control remains poor. Asmerom et al. (1991) extended the profile back to roughly 850 Ma with $^{87}Sr/^{86}Sr$ data from the Shaler Group, northwest Canada. Here, very low ratios (.7056) match those found in the Adrar sequence by Veizer et al. (1983) and also in sulphates from the similar-aged Bitter Springs Formation (Hayes et al., 1992).

Further analytical data for the Nama Group, the Svalbard - east Greenland sequences and the Bitter Springs Formation were presented by Derry et al. (1992). They used trace-element and $\delta^{18}O$ data to select least-altered $^{87}Sr/^{86}Sr$ (and $\delta^{13}C$) values. In the Nama Group, several determinations close to 0.7085 confirmed the results of Veizer et al. (1983).

Narbonne et al. (1994) provide $^{87}Sr/^{86}Sr$ data for the upper Windermere Supergroup, while Kaufman et al. (1993) provide additional data for the Polarisbreen Group (Svalbard - east

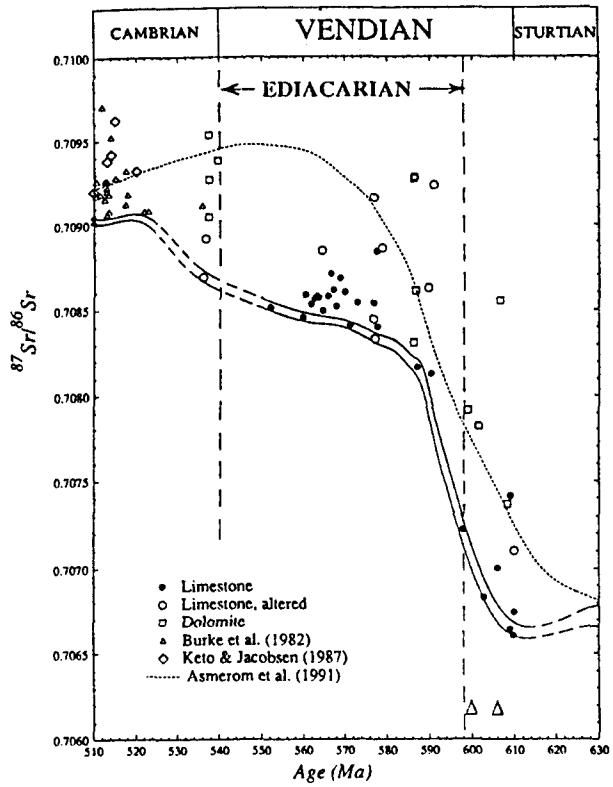

Fig. 1.12: Secular variation in $^{87}Sr/^{86}Sr$ of latest Proterozoic and Cambrian seawater estimated from least-altered carbonates (see text); after Kaufman et al. (1993).

Greenland) and the Witvlei and Nama Groups (Namibia) (Fig. 1.12). Samples were deemed minimally altered in $^{87}Sr/^{86}Sr$ if Mn/Sr < 1.5, $^{87}Rb/^{86}Sr < 0.001$, and $\delta^{18}O > -11$ ‰. This sample set still displays a dispersion of ca. 0.0003 (Fig. 1.12); the lower bounding trend is taken as seawater composition since alteration nearly always increases $^{87}Sr/^{86}Sr$. In the latest Riphean to Varangian Elbobreen Formation, least-altered values are low (0.7066); the Keele Fm, thought to be similar in age, has a minimum value of 0.7071 (for lithostratigraphic succession see Figs. 1.4, 1.5). A limestone sample from the (?basal Ediacarian) 'Tepee dolostone' has $^{87}Sr/^{86}Sr$ of 0.7072. The probably next-youngest reliable data comes from the Witvlei Group, which precedes the first appearance of the Ediacara fauna and has least-altered values of 0.7081 - 0.7082, associated with depleted (-4 to -5 ‰) $\delta^{13}C_{carb}$. Higher, the ^{13}C-enriched, Ediacara-fauna-bearing Zaris Formation has $^{87}Sr/^{86}Sr$ of 0.7084, and slightly higher (0.7085) least-altered values persist up to the base-Cambrian unconformity. Very similar values are found in the Ediacara fauna-bearing Blueflower Formation (0.7084-0.7086). A stratigraphic gap in coverage ensues. The Early Cambrian Nomtsas Formation (Namibia) has a minimum $^{87}Sr/^{86}Sr$ of 0.7087, but this sample may be altered (Kaufman et al., 1993).

The late Proterozoic $^{87}Sr/^{86}Sr$ curve, drawn from information currently available (Fig. 1.13) lacks data in the 630-700Ma interval, and suffers from a sparsity of data in the early Ediacarian and late Ediacarian to middle Cambrian. The inferred steep rise in $^{87}Sr/^{86}Sr$

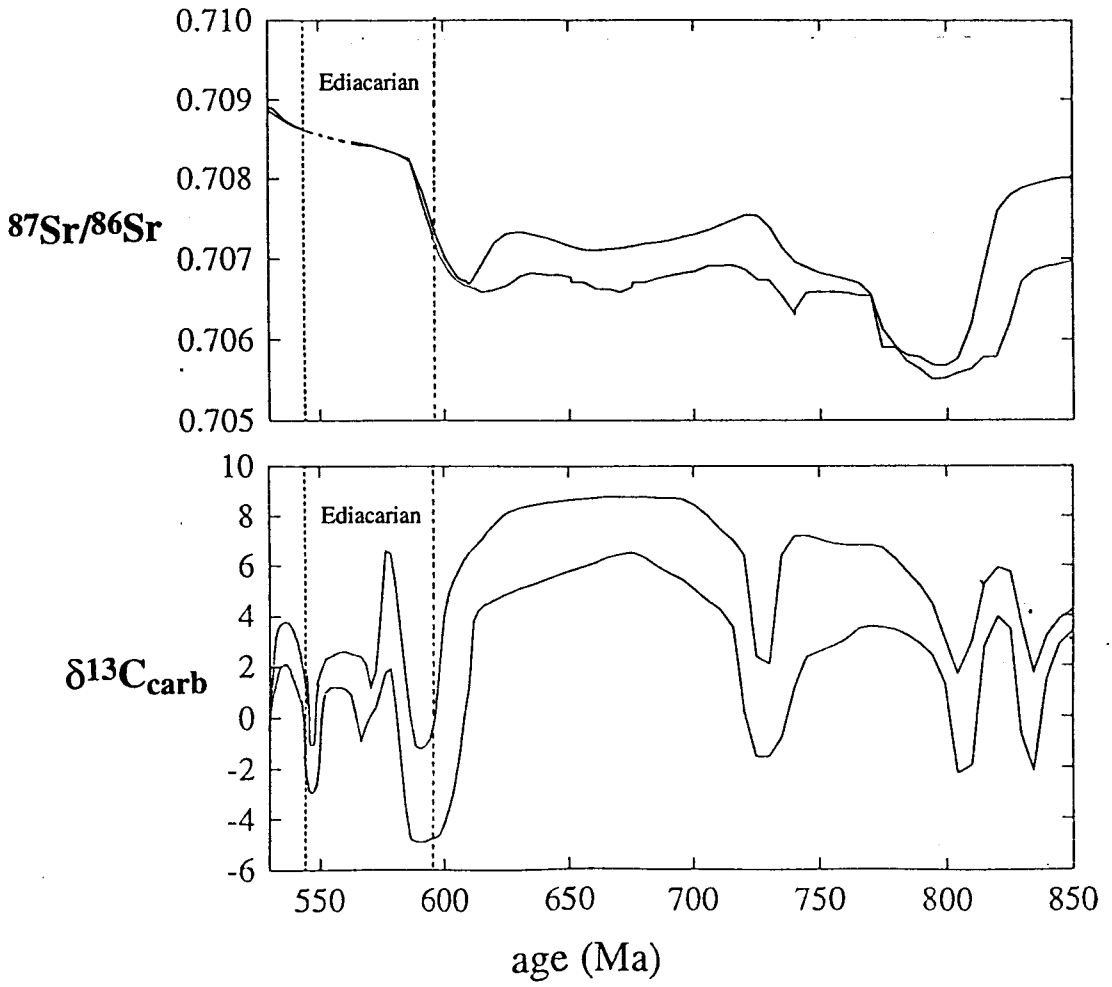

Fig. 1.13: A recent compilation of secular change in (a) $\delta^{13}C$, and (b) $^{87}Sr/^{86}Sr$ of marine carbonates of Cryogenian to early Cambrian age (850 - 530 Ma). From Kaufman & Knoll (1995).

during the early Ediacarian indicates a potential for relatively high resolution chemostratigraphy. Some age curves showing extremely high (0.7095) values in the latest Proterozoic (e.g. Asmerom et al., 1991) are based on samples that may be altered or on samples that may be Cambrian in age (Donnelly et al., 1990). Apparently unaltered $^{87}Sr/^{86}Sr$ values as high as 0.7089 are known in Vendian-aged sequences in southern Africa (Veizer et al., 1983, their Table 4); the Ediacarian of Australia (this study, sections 3.10; 6.3b) and the late Sinian (Lambert et al., 1987). A compilation of numerous Cambrian $^{87}Sr/^{86}Sr$ data (Donnelly et al., 1990) shows no middle Cambrian value below .7090, while early Cambrian data range as low as .7084. No information is available on preservational state of these samples, leaving open the possibility of a late Ediacarian $^{87}Sr/^{86}Sr$ peak (ca. 0.7089) followed by an early Cambrian minimum.

1.3e CONCLUSION: 'GLOBAL' NEOPROTEROZOIC $\delta^{13}C$ AND $^{87}Sr/^{86}Sr$ CURVES

A recent integration of Cryogenian to early Cambrian $\delta^{13}C$ and $^{87}Sr/^{86}Sr$ data is shown as Fig. 1.13. In the Cryogenian, negative excursions in $\delta^{13}C$ coincide with glaciations (Kaufman et al., 1991); and the later part of this period is marked by stronger ^{13}C enrichment than is seen in any younger successions. Low $^{87}Sr/^{86}Sr$ (< 0.7075) serves to differentiate the Cryogenian from most of the Ediacarian and Cambrian.

A common pattern is evident in Ediacarian successions worldwide (Knoll & Walter, 1992). In Australia, Canada and Spitzbergen, 'cap dolostones' immediately overlying Marinoan/Varangian glacigene rocks have depleted carbonate carbon isotopic compositions (-2 to -5 ‰). Similar depletion persists into younger horizons in Spitzbergen and Namibia but the signal is poorly constrained until there is a discrete positive excursion to maximum $\delta^{13}C_{carb}$ values of +5.5 ‰ (Siberia) to +7 ‰ (Canada, South Australia). This is succeeded in several sections by an irregular plateau of moderate ^{13}C enrichment that persists almost to the base of the Cambrian. Ediacara-type metazoan fossil assemblages occur within this zone of moderate $\delta^{13}C_{carb}$ enrichment in China, Siberia, Canada and Namibia, and in the latter two localities they first appear somewhat earlier (just before the $\delta^{13}C$ peak).

A fall to negative $\delta^{13}C_{carb}$ marks the end of the Proterozoic, although the precise timing with respect to the GSSP in Newfoundland is difficult to establish. Negative, then strongly positive $\delta^{13}C_{carb}$ values mark the basal Cambrian 'Nemakit-Daldynian' interval (Fig. 1.8), with the base of the Tommotian coinciding with a steep drop in $\delta^{13}C$.

The Ediacarian $^{87}Sr/^{86}Sr$ curve is constrained by low (< 0.707) Varangian values, a single result of 0.7072 from the 'Tepee Dolostone', and then a plateau of considerably higher (0.7082 - 0.7085) least-altered values. Diverse Ediacara-type metazoan assemblages coincide with values of 0.7084 - 0.7085. As previously discussed, the ensuing rise to the middle Cambrian maximum (0.7090) is very poorly constrained.

It is unlikely that the foregoing represents a complete description of the Ediacarian oceanic carbon and strontium isotopic signals. 'Cap dolostones' are succeeded by thick siliciclastics in Australia, Canada and Svalbard/Spitzbergen in which the $\delta^{13}C_{carb}$ signal is poorly constrained. The Witvlei Group of about this age in Namibia is bounded by unconformities and contains a third. In Canada, South Africa and Siberia there are stratigraphic gaps in the $\delta^{13}C$ signal above the positive excursion. Until this study, no systematic attempt has been made to use the organic carbon isotope signal to fill gaps in the record caused by carbonate-poor intervals.

Another largely unevaluated question is the extent to which a single, apparently continuous section in a basin fully captures the secular marine isotopic signal. A number of studies (e.g. Asmerom et al., 1991; Derry et al., 1992; Kaufman et al., 1993) used a simple basin subsidence model to interpolate ages between 'tie points' for which numerical age data are available. However, stratigraphy is rife with case histories of the chronostratigraphic incompleteness of thick, conformable sedimentary successions (e.g. see Ager, 1973, p. 28 - 34). Sequence stratigraphy (Vail et al., 1977; van Wagoner, 1988) provides a chronostratigraphic model that is a useful qualitative indicator of stratigraphic completeness and patterns of diachroniety (Fig. 1.14). Third-order depositional sequences are of the order of a few million years' duration, significant in terms of possible shifts in marine $\delta^{13}C$. Clearly, individual vertical transects will be very incomplete temporal records, and basinward and shoreward transects will capture different time segments (Fig. 1.14b). There is an obvious need for chemostratigraphic studies to incorporate widespread sections within individual basins to build a more complete picture of secular change, and also for such studies to be integrated with sufficient seismic or mapping data for the geometry of basinal sediment fill to be known at least in outline.

The present study addresses some of these issues. Multiple sections were sampled in each of several Ediacarian basins in Australia, and many examples of local incompleteness were discovered or confirmed, in some cases consistent with sequence-stratigraphic interpretations. Systematic use of $\delta^{13}C_{org}$ in thick siliciclastic successions has revealed a surprising information richness in the organic record, and a utility in correlation equal to that of the carbonate record. Australian Ediacarian successions have a much greater proportional thickness of sediment pre-dating the appearance of the Ediacara fauna than sections in Canada, Namibia, China and Siberia, and it is reasonable to expect that in Australia there may be a more complete record of the lower Ediacarian. This study uncovers additional detail in the $\delta^{13}C$ record for this time. In particular, there appears to be at least one distinctly earlier excursion to enriched (+6‰) carbonate values.

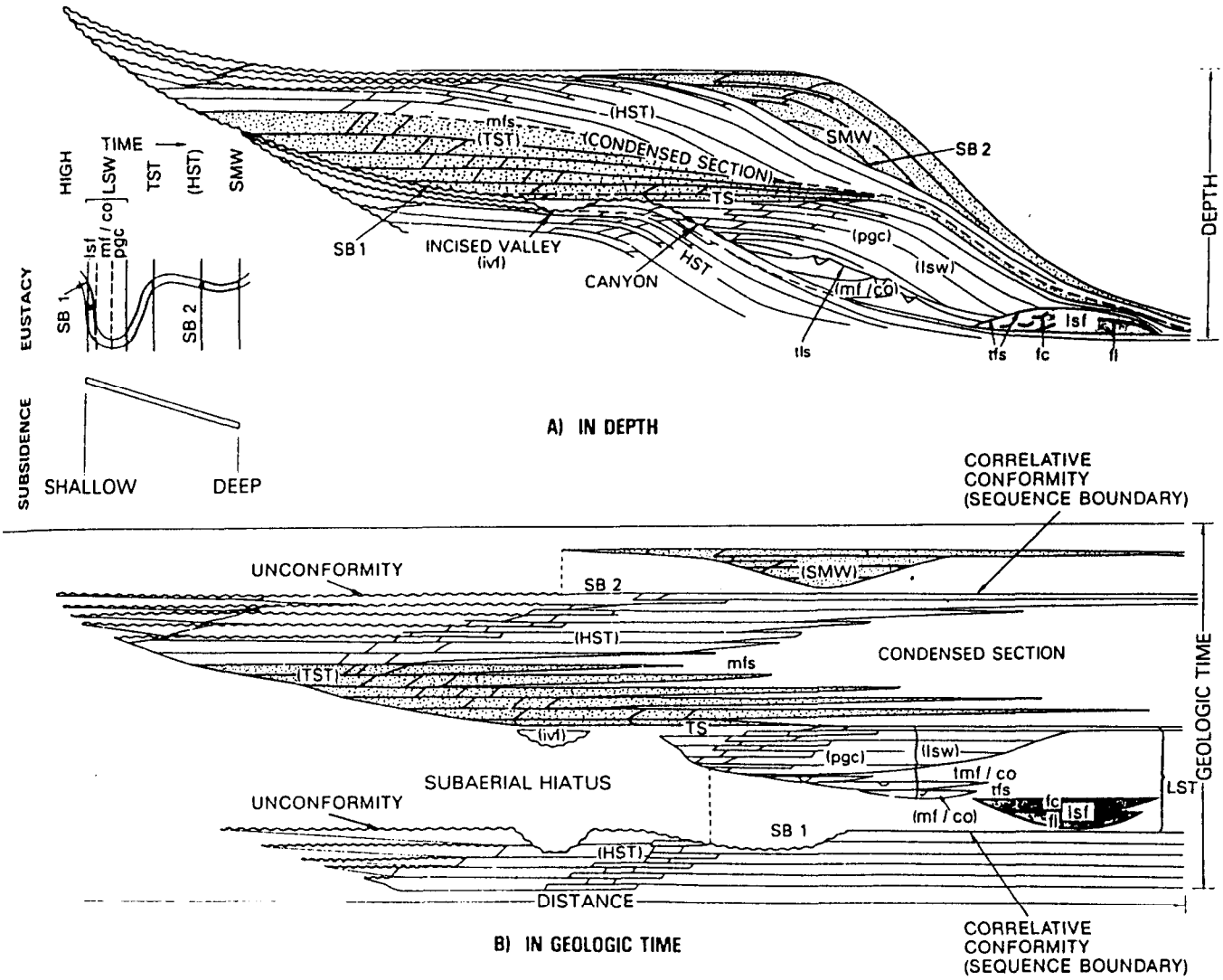

LEGEND

SURFACES

(SB) SEQUENCE BOUNDARIES
- (SB 1) = TYPE 1
- (SB 2) = TYPE 2

(DLS) DOWNLAP SURFACES
- (mfs) = maximum flooding surface
- (tfs) = top fan surface
- (tmf / co) = top mass flow / channel overbank

(TS) TRANSGRESSIVE SURFACE
- (First flooding surface above maximum regression)

SYSTEMS TRACTS

HST = HIGHSTAND SYSTEMS TRACT

TST = TRANSGRESSIVE-SYSTEMS TRACT
- ivf = incised-valley fill

LST = LOWSTAND SYSTEMS TRACT
- ivf = incised-valley fill
- lsw = lowstand wedge
- pgc = prograding complex
- mf / co = mass flow / channel overbank deposits
- lsf = lowstand fan
  - fc = fan channels
  - fl = fan lobes

SMW = SHELF MARGIN WEDGE SYSTEMS TRACT

Fig. 1.14: The depositional model of sequence stratigraphy, shown (a) in relation to depth (with great vertical exaggeration), and (b) in relation to time. From Baum & Vail (1988).

2

Methods in Isotope Chemostratigraphy

2.1 Introduction

This chapter reviews the methods in general use in differentiating primary C and Sr isotopic signals from the 'noise' of post-depositional alteration and initial variability, in the light of which the approaches taken in this investigation are developed. New methodology is developed for elucidating the isotope record of total organic carbon. Sampling protocols and analytical techniques used in this study are outlined in the concluding section.

Isotopes of carbonate carbon and strontium have been the main focus of Neoproterozoic chemostratigraphy, and this study follows methods in common use - including conventional and cathode-luminescence (CL) petrography and trace-element analysis - to distinguish least-altered carbonate phases for C and Sr isotopic analysis (e.g. Veizer et al., 1983; Fairchild et al., 1990; Kaufman et al., 1991, 1993; Narbonne et al., 1994). It is noteworthy, however, that most examples of unusual depletion in $\delta^{13}C_{carb}$ (<-3 ‰) found in this investigation appear to be associated with with particular restricted (yet marine) palaeoenvironments rather than diagenetic alteration, highlighting the prime importance of facies analysis in chemostratigraphic studies.

A large number (ca. 500) of $\delta^{13}C_{org}$ and total organic carbon content (TOC) determinations was undertaken in a systematic attempt to use organic carbon isotope chemostratigraphy in carbonate-poor successions. It has been found useful to apply simple quantitative 'corrections' to raw isotopic data using TOC, H/C and $\Delta\delta$ data as rough indices of kerogen preservation and thermal maturation. A carbonaceous shale facies interpreted to be the result of benthic microbial mat growth is described (see also Schieber, 1986). This facies has a distinct $\delta^{13}C_{org}$ signature. This 'benthic signal' can be more precisely determined by applying a correction to account for mixing with carbon from other (pelagic) sources.

2.2 Carbonate stable isotopes and $^{87}Sr/^{86}Sr$

2.2a Initial Variability

For carbonate carbon isotopes, slight mineralogic effects on isotopic equilibrium, and spatial inhomogeneity of oceanic $\delta^{13}C_{DIC}$, are potential sources of initial variability in the

chemostratigraphic signal even before diagenesis begins. Strontium isotopes, on the other hand, are homogeneously distributed in the oceans and do not undergo measurable natural fractionation, and deciphering the $^{87}Sr/^{86}Sr$ signal is almost wholly concerned with problems of post-depositional alteration.

In general, marine $CaCO_3$ is enriched by 1 to 2 ‰ relative to ambient seawater dissolved inorganic carbon (Anderson & Arthur, 1983). Recent experimental data demonstrate a calcite-bicarbonate enrichment factor ($\varepsilon_{cl\text{-}bicarb}$)of 1.0 ‰ and an aragonite-bicarbonate enrichment factor ($\varepsilon_{ar\text{-}bicarb}$) of 2.7 ‰, and that these are independent of temperature and precipitation rate (Romanek et al., 1992). These differing enrichment factors represent a minor but largely unevaluated source of variability in the $\delta^{13}C_{carb}$ record.

Dolomite should be enriched by ca. 2.4 ‰ in ^{13}C relative to calcite at isotopic equilibrium (Sheppard & Schwarz, 1970) but in general $\Delta^{13}C_{dol\text{-}cal}$ is 1 ‰ or less in modern and ancient examples (e.g. McKenzie, 1981; Rao, 1990; and see fig. 1.9), presumably because the diagenetic environment accompanying dolomitization approaches closure with respect to carbon (Degens & Epstein, 1964; Tucker, 1983). Equilibrium $\Delta^{18}O_{dol\text{-}cal}$ is not precisely known but lies between +1 and +7 ‰ at 25°C (see Land, 1980; 1992). Modern and ancient dolomites are typically 2 to 3 ‰ higher in ^{18}O than closely associated calcites (e.g. McKenzie, 1981; Rao, 1990). Veizer & Hoefs (1976) noted that Proterozoic dolomites are on average 5 ‰ heavier in ^{18}O than coeval limestones, which they attributed to the lower susceptibility of dolomites to post-depositional equilibration with meteoric waters, and to the prevalence of equilibrium effects during penecontemporaneous dolomitization.

With carbon, a significant source of initial variability is the instantaneous spatial inhomogeneity in oceanic $\delta^{13}C_{DIC}$, briefly described in the previous chapter. Present global variation in shallow-water $\delta^{13}C_{DIC}$ of about 1 ‰ (Kroopnick, 1985) probably indicates a fundamental limit to ^{13}C chemostratigraphic resolution. Lateral variability of a few ‰ is to be expected, and is observed, in correlative widespread Neoproterozoic sections (Kaufman & Knoll, 1995) while it has been noted that intrabasinal lateral variability is much less (e.g. Kirshchvink et al., 1991; and see Fig. 1.9).

Depth-related variability in $\delta^{13}C_{DIC}$, maintained by the 'photic pump effect' (Berger & Vincent, 1986) is presently ca. 2 ‰ in most oceans but may have been much greater in times of slower oceanic turnover (previous chapter). In this study, the Ediacarian Wonoka Formation in the Adelaide Geosyncline is shown to have little-altered $\delta^{13}C_{carb}$ as low as -8 ‰ in limestones of mid to outer-shelf environments (see also Urlwin et al., 1993). Sedimentological and indirect palaeogeographic evidence are consistent with deposition

under the lower water layer of a deep, salinity-stratified, semi-isolated marine basin (see section 3.6c). Several other Ediacarian units (Rodda beds, Nuccaleena Formation, Pertatataka Formation) include carbonates with similar, or less strongly depleted isotopic compositions that may have a similar origin (Chapters 3, 4, 6). Other than these examples, known Neoproterozoic carbonates are considered to be characteristic of upper layer or well-mixed oceanic settings (Kaufman & Knoll, 1995). However, there is considerable circumstantial evidence for the existence of ^{13}C-depleted, nutrient-rich deep water masses at times during the Neoproterozoic (e.g. Brasier, 1992; Lambert & Donnelly, 1992; Kaufman et al., 1991).

Anomalous (strongly ^{13}C-depleted) compositions were also found in a quite different depositional setting in the shallow-marine Julie Formation (Amadeus Basin). Here, some apparently little-altered dolostones of evaporative perilittoral environments have $\delta^{13}C_{carb}$ as low as -5.5 ‰, while closely associated open-marine carbonates have $\delta^{13}C_{carb}$ around +5 ‰ (see section 4.6). $\delta^{18}O$ and Sr are relatively high, and Mn is low, in the ^{13}C-depleted horizons; and organic carbon contents are negligible (< 0.1 mg/g). A hypothesis consistent with observations is that the depleted carbonates are ancient analogues of modern ^{13}C-depleted intertidal brine pools documented by Lazar & Erez (1990, 1992).

2.2b Post-depositional Alteration

Carbonate stable isotopes - general observations

The protracted burial history of Proterozoic carbonates suggests caution be exercised in interpreting primary isotopic compositions. There is no primary stable low-Mg calcite in the form of skeletal debris, and Proterozoic carbonates have in general been neomorphosed (e.g. Fairchild et al., 1990). However, several carefully controlled petrographic and isotopic studies of Proterozoic limestones and dolostones show that primary marine carbon isotope compositions are preserved in texturally well-preserved ooids, marine cements and micrites or dolomicrites (e.g.Tucker, 1982, 1983; Burdett et al., 1991; Zempolitch et al., 1988). Microsampling of juxtaposed allochems and early and late cement phases in these rocks shows distinct isotopic compositions and similar patterns of ^{13}C and ^{18}O distribution to those in well-preserved Phanerozoic carbonates, indicating no wholesale isotopic re-equilibration. Solid-diffusion exchange appears to be too slow a process to significantly affect carbonate isotopic compositions (Anderson, 1969).

Bulk-rock isotopic change may have occurred either through cementation (addition of new carbonate) or neomorphism (the latter includes recrystallization and mineralogic

transformation such as dolomitization, and calcitization of aragonite), in porewaters compositionally dissimilar to seawater. Fortunately, seafloor cementation and diagenetic stabilization were evidently commonplace in the Proterozoic (e.g. Knoll & Swett, 1990; Kaufman et al., 1991), the former probably aided by higher seawater carbonate supersaturation (Knoll & Swett, 1990; Grotzinger, 1989). Dolomitization in the Proterozoic typically occurred in waters of marine or near-marine composition (Sibley, 1991). Micritic grainsize and preservation of fine detail in dolostones, a common phenomenon in the Proterozoic (e.g. Tucker, 1982) is considered to be indicative of very early diagenetic or syndepositional dolomitization of metastable precursors (Tucker, 1983; Zempolitch et al., 1988). Late Proterozoic marine stromatolitic carbonate, and the Ediacarian shelly fossil *Cloudina*, exhibit no known carbon isotopic vital effects (Fairchild, 1991; Grant, 1990).

After diagenetic stabilization and lithification, bulk-rock carbon isotopic compositions tend to be inherently stable simply because (except at exceptionally high water-rock ratios) rock carbon vastly outweighs dissolved inorganic carbon in porewaters. Carbonate oxygen, on the other hand, may equilibrate with fluid $\delta^{18}O$ values at relatively low water-rock ratios (e.g. Hudson, 1977). Modelling of water-rock interaction shows that significant shifts in $\delta^{13}C_{carb}$ occur at water-rock ratios *ca.* 10^3 times higher than those required to shift $\delta^{18}O$, and that unless porewater chemistry is exceptional, $^{87}Sr/^{86}Sr$ is intermediate between $\delta^{13}C_{carb}$ and $\delta^{18}O$ in susceptibility to diagenetic alteration (Banner & Hanson, 1990; Land, 1992). In the deeper burial diagenetic environment, neomorphism or addition of cement tends to result in moderate to strong depletion in bulk ^{18}O, mainly due to increased temperature, but only slight depletion in ^{13}C (e.g. Choquette & James, 1987; Algeo et al., 1992).

Several authors have noted that Proterozoic carbonates show surprisingly little difference in $\delta^{13}C_{carb}$ between late cements and early phases, and that whole-rock carbon isotopic compositions have not been significantly altered by diagenetic fluids (Fairchild & Spiro, 1987; Aharon et al., 1987; Burdett et al., 1990; Kaufman et al., 1991). For example, in a study of 101 Neoproterozoic samples from Namibia, Kaufman et al. (1991) found a depletion of only 0.3 ‰ in $\delta^{13}C_{carb}$ and 1.0 ‰ in $\delta^{18}O$ of whole-rock carbonate with respect to the non-luminescent micritic (i.e. petrographically least-altered) components. They attributed this in part to the low initial porosity of these sediments.

However, early lithification and subsequent buffering of $\delta^{13}C_{carb}$ by rock carbon can by no means be universally assumed in Neoproterozoic carbonates. Diagenetic stabilization of aragonite may have been long delayed if the sediments were not exposed to meteoric fliuds in early diagenesis (Tucker, 1986b; Fairchild et al., 1990). On the basis of petrography and

trace-element covariation in a 900 Ma unit in Mauritania, Fairchild et al. (1990) showed that aragonitic carbonates probably survived burial and uplift to be neomorphosed by deeply-circulating meteoric fluids during the Pan-African Orogeny. Open-system (fluid-dominated) diagenesis is postulated to have caused negative shifts of up to 4 ‰ in $\delta^{13}C_{carb}$ and 10 ‰ in $\delta^{18}O$.

Organic and meteoric diagenesis

There are well-documented shifts in stable isotopic composition in sediments subjected during early diagenesis to meteoric fliuds or fluids enriched in organogenic CO_2.

Isotopically anomalous carbonate cements may result from microbial metabolism in newly-deposited, organic-rich, fine-grained sediment. Heterotrophs (chiefly bacterial sulphate reducers) liberate depleted (-25 ‰) CO_2 into porewaters. If labile organic matter survives exhaustion of porewater sulphate, fermentative metabolism will yield enriched ($\delta^{13}C$ +10 to +15 ‰) CO_2 (see Anderson & Arthur, 1983). Cements precipitated from such porewaters may thus depart significantly in ^{13}C content from marine values, and large variations in $\delta^{13}C_{carb}$ may be found over short distances, for example within individual early diagenetic concretions. High TOC, pyrite, phosphate, elevated Mn^{2+} and Fe^{2+}, stability of $\delta^{18}O$ values relative to $\delta^{13}C$, presence of concretions and diagenetic layering are other traits often associated with microbial CO_2 - derived carbonates (Irwin et al., 1977; Mozley & Burns, 1993).

With deeper burial (> ca. 10^3 m), thermal decarboxylation of organic matter contributes ^{13}C-depleted CO_2 to porewaters. Recrystallization in this diagenetic environment has resulted in negative bulk shifts in $\delta^{13}C_{carb}$ of over 10 ‰ in the organic-rich Monterey Formation (Miocene) (Malone et al., 1994). Bulk TOC is three times greater than carbonate carbon content in this unit (ibid.).

Shelfal sediments may be exposed to the influence of meteoric waters through sediment progradation, uplift or eustacy. Meteoric diagenesis in Phanerozoic rocks commonly depletes bulk-rock carbonate $\delta^{13}C$ because of the influence of soil-derived CO_2. Typically, stratigraphic profiles show such depletion commencing a few metres below exposure surfaces and increasing to a maximum (with whole-rock values typically 3 or 4 ‰ below the marine value) at the exposure surface (Allan & Matthews, 1982). A similar pattern in a mid-Proterozoic sequence has been attributed to meteoric diagenesis (Beeunas & Knauth, 1985) but this interpretation is controversial (Vahrenkamp & Rossinsky, 1987) in part because of the presumed lack of land plants in the Proterozoic. In general the effects of meteoric diagenesis in Proterozoic sequences appear to have been muted (Sibley, 1981; Burdett et al.,

1991). There is a more pervasive alteration of oxygen isotopes to prevailing meteoric values (typically around 5 ‰ lower than marine values in low-latitude settings: Hays & Grossman, 1991; Veizer, 1992), which leads to characteristic 'inverted-J' trends on $\delta^{13}C$ - $\delta^{18}O$ crossplots (Lohmann, 1982). Intense evaporation at exposure surfaces may result in localised $\delta^{18}O$ enrichment due to preferential evaporative removal of ^{16}O. As mentioned above, Fairchild et al. (1990) proposed that C and O isotopic compositions in an originally aragonitic, Neoproterozoic unit were pervasively altered by deeply-circulating meteoric fluids. This unit is characterised by strong covariation of decreasing $\delta^{13}C_{carb}$, $\delta^{18}O$ and Sr with increasing Fe and Mn. Such a signature, however, might equally be caused by burial diagenesis.

Strontium isotopes

Seawater strontium isotopic composition is recorded (without fractionation) in marine carbonates, phosphates and sulphates, in which Sr^{2+} substitutes for Ca^{2+}. Aragonite in equilibrium with modern seawater is relatively high in Sr (ca. 8300 ppm) while calcite contains ca. 1100 ppm Sr and dolomite ca. 50 - 550 ppm Sr (Vahrenkamp & Swart, 1990; Baker & Burns, 1985). Substantially lower strontium contents are usual in Proterozoic carbonates. Neomorphism results in a large decrease in Sr content because dissolution-reprecipitation brings about net partitioning of Sr into porewaters. If stabilization is early (with porewaters of near-marine composition) or if water-rock ratios are low (diagenetic environment approaches closure) loss of Sr will be minimised and little change in $^{87}Sr/^{86}Sr$ will result. Meteoric diagenesis little affects $^{87}Sr/^{86}Sr$ despite the loss of most strontium (Banner & Hanson, 1990). It is the deep-burial diagenetic environment in which carbonates appear to be most vulnerable to alteration of $^{87}Sr/^{86}Sr$. Here, recrystallization or cementation in the presence of fluids that have acquired radiogenic Sr from silicates may significantly increase $^{87}Sr/^{86}Sr$ of carbonates (e.g. Chaudhuri & Clauer, 1993). Aluminosilicates are high in ^{87}Sr, which is inherited in detrital components and also derived from post-depositonal decay of ^{87}Rb. Modelling studies show that $^{87}Sr/^{86}Sr$ in carbonate rocks is usually intermediate between $\delta^{13}C$ and $\delta^{18}O$ in susceptibility to equilibration with diagenetic fluids (Banner & Hanson, 1990). Diagenetic change is nearly always towards higher (more radiogenic) ratios (Veizer & Compston, 1976; Burke et al., 1982); but there are rare exceptions (e.g. Fairchild et al., 1990; Gao & Land, 1991).

2.2c READING THE $\delta^{13}C_{carb}$ AND $^{87}Sr/^{86}Sr$ SIGNALS: MONITORING ALTERATION

In the absence of marine fossils, a marine setting in Neoproterozoic sequences must be inferred from broad facies relationships or mineralogical/geochemical indicators (e.g.

presence of glauconite, phosphate; marine $^{87}Sr/^{86}Sr$). Sedimentological observations are important, as variations in $\delta^{13}C_{carb}$ that correlate with facies change must be regarded as suspect, particularly where substantial changes in palaeodepth are involved.

Detection of the primary marine carbon or strontium isotopic signal begins with sample selection for texturally well-preserved ooids, marine cements, and homogeneous micrites or dolomicrites that are neither argillaceous nor organic-rich and avoidance of spar-filled cavities or neomorphic spar (e.g. Tucker, 1982; Kaufman & Knoll, 1995). Essentially all Proterozoic carbonates must have been neomorphosed, but in general a micritic grainsize is an indication that the diagenetic system was more likely to have approached closure, and that the rock has undergone a minimum number of neomorphic events since these nearly always increase grainsize (e.g. Bathurst, 1971, p. 497). Cathodoluminesence petrography can be used to infer the distribution of Mn-enriched (diagenetic) cements: components with Mn > 100 ppm are luminescent (Sippel & Glover, 1965; Marshall, 1988); thus non-luminescent or weakly luminescent micritic carbonate is preferred (e.g. Kaufman et al., 1991).

Trace-element analysis is a useful independent indicator of diagenetic alteration particularly in fine-grained rocks where recrystallization or cementation may be difficult to detect petrographically (Fairchild et al., 1990; Kaufman et al., 1993; Kaufman & Knoll, 1995). Post-depositional alteration in carbonates gives rise to covariant changes in trace-element and isotopic composition: typically, $\delta^{13}C_{carb}$, $\delta^{18}O$, Sr^{2+} and Na^{+} decrease, while Mn^{2+}, Fe^{2+} and $^{87}Sr/^{86}Sr$ increase (Brand & Veizer, 1980, 1981; Veizer, 1983; Banner and Hanson, 1990). Sr^{2+} and Na^{+} decrease because with partition coefficients less than unity, they are partitioned strongly into porewaters with each mineralogic transformation or recrystallization. Mn^{2+} and Fe^{2+} increase because their partition coefficients are greater than 1 and because their solubilities are strongly Eh dependent and much higher in the low-Eh waters of burial diagenetic environments, than in seawater (Tucker & Wright, 1990).

Thus $\delta^{18}O$ and the ratios Mn/Sr and Sr/Ca are commonly used indices of diagenetic alteration in carbon and strontium isotope chemostratigraphic studies (e.g. Derry et al., 1992; Kaufman et al., 1993, Kaufman & Knoll, 1995), with particular, somewhat arbitrary limits chosen to separate altered and 'unaltered' samples. For example, Kaufman & Knoll (1995) consider that $\delta^{13}C_{carb}$ in a given sample is likely to be unaltered if $\delta^{18}O$ is greater than -10 ‰ or if Mn/Sr is less than 10. For the more readily altered $^{87}Sr/^{86}Sr$ ratio, more rigorous limits are required - for example, Mn/Sr < 1.5 and $^{87}Rb/^{86}Sr < 0.001$ for near-primary compositions (Kaufman et al., 1993). Data thus selected still display a scatter of ca. 0.0002 (e.g. Fig. 1.12), and this is therefore the limit of resolution of the Proterozoic $^{87}Sr/^{86}Sr$ record on

present data (see section 6.3b). In general these alteration criteria are empirically derived from large data sets and are chosen to yield consistent and concordant (and hence probably near-primary) $\delta^{13}C_{carb}$ and $^{87}Sr/^{86}Sr$ data.

It would seem sensible to use different $\delta^{18}O$ and Mn/Sr limits in limestones and dolostones for differentiating primary $\delta^{13}C_{carb}$, although this is an issue not broached by the above authors. The distribution coefficient for incorporation of Sr into dolomite is poorly known but may be an order of magnitude lower than that for calcite (Vahrenkamp & Swart, 1990). Proterozoic dolostones also tend to be several ‰ higher in $\delta^{18}O$ than limestones for reasons at least partly concerned with equilibrium fractionation rather than alteration (Veizer & Hoefs, 1976).

Another approach is to seek linear covariance of $\delta^{13}C$ or $^{87}Sr/^{86}Sr$ with one or more of the above variables in a suite of variably-altered samples, allowing identification of least-altered values to be identified through a simple backstripping process (Marshall, 1992; for Proterozoic examples see Fairchild et al., 1990; Kaufman et al., 1992; Derry et al., 1992).

In this study, trace-element data are used as a general guide to understanding diagenesis, but from the viewpoint of ^{13}C chemostratigraphy they must be interpreted in the palaeoenvironmental and petrologic context of the rocks as they may be misleading if considered in isolation. For example, in the previously mentioned Julie Formation, Mn/Sr and $\delta^{18}O$ data considered in isolation point to the most ^{13}C-depleted (as low as -5.5 ‰) carbonates being least-altered (lowest Mn/Sr; highest $\delta^{18}O$), while dolostones with apparently normal marine $\delta^{13}C$ (+5 ‰) have largely 'unacceptable' trace-element credentials (Mn/Sr > 10). Petrography and facies analysis suggest that the ^{13}C-depleted rocks derive their isotopic and trace-element signature from a restricted perilittoral brine pool environment, and that open-marine $\delta^{13}C_{carb}$ signatures are preserved in the carbonates with relatively high (> 10) Mn/Sr ratios (see section 4.6c).

Another approach used to monitor alteration in the $\delta^{13}C_{carb}$ signal is to seek congruent variations in the organic carbon isotope signal. Parallel stratigraphic variation in $\delta^{13}C_{org}$ and $\delta^{13}C_{carb}$ offers powerful evidence of a primary signal, as post-depositional alteration tends to raise $\delta^{13}C_{org}$ while lowering $\delta^{13}C_{carb}$ (Knoll et al., 1986; and see next section). However, there are significant limitations to this method. In practice, a rather wide spread of $\Delta\delta$ (= $\delta^{13}C_{carb}$ - $\delta^{13}C_{org}$) is generally seen (e.g. Knoll et al., 1986; 1995; Margaritz et al., 1992) and it may not be clear whether the 'best-fit' $\Delta\delta$ (Knoll et al., 1986) or maximum $\Delta\delta$ (Knoll et al., 1995) represents the least-altered samples; or indeed whether the organic signal carries any meaningful chemostratigraphic information (see Strauss et al., 1992a). Also, the likelihood

of secular or palaeoenvironmental change in primary $\Delta\delta$ (see next section) means the assumption of original parallelism of $\delta^{13}C_{org}$ and $\delta^{13}C_{carb}$ signals is may be an oversimplification.

Again, palaeoenvironmental context is important in interpreting $\Delta\delta$ data. In the Wonoka Formation, relatively deep-water limestones have unusually depleted $\delta^{13}C_{carb}$ (-8 ‰) and correspondingly very low $\Delta\delta$. There is good evidence that this unusual isotopic signature is not the result of alteration but of deposition below a salinity-stratified water body (see sections 3.6c, 6.2).

In monitoring secondary alteration of $^{87}Sr/^{86}Sr$, the approach used in this study has been to consider only those results with trace-element and $\delta^{18}O$ compositions well within the limits of Kaufman et al. (1993) as being potentially little-altered (see section 6.3b). Since diagenesis nearly always increases the ratio, the lowest results from a suite of closely-related samples thus selected is considered to most closely approach the original marine value. If the two or three lowest $^{87}Sr/^{86}Sr$ values are similar (± 0.0001) then these are considered little - altered (probably within 0.0002 of the original marine value: cf. Fig. 1.12, and see section 6.3b).

2.3 Organic carbon isotopes in chemostratigraphy

2.3a Introduction

Relatively few chemostratigraphic studies have employed organic carbon isotopes, firstly because the analytical technique is more involved than with carbonates and secondly because the isotopic changes associated with the fixation and burial of organic carbon are thought to blur the primary signal considerably (Hayes et al., 1983; Dean et al., 1986; Popp et al., 1989). However, in several studies total organic carbon and carbonate carbon were found to display broadly parallel stratigraphic variation in $\delta^{13}C$, strong evidence for preservation of a primary signal in both phases (Knoll et al., 1986; Hayes et al., 1989; Margaritz et al., 1992; Narbonne et al., 1994). Hayes et al. (1989) found the positive $\delta^{13}C_{carb}$ excursion associated with the Cenomanian-Turonian 'Oceanic Anoxic Event' to be amplified threefold in $\delta^{13}C$ of total organic carbon ($\delta^{13}C_{org}$). In other studies, erratic or anomalously ^{13}C-enriched organic carbon is taken to indicate destruction of the signal by high burial temperatures (Strauss et al.1992a; Kaufman et al., 1991).

Factors affecting $\delta^{13}C_{org}$

The enzyme responsible for the fixation of the bulk of sedimentary organic carbon, RuBP carboxylase ('rubisco'), discriminates in favour of ^{12}C, leading to depletion of primary organic matter of 25 to 30 ‰ in ^{13}C relative to its CO_2 substrate (e.g. Schidlowski, 1988). This fractionation effect, ε_P, is variable and dependent on environmental factors and physiological differences between high-level taxa of primary producers (see review by Hayes, 1993). In subaqueous plants, ε_P is dependent on the concentration of dissolved CO_2, higher $[CO_2(aq)]$ leading to greater depletion in ^{13}C of primary photosynthate (Degens et al., 1968; Mizutani & Wada, 1982; Popp et al., 1989; Hollander & McKenzie, 1991; Freeman & Hayes, 1992). Empirically, the precise ε_P - $[CO_2(aq)]$ relationship appears to be variable for reasons not always well understood, and has variously been taken to be linear (Rau et al., 1989; 1991), logarithmic (Popp et al., 1989; Jasper & Hayes, 1992; Freeman & Hayes, 1992), or hyperbolic (Rau et al., 1992; Hayes, 1993) in form. Nevertheless, crude CO_2 palaeobarometry seems feasible based on reconstructed values of ε_P (Hollander & McKenzie, 1991; Freeman & Hayes, 1992).

As a corollary of the $[CO_2(aq)]$ effect on the isotopic composition of marine photosynthate, temperature and productivity are important factors. If photosynthetic uptake of CO_2 exceeds the rate of replenishment through shifts in carbonate equilibria, decomposition of organic matter, and diffusion of atmospheric CO_2 into surface waters, then drawdown of $[CO_2(aq)]$ and heavier $\delta^{13}C$ of organic matter will result. This effect is important under conditions of unusual nutrient enrichment associated with blooms of primary producers (e.g. Hollander & McKenzie, 1991; Simoneit et al., 1993). In general this productivity effect is not significant in open marine waters (Freeman & Hayes, 1992) largely because phosphorus, not $CO_2(aq)$, is the limiting nutrient (Broecker & Peng, 1982).

There is a temperature effect on the isotopic composition of marine photosynthate because the solubility of CO_2 increases in colder water, and because the fractionation between $CO_2(aq)$ and bicarbonate is notably temperature-dependent, following the relationship

$$\varepsilon_{CO_2\text{-bicarb}} = 24.12 - 9866/T(°K)$$

(Mook et al., 1974). Hence, modern high-latitude phytoplankton have organic carbon depleted by ca. 6 ‰ relative to low-latitude phytoplankton (Rau et al., 1991).

Physiological differences between major taxa of primary producers may result in some ecological effects on the $\delta^{13}C_{org}$ signal (e.g. Hollander & McKenzie, 1991; Strauss et al., 1992d; Hayes, 1993). Green photosynthetic bacteria (the Chlorobiaceae) fix carbon using

reaction mechanisms resulting in ^{13}C enrichment relative to other subaqueous plants and chemoautotrophs which utilise the Calvin cycle involving rubisco (Summons & Powell, 1986; Hayes, 1993). Chemoautotrophic biomass fixed at the oxycline may be relatively ^{13}C-depleted because porewater dissolved CO_2 is there commonly partly organogenic (e.g. Freeman et al., 1990).

Thus, some overprint of the $\delta^{13}C_{org}$ signal by palaeoenvironmental factors can be expected. These may in part be resolved by isotopic analysis of primary photosynthate-derived biomarkers (e.g. see Hayes et al., 1989) but such methods are beyond the purview of this study. However, absence of terrestrial biomass in the Proterozoic simplifies interpretation based on $\delta^{13}C_{org}$ of total organic carbon (cf. Jasper & Hayes, 1990). Of course, changes in $\delta^{13}C_{org}$ related to broad environmental factors such as palaeoclimate or pCO_2 may be of stratigraphic utility while not necessarily reflecting changes in $\delta^{13}C$ of seawater.

Post-depositional processes impose further variability on the organic carbon isotopic signal. Heterotrophic reworking within the water column or within newly deposited sediment leaves residual organic matter slightly ^{13}C-enriched relative to primary photosynthate; while addition of methanotrophic biomass and some differential preservation of isotopically lighter components (lipids), tend to deplete ^{13}C in organic matter (Hayes et al., 1983; 1987; 1989; Freeman et al., 1990; Hayes, 1993). Once the stage of an immature kerogen is reached, however, isotopic shifts are always positive (Hayes et al., 1983). Loss of hydrocarbons during catagenesis and metagenesis leads to progressive ^{13}C-enrichment of residual kerogens (McKirdy & Powell, 1974). This essentially thermally-driven process can be monitored approximately by maturation indices such as kerogen H/C ratio, Rock-Eval T_{max} and illite crystallinity (e.g. Hayes et al., 1983; Strauss et al., 1992c). Proterozoic samples with H/C less than 0.2 or with total organic carbon content (TOC) less than 0.2 mg/g are observed to have erratic and enriched $\delta^{13}C_{org}$ suggesting that the signal is essentially lost in highly degraded kerogens (Fig. 2.1; Knoll et al., 1986; Strauss et al., 1992a; Des Marais et al., 1992). For kerogens with H/C > 0.2, Des Marais et al. (1992) applied a correction factor (derived from the form of the curve on Fig. 2.1) to restore original isotopic compositions (at H/C = 1.5) in a survey of Proterozoic kerogens from widespread localities.

Isotopic compositions of biomarkers derived from primary photosynthate have been shown to track primary $\delta^{13}C$ change with greater fidelity than total organic carbon (Hayes et al., 1989) but such techniques lie outside the field of this study, and in any case may not be generally applicable to thermally mature Neoproterozoic successions (Strauss et al., 1992d).

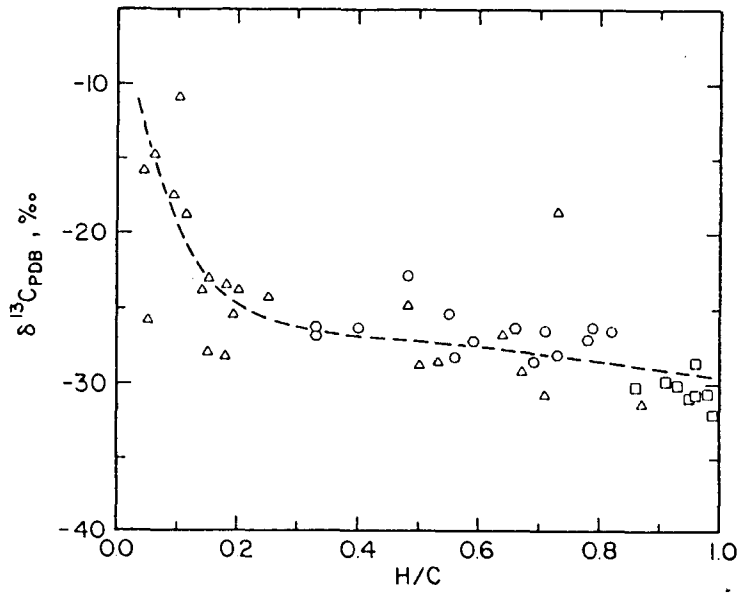

Fig. 2.1: Carbon isotopic composition versus H/C in kerogens with ages of 1.6 Ga or less. From Hayes et al. (1983).

In this study, fossil benthic microbial mats are recognised in certain relatively organic-rich shales. Isotopic composition of the benthic mat carbon tends to be strongly depleted - up to 14 ‰ lower than associated organic carbon of pelagic origin - and appears to yield a discrete and separate chemostratigraphic signal. The 'benthic signal' is more precisely determined by applying a correction to account for mixing with carbon from other (pelagic) sources.

An attempt is made in this study to correct for post-depositional alteration in two ways. Firstly, earlier observations of an inverse correlation of $\delta^{13}C_{org}$ with TOC in Proterozoic sediments (Hayes et al., 1983; Kaufman & Knoll, 1995) are confirmed. This relationship may be due in part to variation in the degree of biological reworking (Hayes et al., 1983). Below, a correction factor derived from the observed inverse $\delta^{13}C_{org}$ - TOC relationship (as determined within short sections of core, thereby excluding the effects of changes in thermal maturation) is applied to $\delta^{13}C_{org}$ data. Results are considered to reflect more closely the primary signal because scatter on chemostratigraphic plots is reduced and congruency with the carbonate signal is enhanced. Secondly, an attempt is made to quantify the effects of regional variation in thermal maturity by using H/C, $\Delta\delta$ and kerogen colour in a systematic way.

2.3b Benthic Microbial Mats

Description

In six marine shaly units covered by this investigation (Table 2.1) there are layers, ranging from thick beds to thin laminae, of dark grey to black shale that are sharply delineated from enclosing, paler shale or carbonate. In thin section (and often to the unaided eye) the darker

Basin Formation *Drillhole*	Occurrence, Stratigraphic range	$\delta^{13}C_{bmm}$ $\Delta p\text{-}b$	Lithological association	Age	Where figured
Amadeus Basin Pertatataka Fm. *Wallara-1*	Black shale as thin laminae to thick beds, 1009-1248m depth	-32 to -36 ‰ *5 to 9 ‰*	Black shale alternates with grey-green shale; rare thick ?turbiditic sandstone beds; wave-formed sedimentary structures in gradationally overlying succession.	early Ediacarian	Plate 2.2; Fig. 4.16
Adelaide Geosyncline Brachina Fm. *BWM1a-1*	Black shale dominantly as thick beds, 145.5-187.5m depth	-36 to -38 ‰ *10 to 11 ‰*	Black shale alternates with lesser grey-green shale; sandy layers absent.	early Ediacarian	Fig. 3.6
Adelaide Geosyncline Brachina Fm. equivalent *SCYW1A*	Very sparse wispy black laminae, 860 - 990 m depth	-38 to -40 ‰ *12 to 14 ‰*	Subequal siltstone and shale, with planar-parallel lamination, ripple cross-lamination, starved ripples.	early Ediacarian	Fig. 3.5
Officer Basin 'Giles Mudstone' *Giles-1*	Single thin black lamina at 1028.85 m depth	-35 ‰ *9 ‰*	Shale with lesser siltstone as thin, graded, ripple cross-laminated or planar-laminated beds.	early Ediacarian	Fig. 3.15
Officer Basin Rodda beds *Munta-1*	Sparse wispy black laminae, 1198 - 1253 and 1438 - 1448 m depth	-28 to -32 ‰ *0 to 6 ‰*	Higher occurrence in dominantly fine-grained sandstone with wave-formed structures; lower in micritic limestone and shale	middle Ediacarian	Fig. 3.16
Smithton Basin Kanunnah Subgroup *Forest-1*	Sporadic thin beds of black shale, 230 - 760m depth	-36 ‰ *5 ‰*	Occur within grey-green silty shale beds, in succession of predominantly volcaniclastic, turbiditic sandstones	Neoproter-ozoic	Plates 2.1, 2.3

Table 2.1: Location, megascopic appearance, generalised isotopic data (from Table 2.2), lithological associations, and ages of six black shale occurrences interpreted to be of benthic microbial mat origin.

colouration is seen to be due to an abundance of weakly anastamosing thin (<50 μ) black layers (Plates 2.1, 2.2). Under high power the layers are seen to consist mostly of pyrite framboids tightly clustered around thin, dark brown organic layers. In adjacent, organic-poor shale beds microlamination is planar-parallel rather than anastamosing (Plate 2.2). Commonly, thin wispy rip-up flakes, 1-10 mm long, of black shale are present in enclosing siltstone or shale (Plate 2.3). Black shale laminae or intraclasts in places exhibit syndepositional folding. Synsedimentary cohesion of the black layers is indicated by sydepositional plastic deformation and their relative abundance as intraclasts. The anastamosing fabric is truncated by minor intraformational erosion surfaces and is present in

disoriented intraclasts, indicating a syndepositional rather than strictly compactional origin. Organic carbon contents of the black shale layers, at up to 7 mg/g, tend to be much higher than associated sediments which average about 1 mg/g (Table 2.2; Fig. 2.2).

Lithological associations suggest mid-shelf depositional environments at or below storm wavebase (Table 2.1). Enclosing successions are predominantly shale or silty shale. A proportion (generally minor) of siltstone and sandstone occurs as thin planar laminae, starved ripples and 'event beds'. In some sections the sand is storm-laid, in others of turbidite origin. The six occurrences are of probably three discrete ages (section 6.2).

section	sample	depth(m)	∂13Cbs	TOCbs	∂13Cbkgd	TOCbkgd	∂13Cbmm	Δp-b
Wallara-1	28.68	1008.80	-30.52	2.30	-27.15	0.80	-32.3	5.2
	28.78	1055.90	-30.64	2.32	-27.10	0.90	-32.9	5.8
	28.80	1066.80	-30.64	1.87	-27.15	0.90	-33.9	6.7
	28.86/1	1083.70	-30.93	2.04	-27.30	0.90	-33.8	6.5
	28.92/1	1115.20	-31.95	2.99	-27.55	1.00	-34.2	6.6
	28.95/1	1127.30	-31.77	4.00	-27.65	1.05	-33.2	5.6
	28.94	1125.60	-32.35	3.59	-27.65	1.05	-34.3	6.6
	28.96	1132.80	-32.23	4.49	-27.70	1.05	-33.6	5.9
	28.100	1152.60	-32.86	3.14	-28.15	1.15	-35.6	7.4
	28.102	1156.00	-32.42	3.23	-28.30	1.15	-34.7	6.4
	28.104	1173.00	-32.30	2.55	-29.65	1.15	-34.5	4.8
	28.105/4	1177.80	-33.37	6.81	-29.90	1.15	-34.1	4.2
	28.106	1181.70	-33.95	5.18	-30.15	1.15	-35.0	4.9
	28.108	1184.40	-33.69	3.73	-30.40	1.15	-35.2	4.8
	28.109/1	1190.00	-33.27	5.85	-30.60	1.15	-33.9	3.3
	28.112/1	1206.50	-34.41	4.35	-30.40	1.15	-35.9	5.5
	28.116	1225.50	-33.38	3.41	-27.15	1.10	-36.3	9.2
	28.118	1232.50	-33.10	3.31	-27.00	1.05	-35.9	8.9
BWM1a-1	20.01	146.50	-32.20	2.50	-26.00	0.98	-36.2	10.2
	20.03/2	157.50	-32.30	2.21	-26.70	0.98	-36.8	10.1
	20.05/1	169.40	-32.70	2.34	-26.70	0.98	-37.5	10.8
SCYW1A	22.47/2	917.60	-29.60	1.10	-25.90	0.82	-40.1	14.0
	22.49	939.50	-29.20	1.19	-25.60	0.82	-37.8	12.5
Giles-1	10.24	1028.85	-30.40	1.10	-26.50	0.60	35.1	8.6
Munta-1	15.39/1	1243.60	-30.00	1.32	-26.50	0.51	-32.1	5.6
Forest-1	F60	321.00	-33.90	1.43	-31.10	0.54	35.6	4.5

Table 2.2: Carbon isotopic composition and TOC of black shales of benthic microbial mat origin ($\delta^{13}C_{bs}$, TOC_{bs}); of associated shales ($\delta^{13}C_{bkgd}$, TOC_{bkgd}); calculated isotopic compositions of benthic microbial mats($\delta^{13}C_{bmm}$) and of isotopic difference between 'pelagic' and 'benthic' carbon (Δ_{p-b}).

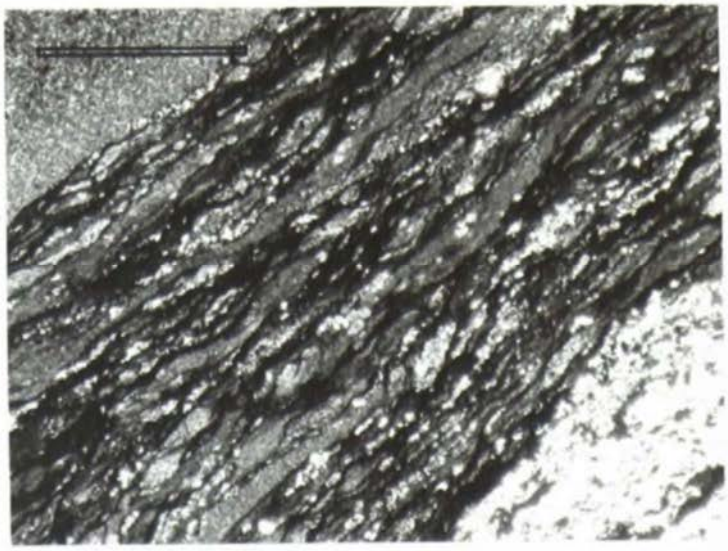

Plate 2.1: Thin section, mudstone with anastamosing organic-rich thin layers interpreted to be remnant benthic microbial mats. Kanunnah Subgroup, sample ABS51, 235 m depth, Forest-1 drillhole, Smithton Basin. Scale bar = 1mm.

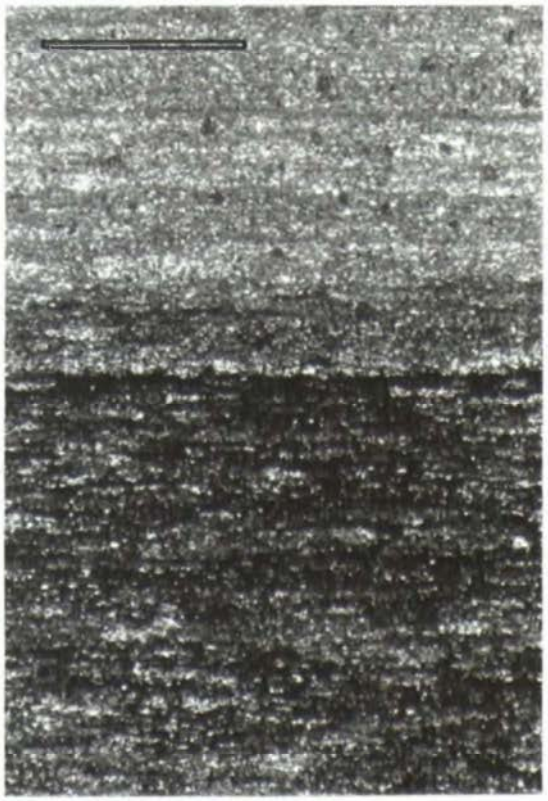

Plate 2.2: Thin section, mudstone with thin, anastamosing, organic-rich laminae (benthic microbial mats) overlain by organic-poor mudstone with planar-parallel lamination. Pertatataka Formation, sample 28.112, 1206.5 m depth, Wallara-1 drillhole, Amadeus Basin. Scale bar = 1mm.

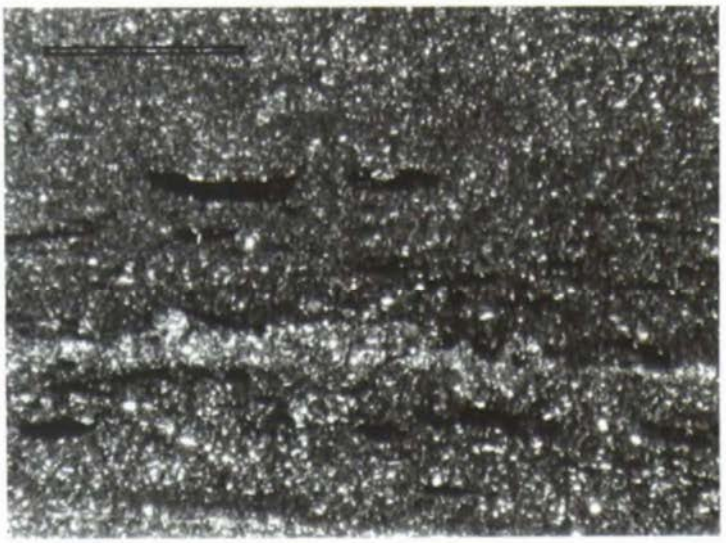

Plate 2.3: Thin section, siltstone with wispy intraclasts of organic-rich mudstone (reworked benthic microbial mat fragments). Kanunnah Subgroup, sample ABS53, 281.3 m depth, Forest-1 drillhole, Smithton Basin. Scale bar = 1mm.

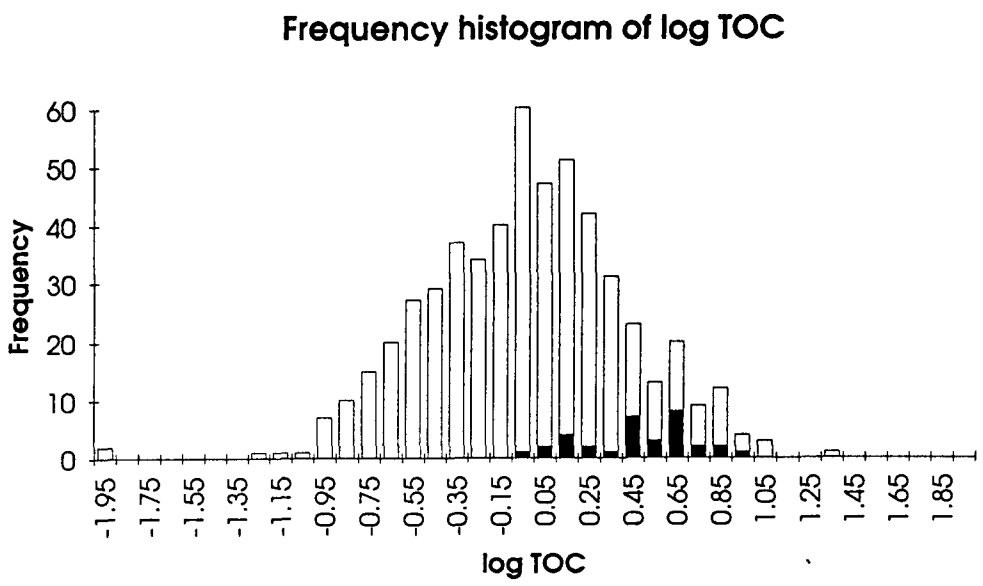

Fig. 2.2: Frequency histogram of log TOC (TOC = total organic carbon content in mg/g); all data of this study. Black bars: 'benthic microbial mat facies' (see text); white bars: all other samples (shales and carbonates). TOC ranges from 0.01 mg/g to 17 mg/g, averaging approximately 1 mg/g.

Very similar black shale layers in the Belt Supergroup, North America, were interpreted as remnant benthic microbial mats ('striped shale facies') by Schieber (1986, 1990). In places these mats are heavily pyritized (Schieber, 1989). Features considered diagnostic of a benthic microbial mat origin (Schieber, 1986) are the wavy microlamination (resulting from the interplay of sediment trapping and binding, and mat growth) and the presence of wispy, sometimes deformed, rip-up flakes indicating coherent mechanical behaviour relative to the associated muds. The benthic microbial mat shales in the Belt Supergroup contain up to 20 mg/g organic carbon. Carbonaceous microlaminae in the Australian examples tend to be thinner and more widely spaced than those figured by Schieber (1986, 1990).

Strew slide observations

Kerogen strew slides, prepared by K. Grey, of typical black shales of this type from the Pertatataka Formation in Wallara-1 (e.g. samples 28.108; 28.116) are marked by an abundance of large, irregular, apparently fragmented and corroded sheets of amorphous dark brown organic matter, crowded with small adhering pyrite framboids (Plate 2.4). Typical microbial mat features (e.g. filaments, coccoids) are not preserved (K. Grey, pers. comm.). There are rare, poorly-preserved leiospherid acritarchs.

Some other palynological residues contain relatively more sparse, but better-preserved mat fragments (e.g. Ungoolya 26.10, 26.46; 26.55; Munta 15.61). These samples contain smaller fragments of moderately to well preserved sheet-like masses of closely-appressed coccoids,

or amorphous sheets with adhering filaments, some with septa (Plates 2.5, 2.6). Pyritization is much less evident. Acritarchs and indeterminate organic matter are relatively abundant in these samples. Of these samples, only one (Munta 15.61) contains thin dark pyritic seams in thin section and an elevated TOC; and none has anomalously depleted $\delta^{13}C_{org}$. Other than in Munta 15.61, the low TOC suggests mat material is not volumetrically large, and the lack of ^{13}C depletion suggests either that the mats comprise only a small proportion of TOC or that they are not isotopically distinct from associated organic matter. The volumetric sparsity, lack of petrographic expression, and fragmented appearance in palynological preparations suggests the mat material in these samples is allochthonous (K. Grey, pers. comm.).

Isotopic composition of mats

Carbon isotopic compositions of the black shale layers range from the same as enclosing layers to (much more commonly) strongly depleted. Depletion is usually much greater than can be accounted for by any inherent TOC - $\delta^{13}C_{org}$ covariation (see below). Thus, two end-member sources of organic carbon can be inferred. Black shale layers are dominated by carbon derived from benthic microbial mats with some carbon of pelagic origin; and other rock-types contain only organic matter of pelagic origin.

Because the fossil benthic organic matter forms such a volumetrically small proportion of the black shales, it is impossible to sample directly without contamination by pelagic carbon, sedimentation of which presumably continued whether or not microbial mats intermittently colonized the sea floor. A closer approximation of the true isotopic composition of the benthic microbial mats can be calculated, however, by a mass-balance equation, since the 'background' (pelagic) TOC and $\delta^{13}C_{org}$ can be inferred from analysis of closely-associated, non-black shale samples:-

$$\delta^{13}C_{bmm} = (\{TOC_{bs} \times \delta^{13}C_{bs}\} - \{TOC_{bkgd} \times \delta^{13}C_{bkgd}\}) / (TOC_{bs} - TOC_{bkgd}) \qquad (1)$$

where subscripts bmm, bs, and bkgd refer to benthic microbial mat, black shale and background, respectively (Table 2.2). 'Background' $\delta^{13}C$ and TOC values are those of lighter-coloured rock immediately adjacent to the black shale or, where adjacent subsamples were not analysed, from averaged, closest-available, non-black shale samples. These values tend to be quite stable, lending credence to the assumption of a relatively constant pelagic flux. The $\delta^{13}C_{bmm}$ calculation is vulnerable to large errors where (TOC_{bs}-TOC_{bkgd}) is very small, and so not all raw black shale data are amenable to this calculation. Both raw ($\delta^{13}C_{bs}$) and refined ($\delta^{13}C_{bmm}$) data are shown in the chemostratigraphic profiles (Chapters 3, 4).

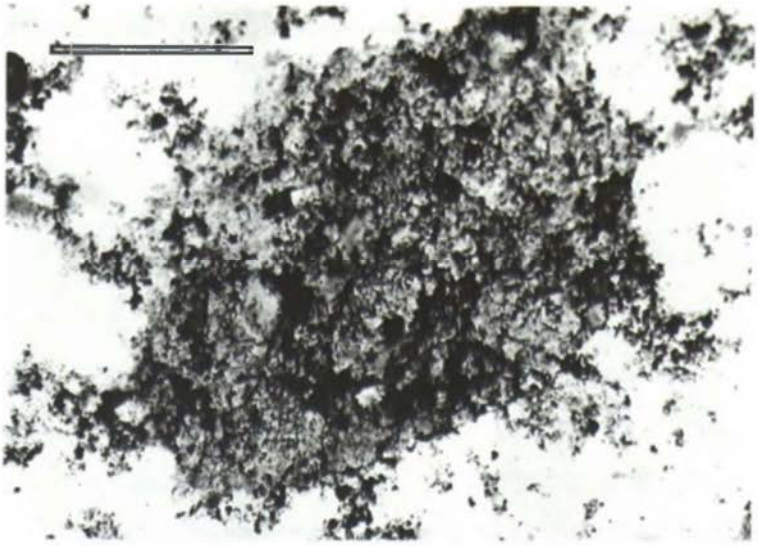

Plate 2.4: Palynological strew slide showing large corroded fragment of amorphous kerogen, probably of benthic microbial mat origin. Pertatataka Formation, sample 28.116, 1225.5 m depth, Wallara 1 drillhole, Amadeus Basin. Scale bar = 100 μ.

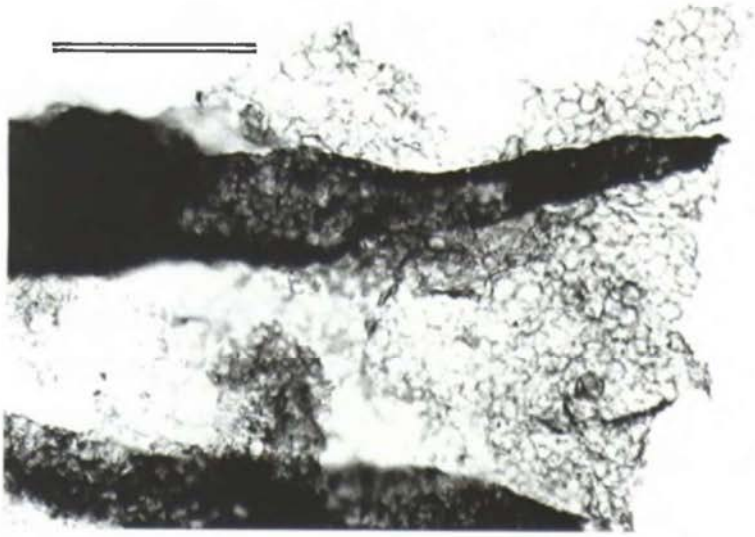

Plate 2.5: Palynological strew slide showing fragment of coccoid sheet. Sample 930112.10, 260.9 m, NJD-1, western Officer Basin. Scale bar = 100 μ.

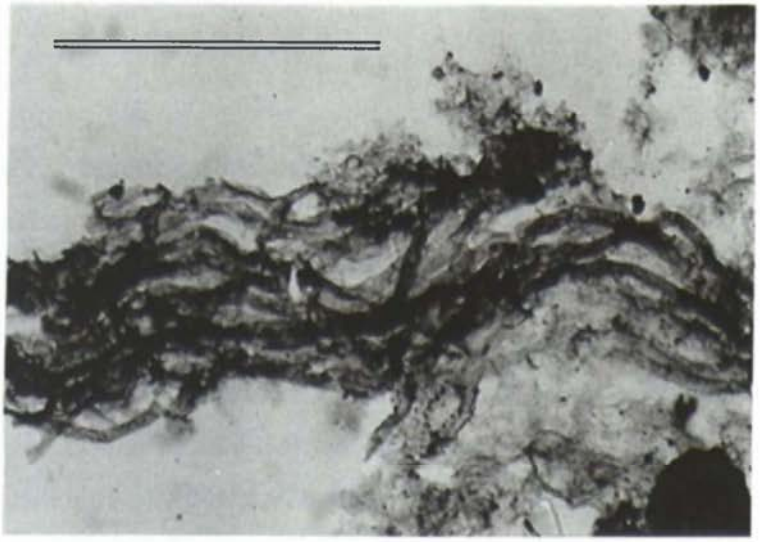

Plate 2.6: Palynological strew slide showing mass of filaments. Rodda beds correlative, sample 26.10, Ungoolya 1 drillhole, Officer Basin. Scale bar = 100 μ.

The difference between $\delta^{13}C_{org}$ of inferred benthic and pelagic origin is a quantity of interest, here defined as

$$\Delta_{p\text{-}b} = \delta^{13}C_{bkgd} - \delta^{13}C_{bmm} \quad (2)$$

$\delta^{13}C_{bmm}$ is as light as -40 ‰, and $\Delta_{p\text{-}b}$ varied from 0 to 14 ‰ (with much narrower ranges typical of individual localities: Tables 2.1; 2.2).

Preliminary carbon isotopic results from biomarkers from benthic microbial mat samples from the Pertatataka Formation (drillhole Wallara 1, see Table 2.1) show that the black shales contain two, isotopically distinct groups of biomarkers: the predominant group consists of even-numbered, long-chain alkanes and certain branched compounds that are around -32 ‰ in $\delta^{13}C$, while odd-numbered and shorter-chain alkanes are 4 to 6 ‰ heavier (G. Logan, pers. comm.). The producers of the isotopically lighter group are thought to have contributed the bulk of the organic matter to form the kerogen (G. Logan, pers. comm.). These results are in good agreement with the two-end-member model presented above.

Pyrite was obtained from twenty representative shales by HF - HCl dissolution (for method see section 2.4b) and analysed for $\delta^{34}S$. Six benthic microbial mat shale samples have $\delta^{34}S_{py}$ of -20 ± 8 ‰; while pyrite from the remaining fourteen shales without benthic microbial mat development has a slightly heavier range of $\delta^{34}S_{py}$ (-16 ± 11 ‰) (see Appendix 1.1 for fully tabulated results). Seawater sulphate isotopic composition during the time of deposition of these shales was +20 to +24 ‰ (see section 6.3c). The slightly lighter $\delta^{34}S_{py}$ of the benthic microbial mat facies is very likely reflects more open-system fractionation associated with a relatively shallow position of sulphate reduction within the sediment pile.

Discussion

Further work is required to fully integrate palynological with petrographic and geochemical observations, but at present it seems that *in situ* benthic microbial mats suffered considerable degradation by sulphate reducers soon after burial, while for resedimented mat fragments, degradation by sulphate reducers was less severe.

Preservation of resedimented organic carbon against attack by sulphate reducers has been observed in modern organic-rich turbidites on the abyssal plains of the NE Atlantic. Despite normal porewater sulphate availability, sulphate reduction appears to be absent in these deposits (Colley et al., 1984; Emerson & Hedges, 1988). Organic matter that has been previously partly oxidised at its original site of deposition may be less prone to attack by sulphate-reducing bacteria (Emerson & Hedges, 1988; Pedersen & Calvert, 1990). Emerson

& Hedges (1988) observe that structural alteration of biochemicals will inhibit subsequent enzymatically catalyzed degradation.

The cause of the strong ^{13}C depletion in the microbial mat facies - up to 14 ‰ lower than organic matter in adjacent beds - is uncertain. The relatively severe corrosion apparent in palynological preparations is symptomatic of heterotrophic reworking that should be accompanied by slight ^{13}C enrichment rather than depletion (Hayes et al., 1983; 1989). In general, it might be expected that pelagic organic carbon has undergone more extensive heterotrophic recycling than benthic mat carbon because of its residence time in the water column, but the isotopic effect should be relatively slight (see below). There appear to be no known mat-forming organisms characterised by unusually large fractionation accompanying carbon fixation. Chemoautotrophs such as sulphide- and ammonia-oxidising bacteria fix dissolved inorganic carbon by means of the C3 pathway and so discriminate to a similar extent to aerobic phototrophs (Strauss et al., 1992a). However it is possible that, growing at the oxycline within or at the top of the sediment, such bacteria fixed CO_2 that was relatively ^{13}C-depleted (Freeman et al., 1990).

Of the anaerobic photosynthetic bacteria, the Chromatiaceae use the C3 pathway while the Chlorobiaceae do not, utilizing instead reaction mechanisms that result in ^{13}C enrichment relative to oxygenic primary producers (Summons & Powell, 1986).

The benthic microbial mats may well have been photosynthetic. The South Australian examples (like those of the Belt Supergroup - Schieber, 1990) grew within storm wavebase but below fairweather wavebase, an environment likely to have been within the photic zone but below the zone of constant wave reworking. Non-photosynthetic sulphur-oxidizing bacterial mats are found in some modern, dysoxic deep marine environments (Williams & Reimers, 1983) but require a high and stable flux of metabolizable organic matter (Arntz et al., 1991). There are no indications of the requisite high organic flux in these organically-lean rocks.

Methane, strongly depleted in ^{13}C (-50 to -80 ‰), may be generated by fermentative processes if labile organic matter remains in the sediment after sulphate ion is exhausted (e.g. Anderson & Arthur, 1983). Aerobic methylotrophs higher in the sediment column will be characterised by strongly ^{13}C-depleted biomass (Hayes et al., 1987; Freeman et al., 1990). In the Eocene Messel Shale, the presence of small amounts of methylotrophic biomass has led to sedimentary total organic carbon with $\delta^{13}C_{org}$ 8 ‰ lower than that of associated oxygenic algae (Freeman et al., 1990).

However, a number of observations argues against methane recapture being the predominant cause of the ^{13}C depletion in the black shales. The preliminary biomarker isotopic results communicated by G. Logan suggest that the depletion seen in the benthic microbial mat facies reflects that of the predominant contributor to the kerogen, itself not sufficiently depleted to have been methylotrophic. Also, benthic microbial mat isotopic compositions from adjacent samples at individual localities are in good agreement, in places delineating patterns of smooth stratigraphic variation (Fig. 4.16). This is a feature suggestive of a palaeoenvironmental control on a predominant producer rather than early diagenetic addition of small amounts of highly depleted methane-derived carbon. Furthermore, there is no significant $\delta^{13}C_{bmm}$ - TOC correlation: in other words, black shale samples with higher TOC (in which fermentative metabolism might be expected to be favoured) are not consistently marked by lighter isotopic compositions.

Strong ^{13}C depletion in the black shales may be due, at least in part, to stratification of the water column. The lower water mass of a stratified water body attains a more depleted $\delta^{13}C_{DIC}$ because of remineralization of sinking pelagic organic matter fixed in the surface layer (e.g. Takahashi et al., 1968; Berger & Vincent, 1986). $[CO_2(aq)]$ will be higher in the lower water mass for the same reason, tending to further deplete ^{13}C in organic matter fixed on the sea floor because of the positive $CO_2(aq)$ - ε_p relationship (see section 2.3a). Other environmental and physiological details might also affect the isotopic composition of the mats in ways not easily predicted. Thus, if water column stratification is the cause of the strong ^{13}C depletion of the benthic microbial mats, $\Delta_{p\text{-}b}$ is unlikely to be a direct measure of the difference in $\delta^{13}C_{DIC}$ between surface and deep water masses.

However, the isotopic composition of carbonates offers some support for a causal relationship between stratification of the water column and large $\Delta_{p\text{-}b}$. The only two samples in which $\Delta_{p\text{-}b}$ approaches zero (Rodda beds, Table 2.1) are interbedded with limestone with enriched (+6 ‰) $\delta^{13}C_{carb}$, suggesting deposition in a well-mixed water column or within the surface layer. No carbonates were found interbedded with black shales with high (6 - 14 ‰) $\Delta_{p\text{-}b}$, but stratigraphically nearby examples in the Adelaide Geosyncline and Amadeus Basin are anomalously depleted (-4 to -8 ‰), consistent with equilibration of the carbonate with a ^{13}C-depleted lower water mass (see section 6.2).

Formation of the mats beneath the chemocline of a stratified water body may be inconsistent with a photosynthetic origin, since the $\delta^{13}C$ chemocline would be expected to coincide roughly with the base of the photic zone. However, photosynthetic benthic mats may have occupied a disphotic environment, within or just below the chemocline, in which

photosynthesis by pelagic organisms had largely ceased, but where the presence of a sedimentary substrate allowed benthic mats to make use of the elevated nutrient levels of the lower water mass.

The lateral distribution of the benthic mat facies offers some support for the view that the organisms were photoautotrophs, being consistent with their development in a relatively narrow preservational-environmental window below the zone of constant wave reworking and above the base of the photic zone. In the Brachina Formation, the facies is present in shelfal localities (the Curnamona Craton and Stuart Shelf) and absent in more distal, probably deeper-water sections in the Flinders Ranges (see section 3.4). In the Pertatataka Formation and its correlatives, the benthic mat facies is known from one locality - drillhole Wallara 1 - where sandstone beds of probable storm origin are interbedded with the upper part of the black shale-bearing succession. Probable time-equivalent parts of sections to the north appear to lack benthic mat developments, are sand-free, more distal and probably of deeper-water palaeoenvironment (see section 4.5).

The consistently relatively high TOC in the black shales of benthic microbial mat origin (Fig. 2.2) suggests they comprise an important hydrocarbon source rock, and that their palaeoenvironmental and palaeogeographic distribution would be worthy of further investigation.

2.3c CORRECTING FOR $\delta^{13}C_{org}$ - TOC COVARIANCE

Using all Precambrian data then available, Hayes et al. (1983) found a weak inverse correlation between TOC and $\delta^{13}C_{org}$. Similarly, Kaufman & Knoll (1995) noted a correspondence between high $\Delta\delta$ (= $\delta^{13}C_{carb}$ - $\delta^{13}C_{org}$) and high TOC. Hayes et al. found that for Proterozoic shales:

$$\delta^{13}C_{org} = - 2.6(\pm 1.8)\log TOC - 29.5(\pm 1.4) \qquad (3)$$

while for Proterozoic carbonates:

$$\delta^{13}C_{org} = - 6.9(\pm 3.2)\log TOC - 29.4(\pm 2.1) \qquad (4)$$

(with TOC in mg/g; indicated uncertainties are 95% confidence levels based on n-2 degrees of freedom).

Data from 47 carbonates analysed by Knoll et al. (1995) also show an inverse correlation:

$$\delta^{13}C_{org} = - 4.0\log TOC - 30.2 \quad (r^2 = 0.33)$$

The total data set in this study is divided into three groups. Firstly, shales interpreted to contain organic matter derived from *in situ* benthic microbial mats (see previous section)

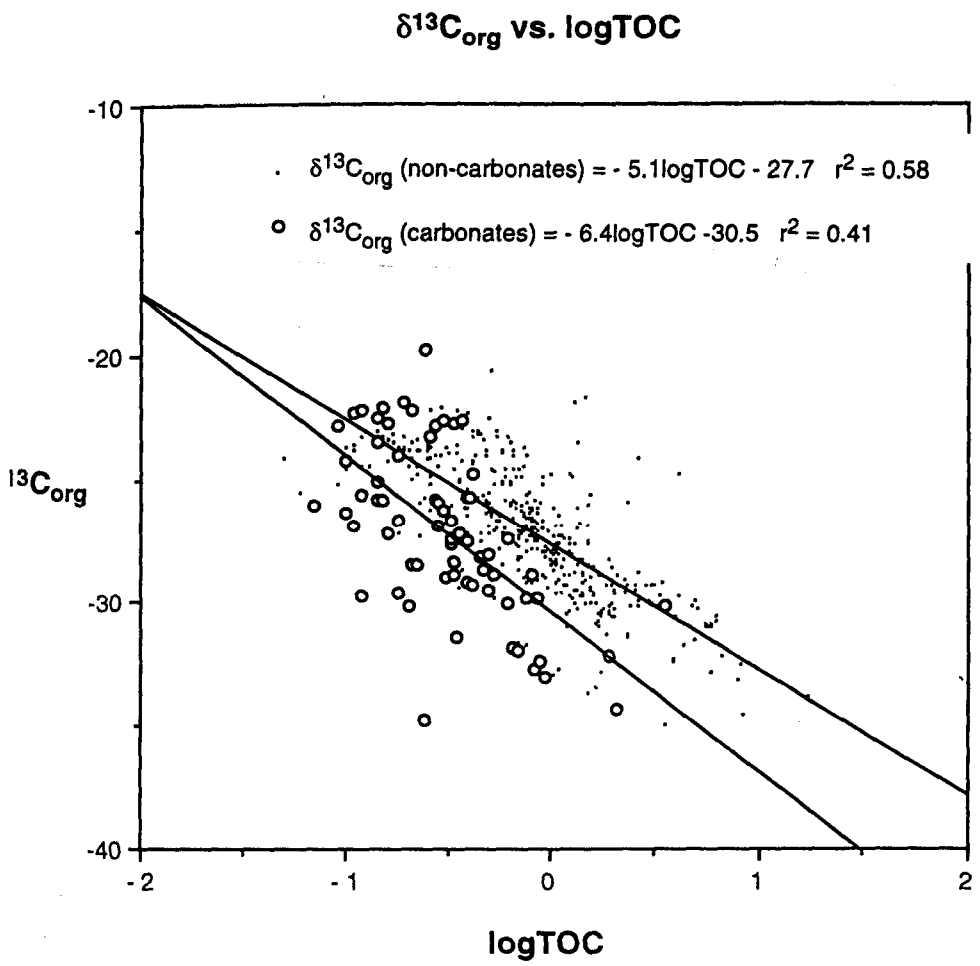

Fig. 2.3(a): Organic carbon isotopic composition versus log TOC; all data of this study; carbonates and non-carbonates (nearly all shales) plotted separately.

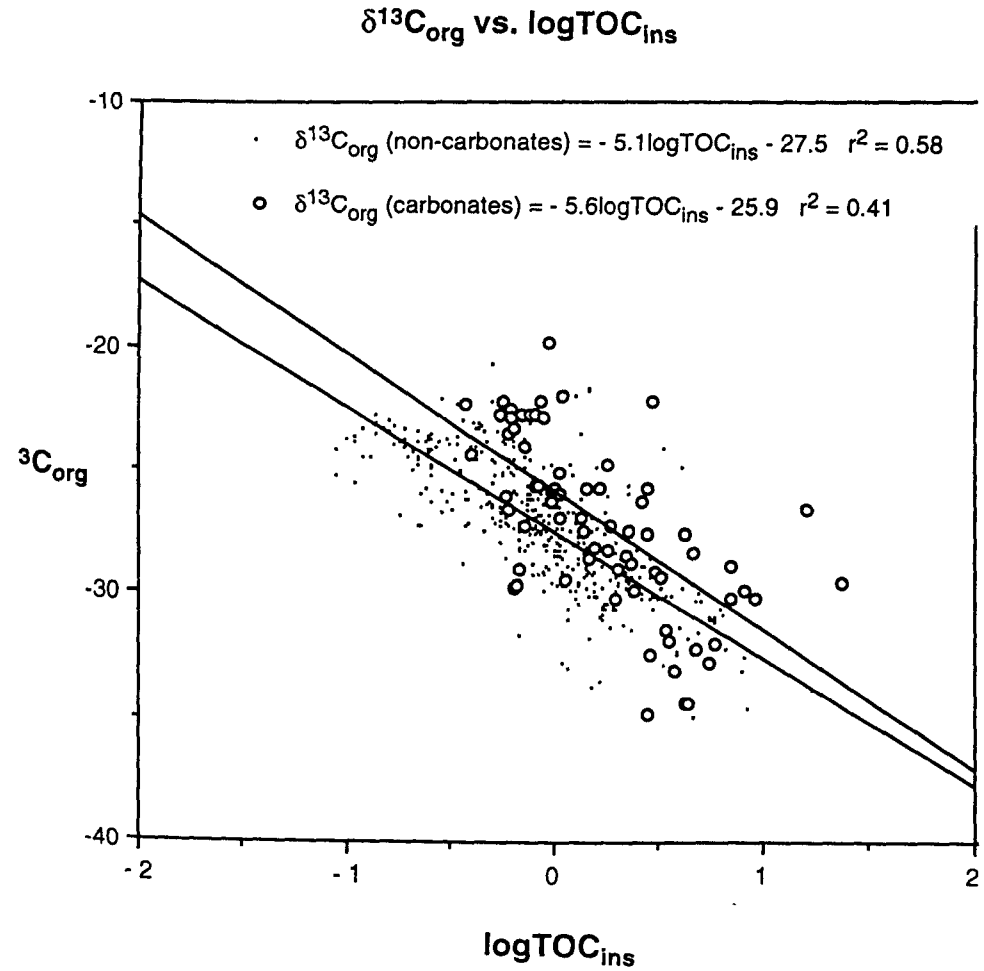

Fig. 2.3(b): As Fig. 2.3(a) but with TOC calculated on a carbonate-free basis (TOC_{insol}).

have isotopic compositions that reflect two distinct sources, and are excluded from the following analysis (n = 34). The second and third groups are shales with less than 50% carbonate (n = 409); and carbonates (more than 50% carbonate; n = 70). The following relationships are obtained (Fig. 2.3a): for non-carbonates,

$$\delta^{13}C_{org} = -5.1 \log TOC - 27.7 \quad (r^2 = 0.58) \qquad (5)$$

while for carbonates,

$$\delta^{13}C_{org} = -6.4 \log TOC - 30.5 \quad (r^2 = 0.41) \qquad (6)$$

A linear fit gives significantly lower correlation coefficients. These results are consistent with those of Hayes et al. (1983), whose data were fewer but more widespread, except that a steeper gradient is here obtained for non-carbonate data. The general inverse TOC - $\delta^{13}C_{org}$ relationship may be attributed to two factors: carbon loss through heterotrophic reworking, and thermal degradation; both processes leading to enrichment of ^{13}C in the residue (Hayes et al., 1983, 1989). However, the reason for the different carbonate and non-carbonate relationships are not clear. TOC on a carbonate-free basis was calculated:

$$TOC_{insol} = (TOC \times 100)/(100 - \%carbonate) \qquad (7)$$

and the replotted results (Fig. 2.3b) show that the carbonate line of best fit is more nearly congruent with the non-carbonate relationship, suggesting that carbonate behaves partly as a simple diluent.

The different factors causing TOC- $\delta^{13}C$ covariation can be separated by analysing variation within small (<100mm) stratigraphic distances. With this approach, the effects of changes in thermal maturity and general scatter caused by secular change in seawater $\delta^{13}C$ should be excluded, as both these factors may be assumed to be constant over such short stratigraphic distances. Accordingly, a number of small (<100 mm) core samples from widespread Australian Ediacarian sequences, each showing some internal apparent variation in TOC, were subsampled. Siltstones and sandstones were avoided: all subsamples consist of shales and silty shales (red, grey, green or black), calcareous mudstones and carbonates. Nearly all samples show an internal, inverse TOC_{insol} - $\delta^{13}C$ relationship (Fig. 2.4). Average gradient by vector addition gives the general relationship

$$\delta^{13}C_{org} = -3.5 \log TOC_{insol} + c \qquad (8)$$

The lower gradient of this relationship can be attributed to the exclusion of the effects of thermal maturation. With raw TOC plotted against $\delta^{13}C$, parallelism is much weaker and gradients flatter for limestone-shale pairs, again suggesting that carbonate acts for the most part as a simple diluent.

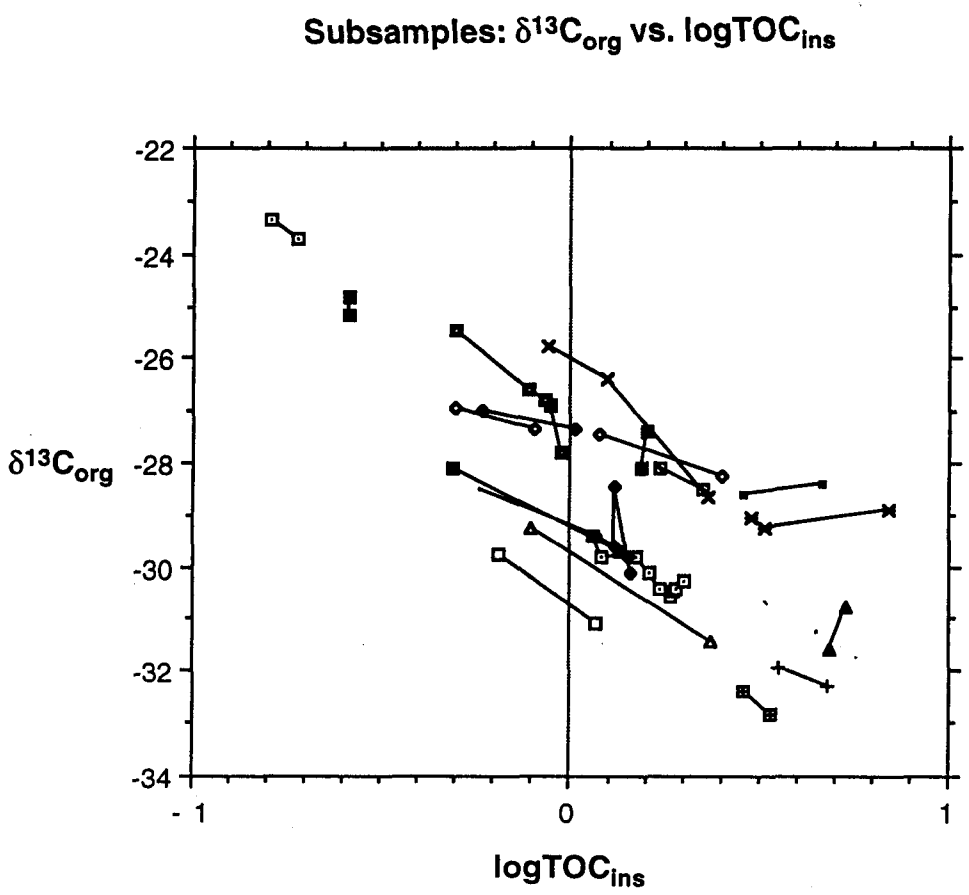

Fig. 2.4: Organic carbon isotopic composition variation with respect to $logTOC_{insol}$ in 19 samples from widespread Ediacarian marine successions; lines join subsamples from individual samples.

The logarithmic relationship allows isotopic change associated with carbon loss to be characterised by the Rayleigh distillation equation

$$R/R_{init} = f^{\{(1/\alpha)-1\}} \quad (9)$$

(R = isotope ratio of residual carbon; R_{init} = initial isotope ratio; f = fraction of carbon remaining; α = fractionation factor of kinetic isotope effect of carbon loss). The fractionation factor associated with this effect (Eq. 8) is calculated at 1.0016.

The data suggest that, superimposed on a rather surprising constancy of productivity and siliciclastic sedimentation rate within samples, a process or processes involving carbon loss with a fractionation factor of 1.0016 was the major factor determining small-scale variation in TOC (and thereby affecting $\delta^{13}C_{org}$). That this phenomenon is not due to systematic experimental error or contamination is shown by the excellent reproducibility of a large number of analytical repeats of varied lithologies, and low organic carbon levels in blanks (see section 2.4b).

This empirical TOC_{insol} - $\delta^{13}C_{org}$ relationship (Eq. 8) allows a correction factor to be systematically applied to $\delta^{13}C_{org}$ data to filter out variation caused by this process, and arrive at a profile that should more closely reflect a primary signal. Measured organic carbon isotopic compositions ($\delta^{13}C_{org}$) are 'normalized' to an arbitrary, constant TOC_{insol} of 1 mg/g (close to the average in most sections studied):

$$\delta^{13}C_{org}{}^{N} = \delta^{13}C_{org} + 3.5 \log TOC_{insol} \quad (10)$$

Both raw ($\delta^{13}C_{org}$) and normalised data ($\delta^{13}C_{org}{}^{N}$) are shown in the chemostratigraphic profiles figured in this study. All data are thus treated except for those from the benthic microbial mat facies which are treated differently as explained in the previous section. Normalized data show considerably less scatter than raw data (e.g. Figs. 3.18; 4.15), but for the most part, qualitative differences in the two data sets are minor. The general practice followed here is to draw freehand a first-order line of best fit with reference to the normalized data. In most sections only a few percent of $\delta^{13}C_{org}{}^{N}$ points fall further than 1 ‰ from the line of best fit. Single outliers are ignored for the purpose of estimating the line of best fit. The reduced scatter of the $\delta^{13}C_{org}{}^{N}$ data, and (on limited data) slightly improved congruency with the $\delta^{13}C_{carb}$ signal (e.g. Fig. 2.5), suggest that the normalised data do indeed more closely approach a primary signal.

The cause of the within-sample covariation in TOC and $\delta^{13}C_{org}$ is uncertain. Organic carbon contents of modern marine sediments are constrained by complex feedback mechanisms such that observed TOC levels are more constant than might be expected from variability in

productivity and sedimentation rate (Emerson, 1985). Heterotrophic reworking of primary photosynthate, both within the water column and after burial, is one factor known to reduce TOC while raising $\delta^{13}C_{org}$ of residual carbon. The isotopic effects accompanying this process can be very roughly quantified by observations showing enrichment of 1 to 1.5 ‰ in total biomass per trophic level (McConnaghy & McRoy, 1979) and a tenfold decrease in biomass with each trophic level (e.g. Broecker & Peng, 1982, p. 9). The corresponding fractionation factor (from Eq. 9), at 1.0004 to 1.0007, is considerably lower than that required to fully account for the observed covariation.

Part of the answer may lie in the selective preservation of relatively ^{13}C-depleted components (lipids) in sediments with high TOC. In modern marine sediments, Harvey et al. (1986) found lipid preservation to be strongly correlated with TOC. This was attributed to sorption onto the organic matrix protecting lipids from microbial attack.

No TOC - $\delta^{13}C_{org}$ covariation is seen in chemostratigraphic studies of the Permo-Triassic (Margaritz et al., 1992; R. Morante, pers. comm) or of the Proterozoic-Cambrian boundary interval (Strauss et al., 1992a).

2.3d Monitoring regional variation in thermal maturation

There is a kinetic isotope effect involving preferential loss of ^{12}C from kerogen during thermal maturation (McKirdy & Powell, 1974), so an assessment of thermal maturation is needed if widely separated organic $\delta^{13}C$ profiles are to be compared. In this study, two independent sets of analytical data - H/C ratios and $\Delta\delta^{N}$ results - are employed that provide quantitative estimates of shifts in carbon isotopic composition attributable to organic maturation. A third criterion, kerogen colour, is a less precise maturation indicator (Marshall, 1990) but provides useful corroborative information. Kerogen strew slides prepared by K. Grey were used for this purpose. Averaged H/C and $\Delta\delta^{N}$ values, and generalised kerogen colour from each section, are used below to generate a rough quantification of relative thermogenic shift in $\delta^{13}C_{org}{}^{N}$ for most of the important sections covered by this investigation. It is assumed that thermal stress was essentially constant over each section or locality. Given a normal geothermal gradient (ca. 30°C.km^{-1}) this should be a reasonable assumption, except possibly for the thick (3 km) Bunyeroo and Brachina Gorge sections.

Kerogen H/C ratios

There is preferential loss of both hydrogen and ^{12}C during thermal maturation , and from an empirically-determined H/C: $\delta^{13}C_{org}$ relationship (Fig. 2.1), Des Marais et al. (1992) derived a quantity, $\Delta\delta_{org}$, representing the total increase in $\delta^{13}C_{org}$ due to thermal maturation:

$$\Delta\delta_{org} = 4.05 - 3.05r + 0.0785/r + 0.0165/r^2 - (0.000879)/r^3 \qquad (11)$$

where $\Delta\delta_{org} = \delta^{13}C_{org}$ (as analysed, H/C = r) - $\delta^{13}C_{org}$ (initial, H/C=1.5). Differences in $\Delta\delta_{org}$ between stratigraphic sections should therefore largely reflect regional differences in thermal maturation. Twenty-four H/C analyses of demineralised residues were undertaken (Appendix 1.3) of which two with less than 4% by weight of carbon are excluded from the following discussion. One published H/C analysis (McKirdy, 1976) - from the Wonoka Formation at Bunyeroo Gorge - is incorporated into the data set (Table 2.3). The lowest observed average H/C value, from Ellery Creek in the Amadeus Basin (Table 2:3), is 0.29, higher than the threshold (0.2) at which loss of the isotopic signal is observed (e.g. Strauss et al., 1992c; Des Marais et al., 1992).

$\Delta\delta^N$

Since $\delta^{13}C_{carb}$ remains unaffected by heat below metamorphic temperatures (e.g. see Kaufman & Knoll, 1995) then $\Delta\delta$ (= $\delta^{13}C_{carb}$ - $\delta^{13}C_{org}$) should, like $\Delta\delta_{org}$, reflect relative differences in regional thermal grade. The possibility of secular change in $\Delta\delta$ (due for instance to changing pCO_2 or palaeotemperature) suggests that regional $\Delta\delta$ comparisons should be restricted to stratigraphically equivalent or near-equivalent units. In this study, $\Delta\delta$ data are very broadly age-correlative. Most data come from the Julie Formation and the correlative middle Rodda beds. Some (Ungoolya-1 samples, and Munta-1 samples from 15.02 to 15.11) are from the upper Rodda beds, but there appears to be no significant change in $\Delta\delta$ between middle and upper Rodda beds (Table 2.4; Fig. 3.20). The Wonoka Formation samples, from the uppermost part of this unit, are probably of similar age or slightly older than the upper Rodda beds (Chapters 3, 6). Since $\delta^{13}C_{org}{}^N$ profiles are to be compared, the quantity $\Delta\delta^N$ (= $\delta^{13}C_{carb}$ - $\delta^{13}C_{org}{}^N$) is calculated and provides the basis for this discussion (where $\delta^{13}C_{org}{}^N$ is organic carbon isotopic composition normalised for TOC, as described in the previous section).

Where a large range of $\Delta\delta^N$ is seen in any one section, values within ca. 2 ‰ of the maximum are selected for this analysis. For example, in the Rodda beds in Munta-1, there is a distinct grouping in the frequency distribution (Fig. 2.5) at $\Delta\delta^N = 32 \pm 1$ ‰, which reflects least-altered carbonates deposited in surface - layer or mixed - layer waters (see Chapter 3).

LOCALITY	FORMATION	SAMPLE	H/C	Δδorg
Ellery Ck	Pertatataka	6.26	0.27	6.3
Ellery Ck	Pertatataka	6.23	0.17	8.5
Ellery Ck	Pertatataka	6.26	0.30	5.9
Ellery Ck	Pertatataka	6.35	0.26	6.4
Ellery Ck	Pertatataka	6.09	0.39	4.9
Ellery Ck	Pertatataka	6.09	0.37	5.2
		Average:	0.29±0.08	6.0±1.3
Wallara 1	Pertatataka	28.115	0.64	3.4
Wallara 1	Pertatataka	28.88	0.35	5.4
Wallara 1	Pertatataka	28.101	0.56	3.8
Wallara 1	Pertatataka	28.138	0.55	3.9
		Average:	0.52±0.13	4.0±0.9
Rodinga-4	Pertatataka	6.18	0.84	2.4
Bunyeroo Gorge	Wonoka	6.06	0.53	3.9
Bunyeroo Gorge	Wonoka	6.09	0.49	4.2
Bunyeroo Gorge	Wonoka	5.52	0.14	9.7
Bunyeroo Gorge	Wonoka	6.05	0.37	5.2
Bunyeroo Gorge	Wonoka	(McKirdy, 1976)	0.47	4.4
Brachina Gorge	Bunyeroo	7.05	0.34	5.4
		Average:	0.39±0.10	4.9±2.2
BWM1A-1	Brachina	20.03/2	0.44	4.6
Munta-1	Rodda beds	15.24/3	0.50	4.2
Munta-1	Rodda beds	15.82	1.13	1.3
Munta-1	Rodda beds	15.99	0.94	2.0
Munta-1	Rodda beds	15.24/1	0.82	2.5
Munta-1	Rodda beds	15.12	0.85	2.4
		Average:	0.85±0.23	2.4±1.1

Table 2.3: H/C ratios and $\Delta\delta_{org}$ (calculated following Desmarais et al., 1992) of samples analysed in this study, together with one analysis from McKirdy (1976). Average results shown for each section/locality; indicated uncertainties are ± one standard deviation.

LOCALITY	FORMATION	SAMPLE	∂13Ccarb	∂13Corg	∂13CorgN	Δ∂	Δ∂N
Munta 1	Rodda beds	15.02	2.4	-31.5	-29.6	33.9	32.0
Munta 1	Rodda beds	15.04	2.2	-31.9	-30.0	34.1	32.2
Munta 1	Rodda beds	15.08	2.1	-32.4	-30.8	34.5	32.9
Munta 1	Rodda beds	15.11	2.9	-30.1	-29.1	33.0	32.0
Munta 1	Rodda beds	15.58	4.2	-27.5	-27.0	31.7	31.2
Munta 1	Rodda beds	15.62	5.0	-26.8	-26.6	31.7	31.6
Munta 1	Rodda beds	15.75	4.7	-28.2	-27.3	32.9	32.0
Munta 1	Rodda beds	15.77	5.4	-28.8	-27.5	34.1	32.8
Munta 1	Rodda beds	15.81	5.5	-28.5	-27.2	34.0	32.8
Munta 1	Rodda beds	15.83	5.4	-28.9	-27.4	34.3	32.8
Munta 1	Rodda beds	15.85	6.0	-28.4	-26.1	34.4	32.0
Munta 1	Rodda beds	15.51	4.0	-27.1	-26.8	31.1	30.8
					average:	33.3±1.2	32.1±0.7
Observatory Hill 1	Rodda beds	14.09	4.3	-30.2	-26.9	34.5	31.1
Observatory Hill 1	Rodda beds	14.12	5.8	-29.9	-26.7	35.7	32.5
					average:	35.1±0.8	31.8±0.9
Ungoolya 1	Rodda beds	26.09	1.4	-31.4	-29.2	32.7	30.6
Ungoolya 1	Rodda beds	26.18	0.9	-32.0	-29.3	32.9	30.2
Ungoolya 1	Rodda beds	26.20	1.5	-32.8	-30.2	34.2	31.6
					average:	33.3±0.5	30.8±0.7
Bunyeroo Gorge	Wonoka Fm.	6.05	0.2	-28.5	-27.9	28.7	28.1
Bunyeroo Gorge	Wonoka Fm.	6.09	0.9	-30.2	-27.3	31.2	28.2
Bunyeroo Gorge	Wonoka Fm.	6.12	2.4	-29.6	-24.7	31.9	27.1
					average:	30.6±1.7	27.8±0.6
Ross River	Julie Fm.	1.01	3.8	-28.4	-26.0	32.2	29.7
Ross River	Julie Fm.	1.02	5.2	-27.6	-25.4	32.8	30.6
Ross River	Julie Fm.	1.13	4.5	-27.6	-25.5	32.1	30.0
Ross River	Julie Fm.	1.29	4.9	-27.2	-26.3	32.1	31.2
Ross River	Julie Fm.	1.51	4.4	-27.0	-26.5	31.3	30.9
Acacia Well	Pertatataka Fm.	1.52	2.6	-28.1	-26.9	30.6	29.5
					average:	31.9±0.8	30.3±0.7
Ellery Creek	Julie Fm.	6.37	4.1	-25.8	-24.8	29.8	28.9
Ellery Creek	Julie Fm.	6.41	4.0	-26.7	-22.3	30.6	26.3
Ellery Creek	Julie Fm.	6.46	1.6	-26.3	-24.7	27.9	26.3
Ellery Creek					average:	29.5±1.4	27.2±1.5
Phillipson Pound	Julie Fm.	24.01	5.0	-26.3	-26.3	31.2	31.3
Phillipson Pound	Julie Fm.	24.17	5.7	-25.8	-24.2	31.5	29.9
Phillipson Pound					average:	31.4±0.1	30.6±1.0

Table 2.4: Selected same-sample organic and carbon isotopic compositions, and derived $\Delta\delta$ and $\Delta\delta^N$ values. Average results shown for each section/locality; indicated uncertainties are ± one standard deviation.

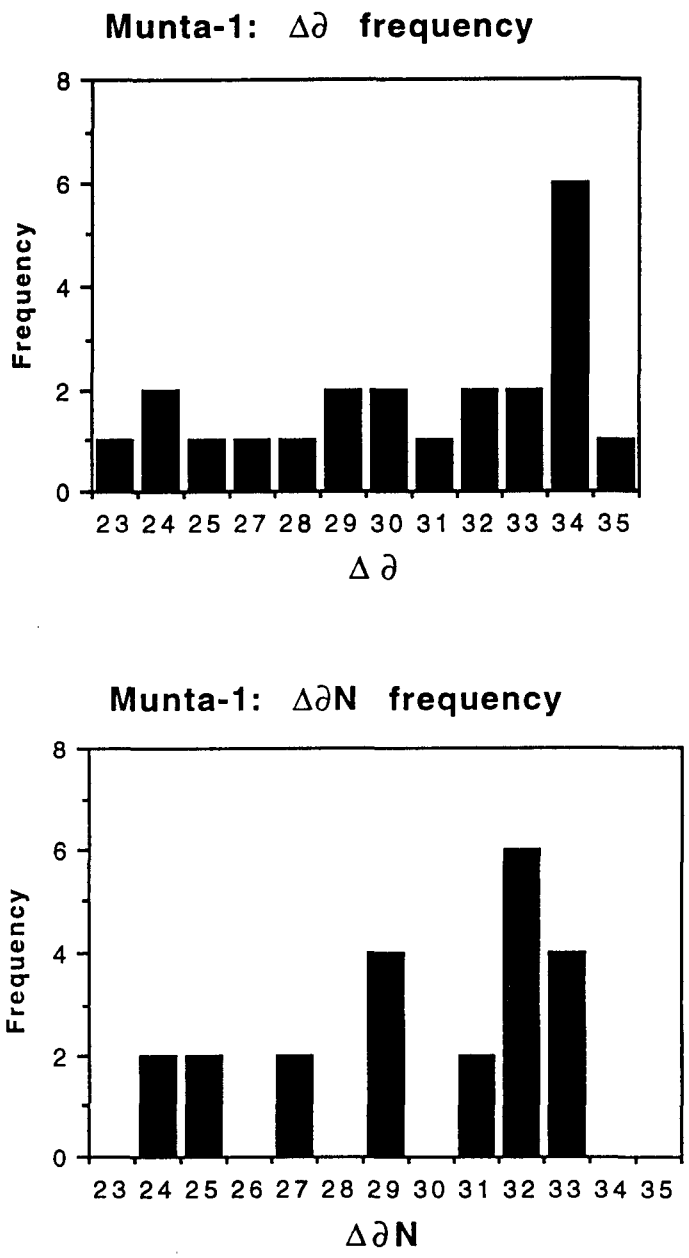

Fig. 2.5: Frequency distribution in Munta-1 (Rodda beds, Officer Basin), of $\Delta\delta$ (above) and $\Delta\delta^N$ (below).

Much lower $\Delta\delta^N$ (15 to 25 ‰) are characteristic of the 'cap dolostones', the lower Pertatataka Formation, most of the Wonoka Formation and much of the Rodda beds (see Chapters 3, 4). These may represent stratified basin setings in which organic and carbonate carbon reflect surface and deeper layer ^{13}C abundances, respectively; these data have no bearing on relative thermal maturation states and are excluded from this discussion. $\Delta\delta^N$ data thus selected are shown in Table 2.4.

Kerogen colour

Kerogen exhibits progressive and irreversible changes in colour with increasing thermal maturity (Marshall, 1990). Several kerogen strew slides from each locality were examined, and comparisons between localities and with a published colour chart (Traverse, 1988) allowed an overall assessment of kerogen colour. This assessment is considered valid as a rough guide to the relative ordering of localities with respect to thermal grade; no attempt is made to derive an independent, absolute measure of maturation from this criterion.

Collation of maturation data

The three data sets are collated in Table 2.5, with localities arranged in inferred order of increasing thermal alteration. There is reasonable agreement (within 1 to 2 ‰) of averaged $\Delta\delta_{org}$ and $\Delta\delta^N$ in terms of differences between sections, and there is broad agreement of these two quantitative data sets with the ordering of localities on the basis of kerogen colour.

On the basis of all three criteria, a value, $\Delta\delta^*$, is selected for each locality that represents inferred $\Delta\delta^N$ for localities where this has not been determined, or 'revised' $\Delta\delta^N$ where the other criteria suggest (slight) revision of the observed, averaged value. In correlation diagrams incorporating multiple $\delta^{13}C$ stratigraphic profiles (Figs. 3.23; 4.36; 4.37) - which represent the most important syntheses of correlation data in this investigation - $\delta^{13}C_{org}{}^N$ and $\delta^{13}C_{carb}$ data in each section are plotted coaxially, with organic data shifted relative to carbonate data by $\Delta\delta^*$. Thus displayed, organic and carbonate signals should be concordant or nearly so within sections, and $\delta^{13}C_{org}{}^N$ signals should be comparable on a common basis between sections.

High Ediacarian $\Delta\delta$

There has been a broad secular change in $\Delta\delta$ through the Proterozoic (Hayes, 1983; Des Marais et al., 1992). For little-altered kerogens, $\Delta\delta$ was near 34 ‰ in the early Proterozoic (Strauss et al., 1992c); 28 to 29 ‰ in the late Proterozoic (Knoll et al., 1986; Strauss et al., 1992c); and near 30 ‰ in the middle Cambrian (Donnelly et al., 1988). In this study, $\Delta\delta$ in least-altered successions (Officer Basin drillholes Munta-1, Observatory Hill-1 and

Locality/section	Δδorg	ΔδN	Kerogen colour	Δδ*
Munta-1 (Officer Basin)	2.4 ± 1.1	32.1 ± 0.7	orange - light brown	**32**
Observatory Hill-1 (Officer Basin)	n. d.	31.8 ± 0.9	orange - light brown	**32**
Ungoolya-1 (Officer Basin)	n. d.	30.8 ± 0.7	orange - light brown	**31**
Rodinga-4 - Phillipson Pound (Amadeus)	2.4	30.6 ± 1.0	light brown - brown	**31**
Ross River area (Amadeus Basin)	n. d.	30.3 ± 0.7	n. d.	**30**
SCYW1-A (Adelaide Geosyncline)	n. d.	n. d.	brown	**30**
DDC-1, 2 (Georgina Basin)	n. d.	n. d.	brown - dark brown	**30**
Wallara-1 (Amadeus Basin)	4.0 ± 0.9	n. d.	brown - dark brown	**30**
BWM1A-1 (Adelaide Geosyncline)	4.6	n. d.	very dark brown - black	**29**
Bunyeroo & Brachina Gorges (Adelaide G.)	4.9 ± 2.2	27.8 ± 0.6	very dark brown - black	**29**
Ellery Creek (Amadeus Basin)	6.0 ± 1.3	27.2 ± 1.5	very dark brown - black	**28**

Table 2.5: Collation of maturation data.

Ungoolya-1) is around 34 ‰. In part, this high value reflects deliberate exclusion of lower values thought to be influenced by organogenic CO_2 in carbonate. (The value of 28.5 ‰ found by Knoll et al., 1986, is a 'best-fit' or averaged Δδ). In agreement with this study, Pell et al. (1993) found a dominant mode in Δδ at 34 ‰ in the Rodda beds, and considered this to represent the primary isotopic separation between coexisting organic and inorganic carbon. Knoll et al. (1995) found Δδ of 32 to 36 ‰ in an Ediacarian - aged succession in NE Siberia. Des Marais et al. (1992) also show relatively high Δδ in the terminal Proterozoic (their Fig. 2). Original, depositional Δδ in the Officer Basin (at H/C = 1.5, using Eq. 11) is inferred to have been around 36 ‰, near the theoretical maximum fractionation of 38 ‰ between carbonates and primary biomass (Roeske & O'Leary, 1984; Hayes et al., 1989). One possible explanation for high Ediacarian Δδ is high atmospheric pCO_2 (cf. Popp et al., 1989; Freeman & Hayes, 1992).

2.4 Sampling protocols and analytical methods followed in this study

2.4a Sampling

Sections in drillcore and outcrop, selected for accessibility, geographic spread, and facies variation (Table 0.1), were systematically logged and sampled. Outcrop sections were measured by 'chain and compass' with appropriate corrections for dip and topography. Sampling interval was roughly 10 m; greater in thick, monotonous successions; much less in

thin, key units such as 'cap dolostones'. Two 'splits' were made of most samples, one for isotope chemostratigraphy (this study); the other for acritarch biostratigraphy (see Grey, in prep). All samples are numbered by a six-figure year-month-day date code (of collection) followed by number (e.g. 920318.34). This is abbreviated in the text to the last three or four digits, with section name where necessary to avoid confusion. Subsamples are suffixed /1, /2 etc.; analytical repeats are suffixed a, b etc.

In sampling for $\delta^{13}C_{carb}$ and $^{87}Sr/^{86}Sr$, the initial visual selection in the field was for purity of carbonate, fineness of grain and textural uniformity. Fortunately, micritic or microsparitic types comprise the bulk of most carbonate units studied; but oolitic, intraclastic and detrital carbonates are locally significant and comprise part of the sample set. Evidence for early (seafloor) lithification, such as hardgrounds and intraclasts, was also noted as a favorable indicator for preservation of marine $\delta^{13}C_{carb}$.

The darkest shales or carbonates were usually selected for $\delta^{13}C_{org}$ (and palynological) analysis, but a considerable amount of sampling was carried out to investigate variation between interbedded rocktypes, e.g. within and between sandy event beds in shale sequences; darker vs. lighter-coloured shale; and carbonate vs. interbedded mudstone (see sections 2.3b,c).

2.4b Analytical Methods

Organic carbon

Organic carbon isotopic analysis was carried out by sealed tube combustion, following Strauss et al. (1992b). Outcrop samples were pre-etched in HF to minimise contamination. About 0.4g of weighed, powdered sample was treated with cold, then hot HCl to destroy carbonate, dried and weighed again to determine percent carbonate; baked at 850°C with CuO in a sealed, evacuated quartz glass tube; then opened *in vacuo* on the gas line and the CO_2 purified cryogenically. Total organic carbon content (TOC) is calculated from the manometrically-determined yield of CO_2. Standards were routinely analysed every 20 to 25 samples. A VG SIRA series II mass spectrometer was used to analyse the CO_2 gas. A large number of analytical repeats showed that precision is ±0.1‰ for samples with more than 1 mg/g organic carbon, and ±0.2‰ for samples with less. Aliquots from three samples were additionally treated with HF and the kerogen separate analysed, with results not significantly different from analysis of the decalcified whole-rock. Five carbon-free blanks (low-density firebrick pre-baked at 850°C) treated as above yielded an average 0.005 ± 0.003 mg carbon,

suggesting an insignificant contribution from laboratory contamination. The CSIRO anthracite standard gives -23.42 ± 0.03 ‰ (n = 7).

In analysing $\delta^{13}C_{org}$ of carbonates, a considerably larger weight of sample (1 - 10g) was acidified, sufficient to yield ca. 0.5g of insoluble residue.

Results are tabulated, together with sample locations and descriptions, in Appendix 1.1.

Kerogen was isolated for H/C analysis from 24 representative samples from widespread sections. The method closely followed Horvath & Jackson (1981). Five to ten grams of powdered sample was treated sequentially with HCl, HF, and hot HCl, washing with distilled water after each treatment. An additional HF - hot HCl teatment was needed for many samples. The residue was then warmed in $NaBH_4$ solution to get rid of (most of the) pyrite. The washed and dried kerogen concentrate was stored in a desiccator until analysed for C, H, S and N on a Carlo-Erba Elemental Analyser. Results are tabulated as Appendix 1.3.

Carbonates

Uncovered thin sections were made of most carbonates. Half of each thin section was stained with alizarin red-S and potassium ferricyanide following Dickson (1966); the other half left unstained for CL observation. Typical fine-grained samples exhibit layering defined by subtle textural or CL variation; and micritic or least-luminescent layers were selected for isotopic analysis. The selected part was identified on the matching face of the hand specimen and a portion excised with a diamond trimming saw or drill. Similarly, ooids or micritic intraclasts were selected and extracted from some grainstones. Ideally an excess (0.3 g) of powdered sample was obtained to allow for stable-isotopic, AAS and $^{87}Sr/^{86}Sr$ analysis.

Stable-isotopic analysis of carbonates followed the traditional method of phosphorolysis (McCrea, 1950). Limestones were reacted overnight with 100% H_3PO_4 at 25°C to liberate CO_2, while dolostones and some impure limestones were reacted at 50°C. $\delta^{18}O$ values are corrected for reaction at 50°C using fractionation factors of 1.00925 for calcite (McCrea, 1950; Wachter & Hayes, 1985) and 1.01066 for dolomite (Rosenbaum & Sheppard, 1986). The precision is ±0.1‰ for both O and C. Approximate percent carbonate was obtained from CO_2 yields. Stable-isotopic analyses of carbonates are tabulated in Appendix 1.1.

Powders from 169 carbonates were leached with 1N HCl and the leaches analysed for major (Ca, Mg) and trace elements (Mn, Sr, some also Fe, Na) by flame atomic absorption spectroscopy. Results are tabulated in Appendix 1.2.

Least-altered carbonates, characterised by low Mn/Sr, high $\delta^{18}O$ and good textural preservation, were selected for $^{87}Sr/^{86}Sr$ analysis. Samples low in insoluble residue were selected to minimise leaching of Sr from silicates during sample preparation. Samples were leached with 0.5N acetic acid, strontium separated using cation exchange columns and the isotopic determination carried out on a thermal ionization mass spectrometer at CSIRO, North Ryde. The $^{87}Sr/^{86}Sr$ ratios are normalized to $^{86}Sr/^{88}Sr = 0.1194$ and to a Standard Reference Material 987 value of 0.710241, following the majority of recent contributions on Neoproteroic strontium isotope chemostratigraphy (Asmerom et al., 1991; Derry et al., 1992; Kaufman et al., 1993; Narbonne et al., 1994).

Rb concentrations were measured by isotope dilution on the soluble fraction of 18 carbonates to evaluate the contribution of radiogenic Sr from decay of incorporated Rb. The maximum calculated contribution to the $^{87}Sr/^{86}Sr$ ratio (the 'age correction', assuming an age of 580 Ma for the Ediacarian samples and 700 Ma for the Black River Dolomite, Tasmania) is 0.000034, the average 0.000008. The age correction is insignificant in these rocks in view of the fact that the Neoproterozoic $^{87}Sr/^{86}Sr$ signal is unlikely to be resolvable beyond the fourth decimal place because of diagenetic alteration (cf. Veizer, 1989). Nevertheless, where obtained, initial (age-corrected) isotope ratios are given in the text. All $^{87}Sr/^{86}Sr$ analytical results and related data are tabulated in Appendix 1.2.

Sulphates

Calcium sulphates, ranging from nodular anhydrite to disseminated gypsum, were collected at many horizons. Impure sulphate samples - such as those finely disseminated in carbonate - were purified by dissolving in 1N HCl, filtering, and precipitating the sulphate as $BaSO_4$. This step was left out for visually pure anhydrites which were simply heated to 100°C for a few hours to ensure complete dehydrogenation. SO_2 for isotopic analysis was evolved by thermal decomposition at 1100°C in the presence of quartz powder and Cu_2O (Holt & Engelkemeier, 1970). The precision of data is ±0.3‰. Results are given in Appendix 1.1.

Thirteen sulphate samples were analysed for $^{87}Sr/^{86}Sr$. 1N HCl was used to solubilise the samples, after which the procedure followed that described above for $^{87}Sr/^{86}Sr$ in carbonates. Rb contents were obtained on the soluble fraction of six sulphates by isotope dilution, as with carbonates, in order to determine the initial $^{87}Sr/^{86}Sr$ ratio.

Sulphides

Twenty pyrite concentrates were obtained of representative shales and limestones in the Pertatataka, Wonoka and Brachina Formations and the Rodda beds. Except for samples from

the Rodinga 4 drillhole section of the Pertatataka Formation, thin sections show disseminated, micron to decimicron-sized framboids and an absence of coarser segregations, so the results should be representative of early diagenetic phases (Berner, 1970; Coleman & Raiswell, 1981; Raiswell, 1982). Pyrite framboids are thought to result from the pyritization of greigite (Fe_3S_4) spheres, and are therefore good evidence of precursor, metastable iron sulphide phases characteristic of bacterial sulphate reduction (Sweeney & Kaplan, 1973). Samples from the Rodinga 4 drillhole section of the Pertatataka Formation show, in addition to framboids, pyritized coiled filaments 20 μ thick and up to 200 μ long (see section 4.5c). Concentrates were obtained by HCl-HF treatment as outlined above for kerogen separation. Some concentrates were palynological residues supplied by K. Grey. Concentrates were mixed with Cu_2O and combusted at 900°C to produce SO_2 for mass spectrometry. Results include some organically-bound sulphur since pyrite and organic carbon could not be successfully separated, but this source is thought to be insignificant.

3

Isotope Chemostratigraphy of Ediacarian Successions in the Adelaide Geosyncline and Officer Basin

3.1 Introduction

The Adelaide Geosyncline contains a thick, mildly deformed but superbly exposed Neoproterozoic succession (Preiss, 1987a). The upper part of the succession is under consideration by a Working Group of the International Stratigraphic Commission as a stratotype for the base of a terminal Proterozoic chronostratigraphic unit of System rank. Two alternative terminal Proterozoic Systems, the Ediacaran (Jenkins, 1981) and Ediacarian (Cloud & Glaessner, 1982), have been defined in the Adelaide Geosyncline (Fig. 0.2), and earlier-established time-rock units - the Adelaidean System and its constituent Stages - have been widely used within Australia (see review by Preiss, 1987b). Flat-lying, well-preserved Ediacarian successions, known mainly from drillcore, are also found in adjacent cratonic areas (the Stuart Shelf and Curnamona Craton) and in the Officer Basin in the northwest of South Australia (Fig. 3.1).

This chapter describes the carbon and strontium isotope chemostratigraphy of the Ediacarian System in these South Australian basins. Isotope stratigraphy of the lower part of the Ediacarian stratotype in the central Flinders Ranges and a number of other correlative and partially correlative sections are documented here. The partly non-marine quartzites and redbeds of the Pound Subgroup, comprising the upper part of the Ediacarian and host to the soft-bodied metazoan 'Ediacara fauna', are for the most part extremely poor in sedimentary carbon and strontium and so are largely excluded from the present study. This investigation was carried out in tandem with a parallel study on acritarch biostratigraphy of the same sections by K.Grey (in prep.).

The multiplicity of sections investigated provides a test of carbon and strontium isotope stratigraphy where sections can be confidently correlated by other means (lithostratigraphy, seismic stratigraphy, palynology, Acraman event layer). Paucity of carbonates has necessitated a focus on organic carbon, and refinements developed in Chapter 2 for the treatment of organic carbon isotope data are utilized. Organic carbon isotopic data yield a well-defined stratigraphic signal that, for the most part, suggests consistent and geologically reasonable correlations. Much carbonate carbon data, on the other hand, is anomalously ^{13}C-

depleted, and part of this chapter is devoted to a discussion of primary versus post-depositional origin for these carbonates. A primary origin, involving deposition beneath a density-stratified marine water body, best satisfies geochemical and sedimentological constraints. The basin stratification concept has important implications for correlation with other basins as well as for Neoproterozoic $\delta^{13}C$ chemostratigraphy and carbon-cycle modelling in general.

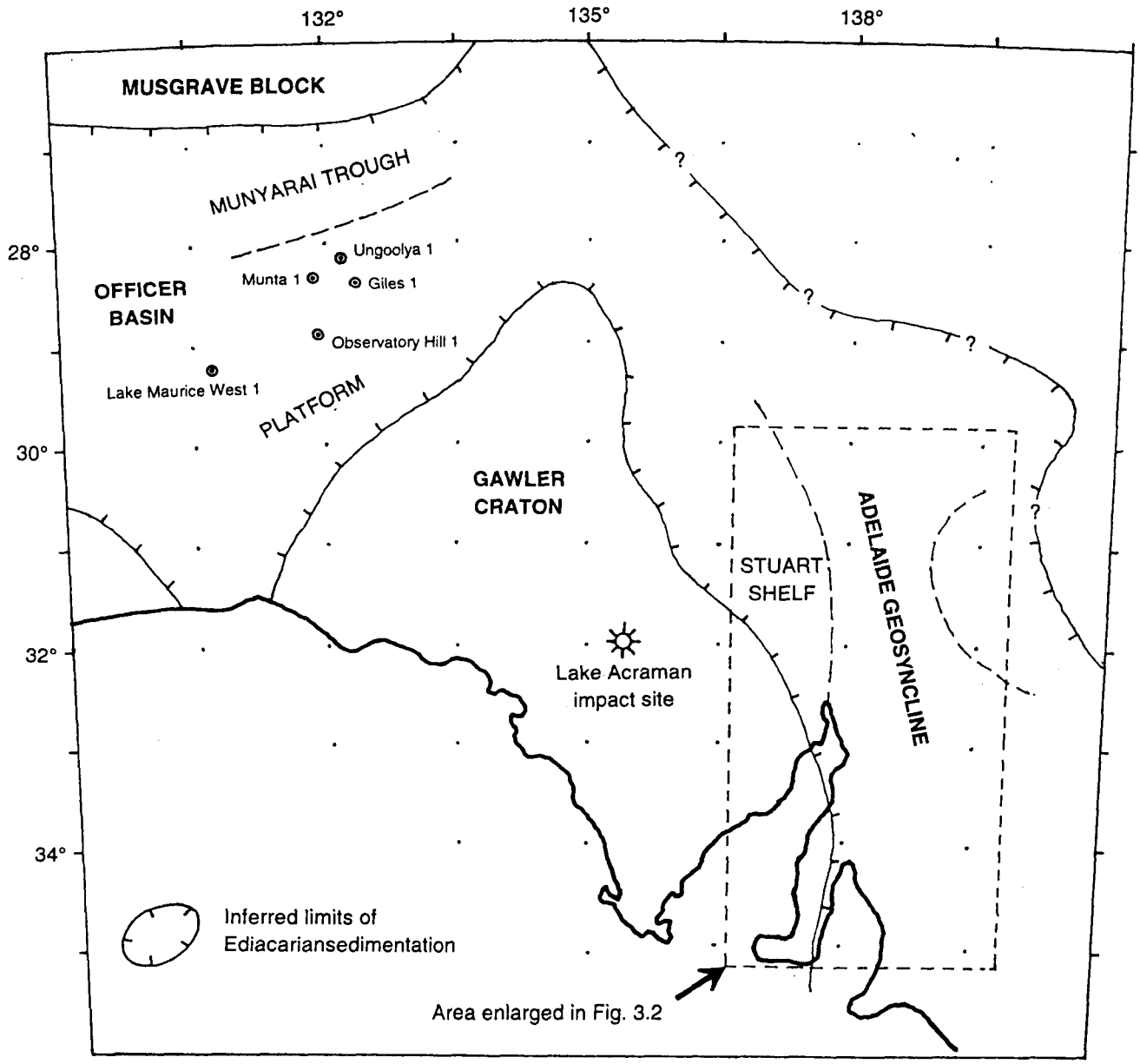

Fig. 3.1: Generalised Ediacarian tectonic elements of South Australia, and locations of Officer Basin drillholes. From Preiss (1993).

In both the Adelaide Geosyncline and Officer Basin, ^{13}C-depleted carbonates are stratigraphically associated with large incised valleys or 'canyons'. The interpreted salinity stratification is consistent with one or more 'Messinian-type' basin desiccation events that are strongly implicated in the development of the canyons in the Adelaide Geosyncline (Christie-Blick et al., 1990; Christie-Blick, 1993).

The strontium and carbon isotope stratigraphy here documented place new constraints on correlation within and between the Adelaide Geosyncline and Officer Basin. Significantly, carbon and strontium data suggest little or no overlap in age between the Rodda beds equivalent of the southeastern Officer Basin and the Pound Subgroup, at variance with some recently published correlation schemes (Sukanta et al., 1991; Pell et al., 1993). Constraints are also placed on correlation with other Australian Neoproterozoic basins (Walter et al., 1995) and overseas sections, issues that are fully explored in Chapters 4 and 6.

3.1a Adelaide Geosyncline - Officer Basin correlation: Previous Work

A remarkable lateral persistence of facies has long facilitated lithostratigraphic correlation within the Adelaide Geosyncline and adjacent cratonic areas, the Stuart Shelf and Curnamona Craton (see Forbes & Preiss, 1987; Preiss, 1984). Correlation of the Ediacarian of the eastern Officer Basin with the Adelaide Geosyncline has been previously made on the basis of lithostratigraphy (Preiss & Krieg, 1992; Wallace et al., 1989), in particular by the occurrence of a unique, isochronous event layer consisting of ejectamenta from a bolide impact whose impact site has been identified at Lake Acraman on the Gawler Craton (Fig. 3.1; Wallace et al., 1989; Gostin et al., 1986). Correlation of the thick Ediacarian succession above the Acraman ejecta layer in the Officer Basin (middle and upper Rodda beds equivalent), however, remains uncertain (Fig. 3.3). Sukanta et al. (1991) correlate the upper Rodda beds with the Pound Subgroup of the Adelaide Geosyncline, on the basis of equating a number of seismic sequence boundaries with an equivalent number of sequence boundaries identified in outcrop in the Wilpena Group.

Jenkins et al. (1992) reported on reconnaissance palynology and carbon-isotope stratigraphy of some Ediacarian units in the Adelaide Geosyncline and Officer Basin, and Pell et al. (1993) provided further $\delta^{13}C$ chemostratigraphic data. In the Rodda beds correlative in the SE Officer Basin, ^{13}C-enriched carbonates associated with a distinctive spiny acritarch flora are succeeded by less strongly positive carbonates and a spheroidal acritarch flora. Broadly similar associations are seen in the Sinian succession in China where the upper units also contain Ediacara-type metazoan fossils (e.g. Lambert et al., 1987; Zang & Walter, 1992). On this basis, Jenkins et al. (1992) and Pell et al. (1993), like Sukanta et al. (1991), propose

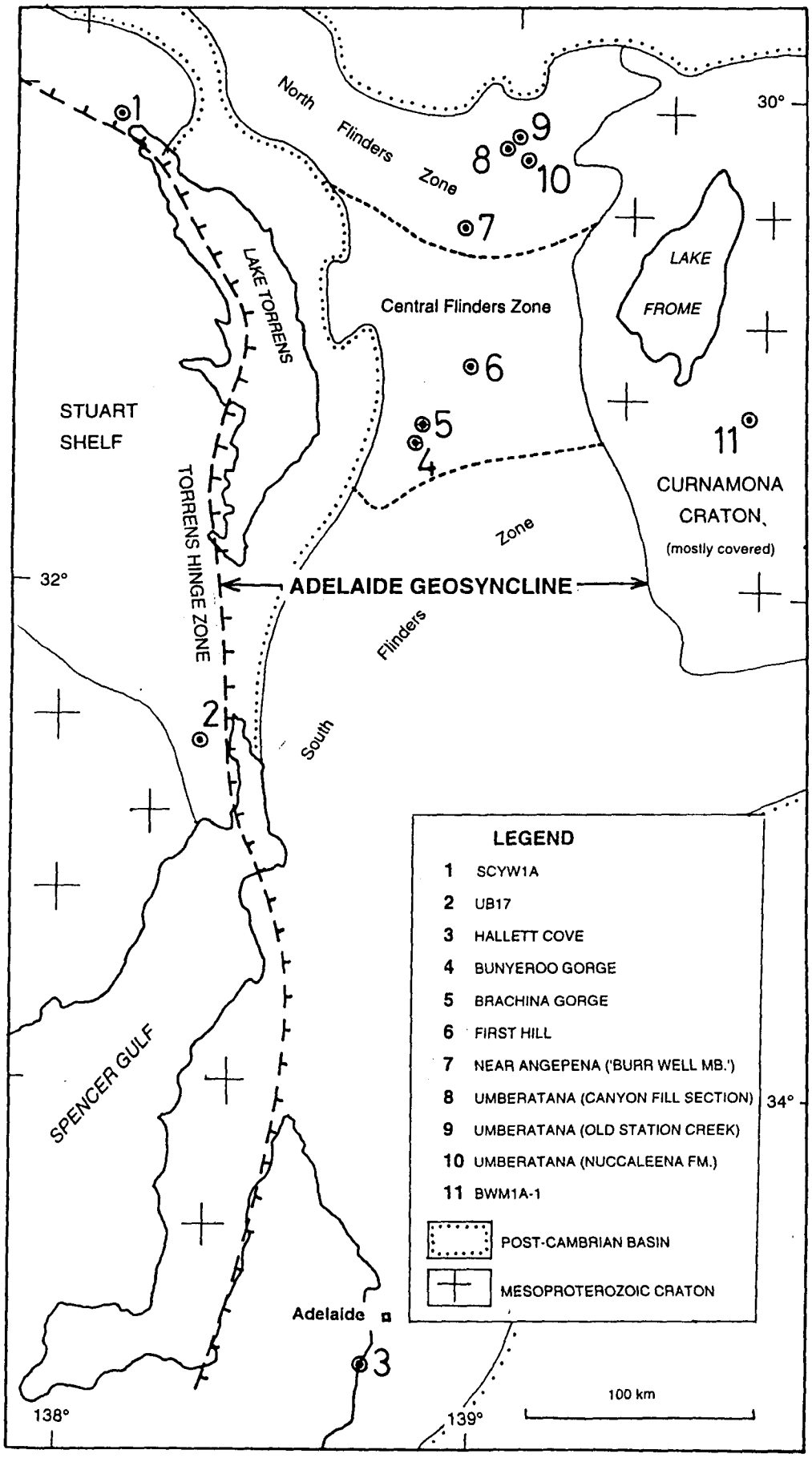

Fig. 3.2: Locality map and main tectonic elements, Adelaide Geosyncline and environs.

correlation of the upper Rodda beds with the Pound Subgroup (Fig. 3.3). (The Pound Subgroup itself is of unsuitable facies to yield acritarchs or $\delta^{13}C$ chemostratigraphic data).

However, the proposed overlap in age between the Rodda beds correlative of the SE Officer Basin and the Pound Subgroup must be regarded as doubtful. The seismic sequences in the upper Rodda beds may be better matched in terms of scale and lithology to lower-order sequences identified within the Wonoka Formation by Dibona et al. (1990). The Rodda beds are a much better match, in terms of facies, to the Wonoka and Billy Springs Formations (Preiss & Krieg, 1992; Walter et al., 1995). The ranges of the acritarch assemblages are as yet poorly known. The synthesis of $\delta^{13}C_{org}$, $\delta^{13}C_{carb}$ and $^{87}Sr/^{86}Sr$ data presented below suggests there may be little or no overlap in age between the Rodda beds correlate of the SE Officer Basin and the Pound Subgroup.

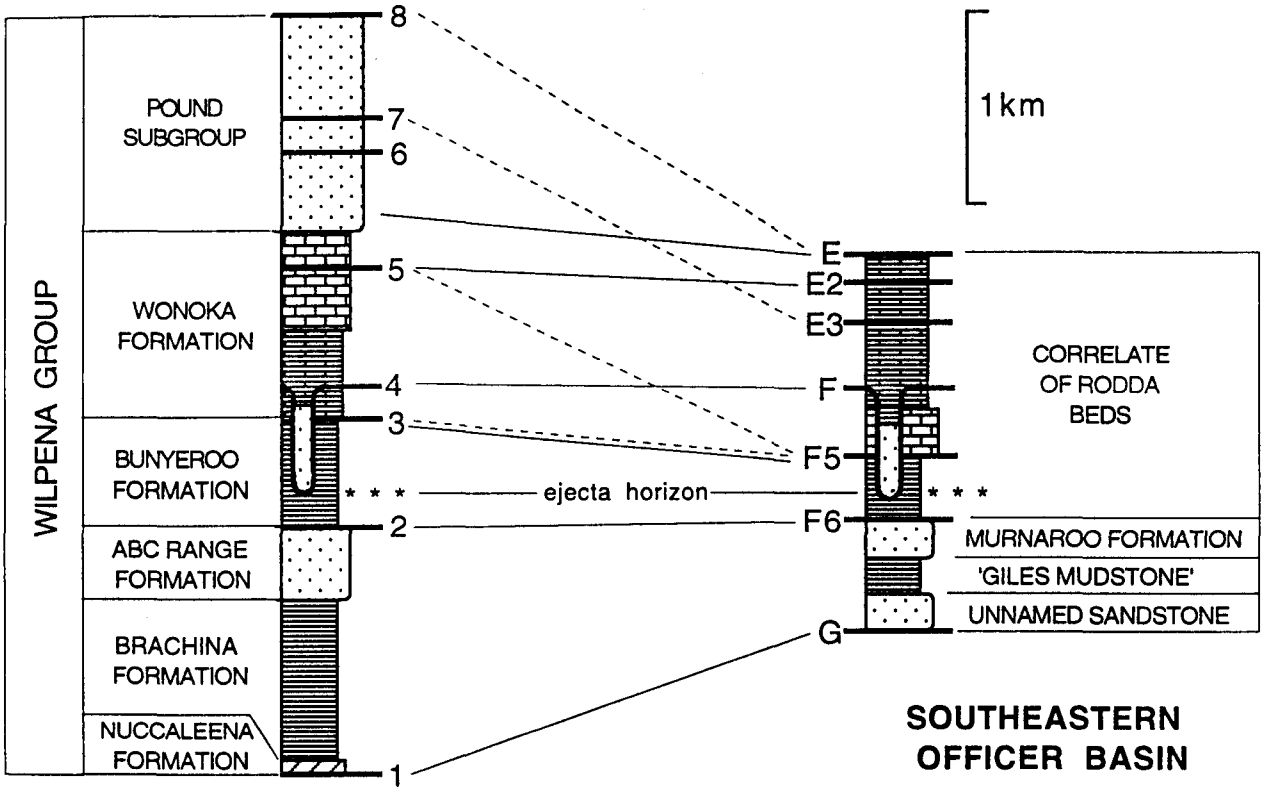

Fig. 3.3: Stratigraphic nomenclature and proposed correlation between the type Ediacarian (Adelaide Geosyncline) and the southeastern Officer Basin. Heavy numbered lines in Adelaide Geosyncline column are depositional sequence boundaries identified in outcrop (from Christie-Blick et al., 1990); those in Officer Basin column are seismic sequence boundaries (from Sukanta et al., 1991). Solid correlation lines: scheme favoured in this study (see also Preiss, 1993); dashed lines: alternative correlations proposed by Jenkins et al. (1992) and Pell et al. (1993). Scale is indicative only.

3.2 Geological Setting: Adelaide Geosyncline

The Adelaide Geosyncline contains a thick, folded syn-rift to post-rift succession of Neoproterozoic to Cambrian age (Preiss, 1987a). The extent and timing of continental break-up is uncertain. An ocean basin may have existed to the SE during the Ediacarian, but the Central Flinders Zone (Fig. 3.2) remained intracratonic (Preiss, 1987a). In the Ediacarian, thinner successions were also laid down on an adjacent small cratonic platform to the east (the Curnamona Craton) and on a larger cratonic platform to the west (the Stuart Shelf) (Forbes & Preiss, 1987) (Fig. 3.1, 3.2). Further west, the Australian Plate was partly covered by a number of broad, interconnected intracratonic basins (Walter et al., 1995) that were also receiving sediment in Ediacarian time. The closest of these was the Officer Basin (Fig. 3.1).

Stratigraphic nomenclature and a generalised lithologic succession for the type section of the Ediacarian System, at Bunyeroo Gorge in the central Flinders Ranges, are shown in Fig. 3.3. The base of the System is defined (Cloud & Glaessner, 1982) as the base of the Wilpena Group that immediately overlies rocks of the Marinoan glaciation. The glaciation may be a correlate of the Varangian of the northern hemisphere (Cloud & Glaessner, 1982; Knoll & Walter, 1992) (but see Eyles (1993) for a contrary view and Chapter 6 for a discussion). Ediacarian and post-Varanger Vendian are thus possibly equivalent, and range from 600 ± 10 Ma to the base of the Cambrian (540 - 545 Ma) (Knoll & Walter, 1992).

3.3 Nuccaleena Formation

3.3a Lithostratigraphy

The Nuccaleena Formation is the 'cap dolostone' that immediately overlies Marinoan glacigene and associated rocks. Six sections were measured and sampled, of which four were from drillcore (Fig. 3.4).

The base is more or less abrupt, in places erosionally disconformable (Plummer, 1979), and is regarded as a depositional sequence boundary (von der Borch et al., 1988). Typically the unit begins with 1-10m of pink to cream-coloured, fine-grained dolostone, usually with planar, thin bedding or lamination (Plate 3.1). Layering becomes thinner up through the formation. There are thin (5-10mm) interbeds of brown-weathering dolomitic mudstone or siltstone that tend to increase in proportion upward. These terrigenous layers often have abrupt and erosional contacts upon dolostone and grade back up, through a few millimetres, into dolostone. The erosional upper surfaces of the dolostone layers may have up to several

millimetres of relief (Plate 3.1) but intraclasts are rare. There is an upper interval, transitional with the Brachina Formation but by original definition included in the Nuccaleena (Coats & Blissett, 1971), of red shale with diffuse layers and nodules of impure dolostone. In SCYW1a (Fig. 3.4) only this latter, shale-dominated facies is present. Dolostone nodules in SCYW1a and BWM1a-1 are early diagenetic concretions, as shown by lamination that can be traced from concretion to matrix and that is strongly deflected by differential compaction about the margins of the concretions (cf. Raiswell, 1971).

An anhydrite nodule, 30 mm in diameter, occurs near the top of the formation in SCYW1a.

At Hallett Cove, several separate thin tongues of dolostone correlative with the Nuccaleena Formation occur within, and at the top of 70 m of predominantly thick-bedded quartz sandstone known as the Seacliff Sandstone (Fig. 3.4) (Dyson & von der Borch, 1986; Forbes & Preiss, 1987; Dyson, 1992; but see Lemon & Gostin (1990) for an alternative stratigraphic interpretation).

Thin sections of dolostones show fine-grained (5-10μ), luminescent dolomicrosparite, sometimes faintly laminated; with rare, rounded dolomicritic peloids up to about 100μ in size. Laminoid to irregular, quartz or dolospar-filled microfenestrae are common, and suggest early cementation but are not diagnostic of palaeoenvironment (Lasemi et al., 1990).

The environment of deposition of the Nuccaleena Formation is controversial. A marine origin seems implicit in the widespread distribution of the Nuccaleena Formation and related cap dolostones (G. Williams, 1979). Intrastratal anticlines resembling peritidal tepee structures are locally abundant, particularly adjacent to zones of possible synsedimentary uplift (Plummer, 1979). 'Tepees', wavy stromatolitic lamination, and the predominantly aphanitic (and therefore probably penecontemporaneous) nature of the dolomite led Plummer (1979), G. Williams (1979) and von der Borch et al. (1988) to propose a predominantly tidal-flat environment for the Nuccaleena and similar, probably correlative units in the Kimberleys, Western Australia. A predominantly warm, and humid or seasonally humid climate was proposed by G. Williams (1979, 1982) on the basis of a range of oxygen isotope compositions similar to those of non-glacial Proterozoic carbonates, and a lack of evaporites.

In contrast, Dyson (1992) and Kennedy & Wallace (1993) argue for a relatively deep-water palaeoenvironment. Dyson (1992) interpreted the dolostone tongues within Seacliff Sandstone at Hallett Cove as representing a transgressive, relatively deep-water facies occurring at the bases of several parasequences that shallow upward from dolostone through submature turbiditic sandstones to hummocky cross-bedded, mature sandstones. The Seacliff Sandstone and Nuccaleena Formation correlative here comprise a transgressive systems tract

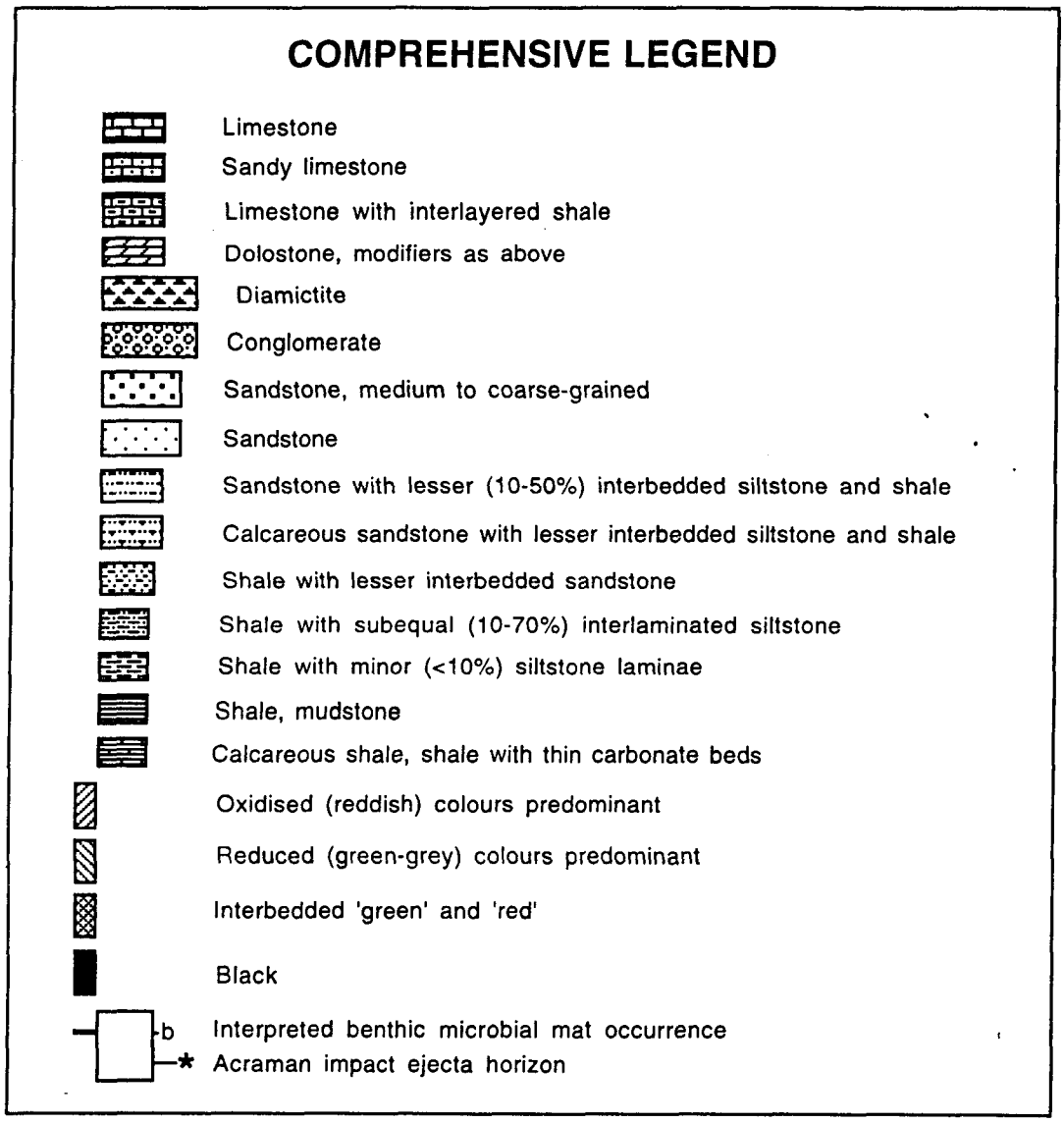

Fig. 3.4 (opposite): Lithologic columns and $\delta^{13}C_{carb}$ profiles of Nuccaleena Formation at six localities.

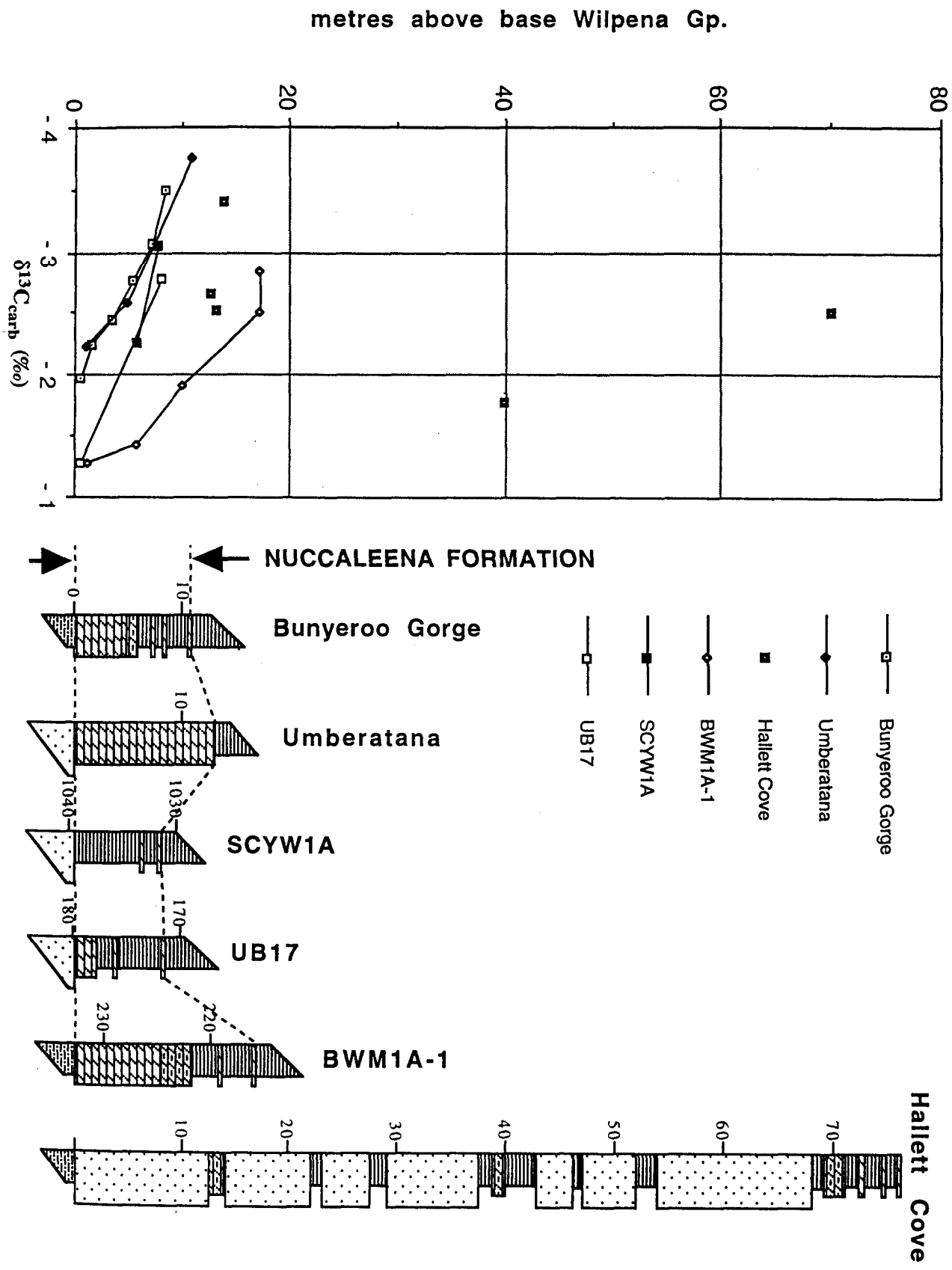
metres above base Wilpena Gp.
0
20
40
60
80
- 4
- 3
- 2
- 1
δ13Ccarb (‰)
NUCCALEENA FORMATION
Bunyeroo Gorge
Umberatana
SCYW1A
UB17
BWM1A-1
Hallett Cove
Bunyeroo Gorge
Umberatana
BWM1A-1
SCYW1A
UB17
Hallett Cove

and thin lowstand systems tract, and the dolostone units may represent intervals of sediment starvation (Dyson, 1992). The thin, persistent graded silt layers with erosive bases may be low-density turbidite deposits that periodically interrupted background carbonate sedimentation (Kennedy & Wallace, 1993). Counting against a tidal-flat environment are the lack of firm evidence for subaerial exposure, the lack of evidence for more than weak current activity, and the fact that the formation grades upward into rocks of deep-water aspect (probably below storm-wavebase: Dyson & von der Borch, 1986; and below). Tepee-like structures observed by the writer in Etina Creek display plastic, not brittle deformation except for localised brittle fracture in the hinges, and do not display the abundant shelter porosity that is characteristic of typical tepees (e.g. Assereto & Kendall, 1977). Lemon & Gostin (1990) remarked that the tepee-like structures are not associated with intraclasts or evidence for exposure and inferred a fully-submerged environment for their formation. Tepee-like structures in a similar, possibly correlative 'cap dolostone' in the Windermere Supergroup of NW Canada (the 'Tepee Dolostone') have been interpreted as deriving from slope movement (J. Aitken, pers. comm.). In the Nuccaleena Formation their abundance near diapirs and their strong preferred meridional orientation (Plummer, 1979, p. 395), parallel to inferred palaeoslope at most localities cited by Plummer, accords with such an interpretation. Syndepositional dolomitization need not imply shallow-water conditions (e.g. Hardie, 1987). Modern seafloor dolomitization is occurring in relatively deep marine environments of very slow sedimentation rate (Mullins et al., 1988).

In this context, the presence of a sulphate nodule at one locality (SCYW1A) remains a puzzle. Possibly, deep basin waters were hypersaline as is suggested for the Wonoka Formation (see later section). Alternatively, reflux of brines generated in evaporative environments to the east may explain this occurrence.

The interpretation of the Nuccaleena Formation as a transgressive systems tract deposited in a middle to outer-shelf environment below wavebase, in conditions starved of siliciclastic sedimentation and under rising relative sealevel (Dyson, 1992; Kennedy & Wallace, 1993) is accepted here. Similarly, the 'Tepee Dolostone' has been attributed to chemogenic sedimentation following post-glacial flooding (Ross, 1991).

3.3b Isotope Stratigraphy

Dolostone in the Nuccaleena Formation is depleted in ^{13}C ($\delta^{13}C$ -1 to -4 ‰) and becomes progressively more depleted toward the top of the unit in all sections except Hallett Cove. The profiles of the Bunyeroo Gorge and Umberatana sections are displaced by 0.5 to 1.5 ‰ towards more negative values relative to the other sections (Fig. 3.4). Uppermost data points

Plate 3.1: Outcrop photograph of Nuccaleena Formation showing irregular, erosive tops to some of the paler, dolostone layers. Uppermost dolostone unit of Hallett Cove section (located at 70 m on Fig. 3.4). Field of view 600 mm wide.

Plate 3.2: Nodular bedding in micritic limestone. 'Karlaya Limestone' unit of Rodda beds correlative, 1661 m depth, Munta 1 drillhole, Officer Basin. Core is 60 mm diameter.

Plate 3.3: Very fine-grained sandstone and siltstone with erosional surfaces and low-angle cross-lamination, Rodda beds correlative, 1233.0 m, 1234.7 m depths, Munta 1 drillhole, Officer Basin. Core is 60 mm diameter.

in SCYW1a and BWM1a-1 are from early diagenetic concretions. Rims and centres of concretions are not significantly different isotopically: the rim and centre of that in SCYW1a are identical in $\delta^{13}C_{carb}$ (-3.1 ‰); the rim and centre in BWM1a-1 differ slightly (-2.5 ‰, -2.9 ‰ respectively). Isotopic compositions of concretions lie on the same stratigraphic trend begun in the bedded dolomites lower down.

At Hallett Cove, the several stratigraphically separate dolostone units show a similar range of carbon isotopic compositions to the other sections but no overall stratigraphic trend is apparent (Fig. 3.4).

Two organic carbon isotope determinations from near the top of the unit in BMW1a-1 and SCYW1a show relatively heavy values (-24 to -25 ‰; Figs. 3.6, 3.8). TOC is very low (0.3 ± 0.1 mg/g).

Oxygen isotope values, from Bunyeroo Gorge, BWM1a-1, SCYW1a and UB17 fall in a narrow range (-8.10 ± 0.32 ‰ (n = 18)). The formation at Umberatana has $\delta^{18}O$ values that are considerably lighter (-11.94 ± 0.76 ‰ (n = 3)), probably a result of recrystallization at relatively high maximum burial temperatures in the Northern Flinders Ranges region (McKirdy et al., 1975). Unlike carbon, there is no systematic stratigraphic variation in $\delta^{18}O$.

At Hallett Cove, $\delta^{18}O$ values are more variable (-4.3 to -10.7 ‰) with heaviest values occurring in the lowest carbonate unit. Only the uppermost unit at Hallett Cove has $\delta^{18}O$ (at -8.24 ‰) within the narrow range of the majority of the other sections, suggesting that only this uppermost unit may be a true Nuccaleena correlative (in accord with the view of Lemon & Gostin, 1990). Further sampling of this uppermost unit needs to be undertaken to see if it displays the characteristic upward-decreasing $\delta^{13}C_{carb}$ of the Nuccaleena Formation.

Six trace-element analyses of dolostones show low Sr (63-174 ppm) and high Mn (1573 - 3734 ppm) giving a range of Mn/Sr from 9 to 45. No correlation of Mn/Sr with either $\delta^{18}O$ or $\delta^{13}C$ is apparent (Table 3.1).

The anhydrite nodule in SCYW1A is +20.4 ‰ in $\delta^{34}S$, and 0.7133 in $^{87}Sr/^{86}Sr$.

3.3c INTERPRETATION

A primary or very early diagenetic origin for the dolostones is indicated by the very fine grainsize (G. Williams, 1979) and evidence for syndepositional lithification (microfenestrae, erosional relief at tops of some beds). The widespread similarity of the decreasing-upward $\delta^{13}C_{carb}$ signature, despite some regional variation in $\delta^{18}O$, suggests a primary signal. There is no evidence for exposure-surface alteration that might produce a similar upward-decreasing $\delta^{13}C_{carb}$ profile (Allan & Matthews, 1982). Three alternative scenarios for the origin of the

upward-decreasing $\delta^{13}C_{carb}$ signal are evaluated below: (i) that the signal is partly diagenetic (organogenic); (ii) that the signal simply reflects secular change in global seawater carbon isotopic composition; (iii) that the signal reflects an increasing degree of stratification of the superincumbent water column, perhaps simply through deepening of the depositional environment.

The presence of early diagenetic dolomite concretions in the upper part of the Nuccaleena Formation raises the possibility that the mildly negative carbon isotopic compositions seen in the formation reflect incorporation of organogenic CO_2. In modern organic-rich hemipelagic sediments, breakdown of organic matter by bacterial sulphate reducers simultaneously decreases sulphate as a potential inhibitor to dolomite precipitation and increases carbonate alkalinity to produce interstitial waters highly supersaturated with respect to dolomite. Nodular and bedded, diagenetic, organogenic dolomites are the result (Baker & Burns, 1985; Compton, 1988).

The Nuccaleena Formation is very poor in organic matter and pyrite, but it is conceivable that a brief phase of sulphate reduction, fed by a small amount of labile organic matter that was quickly exhausted, contributed a small proportion of organogenic carbonate to the dolostones. In this scenario, the decreasing-upward $\delta^{13}C_{carb}$ signature could be a result of an increasing rate of terrigenous (mud) sedimentation which would have increased the amount of organic matter surviving into the zone of sulphate reduction (Emerson, 1985). In the Proterozoic, low O_2 partial pressures and a lack of bioturbation probably resulted in a very shallow (few mm?) upper limit to the zone of sulphate reduction in newly deposited fine-grained sediment. Indeed, sulphate reduction within the water column may have been a general phenomenon

sample	mineralogy	Sr(ppm)	Mn(ppm)	Mn/Sr	87Sr/86Sr	∂13C	∂18O	Rb(ppm)	87/86Srinit
Bunyeroo Gorge									
3.01	dolostone	68	2104	30.9		-2.0	-7.5		
3.03	dolostone	67	1930	28.8		-2.4	-8.1		
3.06	dolostone	63	2846	45.2		-3.5	-7.9		
BWM1A-1									
20.13	dolostone	174	1573	9.0		-1.4	-7.8		
20.14	dolostone	98	1264	12.9		-1.3	-7.3		
20.11/1	dolostone	87	3734	42.9		-2.0	-7.6		
SCYW1a									
22.56	anhydrite	744			0.71308			0.055	0.71308

Table 3.1: Trace-element and strontium isotopic data, Nuccaleena Formation.

(Logan et al., in press). In the Nuccaleena Formation the dolomite layers (if diagenetic) were evidently sufficiently shallow to have been exhumed in some instances by minor phases of seafloor erosion, and the bulk of the carbonate - even in the concretions - must have been supplied by downward diffusion from seawater as shown by the only mildly ^{13}C-depleted compositions.

It is difficult to exclude a partial organogenic origin for the dolostones of the Nuccaleena Formation, but the smoothness of the $\delta^{13}C$ profiles and the widespread consistency of the signal - to some extent independent of facies (compare SCYW1a and Umberatana sections, Fig. 3.4) argues in favour of a wholly primary (ambient seawater) origin for the signal. In contrast, carbonates that are partly organogenic tend to display markedly variable carbon isotopic compositions, typically at the scale of single concretions (e.g. Irwin et al., 1977). The presence of microfenestrae in some dolostone layers also argues against a diagenetic origin.

Regional variation in the $\delta^{13}C_{carb}$ profile corresponds to palaeogeographic position in a way that may provide significant information bearing on the origin of the upward-decreasing $\delta^{13}C_{carb}$ signature. Profiles displaced towards heavier values (BWM1a-1, UB17, SCYW1a) are from shelfal localities - the Curnamona Craton, Stuart Shelf or margin of Stuart Shelf respectively. The Bunyeroo Gorge and Umberatana sections, with 0.5 to 1.5 ‰ lighter overall values, are situated in the axial part of the geosyncline (Fig. 3.2). This is unlikely to be a burial-diagenetic overprint because $\delta^{18}O$ at Bunyeroo Gorge is not significantly different from the shelfal localities.

If the upward-decreasing signal simply reflects secular change in seawater carbon isotopic composition, earlier commencement of sedimentation on the shelves and basinward progradation is implied (Fig. 3.5a). However, basinward progradation does not accord with the sequence-stratigraphic interpretation (see previous section) which requires the retrogradational pattern of sedimentation of a transgressive systems tract (earlier commencement of sedimentation in basinward locations) (cf. Fig. 1.14). The $\delta^{13}C_{carb}$ signature and its regional variation are better explained by retrogradational sedimentation recording progressive deepening of depositional environment in a water body with a strong vertical gradient in $\delta^{13}C_{DIC}$ (Fig. 3.5b). Equally, a strengthening of the vertical $\delta^{13}C_{DIC}$ gradient over time may have played a part in generating the upward-decreasing profile. The carbonates may have equilibrated isotopically with bottom-water $\delta^{13}C_{DIC}$ either by direct precipitation or during syndepositional diagenetic stabilization or dolomitization. Shelfal localities are relatively slightly enriched in ^{13}C because of shallower depositional

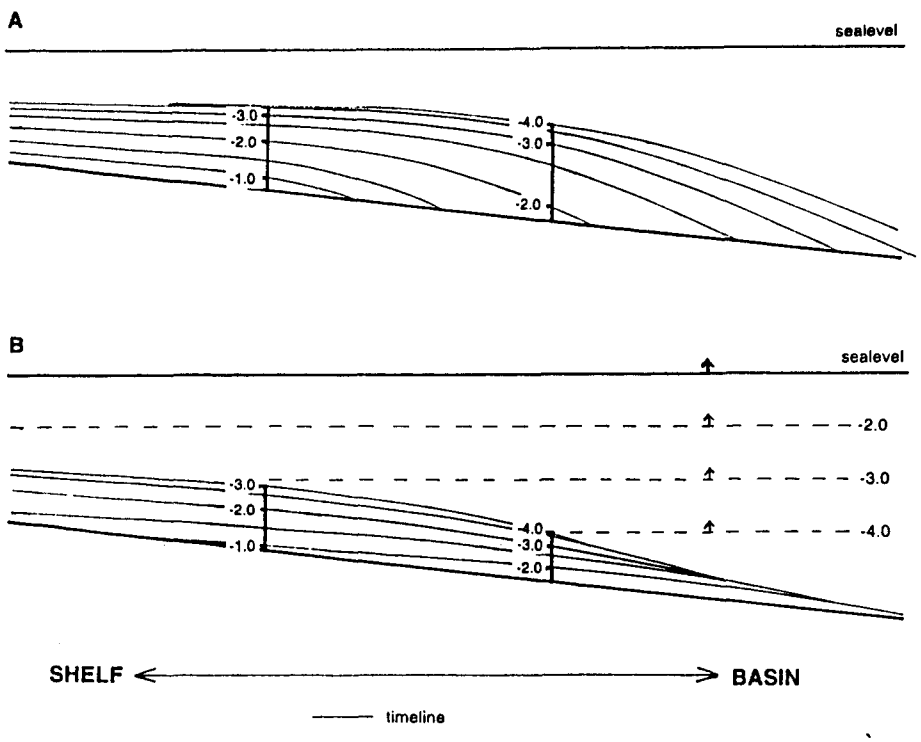

Fig. 3.5: Two models to explain regional vatiation in $\delta^{13}C_{carb}$ profiles in the Nuccaleena Formation. **A:** The sediments prograde from shelf to basin and there is a secular fall in $\delta^{13}C_{DIC}$ in a more or less well mixed water body; time lines are isochemical with respect to $\delta^{13}C_{carb}$. **B:** Shelfward sedimentary retrogradation under rising relative sealevel, in a water body with a strong vertical gradient in $\delta^{13}C_{DIC}$. Timelines are not isochemical; at any time basinward localities have lighter $\delta^{13}C_{carb}$ because palaeoenvironment is deeper. Palaeoslope is maintained by more rapid subsidence in basinward localities.

environments. Thus, $\delta^{13}C_{carb}$ profiles obtained from widespread sections show a pattern of regional variation that cannot be easily reconciled with an interpretation of simple secular change in marine $\delta^{13}C_{DIC}$, if the pattern of retrogradational sedimentation is correctly understood.

Relatively heavy $\delta^{13}C_{org}$ from the upper parts of the Nuccaleena Formation is consistent with stratification of waters, since organic carbon was presumably mainly fixed in surface waters. $\Delta\delta^{N}$ (= $\delta^{13}C_{carb}$ - $\delta^{13}C_{org}{}^{N}$) is 23.8 ‰ and 24.5 ‰ in BWM1a-1 and SCYW1a respectively, several permil lower than the norm for the Ediacarian (see section 2.3d).

Further indirect evidence for intensifying basin stratification comes from the Nuccaleena correlative in the Amadeus Basin, where a complete $\delta^{13}C_{org}$ profile shows a steeply upward-increasing trend, opposite to that of $\delta^{13}C_{carb}$ (see sections 4.4c; 6.2). An overview of several Ediacarian basins shows a loose stratigraphic association of features - ^{13}C-depleted carbonates, low $\Delta\delta$, anomalously ^{13}C-depleted organic carbon of benthic microbial mats, and rare subaqueous evaporite - that are readily explained by salinity stratification, and the falling

$\delta^{13}C_{carb}$ trend in the Nuccaleena Formation is considered to reflect the onset of the first of two Ediacarian phases of stratification (see section 6.2).

Thus, the Nuccaleena $\delta^{13}C_{carb}$ profile has little bearing on the contemporary shallow-marine global $\delta^{13}C_{carb}$ signal except that shallow-marine $\delta^{13}C_{carb}$ was -1 ‰ or greater at the time of commencement of Nuccaleena sedimentation.

3.4 Brachina and ABC Range Formations

3.4a LITHOSTRATIGRAPHY

The Brachina and ABC Range Formations are shale/sandstone, and quartz sandstone-dominated units respectively that on a regional scale intergrade laterally and vertically, representing a single, broadly shallowing-up depositional unit: the highstand systems tract of the first major depositional sequence of the Wilpena Group (Dyson, 1992). Two complete sections (Bunyeroo Gorge and SCYW1a) and one partial section (BWM1a-1) have been examined in this study (Figs. 3.6 - 3.8). The total thickness of the Brachina and ABC Range correlatives in SCYW1a, at the edge of the Stuart Shelf, is less than half that of the Bunyeroo Gorge section.

Although local stratigraphic names have previously been used in SCYW1a (e.g. Damassa & Knoll, 1986; Forbes & Preiss, 1987), the Flinders Ranges nomenclature is used here. Lithostratigraphic correlation between SCYW1a and the type sections in the Flinders Ranges is well-established (Preiss, 1984; Forbes & Preiss, 1987).

At the base of the Brachina Formation in all sections studied is a faintly planar-laminated red shale, 25-40 m thick, that probably represents the deepest palaeoenvironment and probably contains the maximum flooding surface of the first depositional sequence. The proportion of sandstone and siltstone thereafter increases upwards through the Brachina and ABC Range Formations in accordance with an overall shallowing of palaeoenvironment from below storm wavebase to tidally-influenced shallow-marine (Dyson & von der Borch, 1986; Forbes & Preiss, 1987). At Bunyeroo Gorge, the Brachina Formation consists of reddish or greenish silty shales with very fine to fine-grained sandstone that occurs almost entirely as 'event beds' up to 1m thick. The sandstone beds typically have sharp, flute-casted bases, lower parts with internal plane-lamination or HCS, and plane-laminated or wave-ripple cross-laminated tops. Commonly, tops of beds are marked by combined-flow ripples passing gradationally up into in-phase oscillation ripples. Polygonal interference wave ripples are also common on upper bed surfaces. Beds with this suite of sedimentary structures are interpreted as tempestites, and

at Bunyeroo Gorge they are abundant from just above the basal red shale to almost the top of the Brachina Formation (cf. Dyson & von der Borch, 1986; Jenkins, 1993b). Above 950 m above the base of the formation, small clastic dykes become abundant. These resemble the sand-filled 'diastasis cracks' of Cowan & James (1992) or syneresis cracks (Plummer & Gostin, 1983), and are not desiccation cracks. Above 1200 m and within the ABC Range Quartzite, sandstone is coarser (¼ mm) and better sorted. Bedding is lenticular, and shale

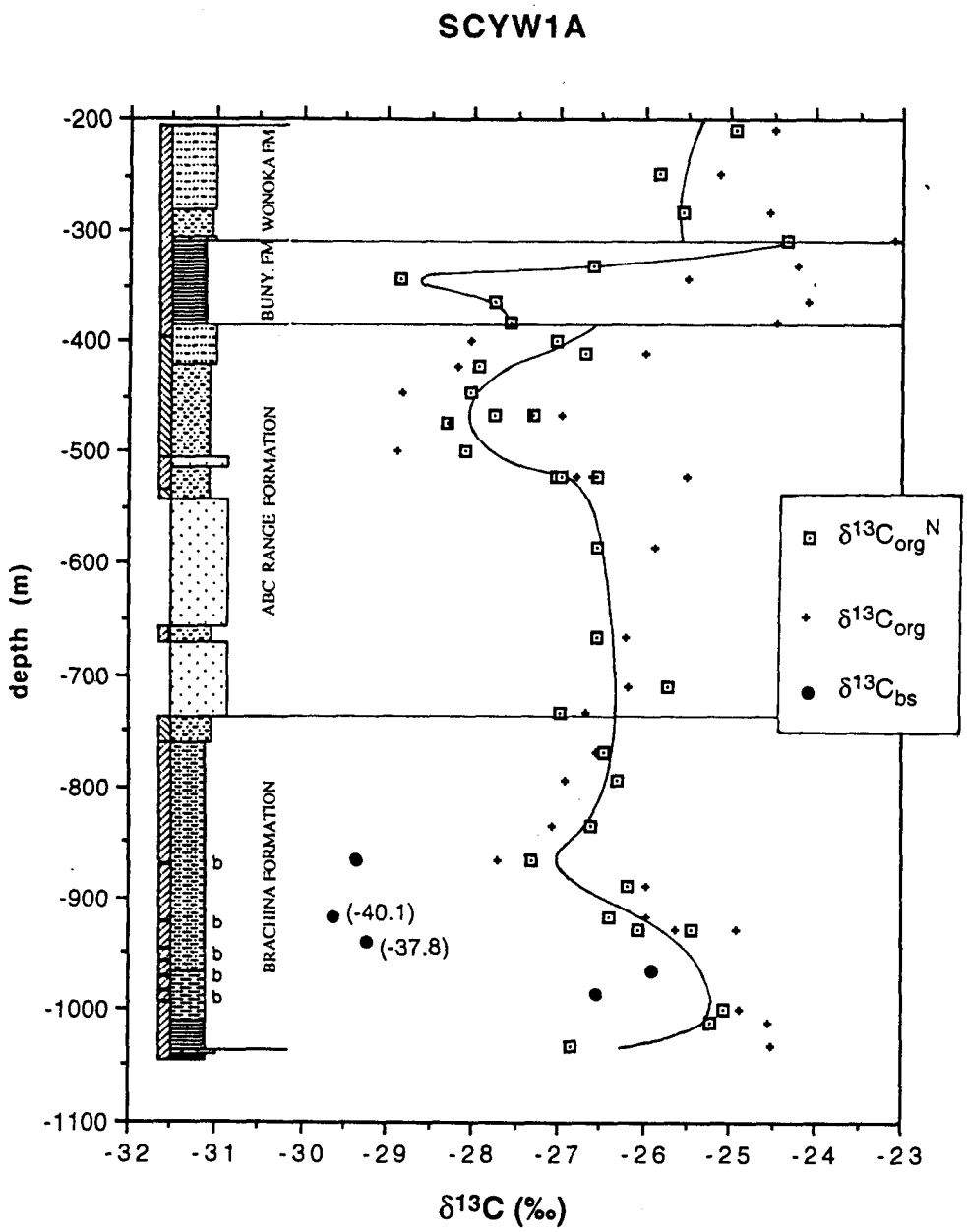

Fig. 3.6: Lithologic column and organic $\delta^{13}C$ data, Brachina, ABC Range, Bunyeroo and lowermost Wonoka Formations, SCYW1a drillhole. Calculated $\delta^{13}C_{bmm}$ indicated adjacent to $\delta^{13}C_{bs}$ points.

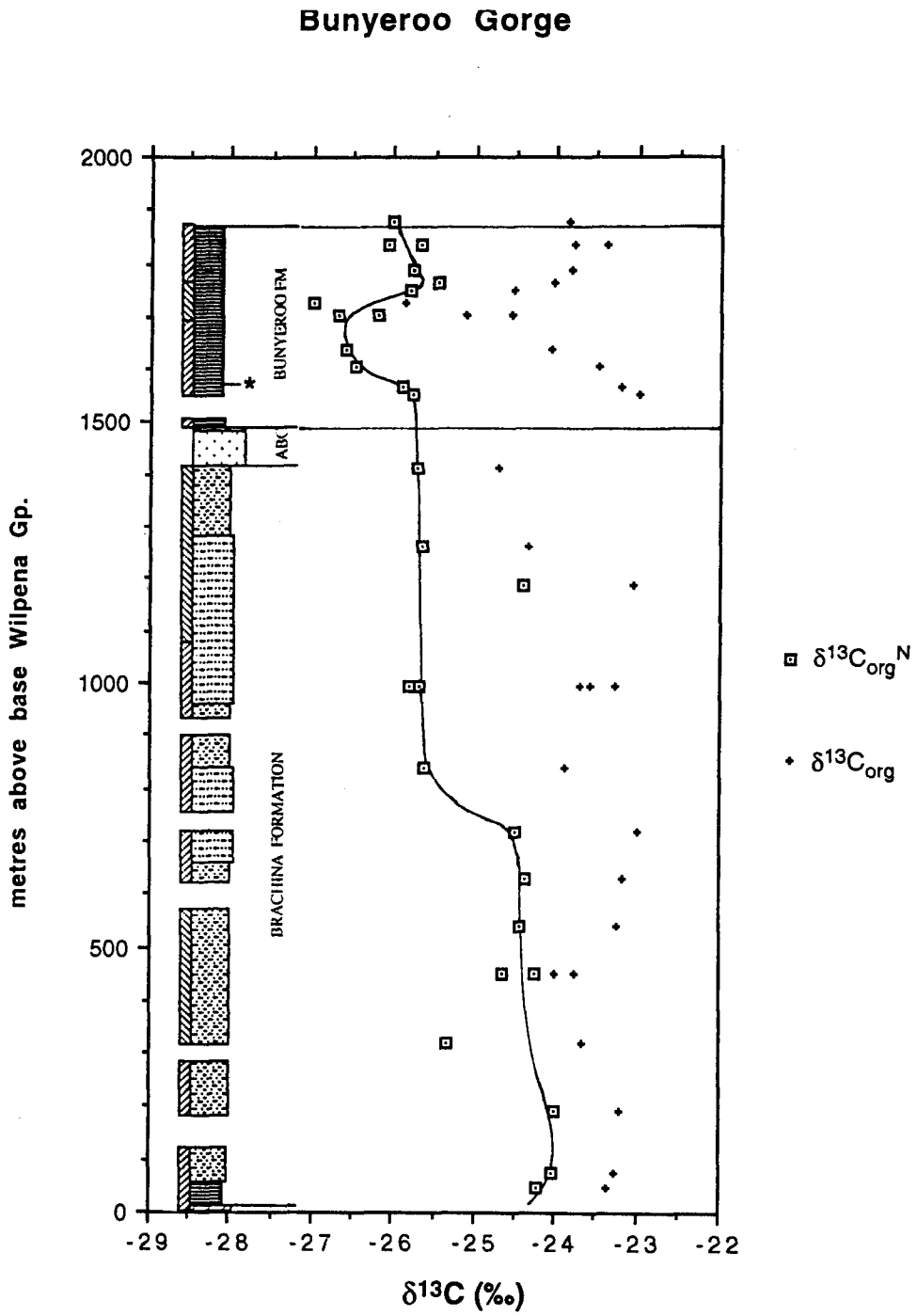

Fig. 3.7: Lithologic column and organic $\delta^{13}C$ data, Brachina and Bunyeroo Formations, Bunyeroo Gorge. Asterisk indicates position of Acraman ejecta layer.

intraclasts ('clay galls') and angle-of-repose cross-bedding with variable current directions are common. A tide-dominated shallow-marine environment is inferred. The top 5 m of the ABC Range Quartzite consists of purple siltstone and a distinctive very coarse, ferruginous lithic sandstone overlying a regionally persistent discontinuity: this surface is sequence boundary 2 of the Wilpena Group (von der Borch et al., 1988; Christie-Blick et al., 1990; Fig. 3.3).

In SCYW1a, the Brachina Formation consists mostly of red shale with 10-50% thin beds and laminae of parallel-laminated or cross-laminated siltstone. Starved ripples are common. Thick sandstone 'event' beds appear only within 50 m of the top of the formation. There are minor thin beds of bluish-grey shale. Between 50 and 170 m above the base of the formation are rare, inconspicuous, very thin laminae of highly ^{13}C-depleted black shale interpreted as remnant benthic microbial mats (see Chapter 2). The ABC Range Formation in SCYW1a consists of fine to medium-grained quartzarenite with angle-of-repose cross-bedding passing up into interbedded, dominantly grey-green, siltstone, shale and cross-bedded sandstone.

In BWM1a-1, all but 69 m of the Brachina Formation has been removed by Cambrian erosion. The basal red shale is gradationally overlain by alternating green and black shale. The black shale beds are sharply-bounded, 20-500mm thick, and display the lithologic and isotopic characteristics of fossil benthic microbial mats (see Chapter 2). They are here much more strongly developed than in SCYW1a.

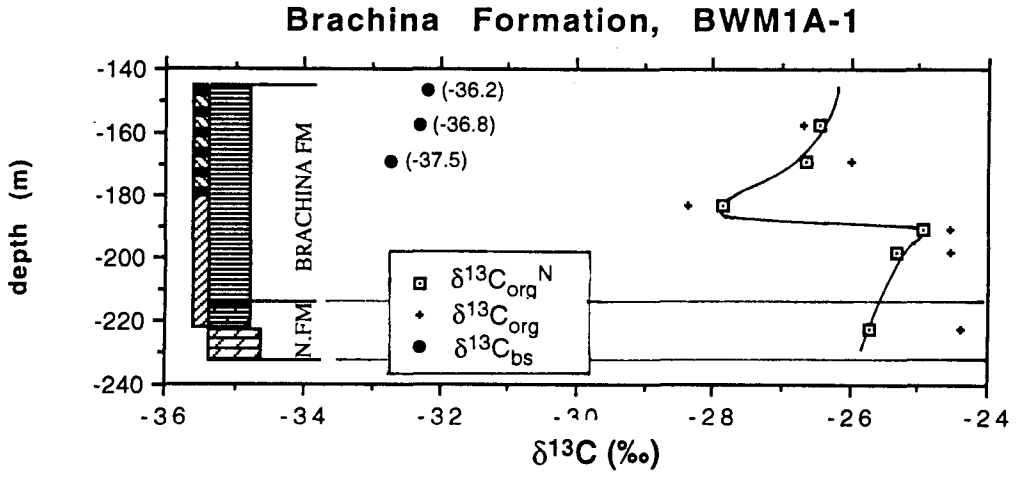

Fig. 3.8: Lithologic column and organic $\delta^{13}C$ data, Nuccaleena and Brachina Formations, drillhole BWM1A-1. Calculated $\delta^{13}C_{bmm}$ indicated adjacent to $\delta^{13}C_{bs}$ points.

3.4b ISOTOPE STRATIGRAPHY

There are no carbonate rocks in the sections studied; carbon isotope data is entirely derived from organic carbon (Figs. 3.6 - 3.8). The most complete record appears to be preserved in SCYW1a (Fig. 3.6). In this section, all normalised data points ($\delta^{13}C_{org}{}^{N}$) lie within 1 ‰ of the indicated first-order curve. (See Chapter 2 for derivation of $\delta^{13}C_{org}{}^{N}$ from raw $\delta^{13}C_{org}$ data). $\delta^{13}C_{org}{}^{N}$ in SCYW1a initially exhibits a positive excursion (-25 ‰), falling to a poorly-defined minimum (-27 ‰) within the Brachina Formation, and there is a second, broader negative excursion within the upper, shaly part of the ABC Range Formation (-28 ‰: Fig. 3.6). Five samples that include benthic microbial mat carbon in the lower Brachina Formation are displaced 1 to 3 ‰ towards lighter values. Isotopic compositions of undiluted benthic microbial mat carbon ($\delta^{13}C_{bmm}$), calculated for two samples as indicated in Chapter 2, are highly depleted (-38,-40 ‰: Table 2.2). The isotopic difference between carbon of inferred benthic and pelagic origin ($\Delta_{p\text{-}b}$) is 12.5 to 14 ‰.

BWM1a-1 also shows a positive excursion up to -25 ‰ in the lower Brachina Formation. The signal then falls sharply to a minimum just below the top of the basal red shale unit. The black shale facies is displaced 5 to 6 ‰ toward more negative values, relative to interbedded green shale. Calculated benthic microbial mat carbon isotopic compositions ($\delta^{13}C_{bmm}$) are -36 to-38 ‰ (Table 2.2). Considering the uncertainties inherent in the calculation, these compositions are similar to those calculated in SCYW1a. Inferred $\Delta_{p\text{-}b}$ is 10 to 11.5 ‰.

The Bunyeroo Gorge section is poorly constrained in terms of density of data, but the lower half of the Brachina Formation has slightly heavier organic carbon than the upper half. No trace of the benthic microbial mat facies was found. TOC's are low (at around 0.4 mg/g, averaging less than half the other sections) and organic carbon is ^{13}C-enriched (-24 to -26 ‰), due at least in part to the higher maximum burial temperatures of the geosynclinal region (McKirdy et al., 1975; and below).

Maturation data

Thermal maturation indices (kerogen colour, H/C ratio: Tables 2.3, 2.5) suggest relatively high degrees of thermal alteration in the Bunyeroo Gorge and BWM1A-1 sections, and less severe thermal effects in SCYW1A. At Bunyeroo Gorge, kerogen H/C ratios are around 0.4 in the Bunyeroo and Wonoka Formations, but no H/C data are available from the Brachina Formation in this section. Maximum burial temperature in the Brachina Formation may have been significantly higher than in the younger formations, perhaps leading to loss of the primary signal (cf. Kaufman et al., 1991), but the preservation of a widespread signal in the Bunyeroo Formation, in samples with comparable or lower TOC than the Brachina Foration

at Bunyeroo Gorge (see next section), gives some confidence that $\delta^{13}C_{org}$ at this locality reflects a primary signal.

3.4c INTERPRETATION

The differences between the SCYW1a and Bunyeroo Gorge signals can be at least partly resolved with an understanding of the pattern of basin fill. Previous studies (Plummer, 1978; Dyson, 1992) suggest that the Brachina-ABC Range succession accumulated as a large, eastward-prograding clinoform (highstand systems tract). In a highstand systems tract, lower parts of proximal sections have time-equivalents that are missing or highly condensed in distal sections; conversely, upper parts of proximal sections can be expected to have greatly thickened time-equivalents in distal sections (see Fig. 1.14). Hence, the lower half of the Brachina Formation in the (more proximal) SCYW1a section, including the black shale-bearing interval, may be missing or highly condensed at Bunyeroo Gorge (probably time-equivalent to part of the basal red shale that comprises the interpreted condensed section). Similarly, the negative excursion in the upper ABC Range Formation in SCYW1a may be time-equivalent to the much thicker interval with relatively low $\delta^{13}C_{org}$ at Bunyeroo Gorge (Fig. 3.26) - although the sparsity and scatter of data in the latter section hardly warrant this as a firm conclusion. $\delta^{13}C_{org}{}^{N}$ at Bunyeroo Gorge is 1 to 2 ‰ heavier than time-equivalent parts of SCYW1A under this scheme. This can be partly attributed to the difference in thermal maturity: independent indicators predict a ca. 1 ‰ enrichment at Bunyeroo Gorge relative to SCYW1A (Table 2.5).

It is simplest to correlate the BWM1a-1 profile directly with the lower part of SCYW1a, although black shale deposition largely precedes the negative excursion in SCYW1a but follows it in BWM1a-1 (Fig. 3.26).

3.5 Bunyeroo Formation

3.5a LITHOSTRATIGRAPHY

The definition of the top of the Bunyeroo Formation has been recently revised downward and is now taken as the base of the Wearing Dolomite Member (Gostin & Jenkins, 1983; Haines, 1990). The Bunyeroo Formation consists almost entirely of structureless or faintly laminated, red or green mudstone. In the Bunyeroo and Brachina Gorges, lower and upper parts of the formation are red, and there is a middle green unit. The red parts have rare, planar, continuous pale green beds. A few green beds have a central planar, persistent lamina of siltstone. The middle green unit of the gorge sections has sparse, large (70cm wide) flattened-

ovoid concretions of impure limestone or calcareous mudstone. Laminae are only slightly deflected by differential compaction at the lateral margins of these concretions, indicating a late diagenetic origin (cf. Raiswell, 1971). In Brachina Gorge the green unit is considerably thicker than at Bunyeroo Gorge, the lower red unit being correspondingly thinner; and here the green unit contains rare beds of black shale and a thick, discontinuous bed of (?diagenetic) impure carbonate (Figs. 3.7, 3.9). In SCYW1a (Fig. 3.6), the Bunyeroo Formation is much thinner than the gorge sections and consists entirely of red shale with rare, very pale green dolomitic mudstone beds.

The Acraman impact ejecta horizon (Gostin et al., 1986) occurs within a green mudstone band 80-100m above the base of the gorge sections but was not located in SCYW1a.

The green layers within the lower red unit are of diagenetic origin, resulting from reduction of Fe^{3+} by low-Eh basinal brines that migrated along permeable horizons provided by the siltstone laminae and by the Acraman ejecta layer (Keays et al., 1992).

A relatively deep environment of deposition, below storm wavebase and starved of coarse sediment, is indicated for the Bunyeroo Formation (Forbes & Preiss, 1987; Haines, 1990).

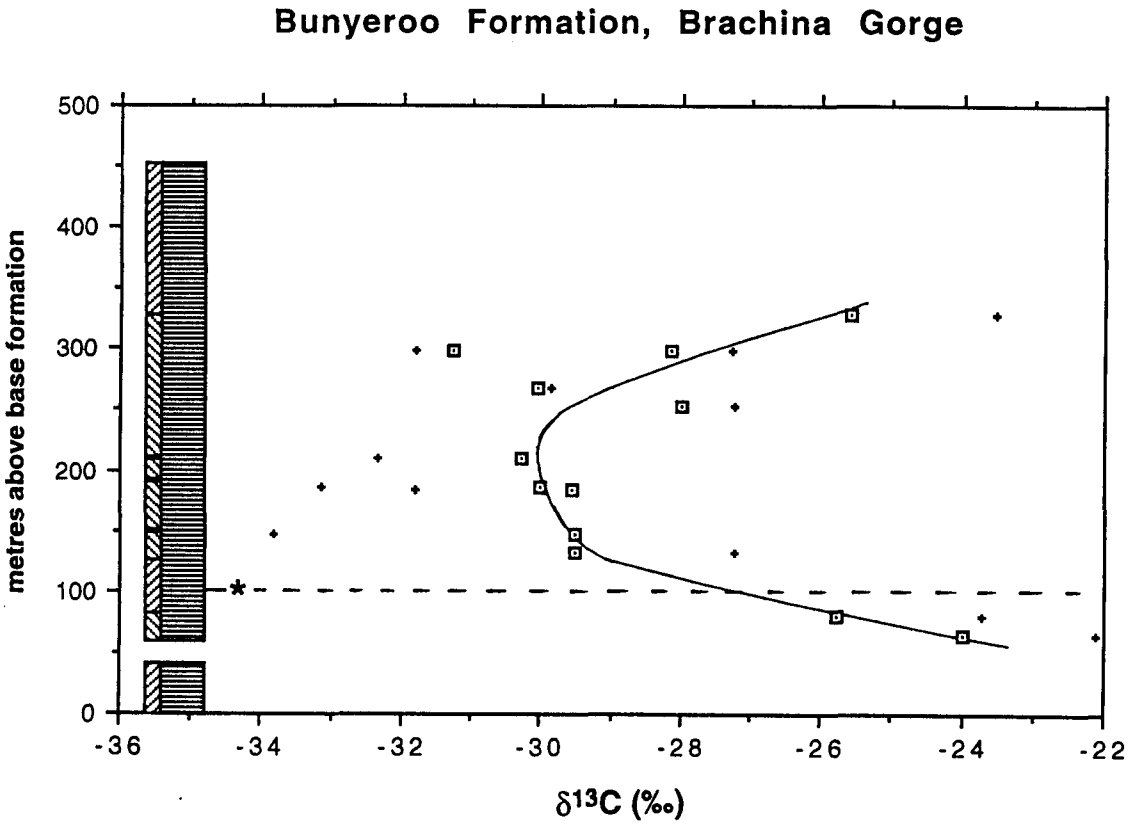

Fig. 3.9: Lithologic column and organic $\delta^{13}C$ data, Bunyeroo Formation, Brachina Gorge. Asterisk indicates position of Acraman ejecta layer.

Localised developments of organic-rich shales in the Bunyeroo Formation have been attributed to syndepositional movement of diapirs and development of peripheral sinks (Forbes & Preiss, 1987, p. 229; Lemon et al., 1992). Heightened preservation of organic matter is considered to be due to local anoxia in depositional lows and enhanced primary productivity over the shoal above the rising salt plug (Lemon et al., 1992). Similarly the lateral facies change from red shale in the lower and middle part of the formation at Bunyeroo Gorge, to green and black shale at Brachina Gorge may be related to local changes in basin topography caused by salt movement at depth.

3.5b Isotope Stratigraphy

Organic carbon isotope profiles of the two gorge sections both show a negative excursion in the middle of the formation, but the magnitude of the shift - as seen in both normalised and raw data - is 2 to 3 times greater in Brachina Gorge (Figs. 3.7; 3.9). Lightest values are found in the central green mudstone unit in both sections, and there is a well-defined decreasing-upward trend in the underlying succession that contains the Acraman ejecta layer.

A negative excursion is also apparent in the SCYW1a section (Fig. 3.6) but data are few and TOCs so extremely low (0.11 ± 0.04 mg/g, n = 5) that the fidelity of this signal must be regarded as doubtful.

One of the late diagenetic concretions from Bunyeroo Gorge has $\delta^{13}C_{carb}$ = - 6.8 ‰ and $\delta^{18}O$ = - 14.9 ‰, suggesting precipitation of carbonate in porewaters at elevated temperature with a component derived from thermal breakdown of organic matter (cf. Irwin et al., 1977).

3.5c Interpretation

The reason for the large size of the negative excursion in Brachina Gorge relative to the other sections (including Officer Basin equivalents: see below) is uncertain. TOC's in the middle green mudstone unit at Brachina Gorge are highly variable (0.18-17 mg/g C), with the trough of the excursion defined by four samples of black shale relatively high in TOC (3.10-17 mg/g). However, with the correction factor applied (see Chapter 2) samples of very high and very low TOC (e.g. at 123 m: 0.18 mg/g) lie roughly on the same trend (Fig. 3.9).

The black shale beds in the Brachina Gorge section of the Bunyeroo Formation are texturally uniform, lacking the wispy microlamination characteristic of benthic microbial mats (Chapter 2); they also lack the characteristic strong depletion of $\delta^{13}C_{org}{}^{N}$ relative to that of associated rocks. These black shales are therefore tentatively identified as accumulations of pelagic organic carbon, preservation of which may have been enhanced in depositional lows created by salt movement at depth (Lemon et al., 1992).

3.6 Wonoka Formation

3.6a LITHOSTRATIGRAPHY

The Wonoka Formation (as redefined by Gostin & Jenkins, 1983) is a broadly shallowing-upward, mixed siliciclastic-carbonate succession about 700 m thick. Large (1 km deep) canyons, of controversial origin, were cut and filled during Wonoka time (Thomson, 1969; von der Borch et al., 1982, 1985; Eickhoff et al., 1988; Christie-Blick et al., 1990). Isotope stratigraphy of two complete sections, Bunyeroo Gorge and First Hill, east of Blinman (Figs. 3.10, 3.11) is documented here. Also sampled were partial sections at Brachina Gorge, Umberatana Syncline and drillhole SCYW1a. Included in this discussion is a dolostone bed in the lowermost Bonney Formation (Pound Subgroup) at Brachina Gorge.

Sections at Bunyeroo Gorge, Brachina Gorge and SCYW1a

Haines (1987, 1988, 1990) described the sedimentology of the Wonoka Formation in the Central Flinders Zone and recognised eleven informal lithological subdivisions, which provide the basis of the following description.

Unit 1

Unit 1 is thin but widespread. At Bunyeroo Gorge the unit consists of 2 m of red and pale green shale with thin, very fine-grained dolostone beds. As is commonly seen in the Nuccaleena Formation, the dolostone layers tend to have gradational bases and sharp, often scoured, tops. Silty dolosparite or intraclastic flat-pebble conglomerate locally fill erosional scours in the tops of dolostone beds. Intraclasts are somewhat rounded, and lithologically identical to subjacent dolostone beds (and also almost identical in $\delta^{13}C_{carb}$ and $\delta^{18}O$ in one comparison in SCYW1a). At Bunyeroo Gorge, Unit 1 has a gradational base and a sharp top, the latter possibly representing a depositional sequence boundary (Christie-Blick et al., 1990).

In SCYW1a, Unit 1 is thinner (1.3 m) but otherwise very similar to Bunyeroo Gorge. Anhydrite occurs in an intraclastic horizon at 310.0 m, as a patchy cement and as isolated crystallites within the mudstone matrix. At Brachina Gorge and First Hill the unit is reduced to a single bed of dolostone with platy intraclasts.

The micritic texture of the dolostone in Unit 1, and the presence of dolostone intraclasts cemented by a marine calcite cement suggests the dolomite is primary or very early diagenetic (Haines, 1990).

Thin, planar bedding and fine grainsize imply deposition below storm wavebase, with perhaps extreme storm activity causing local intraclast conglomerates (Haines, 1990). A quite

different interpretation is given by Gostin & Jenkins (1983) and von der Borch et al. (1989) who regarded the intraclastic conglomerates as evidence of subaerial exposure.

Unit 1 may be a condensed section in sequence stratigraphic terms (von der Borch et al., 1988) and may include a highly attenuated HST with a sequence boundary at the top of the unit (Christie-Blick et al., 1990).

Unit 2

Unit 2 lacks carbonate, consisting of red sandstone turbidite beds and minor storm beds (Haines, 1990) interlayered with red shale and rare green shale. Unit 2 is present in SCYW1a, where it is unconformably overlain by Cambrian rocks. This unit is interpreted as a lowstand systems tract (Christie-Blick et al., 1990) deposited in an outer shelf setting (Haines, 1990). Fanning, east-directed palaeocurrents in the cenral Flinders Ranges area suggest a (?deltaic) point source to the west (Haines, 1990).

Units 3 - 7

Units 3 to 7 comprise a broadly shallowing-upward shelf sequence with an upward-increasing proportion of limestone. Unit 3 is red shale with minor thin, planar, persistent beds of micritic, slightly silty limestone, and siltstone as planar laminae and starved ripples. Many of the thin limestone beds have gradational bases and sharp tops, as in Unit 1. Some limestone beds are ripple cross-laminated. Palaeocurrent directions suggest deposition by contour currents at depths below storm wavebase (Haines, 1990).

Unit 4 contains more and thicker beds of limestone, interpreted as both turbidites and rare storm-deposited layers (Haines, 1990). Units 5 to 7 consist of medium to thick-bedded limestone or sandy limestone with only rare interbedded shale. Hummocky cross-stratification, climbing ripple-lamination, wave-ripple lamination and planar lamination are abundant (Haines, 1988). Intraformational conglomerates are present, in places filling erosional gutters or potholes.

Scattered small (< 1mm) euhedra of gypsum or pseudomorphs of calcite after gypsum are common in Units 4 and 5 (Plates 3.4, 3.5). Previously unrecorded from this part of the Wonoka Formation, the gypsum occurrences may have significant palaeoenvironmental implications (see below). Present in several thin sections, they are also seen on some weathered surfaces as tiny lenticular pits.

Some limestones in Unit 7 are seen in thin section to be very fine-grained calcarenites, consisting of well-sorted, rounded micritic peloids 100μ in diameter in a microspar cement.

Plate 3.4: Lenticular gypsum crystals in calcareous mudstone, sample 5.43, Unit 5, Wonoka Formation, Bunyeroo Gorge. Scale bar = 1mm.

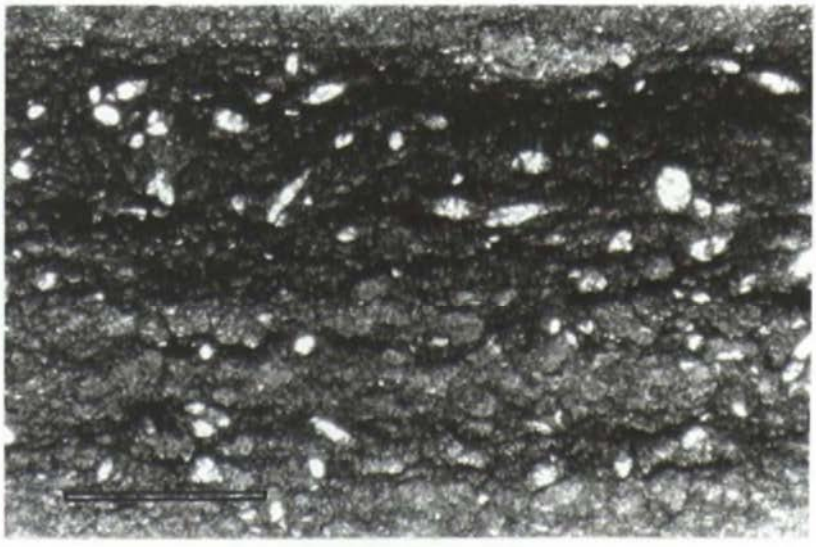

Plate 3.5: Pseudomorphs of calcite after ?gypsum, sample 5.36, Unit 4, Wonoka Formation, Bunyeroo Gorge. Scale bar = 1mm.

The peloids may be of microbial origin (cf. Tucker, 1986b; Chafetz, 1986). Glauconite and francolite grains are present in some limestone beds in Unit 7 (Haines, 1990).

Unit 7 also contains abundant, thick micritic limestone beds pervaded by an unusual, small-scale stylonodular structure consisting of a strongly anastomosing network of overburden stylolites that circumscribe ill-defined 'nodules' a few mm in diameter. Intraformational erosion surfaces cutting these beds have small-scale relief suggesting very early diagenetic initiation of the nodular fabric (Haines, 1988).

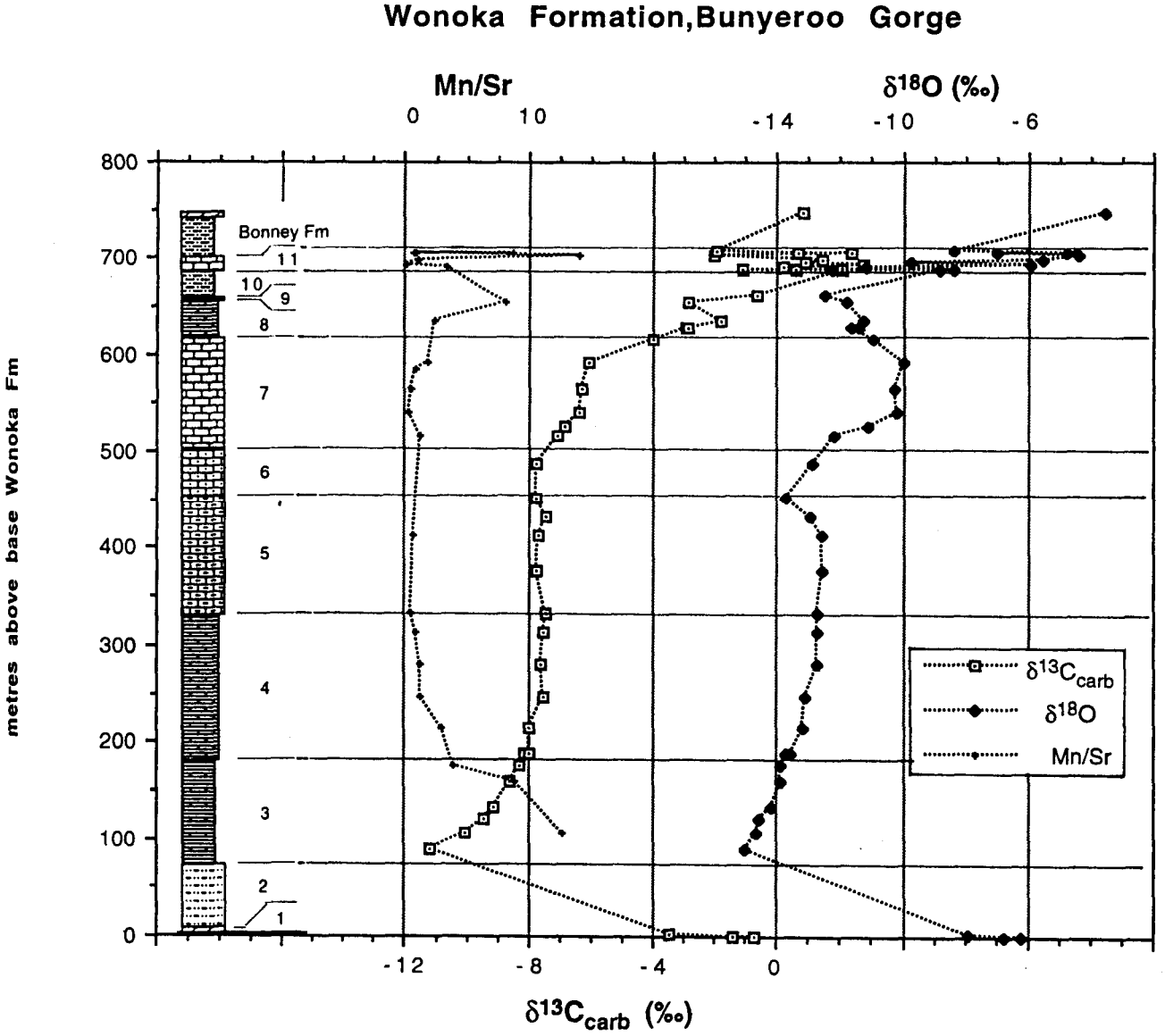

Fig. 3.10: Lithologic column, carbonate $\delta^{13}C$ and $\delta^{18}O$, and Mn/Sr data for Wonoka Formation at Bunyeroo Gorge. Numbered stratigraphic units are after Haines (1990). A few data points in Unit 11 and the lowermost Bonney Fm. are from nearby Brachina Gorge.

Thin sections show the predominant carbonate lithology to be (apart from peloidal calcarenite in Unit 7) weakly to moderately luminescent, calcite microspar (5 - 20μ grainsize) with 10 - 20%, scattered rhombs of slightly coarser dolomite. The microsparitic texture could have originated either by aggrading neomorphism of micrite or by diagenetic stabilization of an aragonite-dominated lime mud (Lasemi & Sandberg, 1984).

Units 4 to 7 record the increasing influence of storm activity concomitant with shallowing of environment from outer to middle shelf (Haines, 1990). The lack of shallow-water grains such as ooids suggests the carbonate was not reworked from shallow banks, but probably formed by direct inorganic precipitation in the middle shelf zone (Haines, 1988).

Units 8 - 11 and dolostone in Bonney Formation

There is an abrupt change at the top of Unit 7 to green shale with beds of glauconitic and in places intraclastic limestone (Unit 8). The Unit 7 - 8 contact is interpreted as a deepening of palaeoenvironment (Haines, 1990) and is considered to be a depositional sequence boundary (Christie-Blick et al., 1990). Storm wave-formed sedimentary structures are still present, such as erosional pot and gutter structures, HCS and climbing oscillation ripples. A tuffaceous marker bed, the 'purple marker bed', is widespread in Unit 8 thoughout the Central Flinders Zone (Haines, 1990), and regional parallelism with the top and base of Unit 8 (see Haines, 1987) suggests Unit 8 is not appreciably diachronous.

Unit 9 - only 1m thick at Bunyeroo Gorge - is an oolitic, shallow-water limestone. Unit 10 is a redbed sandstone and shale sequence with desiccation cracks; it resembles the marginal marine to terrestrial Bonney Formation that overlies the Wonoka Formation. Unit 11 consists of grey and black, oolitic grainstone, fine-grained limestone (microspar) and brown secondary (sucrosic) dolomite. Ooids are preserved as molds filled by coarse centripetal cement and organic matter, suggesting an originally aragonitic mineralogy (see also Haines, 1990). Massive ooid grainstone is predominant in the lower half of the unit in Bunyeroo Gorge. Stromatolite bioherms (*Tungussia* cf. *julia* Walter et al. 1979) occur within the grainstone.

Unit 11 and the lower part of the Bonney Formation (including a thin dolostone unit) were measured and sampled in Brachina Gorge. Here Unit 11 is overlain by 37m of red siltstone and sandstone of the Bonney Formation, then 3m of cream to pink, sandy dolostone, oolitic at the top. Sample points from Brachina Gorge are projected onto the Bunyeroo Gorge section (Fig 3.10).

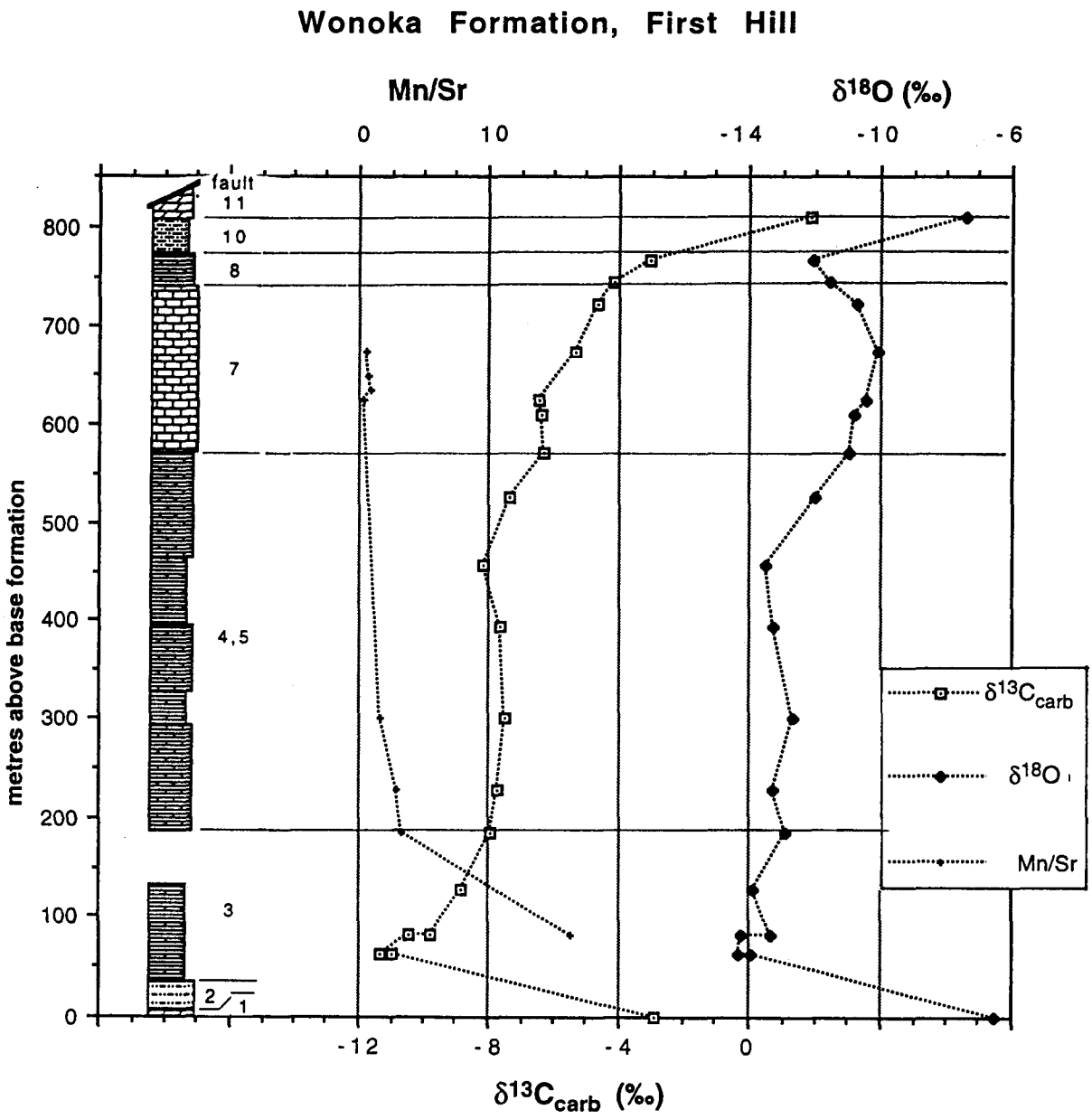

Fig. 3.11: Lithologic column, carbonate $\delta^{13}C$ and $\delta^{18}O$, and Mn/Sr data for Wonoka Formation at First Hill.

Sections at First Hill and Umberatana Syncline

The First Hill section is similar to that at Bunyeroo Gorge except that Unit 5 is represented by a thickened, probably more distal succession of shale with thin limestone beds, resembling units 3 and 4 of the Bunyeroo Gorge section (Fig. 3.11). Unit 11 is here entirely replaced by massive crystalline dolostone in proximity to a fault.

The Wonoka Formation is also thicker and of still more distal aspect in the northern Flinders Ranges. At Umberatana Syncline, about a kilometre thickness of Wonoka Formation was

measured and sampled starting at a stratigraphic level roughly equivalent to the top of the interfluves of large intraformational canyons (see below). This section consists of planar-bedded to massive silty shale with thin, persistent planar beds of microsparry limestone (Fig. 3.12). Pyrite, as euhedra 1 - 3 mm in size, is abundant. There are occasional thick beds of limestone-clast breccia, with chaotic or imbricate fabric; and high in the section there are units, metres to tens of metres thick, of slumped siltstone with pervasive soft-sediment deformation. The base of the slumped interval at 790m (Fig. 3.12) is mapped as a sequence boundary by Dibona (1989), and is considered by him to be a correlate of the sequence boundary at the top of unit 7. A deep (sub-storm wavebase) environment on a rapidly subsiding outer shelf to slope is inferred. Diamictites and pebbly mudstones cropping out nearby at a somewhat higher stratigraphic level, within the lower part of the overlying Billy Springs Formation, were interpreted as glacigene by Dibona (1991) but have not yielded convincing diagnostic glacigene indicators (personal observation; Pell et al., 1993).

The Wonoka 'canyons' and associated facies

During Wonoka time, canyons up to 1 km deep were incised into the lower Wonoka and underlying formations at widespread localities, the erosion beginning from a level approximating the top of Unit 3 (Christie-Blick et al., 1990). These were originally interpreted as submarine canyons (Thomson, 1969; von der Borch et al., 1982; von der Borch et al., 1985); but more recent work has identified features of the sedimentary fill, such as HCS and oscillation ripples, that imply relatively shallow (above storm wavebase) environments (Eickhoff et al., 1988). A canyon fill at Umberatana Syncline is interpreted as predominantly shallow estuarine and fluvial by Christie-Blick (1993). Relative sealevel rise appears to have been sufficiently gradual for sedimentation to have kept pace for much of the filling of the canyons. Classical turbidites are here conspicuously absent: the succession is dominated by current-rippled calcareous siltstone, sandstone and conglomerate that is in places well-stratified and trough cross-bedded.

Because of folding, the canyons are exposed as many, disjunct cross-sections that are located mainly in the North and South Flinders Zones. Possibly as few as two meandering canyon systems can accommodate known canyon outcrops: one flowing NE, the other flowing SE (Haines, 1987). The canyons are evidence for a deep (>1km: oceanic?) basin to the east in Wonoka time.

Possible modes of origin of the canyons are comprehensively discussed by Christie-Blick et al. (1990). The base-level changes required to account for subaerial incision and shallow-water filling of the canyons are implausibly large for a simple eustatic control; likewise,

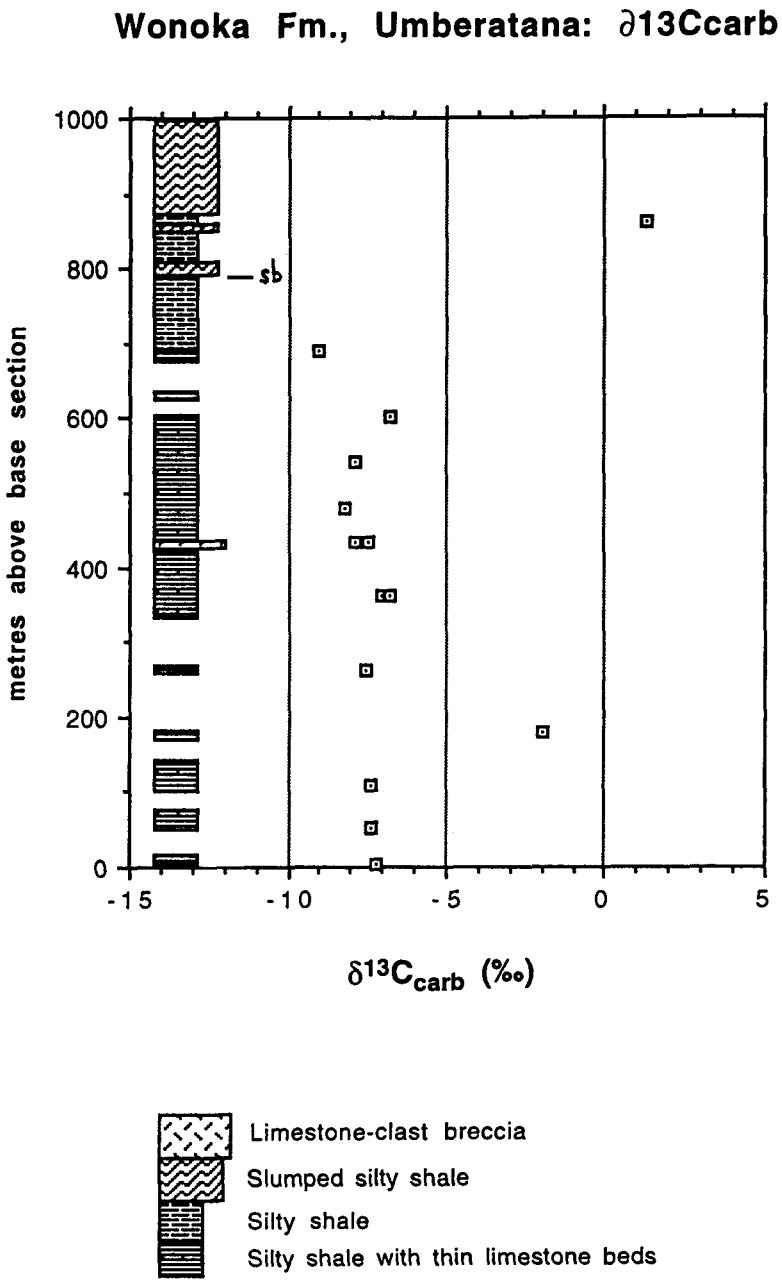

Fig. 3.12: Lithologic column and carbonate $\delta^{13}C$ data for part of Wonoka Formation at Old Station Creek, Umberatana Syncline. 'sb' = sequence boundary mapped by Dibona (1989) and correlated by him with Sequence Boundary 5 (= the top of Unit 7 at Bunyeroo Gorge).

tectonic movements of such magnitude and rapidity are improbable in the light of presently understood mechanisms of basin evolution. A Messinian-style evaporitic lowering of sealevel in an isolated basin (e.g. Hsü et al., 1973) is one favoured hypothesis, though not without its problems (von der Borch et al., 1989; Christie-Blick et al., 1990). Perhaps the most puzzling aspect of any hypothesis involving subaerial incision such as a Messinian-type event is the lack of evidence for subaerial exposure or erosion in the lower to middle Wonoka Formation at localities (such as Bunyeroo Gorge) away from immediate areas of canyon incision.

The first carbonate encountered in the canyon-fill section at Umberatana Syncline is a two metre-thick, brown-weathering silty fine-grained limestone unit 110 m above the base of the canyon-fill (section of Christie-Blick, 1993; his Fig. 15). This unit, sampled in this study, contains thin parallel-laminae, possibly of microbial origin, small slump folds, and rare, small (20mm), isolated domical-stromatolite-like structures. This unit is about 400m stratigraphically below the base of the measured section of Fig. 3.12.

The upper slopes of the canyon erosion surface in the Umberatana Syncline and other localities are in places mantled by a thin (0.5 - 5 m) veneer of cream-coloured, fine-grained, diffusely laminated limestone (the 'wall plaster': Eickhoff et al., 1988; von der Borch, 1993). The origin of this deposit is poorly understood. A subaerial origin, as calcrete or travertine (Eickhoff et al., 1988; von der Borch et al., 1989), and a subaqueous origin (von der Borch, 1993) have been proposed. Ten isotopic analyses by Eickhoff et al. (1988) of the 'wall plaster' and wall plaster-derived clasts from the canyon fill show depleted compositions ($\delta^{13}C_{carb}$ -7 to -10 ‰; $\delta^{18}O$ -14 to -16 ‰) like those expected of a travertine or tufa but also very similar to typical unit 3 and 4 carbonates of the Wonoka Formation (see below).

A lithologically different (but possibly laterally correlative) carbonate unit mantles higher parts of canyon interfluves in the Mt Goddard area ('Burr Well Member' of Dibona, 1989). This unit, in some places resting upon Bunyeroo Formation, in others on unit 3 of the Wonoka Formation, is a metre-thick brown-weathering dolostone locally with pseudomorphs after evaporites and tepee structures (von der Borch et al., 1989; Christie-Blick et al., 1990). On the basis of these features, subaerial exposure on the canyon shoulders is inferred by these authors.

A second horizon characterised by incised valleys up to 200 m deep in the northern Flinders Ranges corresponds to the sequence boundary at the top of unit 7 (Dibona, 1989). These less well-known valleys may be associated with a second basin desiccation event (Christie-Blick et al., 1990).

3.6b ISOTOPE STRATIGRAPHY

Dolostones of unit 1, like the similar Nuccaleena Formation, display a somewhat depleted , decreasing-upward $\delta^{13}C_{carb}$ signature (-0.7 to -3.5 ‰, over 1.6 m, at Bunyeroo Gorge). Determinations from First Hill and SCYW1a fall within this range. $\delta^{18}O$ in unit 1 is -7.2 ± 0.8 ‰ (n = 6), with no covariance with $\delta^{13}C_{carb}$. One trace - element analysis gives the rather high Mn/Sr ratio of 46 (Table 3.2).

Limestones of Units 3 to 7 at Bunyeroo Gorge and First Hill display a remarkably smooth, generally upward-increasing pattern of change in $\delta^{13}C_{carb}$, from -11 ‰ at the base of unit 3 to -5 ‰ at the top of unit 7 (Figs. 3.10, 3.11). There is an extended interval of almost constant values (approximately -7.5 ‰) from low in unit 4 to the base of unit 7. At about the top of unit 7, there is a steep increase to variable values of -4 to -1 ‰ in units 8 and 9, and a further increase to a spread of -2 to +2.5 ‰ in unit 11.

Samples selected for analysis were generally limestones that appeared purest and finest-grained, but other limestone types (e.g. silty, stylonodular, calcarenaceous) do not deviate significantly from the trend. Relatively pure and impure (muddy) limestone samples from the base and top of a single thin bed in Unit 4 have essentially identical isotopic compositions; likewise the centre and rim of a concretion in unit 3.

Stratigraphic variation in $\delta^{18}O$ is somewhat similar, with the most depleted values (-15‰) at the base of unit 3, but with a maximum of -10‰ in the middle of unit 7. A large spread of values, with a maximum of -4.5 ‰, is seen in Unit 11.

At Umberatana Syncline, $\delta^{13}C_{carb}$ exhibits a prolonged, slightly declining trend (-7 to -9 ‰) before rising to 1 ‰ in the uppermost sample (Fig. 3.12). Oxygen, at around -15 ‰, probably reflects exchange with porewaters at high temperature. A considerably higher thermal grade is present in the northern than in the central Flinders Ranges (McKirdy et al., 1975). The lowest limestone unit within the canyon fill, described above, has $\delta^{13}C_{carb}$ = -6.7 ‰, $\delta^{18}O$ = -13.1 ‰.

A sample collected from the 'Burr Well Member' near Angepena is also isotopically depleted ($\delta^{13}C_{carb}$ = -7.8 ‰, $\delta^{18}O$ = -10.4 ‰).

Urlwin et al. (1993) documented $\delta^{13}C_{carb}$ stratigraphic profiles from four widespread sections through the Wonoka Formation. All four profiles show broadly similar features to those described above: most significantly, the extended interval at -7 to -8‰ through the lower and middle part of the formation and the onset of heavier, variable values at approximately the base of unit 8.

sample	Unit	rocktype	Sr(ppm)	Mn(ppm)	Mn/Sr	87Sr/86Sr	∂13C	∂18O	Rb(ppm)	87/86Srinit
Bunyeroo Gorge										
5.16c	Unit 1	dolostone	76	3506	46.1		-1.4	-5.9		
5.23	Unit 3	limestone	172	2200	12.8		-10.1	-14.6		
5.29	Unit 3	limestone	194	1744	9.0		-8.6	-13.9		
5.31	Unit 3	limestone	240	940	3.9		-8.3	-13.9		
5.35	Unit 4	limestone	295	884	3.0		-8.0	-13.2		
5.33b	Unit 4	limestone	246	691	2.8		-8.0	-13.5		
5.36	Unit 4	limestone	577	661	1.1	0.70910	-7.5	-13.1		
5.38	Unit 4	limestone	448	572	1.3		-7.6	-12.7		
5.39	Unit 5	limestone	494	418	0.8		-7.5	-12.7		
5.41	Unit 5	limestone	717	386	0.5	0.70888	-7.5	-12.7		
5.44	Unit 5	limestone	921	577	0.6	0.70868	-7.7	-12.6	0.091	0.70868
5.50	Unit 7	limestone	696	871	1.3		-7.1	-12.2		
5.52	Unit 7	limestone	1420	344	0.2	0.70876	-6.4	-10.2		
5.54	Unit 7	limestone	1064	449	0.4	0.70899	-6.3	-10.3		
5.55	Unit 7	limestone	799	681	0.9					
5.56	Unit 7	limestone	320	559	1.7		-6.0	-9.9		
5.60	Unit 8	limestone	520	1288	2.5		-1.8	-11.2		
6.02	Unit 8	limestone	234	1893	8.1		-2.8	-11.8		
6.05	Unit 11	limestone	259	891	3.4		0.2	-11.2		
6.11	Unit 11	limestone	96	845	8.8		0.7	-4.5		
6.12	Unit 11	limestone	429	269	0.6	0.70901	2.4	-4.7		
6.13	Unit 11	dolostone	115	1609	14.0		-2.0	-4.4		
Brachina Gorge										
7.19	Unit 11	limestone	847	149	0.2	0.70874	2.7	-5.9	0.063	0.70874
7.20	Unit 11	limestone	373	357	1.0		1.4	-5.5		
7.21	Unit 11	limestone	664	612	0.9	0.70888	2.3	-7.0		
7.23	Bonney Fm.	dolostone	58	4402	75.9		0.9	-3.5		
First Hill										
8.05/2	Unit 3	limestone	135	2190	16.2		-9.8	-13.4		
8.10	Unit 3/4	limestone	208	694	3.3		-8.0	-12.9		
8.14	Unit 3/4	limestone	317	961	3.0		-7.7	-13.2		
8.18	Unit 3/4	limestone	325	518	1.6		-7.5	-12.7		
8.35	Unit 7	limestone	1161	451	0.4	0.70876	-6.5	-10.4		
8.36	Unit 7	limestone	763	759	1.0					
8.37	Unit 7	limestone	835	644	0.8					
8.38	Unit 7	limestone	1029	526	0.5	0.70883	-5.4	-10.1		
Umberatana										
10.07		limestone	968	1508	1.6		-8.2	-15.1		
10.15		limestone	1307	664	0.5	0.71103	-6.8	-15.7		
10.22		limestone	1138	592	0.5	0.71571	1.3	-14.9		
10.30		limestone	381	411	1.1	0.71111	-2.0	-4.1		
10.35		limestone	608	959	1.6		-7.3	-15.0		

Table 3.2: Trace-element and strontium isotopic data, Wonoka Formation.

The Mn/Sr ratio varies in a roughly inverse manner to stable isotope composition in Units 3 to 7 (Figs. 3.10, 3.11). Highest Mn/Sr values, of 12 or more, are seen near the base of Unit 3, and decrease rapidly to less than 2 through most of units 4, 5 and 6. Very low values (0.2 to 0.4) are seen in the middle of Unit 7, mirroring the $\delta^{18}O$ peak. Within unit 11, Mn/Sr is variable but again varies inversely with $\delta^{13}C_{carb}$ (Fig. 3.15).

Ten $^{87}Sr/^{86}Sr$ determinations from the Wonoka Formation at Bunyeroo Gorge and First Hill show a minimum of 0.70868 in unit 5 (sample 5.44, Table 3.2); but the oxygen isotopic composition of this sample (-12.6 ‰) is considerably lower than that usually associated with near-primary $^{87}Sr/^{86}Sr$ ratios (cf. Derry et al., 1992). Several samples with heavier $\delta^{18}O$ from the middle of unit 7 were analysed; minimum determinations of 0.70876 were obtained from both Bunyeroo Gorge and First Hill. A very similar value (0.70874) is the lowest obtained from unit 11, from the sample with lowest Mn/Sr and highest $\delta^{13}C_{carb}$ for this unit.

Three $^{87}Sr/^{86}Sr$ determinations from the Umberatana Syncline section show, like $\delta^{18}O$, evidence for considerable diagenetic alteration, ranging from 0.711 to 0.716 (Table 3.2).

Organic carbon isotope profiles are shown for the Bunyeroo Gorge and First Hill sections (Figs. 3.13, 3.14) and the correlate of Units 1 and 2 in SCYW1a (Fig. 3.6). TOC is very low (0.2 - 0.5 mg/g) except for dark limestones in Unit 11. Most of the formation, up to the base of Unit 7, is characterized by ^{13}C-enriched organic carbon (-23 to -25 ‰) relative to older and younger strata. Within and above Unit 7 there are two negative $\delta^{13}C_{org}$ excursions, but the extent and stratigraphic position of the upper excursion are somewhat different at Bunyeroo Gorge and First Hill (Figs. 3.13, 3.14). There is no hint of parallelism with the carbonate carbon profiles; indeed there is a broad inverse relationship with relatively heavy organic carbon in the Unit 3 to 7 interval.

Disseminated pyrite from five samples from Units 5, 7 and 11 at Bunyeroo Gorge has $\delta^{34}S$ of -21 ± 4 ‰. Thin sections show the pyrite to be framboids a few microns in size; an early diagenetic origin is inferred (Berner, 1970; Raiswell, 1982). Disseminated gypsum from one sample from Unit 5 has $\delta^{34}S$ of +9 ‰ (pyrite in the same sample is -19.6 ‰).

3.6c Interpretation: the Dilemma of Low $\delta^{13}C_{carb}$ in the Wonoka Formation

The central problem in the stable isotope geochemistry of the Wonoka Formation is the cause of the marked ^{13}C-depletion in carbonates of Units 3 to 7. The predominant isotopic compositions are significantly lighter than what are generally considered normal marine values (i.e. greater than about -5 ‰: Summons & Hayes, 1992; and see Chapter 1). This problem also has a bearing on the origin of other, less well-known

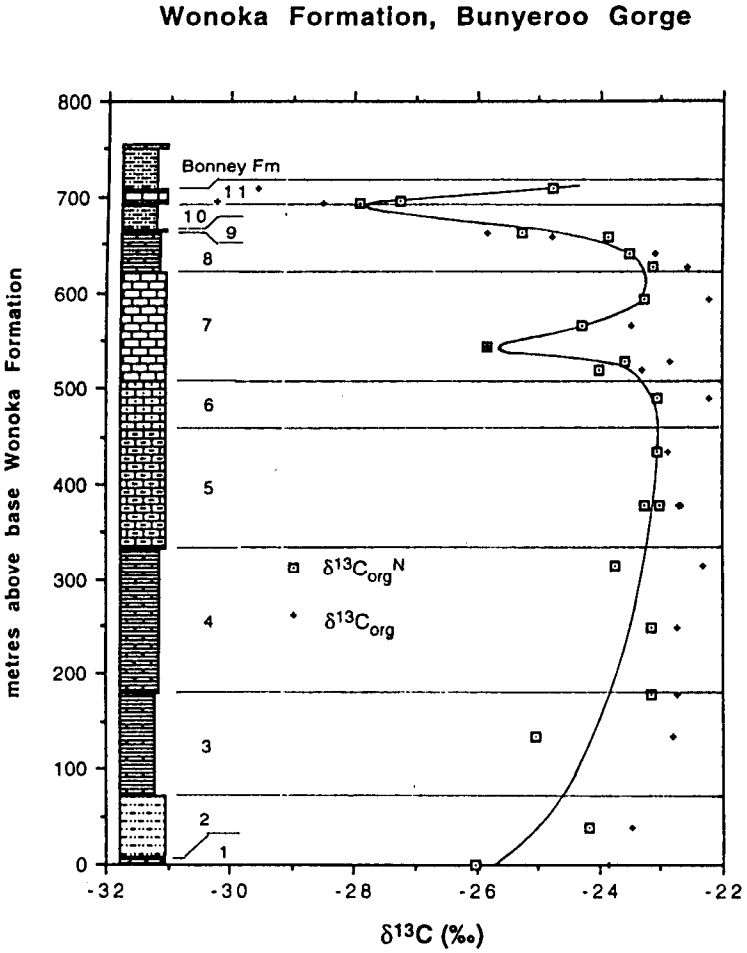

Fig. 3.13: Lithologic column and organic $\delta^{13}C$ data for the Wonoka Formation at Bunyeroo Gorge.

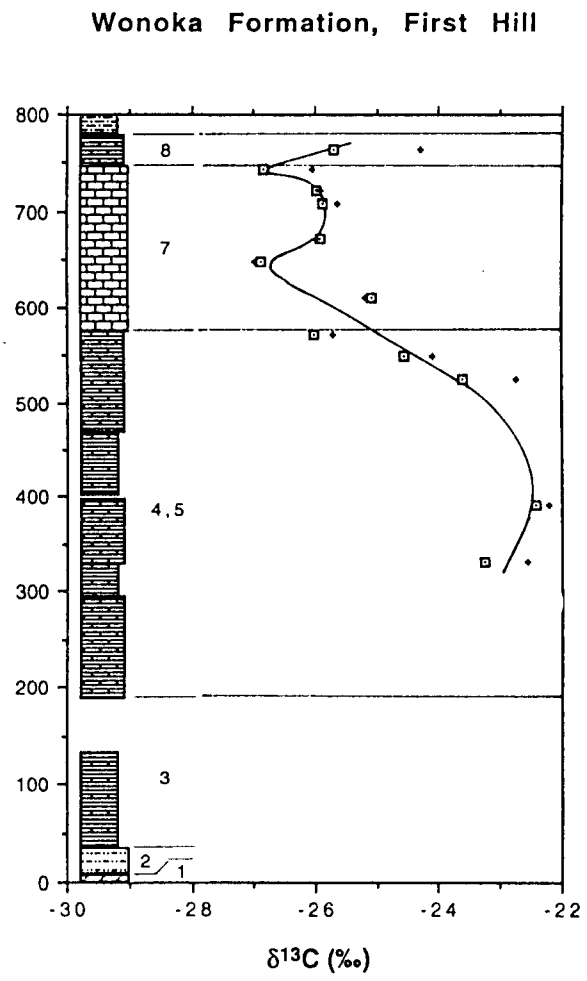

Fig. 3.14: Lithologic column and organic $\delta^{13}C$ data for the Wonoka Formation at First Hill.

^{13}C-depleted carbonates in the Officer Basin and Amadeus Basin, and is therefore treated at some length below.

Urlwin et al. (1993) and Pell et al. (1993) regarded the signal as primary and noted that the negative excursion appears to be a basinwide phenomenon. Pell et al. (1993, p. 159) suggest that the prominent negative excursion reflects recycling of organic matter from primary producers in an oxic water column, but this is not an adequate explanation in view of the absence of parallel depletion in $\delta^{13}C_{org}$ documented here and the magnitude and apparent longevity of the excursion. Internal cycling (fixing and remineralization) of carbon in a well-mixed water column should cause little, if any, net effect on $\delta^{13}C_{DIC}$.

Unit 1

Textural evidence previously mentioned suggests the dolostone of Unit 1 is primary or very early diagenetic, and retention of essentially primary $\delta^{13}C_{carb}$ is likely in spite of high Mn/Sr, bearing in mind that this ratio is inherently high in dolostones (Chapter 2). There is a sedimentological and isotopic similarity of Unit 1 with the Nuccaleena Formation, and there is a similar dilemma in palaeoenvironmental interpretation: Unit 1 was either a littoral deposit (Gostin & Jenkins, 1983) with an isotopic composition reflecting that of shallow marine waters; or a sediment-starved outer shelf deposit (Haines, 1990) with an isotopic composition possibly influenced by ^{13}C-depleted , basinal hypersaline waters. The deep-water alternative is favoured here because there is no compelling evidence for subaerial exposure, and there is no evidence for shallow - water deposition in the enclosing succession. Like the Nuccaleena Formation and Units 3 - 7 in the Wonoka Formation, $\Delta\delta$ is low (20 to 22 ‰), one possible explanation being equilibration of carbonate with the ^{13}C-depleted lower layer of a stratified water body and an origin for organic carbon in pelagic rainout from the upper layer (see discussion below).

Units 3 - 7

Any hypothesis to explain the unusual ^{13}C depletion in the carbonates of Units 3 - 7 must also account for the strong negative excursion in $\delta^{18}O$; the basinwide distribution, apparent synchroneity, and unusual smoothness of the profiles; the presence of apparently-marine $^{87}Sr/^{86}Sr$; and the absence of parallel depletion in $\delta^{13}C_{org}$. Two contending hypotheses are assessed here: (i) that $\delta^{13}C_{carb}$ has been diagenetically altered; or (ii) that $\delta^{13}C_{carb}$ is a primary signature representing equilibration with the bottom waters of a stratified marine body. A third possibility, that basin waters were non-marine, is discounted because of the low

$^{87}Sr/^{86}Sr$, the presence of francolite and glauconite in the succession, and evidence - from the relief of the canyons - for a very large (at least 1 km deep) basin of deposition.

Diagenetic alteration of $\delta^{13}C_{carb}$

Ooid preservation in Unit 11 suggests an original aragonite mineralogy. High Sr contents in Unit 7 (up to 1480 ppm) as well as in Unit 11 (see Table 3.2) may indicate that primary aragonite was predominant throughout this interval, although the Sr contents are nowhere high enough to compellingly suggest an aragonite precursor (i.e. 2000-4000 ppm: Brand & Veizer, 1980).

Deep-water carbonate sediments are buried with marine porewaters with which they are in equilibrium (Choquette & James, 1990). Unlike most shallow-water carbonates, diagenetic stabilization is delayed until pressure and temperature rise with substantial burial (Veizer, 1989; Gieskes et al., 1986). Thus, if sediments are not exposed early to meteoric fluids, aragonite need not be stabilized to calcite until burial to several km (e.g. Tucker, 1986b) or until exposure to meteoric waters during much later uplift (e.g. Fairchild et al., 1990). Delayed diagenetic stabilization may therefore conceivably be responsible for an altered isotopic signature for the deeper-water carbonates (Units 3-7) in contrast to a near-primary, 'normal' marine signature for the shallow-water units (9 and 11).

A 'smoothing' overprint of the original $^{87}Sr/^{86}Sr$ isotopic signal has been documented in ocean-floor sediments (Geiskes et al., 1986; Veizer, 1989). The recrystallization front, at a depth of some hundreds of metres, slowly migrates upwards through the sediment pile with continued subsidence, bringing about diagenetic stabilization through dissolution-reprecipitation. Chemical species entering the solution at this front migrate downgradient, both upwards towards the sediment-water interface and downwards into the sediment; there to be reprecipitated as cements into porespace. The resultant smoothing effect may have an analogue in the $\delta^{18}O$ and $\delta^{13}C_{carb}$ profiles in Units 3 to 7. Data are insufficient to judge whether $^{87}Sr/^{86}Sr$ has been similarly smoothed.

With a normal geothermal gradient, $\delta^{18}O$ of neomorphosing carbonate minerals typically decreases by 5 ‰ per kilometre depth of burial (Algeo et al., 1992). Using this estimate, $\delta^{18}O$ in Units 3 to 7 reflect recrystallization at depths of 2 to 3 km.

However, finding a sufficient source of ^{13}C-depleted carbonate in the diagenetic environment is a serious problem with any hypothesis involving substantial deep-burial shifts in $\delta^{13}C_{carb}$. Assuming the carbonates were deposited with 'normal' middle Ediacarian $\delta^{13}C_{carb}$ of 0 to +5 ‰ (Chapters 1, 6), then a simple mass-balance calculation indicates that a quarter to a third of

the present volume of the limestones must have been replaced by, or added as, organogenic carbonate (-30 to -35 ‰) to give the observed bulk $\delta^{13}C_{carb}$ of -8 ‰ of the interval under consideration. Diagenetic evolution of substantial amounts of ^{13}C-depleted, organogenic carbonate, through sulphate reduction or thermal decarboxylation, is considered unlikely in view of the very organic-poor nature of the Wonoka and enclosing formations. The Wonoka Formation is not pyrite-rich except for some horizons in the Umberatana section. In modern marine sediments there is always a residue of presumably unusable organic carbon that passes through the zone of sulphate reduction to be incorporated eventually into sedimentary rocks (Goldhaber & Kaplan, 1974; Holser et al., 1988). TOC's of the Wonoka Formation are only 0.23 ± 0.15 mg/g ($n = 38$); bulk organic carbon content is thus two to three orders of magnitude lower than carbonate carbon. By comparison, large (10 ‰) negative shifts in $\delta^{13}C_{carb}$ accompanying burial recrystallization of dolomite in the organic-rich Monterey Formation, California, are attributed to a porewater $\delta^{13}C$ chemistry dominated by thermal decarboxylation of organic matter; in these sediments the bulk organic carbon content is three times higher than carbonate carbon (Malone et al., 1994). There is none of the marked, small-scale variation in $\delta^{13}C_{carb}$ associated with evolution of porewaters rich in organic-derived CO_2 (Irwin et al., 1977).

Exposure of Units 3-7 to deeply-circulating meteoric waters may have occurred during the proposed second 'Messinian-style' sealevel drawdown corresponding to the sequence boundary at the top of Unit 7 (Christie-Blick et al., 1990). While the observed ^{18}O depletion may be arguably partly or wholly of meteoric origin, $\delta^{13}C_{carb}$ is most unlikely to have been significantly affected because of the lack of organic matter within the sediment and the likely insignificance of soil-derived, ^{13}C-depleted CO_2. Meteoric depletion of $\delta^{13}C_{carb}$ below an exposure surface has been proposed in a Proterozoic setting, albeit controversially (Beeunas & Knauth, 1985; Vahrenkamp & Rossinsky, 1987) but even below well-developed Phanerozoic soil profiles shifts in bulk-rock $\delta^{13}C_{carb}$ are small and stratigraphically restricted compared to the negative excursion in the Wonoka Formation (cf. Allen & Matthews, 1982). Fairchild et al. (1990) proposed that negative shifts of 3 to 4 ‰ in $\delta^{13}C_{carb}$ occurred in a Neoproterozoic carbonate during open-system diagenesis associated with deep circulation of meteoric fluids, but the source of ^{12}C is unclear.

Textural and geochemical indicators do not fit well with a large diagenetic change in $\delta^{13}C_{carb}$. There is frequent evidence for early lithification of carbonate in Units 3-7 (irregular erosion surfaces, intraclasts). The bulk of the carbonate thus appears to be of depositional or syndepositional origin. Bulk-rock $\delta^{13}C_{carb}$ should therefore be buffered to near-marine values during subsequent diagenetic stabilization or recrystallization events (Marshall, 1992). The

fine, microsparitic grainsize of the carbonates and the low permeability that may be inferred for the enclosing shales, argues against a very open-system diagenetic alteration of $\delta^{13}C_{carb}$ that is required by the magnitude of the depletion and the smoothness of the profile.

By contrast, oxygen isotopic compositions, because of the much greater reservoir of exchangeable oxygen than carbon in porewaters, can be readily altered (at water-rock ratios ca. 10^3 times less than required to alter $\delta^{13}C_{carb}$: Banner & Hanson, 1990). It is perhaps significant that the $\delta^{18}O$ profile does appear broadly related to effective water-rock ratio, covarying with carbonate content: highest values are seen in the middle of Unit 7, richest in carbonate; lowest values in relatively carbonate-poor Unit 3; and a negative excursion is seen in sandy Unit 6 in the Bunyeroo Gorge section (Figs. 3.10, 3.11).

Ratios of Mn/Sr in units 4-7 at Bunyeroo Gorge (Fig. 3.10) and First Hill are nearly all below 2, well below the ratio of 10 considered by Derry et al. (1992) and Kaufman & Knoll (1995) to be the maximum for Neoproterozoic carbonates unaltered with respect to $\delta^{13}C_{carb}$. In Unit 3, initially much higher Mn/Sr values decrease upward, in a close, inverse correspondence with $\delta^{13}C_{carb}$ (Figs. 3.10, 3.11). This close inverse covariance suggests that the very ^{13}C-depleted (-11 to -8‰) composition of Unit 3 may be a partial diagenetic overprint on values originally like Units 4-6 (-7 to -8‰) (cf. Marshall, 1992). A particular vulnerability of Unit 3 to burial-diagenetic change in isotopic and trace-element composition may be expected because of its low bulk proportion of carbonate (<10%) and hence high effective water-rock ratio.

Lowest (least-altered) $^{87}Sr/^{86}Sr$ ratios (coinciding with lowest Mn/Sr : Fig. 3.15; Table 3.2) are essentially identical (~0.7087) in Units 5, 7 and 11 and fall within the range of little-altered marine Ediacarian $^{87}Sr/^{86}Sr$ (Kaufman et al., 1993; and see section 6.3b). Since $^{87}Sr/^{86}Sr$ is, in general, more susceptible than $\delta^{13}C_{carb}$ to equilibration with diagenetic fluids (Banner & Hanson, 1990), this is a further powerful argument for an interpretation of $\delta^{13}C_{carb}$ as near-primary in Units 4-7.

Various independent textural and geochemical criteria thus point to values of -8 to -6 ‰ being an essentially primary $\delta^{13}C_{carb}$ signature for Units 3-7. However, deep - burial neomorphism - possibly involving aragonite-calcite transformation - is indicated by $\delta^{18}O$ which reflects equilibration with high-temperature porewaters, possibly partly rock-buffered in carbonate-rich Unit 7. Unit 7 retains apparently marine $^{87}Sr/^{86}Sr$. $\delta^{13}C_{carb}$ may, like $\delta^{18}O$, have been subjected to a burial diagenetic 'smoothing' overprint, but a large negative diagenetic shift in bulk-rock $\delta^{13}C_{carb}$ is considered untenable for the reasons outlined above.

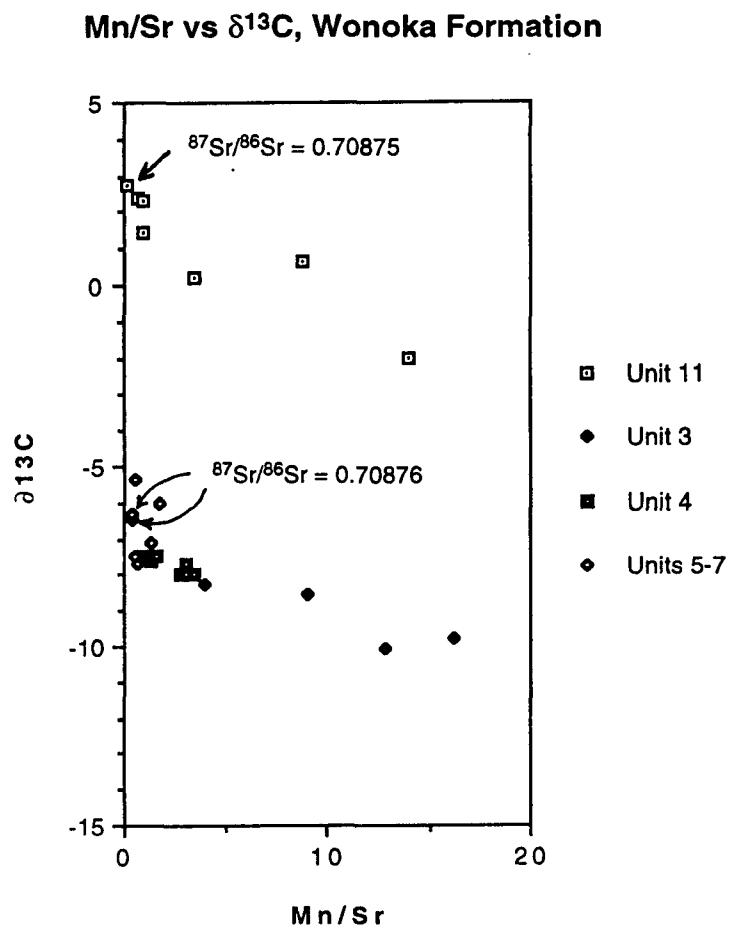

Fig. 3.15: Mn/Sr versus $\delta^{13}C_{carb}$, Wonoka Formation. $^{87}Sr/^{86}Sr$ indicated for least-altered samples (identified on the basis of high $\delta^{18}O$, low Mn/Sr and low $^{87}Sr/^{86}Sr$). Points fall into two distinct groupings separated by about 9 ‰ in $\delta^{13}C_{carb}$, interpreted to represent deposition under the lower layer of a stratified water body (Units 3 to 7) and the upper or mixed layer (Unit 11).

Stratification of the water body

The presence of dispersed gypsum crystals in unit 4 and 5 - in facies of undoubted, relatively deep-water origin (Haines, 1990) - indicates that a regime of salinity stratification in a restricted marine basin may have been operative. Von der Borch et al. (1989, p. 791) foreshadowed an evaporative origin for the carbonate in the Wonoka Formation in the context of a Messinian-type basin desiccation scenario for canyon incision. On sedimentological evidence, Haines (1990) suggested that the bulk of the carbonate in Units 5-7 originated by inorganic precipitation from the overlying water column.

The sulphur isotopic composition of the gypsum (+9 ‰, one determination) is lower than marine sulphates from other early to middle Ediacarian successions analysed in this study (+20 to +25 ‰, see Chapter 6) but considerably higher than pyrite in the Wonoka Formation (-21 ± 4 ‰) and pyrite in the same sample from which the gypsum was extracted (-19.6 ‰).

The gypsum is probably predominantly marine but partly derived from diagenetic oxidation of pyrite. An origin entirely derived from inorganic diagenetic oxidation of pyrite (Bain, 1990) is precluded by the considerable difference in $\delta^{34}S$ between the pyrite and gypsum.

In general, salinity stratification with a marine hypersaline lower water mass requires a silled basin in which evaporation exceeds total freshwater inflow (Scruton, 1953). Stratification develops by sinking of dense, saline surface or shelf water. Such conditions may be common in low-latitude, narrow nascent ocean basins, for example the Cretaceous Angola-Brazil basin (Arthur & Natland, 1979) and the Pleistocene Red Sea (Freidman, 1972). Photosynthetic fixation of carbon takes place mostly in the upper water layer, and sinking particulate organic matter is decomposed to contribute depleted carbon to the dissolved inorganic carbon (DIC) pool of the lower water mass: the so-called 'photic pump effect' (Kroopnick, 1985; Berger & Vincent, 1986), resulting in differentiation in $\delta^{13}C_{DIC}$ between lower and upper water masses. The density gradient between the lower water mass at gypsum saturation and surface water more closely approximating normal salinity would have been sufficiently high to ensure that vertical transport of ions within the pycnocline was extremely slow (cf. Broecker & Peng, 1982, p.327; Sarmiento et al., 1976; and below).

The mechanism of carbonate precipitation is an important consideration. Evaporative precipitation of carbonate in the upper layer is a possible source of relatively ^{13}C-enriched carbonate sediment, but the model would require equilibration with ^{13}C-depleted DIC in the lower layer, perhaps through syndepositional diagenetic stabilisation (dissolution - reprecipitation); or alternatively admixture with a (relatively constant) proportion of strongly ^{13}C-depleted carbonate originating in the lower water mass. The lower water mass was probably suboxic or anoxic (see below) and carbonate precipitation may have been engendered by raised DIC as a result of remineralization of organic matter. In the absence of dissolved O_2, Mn^{4+}, nitrate, Fe^{3+} and sulphate - in that order - are utilised as oxidising agents by heterotrophic bacteria (e.g. Anderson & Arthur, 1983). Manganese and nitrate reduction are important only in pelagic or non-marine environments with a low sedimentation rate (Coleman, 1985). Iron reduction raises pH while liberating HCO_3^- and thus strongly favours carbonate precipitation (Curtis, 1977; Coleman, 1985):

$$4Fe_2O_3 + 2CH_2O + 14H^+ \rightarrow 8Fe^{2+} + 2HCO_3^- + 8H_2O$$

However, iron reduction is slow and Fe^{3+} tends to survive metastably in sediments, in part because of its insolubility (Coleman, 1985); and therefore iron reduction is unlikely to be significant in the water column. Indeed low pyrite in the Wonoka Formation suggests that iron in the water column was limited. The world oceans as a whole were probably aerobic by

the Ediacarian and hence low in Fe^{2+}. In this case sulphate reduction can raise HCO_3^- with a neutral effect on pH:

$$SO_4^{2-} + 2CH_2O \rightarrow H_2S + 2HCO_3^-$$

and thus some carbonate may be precipitated (Goldhaber & Kaplan, 1974; Coleman, 1985). Oxidation of the resultant H_2S at the base of the oxic, upper layer (plausibly by sulphur-oxidising bacteria) - will tend to lower pH:

$$H_2S + O_2 \rightarrow SO_4^{2-} + 2H^+$$

which would tend to inhibit carbonate precipitation and sedimentation from the upper layer. The relative significance of evaporative precipitation (and later re-equilibration in the lower layer), iron reduction and sulphate reduction in sourcing the carbonate in Units 3 - 7 is difficult to evaluate.

Organic carbon isotopic compositions do not show unusual depletion in parallel with $\delta^{13}C_{carb}$ because most organic carbon was fixed in the upper water layer with $\delta^{13}C_{DIC}$ that was close to that of open oceanic surface waters and buffered by interchange with atmospheric CO_2 (see below). Strontium isotopes are not fractionated by biological processes, and so retained essentially the same ratio in the lower water mass (represented by results from units 5 and 7) as in the surface layer (unit 11).

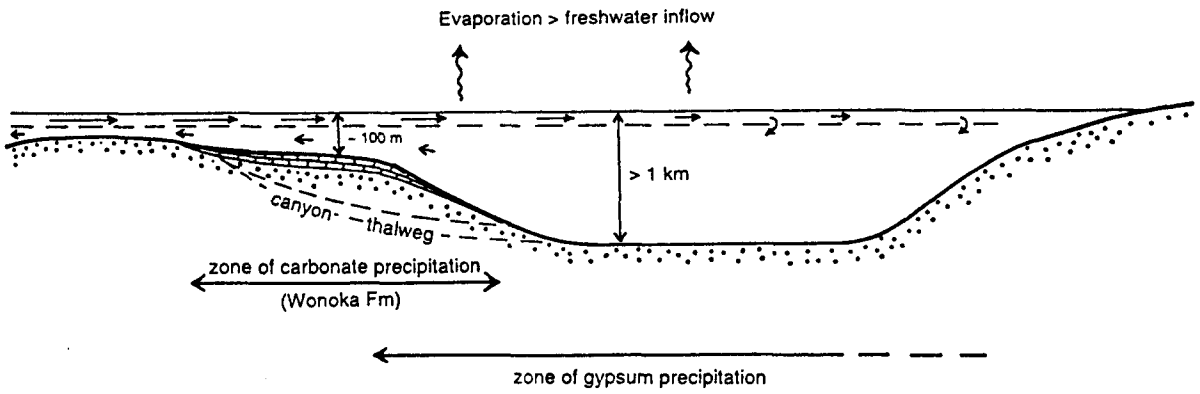

Fig. 3.16: Stratified, evaporative basin model for the deposition of the Wonoka Formation.

There was no overall evolution towards more extreme evaporative conditions throughout the negative $\delta^{13}C_{carb}$ excursion of Units 3-7 (except perhaps for a relatively brief drying up and refilling of the basin associated with canyon incision). Hence two-way exchange across the sill must be inferred, resulting in an areally zoned distribution of evaporite minerals in the basin of deposition, with carbonate in a broad zone closest the ocean connection and more soluble minerals progressively further away (Scruton, 1953). Fig. 3.16 is a hypothetical simple model for a salinity-stratified basin of deposition for the Wonoka Formation. Minimum depth of the basin (1 km) is provided by maximum topographic relief of the canyons. Depth of the pycnocline would have been considerably less than shelf depth (ca. 100 m). Thus the lower water mass must have been considerably more voluminous (at least an order of magnitude, depending also on relative area of deep basin and shelf) than the upper layer. The relatively very large mass and long residence time of the lower water body would have acted to dampen short-term environmental influences on water chemistry, resulting in constant or very slowly changing $\delta^{13}C_{DIC}$ in the lower water layer. This may, at least in part, explain the unusual smoothness of the $\delta^{13}C_{carb}$ profile.

Some quantitative constraints

Some of the fluxes in a simple two-box model of the basin can be roughly estimated assuming seawater composition was similar to today's, to give some semi-quantitative support for the feasibility of the proposed model.

Evaporation excess in modern marginal marine seas such as the Mediterranean, the Red Sea, and the Gulf of California is 0.75 - 2.1 m/yr (Bray, 1988; Friedman & Sanders, 1978). Assuming an evaporation excess of 1 m / yr for the Wonoka basin, a residence time for water in the surface layer of ca. 40 yr is obtained assuming a thickness of 50 m and evaporation to the point of gypsum saturation (i.e. evaporation of 80% of the water). The carbon isotopic replacement time of surface waters by air - sea exchange is presently somewhat shorter (ca. 15 yr: Broecker & Peng, 1982, p. 307) so $\delta^{13}C_{DIC}$ of surface waters would have been buffered to a large extent (but perhaps not fully buffered) by exchange with atmospheric CO_2. During the residence time of water in the upper layer, the model requires (by mass-balance) export of roughly a third of DIC to the lower layer as particulate organic matter where it is nearly all decomposed to release ^{13}C-depleted DIC. It is assumed that essentially all primary productivity is confined to the surface water layer, as in some modern meromictic lakes (e.g. Takahashi et al., 1968). If DIC concentration were similar to today's (28 g/m^3), the required export flux is 12 g/m^2/yr ($\frac{1}{3} \times 28 \times \frac{50}{40}$). Primary productivity would have been much higher since in modern oceans a proportion (70 - 80%) of organic matter is remineralised within the

surface layer (Hargrave, 1972; Wollast, 1983), and this proportion may have been higher in the Precambrian (see below). The required primary productivity using the modern proportion, 40 - 60 $g/m^2/yr$, is nevertheless moderate compared to modern shelfal (164 $g/m^2/yr$) and oceanic (57 $g/m^2/yr$) primary productivities (Tyson & Pearson, 1991).

Assuming that the lower layer approached saturation with respect to gypsum and thus a density of 1.126, and assuming a shelf depth of ca. 100 m, the average vertical density gradient for the water column over the shelf was ca. 8×10^{-4} g/cm^4. Density gradient would have been inhomogeneous, however; probably negligible in the upper layer and at a maximum in the pycnocline. This figure therefore gives a minimum density gradient within the pycnocline, and corresponds to a coefficient of vertical diffusivity, k, approaching that of molecular diffusion (10^{-5} cm^2/sec) (Broecker & Peng, 1982, p. 329). Upward diffusion of DIC across the pycnocline can be modelled by the relation

$$\text{Flux} = k.dc/dz$$

where dc/dz is the DIC concentration gradient. Assuming a five-fold evaporative concentration of DIC to give gypsum saturation in the lower layer (this is a generous maximum since some carbonate would be precipitated), it can be shown that molecular diffusion need be restricted to a layer only 2 m thick to retard upward flux of DIC to a small proportion (ca. 10%) of the modelled downward flux of particulate organic carbon. This calculation, together with the modest levels of primary productivity required by the model as suggested above, means that the 'photic pump' effect need not have been unusually powerful to maintain the inferred $\delta^{13}C_{DIC}$ gradient.

The presence of wave-formed sedimentary structures in Units 4 - 7 appears at first sight to be inconsistent with a density-stratified water column. However, a corollary of the high density gradient within the pycnocline and lower layer is that shear velocities required to induce turbulent vertical transport were relatively high (cf. Quay et al., 1980, p. 212; Jewell, 1993), militating against storm - induced turbulent mixing of surface and deeper waters. A comparison with the model of Jewell (1993), describing the impact of storms on Cretaceous shelf seas with relatively weak (hyposaline over normal marine) density stratification, suggests that storm-induced mixing of the water column in the Wonoka basin was not significant. Studies of the effects of wind on stably stratified lakes (see Fischer et al., 1979) show that in cases of strong stratification (such as is proposed here for the Wonoka basin) the pycnocline and lower water layer are affected by internal waves or seiches but little or no mixing takes place (the pycnocline remains sharp). Sustained wind-induced seiching accompanied by maintenance of a sharp pycnocline has been observed in modern stratified

lakes (Heaps & Ramsbottom, 1966; Thorpe, 1974). By analogy with these observations, evidence for wave action in the Unit 5 - 7 interval (erosional scours, small - scale HCS, oscillation ripples) is here attributed to internal wave motion in which stratification was preserved. The trend to less depleted carbonates upward through Unit 7 may reflect weakening of stratification or increased incidence of storm-induced mixing accompanying the shallowing of depositional environment.

By analogy with modern oceans, an important control on the proportion of DIC photosynthetically fixed in the upper layer, and hence the degree of differentiation in $\delta^{13}C_{DIC}$ that developed between surface and deep water, was nutrient availability. For example, a given volume of modern Pacific deep ocean water contains sufficient nutrients to fix just 10% of DIC once it rises to the photic zone (Broecker & Peng, 1982). The stratified Wonoka basin model, however, requires fixation of about 30% of DIC. Some recycling of nutrients presumably occurred from decomposition of organic matter in the water column, and this recycling may have been more efficient in Precambrian seas than today's (Knoll et al., 1986; Logan et al., in press). Water-column stratification would have hindered efficient nutrient recycling, however, and a significant non-marine (fluvial and aeolian) nutrient source seems likely. Fine-grained siliciclastics throughout the Wonoka Formation attest to such a source. Fluvial nutrient concentrations could have been far higher in the Precambrian than after the development of a substantial terrestrial biomass (Tappan, 1986).

A strong pycnocline within the basin would probably have led to the surface water mass evolving a $\delta^{13}C_{DIC}$ somewhat higher than that of the open ocean, because photosynthesis-induced ^{13}C-enrichment of residual DIC would not have been mitigated by mixing with the lower water mass and perhaps only partly buffered by exchange with the atmosphere (see above). Unusually heavy $\delta^{13}C_{org}$ within the interval of depleted $\delta^{13}C_{carb}$ (units 3-7: $\delta^{13}C_{org}{}^{N}$ mainly -23 to -24 ‰; see Fig. 3.12) may be a reflection of this phenomenon.

Thus, $\Delta\delta$ in the Wonoka Formation is strongly bimodal, with very low values (15-20 ‰) representing the period of basin stratification (units 3-7) and 'normal' (25-30 ‰) values representing sedimentation entirely within a well-mixed, or upper water layer (Units 9-11) (Fig. 3.17).

Other considerations

The Wonoka Formation differs in one important respect from rocks deposited in known hypersaline basins: the lack of evidence for water column anoxia in the form of high TOC and pyrite. The much lower initial solubility of oxygen in hypersaline waters (Kinsman et al., 1973) means anoxia is virtually inescapable in the lower part of the water column in deep

hypersaline basins. Documented examples of deep, hypersaline basins - such as the Cretaceous Angola-Brazil basin (Arthur & Natland, 1979), the Pleistocene Red Sea (Freidman, 1972) and the early Messinian Mediterranean (McKenzie et al., 1979) are characterised by sediments with high organic carbon contents. The latter two examples are characterized by variably and strongly ^{13}C-depleted carbonates (eg. -3.5 to -22 ‰ in the early Messinian Tripoli Formation: McKenzie et al., 1979) that are thought to be derived from calcitization of gypsum, a process fuelled by large amounts of organic matter.

However, while a link between anoxia and high TOC is widely accepted (Demaison & Moore, 1980; Bralower & Thierstein, 1987) an opposing school of thought maintains that productivity is the major control on TOC (see Pedersen & Calvert, 1990; Calvert et al., 1991). Nitrate, Mn^{4+}, Fe^{3+} and sulphate are important marine oxidising agents, and sulphate is present in far greater molar proportion than dissolved oxygen even in oxygen-saturated water.

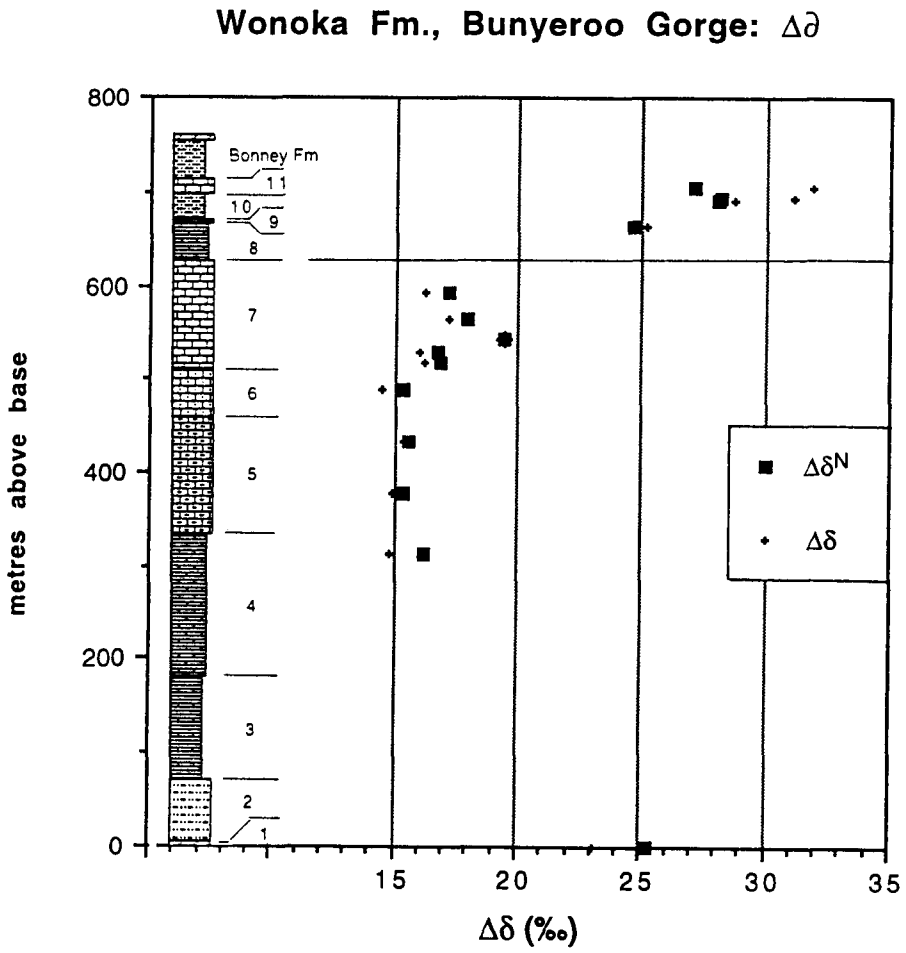

Fig. 3.17: Lithologic column, $\Delta\delta$ and $\Delta\delta^N$ data for the Wonoka Formation at Bunyeroo Gorge.

Remineralization by sulphate-reducing bacteria may be as complete and as rapid as oxic remineralization with the possible exception of refractory lignin-derived terrestrial organic matter (Pedersen & Calvert, 1990; Calvert & Pedersen, 1992, p. 247). The absence of significant terrestrial primary production may thus have been one important difference in Proterozoic carbon cycling. Another significant difference between Phanerozoic and Precambrian oceans was the lack of fecal-pellet packaging of pelagic particulate organic matter in the Precambrian. Smaller particle size would have led to slower sinking rates, in turn favouring more complete decomposition of organic matter in the water column (Knoll et al., 1986; Logan et al., in press).

The model is entirely consistent with the 'Messinian' basin desiccation hypothesis for the origin of the canyons, which requires the same conjunction of palaeogeographic and climatic factors (a silled basin in which evaporation exceeds freshwater inflow). However, the lack of lithological or isotope-stratigraphic evidence at Bunyeroo Gorge or First Hill for a $\delta^{13}C_{carb}$ discontinuity representing the desiccation event, remains puzzling. Conceivably, if the period of desiccation were geologically short, basin bathymetry and climate may have remained little changed to the extent that differentiation of basin waters was not significantly changed from that prior to desiccation. Possibly a burial-diagenetic 'smoothing' effect has obscured $\delta^{13}C_{carb}$ chemostratigraphic evidence for a break. A much closer sampling interval around the Unit 4 - 5 boundary may yet reveal chemostratigraphic evidence for a break. An abrupt step in $\delta^{13}C_{carb}$, or perhaps a short-lived 'spike' in the signal, might be expected to mark the sequence boundary.

The significance of the depleted isotopic compositions of the 'Burr Well Member' (locally mantling canyon interfluves) and the limestone from within the canyon-fill at Umberatana, in the context of the salinity-stratification hypothesis, is uncertain. Both have $\delta^{13}C_{carb}$ and $\delta^{18}O$ broadly similar to the unit 3 to 7 sample suite. Deposition in relatively deep (sub-pycnocline) depths may be the simplest interpretation. However, in the case of the 'Burr Well Member' and the (possibly-related) 'wall plaster', an origin as subaerial travertines fed by refluxing groundwater would also give a depleted stable isotopic composition.

The limestone within the canyon fill occurs in a succession of ripplemarked fine-grained calcareous sandstone and conglomerate, representing depositional environments probably too shallow to be below a marine pycnocline (Christie-Blick, 1993; pers. comm., 1994). However, carbonate accumulating in the estuarine setting proposed by Christie-Blick (1993) may have its origin in pre-existing carbonates transported to the basin as detritus or in

solution. Further study of the sedimentology and geochemistry of the canyon-fill limestones is clearly needed.

Other possible sources of sulphate and ^{12}C

A stratified basin with a ^{13}C-depleted lower water mass does not absolutely require an evaporative setting, as other sources of sulphate and ^{12}C may have been available in the Wonoka basin of deposition. Sedimentary diapirs are known to have breached the seafloor in Wonoka time; in particular, along the northern edge of the Central Flinders Zone (Forbes & Preiss, 1987, Fig. 87; Haines, 1987). The diapirs, presently largely composed of carbonate-cemented breccia, may have originally had a mobilised matrix of evaporite (Lemon, 1985) that led to gypsum saturation of bottom waters.

Diapirs and associated faults may have been pathways for migration of hydrocarbons, particularly methane, into the overlying water body. Biologically oxidised methane may have been a source of strongly ^{13}C-depleted DIC. Small volumes of botryoidal aragonite in North Sea 'pockmarks' (sites of methane outgassing) have $\delta^{13}C_{carb}$ as low as -56 ‰ (Hovland et al., 1987).

Metastable methane clathrates are an important reservoir of methane in modern polar and deep oceanic sediments (e.g. Kvenvolden, 1993), and it is conceivable that clathrates were involved in formation of the ^{13}C-depleted Wonoka carbonates (M. R. Walter, pers. comm.). Liberation of methane from clathrates may have occurred with sealevel fall (Messinian-type desiccation?) or warming but it is difficult to reconcile this mechanism with the apparent longevity of the negative excursion in $\delta^{13}C_{carb}$.

Even if one or more of these alternative sources were significant, a poorly-mixed or stratified water column is still required by low $\Delta\delta$ and marine $^{87}Sr/^{86}Sr$.

Conclusion

By the geochemical and textural criteria usually applied (e.g. Kaufman et al., 1993; Kaufman & Knoll, 1995, Derry et al., 1992), $\delta^{13}C_{carb}$ of units 4 to 7, at -8 to -6 ‰, should be little affected by post-depositional alteration; and there is in any case, as indicated above, a mass-balance problem in finding sufficient ^{12}C in the diagenetic environment to significantly alter $\delta^{13}C_{carb}$ of some hundreds of metres of limestone, in a succession so clearly deficient in organic matter. Burial-diagenetic neomorphism did cause moderate to strong depletion in ^{18}O and a smoothing of the $\delta^{18}O$ and, perhaps, $\delta^{13}C_{carb}$ profiles, but the bulk $\delta^{13}C_{carb}$ of units 4 to 7 is unlikely to have been much affected. The salinity-stratified basin model described above provides a depositional environment of low $\delta^{13}C_{DIC}$ that appears to satisfy known

sedimentological and geochemical constraints. Features that would be unusual in a Phanerozoic context - organic-poor sediments in what must have been an anoxic basin, and the extent of ^{13}C depletion in the lower layer - may be explained by oceanographic characteristics peculiar to the Precambrian: more efficient water-column remineralisation, an absence of refractory lignin-derived organic matter, and a generally more nutrient - rich ocean.

Although diapirs breaching the sea floor may have been the source of some ^{12}C and sulphate, the evaporative basin model has an attractive consonance with the 'Messinian' basin desiccation hypothesis for the origin of the canyons. A genetic link between $\delta^{13}C_{carb}$ depletion and canyon formation is reinforced in the Officer Basin, where similarly ^{13}C-depleted carbonates are found below the canyon unconformity (see later section, this chapter).

The stratification model has important implications for Neoproterozoic $\delta^{13}C$ chemostratigraphy and modelling of the carbon cycle, in which diagenetically unaltered $\delta^{13}C_{carb}$ has been generally assumed to reflect global ocean chemistry (e.g. Kaufman & Knoll, 1995; Derry et al., 1992).

Units 8 - 11 and dolostone in Bonney Formation

The base of Unit 8 marks an increase in water depth (Haines, 1990) accompanied by a rapid shift to heavier $\delta^{13}C_{carb}$. The rise in relative sea level may have substantially enlarged the link to the world ocean, with the result that stratification became much weaker.

Units 9 and 11 and the dolostone bed in the lower Bonney Formation represent the only truly shallow-water carbonates in the Wilpena Group. The far greater range of variation in $\delta^{13}C_{carb}$ (-2.0 to +2.7 in Unit 11) and $\delta^{18}O$ than the deeper-water carbonates of Units 3-7 may be due to the effects of intermittent, early meteoric diagenesis and the lack of a deep-burial 'smoothing' overprint. Lightest $\delta^{13}C_{carb}$ is seen in sucrosic dolostones in Unit 11. There is a weak negative correlation of $\delta^{13}C_{carb}$ with Mn/Sr: lowest Mn/Sr coincides with lowest $^{87}Sr/^{86}Sr$ (0.70874) and highest $\delta^{13}C_{carb}$ (+2.7 in sample 7.19; Fig. 3.15, Table 3.2). These figures represent the best estimates of least-altered $^{87}Sr/^{86}Sr$ and $\delta^{13}C_{carb}$ in Unit 11 in the Bunyeroo and Brachina Gorge sections. Higher values for $\delta^{13}C_{carb}$ (+6 ‰) are known from Unit 11 at some more northern localities (Urlwin et al., 1993; Pell et al., 1993). Unit 11 thickens northwards and the carbon isotopes suggest that Unit 11 may include younger horizons at these latter localities.

3.7 Geological Setting - Officer Basin

The Officer Basin is a large intracratonic depression in the NW of South Australia (Fig. 3.1). Extensive flat-lying subsurface Neoproterozoic sediments in the eastern Officer Basin have hydrocarbon potential, and are known from seismic profiles and a number of fully-cored drillholes (Brewer et al., 1987; Stainton et al., 1988). The thickest Ediacarian succession accumulated in the Munyarai Trough near the northern margin, and a thinner succession was laid down on a wide shelf to the south (Murnaroo Platform).

The generalized lithologic succession is shown in Fig. 3.3. Three formations are considered to be of Ediacarian age: the 'Giles Mudstone', considered equivalent to the Brachina Formation (Sukanta et al., 1991, and below); the Murnaroo Formation (equivalent to the ABC Range Quartzite) and the Rodda beds. The Rodda beds were defined in outcrop in the far northeast Officer Basin but are now recognised to be widespread in the subsurface eastern and southeastern Officer Basin where the base of the unit is taken as the top of the Murnaroo Formation (Brewer et al., 1987). The close lithostratigraphic similarity of the Ediacarian and older successions to those of the Adelaide Geosyncline (Sukanta et al., 1991; Jenkins et al., 1992; Preiss & Kreig, 1992) suggests a connection north of the Gawler Craton (Preiss, 1993), through an area now obscured by younger cover . The lower part of the Rodda beds is a lithostratigraphic correlate of the Bunyeroo Formation, and time-equivalence is proved by the occurrence in both these units of a unique, isochronous marker bed consisting of impact ejecta derived from an astrobleme at Lake Acraman on the Gawler Craton (Gostin et al., 1986; Wallace et al., 1989). As outlined in a previous section, correlation of younger strata is less certain. The middle and upper Rodda beds are lithologically similar to the Wonoka and Billy Springs Formations of the Adelaide Geosyncline (Preiss & Kreig, 1992). Both the Wonoka Formation and the Rodda beds locally contain large intraformational canyons (Sukanta et al., 1991). Equivalence of the upper Rodda beds of the eastern Officer Basin with the Pound Subgroup is proposed by Sukanta et al. (1991) and Jenkins et al. (1992) on the basis of sequence-stratigraphic and indirect chemostratigraphic evidence. However, other interpretations (Walter et al., 1995; and below) suggest there is little, if any, overlap in age between the Rodda beds and the Pound Subgroup.

3.8 'Giles Mudstone'

LITHOSTRATIGRAPHY

The 'Giles Mudstone' is 194 m thick in the Giles 1 drillhole. The formation rests abruptly on massive medium-grained quartz sandstone ('Tarlina beds' of Stainton et al., 1988) with no intervening dolomitic Nuccaleena equivalent. Like the correlative Brachina Formation, there is basal silt-free red shale (here 14 m thick) overlain by a succession with an upward-increasing proportion of siltstone and sandstone, consonant with a general shallowing of the palaeoenvironment.

Above the basal shale is red shale with abundant (10-50%) thin siltstone beds that are internally parallel-laminated, cross-laminated or graded. The upper half of the formation includes abundant (30%) medium to thick beds of very fine-grained sandstone. The sandstone beds have sharp bases and many are gently graded, with internal planar-parallel lamination, cross-laminated upper parts and ripplemarked tops. Other beds have slumped or convolute lamination, and gradational upper contacts. The sandstone and siltstone layers are interpreted as storm beds. Background sediment throughout is red shale (with 0.4-0.6 mg/g TOC) except for rare, thin diffuse layers of grey or green shale (0.7-1.0 mg/g TOC).

Rare, small (10 mm) irregular anhydrite nodules are present in the upper half of the formation.

At 1028.85 m depth, a very thin, slightly wavy but persistent black lamina, anomalously depleted in ^{13}C, is interpreted to be of benthic microbial mat origin (see Chapter 2).

3.8a ISOTOPE STRATIGRAPHY

With the exception of the single black shale sample, organic carbon isotopic compositions are rather constant throughout the unit, at -26 to -27 ‰. Normalized data show a slight negative excursion in the lower half of the unit (Fig. 3.18). The benthic microbial mat organic carbon isotopic composition ($\delta^{13}C_{bmm}$, see Chapter 2) is calculated as -35 ‰, giving an approximate 8 ‰ difference between carbon of benthic and pelagic origin.

An anhydrite nodule (sample 10.32) has a sulphur isotopic composition of 23.1 ‰ and a strontium isotopic composition of 0.7117.

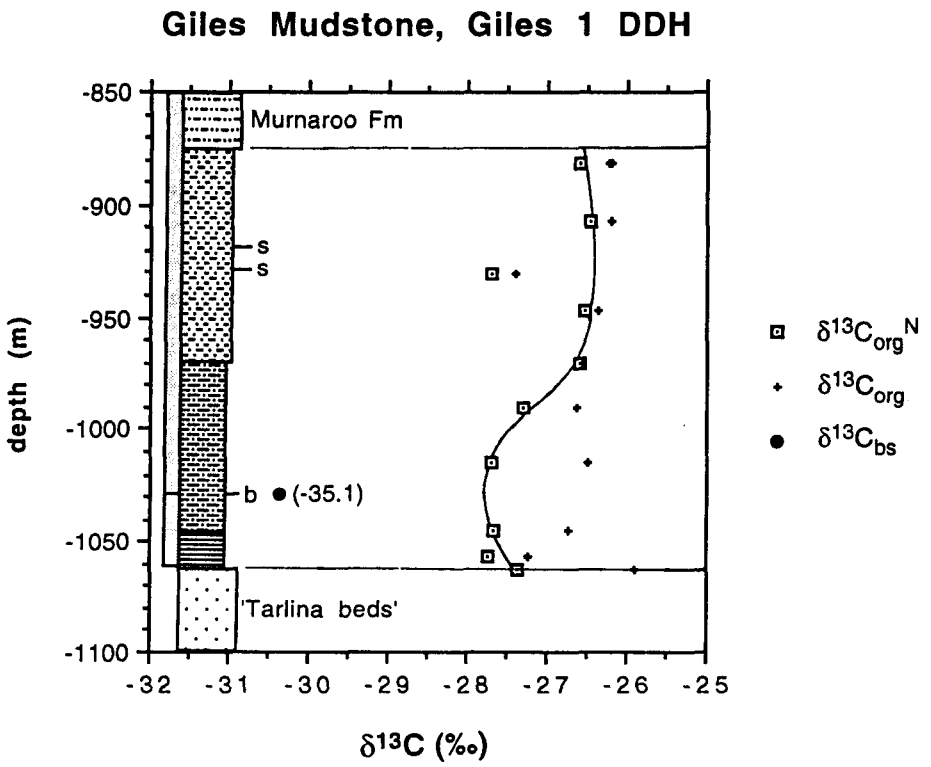

Fig. 3.18: Lithologic column and organic $\delta^{13}C$ data for the 'Giles Mudstone' in drillhole Giles 1. Calculated $\delta^{13}C_{bmm}$ indicated adjacent to $\delta^{13}C_{bs}$ point.

3.9 Murnaroo Formation

3.9a LITHOSTRATIGRAPHY

The Murnaroo Formation, 286 m thick in Giles 1, was not fully logged and sampled in this study. The lowermost Murnaroo Formation in Giles 1 consists of cross-bedded quartz sandstone, and red shale and siltstone with wavy and lenticular bedding. The upper 105 m of the formation was intersected in Munta 1. All except the top 18 m consists of quartz sandstone with angle-of-repose cross-bedding, and red siltstone interbeds. This is abruptly overlain by 2 m of red and green shale, followed by 150 mm of conglomerate, then 16 m of very coarse-grained, feldspathic quartz sandstone. In Observatory Hill 1, the upper 26 m of the Murnaroo Formation consists of thick-bedded, cross-bedded quartz sandstone with a metre of pebble conglomerate at the top.

The formation is lithologically very similar to its correlative, the ABC Range Quartzite. The contact at the base of the coarse-grained unit comprising the uppermost part of the Murnaroo

Formation is interpreted to be equivalent to Sequence Boundary 2 of the Wilpena Group (Fig. 3.3) (Sukanta et al., 1991; Jenkins et al., 1992).

3.9b ISOTOPE STRATIGRAPHY

Two organic carbon isotopic determinations from the upper part of the formation in Munta 1 gave $\delta^{13}C_{org}{}^{N}$ of close to -26 ‰, and lie on the same trend as higher data points in the lower Rodda beds (Fig. 3.20).

3.10 Rodda beds

3.10a INTRODUCTION

In the type area in the Munyarai Trough in the far northeastern Officer Basin, the Rodda beds are a thick (> 3.7 km) succession of dominantly calcareous siltstone with abundant evidence for syndepositional slumping (Preiss & Krieg, 1992). In the SE Officer Basin, a subsurface unit of siltstone, shale and limestone is considered a correlate of the Rodda beds (Brewer et al., 1987). The base of the unit, unknown in the type area, is taken to be the top of the Murnaroo Formation.

Six widespread seismic reflectors, interpreted as sequence boundaries, occur near the base, within, and at the top of the Rodda beds correlate of the SE Officer Basin (Stainton et al., 1988; Sukanta et al., 1991). At the lowest, F6 reflector (considered to be equivalent to Sequence Boundary 2 of the Wilpena Group), seismic onlap of the lower Rodda beds is seen in the southern platform area (Sukanta et al., 1991). Reflector F5 appears to coincide with an intraclastic horizon and probable erosional break at the top of the Bunyeroo Formation correlate. Reflector F is a widespread unconformity associated with the incision of canyons similar in scale to those of the Wonoka Formation. Sukanta et al. (1991) show that the F unconformity is linked to uplift in the southern platform area followed by gravity-driven collapse with detachment along salt horizons at depth, and salt diapirism. Unlike the Wonoka Formation, therefore, a widespread unconformity is associated with the initiation of canyons. The uppermost reflector (E) represents an unconformity at the base of the Cambrian Relief Sandstone.

The Rodda beds were sampled in fully cored drillholes Observatory Hill 1, Munta 1 and Ungoolya 1. Lithologic observations were also made on Lake Maurice West 1. Correlation of important sequence boundaries is shown in Fig. 3.19. In the southern platform area, represented by Observatory Hill 1 and Lake Maurice West 1, most of the formation has been removed by erosion or was never deposited. Munta 1 and Ungoolya 1 are stratigraphically

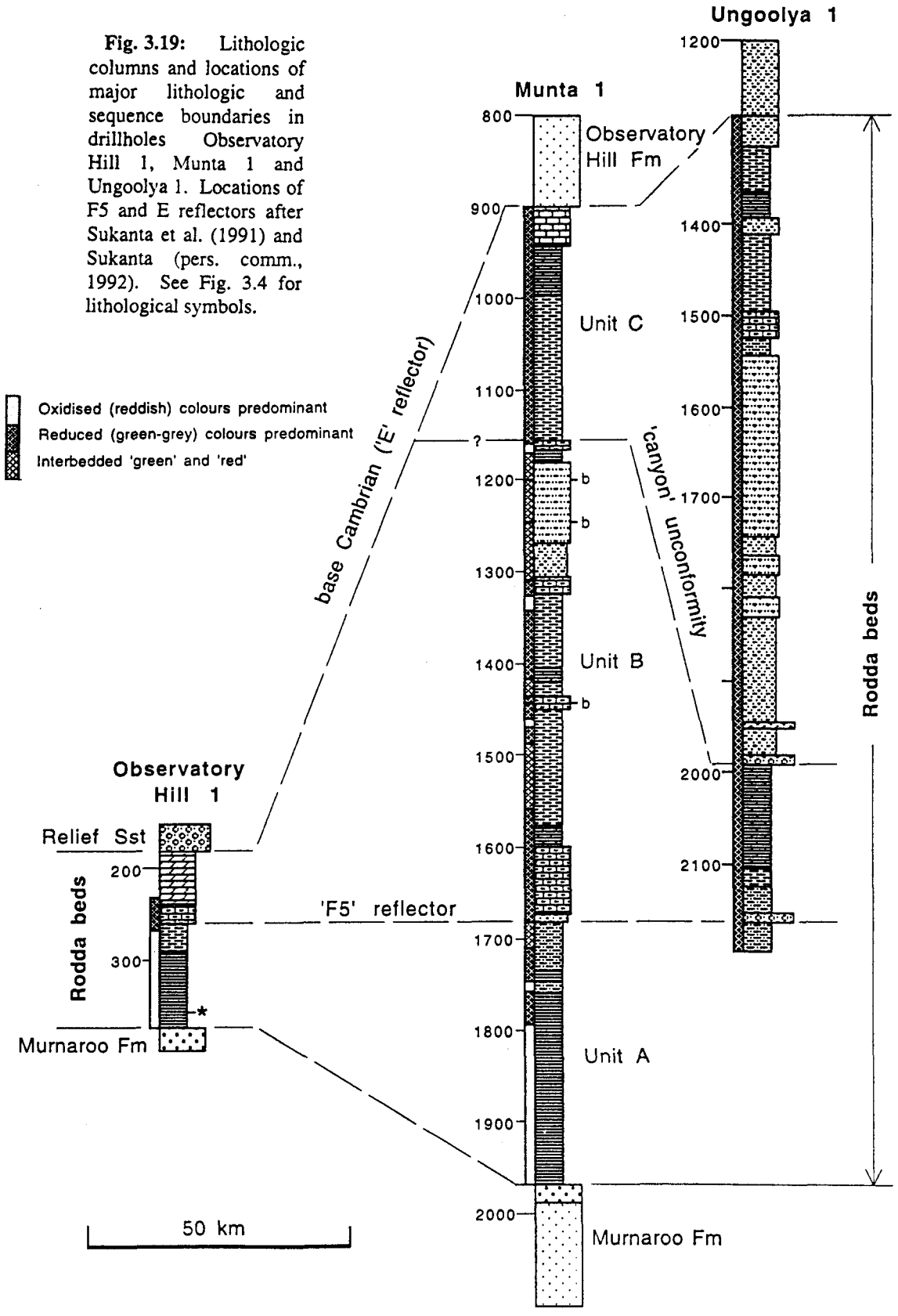

Fig. 3.19: Lithologic columns and locations of major lithologic and sequence boundaries in drillholes Observatory Hill 1, Munta 1 and Ungoolya 1. Locations of F5 and E reflectors after Sukanta et al. (1991) and Sukanta (pers. comm., 1992). See Fig. 3.4 for lithological symbols.

more complete, being situated closer to the Munyarai Trough (Fig 3.1). Ungoolya 1 intersects a canyon: here much of the middle part of the Rodda beds has been removed by a major intraformational erosion event and the upper part of the Rodda beds, including in part the canyon fill, is correspondingly thicker (Sukanta et al., 1991; Fig 3.19).

Sukanta et al. (1991) and Sukanta (pers. comm., 1992) provided interpreted depths of the six seismic reflectors in the drill cores studied (Fig. 3.19). However, in Munta 1 and Ungoolya 1, the 'canyon-cutting' F unconformity is here revised upwards on the basis of compelling stratigraphic and chemostratigraphic evidence detailed below.

The Rodda beds are here divided into informal units, A, B, and C, in order to simplify discussion. The Unit A/B and B/C boundaries are defined at 1679 m (= reflector F5) and 1153.6 m (= revised position of F unconformity), respectively, in Munta 1 (Fig. 3.19).

3.10b Unit A: Lithostratigraphy

Unit A is the correlate of the Bunyeroo Formation of the Adelaide Geosyncline. It is 291 m thick in Munta 1 and 115 m thick in Observatory Hill 1. The lower two-thirds of Unit A in Munta 1, Observatory Hill 1 and Lake Maurice West 1 consists of uniform red mudstone with rare, diffuse pale green beds, and is indistinguishable from typical lower Bunyeroo Formation.

Near the top of the red mudstone interval in Munta 1 is a 0.8 m thick green mudstone bed with a central 150 mm band of black shale. This black shale (sample 15.99, 1810.5 m) has an unusually high TOC (6 mg/g) and is reminiscent of the black shale beds in the Bunyeroo Formation in Brachina Gorge. Like them, it does not have the anomalous ^{13}C-depletion of the black shales of the 'benthic microbial mat facies'.

In Munta 1, Observatory Hill 1 and Lake Maurice West 1, the red mudstone passes up into a succession dominated by grey to green shale with minor siltstone and fine-grained sandstone as planar-parallel laminae and starved ripples. In Munta 1 there is rare limestone and a distinctive, rhythmically-laminated very fine-grained sandstone (1683-1758m). This latter lithology consists of pale sandstone or siltstone thinly interlaminated with red or green shale; superimposed on this small-scale (0.5-1 mm) rhythmicity is a coarser (5-10 mm) alternation of sand-rich and sand-poor layers. This rhythmicity is reminiscent of parts of the Elatina Formation of the Adelaide Geosyncline (Williams, 1989) and of the Cyclops Member of the Pertatataka Formation in the Amadeus Basin (see Chapter 4). The Elatina Formation rhythmites are interpreted as distal ebb-tidal deposits laid down below storm wavebase

(Williams, 1989). Five metres of this distinctive rhythmic facies is also present at a similar stratigraphic level in Lake Maurice West 1.

On seismic evidence (Sukanta, pers. comm., 1992) and chemostratigraphic evidence (below), the lowest 32 m intersected by Ungoolya 1 belongs to Unit A. This interval consists of very dark grey mudstone with minor thin beds of calcareous siltstone. Planar-parallel lamination, low-angle cross-lamination and climbing ripple lamination are evident within the siltstone layers.

Unit A is interpreted as a predominantly deep-water (below storm wavebase) deposit, possibly shallowing in its upper part with the influx of minor amounts of sand.

3.10c Unit A: Isotope Stratigraphy

A fine-grained limestone bed from the upper part of Unit A in Munta 1 has $\delta^{13}C_{carb}$ of 2.0 ‰ (Fig. 3.23). Prevailing $\delta^{13}C_{org}{}^{N}$ here is -29 ‰, giving $\Delta\delta^{N}$ of 31 ‰. (This is very close to the best estimate of 32 ‰ for $\Delta\delta^{N}$ in Units B and C - see below).

Two calcareous siltstone layers from the upper part of Unit A in Ungoolya 1 have depleted $\delta^{13}C_{carb}$: -6 to -7 ‰ (Fig. 3.24). The samples are 20-40% carbonate and the enclosing shales are moderately organic-rich (1.4 to 1.6 mg/g TOC). The isotopic compositions may reflect incorporation of organogenic CO_2 in early diagenesis or equilibration with ^{13}C-depleted bottom waters.

Raw data of $\delta^{13}C_{org}$ show a large spread of values, especially in Munta 1; but normalized points coalesce along a relatively well-defined profile that is very similar in Observatory Hill 1 and Munta 1: a high of -26 ‰ declining to a low of -29 ‰ followed by a slight rise (Figs. 3.20, 3.22). Values of -29 ‰ and rising are also seen in the uppermost part of the unit in Ungoolya 1.

3.10d Unit B: Lithostratigraphy

Unit B is most complete stratigraphically in Munta 1, being largely removed by intraformational canyon erosion in Ungoolya 1 and by Cambrian erosion in Observatory Hill 1 (Fig. 3.19).

In Munta 1, at the F5 sequence boundary defining the base of the unit, quartz sandstone rests abruptly on green mudstone and passes up into a few metres of grey mudstone in turn overlain by a thick (75 m) unit of pale grey, fine-grained limestone (1598 - 1673 m). The limestone is medium to thick-bedded, with thin interbeds of dark grey shale that are often wavy and anastamosing suggesting a partly diagenetic origin to the layering (Plate 3.2). There is rare

intraclastic limestone conglomerate. This limestone unit is named the 'Karlaya Limestone' by Lindsay & Reine (1995).

In Munta 1, the limestone is followed by a thick succession of predominantly grey and red silty shale with minor siltstone laminae that are mostly planar-parallel but in places cross-laminated or lenticular (starved ripples). Here and there are beds of fine-grained limestone and there are two substantial units of limestone (1438-1448 m, 1305-1324.5 m) lithologically similar to the unit at 1598 - 1673 m described above. The lower of these two limestone units contains black shale as sporadic, thinly-laminated layers and wispy intraclasts, interpreted as

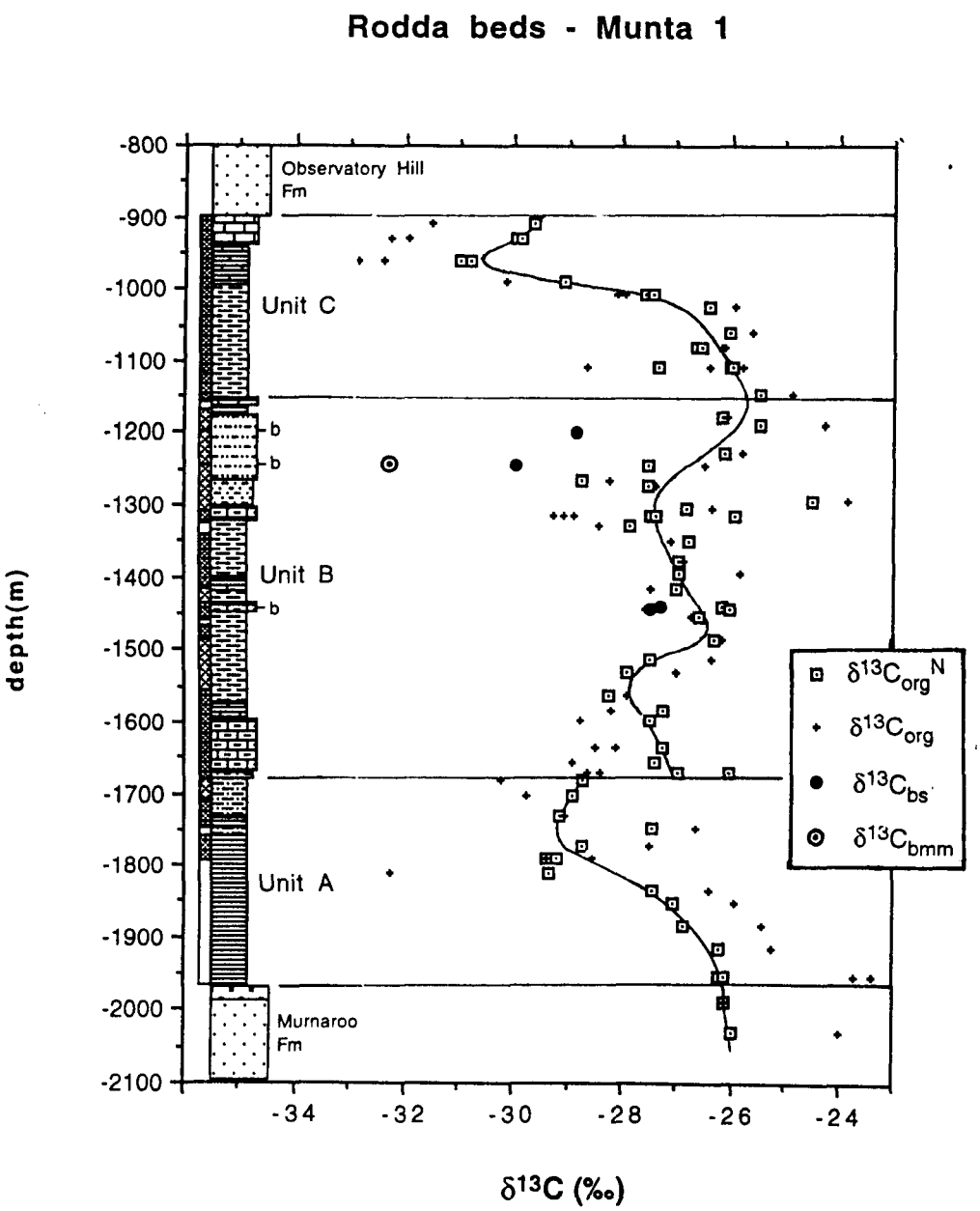

Fig. 3.20: Lithologic column and organic $\delta^{13}C$ data for the Rodda beds and uppermost Murnaroo Formation, drillhole Munta 1.

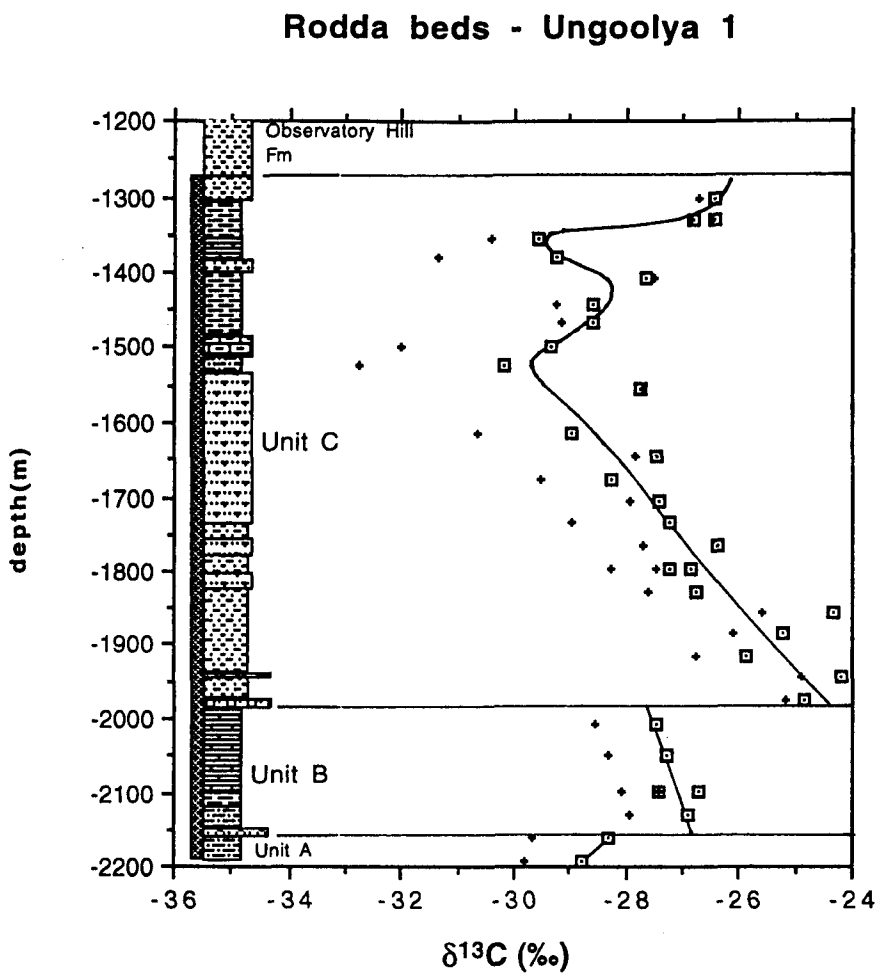

Fig. 3.21: Lithologic column and organic $\delta^{13}C$ data for the Rodda beds, drillhole Ungoolya 1.

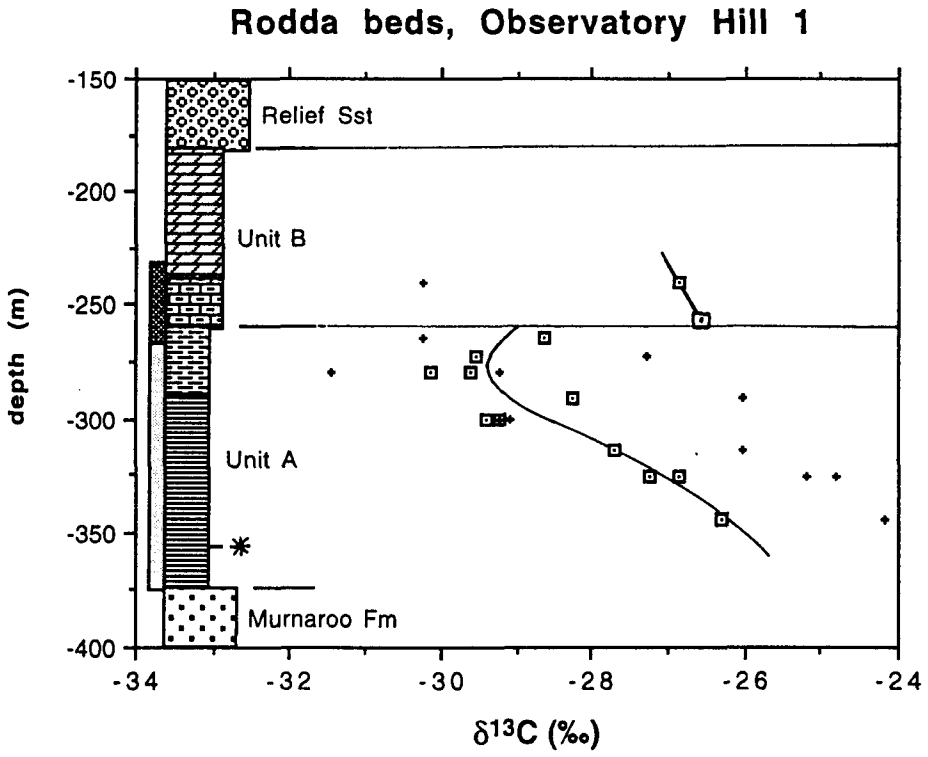

Fig. 3.22: Lithologic column and organic $\delta^{13}C$ data for the Rodda beds, drillhole Observatory Hill 1.

benthic microbial mats. Also present in this limestone unit is a 40mm bed of flat-pebble breccia containing a 10 × 20 mm anhydrite nodule (1441.33m). The nodule has a mudstone coating with a rounded outer profile and is interpreted to have been transported from a more shoreward evaporative environment.

Then follows a substantial unit of interbedded, very fine-grained sandstone and siltstone (1179-1305 m). Sandstone beds are commonly graded, with erosional bases, and pass up into red or green siltstone. The sandstone beds feature abundant planar-parallel lamination and low-angle cross-lamination that may represent hummocky cross-stratification (Plate 3.3). Between 1198 and 1253 m depth there are sporadic remnant benthic microbial mats as very thin black laminae or wispy intraclasts.

The sandy unit is overlain by a few metres of dark grey to green shale, then limestone (1154-1168 m). The limestone is fine-grained, initially pink with red mudstone interbeds; and grey, with grey mudstone interbeds higher up. *In situ* brecciation is common, particularly in the uppermost few metres. This limestone is isotopically similar to the middle part of the Wonoka Formation but no disseminated gypsum was observed in samples collected. The upper contact is an angular unconformity that defines the top of Unit B.

The limestones and silty shales that predominate in Unit B are interpreted to be middle shelf deposits laid down mainly below the reach of storm or wave activity. The sandstone-siltstone unit in the upper part of Unit B (1179-1305m) is interpreted as a storm-dominated inner shelf deposit.

In Observatory Hill 1, the correlative of the thick limestone unit low in Unit B (i.e. 1598 - 1673 m in Munta 1) is an 80 m thick carbonate unconformably overlain by Cambrian Relief Sandstone. The lowest 20 m are micritic limestone identical to that seen in Munta 1. The upper 60 m consists of very pale grey to pinkish, fine-grained dolostone, with common small, irregular vugs possibly after evaporites. Stratiform and small domical stromatolites are present high in the unit. An intertidal, in part sabkha-like depositional environment is envisaged for the dolostone, reflecting the more shoreward setting of Observatory Hill 1.

In Ungoolya 1, the interval of limestone-clast conglomerate and dark grey shale between 2161 and 1988 m is here considered a correlate of the lower part of Unit B in Munta 1, on chemostratigraphic grounds and also because the turbiditic 'canyon-fill' facies does not commence until higher up (above 1988 m). At the base of this interval is 8 m of sandy, thick-bedded limestone-clast conglomerate. A thin section shows common clasts of oolitic grainstone and free ooids in the matrix, indicating derivation - probably by mass-flow processes - from a shallow shelfal environment. The rest of Unit B here consists of dark grey

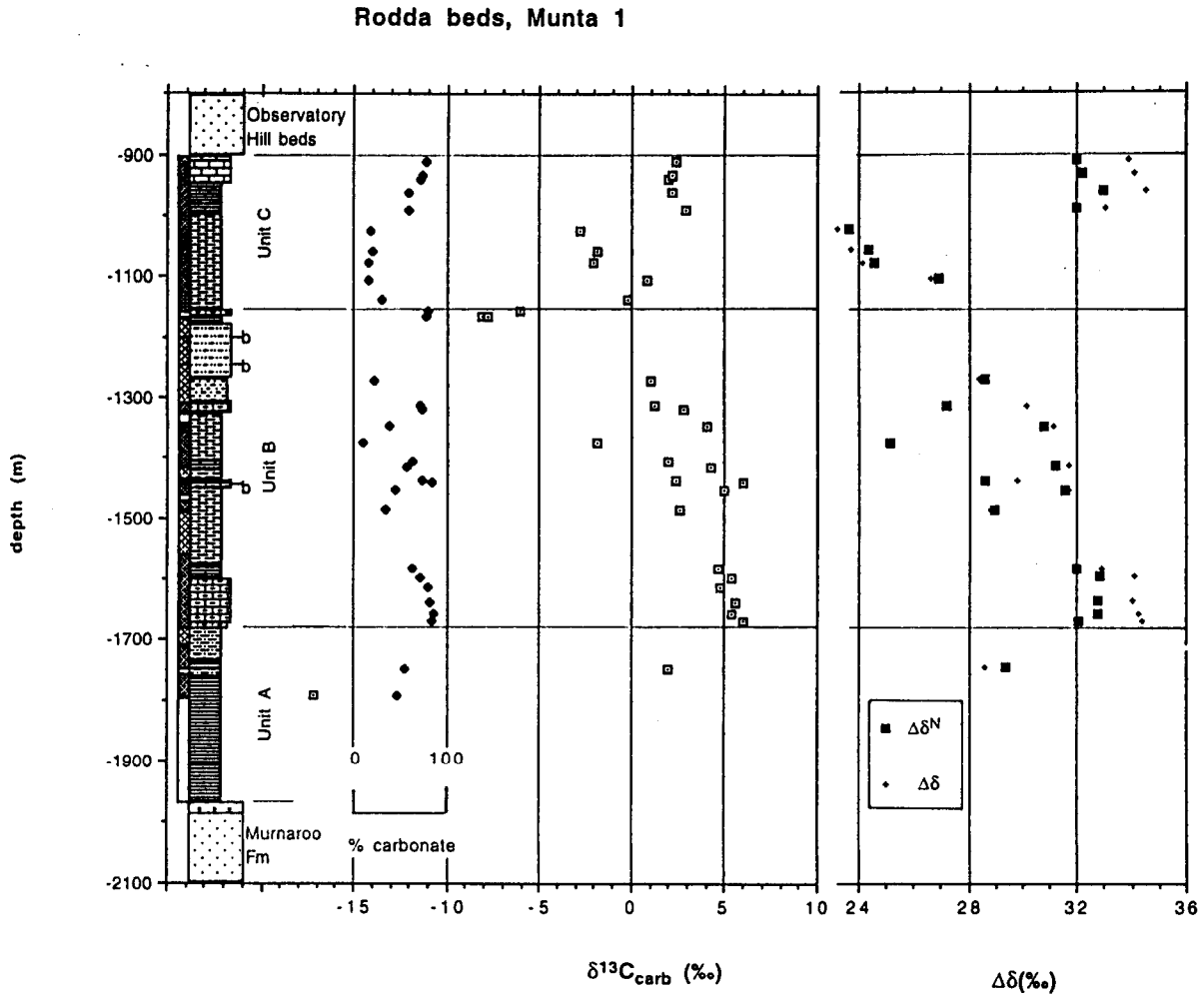

Fig. 3.23: % carbonate, $\delta^{13}C_{carb}$, $\Delta\delta$ and $\Delta\delta^N$ data for the Rodda beds, drillhole Munta 1.

mudstone with minor thin beds of pale grey, fine-grained limestone. Thin beds of calcareous, cross-laminated siltstone are present low in the succession, together with rare, thick graded sandstone beds. Unit B in Ungoolya 1 is interpreted as an upward-deepening, outer shelf to slope deposit, basinward of its calcareous lateral equivalent in Munta 1.

3.10e Unit B: Isotope Stratigraphy

The thick carbonate at the base of Unit B in both Munta 1 and Observatory Hill 1 displays a narrow range of enriched carbon isotopic compositions (+6 to +4 ‰) with a slight upward-decreasing trend apparent (Figs 3.23, 3.25).

Geochemical indicators suggest these $\delta^{13}C_{carb}$ values are very close to primary. Mn/Sr values are low (0.06 - 1.3). Limestones have high Sr contents, up to 1638 ppm, suggesting an aragonite precursor. Oxygen isotope compositions of limestones are moderately high (-5.46 ± 1.96 ‰, n = 8) with one sample as high as -2.59 ‰. Dolostones in Observatory Hill 1 are somewhat lower in ^{18}O (-7.62 ± 0.37 ‰, n = 3) suggesting possible involvement of meteoric waters in dolomitization (mixing-zone dolomitization). Four $^{87}Sr/^{86}Sr$ determinations of limestones show a narrow range (0.70791 - 0.70811) (Table 3.3); with the two lowest values being 0.70795 (Observatory Hill 1) and 0.70791 (Munta 1). Several $\Delta\delta^{N}$ determinations cluster tightly around 32 ‰ (Fig. 3.23, 3.25).

Higher in Munta 1, a number of carbonate isotopic analyses from the middle part of Unit B show a broad range of $\delta^{13}C_{carb}$ (+6 to -2 ‰) (Fig. 3.23). By the usual geochemical indicators of alteration, primary $\delta^{13}C_{carb}$ lies in the heavier end of this range, perhaps +6 ‰ at 1440 m, decreasing to +3 ‰ in the limestone unit at 1305 to 1325 m. The several samples markedly below this trend are impure (< 35% carbonate), have depleted $\delta^{18}O$ (< -9 ‰) or have Mn/Sr > 2; and all have $\Delta\delta^{N}$ < 30 ‰. Two $^{87}Sr/^{86}Sr$ determinations from the limestone unit at 1305-1325 m are 0.7085 and 0.7087; but Mn/Sr values (0.88, 0.75) are higher than those found in other Rodda beds limestones that have low, consistent, and probably near-primary $^{87}Sr/^{86}Sr$. The value 0.7085 must therefore be regarded as a maximum for this horizon.

The limestone unit at the top of Unit B (1168 - 1154 m), immediately below the canyon unconformity, has a markedly depleted carbon-isotopic composition (-6 to -8 ‰) similar to the middle part of the Wonoka Formation (Fig. 3.23). Mn/Sr values are relatively high (~4) and ^{18}O somewhat depleted ($\delta^{18}O$ -7.3 to -8 ‰), but Mn/Sr and $\delta^{18}O$ nonetheless suggest little alteration of $\delta^{13}C_{carb}$ (Derry et al., 1992, and see Chapter 2).

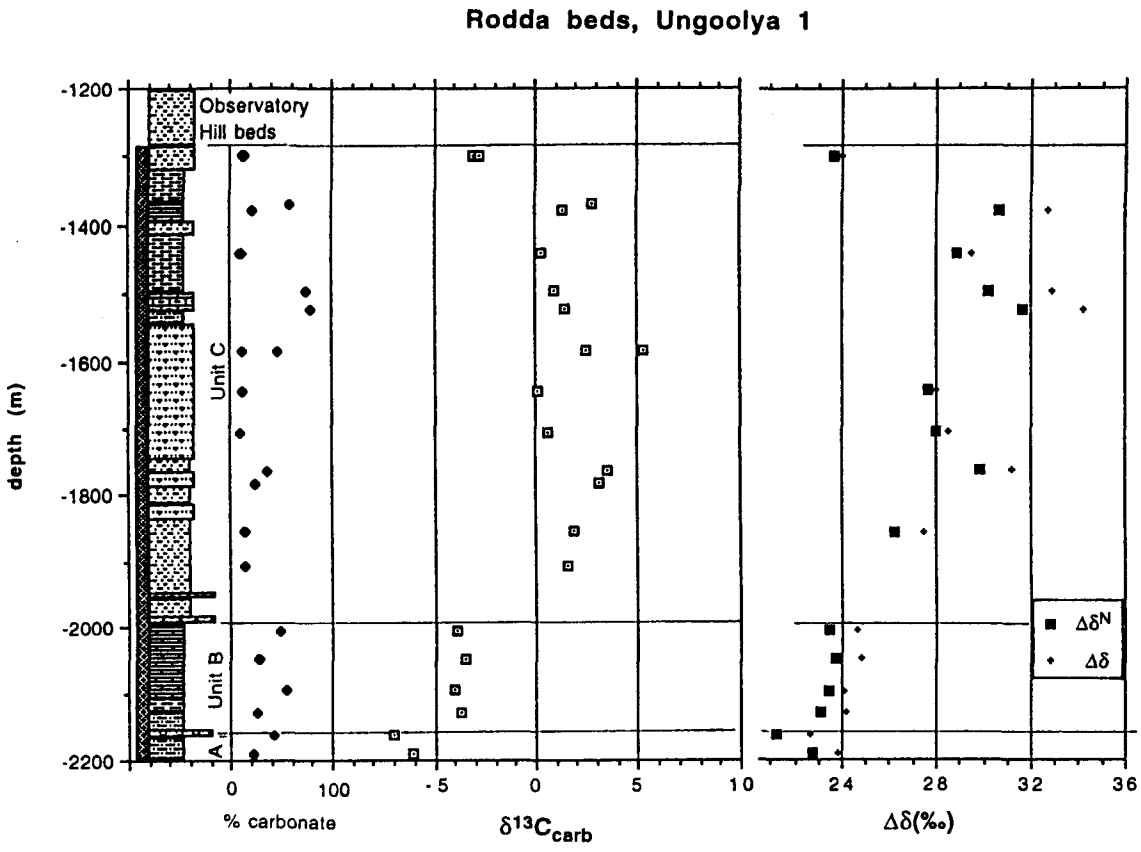

Fig. 3.24: % carbonate, $\delta^{13}C_{carb}$, $\Delta\delta$ and $\Delta\delta^N$ data for the Rodda beds, drillhole Ungoolya 1.

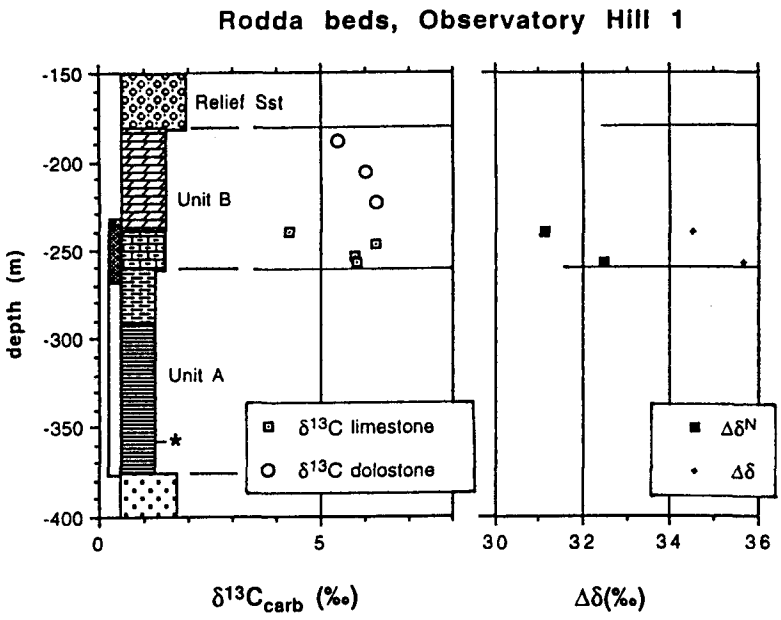

Fig. 3.25: $\delta^{13}C_{carb}$, $\Delta\delta$ and $\Delta\delta^N$ data for the Rodda beds, drillhole Observatory Hill 1.

In Ungoolya 1, Unit B contains thin, impure limestone beds with $\delta^{13}C_{carb}$ consistently close to -4 ‰ (Fig. 3.24). Carbonate purity is variable (25 - 55%), TOC's moderate and $\delta^{18}O$ lies in the range -7.9 to -10.0 ‰. No trace element or $^{87}Sr/^{86}Sr$ data are available.

In all three drillholes there is a jump of +1.5 ‰ to -27 ‰ in $\delta^{13}C_{org}{}^{N}$ at the base of Unit B (Figs 3.20 - 3.22). Then there is an initial gentle decline which parallels that seen in $\delta^{13}C_{carb}$, after which further information is limited to Munta 1 as in the other two sections, Unit B is erosionally truncated. Munta 1 shows a rather complex $\delta^{13}C_{org}$ profile with an overall rise to -26 ‰ at the top of Unit B, with several outlying points (Fig. 3.20).

It is noteworthy that benthic microbial mat-bearing samples at 1440-1450 m have $\delta^{13}C_{org}$ very close to that of enclosing limestone, while those higher up (1198 - 1253 m) have distinctly depleted isotopic compositions relative to the enclosing sequence. Calculated $\delta^{13}C_{bmm}$ for those latter samples are roughly -32 ‰, giving $\Delta_{p\text{-}b}$ of approximately 5 to 6 ‰.

The anhydrite nodule in Munta 1 has a sulphur isotopic composition of 24.4 ‰.

sample	rocktype	Unit	Sr(ppm)	Mn(ppm)	Mn/Sr	87Sr/86Sr	∂13C	∂18O	Rb(ppm)	87/86Srinit
Observatory Hill 1										
14.09	dolostone	Unit B	397	499	1.26		4.3	-8.6		
14.10	limestone	Unit B	320	326	1.02		6.2	-8.5		
14.11	limestone	Unit B	1120	340	0.30	0.70795	5.8	-5.3	0.244	0.70795
14.12	dolostone	Unit B	66	65	0.98		5.8	-5.0		
Munta 1										
15.02	limestone	Unit C	1540	243	0.16	0.70886	2.4	-5.0	0.219	0.70885
15.03	limestone	Unit C	1199	176	0.15					
15.04	limestone	Unit C	1112	219	0.20	0.70886	2.2	-4.7	0.187	0.70885
15.05	limestone	Unit C	1026	274	0.27	0.70899	2.0	-4.5	0.294	0.70898
15.29	limestone	Unit B	170	735	4.32		-6.0	-7.3		
15.30	limestone	Unit B	164	697	4.25		-7.8	-8.0		
15.46	limestone	Unit B	540	403	0.75	0.70866	2.0	9.6		
15.47	limestone	Unit B	323	801	2.48		1.3	-6.7		
15.48	limestone	Unit B	498	440	0.88	0.70852	2.8	-5.7	0.216	0.70850
15.58	limestone	Unit B	228	855	3.75		4.2	-6.4		
15.61	limestone	Unit B	443	528	1.19					
15.62	limestone	Unit B	199	836	4.20		5.0	-7.1		
15.66	limestone	Unit B	7699	682	0.09	0.71202	6.0	-9.8		
15.79	limestone	Unit B	794	789	0.99		4.8	-5.2		
15.81	limestone	Unit B	944	212	0.22	0.70806	5.5	-4.6	0.16	0.70805
15.83	limestone	Unit B	1638	102	0.06	0.70791	5.4	-2.6	0.171	0.70791
15.84	limestone	Unit B	373	195	0.52					
15.85	limestone	Unit B	906	163	0.18	0.70812	6.0	-4.0	0.425	0.70811

Table 3.3: Trace-element and strontium isotopic data, Rodda beds correlative.

3.10f UNIT C: LITHOSTRATIGRAPHY

In Munta 1, an angular unconformity defines the Unit B-C boundary. Below this contact, beds dip at ~25° (assuming vertical drillcore); above it, dips are consistently less than 10°. The unconformity is directly overlain by a thick (1154 - 997 m depth) succession of dark grey-green silty shale with minor (< 10%) thin beds or laminae of paler calcareous siltstone or very fine-grained sandstone. Many of these layers are internally plane-laminated, ripple cross-laminated or slumped. Thin planar siltstone laminae in many places exhibit a bundled distribution. Above 997 m, the succession becomes increasingly calcareous, with thin diffuse limestone beds in dark grey calcareous mudstone, succeeded by grey, fine-grained limestone (943 - 898 m, top of Rodda beds). A deep, sub-wavebase, outer-shelf environment is inferred for unit C, possibly with shallowing represented by the upper carbonate. Many of the thin sandy layers may be turbidites.

Unit C is much thicker in Ungoolya 1, consisting largely of canyon fill. Unit C begins with 8 m of limestone-clast conglomerate and coarse-grained sandstone. Then follows over 400 m (1980 - 1544 m depth) of interbedded calcareous sandstone and dark grey-green mudstone. Sandstone beds, up to 1 m thick, are usually graded, mostly structureless but in places showing parallel-lamination, ripple cross-lamination, convolute lamination or soft-sediment slumping. Detrital carbonate is present in the sandstone. This turbiditic sandstone-dominated interval is succeeded by a unit of thick-bedded, fine-grained limestone with diffuse dark grey mudstone interbeds, including several metres of slumped, pebbly calcareous siltstone (1525 - 1497 m). Seismic-stratigraphic interpretation by Sukanta (pers. comm., 1992) correlates this limestone with the limestone unit at the top of Unit C in Munta 1, and this is corroborated by chemostratigraphy (below). The upper 216 m of Unit C in Ungoolya 1 are therefore not represented in Munta 1. This interval is dominated by dark grey-green mudstone; there are minor thin beds of calcareous siltstone, and, in places, thick sandstone turbidite beds. There are intervals up to 10 m thick displaying pervasive soft-sediment slumping. A deep-water, outer-shelf environment is envisaged for Unit C in Ungoolya 1. There are no features suggestive of shallow-water deposition for the canyon-fill, as is seen in the Wonoka Formation (Christie-Blick, 1993), but the oldest part of the canyon fill is not intersected in Ungoolya 1 (Stainton et al., 1988; Sukanta et al., 1991, Fig. 12).

3.10g UNIT C: ISOTOPE STRATIGRAPHY

In Munta 1, $\delta^{13}C_{org}{}^{N}$ declines from -26 ‰ low in Unit C to a minimum of -31 ‰ just below the limestone unit (Fig. 3.20).

In Ungoolya 1, as might be expected, the decline is seen over a much more prolonged stratigraphic interval, and beginning at a heavier value (~ -24.5 ‰) than seen in Munta 1 (Fig. 3.21). There is a large jump in the $\delta^{13}C_{org}{}^{N}$ profile at the base of Unit C in accordance with a major erosional break (and base of the canyon-filling sequence) at 1988 m. The decline reaches a minimum (as in Munta 1) of about -31 ‰ at the base of the limestone unit, supporting Sukanta's seismic correlation of the limestone between the two drillholes. Thereafter the profile climbs irregularly to ~ -26 ‰ in Ungoolya 1.

Calcareous siltstones from the lower part of Unit C in Munta 1 have a spread of $\delta^{13}C_{carb}$ (-3 to +1 ‰). These samples are relatively low in carbonate (16 - 30%); $\Delta\delta^{N}$ values are low (Fig. 3.23); and almost certainly the carbon isotopic compositions reflect a degree of diagenetic incorporation of organogenic CO_2. In contrast, limestones higher up have a narrow range of $\delta^{13}C_{carb}$ (+2 to +3 ‰); here geochemical indicators point to the likelihood of preservation of primary $\delta^{13}C_{carb}$. Strontium contents are high - up to 1540 ppm - and Mn/Sr ratios are low (0.15-0.27). $\Delta\delta^{N}$ values lie close to 32 ‰ (Fig. 3.23). Three $^{87}Sr/^{86}Sr$ determinations show a narrow range with the two lowest in agreement at the fifth decimal place (0.70885) (Table 3.3).

In Ungoolya 1, calcareous rocks from the sandstone-dominated lower part of Unit C (the canyon-filling succession) show a range of $\delta^{13}C_{carb}$ values (0 to +5 ‰) that show a positive correlation with % carbonate (10 - 50%) (Fig. 3.24). Probably, these compositions reflect a mixture of primary carbonate, early diagenetic organic-derived carbonate and detrital carbonate; and may mean little in terms of a useful chemostratigraphic signal. The limestone unit has slightly lower $\delta^{13}C_{carb}$ (+1 to +2 ‰) than its correlate in Munta 1. Higher, a point at +3 ‰ at 1369.9 m is a calcareous sandstone that may contain significant detrital carbonate.

A collation of previous $\delta^{13}C_{carb}$ chemostratigraphic data from Unit C in Ungoolya 1 (Jenkins et al., 1992; Zang, 1988) with this study shows scattered results, suggesting that the primary signal is obscured by 'noise' from detrital and diagenetic sources except perhaps for the limestone at 1525 - 1497 m. Greater reliance is therefore placed upon the organic carbon isotopic signal in the following synthesis.

3.11 Adelaide Geosyncline - Officer Basin correlation

A correlation scheme linking all major sections in the Officer Basin and Adelaide Geosyncline region is shown as Fig. 3.26. Organic carbon data are shown as lines of best fit through $\delta^{13}C_{org}{}^{N}$ from preceding figures. Only trends of least-altered $\delta^{13}C_{carb}$ from carbonates interpreted to have been deposited in shallow or mixed-layer environments are

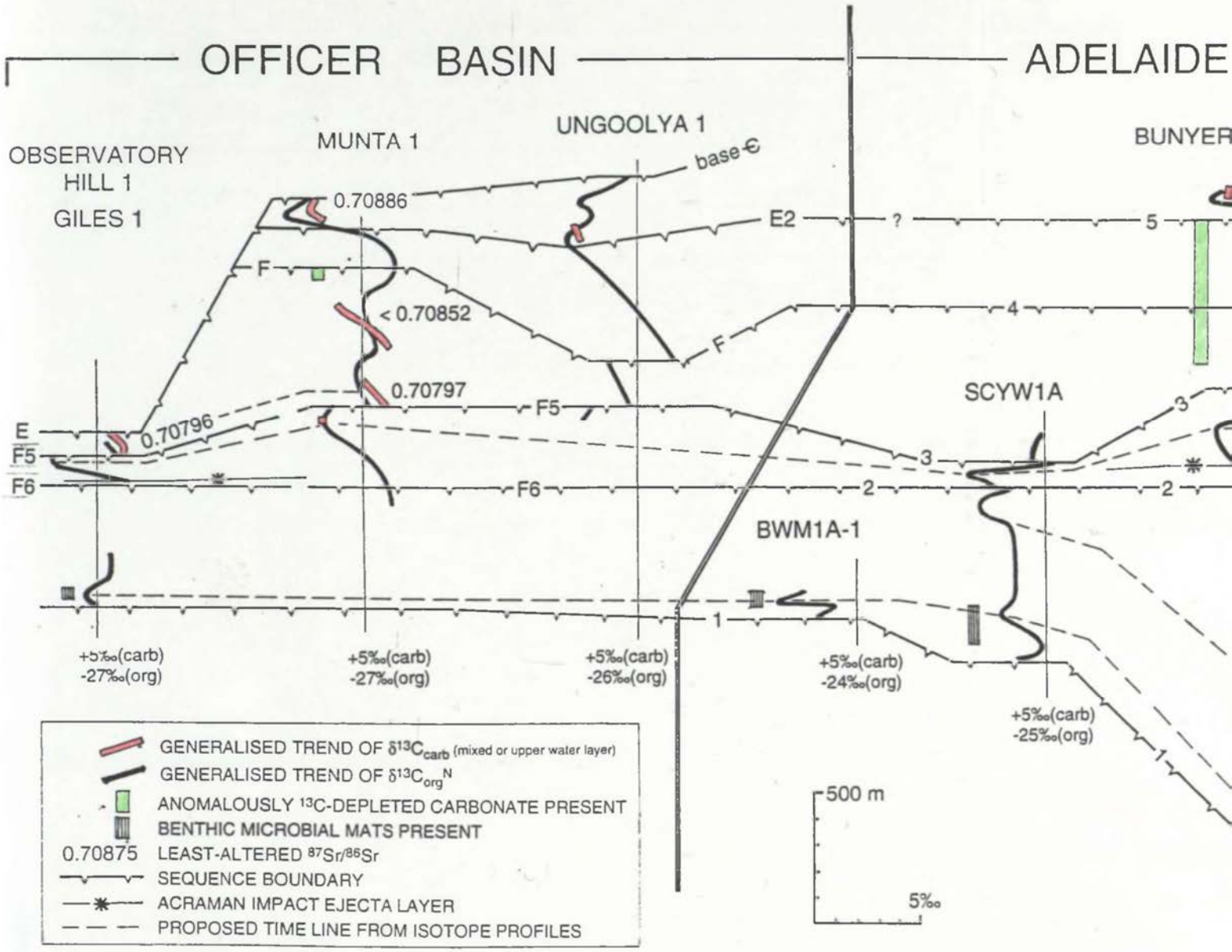
OFFICER BASIN
ADELAIDE
OBSERVATORY HILL 1
GILES 1
MUNTA 1
UNGOOLYA 1
BUNYER
SCYW1A
BWM1A-1
base €
0.70886
< 0.70852
0.70797
0.70796
E
F5
F6
F
E2
?
5
4
3
2
1
+5‰(carb) -27‰(org)
+5‰(carb) -27‰(org)
+5‰(carb) -26‰(org)
+5‰(carb) -24‰(org)
+5‰(carb) -25‰(org)
GENERALISED TREND OF δ13Ccarb (mixed or upper water layer)
GENERALISED TREND OF δ13Corg N
ANOMALOUSLY 13C-DEPLETED CARBONATE PRESENT
BENTHIC MICROBIAL MATS PRESENT
0.70875 LEAST-ALTERED 87Sr/86Sr
SEQUENCE BOUNDARY
ACRAMAN IMPACT EJECTA LAYER
PROPOSED TIME LINE FROM ISOTOPE PROFILES
500 m
5‰

FIG. 3·26 – FOLDS OUT

plotted. Organic and carbonate carbon data in each section are shifted relative to each other by an amount ($\Delta\delta*$) intended to superimpose the two carbon signals. $\Delta\delta*$ is an inferred or generalised $\Delta\delta^N$ ($= \delta^{13}C_{carb} - \delta^{13}C_{org}{}^N$) for each section derived from a collation of thermal maturation data (H/C, $\Delta\delta^N$, and kerogen colour: see section 2.3d; Table 2.5). The lowest $\Delta\delta*$ (29 ‰), interpreted to reflect the greatest degree of thermal maturation, is seen in the Adelaide Geosyncline (Brachina and Bunyeroo Gorge sections) and the Curnamona Craton (BWM1A-1) (Table 2.5). A similar $\Delta\delta*$ is assumed for the First Hill section from which no thermal maturation data are available. The SCYW1a section has suffered slightly less thermal stress ($\Delta\delta* = 30$ ‰). A distinctly lower thermal grade is inferred in the Officer Basin, where $\Delta\delta*$ of 31 to 32 ‰ are seen. Thermal maturation data of this study (Table 2.5) are in good agreement with previously published work on regional thermal maturation in the Adelaide Geosyncline (McKirdy & Powell, 1974) and the Officer Basin (McKirdy et al., 1992).

The distribution of benthic microbial mats, and of anomalously depleted carbonates (inferred to have been deposited under stratified water columns) are also indicated on Fig. 3.26. Also shown are least-altered $^{87}Sr/^{86}Sr$ ratios.

Sequence boundaries identified by Sukanta et al. (1991), Sukanta (pers. comm. 1992, as revised herein) and Christie-Blick et al. (1990) provide a framework for the correlation scheme. Sequence boundaries (and unconformities in general) have chronostratigraphic significance because (with very few exceptions) there is no age overlap between strata above and below a sequence boundary (Christie-Blick, 1991). An important constraint is thereby placed on large-scale diachroniety of units. A horizon of critical chronostratigraphic significance in this scheme is the Acraman ejecta layer, found in Observatory Hill 1 and the Bunyeroo and Brachina Gorge sections. Sequence boundaries that can be confidently correlated are those numbered 1 (base of the Ediacarian), 2 and 3 (below and above the Acraman ejecta layer). Correlation of boundaries 4 and 5 between the Officer Basin and the Adelaide Geosyncline is less certain. The most economical interpretation, followed here, is to correlate sequence boundary 4 of the Adelaide Geosyncline (the main 'canyon-cutting' surface) with the canyon unconformity in the Officer Basin (Sukanta et al., 1991). However, the isotopic data presented here would also be consistent with a correlation of sequence boundary 5 (which is associated with incised valleys of smaller dimensions at the top of Wonka Formation Unit 7: Christie-Blick et al., 1990) with the canyon unconformity in the Officer Basin.

Here, sequence boundary 5 of the Adelaide Geosyncline is correlated with reflector E3 within the upper part of the Rodda beds (Unit C of this study). This is at variance with Sukanta et al.

(1991) who correlate the E3 reflector with a surface within the Pound Subgroup. The revised correlation is favoured because of consistency with isotopic results (see below) and because the upper Rodda beds have a much stronger lithologic resemblance to the Wonoka and Billy Springs Formations than the Pound Subgroup (see also Preiss & Krieg, 1992).

A negative $\delta^{13}C_{org}{}^{N}$ excursion low in the first sequence is flagged by the occurrence of benthic microbial mats in Giles 1, BMW1A-1 and SCYW1a. Correlation of this excursion is proposed, while recognising that benthic mat distribution was probably environmentally controlled. Absence of benthic microbial mats and accompanying $\delta^{13}C_{org}{}^{N}$ detail from the Bunyeroo Gorge section may be due (as explained above: section 3.4c) to the distal position of this section with respect to the east-prograding clinoform of the Brachina and ABC Range Formations.

The Bunyeroo Formation and its correlates, bounded by sequence boundaries 2 and 3, are everywhere marked by a negative excursion in $\delta^{13}C_{org}{}^{N}$. The large amplitude of the excursion at Brachina Gorge (6 ‰) relative to other sections (2-3 ‰) may be due to preservational or environmental factors associated with the local facies change to more organic-rich sediments in the Brachina Gorge section. The truncated profile in the Officer Basin sections suggests that sediments equivalent to the upper part of the Bunyeroo Formation were eroded or not deposited. Shelfal localities in both basins (Observatory Hill 1, SCYW1a) are lithologically indistinguishable from more basinward localities (Munta 1, Bunyeroo Gorge) but are considerably thinner, and chronostratigraphically condensed as indicated by the vertically compressed $\delta^{13}C_{org}{}^{N}$ profiles. An essentially isochronous, 'layer-cake' mode of sedimentation is implied - consistent with the deep-water, starved basin palaeoenvironment suggested (Forbes & Preiss, 1987) for the Bunyeroo Formation.

Carbon and strontium isotopic data immediately below and above sequence boundary 3 are essentially identical in the three Officer Basin sections, except that no $^{87}Sr/^{86}Sr$ or useful $\delta^{13}C_{carb}$ data are available from Ungoolya 1. Anomalously depleted carbonates, probably laid down beneath the lower layer of a stratified water column, appear below ('canyon-cutting') sequence boundary 4 in the Officer Basin (Munta 1) and in the Adelaide Geosyncline, and persist through a considerable thickness of sediment above boundary 4 in the latter basin.

The stratified basin model suggests a significant reinterpretation of a previous $\delta^{13}C$ chemostratigraphic correlation (Pell et al., 1993) between the Adelaide Geosyncline and the Officer Basin. Clearly the model allows synchronous deposition of relatively ^{13}C-enriched cabonates in shallower shelfal environments and strongly depleted carbonates in more offshore environments. The assumption, implicit or explicit, that $\delta^{13}C_{carb}$ reflects surface-

layer or well-mixed ocean chemistry (e.g. Kaufman & Knoll, 1995) led to an interpretation that chronostratigraphic equivalents of Units 3 to 7 of the Wonoka Formation were absent from the Rodda beds (Pell et al., 1993). Recognition of a strong palaeoenvironmental overprint on $\delta^{13}C_{carb}$ allows the correlation shown (Fig. 3.26), in better accord with sequence stratigraphic (Sukanta et al., 1991) and lithostratigraphic considerations, and with $\delta^{13}C_{org}$ and $^{87}Sr/^{86}Sr$ data.

A strong positive excursion in $\delta^{13}C_{org}{}^{N}$ coincides with the ^{13}C-depleted carbonate interval in the Wonoka Formation, and similarly, a positive $\delta^{13}C_{org}{}^{N}$ excursion corresponds to the shorter interval of ^{13}C-depleted carbonates in the Rodda beds in Munta 1 (Fig. 3.26). Since enriched organic carbon is a likely corollary of the stratified basin model (see section 3.6c), these excursions too may not be of extrabasinal significance. Above sequence boundary 5 and its probable correlative the E3 reflector, widespread similarity is seen in carbon and strontium data. Least-altered $\delta^{13}C_{carb}$ is close to +2.5 ‰ (Unit 11, Wonoka Formation; uppermost limestone units in Munta 1 and Ungoolya 1); coinciding with a negative excursion in the more complete organic record. Least-altered $^{87}Sr/^{86}Sr$ at Bunyeroo Gorge (0.70874) is sufficiently similar to that in Munta 1 (0.70885) to support this correlation given the vagaries of post-depostional alteration of $^{87}Sr/^{86}Sr$ (see section 6.3b). The rising trend seen higher up in Ungoolya 1 (not preserved in the other Officer Basin sections) may be reflected in the Adelaide Geosyncline by enriched (+6 ‰) carbonates in possibly younger parts of Unit 11 (Pell et al., 1993; Urlwin et al., 1993).

Thus the isotope-chemostratigraphic data are best interpreted by a scheme involving little or no overlap in age between the Pound Subgroup and the Rodda beds correlate of the SE Officer Basin. Younger parts of the Rodda beds are probably preserved, however, in more basinward localities such as the type area where a thick (3.7 km) succession resembles the Billy Springs Formation of the northern Flinders Ranges (Preiss & Krieg, 1992). The Billy Springs Formation may be a distal equivalent of the lower part of the Pound Subgroup (Forbes & Preiss, 1987).

4

Isotope Chemostratigraphy of Ediacarian Successions in the Amadeus and Georgina Basins

4.1 Introduction

Neoproterozoic successions comprise much of the fill of the Amadeus Basin and the nearby southwestern part of the Georgina Basin. In the Amadeus Basin, the Ediacarian System is constrained at its base by a glacigene succession of probable Marinoan age (Wells et al., 1970; Preiss et al., 1978), and there are rare occurrences of the soft-bodied metazoan 'Ediacara fauna' in both basins (Daily, 1972; Glaessner & Walter, 1975; Wade, 1970; Walter, 1980). There is a broad lithostratigraphic resemblance between the presumed Ediacarian successions of the Amadeus and Georgina Basins, and the type Ediacarian (Cloud & Glaessner, 1982) of the Adelaide Geosyncline (see Chapter 3). Lithostratigraphic correlation at formation level with the Adelaide Geosyncline succession was proposed by Preiss et al. (1978), and correlation between the Amadeus and Georgina Basins was proposed by Walter (1980). This essentially lithostratigraphic scheme (Fig. 4.1a) has been followed in the regional overviews of Preiss & Forbes (1981), Forbes & Preiss (1987) and Walter et al. (1995). The apparent persistence of facies between separate present-day structural basins suggests lateral continuity of the original depositional system (Fig. 4.2; Preiss et al., 1978; Walter et al., 1995).

There are few chronostratigraphic constraints on these correlations. The diverse acritarch flora recently discovered in the Pertatataka Formation of the Amadeus Basin (Zang & Walter, 1989; 1992) has not been found in the Adelaide Geosyncline, probably because of preservational factors (Grey, in prep.). Elements of this flora are known, however, from the Officer Basin (Jenkins et al., 1992; Grey, in prep.) The Acraman impact ejecta layer (Gostin et al., 1986; Wallace et al., 1989) has not been detected in the Amadeus or Georgina Basins, probably because these basins are too distant from the impact site (Fig. 4.2). Sequence-stratigraphic correlation is hampered by particular difficulties in recognising and differentiating sequence boundaries in these intracratonic basins (Kennard & Lindsay, 1991; Lindsay & Korsch, 1991).

The formation-level lithostratigraphic correlation (Fig. 4.1a) obscures significant regional variations in lithostratigraphic detail within and between basins, variations that have led to a number of uncertainties in correlation (Preiss et al., 1978; Field, 1991; Freeman et al., 1991; Jenkins et al., 1992; Jenkins, 1993b; Preiss, pers. comm., 1993). One significant published difference of opinion concerns an angular unconformity at the base of the Gaylad Sandstone in the NE Amadeus Basin (Fig. 4.1; Freeman et al., 1991). This is interpreted by Jenkins et al. (1992) and Jenkins (1993b) to represent a significant time break, a corollary being that the Pertatataka Formation is entirely younger than the Brachina Formation (Fig. 4.1b), perhaps even wholly younger than the Bunyeroo Formation (Jenkins, 1993b), instead of being the broad equivalent of both. Another problem concerns the age of the Grant Bluff and Elkera Formations in the Georgina Basin. Jenkins (1993b, Fig. 26, and pers. comm.) considers the presence of simple trace fossils in these units as evidence of correlation with the metazoan-bearing lower Arumbera Sandstone and Pound Subgroup (Fig. 4.1b). In contrast, there is good lithostratigraphic evidence for correlation of the Grant Bluff Formation with the Cyclops Member and the calcareous part of the Elkera Formation with the Julie Formation (Walter, 1980; Fig. 4.1a).

This chapter is a systematic isotope-chemostratigraphic survey of the Ediacarian of the Amadeus and Georgina Basins, not including the upper, redbed-dominated formations in both basins (Arumbera Formation, Central Mt Stuart Formation) which are very poor in sedimentary carbon and strontium. The better-known and more extensive Ediacarian successions of the Amadeus Basin are the main focus of the study. In the Amadeus Basin, a large number of outcrop and drillcore sections was measured or logged (Fig. 4.4), and isotopic data were extracted from most of these. Three overlapping drillcore sections from the southwest Georgina Basin were logged and sampled. Fieldwork was carried out in collaboration with K. Grey, who undertook duplicate sampling of most sections for a parallel study in acritarch biostratigraphy (Grey, in prep.). Sedimentological descriptions and inferred palaeoenvironments are given for units studied, based on field observations, petrography and geochemistry. In most cases little previous detailed sedimentological work has been carried out on these successions.

Sampling and analytical methods are detailed in Chapter 2. Carbon isotopes are the main focus of this work, but isotopes of oxygen, sulphur and strontium have yielded important supplementary chemostratigraphic information. As in the type Ediacarian, most of the succession lacks primary carbonates and it has been necessary to rely heavily on organic ^{13}C data. Although generally perceived as a less reliable

a)

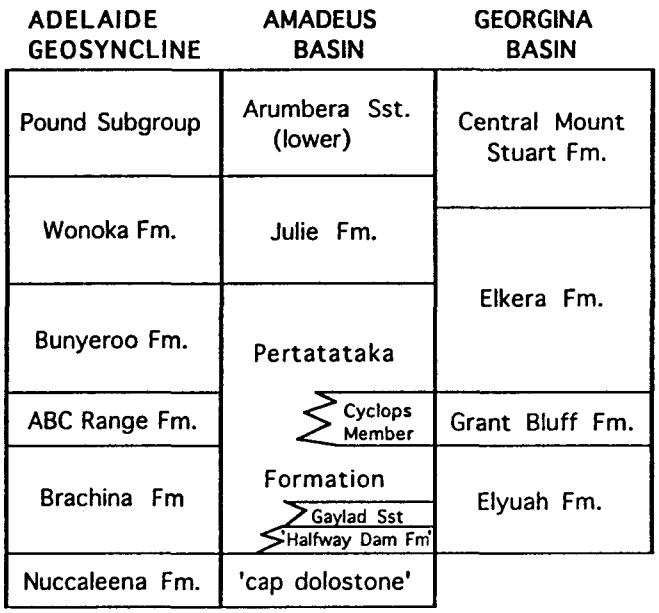

b)

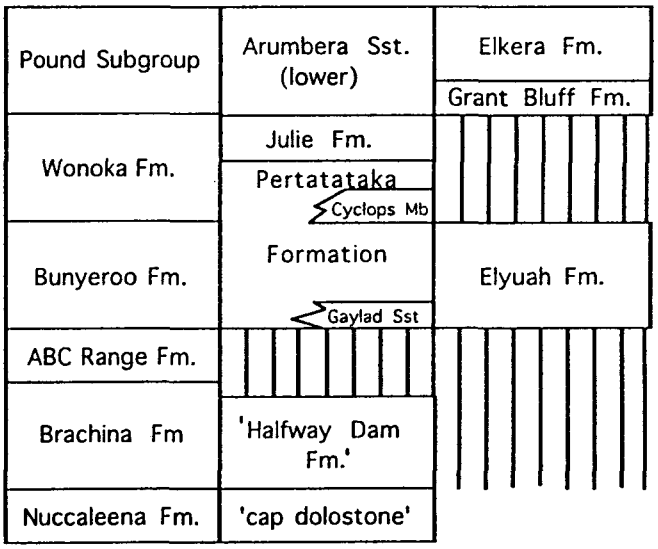

Fig. 4.1: Stratigraphic nomenclature and proposed correlation between the type Ediacarian (Adelaide Geosyncline), the northern Amadeus Basin and the southwestern Georgina basin; (a) after Preiss et al. (1978) and Walter (1980); (b) after Jenkins (1993).

chemostratigraphic signal carrier than carbonate ^{13}C (eg. Kaufman & Knoll, 1995), the organic data here (together with Chapter 3) provide further empirical evidence for the utility of organic ^{13}C stratigraphy in Ediacarian successions. Methods of organic $\delta^{13}C$ data treatment to better resolve the organic $\delta^{13}C$ signal by correcting for variation caused by changes in TOC, regional variation in thermal maturity, and mixing of

benthic and planktonic end-member sources, are utilized (see section 2.3 for a full explanation of these methods). Cathode luminesence, plane-light petrography, and trace-element (Mn, Sr) analyses of a large number of representative samples were used to assess diagenetic alteration in carbonates.

The isotopic data are in broad agreement with the correlations suggested by Preiss (1978) and Walter (1980), as depicted in Fig. 4.1a. In the Amadeus Basin, the data support correlation of the (pre-Ediacarian part of the) Pioneer Formation with the partly glacigene Olympic Formation. The 'cap dolostone' of the NE Amadeus Basin has a markedly similar stable isotope profile to the Nuccaleena Formation of the Adelaide

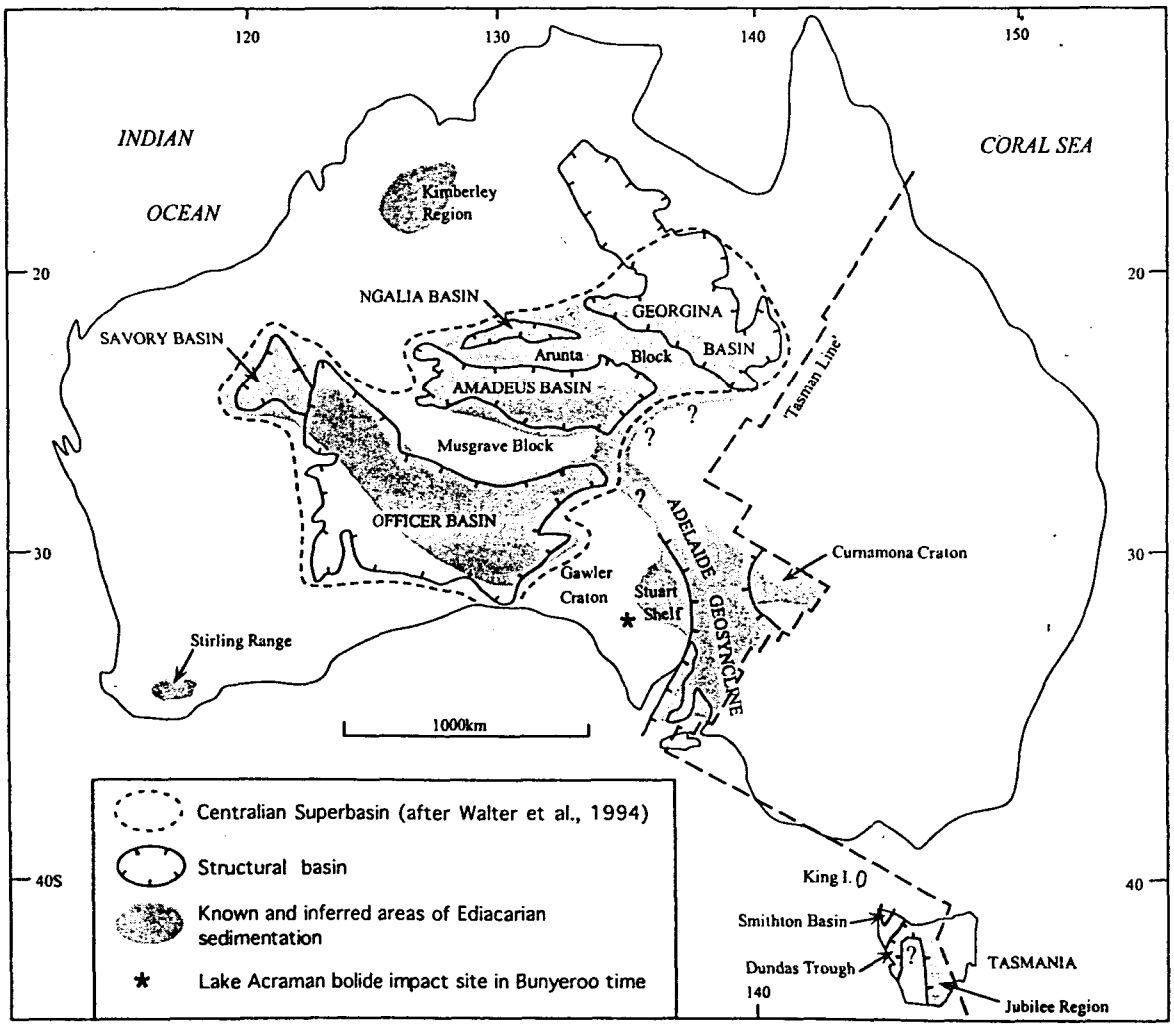

Fig. 4.2: Known and inferred extent of Ediacarian sedimentation in Australia; inferred limits of Neoproterozoic Centralian Superbasin; major present structural basins and Lake Acraman bolide impact site. From Walter et al.(1995); Preiss & Forbes (1981); Cruse et al.(1993); Gostin & Williams (1986).

Geosyncline. The data are most simply interpreted if the Pertatataka Formation is correlative with the Brachina, ABC Range, and Bunyeroo Formations. Apparent lateral change in the $\delta^{13}C_{org}$ profiles in the Pertatataka Formation between the central and northern part of the Amadeus Basin are consistent with lateral variations in sedimentation rates that may be expected *a priori* from a sequence-stratigraphic framework based on basin geometry, palaeocurrents and facies change. The Julie Formation is probably older than the upper part of the Wonoka Formation. Isotopic evidence supports correlation of the Elyuah and Grant Bluff Formations of the Georgina Basin with the lower and middle parts of the Pertatataka Formation. Correlation of the Elkera Formation is problematic. It may be partly younger than the type Julie Formation.

In the Amadeus Basin, carbonates associated with Marinoan glacigene rocks are enriched in ^{18}O relative to cap dolostones and younger Ediacarian carbonates, consistent with a ca. 20°C temperature rise at the close of the glaciation. A period of stratification of basin waters early in the Ediacarian is suggested by strongly ^{13}C-depleted organic carbon of benthic microbial mat origin and ^{13}C-depleted carbonates in relatively deep-water environments low in the succession.

4.2 Geological Setting: Amadeus Basin

The Amadeus Basin is one of a number of intracratonic basins in which Neoproterozoic successions are preserved on the Australian plate (Fig. 4.2). These basins are structural and erosional remnants of an originally much larger depositional system named the Centralian Superbasin (Walter et al., 1995) (Fig. 4.2). In the Amadeus basin the successions are predominantly marine; and a connection to the open ocean probably existed to the east (Lindsay, 1989). During the Ediacarian, the Musgrave Block to the south of the Amadeus Basin was emergent and a major source of sediment, and parts of the Arunta Block were a lesser source from the north (Wells et al., 1970; Walter et al., 1980).

Ediacarian basin geometry was evidently complex. There was a larger, southern sub-basin with a southward-thickening sediment prism (Wells et al., 1970, their Fig. 11), and a smaller, generally shallower northern sub-basin with two depocentres (Fig. 4.3). A narrow, east-west structural high, the Central Ridge, was emergent at times.

Lindsay et al. (1987) proposed that the Amadeus Basin evolved through two phases of thermal subsidence following periods of crustal extension at 900 Ma and 600 Ma.

However, Shaw et al. (1991) and Oaks et al. (1991) convincingly argue for a more complex history of basin tectonics. Shaw et al. propose a regional, N-S horizontal compressive regime for the Olympic-Pertatataka-Julie sequence, with which this study is primarily concerned. There was a steep thrust fault along the southern margin of the basin, and lithospheric downwarping was enhanced by sediment loading . The Central Ridge is interpreted as a peripheral arch separating the larger, southern, southward-thickening sediment prism from the smaller northern sub-basin (Fig. 4.13b). However, the Central Ridge was topographically subdued during Pertatataka time (Fig. 4.13c, and see later discussion), and the peripheral arch may instead have coincided with the broad area of relatively thin Pertatataka Formation in the northern part of the basin.

There was uplift along the Central Ridge during the Petermann Ranges Orogeny at the close of the Proterozoic. At the same time, gentle folding and uplift in the southern sub-basin caused erosion of much of the Ediacarian succession from this area (Wells et al., 1970; Oaks et al., 1991).

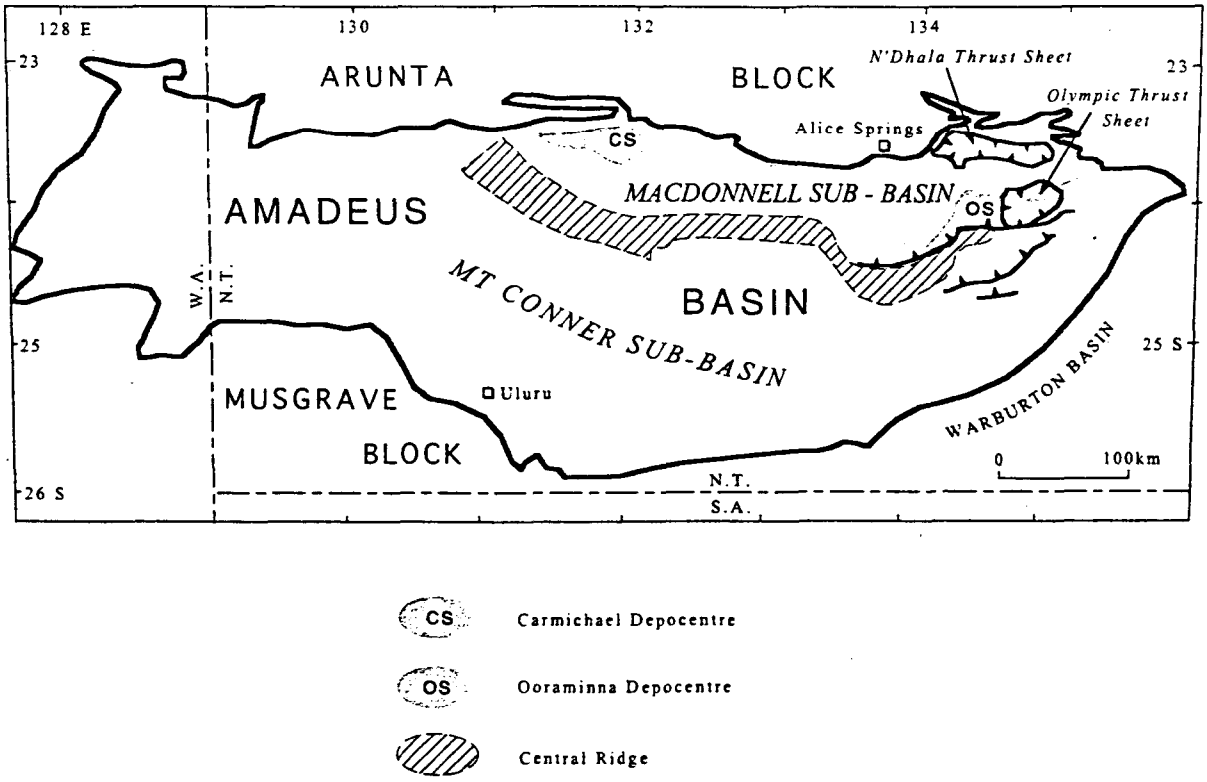

Fig. 4.3: Tectonic elements of the Amadeus Basin. Nomenclature after Oaks et al. (1991).

The Alice Springs Orogeny affected the northern sub-basin in the Devonian, causing gentle folding and southward-directed thrusting. A number of important localities in the NE Amadeus Basin are located on rootless thrust sheets emplaced at this time (Fig. 4.4). Transport distances for these nappes are controversial (Stewart et al., 1991). Oaks and Deckelman (in Stewart et al., 1991) convincingly argue for relatively short (~10 km) transport distances on the basis of distributions of laterally restricted facies variants in several units. This interpretation obviates the need for major palinspastic readjustment. The alternative interpretation, by Stewart & Shaw (in Stewart et al., 1991) involves a minimum of 60 km of southward movement of the N'Dhala and Olympic thrust sheets.

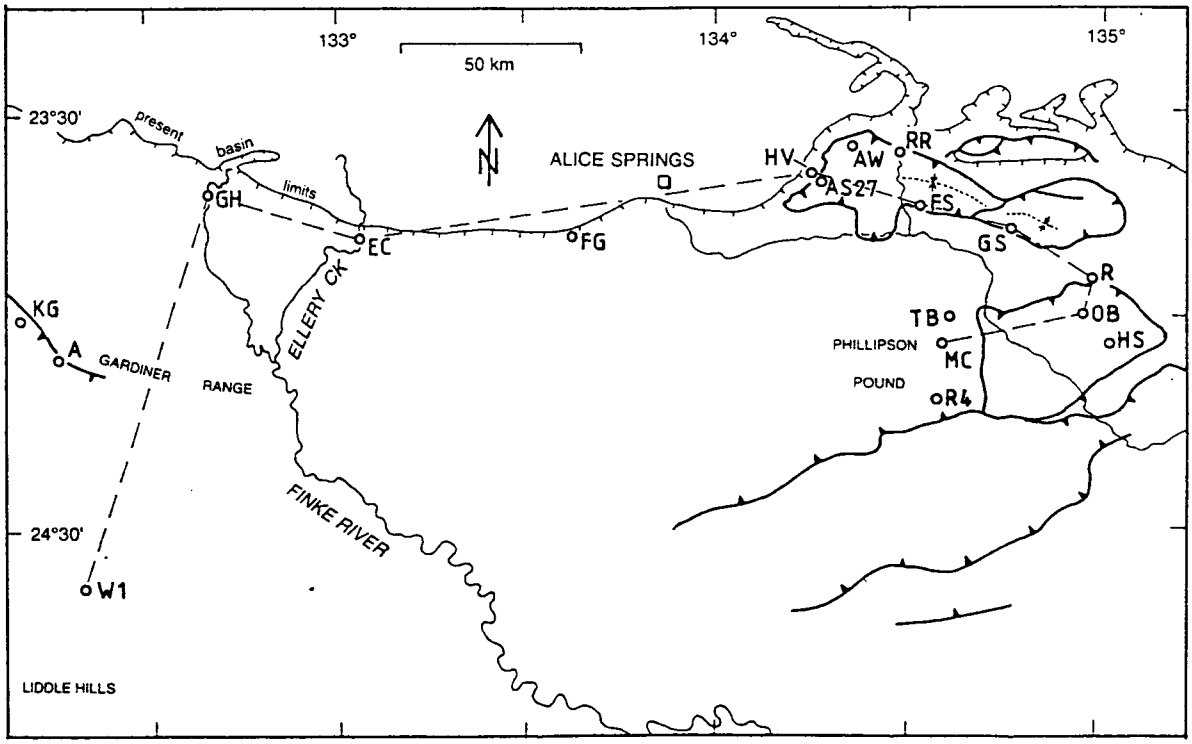

Fig. 4.4: Locality map, northeastern Amadeus Basin. Dashed line links sections shown in Fig. 4.21. Individual localities/sections are: **A:** Areyonga; **AS27:** Alice Springs 27 drillhole; **AW:** Acacia Well; **EC:** Ellery Creek; **FG:** Fenn Gap; **FS:** Fergusson Syncline; **GH:** Glen Helen; **GS:** Gaylad Syncline; **HS:** Hijinx Syncline; **HV:** Hidden Valley; **KG:** Katapata Gap; **MC:** Mt. Capitor; **OB:** Olympic Bore; **R:** 11 km S of Ringwood Station; **RR:** Ross River; **R4:** Rodinga 4 drillhole; **TB:** Twin Bore; **W1:** Wallara 1 drillhole.

4.2a Correlation of the Ediacarian Succession: Previous Work

A number of techniques - lithostratigraphy, biostratigraphy, sequence-stratigraphy and radiometric dating - have yielded information concerning correlation of the Ediacarian succession in the Amadeus Basin.

The Ediacarian System is constrained at its base by the upper of two Neoproterozoic glacigene units (Wells et al., 1970; Preiss et al., 1978) and at its top by the base of the Cambrian, identified within the Arumbera Sandstone that has rare elements of the soft-bodied metazoan Ediacara fauna in its lower part and early Cambrian trace fossils in its upper part (Daily, 1972; Glaessner & Walter, 1975; Walter et al., 1989). Lindsay (1989) proposed a non-glacial origin for the diamictites of the Olympic Formation, thereby casting doubt on a correlation with the Marinoan glacials of the Adelaide Geosyncline. However, evidence for ice rafting (Field, 1991), lithologic resemblance with the Elatina Formation diamictite and the presence in both basins of lithologically similar overlying cap dolostones (Preiss et al., 1978) are strong evidence in favour of the correlation.

In the N and NE parts of the basin, the Ediacarian sedimentary succession is broadly similar to the type Ediacarian (Cloud and Glaessner, 1982) of the Adelaide Geosyncline, beginning with a cap dolostone overlying the glacigene rocks, followed by thick shales (Pertatataka Formation), carbonates (Julie Formation), and redbeds (Arumbera Sandstone). The close resemblance of the cap dolostone to the Nuccaleena Formation of the Adelaide Geosyncline is particularly noteworthy (Preiss et al., 1978). A straightforward lithostratigraphic correlation as shown in Fig. 4.1a has been widely accepted (Preiss et al., 1978; Preiss & Forbes, 1981; Forbes & Preiss, 1987; Walter et al., 1995).

However, the succession is here much thinner than the type Ediacarian (approximately one-quarter to one-half the thickness) and there are significant differences of detail. For example, the Julie Formation (mostly shallow-water dolostone) is unlike all but the topmost part of the Wonoka Formation. The Gaylad Sandstone and its basal unconformity, which occur low in the Ediacarian in the NE Amadeus Basin (Freeman et al., 1991), have no clear equivalent in the Adelaide Geosyncline.

Regional facies variation within the Amadeus Basin has led to uncertainties in intrabasinal correlation. Preiss et al. (1978) proposed equivalence of the predominantly glacigene Olympic Formation with the sandy Pioneer Formation, and this is confirmed by recent unpublished mapping by M. R. Walter and R. J. F. Jenkins (Jenkins, 1993b).

This correlation, however, has recently been questioned (Field, 1991; Preiss, pers. comm.). There has been confusion of some cap dolostone occurrences with older dolostone units (eg. see Freeman et al., 1991). Cap dolostone occurrences are lithologically variable from place to place and their mutual equivalence is not always certain (e.g. Preiss et al., 1978). How the Gaylad Sandstone and the underlying shale unit, the Halfway Dam Formation, relate to the type Pertatataka Formation in the central-north Amadeus Basin, is also controversial (Field, 1991; Freeman et al., 1991; Jenkins, 1993b). Three alternative proposed within-basin lithostratigraphic correlation schemes are presented as Fig. 4.21.

A distinctive assemblage of large, spiny acritarchs occurs near the top of the Pertatataka Formation (Zang & Walter, 1989, 1992); elements of which are also found in the Rodda beds of the Officer Basin at a stratigraphic level above the correlate of the Bunyeroo Formation (Jenkins et al., 1992). Important new biostratigraphic data are emerging from the systematic acritarch study by Grey (in prep.). Preliminary data from Grey (in prep.) provide significant corroborative chronostratigraphic information for some of the correlations proposed below.

A stromatolite from the Julie Formation (*Tungussia julia* Walter & Krylov in Walter et al., 1979) is possibly conspecific with a form (*Tungussia cf. julia)* from the uppermost Wonoka Formation (Walter et al., 1979). The lower Arumbera Formation contains *Charniodiscus* and other metazoan body fossils of the Ediacara fauna (Glaessner, 1969; Jenkins & Gehling, 1978). The upper Arumbera Formation contains a diverse trace fossil assemblage (assemblage 3 of Walter et al., 1989) indicating an Early Cambrian age.

Several Rb/Sr dates on the Pertatataka Formation range from 822 Ma to 715 Ma (Compston & Arriens, 1968; Bofinger in Wells et al., 1970; and Preiss & Forbes, 1981) but for various reasons these dates are now considered unreliable (Walter, 1972; Walter et al., 1995).

Sequence-stratigraphy in Neoproterozoic successions is a potentially useful chronostratigraphic technique (eg. Christie-Blick et al., 1988; Sukanta et al., 1991). In the Amadeus Basin, identification of sequence boundaries is hindered by the prevailing parallelism of seismic reflectors, a function of the slow, regular subsidence of the intracratonic setting and of the non-preservation of original basin margins where differential subsidence is instrumental in generating patterns of stratal onlap and offlap (Lindsay & Korsch, 1991; Kennard & Lindsay, 1991). Sequence boundaries have been

identified at mapped unconformities and prominent facies discontinuities (Lindsay, 1989; Lindsay & Korsch, 1991). In the succession of interest here, the disconformable, locally unconformable base of the Olympic Formation is considered a sequence boundary (Lindsay & Korsch, 1991; Oaks et al., 1991). A second boundary has been identified at the unconformable base of the Gaylad Sandstone, a unit present only in the NE Amadeus Basin (Fig. 4.21) (Freeman et al., 1991; Jenkins et al., 1992). A third has been proposed at the prominent facies discontinuity at the top of the Julie Formation (Lindsay, 1989; Lindsay & Korsch, 1991). The base of the cap dolostone has been interpreted as a transgressive surface (Lindsay, 1989; Lindsay & Korsch, 1991), in contrast to the (probably correlative) base of the Nuccaleena Formation in the Adelaide Geosyncline where a sequence boundary has been convincingly identified (Christie-Blick et al., 1988; Dyson, 1992).

Only two intra-Ediacarian depositional sequence boundaries have therefore been identified, compared to five or more in the Adelaide Geosyncline (Christie-Blick et al., 1990). Jenkins et al. (1992) proposed correlation of the base-Gaylad sequence boundary with the first intra-Ediacarian sequence boundary at the top of the ABC Range Formation in the Adelaide Geosyncline (Figs. 4.1b, 4.21). The type Pertatataka Formation would then be entirely younger than the ABC Range Formation of the Adelaide Geosyncline. Recently Jenkins (1993b, p 57) has raised the possibility of an even younger (wholly post-Bunyeroo) age for the Pertatataka Formation.

Unfortunately, interbasinal sequence correlation cannot be regarded as reliable in the absence of corroborative age control (e.g. Miall, 1992). (Neoproterozoic sequence correlation between the Officer Basin and the Adelaide Geosyncline is aided by a unique, isochronous marker bed, the Acraman impact ejecta layer (Sukanta et al., 1991)). Furthermore, the assumption of a global, eustatic control on sequence development (Vail et al., 1977) is doubtful where local tectonism may have influenced relative sea-level change - as shown, for instance, by angular unconformities or evidence for salt tectonics (Galloway, 1989). By these criteria, the base-Olympic and base-Gaylad unconformities may not be regionally correlatable surfaces. There is good evidence for salt movement in the Amadeus Basin around this time (Kennedy, 1993).

4.3 Olympic and Pioneer Formations, excluding cap dolostone

4.3a Introduction

The Olympic and Pioneer Formations are conglomeratic and sandy equivalents, respectively, of the Marinoan glacial phase (Preiss et al., 1978). These formations were defined (Preiss et al., 1978) to include the cap dolostone (the basal unit of the Ediacarian), but it is clear that the cap dolostone is fundamentally dissimilar to the underlying successions (e.g. Coats & Preiss, in Preiss et al., 1978, p. 47) and accordingly this unit is treated in a separate section below. The base of the cap dolostone is a prominent facies discontinuity; it is everywhere abrupt and in places is an erosional disconformity. This surface is probably a sequence boundary correlative with the base-Ediacarian sequence boundary in the Adelaide Geosyncline (see next section). Rocks treated in this section are considered pre-Ediacarian but include units similar to cap dolostone.

The Olympic Formation crops out in the NE Amadeus Basin, and includes diamictites and pebbly mudstones widely accepted as being of glacial origin (Wells et al., 1970; Preiss et al., 1978; Field, 1991; but see Lindsay (1989) for an alternative view). Preiss et al. (1978) proposed on lithostratigraphic grounds that the sandy Pioneer Formation, widespread elsewhere in the Amadeus Basin, is a lateral equivalent of the Olympic Formation. Supporting this view is the observation that thick-bedded, cross-bedded feldspathic sandstones in the upper part of the Olympic Formation at Mt Capitor are essentially identical to sandstones of the Pioneer Formation at Ellery Creek and Glen Helen (Freeman et al., 1991, p. 146; Jenkins, 1993b, p. 54). Mapping by Walter & Jenkins (unpubl.) provides further confirmation that the two formations are lateral facies equivalents.

4.3b Olympic Formation

Wells et al. (1967), Field (1991) and Freeman et al. (1991) provide detailed descriptions of the Olympic Formation, which consists of a laterally variable succession, up to 300 m thick, of shale, sandstone, conglomerate, diamictite and minor dolostone. Carbonates from two sections, at Hijinx Syncline and Mt Capitor (Fig. 4.4) were sampled in this study.

At Hijinx Syncline a six metre-thick sandy dolostone unit at [5040 73407] constitutes the youngest exposed unit in the core of the syncline. This unit was regarded by Preiss

et al. (1978, their Fig. 3) as cap dolostone, but Freeman et al. (1991, p.145) present lithostratigraphic evidence that the unit belongs to the older Olympic Formation, a conclusion supported here by isotope chemostratigraphy. Freeman et al. and Oaks et al. (1990) show that the sandy dolostone belongs to a lower, shale and siltstone-dominated, mappable subunit (Puf_1) which is regionally overlain (e.g. at nearby South Bore and at Mt Capitor) by an upper, sandstone and conglomerate-dominated subunit (Puf_2) of the Olympic Formation.

At Hijinx Syncline the dolostone abruptly overlies a probably glaciomarine succession of pebbly siltstone, sandstone and diamictite of which a total thickness of about 30 m is exposed. Low in the dolostone unit (Fig. 4.5), there are thick, sharp-based, irregular beds of impure, brown-weathering, poorly sorted, sandy dolostone that may be debris-flow deposits. Thin sections show small (1mm) euhedral voids, some calcite-lined, possibly after gypsum. Most of the unit consists of thin-bedded, slightly sandy, fine-grained dolostone, with a bed of creamy dolomicrite 3.1 to 3.2 m above the base. In thin section the dolomicrite is seen to be partly open-framework breccia with sparse angular fragments of denser dolomicrite; and there are sparse irregular vugs of uncertain origin filled with calcite spar.

At the base of the large cliff section at Mt Capitor there is a dolomitic unit correlated by Freeman et al. (1991) with that at Hijinx Syncline (their Figs. 8, 13). (The thicker dolostone unit high in the Mt Capitor section (Fig. 4.6a) is cap dolostone (Jenkins, 1993b), not part of the older Olympic Formation as indicated by Freeman et al. (1991, their Fig. 13) and Field (1991, his Fig. 2)). The dolomitic unit at the base of the cliff section consists of 2 m of breccia composed of angular, creamy dolomicrite clasts and red and grey chert pebbles in a sandy dolostone matrix. This bed, possibly a debris-flow deposit, is overlain by a thin continuous bed of creamy dolomicrite. The unit is overlain by 200 m of thick-bedded, cross-bedded feldspathic quartzarenite and minor diamictite belonging to the upper subunit of the Olympic Formation (Freeman et al., 1991).

Isotope Stratigraphy

At Hijinx Syncline sandy dolostone (50% carbonate) from low in the dolostone unit has a moderately depleted isotopic composition (Fig. 4.5) but carbonate in this lithology is probably at least partly detrital in origin. The two stratigraphically higher samples analysed are moderately ^{13}C-enriched and also relatively high in ^{18}O. Micritic texture and Mn/Sr ratios below 10 suggest preservation of near-primary $\delta^{13}C_{carb}$ values. A

sample from the dolomicrite bed ($\delta^{13}C_{carb}$ = +3.1 ‰; $\delta^{18}O$ = -0.6 ‰) probably preserves stable isotopic composition closest to depositional values on the basis of textural preservation, heaviest isotopic composition and relatively low $^{87}Sr/^{86}Sr$ (Table 4.1). The $^{87}Sr/^{86}Sr$ ratio of this sample, at 0.7090 , is probably a slightly altered marine composition (see below). Sr content of this sample is low (75 ppm) so some vulnerability of $^{87}Sr/^{86}Sr$ to diagenetic alteration is to be expected.

The dolomicrite bed at Mt Capitor has an almost identical stable-isotopic composition ($\delta^{13}C$ = +3.2 ‰, $\delta^{18}O$ = 0.1 ‰) to the dolomicrite bed at Hijinx Syncline, supporting the correlation of Freeman et al. (1991) of these two sections.

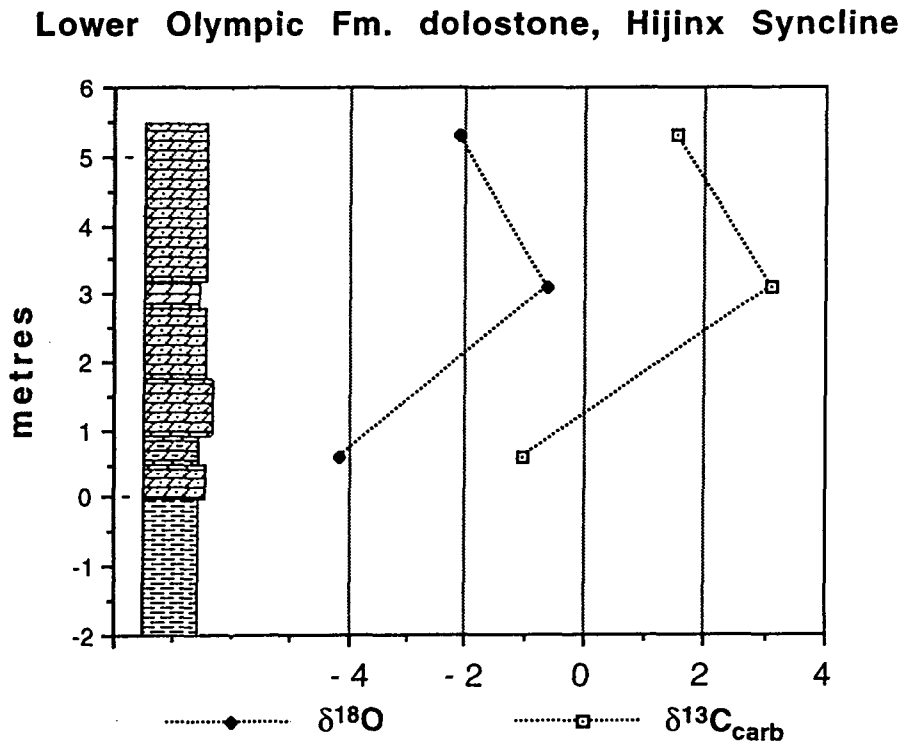

Fig. 4.5: Lithologic column and carbonate $\delta^{13}C$ and $\delta^{18}O$ profiles, dolostone unit within Olympic Formation, Hijinx Syncline. (For key to lithological symbols see Fig. 3.4).

4.3d Pioneer Formation

The Pioneer Formation was examined in its type section at Ellery Creek, at Glen Helen, Hidden Valley and in Wallara 1. In addition, isolated outcrops of carbonate at Fenn Gap and Mt Conner are here regarded as correlatives of the Pioneer Formation on the basis of isotopic composition and inferred stratigraphic position.

In Wallara 1 (Calver, 1993), at Ellery Creek and Glen Helen, the Pioneer Formation consists mainly of feldspathic, gritty quartz sandstone. At Ellery Creek and Glen Helen, large-scale (1 m) cross-bedding is common and there is upward gradation into

sample	rocktype	Sr(ppm)	Mn(ppm)	Mn/Sr	87Sr/86Sr	∂13C	∂18O
Olympic Fm., Hijinx Syncline							
23.14	dolostone	75	704	9.43	0.70898	3.1	-0.3
23.15	dolostone	180	774	4.30	0.71157	1.5	-2.1
Correlate of Pioneer Fm., Fenn Gap							
6.62	dolostone	150	1689	11.25	0.70775	1.6	-2.5
6.64	dolostone	249	706	2.84		2.2	-1.5
?Correlate of Pioneer Fm., Mt Conner							
7.01	dolostone	151	1408	9.30	0.71003	-1.1	-1.5
7.06	dolostone	219	2393	10.91	0.71032	-1.6	-1.2
'Cap dolostone', Wallara 1							
28.128	dolostone				0.70959		
28.129	dolostone				0.70924	-3.5	-7.7
28.132	dolostone				0.70898	-3.3	-7.7

Table 4.1: Trace-element and strontium isotopic data, carbonates of Olympic and Pioneer Formations including cap dolostone from Wallara 1.

texturally and compositionally more mature quartzarenite. At Ellery Creek, this upper quartzarenite unit - only 6 m thick of a total 160 m - has medium-scale (0.1 m) tabular herringbone cross-bedding. Here, the quartzarenite is partly dolomite-cemented and locally contains large (100 mm) platy intraclasts of sandy dolostone and rare ooids (Walter & Bauld, 1983). The upper contact of the quartzarenite is an erosional surface overlain by cap dolostone.

The feldspathic sandstone at Ellery Creek and Glen Helen is probably predominantly fluvial or fluvioglacial and possibly partly aeolian (Freeman et al., 1991), while the quartzarenite at Ellery Creek is interpreted as tide-influenced shallow-marine.

An isolated outcrop of dolostone and sandstone at Fenn Gap is appropriately located to be a Pioneer Formation correlative (M R Walter, pers. comm.). The section (Fig. 4.7) begins with 2 m of quartzarenite with medium-scale cross-bedding and carbonate intraclasts, resembling the upper part of the Pioneer Formation at Ellery Creek. Then follows about 40 m of predominantly thin-bedded and laminated, grey-brown silty dolostone, with several stromatolitic beds. These beds consist of close-spaced domical, cumulate and turbinate stromatolites with platy-intraclast conglomerate filling intercolumnar spaces. Many stromatolites appear to have nucleated on edgewise clusters of intraclasts. A shallow-marine, probably intertidal environment of deposition is inferred. Strontium isotopic composition confirms a marine environment (see below).

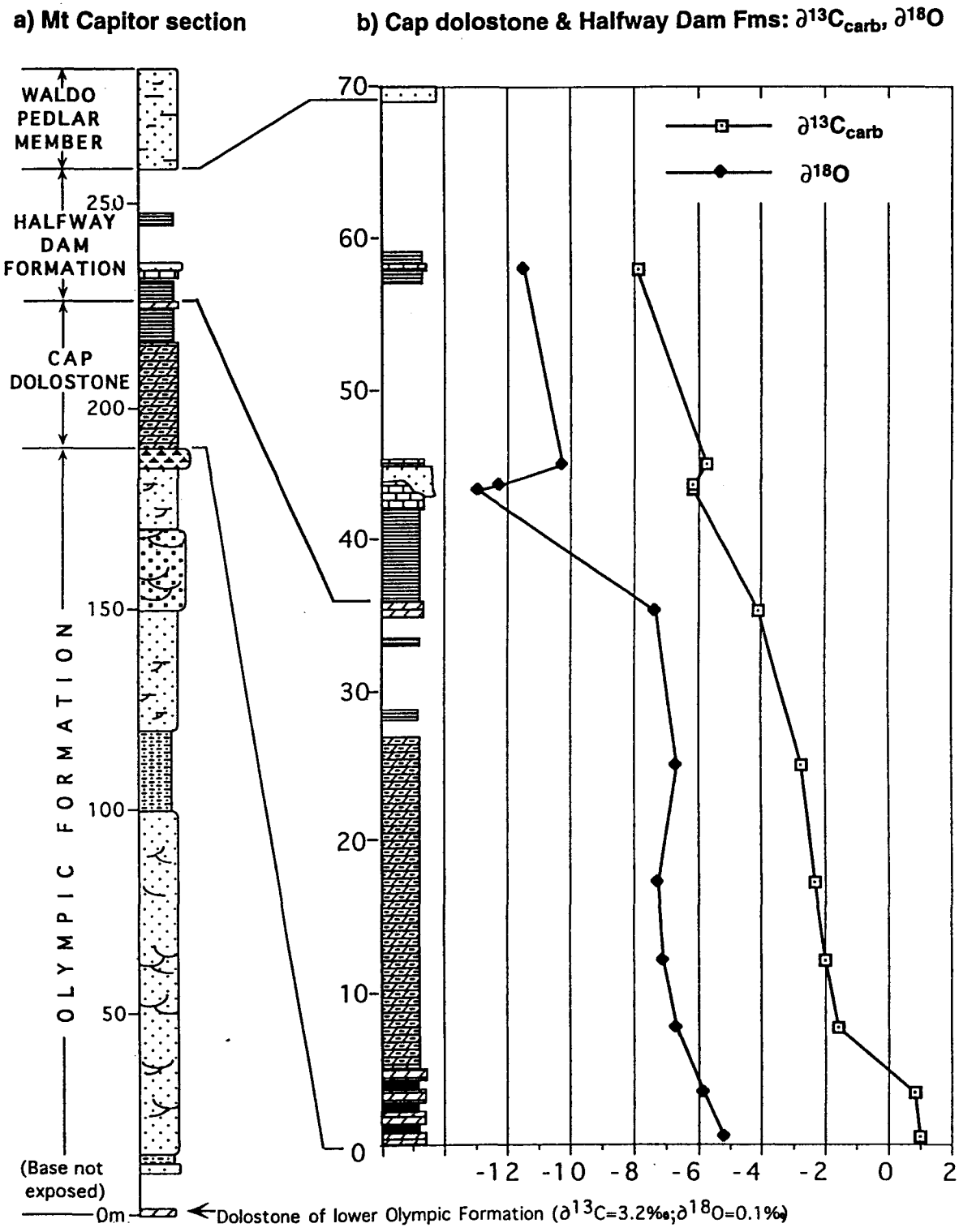

Fig. 4.6: (a) Lithologic column, eastern face of Mt Capitor; (b) carbonate $\delta^{13}C$ and $\delta^{18}O$ profiles of cap dolostone and 'Halfway Dam Formation'.

Further east, at Hidden Valley, a thin (5-10 m) unit of sandstone and silty dolostone, a probable correlative of the Pioneer Formation, rests gradationally upon a thick (700 m) succession of siltstone and poorly-sorted sandstone that has been described and named the 'Undoolya sequence' by Kennedy (1993). The Undoolya sequence is very localised in distribution, and is interpreted by Kennedy as the fill of the peripheral sink of a salt diapir rising from the underlying Bitter Springs Formation. The Pioneer correlative (Fig. 4.8) consists of interbedded brown-weathering silty dolostone and quartz sandstone that becomes coarser-grained upwards. A thin section of the silty dolostone has 40% quartz silt grains and shows that the dolomite is recrystallised (50 μ grainsize) and probably includes both detrital carbonate and cement. The uppermost bed of the Pioneer correlative is an unusual sedimentary breccia of probable slump origin consisting of angular, ragged fragments of quartz sandstone in a brown-weathering sandy dolostone matrix. A thin section shows a recrystallised, xenotopic dolomite mosaic of 50 - 100 μ grainsize with floating, rounded quartz sand grains. The upper contact of this breccia bed (the surface here considered to represent the base of the Ediacarian) has a mounded topography with up to a few metres of relief. The mounds are slightly elongate in a down-dip (W-E) direction. Some have southern flanks that are vertical to oversteepened with respect to bedding, suggesting an origin by S-directed slump movement. The mounds are encrusted by a continuous bed of stromatolitic chert, here regarded as the basal Ediacarian cap dolostone correlative. The steepness of the mound flanks suggests the former presence of supporting superincumbent sediments that were also involved with slump movement. The dolostone-sandstone breccia perhaps became lithified prior to a phase of erosion that removed the overlying sediments to uncover the undulose upper surface of the bed, which then became the substrate for stromatolite growth at the commencement of the Ediacarian marine transgression.

The Pioneer Formation correlative here represents the final shoaling phase of the deep-water, turbiditic fill of a localised salt-withdrawal basin (Kennedy, 1993). Slumping at the top of the formation may be related to salt tectonics.

Near Mt Conner in the southern Amadeus Basin, an isolated exposure of dolostone is situated roughly 300 m stratigraphically above the nearest outcrop of quartz sandstone mapped as (pre-Ediacarian) Inindia beds (Wells et al., 1970), and 200 m below nearest outcrop of Winnall beds (correlative of the Pertatataka Formation) (Fig. 4.14). The dolostone is exposed over a broad area but regional dips are gentle and the unit may be

only a few metres thick. Outcrops consist of bioherms a few metres wide composed of large, broadly domical stromatolites individually up to 2 m wide. As at Fenn Gap, stromatolites are associated with flat-pebble breccia, and many have nucleated on upturned edges of intraclasts.

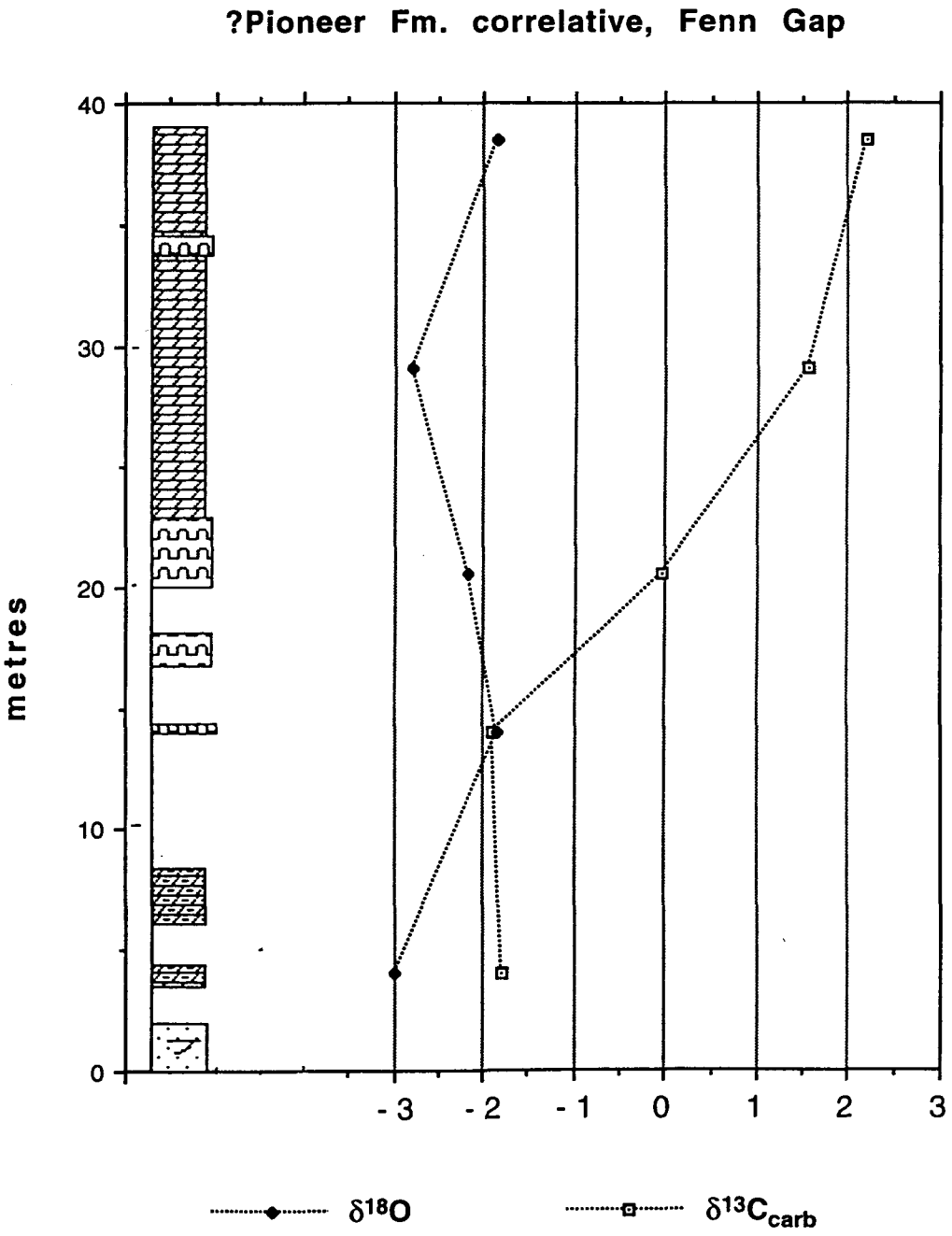

Fig. 4.7: Lithologic column and carbonate $\delta^{13}C$ and $\delta^{18}O$ profiles of a dolostone unit (probable Pioneer Formation correlative) at Fenn Gap.

Isotope Stratigraphy

The carbonates at Fenn Gap, Hidden Valley and Mt Conner have $\delta^{13}C_{carb}$ within the range -2 to +2 ‰. The thickest carbonate section at Fenn Gap displays an upward-increasing trend through this range (Figs 4.7, 4.8). Mt Conner and Fenn Gap are characterised, like the Olympic Formation carbonates, by $\delta^{18}O$ that is heavy (-3 to -1.2 ‰) relative to cap dolostone and most younger Ediacarian carbonates (Fig 4.10). The micritic texture, heavy $\delta^{18}O$, and moderate Mn/Sr ratios (range 2.8 to 11.3, n = 4, Table 4.1) suggest carbon isotopic compositions at Mt Conner and Fenn Gap are not significantly altered. Relatively coarsely recrystallized textures and low $\delta^{18}O$ in the two samples analysed from Hidden Valley, however, mean that $\delta^{13}C_{carb}$ results from this locality may be altered.

One $^{87}Sr/^{86}Sr$ determination from Fenn Gap, at 0.7078, is sufficiently low to indicate a marine origin for the carbonate, but the ratio is slightly higher than accepted Marinoan-age marine $^{87}Sr/^{86}Sr$ (0.7066 - 0.7072: Kaufman et al., 1993) and so may be slightly altered. Two determinations from Mt Conner give values (~.710) that are clearly altered, if originally marine (Table 4.1).

4.3e INTERPRETATION

Lithostratigraphic and isotopic evidence, taken together, suggest two episodes of carbonate deposition in pre-Ediacarian Pioneer/Olympic time: an older unit of sandy, brecciated and micritic dolostone, partly of debris-flow origin, in the middle of the Olympic Formation (at Hijinx Syncline and Mt Capitor); and a younger unit of stromatolitic dolostone within the Pioneer Formation, associated with quartz sandstone at Fenn Gap and Hidden Valley and possibly represented by sandy dolostone intraclasts within quartz sandstone near the top of the formation at Ellery Creek. The dolostone near Mt Conner is a probable correlative of this younger unit on the basis of similar lithology, similar stromatolite morphology and microstructure (K. Grey, pers. comm.), and similar stable-isotopic composition.

Stable-isotope compositions of the two units are similar, consistent with the view that the Olympic and Pioneer Formations are correlative. However, the unit in the Olympic Formation may be slightly older as it occurs below a substantial unit of thick-bedded feldspathic sandstone at Mt Capitor (Fig. 4.6a); while the second unit is probably younger than a similar sandstone at Ellery Creek, and is found immediately below the base of the Ediacarian at Hidden Valley.

These dolostones are for the most part more enriched in ^{13}C and ^{18}O than cap dolostones, with only a small overlap of fields on a $\delta^{13}C$ - $\delta^{18}O$ crossplot (Fig 4.9). If the two texturally altered samples with lowest $\delta^{18}O$ (from Hidden Valley) are excluded, overlap of fields becomes negligible. Stable isotope analysis thus offers a means of differentiating these units where disagreement has existed in the past (e.g. compare Preiss et al., 1978; Freeman et al., 1991; and Jenkins, 1993b).

?Pioneer Fm correlative and cap dolostone, Hidden Valley

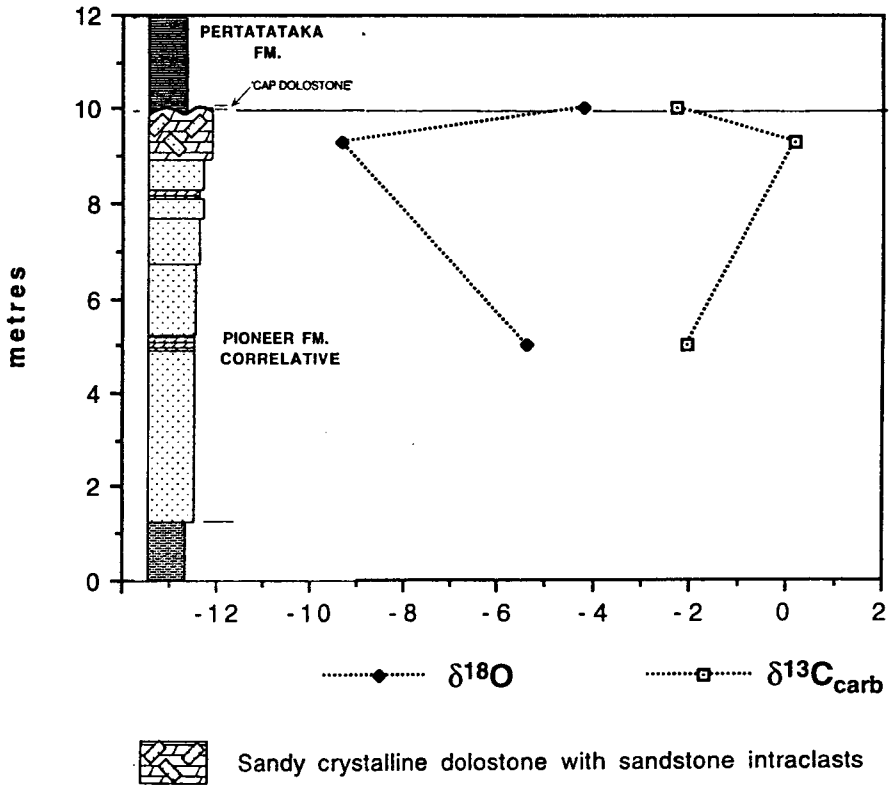

Fig. 4.8: Lithologic column and carbonate $\delta^{13}C$ and $\delta^{18}O$ profiles of a sandstone and dolostone unit (probable Pioneer Formation correlative) and overlying stromatolitic chert bed (probable cap dolostone) at Hidden Valley. Cap dolostone isotopic data from locality 2km SE of Hidden Valley. Upper two samples are recrystallised and possibly altered in $\delta^{13}C_{carb}$. Carbonate in lowest sample is partly detrital (see text).

$\delta^{18}O$ and palaeoclimate

The relatively ^{18}O-enriched compositions of these rocks suggests either preservation of little-altered marine values or evaporative enrichment of ^{18}O in a lacustrine setting. Least-altered $^{87}Sr/^{86}Sr$ ratios from both the Olympic Formation (0.7090) and Pioneer Formation (0.7078) indicate a marine origin because, given that the ratio increases with diagenetic alteration (Veizer & Compston, 1974), these ratios are unlikely to be derived

from depositional meteoric values. $^{87}Sr/^{86}Sr$ in the dissolved load of modern meteoric waters averages 0.7101 (Goldstein & Jacobsen, 1987) but is highly variable depending on Rb content and age of catchment areas. The ratio in meteoric waters draining the ancient felsic terranes of the Arunta and Musgrave Blocks - likely source areas to these sediments - is likely to have considerably exceeded this average, even 600 Ma ago.

An attractive explanation for the observed ^{18}O enrichment in these rocks is low palaeotemperatures, consistent with the observed association with glacigene rocks. The roughly 5‰ difference in $\delta^{18}O$ between the Pioneer/Olympic dolostones and the cap dolostones (Fig. 4.10) may be accounted for by a ca. 20°C temperature rise at the beginning of the Ediacarian. It is argued below that the cap dolostones are marine and that their oxygen isotopic compositions have been little altered by diagenesis. Deglaciation is the only mechanism capable of rapidly lowering oceanic $\delta^{18}O$, but in the Pleistocene this was limited to 1.5‰ (Shackleton, 1968).

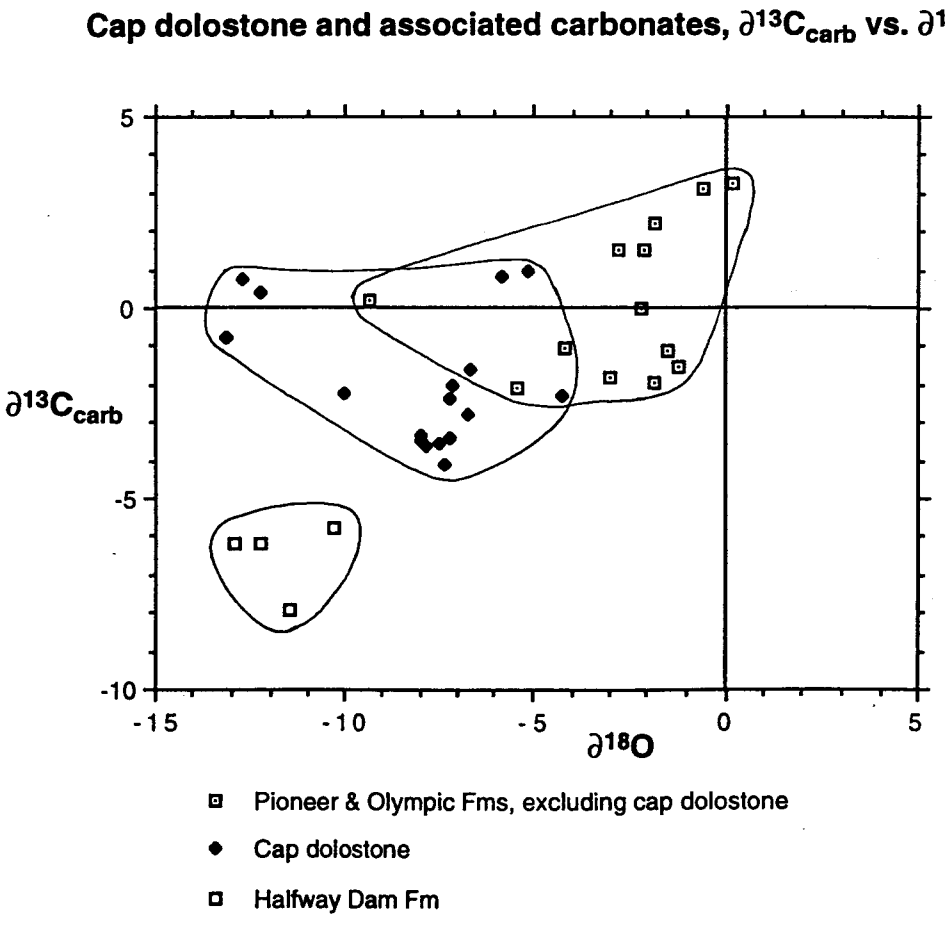

Fig. 4.9: $\delta^{13}C$ - $\delta^{18}O$ crossplot incorporating cap dolostones, (older) Pioneer/Olympic Formation. carbonates and limestones of the Halfway Dam Formation.

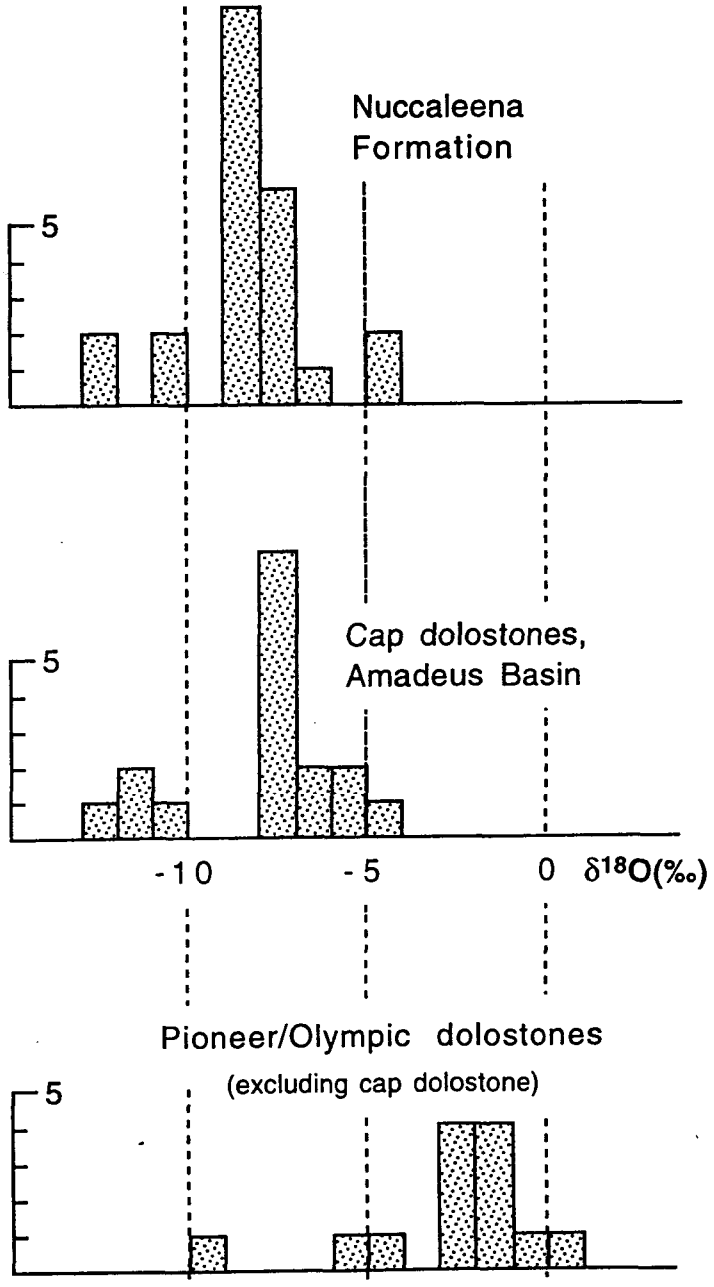

Fig. 4.10: $\delta^{18}O$ frequency distributions of cap dolostones, older Pioneer/Olympic dolostones, Julie Formation and Elkera Formation.

4.4 Cap dolostone

4.4a Introduction

'Upper marker cap dolomite' is the term used by Preiss et al. (1978) to denote the dolostone unit correlative with the Nuccaleena Formation of the Adelaide Geosyncline and (implicitly) the basal unit of the Ediacarian in the Amadeus Basin. 'Cap dolostone' is the term used for the sake of brevity here.

There has been some disagreement over identification of cap dolostone in different parts of the Amadeus Basin (Preiss et al., 1978; Freeman et al., 1991; Jenkins, 1993b). Here, thin cherty units at Ellery Creek and Hidden Valley are included together with more Nuccaleena-like laminated dolostones at Mt Capitor and Wallara 1, although as a lithostratigraphic correlation this must be regarded as tentative. There is strong evidence, both lithologic (Jenkins, 1993b) and isotopic (below), that dolostone at Mt Capitor is a correlative of the Nuccaleena Formation and hence a true cap dolostone, but Freeman et al. (1991) and Field (1991) included it as part of the older Olympic Formation. Conversely, dolostone outcrop in the Hijinx Syncline, originally shown by Preiss et al. (1978) as 'upper marker cap dolomite', is an older unit within the pre-Ediacarian Olympic Formation (see previous section).

4.4b Lithostratigraphy

Mt Capitor

At Mt Capitor, thick-bedded sandstone and diamictite of the Olympic Formation is abruptly overlain by an unusually thick (36 m) development of cap dolostone (Fig. 4.6a). The lowest 5 m consists of maroon shale with about 30% resistant, grey-brown, dolomitic, very fine-grained sandstone beds. These beds have sharp, planar bases and planar-parallel internal lamination passing up into wave-ripple lamination; and sharp, ripplemarked tops. A thin section shows about 50% quartz and about 50% granular, in part detrital, dolomite (Plate 4.1).

Then follows 22 m composed of thin, planar persistent beds of yellow-brown-weathering, pinkish-grey, very fine-grained dolostone interbedded with about 30% maroon shale. This part of the succession is strikingly similar to the Nuccaleena Formation (see previous chapter). As in the Nuccaleena Formation, the thin dolostone beds tend to have sharp tops and gradational bases on shale, and the tops of some dolostone beds are scoured with a few millimetres of relief. A thin section from 17.5 m

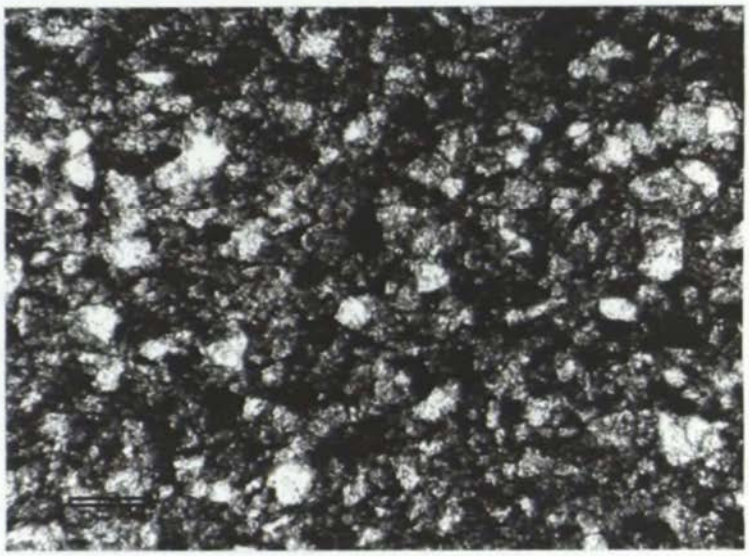

Plate 4.1: Thin section of silty dolostone from 0.5 m above base of 'cap dolostone' at Mt Capitor, showing clearly detrital nature of most carbonate. Sample 22.03. Scale bar = 100 μ.

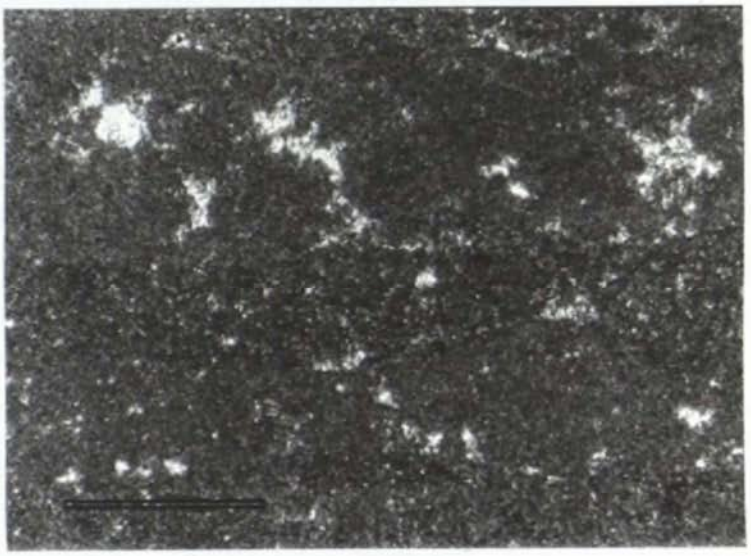

Plate 4.2: Thin section of 'cap dolostone' showing dolomicrosparite with microfenestrae, filled with clear dolospar and barite. Sample 22.09, 17.4 m above base of cap dolostone at Mt Capitor. Scale bar = 1mm.

Plate 4.3: Thin section showing small-scale erosional scour in the top of a dolostone bed in 'cap dolostone', sample 28.126, 1272.4 m depth, Wallara 1 drillhole, Amadeus Basin. Scale bar = 1mm.

above the base shows dolomicrosparite (5 - 10 μ grainsize) in places with abundant irregular microfenestrae, 10 - 100 μ in size, filled with dolospar and barite (electron microprobe determination) (Plate 4.2). At 25-30 m above the base of the cap dolostone (Fig. 4.6b) the succession becomes more thinly layered and shale-rich, and grades up into red shale. There is a final silty dolostone bed with ripple cross-lamination at 35 m, that is here taken as the top of the cap dolostone. The overlying succession, of shale with minor limestone and sandstone, is assigned to the 'Halfway Dam Formation' (Jenkins, 1993b), considered here to be a correlative of the lower Pertatataka Formation (see later section).

As in the Nuccaleena Formation, the cap dolostone at Mt Capitor (and Wallara 1 - see below) is interpreted as a transgressive systems tract deposited under a deepening water body, starved of siliciclastic input, mostly below storm wave-base (Wallace & Kennedy, 1993). The lowest 5 m of the unit at Mt Capitor, with thick silty dolostone 'event beds', is a facies not seen elsewhere in the Amadeus Basin or Adelaide Geosyncline. This interval represents storm-influenced sedimentation at shallower depths.

Wallara 1

In Wallara 1, cap dolostone rests abruptly on quartz sandstone (lower Pioneer Formation) at 1279.16 m. An initial bed of dark grey shale, sandy at the base, passes up into 6.5 m of thin-bedded, very pale yellow-brown dolomicrite with 5-10% interbeds of dark grey shale. Dolostone-shale contacts are sharp and planar to undulose. Irregular scoured tops of dolostone beds are seen in places (Plate 4.3). There is a 1.4 m thick interval, transitional with the overlying Pertatataka Formation, of red shale with sparse, diffuse dolostone nodules and layers (Plate 4.4).

Thin sections show texturally uniform dolomicrosparite of 5-10 mm grainsize with dull to bright luminescence. Analysis of adjacent dull and bright layers showed no significant stable-isotopic difference (sample 28.126 at 6.4 m on Fig. 4.11). Shale beds contain very thin (0.1 mm) planar to gently lenticular lenses of siltstone.

Ellery Creek

At Ellery Creek, the base of the cap dolostone is an erosional surface with up to 20 cm of relief. The underlying quartz sandstone is penetrated by narrow, dolostone-filled Neptunian dykes governed by pre-existing joints, indicating that the sandstone was fully lithified prior to deposition of the cap dolostone. The cap dolostone is a metre

thick and consists of pale pinkish-grey finely crystalline dolostone, with lenses of red chert in its lower half. Some chert lenses have an ill-defined fragmental fabric; others are crowded with the small finger-like stromatolite *Elleria minuta* Walter et al. (1979). Some *Elleria* chert lenses encrust the surface of the erosional disconformity; others are enclosed by dolostone.

The dolostone in thin section has a recrystallized fabric of hypodiotopic dolomite crystals 50 μ in size, with rare euhedral barite crystals. Some chert lenses contain pseudomorphs of chert after probable anhydrite and gypsum (Walter & Bauld, 1983).

Hidden Valley

Here the cap dolostone is represented by a continuous layer of stromatolitic chert, 1-10 cm thick, that encrusts the mounded surface that here comprises the top of the pre-Ediacarian Pioneer Formation correlative (see previous section). The chert is crowded with small columnar stromatolites very similar to the type *Elleria minuta* at Ellery Creek. The chert is abruptly overlain by red shale of the Pertatataka Formation.

Two kilometres to the SE, at a locality on the N'Dhala Thrust Sheet, the chert layer has overstepped older units and rests directly on Bitter Springs Formation. The chert layer is very similar to that at Hidden Valley except that coarse-grained sandstone fills the narrow intercolumnar spaces, and there is a thin (10 mm) layer of dolostone within the chert bed. A thin section shows the dolostone to be a hypidiotopic 50 μ dolospar mosaic similar to the dolostone at Ellery Creek. The stromatolites at this locality have been described as *Anabaria [Kotuikania] juvensis* Cloud & Semikhatov (1969), but this is probably synonymous with *E. minuta* (M. R. Walter, pers. comm.). Prior to thrusting, this locality lay north of the Hidden Valley section. Oaks & Deckelman (in Stewart et al., 1991) estimate 10 km of southward movement for the N'Dhala Thrust Sheet.

4.4c Isotope Stratigraphy

At Mt Capitor, dolomitic sandstone beds in the basal 5 m of the section have a $\delta^{13}C_{carb}$ of around +1 ‰, but as the carbonate is partly detrital this composition is of little relevance to chemostratigraphy. Carbon isotopic compositions in the fine-grained, thin-bedded dolostones above 5 m delineate a falling trend from -1.6 ‰ to a minimum of -4 ‰ in the topmost dolostone bed (Fig. 4.6). $\delta^{18}O$ is fairly constant through this interval (-7 ‰). $\delta^{13}C_{carb}$ in limestones in the overlying 'Halfway Dam Formation' continues the upward-decreasing trend (Fig 4.6).

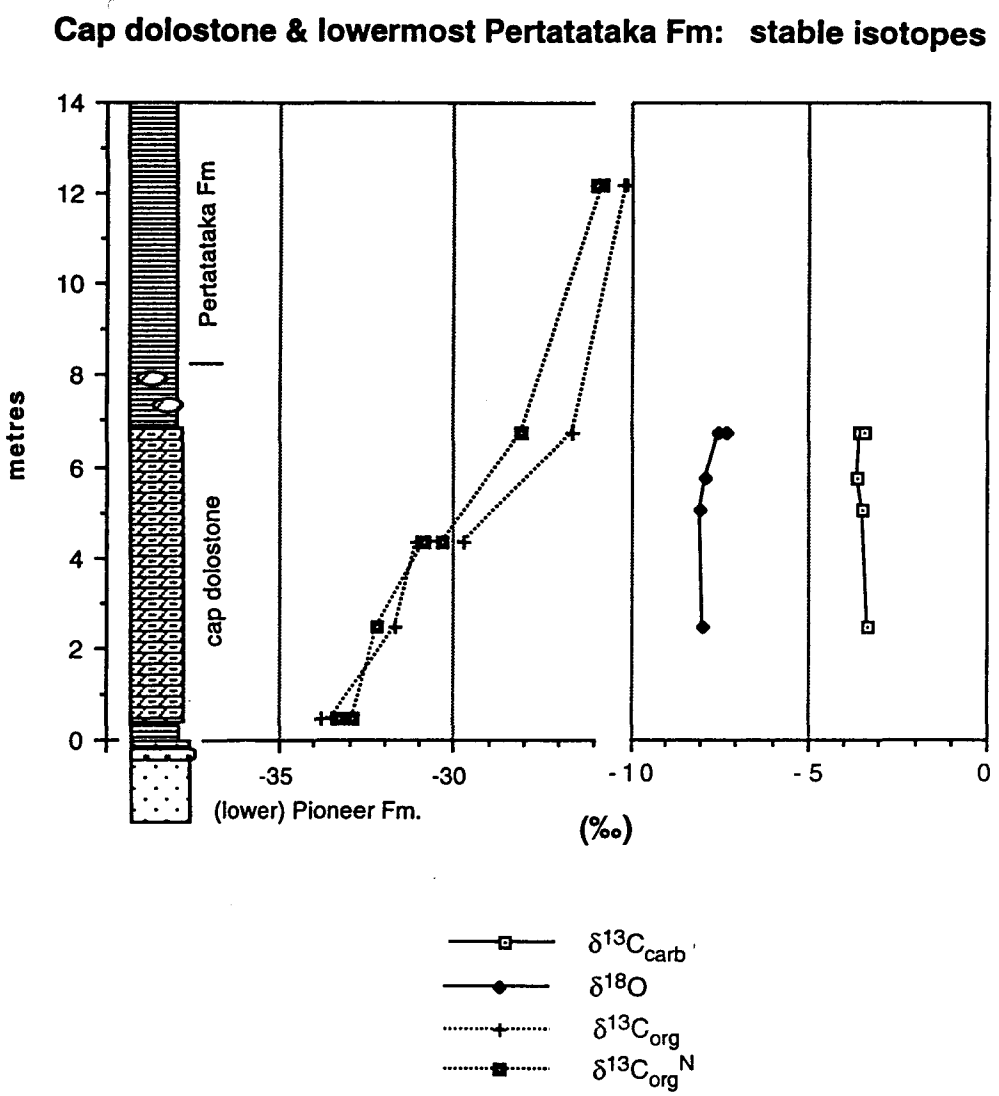

Fig. 4.11: Lithologic column, carbonate $\delta^{13}C$ and $\delta^{18}O$ profiles and organic $\delta^{13}C$ data of cap dolostone and lowermost Pertatataka Formation, Wallara 1 drillhole.

In Wallara 1, carbonate isotopic compositions are relatively constant, clustering closely around -3.5 ‰ ($\delta^{13}C_{carb}$) and -8 ‰ ($\delta^{18}O$) (Fig. 4.11), closely matching the upper part of the Mt Capitor profile.

Cap dolostone at Ellery Creek has relatively heavy $\delta^{13}C_{carb}$ (+0.7 to -0.7 ‰). $\delta^{18}O$ is, however, strongly depleted (-12 to -13 ‰) suggesting involvement of meteoric water or that the relatively coarse recrystallization observed in thin section took place during deep-burial diagenesis. The thin dolostone layer from the locality 2 km SE of Hidden Valley, where the presence of *Elleria*-bearing chert suggests a similar palaeoenvironment to Ellery Creek, is isotopically rather different with $\delta^{13}C_{carb}$ at -2.3 ‰ and $\delta^{18}O$ at -4.3 ‰. This sample is also relatively coarsely recrystallised.

Three $^{87}Sr/^{86}Sr$ determinations from Wallara 1 give elevated, variable results (0.7092 - 0.7096), the lowest of which suggests a marine rather than freshwater origin, but is apparently altered with respect to expected basal Ediacarian marine values.

Organic carbon isotopic compositions ($\delta^{13}C_{org}$) were obtained from relatively organic-rich (1 mg/g TOC) dark shale interbeds in Wallara 1. The trend is distinctly different from the carbonate C signal, with a systematic upward increase of 7‰ (from -34 to -27‰) in $\delta^{13}C_{org}$, and 5‰ (from -33 to -28 ‰) in $\delta^{13}C_{org}{}^{N}$ (Fig 4.11) [see Chapter 2 for derivation of organic carbon isotopic compositions normalized with respect to variation in TOC ($\delta^{13}C_{org}{}^{N}$)]. $\delta^{13}C_{org}{}^{N}$ of a dolostone bed is slightly heavier but not significantly different from an adjacent shale bed (sample 28.130 at 4.2 m on Fig 4.11). There is no petrographic evidence of benthic microbial mat development in the lower samples, which elsewhere is associated with anomalously ^{13}C-depleted isotopic compositions.

4.4d Interpretation

Three uncertainties are attendant on the interpretation of the C-isotope record of the cap dolostones: (i) whether primary $\delta^{13}C_{carb}$ compositions are recorded; (ii) whether all sections described are mutually correlative; and (iii) if the foregoing are affirmative, whether the observed geographic and stratigraphic variation represents secular change in seawater isotopic composition or palaeoenvironmental variation.

In Mt Capitor and Wallara 1 very fine-grained, microsparitic and micritic textures, and concordant $\delta^{13}C$ suggest preservation of depositional $\delta^{13}C_{carb}$ except for the partly detrital carbonates in the lowest 5 m at Mt Capitor. As in the Nuccaleena Formation, $\delta^{18}O$ values are also concordant and are mostly -7 to -8 ‰ - compositions that are conceivably primary or only mildly altered (see below), supporting an interpretation of minimal $\delta^{13}C_{carb}$ alteration since burial-diagenetic $\delta^{18}O$ alteration nearly always precedes that of $\delta^{13}C_{carb}$ (Banner & Hanson, 1990). The upward-decreasing $\delta^{13}C_{carb}$ and relatively constant $\delta^{18}O$ are reminiscent of meteoric-diagenetic profiles (Allan & Matthews, 1982) but interpreted palaeoenvironments are not consistent with subaerial exposure. The heavier $\delta^{18}O$ and $\delta^{13}C_{carb}$ in the detrital carbonates comprising the lowest 5 m at Mt Capitor is consistent with partial derivation from the relatively enriched carbonates of the underlying Olympic Formation (see previous section).

The marked rise in $\delta^{13}C_{org}$ within the Wallara 1 cap dolostone (the only cap dolostone for which a complete organic profile was obtained) is a strikingly different trend to the

carbonate signal. Other factors remaining equal, strongly rising palaeotemperatures may have brought this about by lowering the solubility of CO_2 and hence lowering ε_P (the fractionation factor associated with photosynthesis) (eg. Rau et al., 1991). However, carbonate $\delta^{18}O$ values in Wallara 1 remain relatively constant and thus cannot be interpreted to indicate such a rise in temperature. Conceivably, the rise in $\delta^{13}C_{org}$ represents a warming of only the surface layer of the ocean (where most photosynthetic fixation takes place) - an increasing degree of temperature stratification of the water body would then be implied. Perhaps the simplest, and favoured explanation for the divergent organic and carbonate $\delta^{13}C$ trends is one of intensifying $\delta^{13}C_{DIC}$ stratification of the water column, with increasingly ^{13}C-enriched organic carbon reflecting evolution of the surface layer and steady (Wallara 1) to falling (Mt Capitor) bottom-water $\delta^{13}C_{DIC}$ reflected in the carbonate. Further circumstantial evidence exists for stratification during and after cap dolostone time (see below).

The relatively coarse recrystallization in the Ellery Creek cap dolostone is reflected in strongly depleted $\delta^{18}O$; consequently $\delta^{13}C_{carb}$ must be regarded as possibly altered. Since the usual trend of diagenesis is toward lower $\delta^{13}C_{carb}$, the heaviest value (+0.7 ‰) is probably the least-altered; however, since primary textures are not preserved a partly detrital origin (like the lower part of the Mt Capitor section) is difficult to rule out.

The carbon isotopic composition of the thin dolostone layer within chert at the locality 2 km SE of Hidden Valley (-2.3 ‰) may be near-primary in view of the relatively heavy $\delta^{18}O$; however, the recrystrallised texture suggests the possibility of some alteration of stable isotopic compositions.

The Mt Capitor cap dolostone is very similar to the Nuccaleena Formation in lithology, superposition and stable-isotopic composition, differing mainly in that the lowest 5 m at Mt Capitor is thicker-bedded, largely detrital and probably of shallower palaeoenvironment than any known Nuccaleena Formation. The Wallara 1 cap dolostone is a good match, lithologically and isotopically, for the Nuccaleena Formation and the middle to upper parts of the Mt Capitor section. Shales in Wallara 1 are more organic-rich, at least in part because of lack of weathering in drillcore. Both the Mt Capitor and Wallara 1 cap dolostones are therefore here regarded as firm Nuccaleena equivalents and base-Ediacarian units.

An element of doubt exists as to whether this correlation can be extended to the stromatolitic chert-bearing units along the northern margin of the Amadeus Basin at

Ellery Creek and Hidden Valley (Preiss et al., 1978, p. 46; Jenkins, pers. comm., 1993b; Preiss, pers comm., 1993). Carbon isotopic compositions of these units fall within the total range exhibited by the Mt Capitor section, but as this range is large (+1 to -4 ‰), this is not compelling evidence for correlation. A stronger case can be made if the likely causes of regional and stratigraphic variation in $\delta^{13}C_{carb}$ are considered.

In the previous chapter, it was proposed that variation in $\delta^{13}C_{carb}$ in the Nuccaleena Formation primarily reflects increasing depth of palaeoenvironment in a basin with stratified isotopic composition of dissolved inorganic carbon ($\delta^{13}C_{DIC}$) or sedimentation under a water body that became increasingly stratified over time. Extending this model to the cap dolostones of the Amadeus Basin, the probably-intertidal units at Ellery Creek and Hidden Valley should be representative of the relatively ^{13}C-enriched upper water layer and, if broadly correlative with Mt Capitor, should have $\delta^{13}C_{carb}$ similar to, or greater than, the heaviest values at Mt Capitor (-1.6 ‰, ignoring the detrital carbonates in the basal 5 m). $\delta^{13}C_{carb}$ at Ellery Creek (-0.7 to + 0.7 ‰) and the single sample from near Hidden Valley (-2.3 ‰) are in fair agreement with the model, although the poor textural preservation at these localities casts some doubt on this interpretation.

If, on the other hand, the pattern of change in $\delta^{13}C_{carb}$ at Mt Capitor represents simple secular decrease in $\delta^{13}C_{DIC}$ of a well-mixed water body, then the implication is that sedimentation began at Mt Capitor and Ellery Creek before the cap dolostones at Hidden Valley and Wallara 1. The sample from near Hidden Valley does not readily fit this scenario: one might expect that, if the cap dolostones are part of a transgressive systems tract, that sedimentation commenced earlier in northern localities (Ellery Ck and Hidden Valley)(compare Figs 4.12 and 4.13c).

The relative thinness and shallow palaeoenvironment of the cap dolostones along the northern margin of the Amadeus Basin (Ellery Creek, Hidden Valley) can be understood in terms of the interpreted basin geometry (Fig. 4.13c). Northern localities were situated on or near a nascent, barely emergent peripheral arch (Fig 4.12), remote from the main siliciclastic source area on the Musgrave Block. Erosional surfaces at the base of the cap dolostones at Ellery Creek and Hidden Valley probably represent ravinements that accompanied transgression onto a land surface that was (as shown by the lack of siliciclastic detritus in the overlying cap dolostones) very limited in area and relief. The cap dolostones at Wallara 1 and Mt Capitor, on the other hand, are situated in a part of the basin where more rapid subsidence enhanced the rate of relative sealevel

rise, and where a small amount of siliciclastic detritus was available. It is suggested that these factors contributed to the evidently deeper palaeoenvironment and greater thickness of the cap dolostones here.

In summary, isotopic compositions of the cap dolostones described here are strong evidence that the Mt Capitor and Wallara 1 sections are correlatives of the Nuccaleena Formation. Isotopic data are permissive of the view that the cherty units at Ellery Creek and Hidden Valley are also Nuccaleena correlatives, but the evidence is not compelling on this point. Further support for the proposed correlation comes from evidence for correlation of units underlying the cap dolostones (see previous section) and of units overlying them (next section). Either secular change or palaeoenvironmental variation may be responsible for the observed regional and stratigraphic variation in $\delta^{13}C_{carb}$. However, a palaeoenvironmental model (increasing depth of palaeoenvironment in a basin with stratified isotopic composition of dissolved inorganic carbon ($\delta^{13}C_{DIC}$) or sedimentation under a water body that became increasingly stratified over time) is favoured here. This is because such a model explains the divergent $\delta^{13}C_{org}$ and $\delta^{13}C_{carb}$ signals; and because there is further circumstantial evidence from the Nuccaleena Formation and from the overlying lower Pertatataka Formation for basin stratification: notably, ^{13}C-depleted carbonates with low $\Delta\delta$, anomalously-depleted organic carbon of benthic microbial mats, and rare subaqueous evaporite (see sections 3.3c (Nuccaleena Formation) and 6.2 (synthesis)).

The least-altered $^{87}Sr/^{86}Sr$ ratio is good evidence for a marine origin for these rocks, a significant finding in view of a previous proposal of lacustrine palaeoenvironments (Walter & Bauld, 1983).

$\delta^{18}O$ and palaeoclimate

Oxygen isotopic compositions remain relatively constant or decrease slightly upwards in Wallara 1 and Mt Capitor (Figs 4.6b, 4.11). There is a close resemblance in the frequency distribution of oxygen isotopic compositions between the Amadeus cap dolostones and the Nuccaleena Formation, with the majority of values at -7 to -8 ‰ (Fig. 4.10). Outliers more depleted than this are associated with either petrographic evidence for recrystallization (Ellery Creek) or with higher regional thermal grade (Umberatana section of the Nuccaleena Formation, see Chapter 3). The remarkable regional uniformity in $\partial^{18}O$, particularly evident in the Nuccaleena Formation, suggests that values of -7 to -8 ‰, together with a few more enriched values, may be primary. Regional diagenetic resetting of $\delta^{18}O$ would be expected to have affected the older

(Pioneer/Olympic) dolostones of the Amadeus Basin but these retain compositions around -2 ‰ (Fig. 4.10). G. Williams (1979) observed that oxygen isotopic compositions of cap dolostones were similar to those of Proterozoic warm-water carbonates and inferred a non-glacial palaeoclimate. This larger data set (Fig. 4.10) bears out his observations, and suggests that the cap dolostones were deposited in marine waters ca. 20°C warmer than the older (Pioneer/Olympic) dolostones.

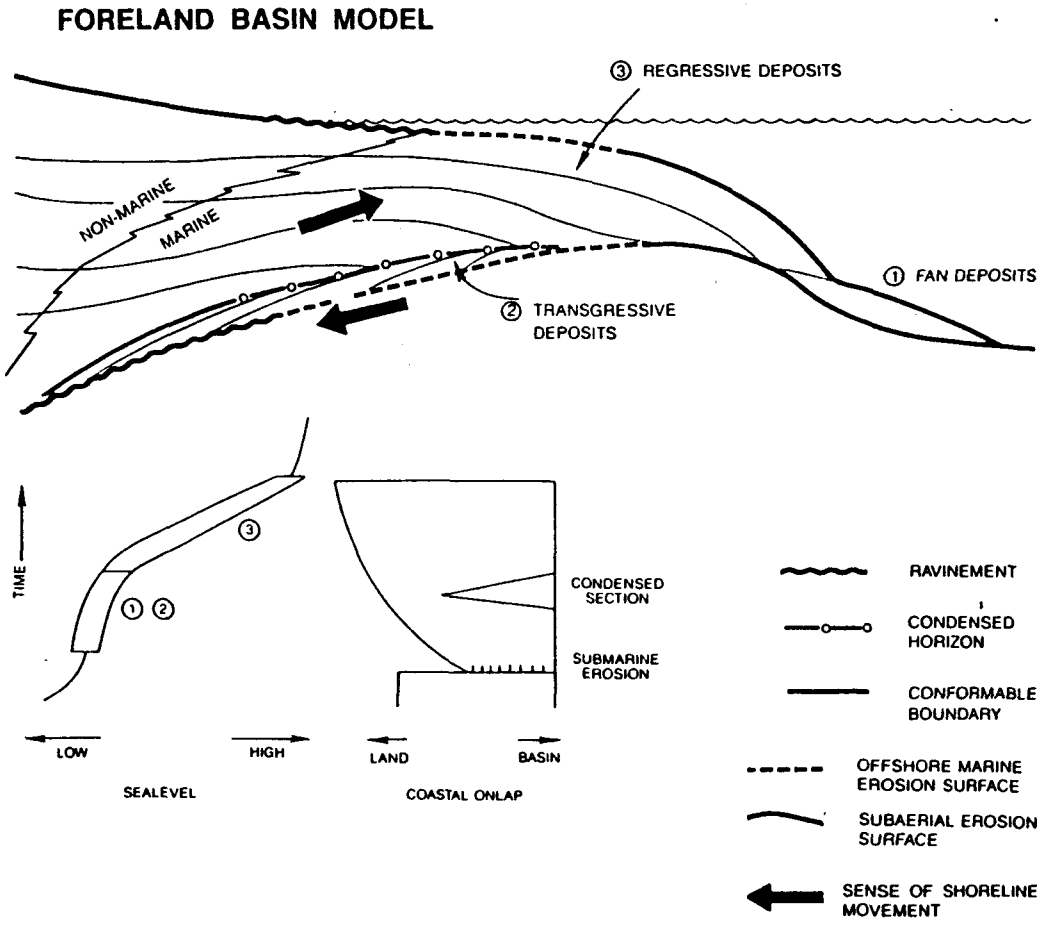

Fig. 4.12: Sequence architecture in foreland basin: model of Swift et al. (1987). Compare with passive-margin model shown in Fig. 1.14.

4.5 Pertatataka Formation and correlatives

4.5a INTRODUCTION

The Pertatataka Formation, as redefined by Preiss et al. (1978), is the thick (300-1000 m) recessive unit of shale and siltstone that overlies cap dolostone and underlies Julie Formation in the N and NE Amadeus Basin. The type section is near Ellery Creek at the central-northern margin of the basin. The formation includes minor, impersistent sandstone units (the Cyclops Member, the Waldo Pedlar Member and at least one un-named unit: Wells et al., 1967; Preiss et al., 1978). The Gaylad Sandstone (Freeman et al., 1991) occurs near the base of the succession in part of the NE area, and the 'Halfway Dam Formation' is the name given to the shale unit between cap dolostone and Gaylad Sandstone (Figs 4.1, 4.21; Jenkins, 1993b). Jenkins et al. (1992), Jenkins (1993b) and Freeman et al. (1991) proposed that one or both these formations are older than the Pertatataka Formation. It is shown below, however, that chemostratigraphic and lithostratigraphic evidence are more consistent with Gaylad and 'Halfway Dam Formation's being correlatives of the lower part of the Pertatataka Formation (Fig. 4.21a). Fig. 4.21b and 4.21c show an alternative ways of correlating these units, to be fully discussed below.

In the central Amadeus Basin, the Pertatataka Formation passes south and west into the sandy, more proximal facies of the Winnall beds (Fig. 4.13; Wells et al., 1970; Freeman et al., 1991).

Systematic sampling and analysis have been carried out at Ellery Creek, Hidden Valley and in fully-cored drillholes Wallara 1, Rodinga 4 and Alice Springs 27. A few samples were collected from Mt Capitor and Acacia Well. Below, brief descriptions are also included of lithological observations made at Glen Helen, Ross River, Areyonga and Mt Conner (Fig. 4.4).

Basin Geometry

An understanding of basin geometry and the pattern of sedimentary fill aids in predicting patterns of diachroniety that may helpful in chemostratigraphic interpretation.

The Pertatataka Formation is relatively thin (300 m) in the central-north of the basin, and thickens to the W and E in the Carmichael and Ooraminna depocentres (Fig. 4.13). The formation also thickens southward and passes south and west, through an observed

lateral facies change (Wells et al., 1970; Freeman et al., 1991), into the sandstone-dominated Winnall beds. This facies transition lies south of the Central Ridge (Fig. 4.13a). The Pertatataka Formation and Winnall beds, south of the Central Ridge, form a southward-thickening wedge with a maximum thickness of 2.5 km near the southern margin of the basin (Wells et al., 1970).

The Pertatataka Formation is imaged on petroleum exploration seismic profiles north of the Central Ridge. In nearly all profiles examined in this study (Fig. 4.13a), the formation is characterised by weak, discontinuous, parallel reflectors. At the southwestern side of the Carmichael depocentre, however (line P81-U1), a large prograding clinoform with an easterly apparent dip is evident that encompasses much or most of the thickness of the formation (Kennard & Lindsay, 1991, their Fig. 10). A very gentle north-prograding clinoform is also evident just north of the Central Ridge between the two northern depocentres (lines W. Dingo 1, 2, and 3).

The pattern of basin fill thus resembles that of a foreland basin, with maximum subsidence taking place closest to the main source area in the south. In the compressional fault block model of Shaw et al. (1991) a peripheral arch is predicted which is equated with the Central Ridge. However, the Central Ridge was probably not emergent in Pertatataka time. Shaw et al. (1991) cite widespread transgression during Pertatataka deposition, but do not state whether the Central Ridge was covered at this time. In support of a non-emergent Central Ridge (Fig. 4.13c), the lateral facies change between Winnall beds and Pertatataka Formation does not coincide with the Central Ridge (Fig. 4.13a). The Pertatataka Formation observed just south (Wallara 1) and just north (Areyonga) of the Central Ridge appears very similar, in both places consisting of shale with subordinate storm-laid and turbidite sandstone beds (see below). Northward palaeocurrents at Areyonga (Korsch, 1986b) suggest derivation from the Musgrave Block rather than the Central Ridge which would presumably have been too small and too close (10 km) to have been the source of large volumes of fine-grained sediment. The Pertatataka Formation is absent from the Central Ridge because of uplift and erosion at the close of the Proterozoic (Wells et al., 1970), rather than non-deposition on a topographic high.

Fig. 4.13 (opposite): (a) Elements of palaeogeography of the Amadeus Basin in Pertatataka time; (b) Diagrammatic S-N cross-section showing basin geometry for Olympic-Pertatataka-Julie sequence, from Shaw et al.(1991); (c) Proposed cross-section for Pertatataka time with subdued Central Ridge.

a) Basin geometry and palaeogeography in Pertatataka time

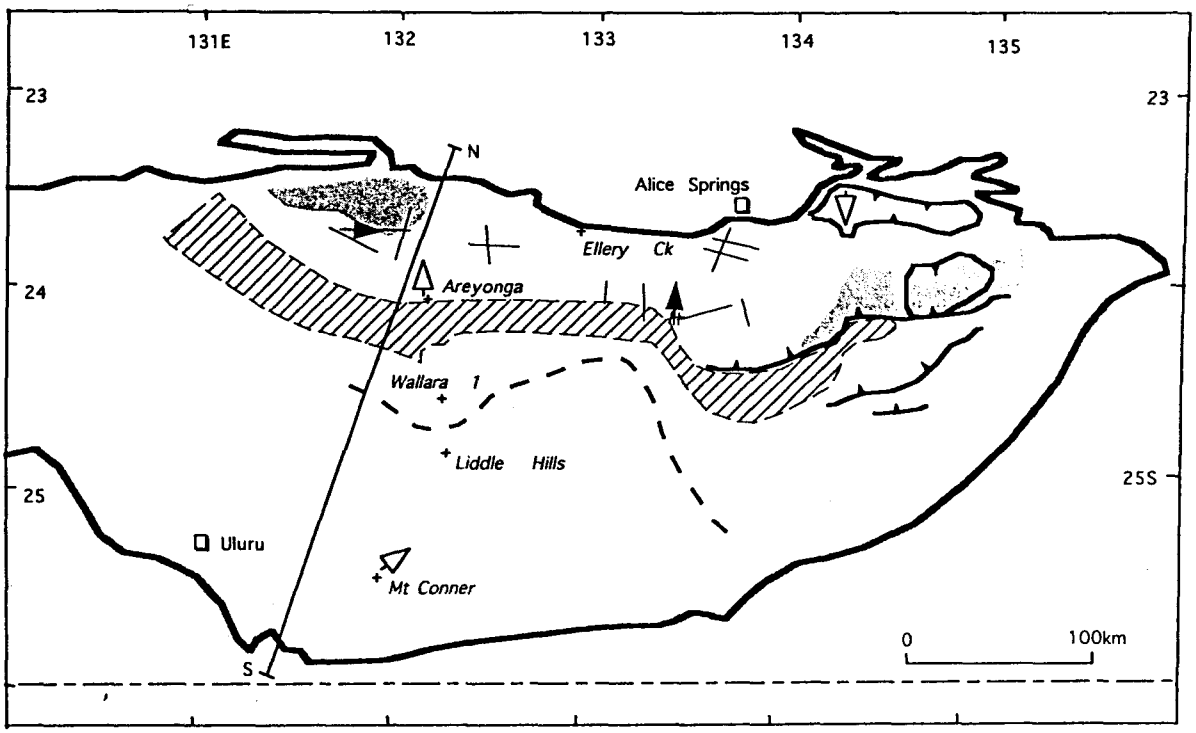

Approximate position of northward transition from Winnall Beds to Pertatataka Formation (partly after Wells et al., 1970; Oaks et al., 1991)

Siesmic reflection profile showing weak, parallel reflectors in Pertatataka Formation

Siesmic reflection profile showing direction of progradation of clinoforms within Pertatataka Formation

Generalised palaeocurrent directions in Pertatataka Formation (after Korsch, 1986a,b) and Winnall beds

Central Ridge

Carmichael and Ooraminna depocentres

b) S-N section showing basin geometry after Shaw et al., 1991

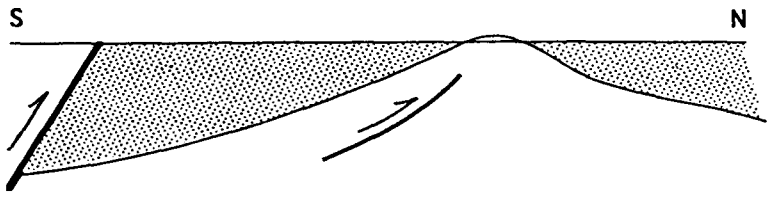

c) Revised basin geometry (with non-emergent Central Ridge)

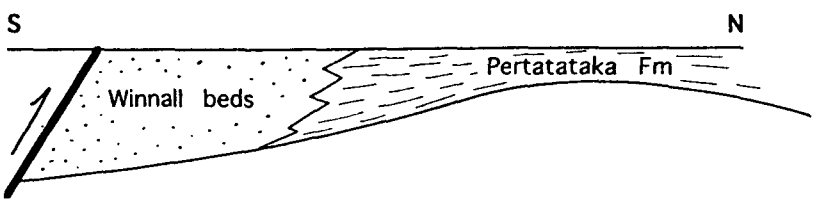

The proposed basin shape in Pertatataka time (Fig. 4.13c) closely resembles a foreland basin, and the sequence stratigraphic model of Swift et al. (1987) (Fig. 4.12) should be a guide to chronostratigraphic patterns within the formation (continuous lines in this figure approximate timelines). The cap dolostone is part of a transgressive systems tract (see above). There is evidence for an overall pattern of upward-shallowing in the Pertatataka Formation in Wallara 1; hence in the central Amadeus Basin, most or all of the formation consists of a highstand systems tract (HST). Clinoforms seen on seismic profiles presumably belong to this HST. A condensed section may be inferred to exist close to the base of the formation (Fig. 4.12). This disposition of sequence tracts is closely analagous to the Nuccaleena-Brachina -ABC Range interval of the Adelaide Geosyncline (Chapter 3; Dyson, 1992). However the stratigraphic position of the sequence boundary at the top of the HST is uncertain in northern localities such as the type section at Ellery Creek. A sequence boundary has been recognised at the top of the Julie Formation (Lindsay & Korsch, 1991), but one or more cryptic sequence boundaries may be present at lower levels.

4.5b LITHOSTRATIGRAPHY

Ellery Creek

The Ellery Creek section (Fig. 4.15) is 5 km E of the type section of the Pertatataka Formation (Preiss et al., 1978; Pritchard & Quinlan, 1962). The formation is 294 m thick here. In the lowest 10 m of the formation, thin (50 mm), sharply-bounded fine-grained sandstone beds within poorly-exposed red shale are probably storm beds. Uniform, red and grey-green shale predominates through the rest of the formation. Between 170 and 210m there are minor (< 10%) planar-parallel laminae of quartz, siltstone, and a metre-thick unit of laminated, fine-grained quartz sandstone. This interval may be an equivalent of the sandy Cyclops Member of the NE Amadeus Basin. Siltstone reappears as thin beds in the uppermost 30 m of the formation, together with minor (20%), thick beds of fine-grained quartz sandstone. Shale intraclasts and cross-bedding are present in some sandstone beds.

The lowest 10 m of the formation probably represents an environment transitonal between peritidal cap dolostone and sub-storm wavebase shales of the lower Pertatataka Formation; and is interpreted to represent, together with the cap dolostone, a transgressive systems tract.

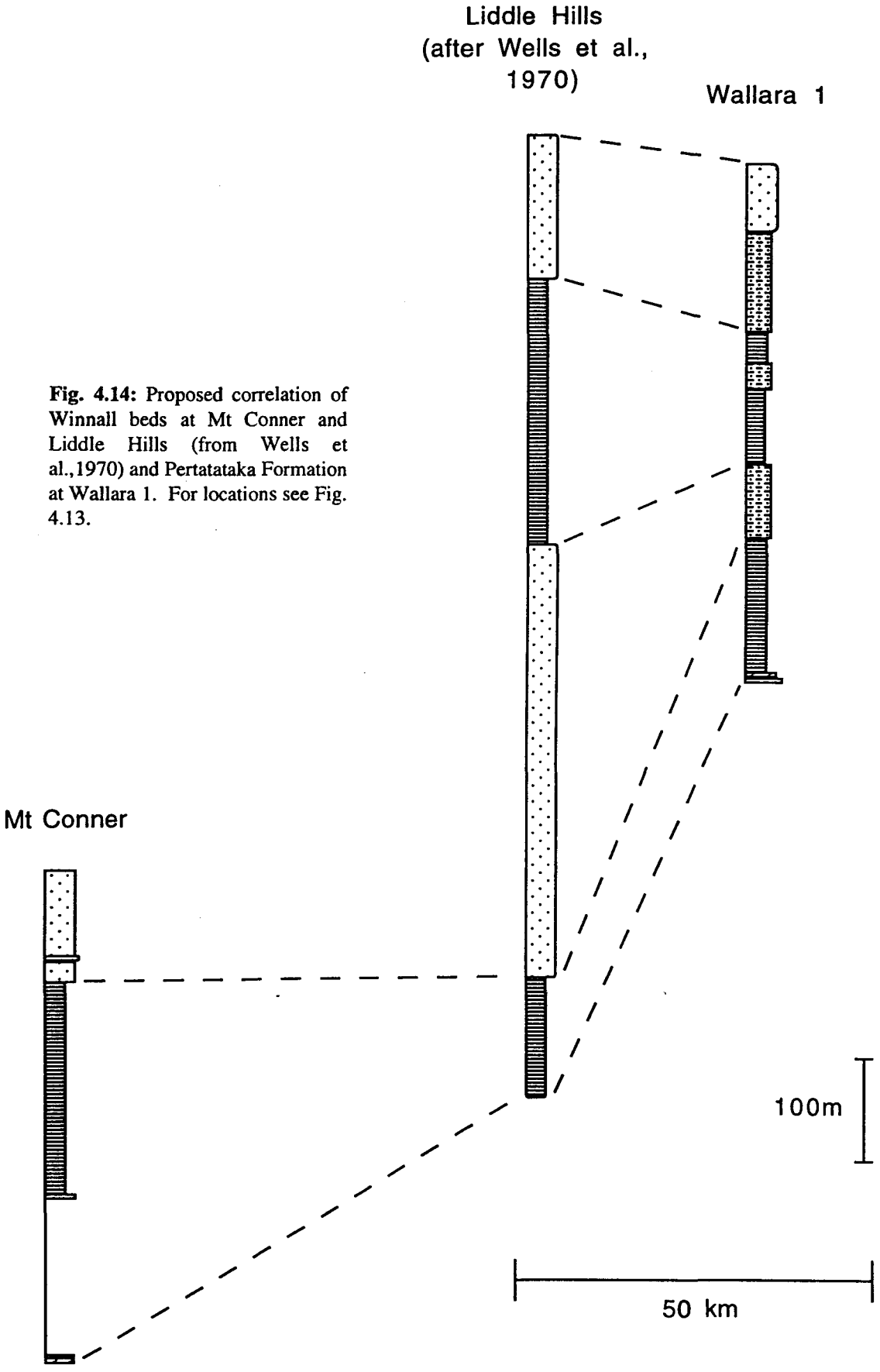

Fig. 4.14: Proposed correlation of Winnall beds at Mt Conner and Liddle Hills (from Wells et al.,1970) and Pertatataka Formation at Wallara 1. For locations see Fig. 4.13.

Glen Helen

Here, 44 km west of Ellery Creek, the Pertatataka Formation is exposed along the Finke River. The formation is here considerably thicker (570 m): the locality is close to the Carmichael depocentre. Uniform red shale is poorly exposed in the lower part of the formation, and a 10 m-thick unit of thick-bedded, fine-grained, cemented quartzarenite occurs 150 m above the base. This unit crops out as a prominent, wall-like outcrop for many kilometres. Eleven kilometres east of Glen Helen this unit remains the same stratigraphic distance above the base of the formation, showing no indication of eastward convergence with the base of the Pertatataka Formation, as might be expected if the unit were a correlate of the upper part of the type Pioneer Sandstone (cf. Fig. 4.21c). Also, the upper contact of the unit is here exposed and is seen to grade rapidly upward into silty shale with no sign of cap dolostone.

Higher in the Glen Helen section, there is a considerable thickness of featureless grey-green shale, with minor (10%) thin storm beds of fine-grained sandstone occuring above 350 m. Thick beds of coarse-grained, trough-cross-bedded quartzarenite appear near the top of the formation. The quartzarenite is supermature, with polymodal current directions; and probably represents tidally-worked sandbodies in a shallow sublittoral environment. There is an upward transition into the Julie Formation; silty shale and quartzarenite remain predominant above the first dolostone bed that is taken as the base of the Julie Formation.

Areyonga Creek

This locality is situated just north of the Central Ridge. Here, the Julie Formation and an indeterminate thickness of the upper Pertatataka Formation have been removed at an unconformity at the base of the Arumbera Sandstone. The total thickness of the Pertatataka Formation here is roughly 500 m and the lower 200 m is not exposed. The exposure consists of grey-green micaceous silty shale with planar, persistent beds of fine-grained quartz sandstone. Plane lamination, wave-ripple cross-lamination, small-scale HCS and convolute lamination are common in sandstone beds. A few beds are slumped; a few have loadcasted bases, but most have sharp, planar bases and sharp, sometimes ripplemarked tops. Some beds are poorly-sorted and structureless or graded. Most sandstone beds are probably storm beds, but many appear to be turbidites. Korsch (1986b) interpreted beds in the lowest 100 m of this section as distal turbidites, and noted north-directed palaeocurrents.

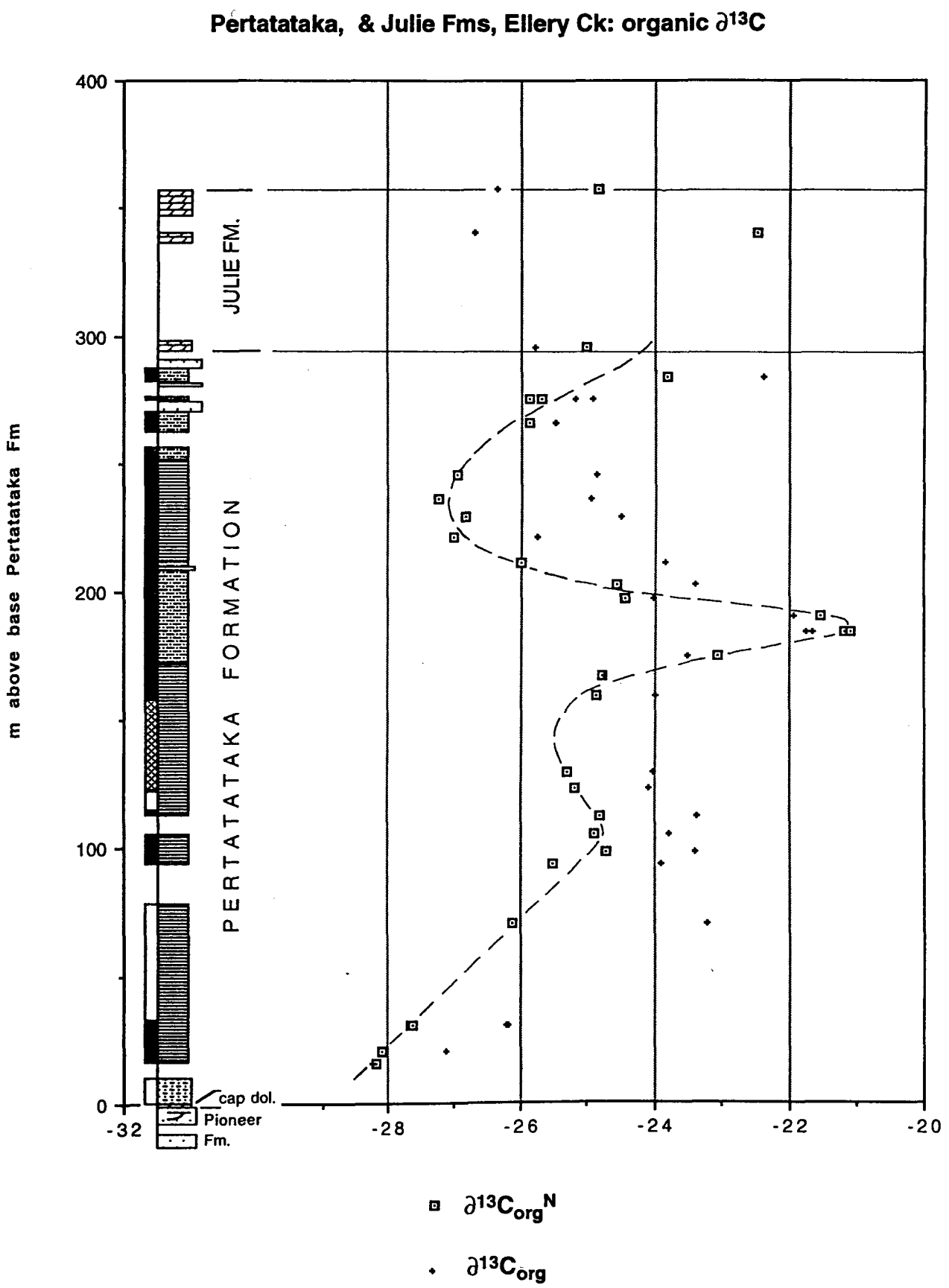

Fig. 4.15: Lithologic column and organic $\delta^{13}C$ data, Pertatataka and Julie Formations, Ellery Creek.

Wallara 1

Wallara 1 was drilled south of the Central Ridge in the centre of the Amadeus Basin (Fig. 4.4, 4.13). As at Areyonga Creek, the Arumbera Sandstone unconformably overlies the Pertatataka Formation. The Pertatataka, at 557 m thick, is thicker that at most northern localities; nonetheless, chemostratigraphic and biostratigraphic correlations (below) indicate that here much of the formation was removed by erosion (or not deposited) prior to deposition of the Arumbera Sandstone.

The Pertatataka Formation gradationally overlies cap dolostone, and begins with 23 m of featureless red mudstone (Plate 4.4). Then follows 158 m (1090-1248 m depth) of alternating grey-green and black shale (Plate 4.5). The green shale contains rare very thin planar siltstone laminae and averages 1 mg/g total organic carbon (TOC). The black shale layers contain 2-6 mg/g TOC that is strongly ^{13}C-depleted relative to organic carbon in the green shale beds (see below). Thin sections of the black shale show weakly anastamosing, pyritic, organic-rich microlaminae: these are interpreted as remnant benthic microbial mats (Plate 2.2; fully discussed in Chapter 2). In the upper half of this unit, a few percent thin beds and laminae of siltstone are present, and here and there, thick graded sandstone beds.

Overlying the grey-green and black shale unit is a thick succession (ca. 250m) of predominantly grey-green and reddish-grey shales, with siltstone and fine-grained sandstone occurring as thin planar laminae, starved ripples or thin cross-laminated beds (Plate 4.6), and as thicker beds with partial Bouma sequences. Wave-ripple cross-lamination and HCS may be present but are difficult to unequivocally identify in drillcore. Many sandstone beds are glauconitic. Rare black shale laminae (benthic microbial mat facies) are found as high as 1009 m. Deposition by turbidity currents (predominantly low-density), and hemipelagic processes is inferred. Depositional environment was probably never very deep (<150 m?) considering the vertical and lateral facies transitions into shallow-water sediments and the intracratonic basin setting. In the uppermost 100 m or so of the Pertatataka Formation in Wallara 1, sandstone becomes predominant, and more complete and coarser-grained Bouma sequences are seen; and high in this interval, cross-bedding and ripple cross-lamination and abundant wavy, lenticular and flaser bedding suggest deposition within fairweather wavebase (Plate 4.7). The contact with the overlying Arumbera Sandstone is abrupt and erosional.

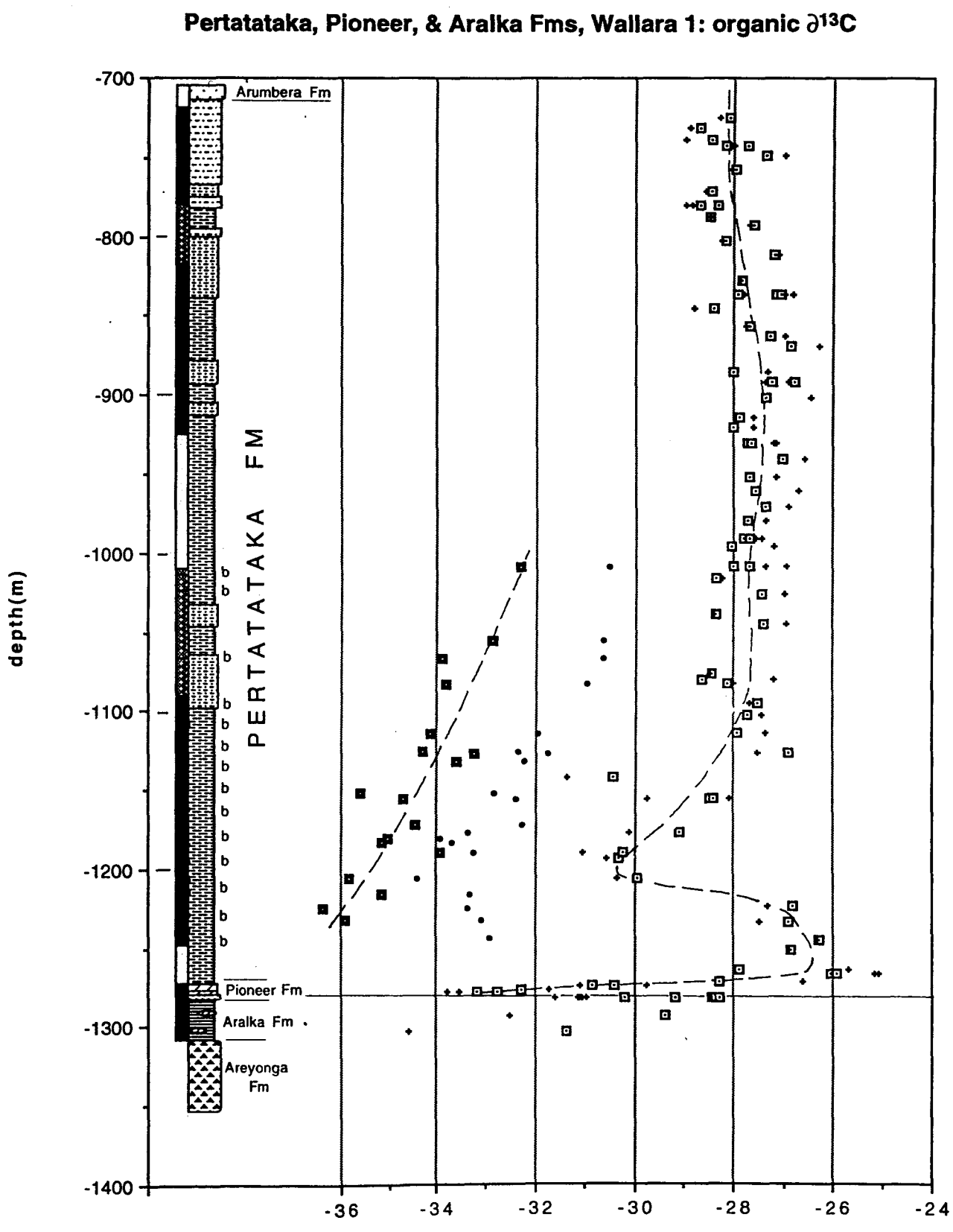

Fig. 4.16: Lithologic column and organic $\delta^{13}C$ data, Pertatataka Formation, Pioneer Formation (including cap dolostone), and Aralka Formation, Wallara 1.

Rare thin beds of calcite-cemented siltstone are present, but carbonate is otherwise absent.

South of Wallara 1 is a facies transition to sandstone-dominated Winnall beds. At the Liddle Hills 30 km S of Wallara 1, 1200 m of Winnall beds is present, consisting of four units: thin-bedded siltstone, cross-bedded quartz sandstone, variegated thin-bedded siltstone, and poorly-sorted sandstone (Wells et al., 1970). Conceivably, these four units correspond to relatively shale-rich and sand-rich units in Wallara 1 (Fig. 4.14).

Mt Conner

Seventy kilometres S of the Liddle Hills, the Winnall beds crop out at Mt Conner. A section was measured in a N-S line north of the eastern edge of the Mt Conner plateau, beginning at the stromatolitic dolostone tentatively correlated with the Pioneer Formation (previous section). There is a covered interval for roughly 200 m of stratigraphic thickness above the dolostone (Fig. 4.14). The first outcrop of Winnall beds is a prominent, 4 m thick unit of thick-bedded fine-grained quartz sandstone. Higher, there is a considerable thickness (300 m) of poorly-exposed reddish-brown shale with planar, persistent beds of purplish-brown lithic sandstone. The sandstone beds are graded, have loadcasted bases, and are probably turbidites. At the top of this interval, sandstone beds become thicker and amalgamate to form a 30 m thick unit of thick-bedded, cross-bedded sublithic quartz sandstone. Beds have erosive bases, and heavy minerals are concentrated along bottomsets. In the upper 10 m of this unit, cross-bedding indicates palaeocurrents from the W and SW. There is an upward increase in textural and compositional maturity through this unit. The top is an erosional surface overlain by 1.5 m of conglomerate, then 150 m of pink, cross-bedded quartzarenite with minor pebbly horizons. The quartzarenite forms the prominent, cliff-bound plateau of Mt Conner, and is thought to be equivalent to the lower of the two sandstone units of the Liddle Hills section (Wells et al., 1970). A comparison of the Wallara, Liddle Hills and Mt Conner sections highlights the southward-thickening trend south of the Central Ridge (Fig. 4.14).

Hidden Valley - Ross River

At Hidden Valley, on the northern margin of the basin 120 km E of Ellery Creek, the Pertatataka Formation is 460 m thick (Fig. 4.17). There is a basal 55 m of uniform red mudstone that rests abruptly on the stromatolitic chert bed considered correlative with the cap dolostone. Poorly-exposed grey-green shale comprises the rest of the formation

Plate 4.4: Drillcore showing upward gradation from pale buff-coloured, laminated 'cap dolostone' into massive red mudstone of the basal Pertatataka Formation. Note diffuse nodules and layers of dolostone in basal part of red mudstone. Wallara 1 drillhole. Core is 60 mm diameter.

Plate 4.5: Drillcore showing interbedded black shale (benthic microbial mat facies) and grey-green shale in lower part of Pertatataka Formation, 1236-1241 m depth, Wallara 1 drillhole. Core is 60 mm diameter.

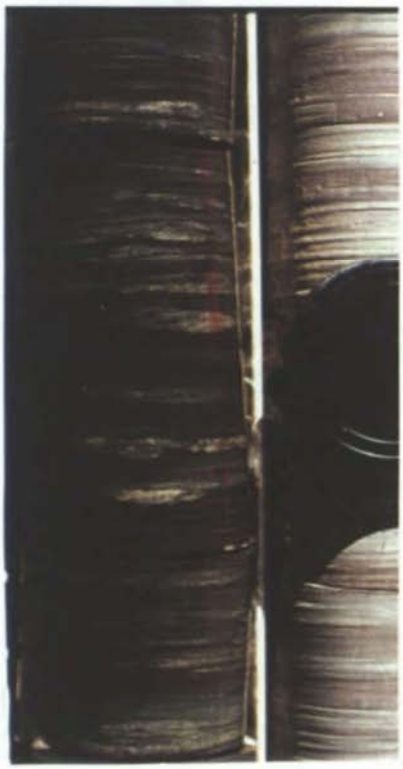

Plate 4.6: Thin laminae and starved ripples of quartz siltstone in red and green shale, Pertatataka Formation. 943 m depth, Wallara 1 drillhole. Core is 60 mm diameter.

Plate 4.7: Lenticular bedding in fine-grained sandstone and shale, upper Pertatataka Formation, 734 m depth, Wallara 1 drillhole. Core is 60 mm diameter.

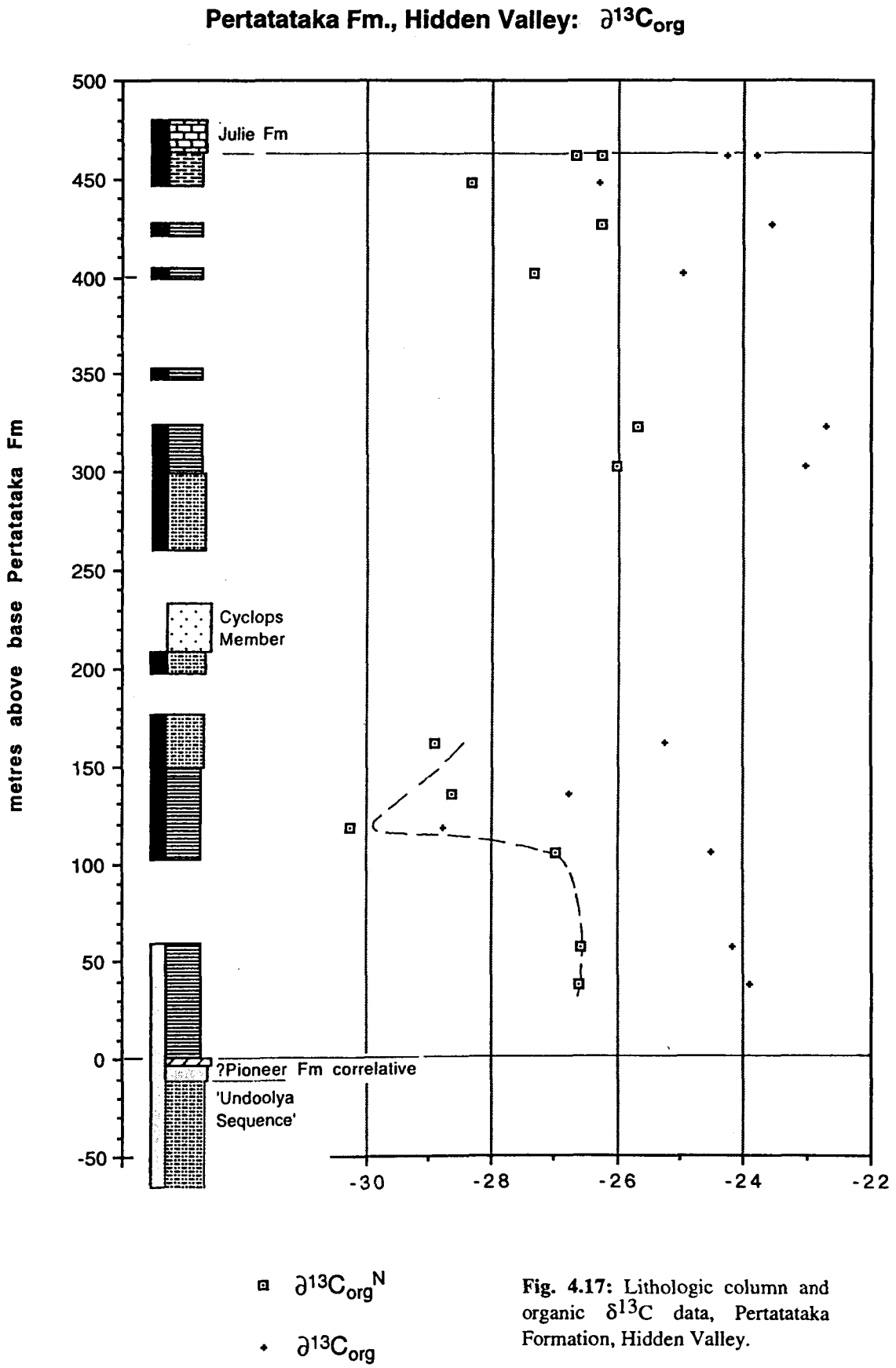

Fig. 4.17: Lithologic column and organic $\delta^{13}C$ data, Pertatataka Formation, Hidden Valley.

except for the central 50 m that constitutes the Cyclops Member, and a few thin fine-grained sandstone beds in the uppermost few metres of the formation.

The Cyclops Member is a distinctive laminated quartz siltstone and very fine-grained sandstone extending from Jay Creek (40 km E of Ellery Creek) to Ringwood (Fig 4.4), and possibly also occurring in the Gardner Range (Wells et al., 1970). It is characterised by evenly-spaced (rhythmic), planar-parallel pelitic partings a few millimetres apart. In some outcrops a smaller scale (sub-millimetre) rhythmicity is apparent. The twofold rhythmicity resembles that of the Elatina Formation (Williams, 1989) and a sandstone in the lower Rodda beds of the southeastern Officer Basin (see Chapter 3). The Elatina Formation rhythmite is interpreted as a distal ebb-tidal deposit recording semidiurnal and fortnightly cycles (Williams, 1989). The top and base of the Cyclops Member at Hidden Valley are gradational over several tens of metres.

A few kilometres S of Hidden Valley, on the N'Dhala Thrust Sheet, drillhole Alice Springs 27 intersected the lowermost 52 m of the Pertatataka Formation (Fig 4.18). This succession (like the basal 55 m at Hidden Valley) consists of uniform red mudstone with a few pale green, diffuse reduction spots and rare pale green mudstone beds.

At Acacia Well, a half metre-thick bed of plane-laminated brown-weathering silty limestone occurs 80 m below the top of the formation, and is the only carbonate found in this study, within the Pertatataka Formation *sensu stricto*. This rock is a weakly luminescent ferroan microsparite with about 10% dolomite and is probably a recrystallized dolomitic micrite.

Along the northern margin of the N'Dhala Thrust Sheet between Acacia Well and Ross River, the Cyclops Member is more thickly layered (15 mm) than at Hidden Valley, and the smaller-scale rhythmicity is well-developed. Current-ripples are present that indicate palaeocurrent directions from the north (Korsch, 1986a). Given the southward movement of the N'Dhala Thrust Sheet, these outcrops were originally closer to the source area than Hidden Valley.

The uppermost few metres of the Pertatataka Formation at Ross River Homestead consists of silty shale with thin beds of fine-grained quartz sandstone with small-scale HCS. The base of the Julie Formation is marked by an abrupt lithological change to silty limestone, but small-scale HCS persists into the lower part of the Julie Formation.

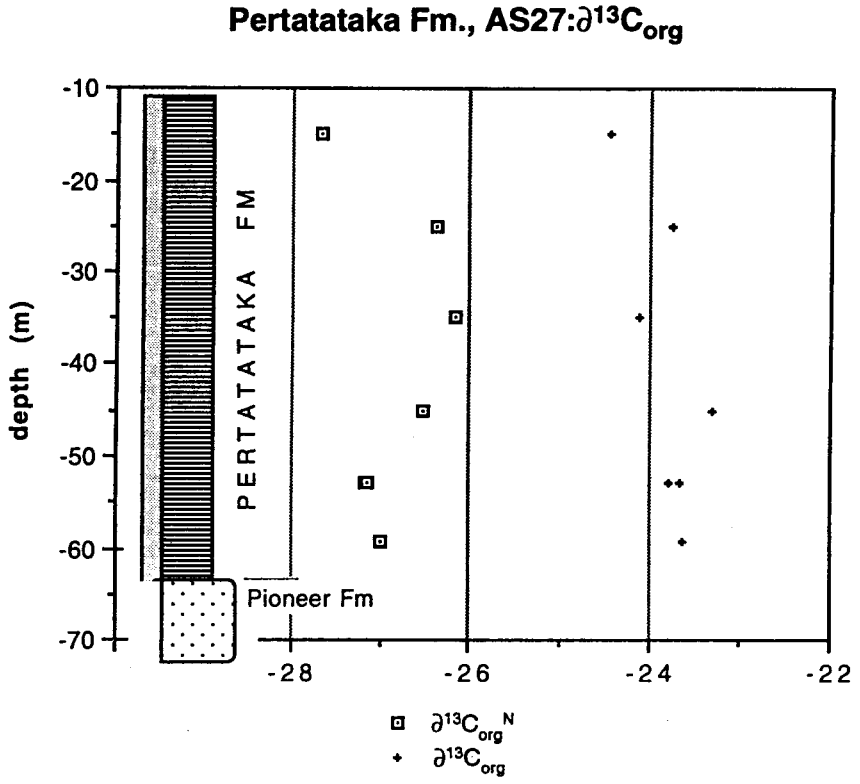

Fig. 4.18: Lithologic column and organic $\delta^{13}C$ data, lower Pertatataka Formation, Alice Springs 27.

Ringwood area - Mt Capitor

The 'Halfway Dam Formation' (Jenkins, 1993b) overlies cap dolostone in the Ringwood area and at Mt Capitor, and consists of grey-green shale with thin limestone beds. It is overlain by the Waldo Pedlar Member at Mt Capitor and unconformably by Gaylad Sandstone, west of Ringwood. Eleven km S of Ringwood, no sandstone is present and the formation passes up at an indeterminate level (Jenkins, 1993) into shales of the Pertatataka Formation (Fig. 4.21). The 'Halfway Dam Formation' is shown as uppermost Olympic Formation (subunit Puf_{2C}) by Freeman et al. (1991, their Fig. 10, 13) but as the unit overlies firmly identified cap dolostone, a post-Olympic, Ediacarian age is well established (Jenkins, 1993b; and previous section).

At Mt Capitor (Fig. 4.6a) the 'Halfway Dam Formation' is conformable upon cap dolostone, and the base of the unit is here taken as the top of the last dolostone bed. Red shale of the basal 6 m passes up into grey-green shale with pale grey, micritic limestone beds. Eight metres above the base, limestone is abruptly overlain by a thick bed of quartzarenite. The contact is irregular and erosional, neptunean dykes penetrate the limestone, and in places there are large (up to 1 m long) locally-derived tabular limestone clasts within the quartzarenite. The clasts are haphazard and matrix-supported, suggesting a debris-flow origin. The quartzarenite is graded, has internal

plane-lamination, and in places contains angle-of-repose cross-bedding at the top, indicating E-directed palaeocurrents. The quartzarenite is overlain by a thin bed of brown-weathering limestone, and then a poorly-exposed interval of grey-green shale with rare, thin grey-green limestone beds. The base of the Waldo Pedlar Member is abrupt. This unit consists of about 20 m of fine-grained muscovitic quartz sandstone. Thick (1-2 m), internally uniform beds alternate with flaggy, thin-bedded intervals in which current lineation, flute casts, and climbing ripples are common. Palaeocurrents are east-directed.

Outcrop of the Gaylad Sandstone is essentially limited to the southern, eastern and northeastern margins of the N'Dhala Thrust Sheet (Freeman et al., 1991). Along the SE margin, in the vicinity of the type section 20 km W of Ringwood (Figs. 4.4, 4.21), the formation is roughly 100 m thick and consists of a lower, thicker subunit of poorly-sorted pebbly arkosic grit, probably of fluvial origin; and an upper, thinner subunit of coarse-grained glauconitic quartz sandstone of shallow-marine origin (Freeman et al., 1991). The contact upon 'Halfway Dam Formation' is locally conformable but in places is an unconformity with a moderate angular discordance of bedding (ranging from 12° to 36°: Field, 1991, his Fig. 10B). The Gaylad Sandstone is conformably overlain by red shale of the Pertatataka Formation.

Along the northeastern margin of the N'Dhala Thrust Sheet, the Gaylad Sandstone is thinner and rests unconformably upon Bitter Springs Formation. The Gaylad Sandstone evidently represents a short-lived southward progradation of deltaic sands and gravels caused by uplift to the north, followed by marine transgression. Uplift may have been caused by post-glacial rebound and related flowage of subsurface salt in the Bitter Springs Formation (Freeman et al., 1991). Subsidence was greater to the south (Ooraminna depocentre) and the Gaylad Sandstone is replaced by offshore shales south of Ringwood. The storm-laid marine sandstone of the Waldo Pedlar Member may be an offshore lateral equivalent of the Gaylad Sandstone in the Mt Capitor area.

Rodinga 4

Fully cored drillhole Rodinga 4, 15 km S of Mt Capitor, intersected the interval from 35 to 205 m below the top of the Pertatataka Formation. The cored interval approximates the upper third of the Pertatataka Formation at this locality.

Unusual assemblages of very large sphaeromorph and acanthomorph acritarchs were first described from Rodinga 4 (Zang & Walter, 1989, 1992; and see Grey, in prep.).

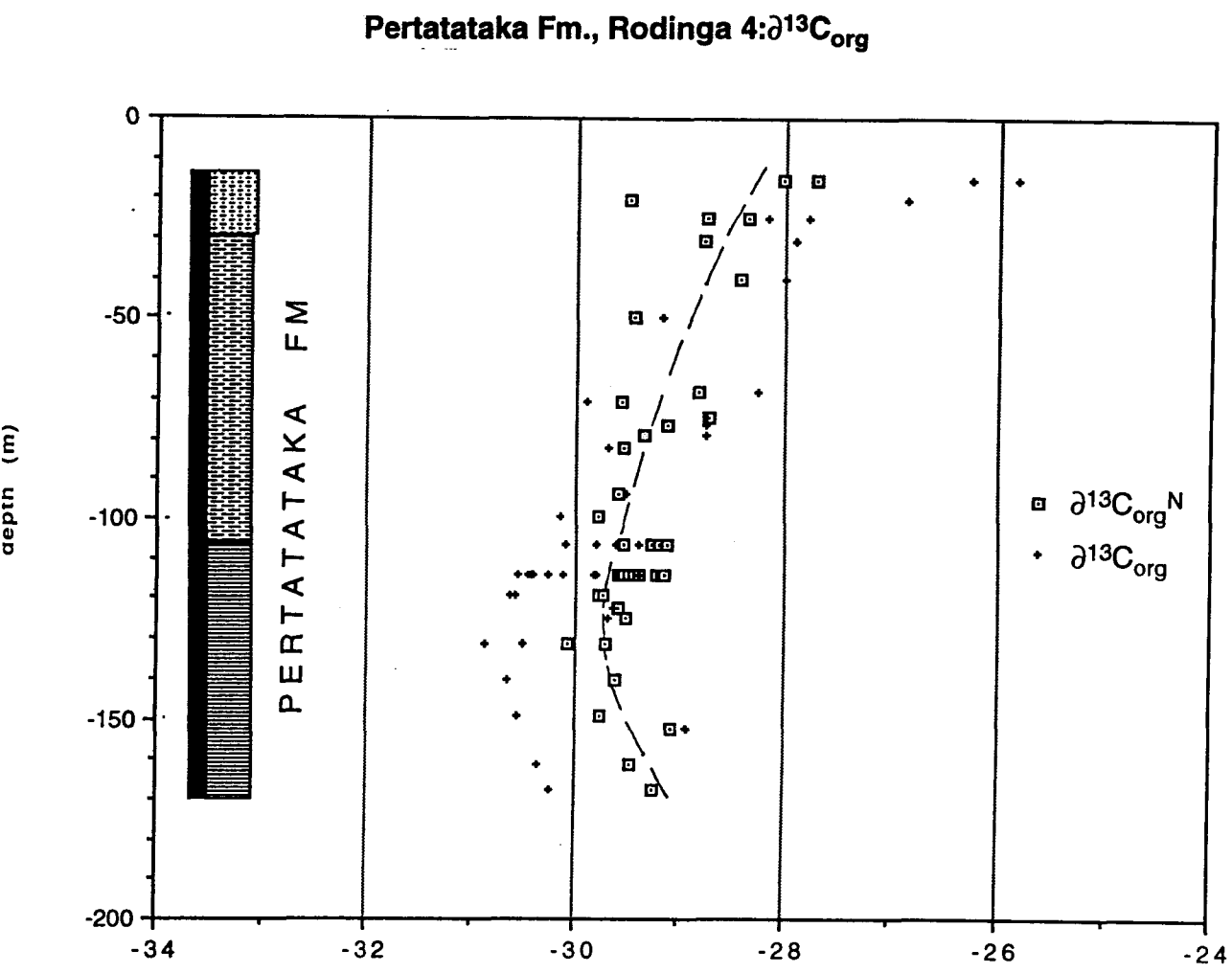

Fig. 4.19: Lithologic column and organic $\delta^{13}C$ data, Pertatataka Formation, Rodinga 4.

The cored section is predominantly shale, with an upward-increasing proportion of siltstone and very fine-grained sandstone. The lowest 40 m (130-170 m below collar of hole, Fig. 4.19) is dark grey, faintly laminated shale; less than one percent is very thin (0.1-1 mm), planar, paler siltstone laminae with a loosely bundled distribution. Higher, the core contains several percent siltstone or very fine-grained sandstone, as planar laminae, lenses (starved ripples), and as thin (all < 50 mm, and most < 10 mm thick), graded layers.

Above 65 m, siltstone and very fine-grained sandstone increase in proportion upward to 20-50% of the core. Low-angle erosional truncations are common, and clastic dykes of silt or very fine sand in mudstone are common (these features, 'diastasis cracks' of Cowan & James (1992) or 'syneresis cracks' of Plummer & Gostin (1981), have no particular palaeoenvironmental significance). Small-scale slumps are common. Shale

throughout is medium to dark grey except above 23 m where a change to pale greenish-brown is probably due to weathering.

The lower part of the Rodinga 4 section records deposition of hemipelagic muds below storm wavebase with occasional low-density turbidity currents or nepheloid flows. Higher, the palaeoenvironment becomes shallower, with evidence of bottom currents (storm-induced?) periodically reworking sediment and introducing more silt and sand.

4.5C ISOTOPE STRATIGRAPHY

Carbonate carbon and oxygen

Known occurrences of carbonates in the Pertatataka Formation and its correlatives are the limestone beds of the 'Halfway Dam Formation' and the limestone bed 80 m below the top of the Pertatataka Formation at Acacia Well. Two calcite-cemented siltstone samples from Wallara 1 have highly depleted $\delta^{13}C_{carb}$ (-16.1‰, -17.7‰), and clearly reflect cementation by diagenetic, partly organogenic carbonate.

At Mt Capitor, the 'Halfway Dam Formation' is characterised by strongly depleted (-6 to -8 ‰) $\delta^{13}C_{carb}$, in an upward-decreasing pattern that continues the trend of the underlying cap dolostone (Fig. 4.6b). These limestones are microsparitic and uniformly-textured but no trace-element data are available to support an interpretation of lack of diagenetic overprint. $\delta^{18}O$ is also relatively low (-10 to -13 ‰). A single organic carbon isotopic determination from 5.9 m above the base of the formation is -25.0 ‰ ($\delta^{13}C_{org}{}^{N}$ = -26.6 ‰); and $\Delta\delta$ from the nearest carbonate determination is 21 ‰ ($\Delta\delta^{N}$ = 22.6 ‰).

Jenkins (1993b) reports $\delta^{13}C_{carb}$ values of -5.1 to -7.4 ‰ from the 'Halfway Dam Formation' at Olympic Bore and at Ringwood.

The limestone bed at Acacia Well has $\delta^{13}C_{carb}$ of +2.6 ‰. Mn/Sr (at 3.2) and $\delta^{18}O$ (at -8.8 ‰) of this sample are within the range considered typical of Neoproterozoic carbonates minimally altered with respect to $\delta^{13}C_{carb}$ (Kaufman & Knoll, 1995). $\delta^{13}C_{org}$ of the same sample is -28.1‰, giving $\Delta\delta$ of 30.6 ‰ and $\Delta\delta^{N}$ of 29.5‰ Table 2.4). The $\Delta\delta^{N}$ value is the same as the average for the Julie Formation (next section). $^{87}Sr/^{86}Sr$ of this sample is considerably altered (0.7108, Table 4.2).

Organic carbon

Systematic organic carbon isotopic determinations were made on three cored sections (Wallara 1, Rodinga 4, Alice Springs27) and on the outcrop section at Ellery Creek. A

few samples were also analysed from the more poorly outcropping Hidden Valley section, and one sample each from Acacia Well and Mt Capitor (discussed above).

Ellery Creek samples are texturally uniform shales; most are grey-green, a few are red. TOC's are low (0.58 ± 0.36 mg/g, n = 35). $\delta^{13}C_{org}{}^{N}$ values are remarkably concordant and a curve of best fit can be drawn from which only the topmost sample deviates more than 0.5 ‰ (Fig. 4.15) (samples from the overlying Julie Formation yield apparently more scattered results but data are few). The lowest $\delta^{13}C_{org}{}^{N}$ of -28 ‰ is seen in the lowest sample, from 15 m above the base of the formation. Thereafter, there is a uniform rise to a plateau (-25 ‰) and an abrupt positive excursion (-21 ‰) in the lower part of the central, silty interval (possible Cyclops Member correlative). Three samples that have heaviest $\delta^{13}C_{org}$ and which essentially define this positive excursion are marked by relatively high TOC (1.3 - 1.5 mg/g), the highest seen in this section.

Then follows an abrupt fall to -27 ‰ just above the silty interval, and then a rising trend towards the top of the formation. Raw $\delta^{13}C_{org}$ values show more scatter, and the negative excursion in the upper part of the formation is not apparent in the raw data.

Distinctive black shales (benthic microbial mat facies) in the lower half of the Wallara 1 section yield a distinct, separate, more depleted signal (Fig. 4.16). All other, lighter-coloured (grey-green, red) shales, with organic carbon considered to be predominantly of pelagic origin, yield $\delta^{13}C_{org}{}^{N}$ data points that, while more scattered than Ellery Creek data, nearly all lie within 1 ‰ of the indicated line of best fit (Fig. 4.16).

The 'pelagic' signal initially continues the relatively heavy values seen in the top of the cap dolostone ($\delta^{13}C_{org}{}^{N}$ = -26 to -27 ‰). This maximum persists through the basal red mudstone and into the lower part of the interbedded grey-green and black shale unit; then at 1220 m there is a sudden fall to a minimum ($\delta^{13}C_{org}{}^{N}$ = -30.5 ‰) followed by a gentle rise through the remainder of the banded black/green shale unit. The prolonged plateau (-27.5 ‰) through the remaining 400 m of the formation has a slight fall towards the top. The apparently scattered points may in places be distributed according to a higher-order variation - for example, possible variation of amplitude 2 ‰ and wavelength 50 m in the 720-840 m interval. Raw $\delta^{13}C_{org}$ data show essentially the same pattern, with slightly greater scatter of points (Fig. 4.16).

Isotopic data from the black shale 'benthic microbial mat' facies are treated differently to those of other rocktypes, in a manner fully discussed in Chapter 2. Briefly, two end-member sources of organic carbon are presumed to be present in the black shale beds: relatively ^{13}C-depleted carbon of benthic origin and relatively ^{13}C-enriched carbon of

pelagic origin. A simple mass-balance relationship allows calculation of a closer approximation of the benthic organic carbon end-member ($\delta^{13}C_{bmm}$). (The pelagic carbon end-member composition is obtained from the interbedded green shales). Another quantity of interest, $\Delta_{p\text{-}b}$, the difference between pelagic and benthic end-members, can then also be calculated.

Benthic microbial mat organic carbon isotopic compositions ($\delta^{13}C_{bmm}$) show an upward stratigraphic increase from around -36 to -32 ‰ (Fig. 4.16). These values are roughly 2 ‰ lighter than the raw black shale isotopic compositions ($\delta^{13}C_{bs}$). Curiously, the most depleted, stratigraphically lowest benthic microbial mats lie within the initial, positive excursion in the pelagic signal ($\delta^{13}C_{org}{}^{N} = -27$ ‰); and the rapid fall in $\delta^{13}C_{org}{}^{N}$ at 1220m is not reflected in $\delta^{13}C_{bmm}$. Higher up, however, the rising trends in 'benthic' and 'pelagic' signals are roughly parallel. Δ_{pb} is initially 9‰ but decreases abruptly at 1220 m to roughly 5 ‰, which value persists through most of the black-shale-bearing succession (Fig. 4.16).

Shales from Rodinga 4 contain 1.20 ± 0.52 mg/g TOC (n=36), and no benthic microbial mat facies is present. $\delta^{13}C_{org}{}^{N}$ points delineate an initial slight fall to a minimum of -30 ‰ followed by a more prolonged rise to -28 ‰ (Fig. 4.19). The amount of scatter (~± 1 ‰ from the line of best fit) is about the same as in Wallara 1. The uppermost three samples analysed are from the bleached, weathered zone; TOC's are very low and $\delta^{13}C_{org}{}^{N}$ are 1 to 1.5 ‰ heavier than the preceding trend.

Raw $\delta^{13}C_{org}$ data display a similar, but more exaggerated upward rise in isotopic composition (Fig. 4.19), a reflection of the fact that an upward fall in TOC accompanies the increase in $\delta^{13}C_{org}$.

Systematic analysis of the Hidden Valley section was hindered by very low TOC (0.21 ± 0.07 mg/g, n = 14) and poor outcrop. A total of twelve samples yield an apparently coherent signal below and just above the Cyclops Member (itself not analysed); but the scatter and sparsity of the upper four samples makes the continuation of the trend difficult to constrain (Fig. 4.17).

Normalised ($\delta^{13}C_{org}{}^{N}$) values are consistently about 2 ‰ lighter than raw data because of the uniformly low TOC. $\delta^{13}C_{org}{}^{N}$ in the basal red shale unit is -27 ‰, a value that continues into the overlying green shale. At about 100 m above the base of the section there appears to be a sharp decline followed by a gentler rise (Fig. 4.17). Immediately above the Cyclops Member are heavier values (-26 ‰); scattered points higher up

suggest a slight overall decline but data are clearly inadequate to constrain the signal with any precision.

Drillhole AS27 penetrated the lowest 60 m of the Pertatataka Formation. Six green bands within the predominant uniform, red mudstone have an average 0.14±0.05 mg/g TOC and $\delta^{13}C_{org}{}^{N}$ close to -27‰ (Fig. 4.18), essentially identical to the basal red mudstone unit at Hidden Valley.

Thermal grade

There is a kinetic isotope effect involving preferential loss of ^{13}C from kerogen during thermal maturation (McKirdy & Powell, 1974), so an assessment of thermal maturation is needed if widely separated organic $\delta^{13}C$ profiles are to be compared. Three independent sets of analytical data are employed that provide quantitative estimates of shifts in carbon isotopic composition attributable to organic maturation (see Chapter 2 for a full discussion): kerogen H/C ratios; $\Delta\delta$, the difference between carbonate and organic carbon isotopic composition ($\delta^{13}C_{carb}$-$\delta^{13}C_{org}$); and kerogen colour. This information, summarised in Table 2.5, indicates that thermal maturation in Wallara 1 has caused a ca. 1 ‰ enrichment in $\delta^{13}C_{org}$) relative to the Rodinga 4 Phillipson Pound area and the Ross River area; and that Ellery Creek should be 2 ‰ enriched relative to Wallara 1.

The data from Wallara 1, Ellery Creek and the Rodinga 4 - Phillipson Pound area are broadly consistent with the basin-wide assessment of maturation data by Jackson et al. (1984). In general, thermal maturity increases northwards in the Amadeus Basin. The Pertatataka Formation of Wallara 1 and Phillipson Pound - Rodinga 4 lie within the 'oil window' (0.6-1.3% VRE) with Wallara 1 closer to the 1.3% contour (see Figs 7, 8 of Jackson et al., 1984). Ellery Creek at the northern edge of the basin is distant from control points but by extrapolation has a significantly higher thermal maturity. Their data are sparse in the Ross River area area but suggest somewhat higher thermal maturity relative to Phillipson Pound than is indicated here.

R. S. Nicoll (pers. comm.) found conodont colour alteration indices from Ordovician units in Ellery Creek, ca. 2 km south of the Pertatataka section, to be surprisingly low (1 - 1.5, equivalent to less than 0.8% VRE). These data, taken at face value, indicate that either peak thermal conditions (under a high geothermal gradient) predated folding (at odds with current ideas on the evolution of the basin: Jackson et al., 1984); or that the maturation indices used above may be in error at Ellery Creek. Kerogen colour and H/C data were derived from outcrop samples at Ellery Creek and drillcore at other

localities. Possibly, the effects of weathering on kerogen colour and chemical and isotopic composition in shales mimic those of thermal maturation.

Sulphide sulphur isotopes

Nine pyrite sulphur isotopic analyses were carried out on randomly selected samples from Wallara 1 and Rodinga 4. Pyrite was concentrated using HF and HCl demineralization (see Chapter 2). Most samples thus treated are palynological residues provided by K. Grey.

Pyrite is generally not visible to the unaided eye in the Pertatataka Formation, but is seen in thin sections as framboids 2-20 μ in diameter, comprising much less than 1% of the rock. Pyritized coiled filaments are also seen in bedding-parallel thin sections from Rodinga 4. These structures are ~ 20 μ thick and up to 200 μ long, usually lying in irregular loops or coils. In black shale in Wallara 1 (benthic microbial mat facies) pyrite is abundant; in places lenticular segregations of fine-grained pyrite are visible. In thin sections pyrite is seen to be heavily concentrated along organic-rich, anastamosing seams thought to be remnant benthic microbial mats (see Chapter 2). All pyrite is considered to be early diagenetic in origin.

Results (Fig. 4.20) are considered to reflect environmental/diagenetic factors rather than secular change in marine $\partial^{34}S_{sulphate}$. Results from the benthic microbial mat facies show a broad spread of $\partial^{34}S$ values: -8 to -28 ‰ (Fig. 4.20). Results from other shales show a narrower spread of mostly heavier values ($\partial^{34}S$ = 0 to -10 ‰).

Pyrite evolves towards heavier $\partial^{34}S$ during early diagenesis through a Rayleigh distillation effect as sulphate-reducing bacteria use up porewater sulphate. Sulphate reduction does not commence in sediments until oxygen, nitrate, manganese and ferric iron are exhausted as oxidising agents (Anderson & Arthur, 1983). Heavier pyrite in the organic - poor samples in the Pertatataka Formation may reflect relatively late onset of sulphate reduction and lower sulphate availability. Sulphate availability would have been reduced because of deeper burial and decreased diffusive renewal from sea water, and reduced pore volumes due to compaction. In relatively organic-rich samples, by contrast, the other oxidising agents were more rapidly depleted, allowing sulphate reduction to proceed at relatively shallow sediment depths where freer diffusive renewal of sulphate was possible.

The Pertatataka Formation evidently does not share the strong (and enigmatic) enrichment of sulphide $\partial^{34}S$ seen in many older (Sturtian) Proterozoic units.(Hayes et

al., 1992). The observed range of sulphide $\partial^{34}S$ compositions would be not unusual in the Phanerozoic.

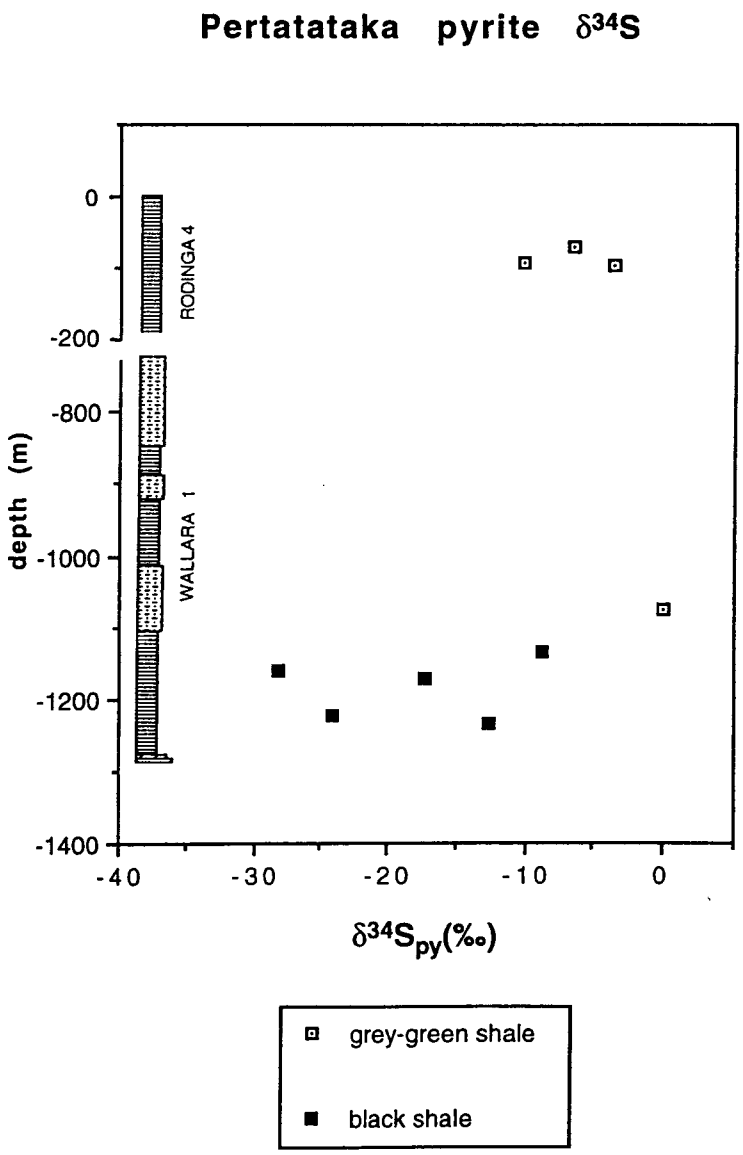

Fig. 4.20: Stratigraphic variation in pyrite $\delta^{34}S$ in the Pertatataka Formation (composite section of Wallara 1 and Rodinga 4 correlated as in Fig. 4.37).

4.5d INTERPRETATION

Correlation of the Pertatataka Formation within the Amadeus Basin

Alternative ways of correlating the Pertatataka Formation and associated units between the sections described above and with the type Ediacarian may be encapsulated in three correlation diagrams (Fig. 4.21). Shaded areas on these diagrams correspond approximately to the Nuccaleena-Brachina interval of the type Ediacarian. There is general agreement that cap dolostones in Wallara 1 and in the NE Amadeus Basin are Nuccaleena correlatives, and that transitionally overlying shales at these localities are Brachina correlatives. It is shown here that the isotopic-chemostratigraphic data support correlation of the Wallara 1 Pertatataka section with the lower part of the Ellery Creek and Hidden Valley sections, and that the Wallara 1 Pertatataka section can be firmly correlated with the Brachina Formation. Correlation scheme A (Fig. 4.21a) is therefore best supported by the evidence presented in this study.

Scheme A

This scheme is essentially an extension of Preiss et al. (1978). In this scheme, the Olympic Formation and the type Pioneer Formation at Ellery Creek are lateral correlatives, for which there is good lithologic evidence and some chemostratigraphic evidence (reviewed in previous section). The cherty, *Elleria*-bearing cap dolostones at Ellery Creek and Hidden Valley are correlatives of the cap dolostones in the Ringwood, Mt Capitor and Wallara 1 sections. Stable isotopes offer permissive but not conclusive support for this correlation (see previous section). The Gaylad and Halfway Dam Formations are, in this scheme, time-equivalents of an undefined (possibly condensed) interval low in the type Pertatataka. The base-Gaylad unconformity is only a local development and passes into conformity elsewhere in the basin. In support of this scheme, uniform red mudstones low in the Pertatataka Formation in the Hidden Valley and Ellery Creek sections are lithologically identical to the basal 23 m of the formation in Wallara 1, and to the basal part of the Brachina Formation (see Chapter 3).

Scheme B

This scheme is derived from Jenkins et al. (1992), Jenkins (1993b) and Jenkins (pers. comm. 1993). As in Scheme A, the type Pioneer and Olympic Formations are correlative, but the sandstone unit above the Undoolya sequence at Hidden Valley is a Gaylad Sandstone correlative rather than Pioneer Formation. The Undoolya sequence, 'Halfway Dam Formation' and Pertatataka Formation in Wallara 1 are correlatives and

Brachina equivalents, and are not represented in the type Pertatataka at Ellery Creek. The base-Gaylad surface is represented by the abrupt base of the 'cap dolostone' at Ellery Creek, which is then considerably younger than the Nuccaleena-correlative cap dolostones of the Wallara 1, Ringwood, Olympic Bore and Mt Capitor sections. The base-Gaylad unconformity is a sequence boundary correlated with the sequence boundary near the top of the ABC Range Quartzite in the Adelaide Geosyncline. In support of this scheme, Nuccaleena-like cap dolostones at Wallara 1 and in the NE Amadeus Basin (cd1 in Fig. 4.21b) need not be correlated with lithologically dissimilar, cherty units (cd2) at Ellery Creek and Hidden Valley. Also, red mudstone low in the Pertatataka Formation overlying Gaylad Sandstone in the Gaylad Syncline section resembles that at Hidden Valley, and is typical of the Bunyeroo Formation of the type Ediacarian. (Note, however, that identical red mudstones are also seen at the base of the Brachina Formation and agreed correlatives such as the Wallara 1 section). The base-Gaylad unconformity may alternatively represent an amalgamation of sequence boundaries and the Gaylad and Pertatataka Formations may be equivalent to the Wonoka Formation and/or Billy Springs Formation (Jenkins, 1993b, p. 56-57).

Scheme C

This scheme was recently proposed by Preiss (pers. comm. 1993). It is similar to Scheme B except that the type Pioneer is a Gaylad correlate, as is the thin, prominent sandstone unit at Glen Helen. Arguments against correlation of this sandstone unit with the type Pioneer are presented above (section 4.5b, *Glen Helen*).

Chemostratigraphic correlation

The organic carbon isotope profile of Wallara 1 is similar in part to that of the lower half of the type section at Ellery Creek (Fig. 4.15, 4.16). Differences between the profiles can be explained in terms of relative position within the depositional system, and a higher degree of thermal maturity at Ellery Creek.

The distinct $\delta^{13}C_{org}$ signal of the black shale (benthic microbial mat facies) in Wallara 1 can be ignored for the purpose of this discussion, since this facies is unknown elsewhere in the Pertatataka Formation.

The minimum (-30.5 ‰), ensuing rise and plateau (-27.5 ‰) in Wallara 1 are here interpreted as equivalent to the initial minimum (-28 ‰), rise and plateau (-25 ‰) at Ellery Creek. The heavier isotopic compositions (by 2.5 ‰) at Ellery Creek correspond

a) CORRELATION SCHEME A

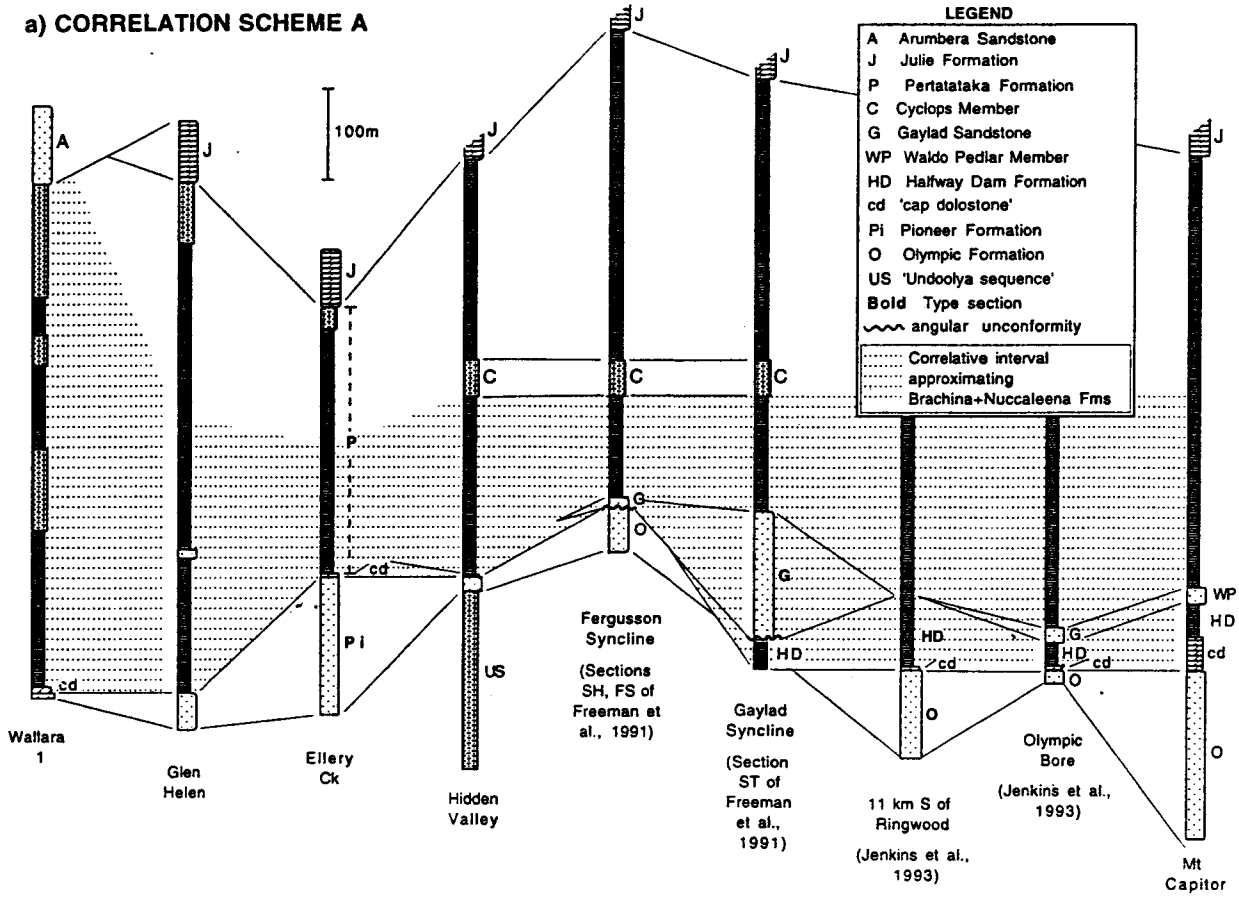

b) CORRELATION SCHEME B

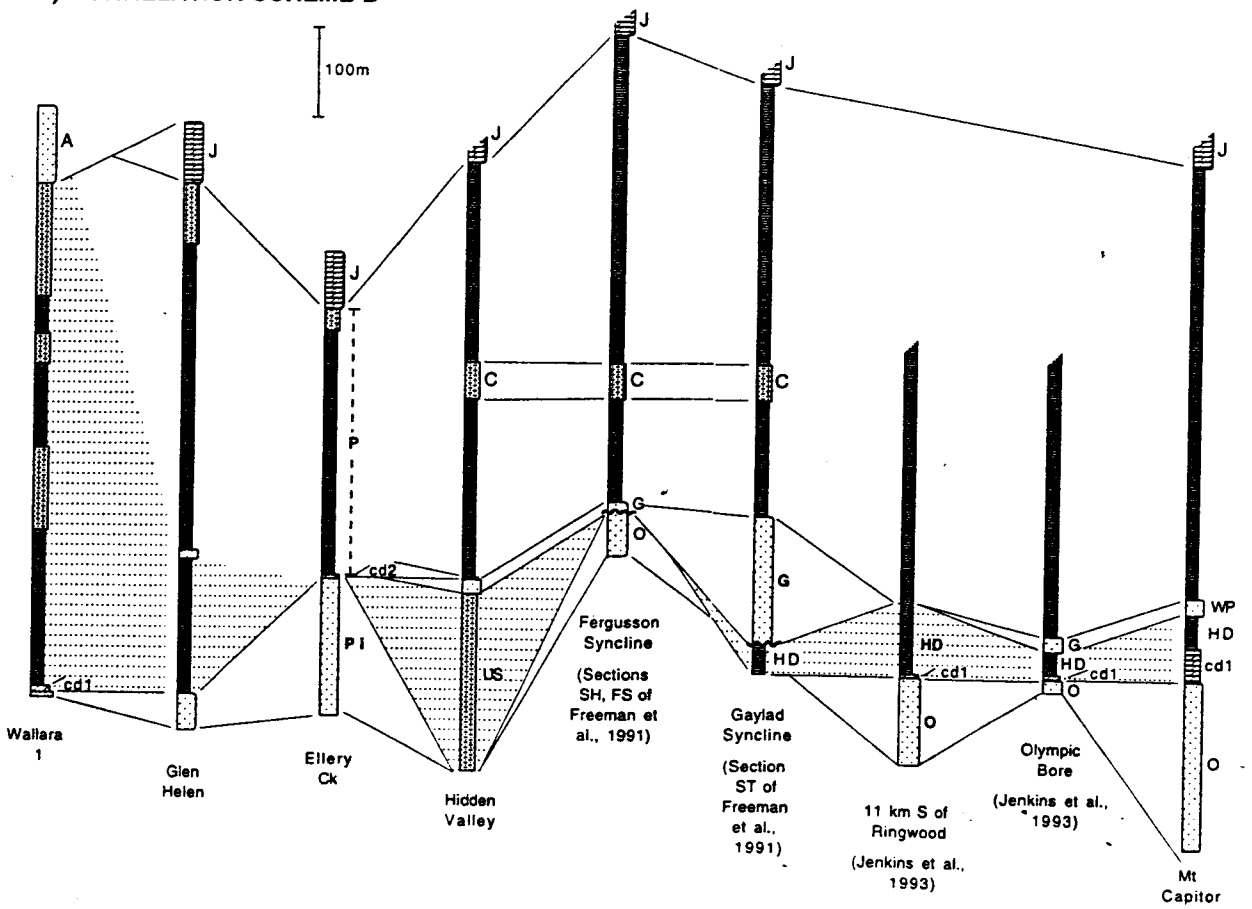

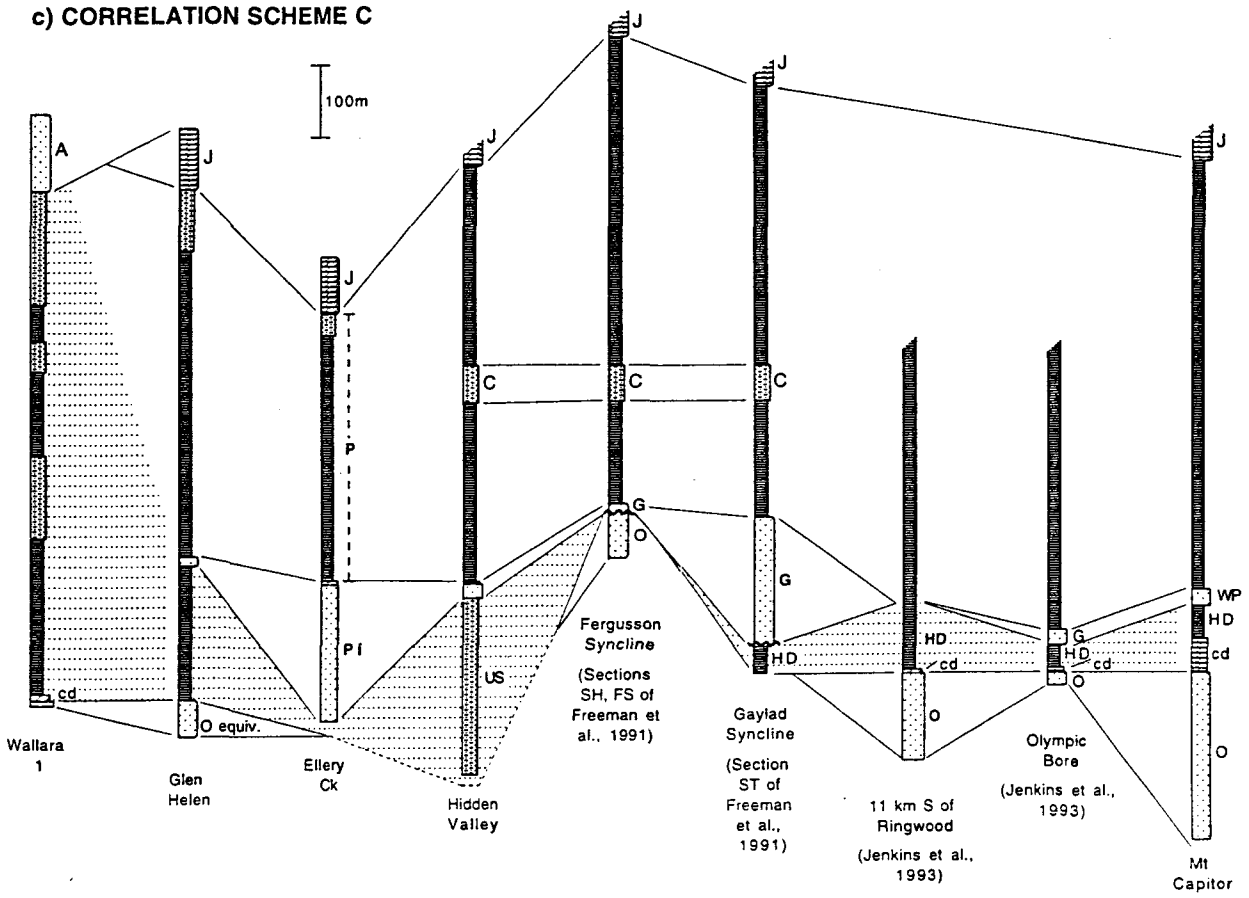

Fig. 4.21 (opposite, and above): Alternative correlation schemes for the Pertatataka Formation and associated units. (a) As proposed in this study, and in part by Preiss et al. (1978); (b) as proposed in part by Jenkins et al. (1992) and Jenkins (pers. comm., 1993); (c) as proposed by Preiss (pers. comm., 1993). Patterned area between columns indicates interval thought to correlate with Nuccaleena and Brachina Formations of the Adelaide Geosyncline.

closely to the relative thermogenic enrichment (2.0 ‰) predicted from H/C data (Table 2.5).

The remaining differences between the profiles are the apparent absence, at Ellery Creek, of the basal positive excursion at Wallara 1, and the apparently greatly condensed nature, at Ellery Creek, of the prolonged plateau in the Wallara 1 profile.

Above (section 4.5a) it is established from a synthesis of seismic, palaeogeographic and palaeocurrent data that the Pertatataka Formation in the central-north Amadeus Basin incorporates a major, north-prograding highstand systems tract with a condensed section near the base of the formation (Figs. 4.12, 4.13). Fig. 4.22 shows the proposed chronostratigraphic relationship between the Wallara 1 and Ellery Creek sections, based on this sequence stratigraphic framework and the general model of Swift et al. (1987) (Fig. 4.12). The condensed section (downlap surface) in the more distal locality (Ellery Creek) is predicted to incorporate a longer time interval than in the more proximal locality (Wallara 1) (Fig. 4.12). In this interpretation, the positive excursion in Wallara 1 is is incorporated into the condensed section at Ellery Creek. This probably lies within the unexposed interval 10-15 m above the base of the formation, above sandsone beds that occur in the basal 10 m (part of the TST) and below the first analysed sample. The condensed section in Wallara 1 is interpreted to occur within the basal, uniform red mudstone unit. Sedimentological evidence is consistent with this: there is no evidence for current action or introduction of silt or sand into this uniformly fine-grained, 23 m-thick unit, while the same cannot be said of anywhere higher or lower in the succession.

The gentle upward climb above the minimum in the profiles of both sections occupies about the same stratigraphic thickness (100 m). This was an interval of shale sedimentation with only rare silt or sand in both localities, with benthic microbial mats common at Wallara 1. A period of slow sedimentation largely from suspension is implied, and consequently there is little, if any, condensation of the profile in the more distal section.

Higher in the Wallara section, the prolonged plateau in the profile coincides with the appearance of considerable silt and fine-grained sand which marks a change to a prodelta setting (R. J. Korsch, pers comm to M. R. Walter) with sands transported basinward by turbidity currents or storms. A greater sedimentation rate and steepening clinoforms seem probable on sedimentological evidence. At Ellery Creek, however, the plateau corresponds to continuing shale sedimentation with very little silt or sand. Thus this part of the profile is condensed relative to Wallara 1.

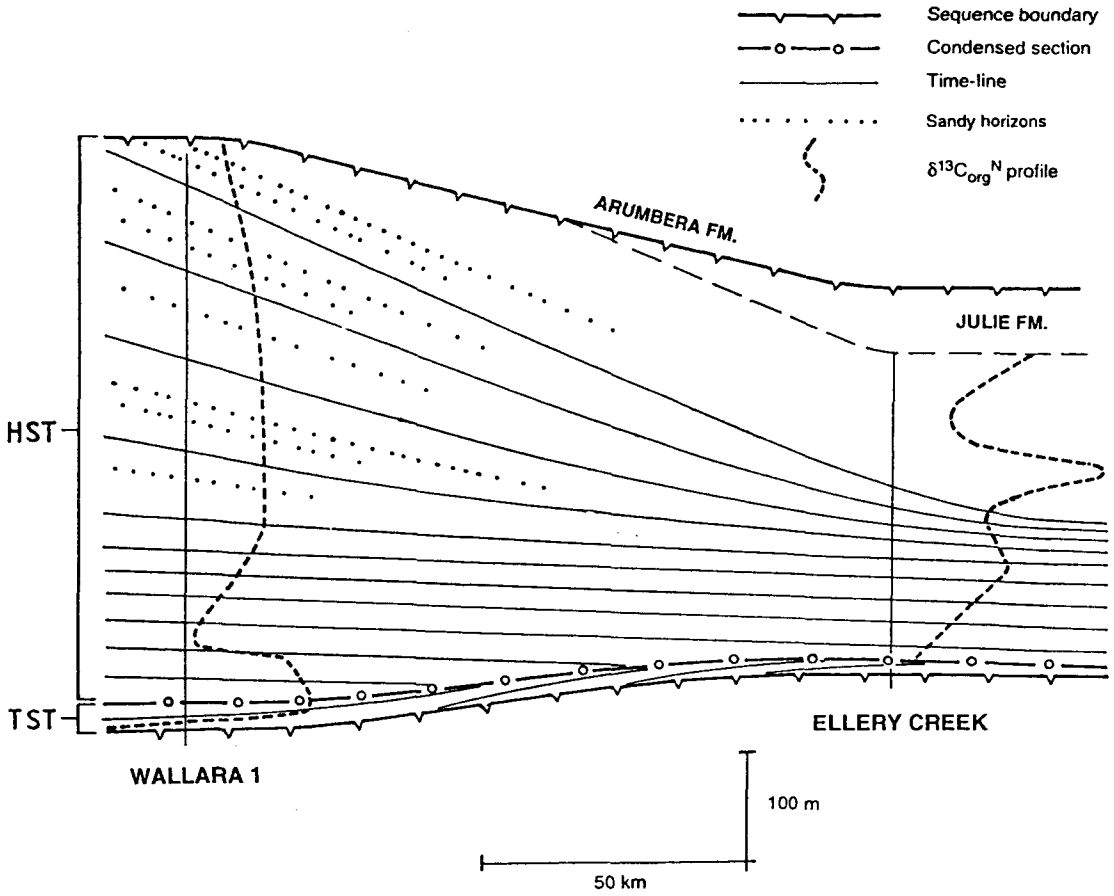

Fig. 4.22: Proposed chronostratigraphic correlation of Wallara 1 and Ellery Creek Pertatataka sections, showing relaltionship of sequence-stratigraphic framework to $\delta^{13}C_{org}{}^{N}$ chemostratigraphic profiles. HST: highstand systems tract; TST: transgressive systems tract. Chemostratigraphic profiles from Figs. 4.15, 4.16.

The proposed correlation (Fig. 4.22) relies on a highly interpretive and possibly oversimplified model of basin fill. Confirmation by an independent chronostratigraphic technique, or chemostratigraphic profiling at intermediate sections, is required. However, the good agreement of absolute values (once the difference in thermal grade is accounted for), and the consonance with sedimentological data, suggest that this interpretation is the best interpretation possible at present.

Data at Hidden Valley are sparse but the profile in the lower third of the formation (Fig. 4.17) is similar to the lower part of the Wallara 1 profile (Fig. 4.16). It is noteworthy that the initial high (-26.5‰) in the Hidden Valley $\delta^{13}C_{org}{}^{N}$ profile coincides with a unit of uniform red mudstone identical to that comprising the basal unit at Wallara 1, and which has essentially identical $\delta^{13}C_{org}{}^{N}$. However in both sections it is seen that the positive excursion is not lithologically governed as high $\delta^{13}C_{org}{}^{N}$ extends upward into grey-green silty shales in both cases. No thermal maturation data are available from Hidden Valley, but $\Delta\partial$ data from nearby localities on the N'Dhala Thrust Sheet suggest that Wallara 1 should exhibit a roughly 1‰ enrichment due to thermal effects,

relative to Hidden Valley. Thermal maturation data therefore allow the proposed correlation, given the uncertainties in $\Delta\partial$ and the correction factor used in $\delta^{13}C_{org}{}^{N}$ calculation (here significant because of very low TOC at Hidden Valley).

The initial plateau in $\delta^{13}C_{org}{}^{N}$ in the Hidden Valley profile has twice the stratigraphic extent than that at Wallara 1, and the basal uniform red mudstone unit is also thicker (55 m vs 23 m). There is no obvious explanation for this; however the Pertatataka Formation in the NE Amadeus Basin probably belongs to a different (north-sourced) depositional system than that proposed for the central and northern parts of the basin (Fig. 4.22). Palaeocurrents in the Gaylad Sandstone and Cyclops Member in the NE Amadeus Basin are predominantly from the north (Freeman et al., 1991; Korsch, 1986a).

The basal 50 m of the Pertatataka Formation in Alice Springs 27 (Fig. 4.18) is a good lithologic and isotope-chemostratigraphic correlate of the basal part of the formation at nearby Hidden Valley.

The profile from Rodinga 4 (Fig. 4.19) spans the upper third of the Pertatataka Formation, and is similar to the $\delta^{13}C_{org}{}^{N}$ profile from the upper third of the formation at Ellery Creek (Fig. 4.15). There is a ca. 3‰ difference between the sections in the minimum of the negative excursion (ca. -30‰ at Rodinga 4 vs. -27‰ at Ellery Creek). This corresponds to the predicted thermal maturation effect (Table 2.5).

An upward trend in marine $\delta^{13}C_{DIC}$ during deposition of the uppermost Pertatataka is supported by carbonate data. The limestone bed 80 m below the top of the formation at Acacia Well has $\delta^{13}C_{carb}$ of +2.6‰; while the lowermost Julie Formation exhibits a regionally uniform +5‰. There is no detectable diachrony in the Pertatataka - Julie transition, from data at Ellery Creek, the Rodinga 4 area, and Acacia Well - Ross River.

The organic carbon isotope profiles are thus readily accommodated by correlation of the Pertatataka Formation in Wallara 1 with the lower part of the type section at Ellery Creek, and with the lower part of the formation at Hidden Valley. Correlation scheme A (Fig. 4.21a) is therefore favoured. This conclusion is indirect support for the correlation of the cap dolostones as proposed in the previous section.

One consequence of the proposed correlations is that a considerable part of the upper Pertatataka Formation has been eroded (or was not deposited) at Wallara 1. Independent support for this interpretation comes from acritarch biostratigraphic work

that suggests no temporal overlap between Rodinga 4 and Wallara 1 Pertatataka sections (Grey, in prep).

Stratification of basin waters early in Pertatataka time

In this and the previous chapter it is suggested that depleted carbonate carbon isotopic compositions in cap dolostones may reflect deposition under the bottom layer of a stratified marine water body. ^{13}C-depleted limestones in the 'Halfway Dam Formation', and ^{13}C-depleted organic carbon of benthic origin in the lower Pertatataka Formation in Wallara 1 are evidence that stratification may have persisted through this time. There is no trace-element or Sr-isotope data from the 'Halfway Dam Formation' limestones to assess the possibility of diagenetic shifts in $\partial^{13}C_{carb}$, but the fine grainsize, evidence for early lithification (intraclasts, Neptunean dykes), and low TOC suggest that the values (-5 to -8‰) have been little altered by burial or organic diagenesis. A $\Delta\partial$ determination at Mt Capitor from separate (but closely adjacent) samples is 21‰, which is 10‰ lower than is seen in nearby Julie Formation (Table 2.4). Elsewhere (Chapter 3) it is postulated that some anomalously low $\Delta\partial$ in relatively deep- water environments (e.g. Wonoka Formation) are due to stratification of the water body that results in simultaneous deposition of organic carbon fixed in the (relatively ^{13}C-enriched) surface layer and carbonate precipitated from, or equilibrated with, the ^{13}C-depleted lower layer. If the heaviest $\partial^{13}C_{carb}$ values from the cap dolostone (+1 ‰) reflect surface-water $\partial^{13}C_{DIC}$ in lower Pertatataka time, then a difference of up to 9 ‰ in composition between surface and lower water layers is implied. This is in rough agreement with the observed shortfall in $\Delta\partial$ at Mt Capitor and with the observed difference in composition (9 ‰) between carbon of pelagic and benthic origin (Δ_{pb}) in the lowermost part of the Wallara 1 section. Interpretation of the benthic microbial mats in the light of the basin stratification hypothesis is fully discussed in Chapter 2.

4.6 Julie Formation

4.6a STRATIGRAPHY

The Julie Formation is mainly carbonate, is widespread in the N and NE Amadeus Basin, and conformably overlies the Pertatataka Formation. It is absent south of the Central Ridge where it has been presumably removed by uplift and erosion at the end of the Proterozoic. The formation is 50-100 m thick over most of its extent, but it thickens markedly in the Phillipson Pound area (Ooraminna depocentre), where 500-600 m are

present between Mt Capitor and the Rodinga 4 drillsite. Four sections were systematically sampled: Ross River Homestead (the type section: Wells et al., 1967), Ellery Creek, Katapata Gap (near Areyonga), and Phillipson Pound (a composite section in which the lower part of the formation was sampled N of the Rodinga 4 drillsite, and the upper part at Twin Bore, just N of Mt Capitor) (Fig. 4.4).

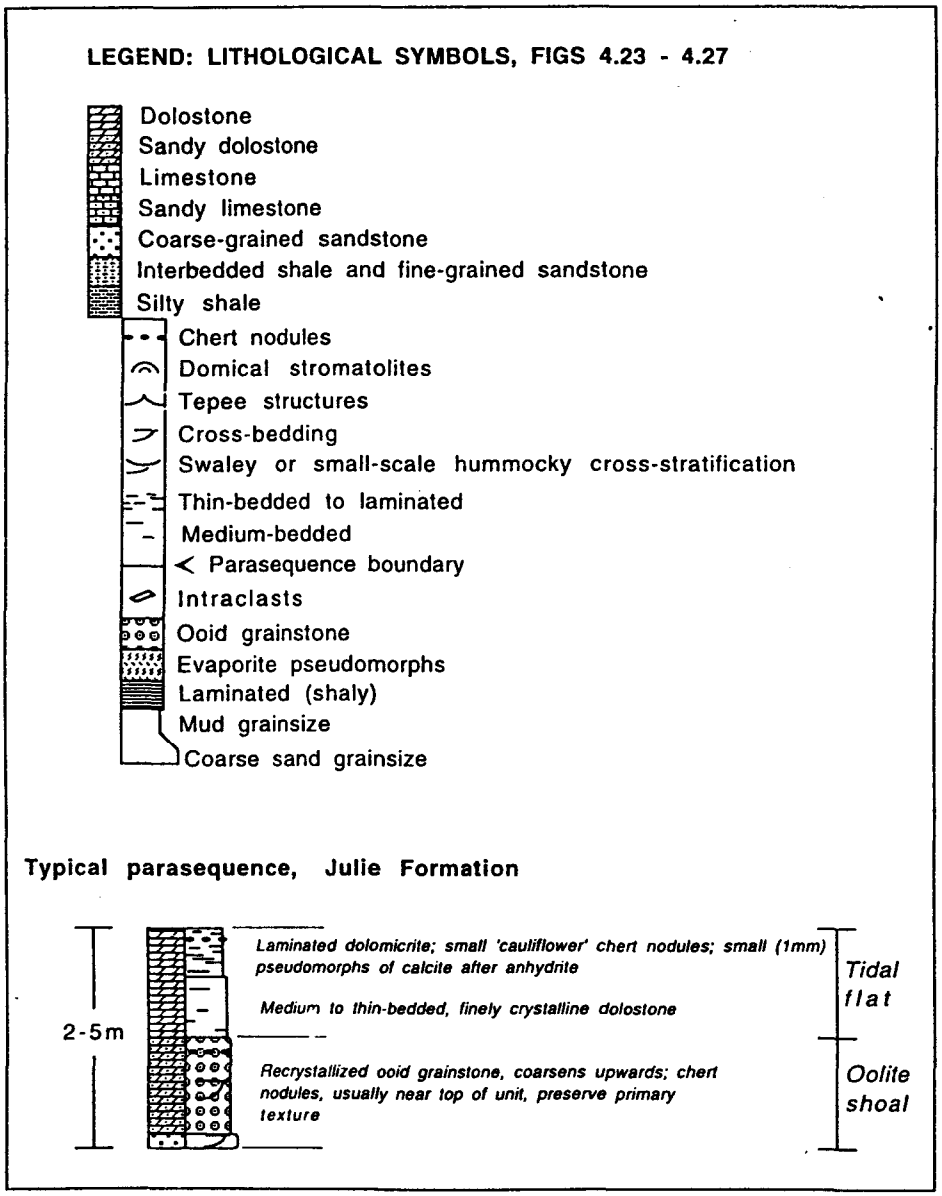

Fig. 4.23 (above): Typical parasequence of Julie Formation, and lithologic symbols used in Figs. 4.23 - 4.27.

Fig. 4.24 (opposite): Lithologic column and carbonate $\delta^{13}C$ and $\delta^{18}O$ data, Julie Formation, Ross River (type section).

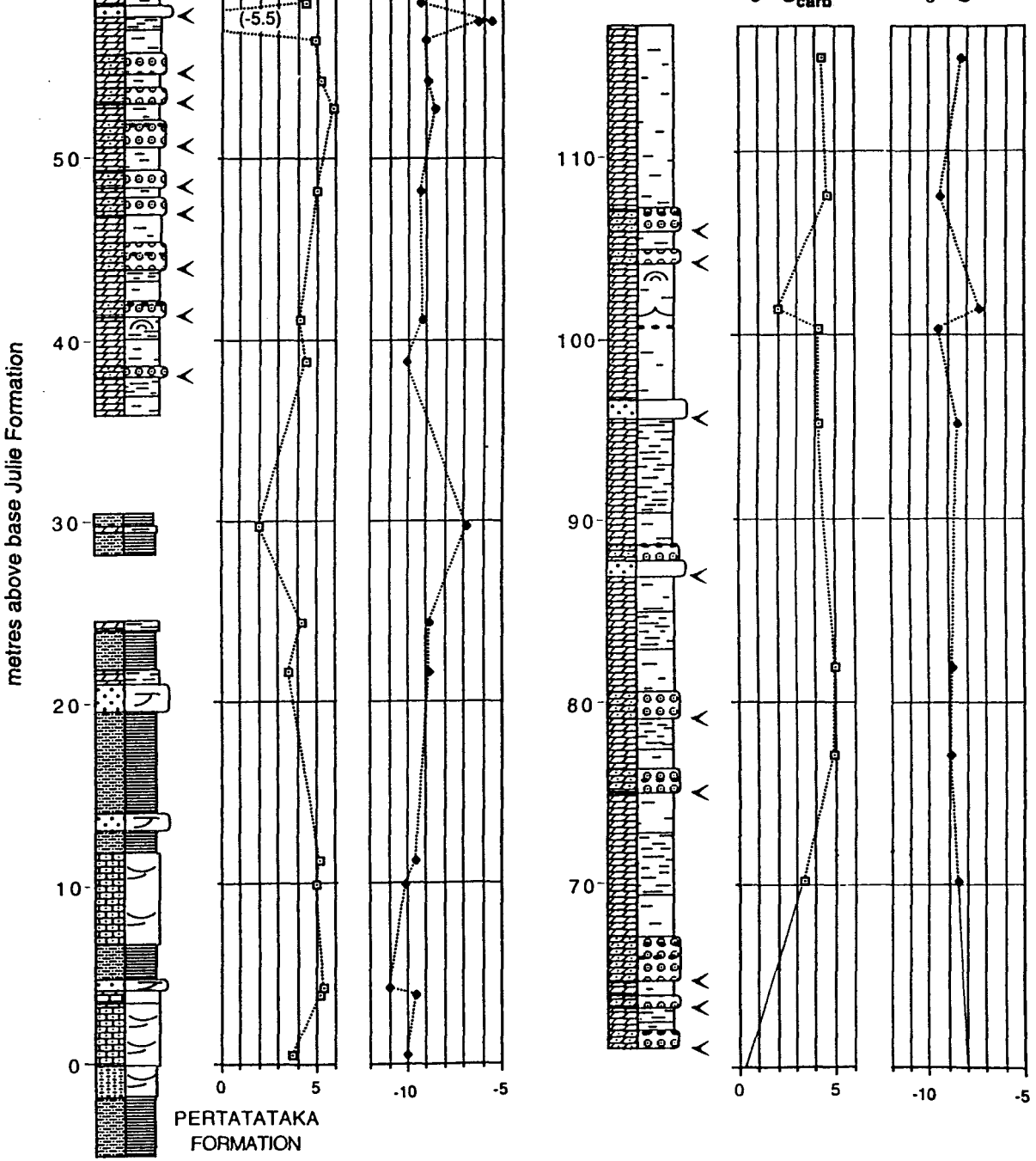
metres above base Julie Formation
(-5.5)
50
40
30
20
10
0
0
5
-10
-5
PERTATATAKA
FORMATION
110
100
90
80
70
0
5
-10
-5

Ross River

The type section is well-exposed on the ridge immediately south of the Ross River homestead. This section is 117 m thick (Fig. 4.24). The contact upon Pertatataka Formation is abrupt but conformable. An abrupt upward increase in bedding thickness accompanies the lithologic change from shale to sandy limestone. Small-scale HCS, present in thin sandstone beds in the uppermost Pertatataka formation, persists into the lower part of the limestone.

The lowest 12 m of Julie Formation consists of dark grey, sandy and silty, well-bedded limestone, in places with low-angle, polymodal (swaley?) cross-stratification. One bed 4m above the base contains a small-scale stylonodular fabric similar to that of Unit 7 of the Wonoka Formation (see Chapter 3). Thin sections of the limestone show moderately to weakly luminescent xenotopic microspar of 20-50μ grainsize with 10-40% dolomicrospar.

Then follows a recessive unit (12 - 36 m on illustrated section) of siltstone, cross-bedded coarse-grained quartzarenite and minor dolostone with small 'cauliflower' chert nodules (probably after evaporites). The rest of the formation (36 - 117 m) consists essentiallly of alternating sandy, recrystallised ooid dolograinstone and fine-grained dolostone with minor coarse-grained sandstone. These lithologies are arranged in shallowing-upward cycles or parasequences (Fig. 4.23, 4.24; Plate 4.8). The erosional bases of parasequences are typically overlain by a thin (<100 mm) layer of very coarse-grained quartz sandstone. Then follows 1 - 2 m of dolograinstone with coarse, fabric-destructive recrystallization. Individual grainstone units tend to coarsen upwards and in places have cross-bedding. The coarsening-upward trend indicates that the oolitic units represent ooid shoals rather than tidal channel-fills. The original oolite fabric is well-preserved within large (100 - 200 mm) ovoid chert nodules that tend to occur toward the tops of the grainstone units. The upper part of each parasequence consists of medium to thin-bedded, fine-grained pale grey dolostone and dolomicrite, with common small 'cauliflower ' chert nodules and small (< 1mm) calcite pseudomorphs after anhydrite. Wavy lamination of possible microbial origin occurs in the upper parts of parasequences. In places, tepee structures and poorly-preserved domical stromatolites are present. Each parasequence probably represents a tidal flat complex prograding over an oolite shoal.

Thin sections of grainstone show a coarsely recrystallised (100 μ) xenotopic mosaic with poorly-preserved ooids. This lithotype was not selected for isotopic analysis,

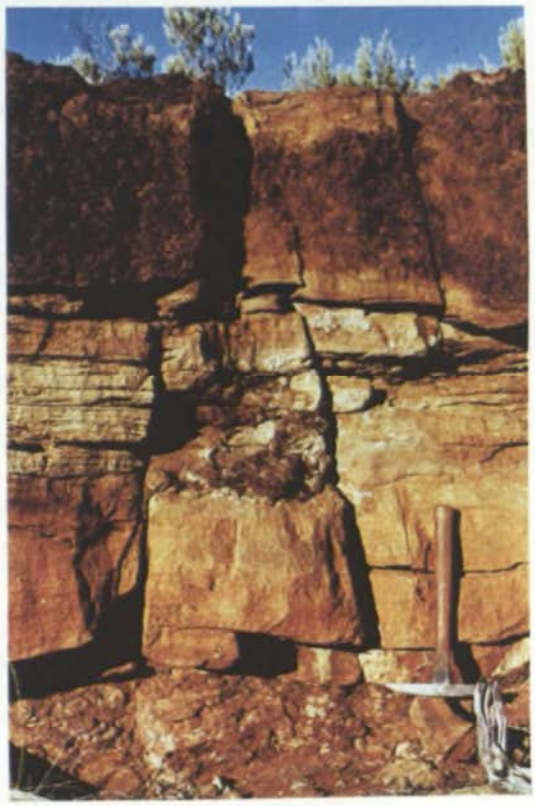

Plate 4.8: Part of two parasequences, Julie Formation, Ross River section. Lower part of outcrop, showing massive, then laminated fine-grained dolostone, is the upper part of earlier parasequence; upper part of outcrop - massive, brown, sandy, recrystallised dolomite oolite - is lower part of the next parasequence.

Plate 4.9: Low-angle and swaley cross-stratification in sandy limestone, lower Julie Formation, Phillipson Pound section. Lens cap 50 mm diameter.

preference being given instead to the fine-grained rock-types of the middle and upper parts of parasequences. Uniform medium-bedded dolostone from the middle parts of parasequences are fine-grained, slightly silty dolomicrosparites(5-20μ grainsize). Laminated rock from upper parts of parasequences are dolomicrite or interlaminated dolomicrite and silty dolomicrosparite; desiccation cracks and small vugs - possibly after evaporites - are filled with coarse calcspar.

The basal limestone unit was deposited in a sublittoral environment, within storm wavebase, perhaps at fairweather wavebase. Most of the remainder of the formation represents dolomitic-evaporitic tidal mudflats and oolite shoals. Shallowing upwards cyclicity is a very common pattern of sedimentation in platformal carbonates (e.g. Wilson, 1975, p 281) but whether this pattern is due predominantly to eustatic cycling or to some autocyclic mechanism, is a matter of ongoing debate.

It is noteworthy that parasequences become thinner upwards towards 64.5m (Fig. 4.24), suggesting this horizon is the top of a highstand systems tract (a depositional sequence boundary) (e.g. Posamentier & Vail, 1988); thicker parasequences higher up suggest more rapidly rising relative sealevel and a transgressive systems tract. Parasequence stacking patterns at Ross River are thus not consistent with the proposed (Lindsay & Korsch, 1991) sequence boundary at the top of the Julie Formation.

Silicification to form the chert nodules in the upper parts of grainstone units may have been early diagenetic, evidently preceding compaction and recrystallisation. Seawater may have been the source of silica, which was more abundant in Precambrian seawater than today's (Maliva et al., 1990).

Ellery Creek - Glen Helen

At Ellery Creek the formation is 63 m thick. It begins with two thick beds of pale grey, laminated dolomicrite, followed by a covered interval of 40 m (probably consisting of recessive shale, siltstone and sandstone judging by nearby exposure). The upper 20 m consists of pale grey dolomicrite with two thick beds of ooid dolograinstone. Lithologies are arranged as two, perhaps three parasequences similar to those at Ross River. At the parasequence boundary at 43.7 m, for example, ooid grainstone abruptly overlies thin-bedded creamy dolomicrite with calcite-after-anhydrite pseudomorphs (Fig. 4.25). The grainstone bed coarsens upwards and has chert nodules in its upper part. Ooids are concentric, often compound, with micritic cortices and sparry centres. There is a lens of dark grey, peloidal lime grainstone in the upper part of this bed. In thin section this is a recrystallized microspar of 20-50 μ grainsize. There are three

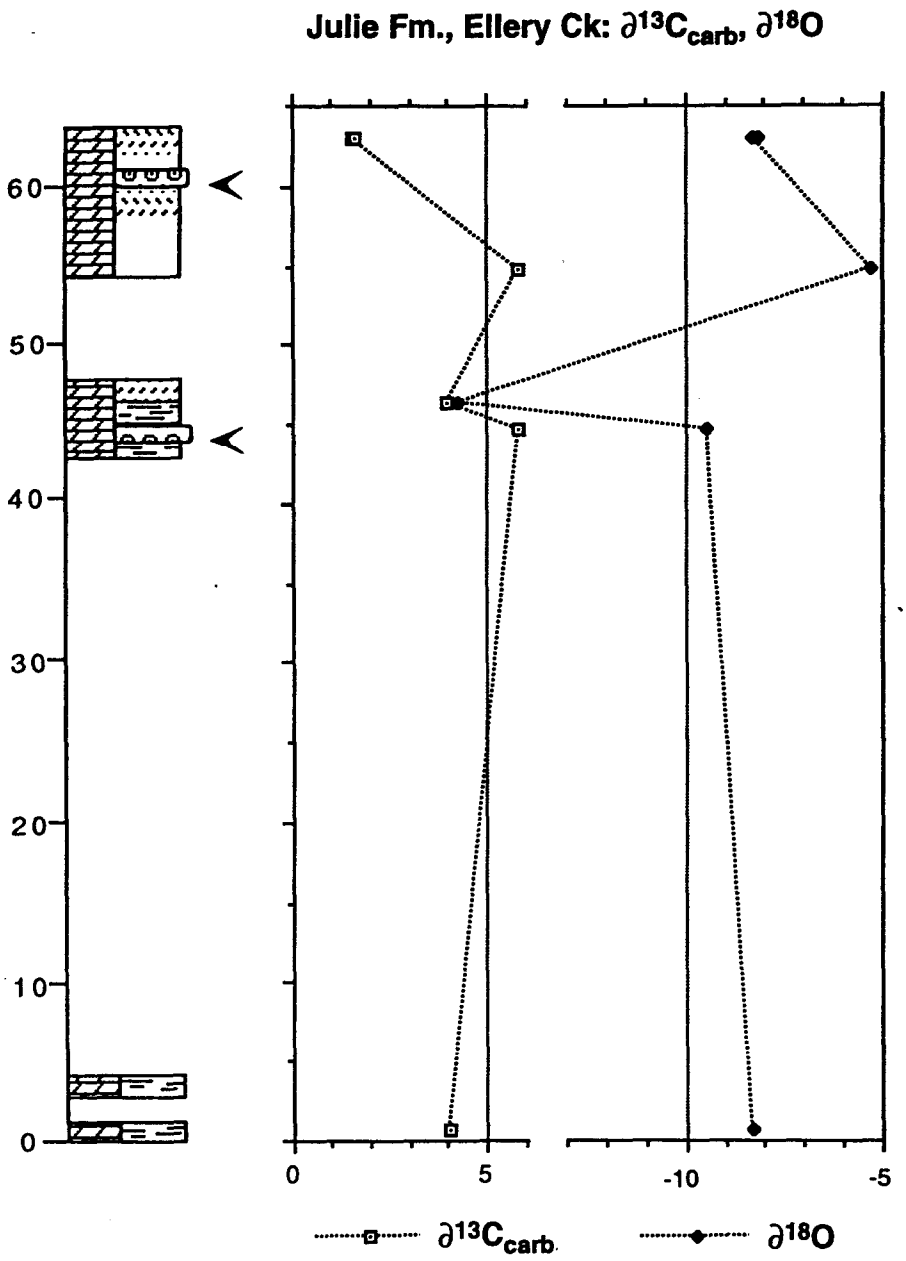

Fig. 4.25: Lithologic column and carbonate $\delta^{13}C$ and $\delta^{18}O$ data, Julie Formation, Ellery Creek.

horizons where dolomicrite contains scattered, small (1-2 mm) pseudomorphs of calcite after anhydrite (Plate 4.10).

44 km further west, at Glen Helen, the Julie Formation is 65 m thick and carbonate is minor. The lower 40 m comprises beds of fine-grained dolostone in a predominantly red shale and siltstone succession. Then follows a prominent unit, 6 m thick, of thick-bedded oolitic dolograinstone. Irregular vugs in this unit, 10-20 mm in size, may be after evaporites. This is succeeded by recessive, thin-bedded silty dolostone and shale(14 m) and then a prominent 6 m-thick unit of coarse-grained quartzarenite that comprises the topmost part of the Julie Formation. The base of the Arumbera

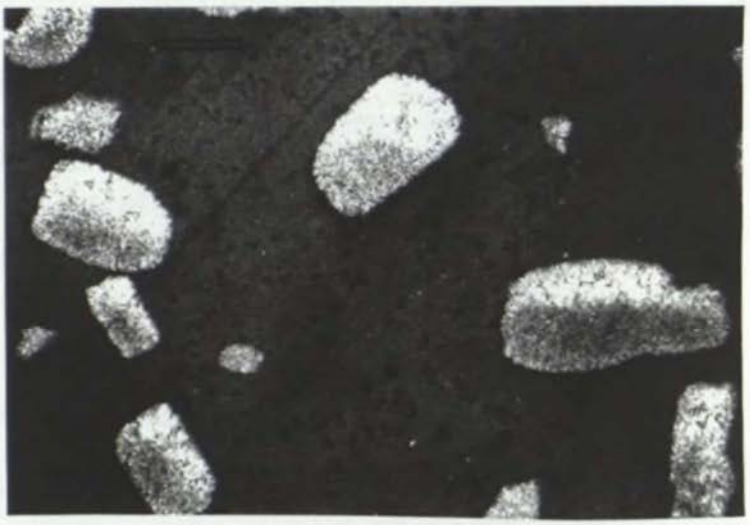

Plate 4.10: Thin section of dolomicrite with calcite-after-anhydrite pseudomorphs with geopetal internal sediment. Sample 6.42, 47 m above base of Julie Formation, Ellery Creek section. Scale bar = 1mm.

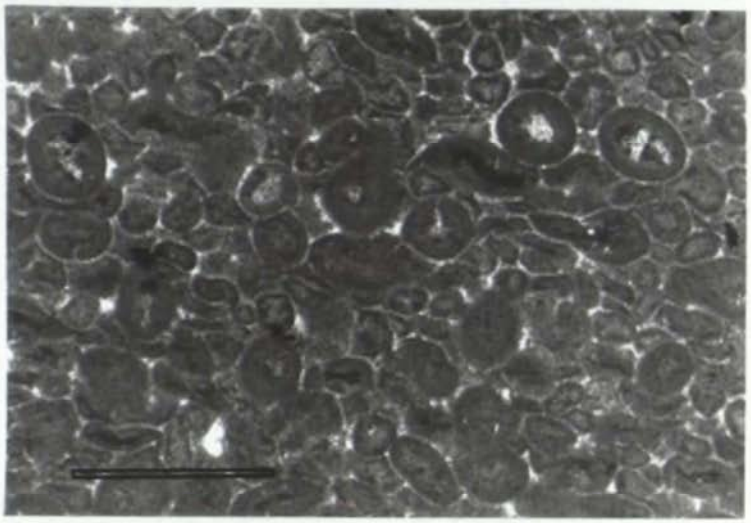

Plate 4.11: Thin section showing texturally well-preserved micritic ooids, deformed by compaction so that cement is negligible apart from a very thin isopachous early (marine?) phase. Sample 24.21, upper Julie Formation, Phillipson Pound section. Scale bar = 1mm.

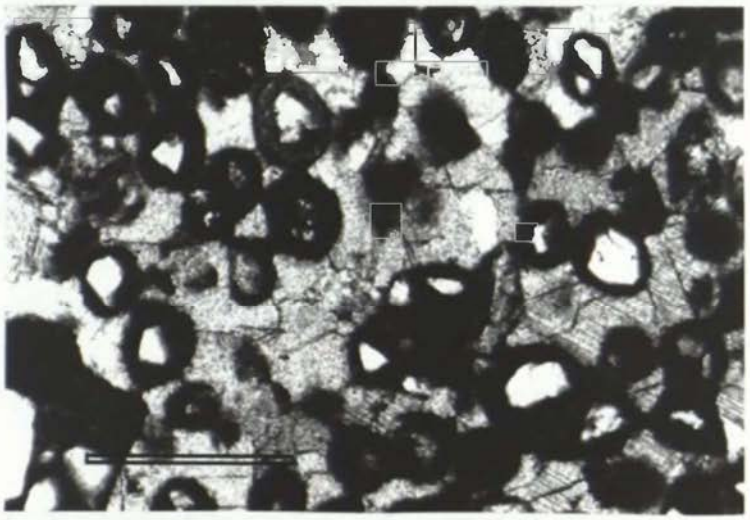

Plate 4.12: Thin section of anhydrite-cemented oolitic dolostone, Elkera Formation, Georgina Basin. Ooid cores are detrital quartz. Sample 31.26, 468.8 m depth, DDC 1 drillhole. Scale bar = 1mm.

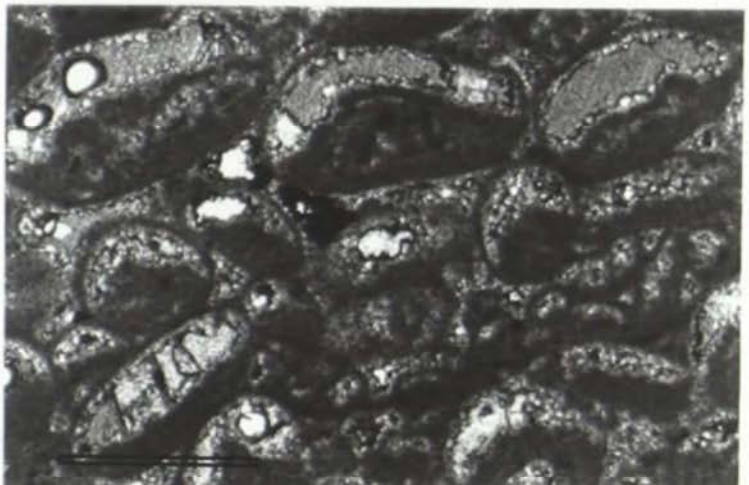

Plate 4.13: Thin section of 'half-moon' ooids, uppermost Elkera Formation. Pore space is mostly void. Sample 31.12, 381.3 m depth, DDC 1 drillhole. Scale bar = 1mm.

Sandstone is marked by a sudden change to weathered, soft black silty mudstone(0.5 m), gradationally overlain by several tens of metres of red shale. The black mudstone, possibly a condensed section deposit, contains 50% quartz, 25% illite and 15% kaolinite (XRD analysis).

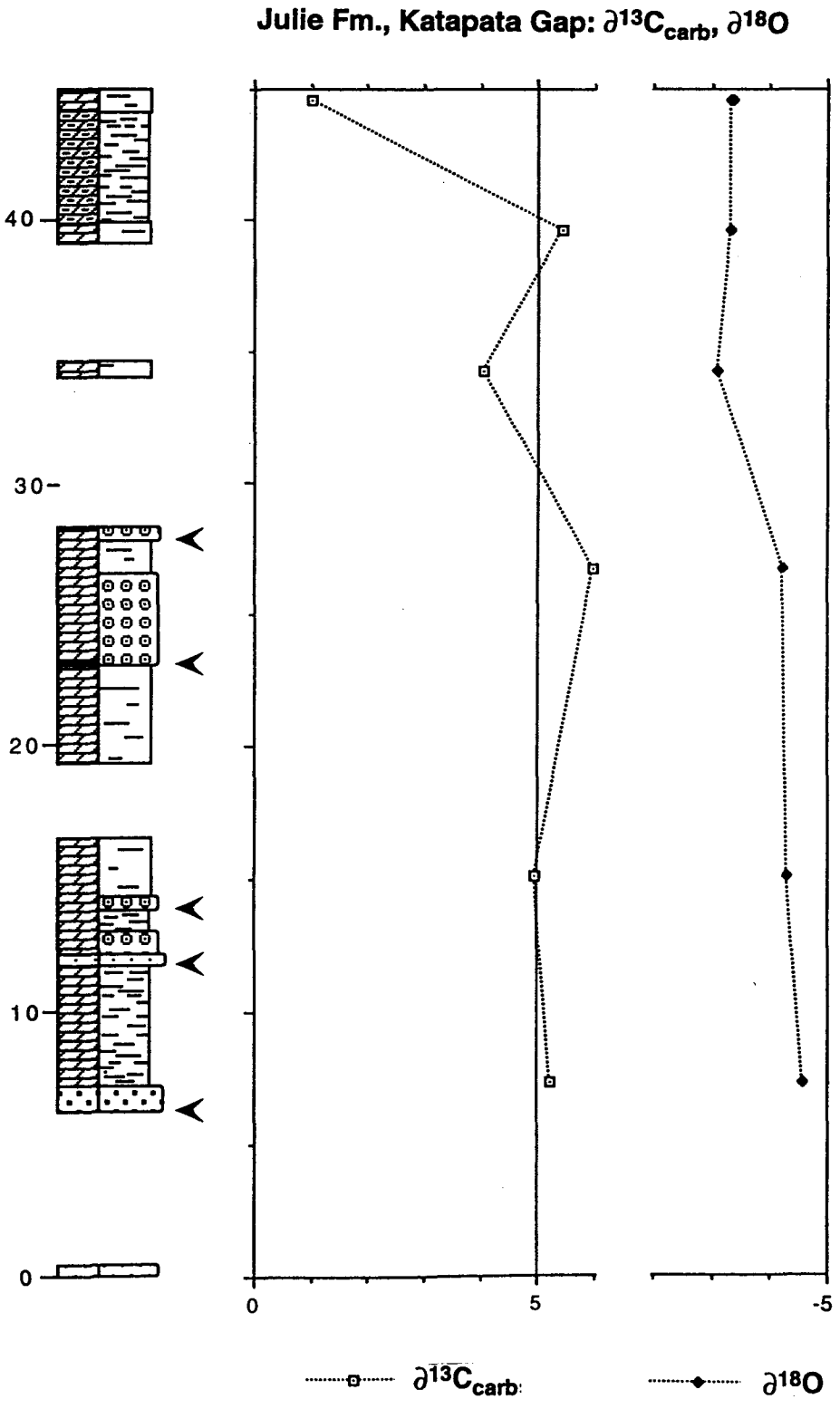

Fig. 4.26: Lithologic column and carbonate $\delta^{13}C$ and $\delta^{18}O$ data, Julie Formation, Katapata Gap section.

Katapata Gap

The southernmost exposure of Julie Formation in the central-northern Amadeus Basin is near Katapata Gap, 14 km NW of Areyonga. Further south, the unit has been removed by end-Proterozoic erosion. The section here is 38 m thick, and is lithologically similar to the upper (dolostone) part of the type section, consisting of alternating dolomicrite and sandy ooid grainstone (Fig. 4.26). 'Cauliflower' chert nodules and small (1mm) calcite pseudomorphs after evaporites are present in the dolomicrite. Several parasequences are probably present, but poor exposure precludes elucidation of stacking patterns.

Phillipson Pound

On the SE side of Phillipson Pound the Julie Formation attains its maximum thickness (≈500 m). The lower 260 m of the illustrated section (Fig. 4.27) was measured directly north of the Rodinga 4 drillsite; the top 27 m was examined near Twin Bore (8 km N of Mt Capitor). Stratigraphically between these two intervals is a thick (≈200 m) poorly outcropping succession that includes a unit mapped by Oaks et al. (1990) as a tongue of Arumbera Sandstone (see also Freeman et al., 1991, their Fig. 8).

The lower 75 m of the formation consists of interbedded, fine to medium-grained sandy lime grainstone and medium to coarse-grained quartzarenite. Cross-bedding is abundant, including swaley cross-stratification and probable hummocky cross-stratification (Plate 4.9). There are rare intraclasts of both dolomicrite and micrite. Thin sections show well-rounded quartz sand grains and rare micritic ooids in a calcite microspar matrix.

Higher up (80 - 100 m) there is coarse-grained quartz sandstone interbedded with sandy dolostone. Creamy dolomicrite clasts are very abundant at some horizons. At 97 m is a sandy dolomicrite bed with probable tepee structures and desiccation cracks filled with calcite spar. Red sandstone at the top of this interval has abundant small vugs possibly after evaporites. A covered interval is succeeded by dolomitic limestone (190 - 200 m). This is microspar (≈ 40 μ grainsize) with 40% dolomicrospar, and has irregular chert nodules that contain tabular vugs possibly after euhedral anhydrite. There is minor oolitic grainstone. This dolomitic limestone unit has the least-altered (lowest) $^{87}Sr/^{86}Sr$ ratios found in the Julie Formation (see next section).

Fig. 4.27(opposite): Lithologic column and carbonate $\delta^{13}C$ and $\delta^{18}O$ data, Julie Formation, Phillipson Pound composite section. Large stratigraphic gap between sections is 'tongue of Arumbera Formation' (Freeman et al., 1991; Oaks et al., 1990).

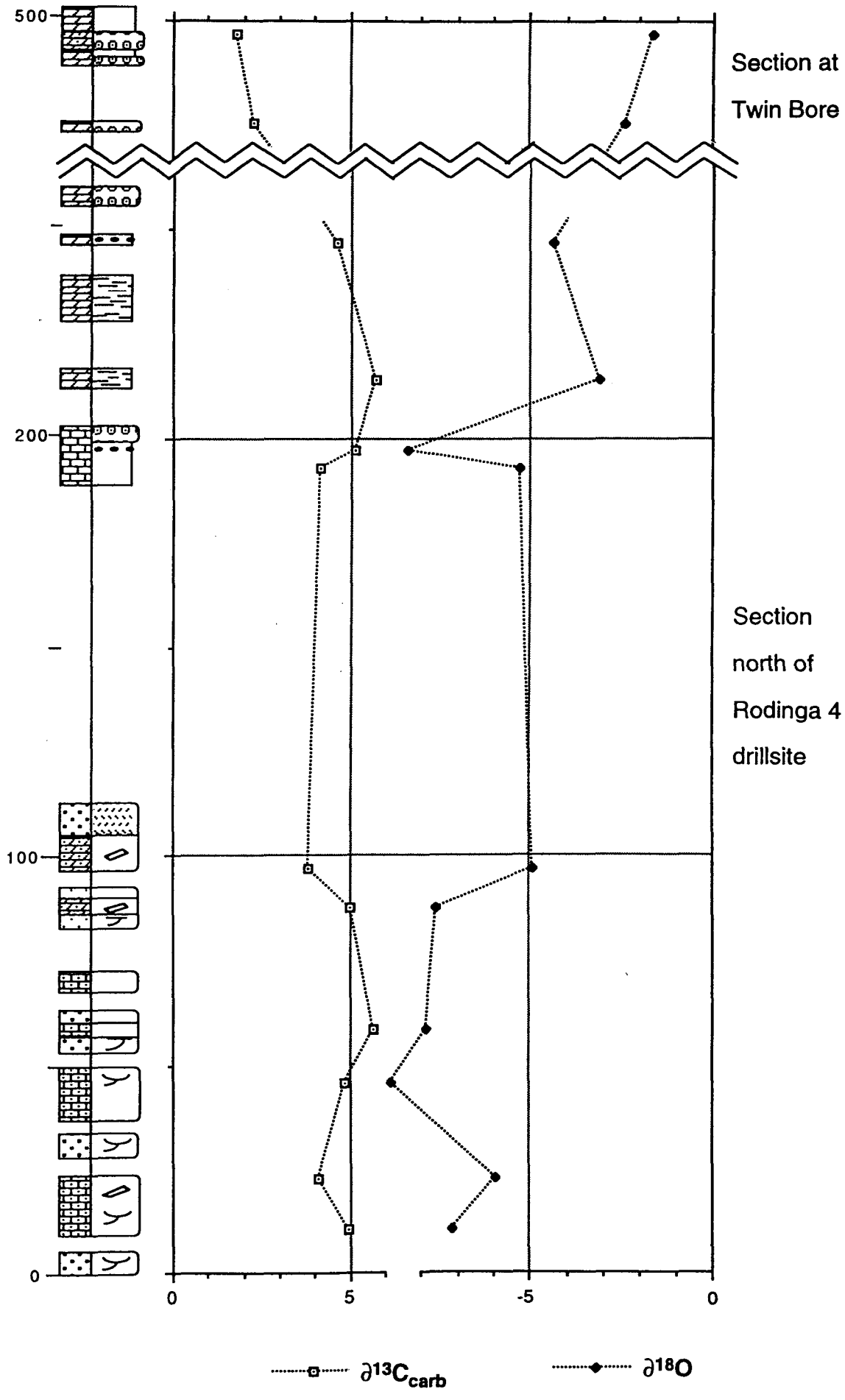
Julie Fm., Phillipson Pound: ∂13Ccarb, ∂18O
500
200
100
0
0
5
-5
0
Section at Twin Bore
Section north of Rodinga 4 drillsite
∂13Ccarb
∂18O

Higher (215-260 m) is a poorly exposed interval of creamy grey thin-bedded dolomicrite with abundant cauliflower chert nodules, and ooid dolograinstone at the top.

The topmost part of the Julie Formation at Twin Bore consists of ooid dolograinstone, intraclastic and sandy in places, and pink micritic dolostone. Here the grainstones are texturally particularly well-preserved in thin section. Ooids have cores of microspar or detrital quartz and micritic cortices. There is an early, fibrous isopachous nonluminescent dolospar cement and a later, moderately luminescent coarser dolospar cement. Ooids are plastically deformed by compaction to varying degrees. Compaction occurred after the first cement phase but before the second. The most compacted horizons (containing negligible late cement, see Plate 4.11) were selected for isotopic analysis.

The Julie Formation in the Rodinga 4 - Twin Bore area is divided, like the type section at Ross River, into a lower limestone unit with wave-formed sedimentary structures - here coarser-grained and much thicker than the type section - and an upper, predominantly dolostone unit deposited in evaporitic-peritidal and ooid-shoal environments. The presence of the Arumbera Formation 'tongue' raises the question of whether the Twin Bore section may be wholly younger than the type Julie Formation.

The basal limestone unit is also present at Hidden Valley and is apparently widespread in the NE Amadeus Basin but is absent in north-central and western sections such as Ellery Creek and Katapata Gap.

4.6b Isotope Stratigraphy

Carbonate carbon and oxygen

The Julie Formation exhibits widespread uniformity of $\delta^{13}C_{carb}$ at +5 ‰, but there are local marked departures attributable to diagenetic or environmental factors.

In the type section at Ross River Homestead, $\delta^{13}C_{carb}$ in the basal limestone unit is close to +5 ‰. Higher up, most dolostone $\delta^{13}C_{carb}$ results are similar, lying between +4 and +6 ‰ except for anomalously depleted samples at 29.7 m, 57.5 m, 60.7 m and 101.4 m. The most depleted of these is -5.7 ‰. Three of these samples coincide with the uppermost parts of parasequences, consisting of laminated dolomicrite with probable remnant evaporites; a fourth (at 29.7 m) cannot be assigned a parasequence position but the lithology is similar. Uppermost parts of other parasequences do not display ^{13}C-depleted compositions, for example +4.1 ‰ at 41.1 m.

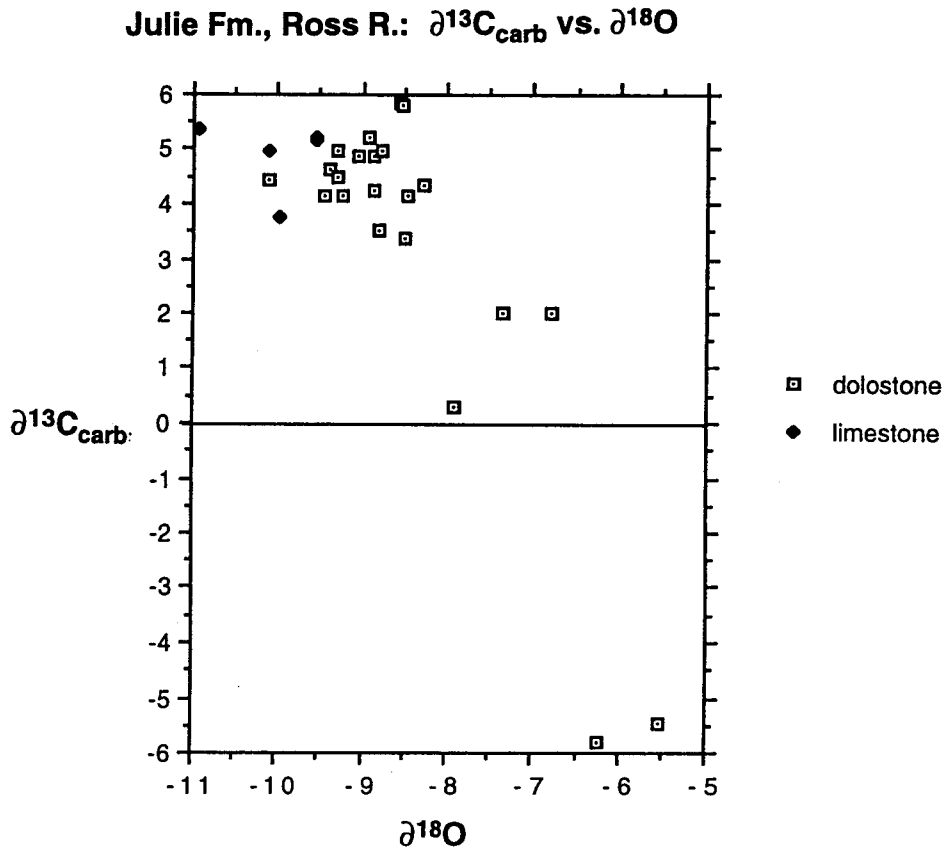

Fig. 4.28: $\delta^{13}C$ - $\delta^{18}O$ crossplot for the Julie Formation at Ross River.

Mn/Sr of limestone samples are moderate (1 to 4, see Table 4.2) and the two limestone samples with Mn/Sr<2 have the highest $\delta^{13}C_{carb}$ (+5.2, +5.4 ‰) suggesting these values are least-altered. $\delta^{18}O$ of the limestone, at -9.5 to -11 ‰, are low (altered) but within the acceptable limits for minimal $\delta^{13}C_{carb}$ alteration cited by Kaufman et al. (1993).

Most dolostones have $\delta^{18}O$ of -8 to -10 ‰ but the ^{13}C-depleted samples have relatively heavy $\delta^{18}O$ (e.g. -6 ‰ for the sample with $\delta^{13}C_{carb}$ of -5.5‰). The anomalous results define a steep inverse $\delta^{13}C_{carb}$-$\delta^{18}O$ relationship (Fig. 4.28). If the four outliers with high $\delta^{18}O$ and low $\delta^{13}C_{carb}$ are excluded from this plot, however, the correlation is weak or non-existent in the remaining points.

Dolostones mostly have rather constant and low Sr contents of 30-40 ppm and several hundred ppm Mn giving Mn/Sr values of 10 to 17, greater than the limit of 10 suggested by Derry et al. (1992) as the maximum for carbonates with unaltered $\delta^{13}C_{carb}$. The only two exceptions amongst those samples analysed are the anomalously ^{13}C-depleted samples from 57.5 m and 101.4 m, which both have markedly higher Sr and lower Mn (Table 4.2). A minimum Mn/Sr value of 0.4 is seen

in the most ^{13}C-depleted sample at 57.5 m. *Upper parts of some parasequences at Ross River thus display a distinctive geochemical fingerprint of depletion in ^{13}C, enrichment in ^{18}O and low Mn/Sr.*

Other sampled sections (Figs 4.25 - 4.27), like Ross River, have a predominance of $\delta^{13}C_{carb}$ values between +4 and +6 ‰. A sample from the lowermost bed of the Julie Formation at Glen Helen has $\delta^{13}C_{carb}$ = +5.5 ‰, $\delta^{18}O$ = -5.4 ‰ (not figured). No anomalous ^{13}C-depletion was found. However, the topmost one or two samples in each section are lighter (+1 to +2 ‰). The topmost sample at Ellery Creek has a very high Mn/Sr ratio (97) and must therefore be regarded as possibly altered. Both analysed samples from Twin Bore (the uppermost part of the Phillipson Pound section, Fig. 4.27) are lower in ^{13}C, raising the possibility of secular fall in marine $\delta^{13}C$ towards the end of Julie time. Perhaps also of chemostratigraphic significance, these two samples have the highest $\delta^{18}O$ seen in the Julie Formation. The lack of cement in the grainstones at Twin Bore may indicate lack of meteoric recharge and hence aridity (Hird & Tucker, 1988); a causal link with high $\delta^{18}O$ (a possible evaporative signature) seems plausible. Generally in these other sections, $\delta^{18}O$ is somewhat heavier than at Ross River, a notable exception being a very depleted result (-15.7 ‰) from the limestone bed at Ellery Creek.

Dolostones from these sections have variable, and locally high Mn/Sr values mainly because of elevated Mn (e.g. 4646 ppm, sample 6.46, Ellery Ck). There is a weak negative correlation of Mn/Sr with $\delta^{13}C_{carb}$ at Katapata Gap and Phillipson Pound (Fig. 4.29). Limestones from the Phillipson Pound section have low Mn/Sr (<1) and oxygen and carbon isotopic compositions comparable with associated dolostones (Fig. 4.27; Table 4.2).

Organic carbon

Organic carbon contents in the Julie Formation are low (0.15 ± 0.15 mg/g, n = 11) with the highest TOC (0.55 mg/g) found in the basal limesone unit at Ross River. $\delta^{13}C_{org}$ values do not exhibit any consistent stratigraphic change. The average $\delta^{13}C_{org}$ is -26.86 ± 0.82‰ (n=10) [excluding an unusually heavy value of -21.96‰ from the horizon with most strongly ^{13}C-depleted carbonate (sample 1.30 at Ross River, with $\delta^{13}C_{carb}$ = -5.7‰); these carbon isotopic compositions probably reflect unusual local environmental conditions - see below]. $\Delta\delta$ values are shown in Table 2.4. Average value for $\Delta\delta$ is 31.15 ± 1.36 ‰ (n = 10); average $\Delta\delta^N$ is 29.50 ± 1.75 ‰ (n = 10). These values are higher than previously documented 'typical' Neoproterozoic $\Delta\delta$ of

sample	rocktype	Sr(ppm)	Mn(ppm)	Mn/Sr	87Sr/86Sr	∂13C	∂18O	Rb(ppm)	87/86Srinit
Pertatataka Fm., Acacia We									
1.52	limestone	405	1285	3.17	0.71080	2.6	-8.8		
Julie Fm., Ross River									
1.01	limestone	136	549	4.04	0.71037	3.8	-10.0		
1.02	limestone	371	360	0.97	0.70905	5.2	-9.6		
1.03	limestone	182	336	1.85	0.70940	5.4	-11.0		
1.06	limestone	118	336	2.85		5.0	-10.1		
1.09	dolostone				0.71174	3.5	-8.8		
1.11	dolostone	41	619	15.10		2.0	-6.8		
1.13	dolostone	42	422	10.11	0.71031	4.5	-10.1		
1.24	dolostone	33	422	12.78	0.70951	5.0	-9.3		
1.25	dolostone	36	422	11.87	0.71030				
1.27	dolostone	33	585	17.73		5.8	-8.9		
1.28	dolostone	33	422	12.86	0.71021	5.2	-9.2		
1.30	dolostone	137	56	0.41		-5.5	-5.8		
1.32	dolostone	40	422	10.56	0.71053				
1.37	dolostone	38	508	13.37	0.71005	4.9	-9.2		
1.38	dolostone	32	493	15.48	0.71045	5.0	-9.1		
1.42	dolostone	47	649	13.81	0.71096	4.2	-8.8		
1.45	dolostone	67	392	5.85		2.0	-7.6		
Julie Fm., Ellery Creek									
6.40	dolostone	55	563	10.21	0.71254	5.8	-9.2		
6.41	limestone	47	567	12.06		4.0	-15.7		
6.42	dolostone	65	634	9.73	0.71120				
6.43	dolostone	59	1408	23.70		5.8	-5.0		
6.46	dolostone	48	4646	97.80	0.71035	1.6	-8.0		
Julie Formation, Katapata Gap									
21.18	dolostone	54	1267	23.54	0.70955	5.0	-5.4		
21.21	dolostone	43	774	18.18	0.70927	6.0	-5.5		
21.22	dolostone	48	1267	26.39	0.70946	4.0	-6.6		
21.24	dolostone	43	1267	29.40	0.70928	1.0	-6.4		
Julie Fm., Phillipson Pound									
24.09	limestone	221	164	0.74		5.7	-7.9		
24.14	dolostone	61	352	5.78	0.70972				
24.17	dolostone	61	282	4.64	0.70892	5.7	-2.8		
24.18	limestone	247	133	0.54	0.70843	5.1	-8.4	0.135	0.70842
24.19	limestone	246	110	0.45	0.70836	4.2	-6.3	0.092	0.70835
24.21	dolostone	75	1619	21.61	0.70980	2.3	-2.1		
24.22	dolostone	96	1126	11.77	0.71175				
24.24	dolostone	73	1337	18.40	0.70971	1.8	-1.3		

Table 4.2: Trace-element and strontium isotopic data, Julie Formation and limestone from upper Pertatataka Formation at Acacia Well.

28.5‰ (Knoll et al., 1986; Kaufman & Knoll, 1995); but are slightly lower than those of the Ediacarian of the Officer Basin (Chapter 3). Although data are few and scatter of data is great, regional change in $\Delta\delta$ and $\Delta\delta^N$ is interpreted to reflect variation in thermal maturation (see section 2.3d).

$^{87}Sr/^{86}Sr$

Twenty-six $^{87}Sr/^{86}Sr$ analyses were carried out. Results range widely (0.70835 - 0.71254) and while of limited chemostratigraphic value, these data provide useful information on diagenetic alteration.

$^{87}Sr/^{86}Sr$ shows distinct and different correlations with $\delta^{13}C_{carb}$ and $\delta^{18}O$ at different localities, perhaps suggesting regional differences in diagenetic fluid chemistries (Figs. 4.30, 4.31). $^{87}Sr/^{86}Sr$ - $\delta^{13}C_{carb}$ trends at Ross River and Phillipson Pound converge toward least-altered compositions of $^{87}Sr/^{86}Sr < 0.7085$ and $\delta^{13}C_{carb} > 5.5‰$. Limestones almost always have distinctly lower (less altered) $^{87}Sr/^{86}Sr$, in spite of having generally lower $\delta^{18}O$. A plot of $\delta^{18}O$ against $^{87}Sr/^{86}Sr$ (Fig. 4.31) indicates that the Phillipson Pound section has suffered the least diagenetic alteration, Ellery Creek and Ross River the most.

The lowest (least-altered) $^{87}Sr/^{86}Sr$ ratios in the Julie Formation were found in the second limestone unit at Phillipson Pound, which yielded two initial $^{87}Sr/^{86}Sr$ results in close agreement (0.70842, 0.70835; Table 4.2). Sr contents of these samples, however, are low (247, 246 ppm) relative to samples that yield consistent and probably marine isotopic ratios in other basins (≈1000 ppm). These values are therefore regarded as maximum values for contemporaneous seawater.

4.6c INTERPRETATION

Correlation

The fine grainsize and good textural preservation of those carbonates selected for $\delta^{13}C$ analysis, and the regional consistency and great predominance of results between +4 and +6 ‰ are strong indications that these values were near equilibrium with contemporaneous seawater. The higher end of this range (+5 to +6 ‰) may be a more precise estimate, on the principle that alteration generally depletes ^{13}C, and also on the evidence of a weak negative $\delta^{13}C_{carb}$ - Mn/Sr correlation (at Katapata Gap and Phillipson Pound) and negative $\delta^{13}C_{carb}$ - $^{87}Sr/^{86}Sr$ correlation (at Ross R. and Phillipson Pound) (Figs.4.29, 4.30).

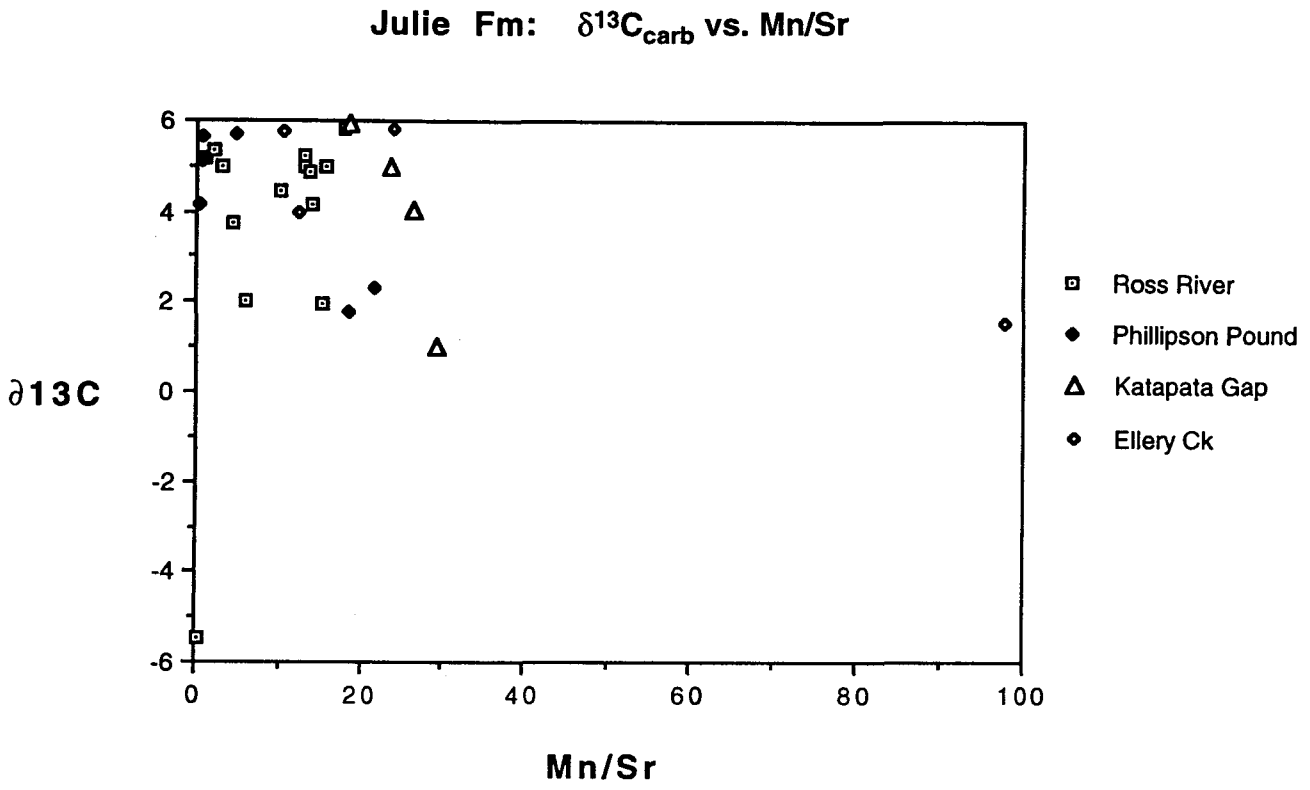

Fig. 4.29: Mn/Sr versus $\delta^{13}C_{carb}$, Julie Formation, differentiated according to locality.

The topmost samples at Ellery Creek, Katapata Gap and Phillipson Pound are lighter (+1 to +2 ‰) and may reflect secular fall in marine $\delta^{13}C$. The evidence for this is firmest at Phillipson Pound where both samples analysed in the upper 27 m (Twin Bore section) are +1 to +2 ‰; and these samples are ooid dolograinstone (free of late cement) rather than evaporitic dolomicrite that locally exhibits anomalous ^{13}C depletion at Ross River. These samples are texturally well-preserved (Plate 4.11) and have $\delta^{18}O$ that is unusually high for the Julie Formation, suggesting preservation of depositional $\delta^{13}C_{carb}$ despite high Mn/Sr and high $^{87}Sr/^{86}Sr$. The Twin Bore section is a good lithologic and stable-isotopic match for the uppermost Elkera Formation of the Georgina Basin, and it therefore is possible that the Twin Bore section is substantially younger than the type Julie Formation, and thus a chronostratigraphic correlative of part of the lower Arumbera Formation (Fig. 4.36).

Geochemical and isotopic variation, Ross River section

As noted above, in the cyclic peritidal dolostones at Ross River, $\delta^{13}C_{carb}$ as low as -5.5‰ coincides with the uppermost parts of some parasequences, and is associated with relatively high $\delta^{18}O$ and low Mn/Sr. Very low TOC suggests no early diagenetic

incorporation of organogenic carbonate. The anomalous ^{13}C depletion evidently reflects local environmental conditions during deposition or very early diagenesis.

The relatively high levels of strontium at these horizons, and their sedimentology, suggests they underwent penecontemporaneous dolomitization under evaporitic conditions. Lower parts of parasequences display lower [Sr], lower $\delta^{18}O$ and microsparitic textures suggestive of mixing-zone or burial dolomitization that post-dated metastable carbonate into calcite (e.g. Hird et al., 1987).

Association with the upper parts of parasequences suggests that exposure-surface alteration, under an evaporitic regime, may be responsible for the observed shifts in $\delta^{13}C_{carb}$ and $\delta^{18}O$ (cf. Allan & Matthews, 1982). ^{13}C depletion due to incorporation of soil-derived carbon below subaerial exposure surfaces has been proposed in rocks as old as mid-Proterozoic (Beeunas & Knauth, 1985). However, the observed shifts in $\delta^{13}C_{carb}$, even below well-developed Phanerozoic soil profiles, are only 3 to 4 ‰ (Allan & Matthews, 1982).

Extreme ^{13}C depletion has been observed in modern seawater-derived brine pools overlying microbial mats (Lazar & Erez, 1990). Intense photosynthetic activity rapidly lowers dissolved inorganic carbon (DIC) and this is postulated to cause a strong negative fractionation of CO_2 crossing the air-brine interface. Low DIC also leads to lowering of ε_P and enrichment of $\delta^{13}C_{org}$ in the microbial mats (see also Schidlowski et al., 1992). $\delta^{13}C_{DIC}$ as low as -12 ‰, and $\delta^{13}C_{org}$ as high as -11 ‰ are seen (Lazar & Erez, 1990). This phenomenon is an attractive explanation for the observed strong depletion in ^{13}C together with mild relative ^{18}O enrichment and sedimentology indicative of an evaporative tidal-flat environment. Further tentative support is provided by the relatively heavy $\delta^{13}C_{org}$ of -22 ‰ for the sample with greatest carbonate carbon depletion (Appendix 1.1), but TOC of this sample was very low (0.03 mg/g). The paradox of low TOC in an environment once dominated by microbial mats may be explained by the observation that modern mats effectively recycle carbon (Jorgensen et al., 1992).

4.7 Boord Formation

The Boord Formation crops out in far north-west of the Amadeus Basin. About 800 m thick, it disconformably overlies the Bitter Springs Formation and consists of diamictite of probable glacial origin passing up into interbedded shale, siltstone and carbonate (Wells et al., 1970). Wells et al. (1970) and Preiss & Forbes (1981) correlated the

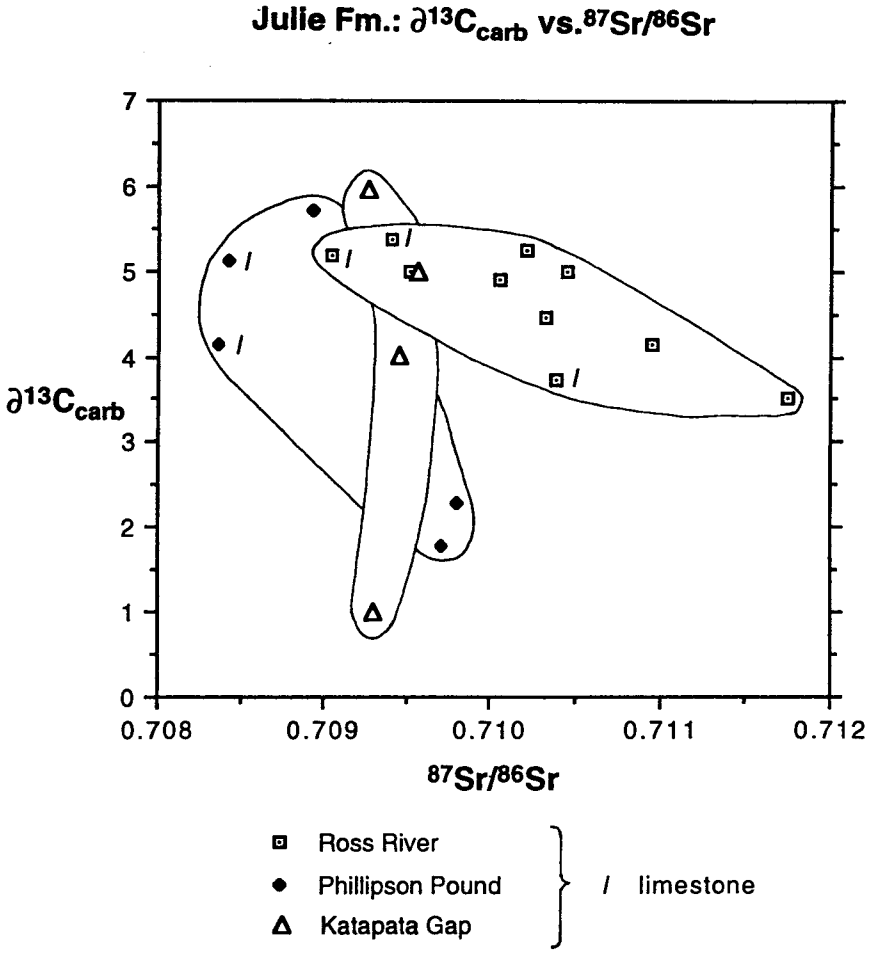

Fig. 4.30: $^{87}Sr/^{86}Sr$ versus $\delta^{13}C$, Julie Formation, differentiated according to locality.

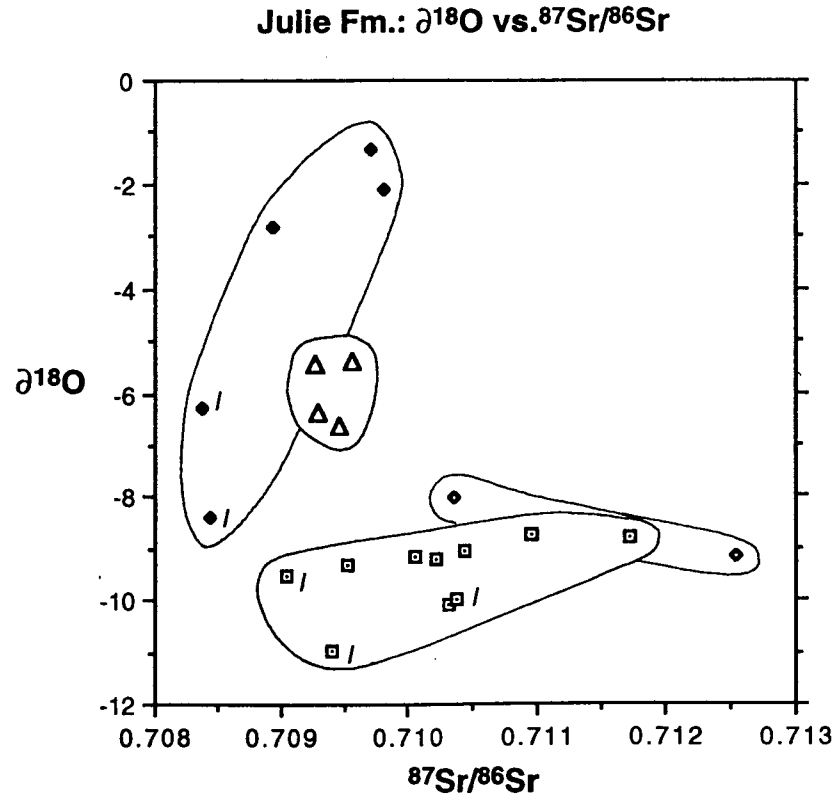

Fig. 4.31: $^{87}Sr/^{86}Sr$ versus $\delta^{18}O$, Julie Formation, differentiated according to locality.

Boord Formation with the (pre-Ediacarian) Inindia beds and Areyonga Formation, but Walter et al. (1994, 1995) on broad lithostratigraphic grounds regard the diamictite as a correlate of the Olympic Formation and the overlying succession as a correlate of the Pertatataka and Julie Formations.

Four samples of stromatolitic limestone were analysed (Appendix 1.1). All were collected from 4.8 km east of Mt Greene (Walter et al., 1979). The samples, all of which are texturally well-preserved, micritic, microbially laminated limestones, display a narrow range of stable isotopic compositions: $\delta^{13}C_{carb}$ of +3.2 to +4.1 ‰ and $\delta^{18}O$ of -5.9 to -7.4 ‰.

As evidence for correlation of the Boord Formation, these carbon isotopic compositions are ambiguous. They are slightly depleted relative to the type Julie Formation (+4 to +6 ‰) but lie within the range seen in the upper part of the Julie Formation in some sections (Phillipson Pound, Ellery Creek). They are slightly enriched relative to $\delta^{13}C_{carb}$ seen in part of the Aralka Formation, a pre-Ediacarian unit overlying the Areyonga Fromation in the northeastern Amadeus Basin (S. Grant, pers. comm. 1995).

$^{87}Sr/^{86}Sr$ chemostratigraphy might resolve the problem of correlation of the Boord Formation, if little-altered ratios could be obtained.

4.8 Georgina Basin - Geological Setting

The Georgina Basin has a fill of mostly Palaeozoic age, but Neoproterozoic successions are present in the SW part of the basin. The most recent detailed account is that of Walter (1980). These sediments wedge out northwards against higher basement; while to the south, sedimentation was originally continuous into the Amadeus Basin (Walter et al., 1995). The Neoproterozoic successions fill deep meridional troughs (half-grabens). The Ediacarian Mopunga Group overlaps the troughs to cover most of the intervening basement highs (Walter, 1980).

Lithostratigraphy (Walter, 1980), limited fossil evidence (Wade, 1970; Walter, 1980; Walter et al., 1989; Jenkins et al., 1992; Walter et al., 1995) and limited magnetostratigraphic evidence (Burek et al., 1979) suggest that the Ediacarian System is here represented by the Mopunga Group. No glacigene rocks of definitive Marinoan age are known but thick arkose units of the Keepera Group are considered to be glacial outwash deposits comparable to the Pioneer Formation of the Amadeus Basin (Walter,

1980). The overlying Wonnadinna Dolomite, not sampled in this study, may be a correlative of the cap dolostone (Nuccaleena Formation equivalent) but is much thicker and lithologically unlike cap dolostones in the Amadeus Basin and Adelaide Geosyncline (Walter et al., 1995). A thick, locally-developed arkose (the Gnallan-a-Gea Arkose) at the base of the Mopunga Group resembles the Gaylad Sandstone (Walter et al., 1995). Lithostratigraphic considerations suggest the more widely distributed Elyuah, Grant Bluff and Elkera Formations are correlatives of the lower Pertatataka Formation, Cyclops Member, and Julie Formation, respectively (Burek et al., 1979; Walter, 1980) (Fig. 4.1a). The Central Mt Stuart Formation contains a soft-bodied metazoan fauna (Wade, 1970; Walter, 1980) and trace fossils (Walter et al., 1989) consistent with correlation with the lower Arumbera Sandstone. Walter et al. (1989) and Jenkins et al. (1992) report simple trace fossils from the Elkera and Grant Bluff Formations. Those in the Grant Bluff Formation are the oldest known trace fossils in Australia if the lithostratigraphic correlation (Fig. 4.1a) is valid. However, despite many searches, no trace fossils have been found in supposedly correlative parts of the Amadeus Basin succession (Cyclops Member, upper Pertatataka, and Julie Formations). Accordingly Jenkins (1993b, Fig. 29) regards the trace fossils as evidence for a substantially younger (Arumbera 1-2) age for the Elkera and Grant Bluff Formations (Fig. 4.1b).

Systematic sampling for isotopic analysis was carried out on the Elyuah, Grant Bluff and Elkera Formations in three fully-cored drillholes in the southwestern Georgina Basin: Centamin DDC 1, Centamin DDC 2 and Huckitta 7. DDC 1 was drilled 1 km east of Mt Skinner at 22° 14' 44" S, 134° 19' 55" E; DDC 2, 5 km east of Mt Skinner (22° 15' 0" S, 134° 23' 27" E). Huckitta 7 was drilled 132 km to the ESE of Mt Skinner (22° 39' 38" S, 135° 32' 0" E). The Central Mt Stuart Formation, logged in DDC 1, contained suitable lithologies for analysis at only a few horizons.

4.9 Elyuah and Grant Bluff Formations

4.9a Lithostratigraphy

The Elyuah and Grant Bluff Formations were sampled in DDC 1 and DDC 2. DDC 2 reached basement beneath the Elyuah Formation; DDC 1 stopped just short of basement. The Elyuah Formation, of shale, is transitionally overlain by the sandier Grant Bluff Formation.

The Elyuah Formation in DDC 2 begins with 1m of conglomerate resting on Mesoproterozoic granitic basement. The rest of the formation, here 93 m thick, consists of dark grey shale with several percent thin beds and laminae of quartz sandstone and siltstone. Scattered quartz and feldspar granules are present in the lowest 30 m. Siltstone laminae tend to be planar-parallel; thicker sandstone layers are lenticular and ripple cross-laminated, and some are starved ripples. There are rare graded sandstone beds up to 10 cm thick. In DDC 1, which intersected 64 m of Elyuah Formation, the unit is similar, but with less (~ 2%) silt and sand.

The base of the Grant Bluff Formation is taken as the base of the first substantial unit of siltstone or sandstone, at 438 m depth in DDC 2. The Grant Bluff Formation is 126 m thick in DDC 1 and 103m thick in DDC 2. The formation contains about 30% sandstone interbedded with predominant dark grey shale. In places there are units several metres thick of thick-bedded, coarse-grained quartz sandstone. Thinly interbedded shale and sandstone in places resembles flaser bedding and wavy bedding *sensu* Reineck & Singh (1973). The volumetrically predominant lithology in the Grant Bluff Formation in DDC 1 and DDC 2 remains dark grey shale with a few percent siltstone laminae, like the Elyuah Formation. A sandstone unit in DDC 1 (611 - 625 m) may correlate with that at 360 - 376 m in DDC 2. In the uppermost 20 m or so of the formation in both drillholes, shale becomes red and green. The topmost few metres in DDC 1 contains anhydrite, probably remobilized from the overlying Elkera Formation.

The Elyuah Formation and the shaly parts of the Grant Bluff Formation represent sedimentation in a quiescent environment below storm wavebase. Thin silt laminae were laid down by low-density turbidity currents, nepheloid flows and perhaps aeolian processes. Sandy intervals of the Grant Bluff Formation probably represent shallower, sublittoral conditions, probably largely within wavebase.

4.9b Isotope Stratigraphy

No carbonates are present; samples were selected and analysed for $\delta^{13}C_{org}$. Organic contents are higher than is usual in the Pertatataka Formation, averaging 2.6 ± 1.3 mg/g in these two formations.

Fig. 4.32 (opposite): Lithologic column and organic $\delta^{13}C$ data, Elyuah, Grant Bluff and Elkera Formations, DDC1 drillhole. 'e' indicates presence of anhydrite.

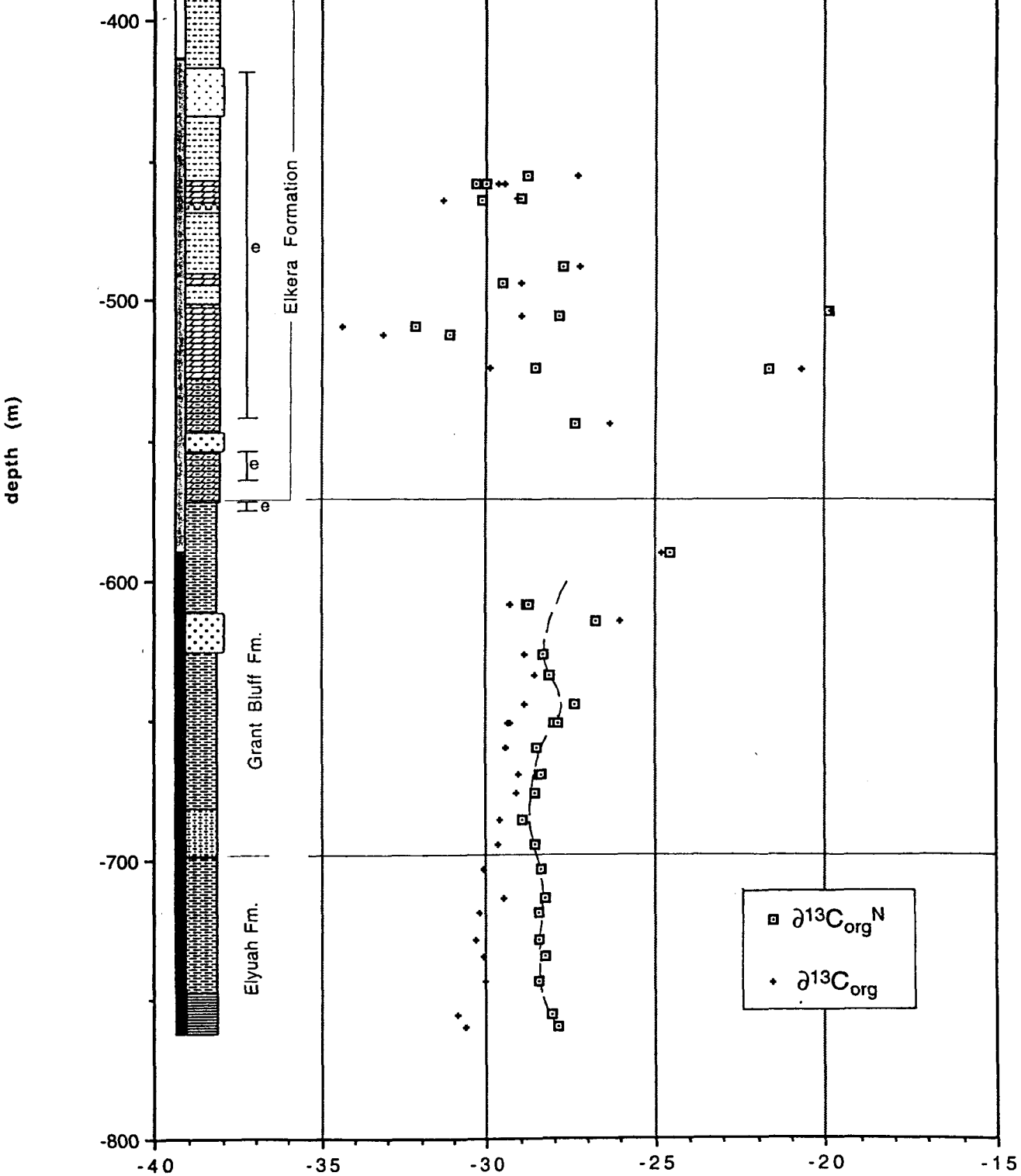
depth (m)
-400
-500
-600
-700
-800
-40
-35
-30
-25
-20
-15
Elkera Formation
e
e
e
Grant Bluff Fm.
Elyuah Fm.
∂13Corg N
∂13Corg

The lowest three samples in DDC 2 define a steep upward increase in $\delta^{13}C_{org}{}^{N}$ from -33 to -29 ‰; thereafter in both drillholes, data points fall in a tightly constrained plateau at around -28 ‰ (Fig. 4.32, 4.33). The topmost sample in DDC 1 is several permil heavier.

Thermal maturation

No quantitative data related to thermal maturity are available from DDC 1 or DDC 2. The utility of $\Delta\delta$ values from the Elkera Formation is negated by the apparently erratic behaviour of $\delta^{13}C_{org}$ in that unit (see below). However, kerogen colour was gauged from palynological strew slides prepared by K. Grey, and is similar to that of the Pertatataka Formation in Wallara 1 in the Amadeus Basin.

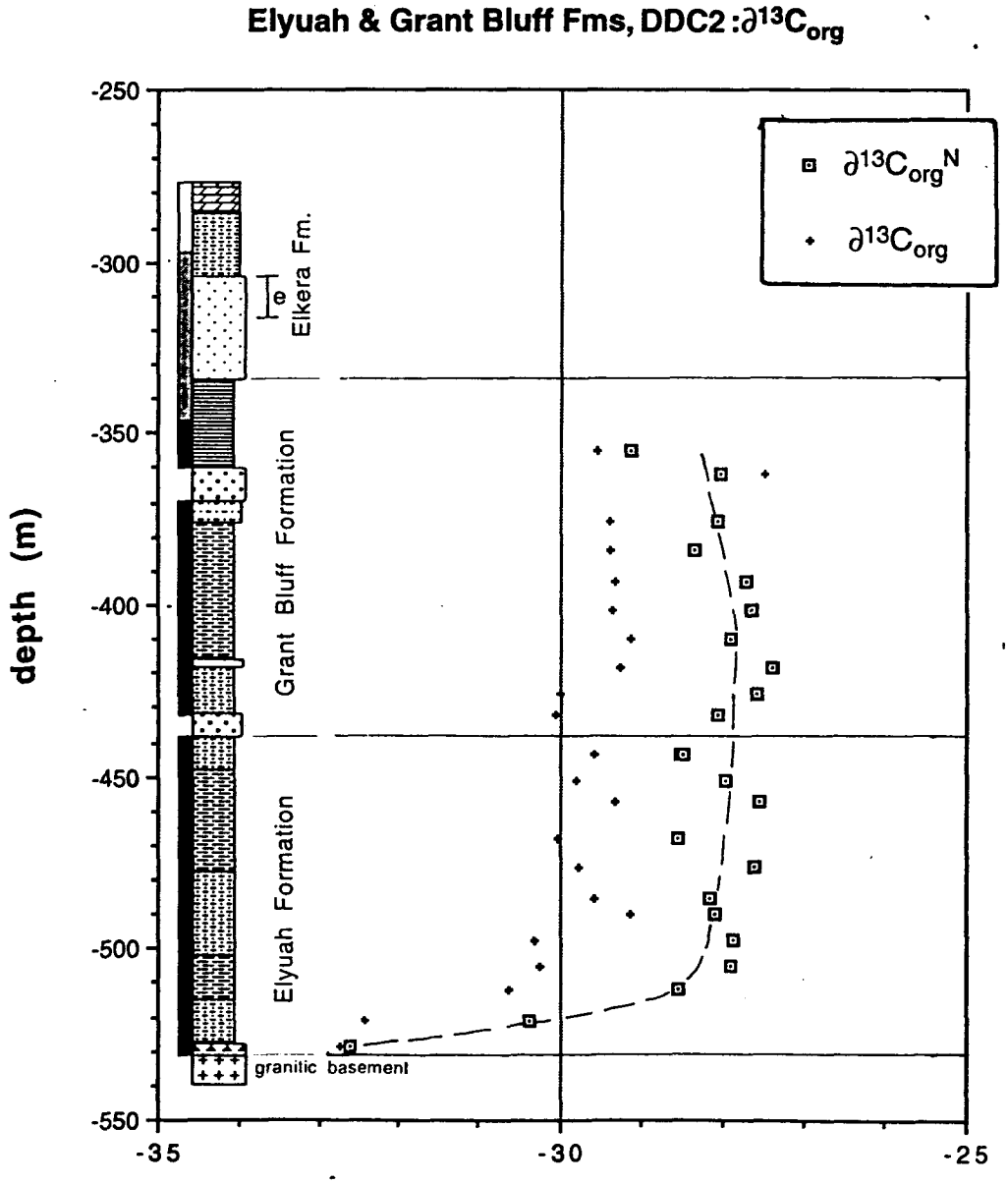

Fig. 4.33: Lithologic column and organic $\delta^{13}C$ data, Elyuah Formation, DDC2 drillhole.

4.10 Elkera Formation

4.10a Stratigraphy

An unconformity may be present at the base of the Elkera Formation in the three drillholes examined. The base of the formation in all three holes is abrupt and in Huckitta 7 the contact, at 204 m depth, is erosional with a slight angular discordance of bedding above and below.

A complete section of Elkera Formation, 192 m thick, was intersected in DDC 1 (Figs. 4.32, 4.34). It consists of a lower, carbonate-dominated unit (491 - 572 m) and an upper, sandstone- dominated unit (380 - 491 m). The lower unit is pale grey to red, fine-grained dolostone, mostly thin-bedded to laminated; interbedded with lesser siltstone, sandstone and shale. Anhydrite nodules constitute several percent by volume of the lower unit in DDC 1. Brecciated dolostone at 510 - 519 m may be an evaporite collapse breccia.

The upper unit is grey to red, fine-grained sandstone to siltstone and minor dolostone. Anhydrite is present as small disseminated nodules throughout the lower two-thirds of the upper unit. Coarse-grained saddle dolomite has replaced anhydrite between 428 and 445 m. Dolostone at 458 - 469 m contains small domical and columnar stromatolites and minor ooid grainstone. Thin sections are predominantly very weakly luminescent, sandy and silty dolomicrite. Grainstone consists of small (¼mm), micritic ooids with porespace entirely occluded by compactive deformation, or in one sample (Plate 4.12), by an abundant cement of coarse poikilitic anhydrite. Anhydrite also occurs as possible desiccation crack fills in dolomicrite and filling fenestrae in grainstone.

The top 6 m of the upper unit consists of creamy, sandy dolomicrite passing up into ooid dolograinstone. A thin section of the dolograinstone shows weakly luminescent micritic envelopes and ooid cores (Plate 4.13). Ooid cores have fallen to the bottom of intra-ooid porespaces after dissolution of the ooid cortices (originally presumably aragonite or evaporite). These are 'half-moon' ooids of Carozzi (1963), considered to be typical of evaporitic settings. Micritic envelopes are deformed plastically, in places brittly, by compaction; and a thin, blocky isopachous dolomite cement post-dates compaction. Most inter- and intra- particle porosity remains unfilled; some is filled by coarse anhydrite or rare euhedral dolospar. Whole-rock stable-isotopic analysis of this

rock gave $\delta^{13}C_{carb}$ 0.4 ‰ lighter, and $\delta^{18}O$ 4 ‰ lighter than the immediately underlying dolomicrite unit, possibly because of the presence of some late cement.

The lithologic and $\delta^{13}C$-chemostratigraphic correlative of the lower unit was logged and sampled in drillhole Huckitta 7, 130 km east of DDC 1 and 2. This succession consists of pink to grey micritic dolostone with minor fine to coarse-grained sandstone. Evaporites are absent. Columnar stromatolites are common, some of those at 129 - 146 m depth being attributable to *Georginia howchini* (K. Grey, pers. comm.), a form unknown outside the Georgina Basin.

4.10b Isotope Stratigraphy

Carbonate carbon and oxygen

$\delta^{13}C_{carb}$ data points in DDC 1 exhibit a well-defined signal in the lower half of the formation, with little of the scatter seen in some other shallow-water carbonates such as the Julie Formation and unit 11 of the Wonoka Formation (see Chapter 3). There is a positive excursion to +5 ‰ in the lower half of the lower (dolostone) unit (Fig. 4.34). Then follows a decline to a prolonged negative excursion near 0 ‰ (defined only by a few points) that lasts throughout most of the upper, sandy unit. The carbonate at the top of the formation is +2 to +2.5 ‰.

Two samples of saddle dolomite are not included in the chemostratigraphic profiles as they are clearly of diagenetic origin (Radke & Mathis, 1981); these, collected from 433 m and 440 m in DDC 1, have $\delta^{13}C_{carb}$ -0.4 and -0.8 ‰; $\delta^{18}O$ -10.9 and -11.7 ‰, respectively.

Huckitta 7 displays the initially heavy (+5 ‰) carbonate and the ensuing decline in parallel with the lower unit in DDC 1 (Fig. 4.35).

Oxygen isotopic compositions of the carbonates from these two sections nearly all lie in the range -7 to -3 ‰, with half of the samples being heavier than -4 ‰. There is no coherent pattern of stratigraphic variation or correlation with $\delta^{13}C_{carb}$ as is locally seen in dolostones of the Julie Formation.

Reconnaisance trace-element analyses of dolostones were undertaken: five out of seven samples, distributed across the $\delta^{13}C$ profile, have Mn/Sr < 10. Sr contents are mostly low (50 - 70 ppm).

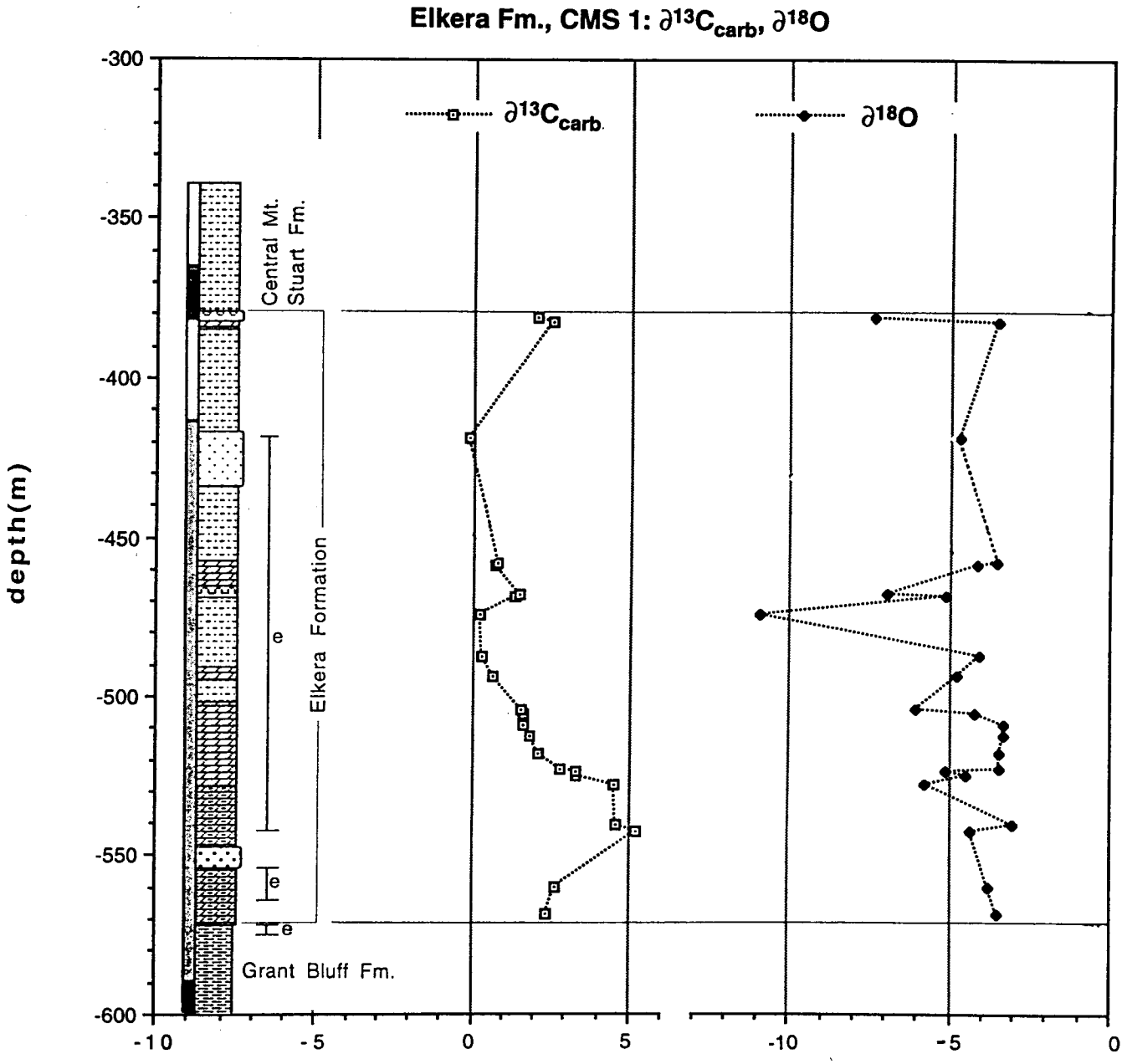

Fig. 4.34: Lithologic column and carbonate $\delta^{13}C$ and $\delta^{18}O$ profiles, Elkera Formation, DDC1 drillhole. 'e' indicates presence of anhydrite.

$^{87}Sr/^{86}Sr$

Eleven $^{87}Sr/^{86}Sr$ ratios from dolostones are scattered, and high relative to expected marine values (Table 4.3). The lowest ratio obtained was 0.7100 (sample 12.05). Ratios obtained from DDC 1 included the highest obtained in the course of this project, suggesting diagenetic incorporation of highly radiogenic strontium from the ancient felsic terrain of the Arunta Block. Emergent basement was probably not far away during sedimentation. Detrital, Rb-rich minerals (K-feldspar and coarse muscovite) are

abundant in most thin sections of carbonates. $^{87}Sr/^{86}Sr$ ratios from DDC 1 average 0.7153 ± 0.0020 (n = 5); and from Huckitta 7, 0.7113 ± 0.0018 (n = 6) There is no correlation of $^{87}Sr/^{86}Sr$ with either $\delta^{13}C_{carb}$ or $\delta^{18}O$. $^{87}Sr/^{86}Sr$ ratios of ten anhydrite samples from DDC 1 are somewhat higher: 0.7200 ± 0.0058 (n = 10). The highest value obtained from anhydrite was 0.7295 (sample 31.19). Anhydrite thus appears to have been, in general, more susceptible to $^{87}Sr/^{86}Sr$ alteration than dolostone in spite of its higher strontium content (ca. 1000 ppm).

Organic carbon

No coherent stratigraphic pattern emerges from $\delta^{13}C_{org}$ results obtained from the Elkera Formation in DDC 1 (Fig. 4.32). Results are widely scattered: $\delta^{13}C_{org}$ ranges fom -20 to -34 ‰. TOC is variable (0.2 - 2.1 mg/g) and there is a weak negative TOC-$\delta^{13}C_{org}$ correlation but data points normalised for variation in TOC using the constant developed in Chapter 2 ($\delta^{13}C_{org}{}^{N}$) show only slightly less scatter than raw data (Fig. 4.32).

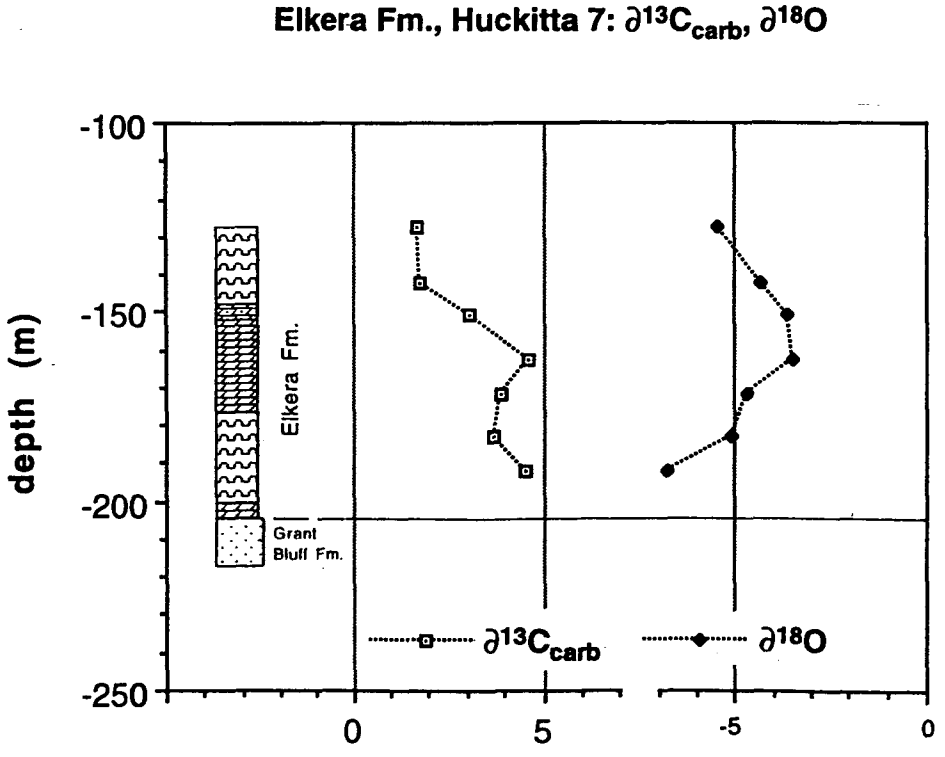

Fig. 4.35: Lithologic column and carbonate $\delta^{13}C$ and $\delta^{18}O$ profiles, Elkera Formation, Huckitta 7 drillhole.

sample	rocktype	Sr(ppm)	Mn(ppm)	Mn/Sr	87Sr/86Sr	∂13C	∂18O	Rb(ppm)	87/86Srinit	∂34S
Georgina Basin, Huckitta 7: Elkera Fm.										
12.05	dolostone	50	493	9.92	0.71004	1.7	-5.1			
12.10	dolostone				0.71052	3.1	-3.6			
12.11	dolostone	69	493	7.15	0.71058					
12.12	dolostone				0.71085					
12.15	dolostone	69	563	8.22	0.71096	4.5	-6.5			
12.16	dolostone	63	563	8.99	0.71539					
12.17	dolostone	50	634	12.75	0.71050					
Georgina Basin, DDC(Mt Skinner) 1: Elkera Fm.										
31.13	dolostone	65	2675	41.43	0.71281					
31.15	anhydrite	860			0.71100			0.091	0.71099	25.7
31.19	anhydrite				0.72951					29.2
31.21	dolostone				0.71857	0.8	-3.2			
31.27	anhydrite				0.72718					27.7
31.28	anhydrite				0.72257					26.9
31.30	anhydrite	1241			0.72040			0.769	0.72039	25.8
31.31	anhydrite				0.71933					25.9
31.33	anhydrite	612			0.72359			0.106	0.72358	25.3
31.35	anhydrite	1017			0.71314			0.05	0.71314	25.8
31.39	anhydrite				0.71401					
31.39	dolostone				0.71409	4.5	-5.4			
31.40	anhydrite	537			0.71793			0.474	0.71790	25.4
31.41	dolostone				0.71447	4.6	-2.7			
31.42	anhydrite					5.2	-4.4			26.4
31.45	anhydrite				0.71739					
31.48	dolostone	297	2393	8.05	0.71657					

Table 4.3: Trace-element and strontium and sulphur isotopic data, Elkera Formation.

This great degree of scatter in $\delta^{13}C_{org}$ in the Elkera Formation contrasts markedly with the well-defined signal from the Elyuah and Grant Bluff Formations (Figs. 4.32, 4.33), and indeed with the relatively well-defined signals from other Ediacarian units in this study. The cause of the scatter is not understood. Compositional immaturity of terrigenous sand in thin sections implies proximity to eroding basement and presence of possibly significant amounts of reworked kerogen or graphite. Also, evaporitic tidal-flats may be characterised by strong local variations in $\delta^{13}C$ geochemistry characteristic of isolated brine pools floored by benthic microbial mats (Lazar & Erez, 1990).

Sulphur

Twelve anhydrite samples were analysed for $\delta^{34}S$ (Table 4.3). Eight results fall in a narrow range (+25 to +26 ‰; average = 25.6 ± 0.2‰). The remaining four samples have more ^{34}S-enriched compositions, up to a maximum of +29.2 ‰. There is a weak positive correlation of $\delta^{34}S$ with $^{87}Sr/^{86}Sr$, with three of the four ^{34}S-enriched samples having high (> 0.72) $^{87}Sr/^{86}Sr$.

Isotopic compositions of early diagenetic sulphate may be perturbed towards more ^{34}S-enriched compositions by formation of pyrite which sequesters ^{32}S. There is no visible pyrite in the relatively enriched samples, however, and no significant lithologic difference from the other samples. Positive correlation with $^{87}Sr/^{86}Sr$ suggests burial-diagenetic dissolution-reprecipitation caused locally elevated $\delta^{34}S$, and the narrow range of results from the eight lightest samples (+25 to +26 ‰) is considered least-altered.

4.11 Central Mt Stuart Formation

Drillhole DDC 1 was collared in Central Mt Stuart Formation, and the hole intersected 380 metres of the formation. The base is an abrupt erosional contact on dolostone of the Elkera Formation. Pink to grey, quartz sandstone predominates, with frequent intervals of red shale interlaminated with sandstone, particularly below 200 m. The thinly layered shaly intervals feature ripple cross-lamination, undulose bedding and flaser bedding. There is rare dark grey shale.

Only a single shale sample was analysed for $\delta^{13}C_{org}$ from 1m above the base of the formation (Fig. 4.32).

4.12 Chemostratigraphic correlation within the Georgina Basin

Chemostratigraphic correlation between the three drillholes is clear-cut. The proposed correlations follow lithostratigraphy in a straightforward manner. The initial steep rise in $\delta^{13}C_{org}{}^{N}$ in DDC 2 is missing in DDC 1 which stopped short of basement. The level of the ensuing 'plateau' in both sections is essentially identical. The smooth continuity of the profile across the Elyuah- Grant Bluff Formation boundary - which also appears gradational in a lithostratigraphic sense - strongly suggests that there is no major hiatus or sequence boundary at this horizon in contrast to the suggestion of Jenkins (1993b) (Fig. 4.1b). The $\delta^{13}C_{carb}$ profile in the lower Elkera Formation is very similar in Huckitta 7 and DDC 1, notwithstanding somewhat different facies and the 130 km separation of these sections.

4.13 Correlation scheme - Amadeus and Georgina Basins

A correlation scheme linking all major Ediacarian sections in the Amadeus and Georgina Basins is shown as Fig. 4.36. Organic and carbonate carbon data are plotted coaxially with the offset between $\delta^{13}C_{org}{}^{N}$ and $\delta^{13}C_{carb}$ axes corresponding to $\Delta\delta^{*}$ for each locality. $\Delta\delta^{*}$ is a generalised figure intended to reflect the thermogenic shift in $\delta^{13}C_{org}{}^{N}$ at each locality; it is derived from observed $\Delta\delta^{N}$ (= $\delta^{13}C_{carb}$ - $\delta^{13}C_{org}{}^{N}$), kerogen H/C data, and kerogen colour (see Chapter 2 for a full discussion). As previously discussed, no $\Delta\delta$ or H/C data are available from DDC 1 and DDC 2, but on the basis of kerogen colour, thermal grade is inferred to be similar to that of the Pertatataka Formation in Wallara 1. Differences in $\Delta\delta^{*}$ between sections should accommodate thermogenic shifts in $\delta^{13}C_{org}{}^{N}$ so that organic profiles from widely separated localities have, in effect, a common baseline. Organic carbon data are shown as lines of best fit through $\delta^{13}C_{org}{}^{N}$ from preceding figures. Only $\delta^{13}C_{carb}$ data considered representative of surface or well-mixed oceanic water are included. Hence data thought to be possibly altered are excluded (i.e. topmost sample, Julie Formation, Ellery Creek); as are data considered reflective merely of local environmental conditions. As discussed in previous sections, into this second category fall depleted Julie Formation samples that may be affected by locally isolated brine-pool chemistry; and all but the most enriched (and relatively shallow-water) cap dolostone samples. Least altered Julie Formation $\delta^{13}C_{carb}$ signature is taken to be +5 to +6 ‰ with the exception of the uppermost part of the Phillipson Pound section.

The most enriched cap dolostone samples (ca. +1 ‰ to -1 ‰), at the very base of the Ediacarian at Ellery Creek and Mt Capitor, may reflect the composition of either the upper layer or a well-mixed marine water column. Thereafter, throughout the Pertatataka Formation and its correlatives, only an organic carbon chemostratigraphic signal is available (except for the single carbonate point from Acacia Well). Isotopic compositions of carbonates from cap dolostones at Mt Capitor and Wallara 1, and from the 'Halfway Dam Formation' (lowermost Pertatataka equivalent) are interpreted to reflect deposition under a deepening and increasingly stratified marine water body. In the lower Pertatataka Formation in Wallara 1, strong ^{13}C-depletion in organic carbon of benthic origin suggests that stratification persisted for a substantial period, and became less intense during this time (Δ_{pb}, the inferred difference in $\delta^{13}C$ between organic carbon of benthic and pelagic origin, changes upsection fairly abruptly from 9 to 5‰).

Within and immediately above cap dolostone in Wallara 1 there is a large and rapid rise in $\delta^{13}C_{org}{}^{N}$, followed by a brief maximum and rapid fall. The maximum and rapid decline are also seen at Hidden Valley, a correlation that is supported by a distinctive uniform red mudstone unit (probably incorporating, in sequence-stratigraphic terms, a condensed section or maximum flooding surface) in the lower part of the positive excursion at both places. This part of the profile is absent fom the Ellery Creek section, a fact consistent with the proposed sequence-stratigraphic framework and the more distal setting of Ellery Creek relative to Wallara 1. The negative excursion in $\delta^{13}C_{org}{}^{N}$ in Wallara 1 and Hidden Valley is seen as an initial minimum at Ellery Creek and DDC 2 (Georgina Basin). The stratigraphic extent of the ensuing plateau, seen in Wallara 1, Ellery Creek and DDC 1 and 2, roughly corresponds to the proportion of sandstone (and hence sedimentation rate), again consistent with the relatively distal palaeogeographic setting of the Ellery Creek section.

An alternative possibility for the correlation of the Elyuah and Grant Bluff Formations than that shown in Fig. 4.36, and one that accords better with the strong depletion seen in the lowermost samples, is that these units correlate with the cap dolostone and lowermost Pertatataka (below the negative excursion) in Wallara 1 and Hidden Valley. However, lithostratigraphy fits better with the correlation indicated, with deep-marine shales passing up into sandier successions characteristic of this interval in both basins.

Fig. 4.36 (opposite, folds out): Correlation scheme linking major sections in the Amadeus and Georgina Basin. See text for full explanation.

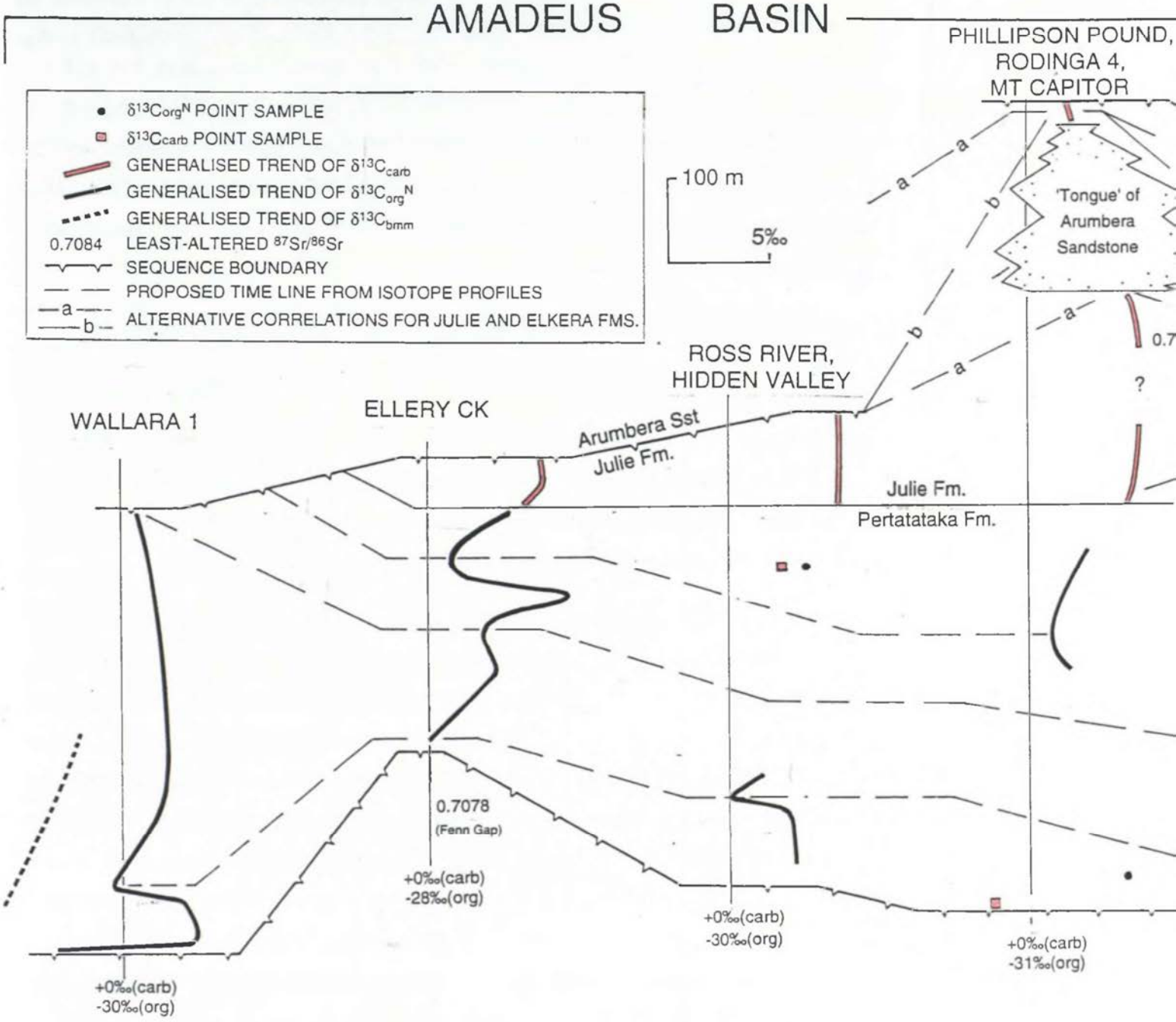

Fig. 4.36: Correlation scheme linking major sections in the Amadeus and Georgina Basin. See text for full explanation.

A mild negative excursion is seen in $\delta^{13}C_{org}{}^{N}$ near the top of the Pertatataka Formation at Ellery Creek and Rodinga 4. Absence of time-equivalents of this part of the succession from Wallara 1 is supported by acritarch biostratigraphy (Grey, in prep). The Julie Formation is marked everywhere by enriched (+5 to +6 ‰) carbonate except for lighter values at the top of the Phillipson Pound section. Given the presence of a thick sandsone unit attributed to the Arumbera Formation in this section (Fig. 4.36; Freeman et al., 1991; Oaks et al., 1990) it is possible that the top of the Phillipson Pound section belongs temporally to the Arumbera Sandstone and is substantially younger than the type Julie Formation ('a' timelines on Fig. 4.36). Alternatively, the Phillipson Pound section is simply a greatly thickened equivalent of the type section with an Arumbera-like facies tongue ('b' timelines).

Correlation of the Elkera Formation is problematic. There are three possibilities.

(i) The $\delta^{13}C_{carb}$ profile of the Elkera Formation closely resembles the organic carbon profile from the upper Pertatataka Formation at Ellery Creek. However, the two units are lithologically quite dissimilar, and a correlation of all or part of the Elkera Formation with the lithologically similar Julie Formation can also accommodate the $\delta^{13}C$ data, and is considered preferable (below).

(ii) The unconformity at the base of the Elkera Formation suggests the possibility of a substantial time break, and as shown in Fig. 4.36, the Elkera Formation could be a partial correlative of the Julie Formation. Alternative correlations with the Phillipson Pound section, indicated with 'a' and 'b' timelines, seem equally possible. Inherent in both these possibilities is the conclusion that the upper two-thirds of the Elkera Formation is younger than the type Julie Formation (Ross River section). Tenuous support for a correlation with the Julie Formation comes from sulphur isotope chemostratigraphy. The sulphate sulphur isotopic compositions found in the Elkera Formation (+25 to +26 ‰) are not significantly different than a single $\delta^{34}S_{sulphate}$ result (+24.3 ‰) from a level in the Rodda beds of the Officer Basin thought to be roughly correlative with the Julie Formation (see later section).

(iii) The Elkera Formation, as indicated by Jenkins (1993b), is entirely younger than the type Julie Formation. ^{13}C-enriched carbonates such as those of the Julie Formation and lower Elkera Formation were probably deposited more than once during the Ediacarian (see later chapter) and thus these units need not be correlative. Tenuous support for this this third possibility comes from oxygen isotopes. In the Elkera Formation there is a

preponderance of oxygen isotopic compositions around -3 ‰ and no values heavier than this, suggesting this value represents primary $\delta^{18}O$. Nearly all $\delta^{18}O$ values in the Julie Formation are substantially lighter than this except for the uppermost Phillipson Pound samples which may, as indicated above, be temporally part of the lower Arumbera Formation.

Further isotope work could probably resolve this dilemma. Were well-preserved limestones to be found in the Elkera Formation, this would enable $^{87}Sr/^{86}Sr$ results close to primary values to be obtained. In the Julie Formation, microsampling of micritic ooids in the lower Philipson Pound section for $^{87}Sr/^{86}Sr$ analysis would probably yield improved (less altered) results. A search for preserved sulphates in the Julie Formation, for $\delta^{34}S_{sulphate}$ analysis, may provide corroborative data.

4.14 Correlation with Adelaide Geosyncline and Officer Basin

With this resolution of the problems of correlation within the Amadeus and Georgina Basins (Fig. 4.36), chemostratigraphic correlation with the Officer Basin and type Ediacarian of the Adelaide Geosyncline can be attempted. For the purposes of this discussion, consecutive positive excursions in the $\delta^{13}C$ profiles are designated Cycle I, II etc (Fig. 4.37).

Cap dolostones at Mt Capitor, Wallara 1 and in the Adelaide Geosyncline (Nuccaleena Formation) are mutually correlative on strong lithologic and $\delta^{13}C_{carb}$ - chemostratigraphic evidence (section 4.4d). A positive excursion in $\delta^{13}C_{org}$ above cap dolostone - Cycle I - is seen in Wallara 1, Mt Capitor (sparse data), Hidden Valley and in BWM1a-1 and SCYW1a in the Adelaide Geosyncline. Cycle 1 appears to be absent from some localities distal from source areas (Ellery Creek, Bunyeroo Gorge) becauseof non-deposition at a condensed section or maximum flooding surface as explained above (sections 3.4c, 4.5d). The condensed section is inferred to lie within the lower part of a widespread, silt-free red shale near the base of the Brachina and Pertatataka Formations. (for example at Bunyeroo Gorge, BWM1a-1, SCYW1a, Wallara 1, Hidden Valley). Conversely, Cycle I may be absent form Giles 1 (Officer Basin) becauseof depositional onlap towards the southern basin margin.

The negative excursion defining the top of Cycle I is marked by the widespread appearance of benthic microbial mats in three basins: the Officer Basin, the Adelaide Geosyncline and the Amadeus Basin. Cycle II is of greater stratigraphic extent and

attains a lower maximum than Cycle I (see Wallara 1, SCYW1a). The very short Cycle III is fully delineated only at Ellery Creek - in an interval not sampled anywhere else except the Adelaide Geosyncline, where a weaker positive excursion coincides with Sequence Boundary 2 (at the top of the ABC Range Fomation) in SCYW1a. The sequence boundary suggests a possible lacuna here. Cycle III appears to be absent form the more sparsely-sampled Bunyeroo Gorge section. This correlation implies that the Cyclops Member (Amadeus Basin) is a correlative of the ABC Range Formation (since a silty interval probably correlative with the Cyclops coincides with Cycle III at Ellery Creek), supporting the correlation of Preiss et al. (1978). Another implication is that Sequence Boundary 2 (and the correlative F6 surface in the Officer Basin) is 'cryptic' in the Amadeus Basin.

The negative excursion defining the top of Cycle III occurs widely in the Amadeus Basin (Ellery Creek, Rodinga 4), in the Officer Basin (Observatory Hill 1, Munta 1) and in the Adelaide Geosyncline (SCYW1a, Bunyeroo and Brachina Gorges). The Acraman Impact Ejecta Layer links the Officer Basin and Adelaide Geosyncline profiles at a horizon just below this negative excursion, and at a slightly younger level the incoming of the complex spiny acritarch flora roughly coincides with the negative excursion in the Amadeus Basin (Rodinga 4) and the Officer Basin (Munta 1, Observatory Hill 1) (Grey, in prep).

Sequence Boundary 3 (= F5 in the Officer Basin), above the negative excursion, is 'cryptic' in the Amadeus Basin. The carbon isotope profiles suggest the presence of a lacuna at this surface in the Officer Basin, but more or less continuous deposition may have occurred in the Amadeus Basin. This sequence boundary is inferred to lie within the uppermost Pertatataka or Julie Formation in the Amadeus Basin. One possible candidate is the sequence boundary inferred on the basis of parasequence stacking patterns within the Julie Formation (see section 4.6a).

Cycle IV is defined by $\delta^{13}C_{carb}$ data peaking at +5 to +6 ‰ in the Amadeus Basin (Julie Formation), Georgina Basin (lower Elkera Formation) and Officer Basin (lower Unit B of the Rodda beds correlative). At this time in the Adelaide Geosyncline (Wonoka Formation) strongly anomalously depleted $\delta^{13}C_{carb}$ (and possibly moderately anomalously enriched $\delta^{13}C_{org}$) are thought to be a consequence of stratification of basin waters (section 3.6c).

Fig. 4.37 (opposite, ~~folds out~~): Correlation scheme for Ediacarian successions in Adelaide Geosyncline, and Officer, Amadeus and Georgina Basina, based on Figs. 4.36 and 3.26.

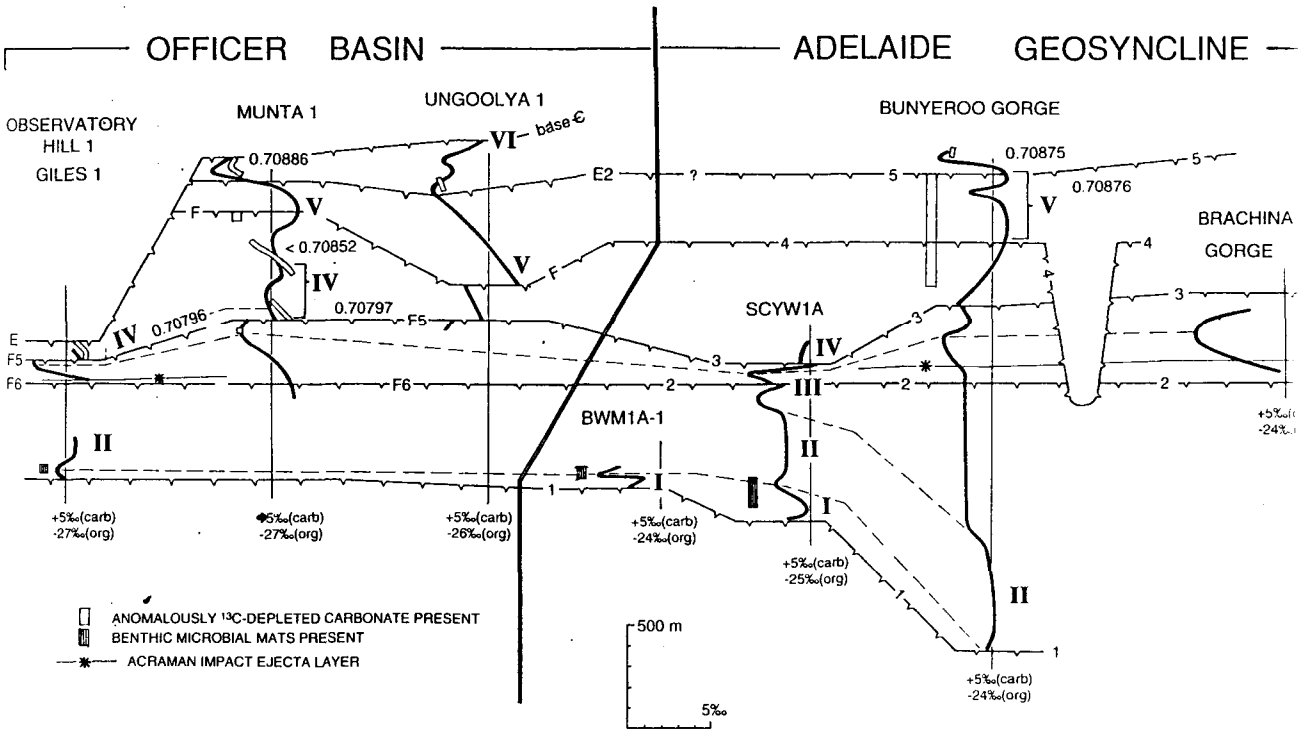
OFFICER BASIN
ADELAIDE GEOSYNCLINE
OBSERVATORY HILL 1
GILES 1
MUNTA 1
UNGOOLYA 1
BUNYEROO GORGE
BRACHINA GORGE
SCYW1A
BWM1A-1
0.70886
< 0.70852
0.70796
0.70797
0.70875
0.70876
VI
base €
E2
F
E
F5
F6
+5‰(carb) -27‰(org)
+5‰(carb) -26‰(org)
+5‰(carb) -24‰(org)
+5‰(carb) -25‰(org)
ANOMALOUSLY ¹³C-DEPLETED CARBONATE PRESENT
BENTHIC MICROBIAL MATS PRESENT
ACRAMAN IMPACT EJECTA LAYER
500 m
5‰

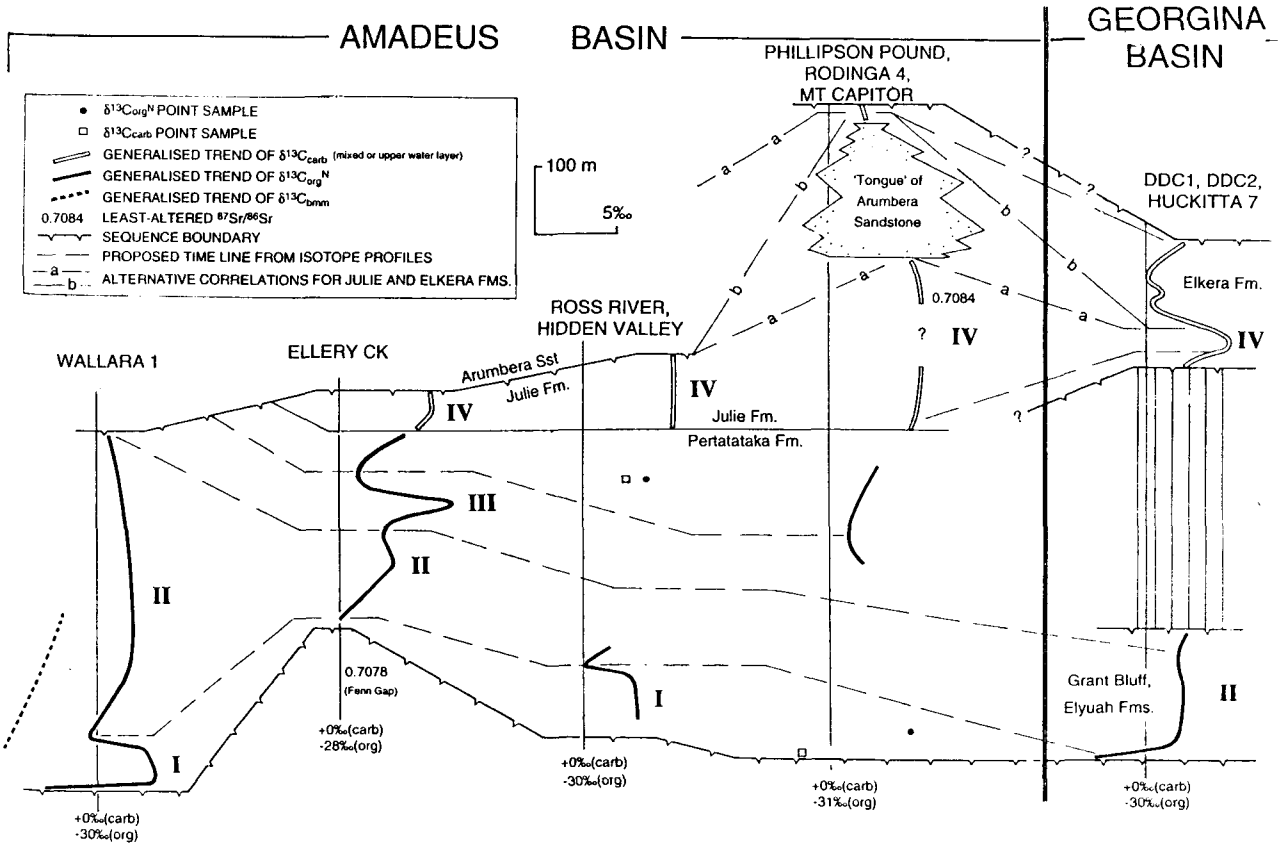
AMADEUS BASIN
GEORGINA BASIN
δ¹³C_orgN POINT SAMPLE
δ¹³C_carb POINT SAMPLE
GENERALISED TREND OF δ¹³C_carb (mixed or upper water layer)
GENERALISED TREND OF δ¹³C_orgN
GENERALISED TREND OF δ¹³C_bmm
0.7084 LEAST-ALTERED ⁸⁷Sr/⁸⁶Sr
SEQUENCE BOUNDARY
PROPOSED TIME LINE FROM ISOTOPE PROFILES
ALTERNATIVE CORRELATIONS FOR JULIE AND ELKERA FMS.
100 m
5‰
PHILLIPSON POUND, RODINGA 4, MT CAPITOR
'Tongue' of Arumbera Sandstone
DDC1, DDC2, HUCKITTA 7
ROSS RIVER, HIDDEN VALLEY
WALLARA 1
ELLERY CK
Arumbera Sst
Julie Fm.
Pertatataka Fm.
Elkera Fm.
Grant Bluff, Elyuah Fms.
0.7084
0.7078 (Fenn Gap)
+0‰(carb) -28‰(org)
+0‰(carb) -30‰(org)
+0‰(carb) -31‰(org)

Strontium isotopes are significant in correlating the Julie Formation. On present data, marine $^{87}Sr/^{86}Sr$ increased monotonically through the Ediacarian (Kaufman et al., 1993; and see section 6.3b). Strontium isotopes therefore suggest that the Julie Formation (primary $^{87}Sr/^{86}Sr < 0.7084$) is older than both Rodda beds Unit C ($^{87}Sr/^{86}Sr = 0.70886$) and Unit 7 of the Wonoka Formation (0.70876). However, it is not entirely clear whether the Julie Formation correlates with the whole of Rodda beds Unit B (interval between F5 and F) or only part of Unit B. The preferred correlation here is that the Julie Formation correlates with the carbonate unit at the base of Unit B (1598 - 1673 m in Munta 1: this unit is called the "Karlaya Limestone" by Lindsay & Reine, 1995). The "Karlaya Limestone" is a good lithologic correlative of the Julie Formation, because in southern (shoreward) settings (e.g. Observatory Hill 1, Lake Maurice West 1) it consists (like the Julie Formation) of a lower subtidal limestone member and an upper, shallow-water dolostone member. Also, in the type Julie Formation, least-altered $\delta^{13}C_{carb}$ is stable at +5 to +6 ‰, and there is no indication of a downward trend to +3 ‰, as there is in the upper part of Rodda beds Unit B.

Implications of this correlation are:

(i) that the Julie Formation (and the uppermost Pertatataka Formation) lie within the lower part only of the range of the large acanthomorph acritarchs (which extends throughout Rodda beds Unit B: Grey, in prep); and

(ii) the canyon-forming unconformity ('F' surface) in the Officer Basin - and its probable correlative surface, Sequence Boundary 4 in the Adelaide Geosyncline - lies above the Julie Formation. The oldest part of the Arumbera Formation - a thick succession of marine red shale and siltstone in the Ooraminna and Carmichael Depocentres (Lindsay, 1987) - may correlate with the upper Rodda beds, or the Julie - Arumbera contact may represent a more substantial hiatus.

Correlation of the negative excursion in $\delta^{13}C_{carb}$ (to 0 ‰) in the upper Elkera Formation is not clear. There is no evidence for a corresponding negative excursion in Rodda beds Units B or C. (^{13}C-depleted carbonates just below the F unconformity are associated with relatively enriched $\delta^{13}C_{org}$ and are attributed to basin stratification: see section 3.11). However, the data do not entirely preclude such a negative excursion either: basin stratification may be expected to perturb $\delta^{13}C_{org}$ towards anomalously positive values as well as $\delta^{13}C_{carb}$ to negative ones (sections 3.6c; 6.2). Also, the 'F' uncomformity may represent a considerable time break. Hence the negative excursion in the Elkera Formation may correspond approximately with the 'F' unconformity or to

some interval not represented in the Rodda beds of the southeastern Officer Basin.

5

Isotope chemostratigraphy of some Tasmanian Neoproterozoic successions

5.1 Introduction

Widespread Neoproterozoic successions deposited on, or marginal to the Australian craton are sufficiently similar to allow broad lithostratigraphic correlation across the continent (e.g. Preiss & Forbes, 1981; Walter et al., 1995) and even into Laurentia, then adjoining Australia to the east (Moores, 1991; Young, 1992; Brookfield, 1993). However, Tasmanian Neoproterozoic successions are not easily matched with either mainland Australia or North America. Tasmanian Proterozoic rocks have traditionally been interpreted as *in situ* basement (Williams, 1976; 1989) perhaps linked to the Australian craton (Veevers, 1984, p. 280) but on continental reconstructions the Cambro-Ordovician Kanmantoo Fold Belt and Ross Orogen separate Tasmania from the pre-Adelaidean cratonic areas of Australia and east Antarctica (e.g. Leaman et al., 1994). Within Tasmania, there are several spatially or structurally separated Proterozoic inliers or terranes whose interrelationships are mostly obscure (see Turner et al., 1989), largely because of Cambrian and Devonian tectonism. Some recent interpretations suggest that these terranes are allochthonous fragments accreted into the Tasman Fold Belt during the early Palaeozoic (Powell, 1992; Leaman et al., 1994). Chemostratigraphy is one means of providing much-needed age constraints for some of the Proterozoic successions. This chapter is an initial study.

The focus of this chapter is the gently deformed, late Neoproterozoic Togari Group (< 725 Ma?) of the Smithton Basin in far NW Tasmania (Figs. 5.1, 5.2). There are no known Ediacara-type metazoan fossils or clearly established Early Cambrian fossils in Tasmania, but indirect evidence from radiometric dating suggests a late Cryogenian to Ediacarian age for the Togari Group. This chapter presents C and Sr isotope chemostratigraphic data for the Togari Group, and also provides a body of new information on the sedimentology of the succession. A synthesis of chemostratigraphic and other data suggests a Torrensian age for the lower part of the Group (Black River Dolomite) and an Ediacarian age for the upper part (Smithton Dolomite). An

Ediacarian age for the Smithton Dolomite suggests a substantial hiatus at the base of the overlying Middle to Late Cambrian Scopus Formation.

Reconnaissance C-isotopic data were also gathered from the Jubilee Region in central-south Tasmania, a structurally complex area where a thick Proterozoic dolostone-dominated succession, the Weld River Group, includes diamictites of probable glacial origin (Calver, 1989c; unpubl.). Correlation of the Weld River Group with the Smithton Dolomite best accommodates the chemostratigraphic data, but corroborative information (from Sr isotopes and palaeontology) is needed.

A dolostone unit overlying diamictite on King Island has a carbon-isotopic composition similar to 'cap dolostones' overlying glacial units on mainland Australia.

5.2 Geological framework

The western two-thirds of Tasmania comprise Proterozoic to mid-Palaeozoic rocks deposited in a variety of tectonic settings.

There are three main Proterozoic regions: the largely unmetamorphosed Rocky Cape region in the north-west; the central Tyennan region, mainly of metasedimentary rocks; and the mostly unmetamorphosed Jubilee region in the southeast (Fig. 5.1). The Rocky Cape and Tyennan regions are separated by the Dundas Trough, filled mainly with a thick, deformed pile of middle to late Cambrian sediments and volcanics. The trough succession includes structurally-emplaced ultramafic/mafic igneous rock associations of oceanic forearc origin (Brown & Jenner, 1988; Brown, 1989, Crawford & Berry, 1992); and a narrow calc-alkaline volcanic arc, the Mount Read Volcanics (Corbett & Solomon, 1989). Cambrian rocks including ultramafics also partly separate the Tyennan and Jubilee regions. A major unresolved question is whether there has been substantial convergence of the Proterozoic terranes, for example by subduction (Griffiths & Solomon, 1974; Corbett & Lees, 1989) or shallow thrusting (Leaman et al., 1994) (see Corbett & Turner, 1989 for a review). Berry & Crawford (1988) and Crawford & Berry (1992) proposed that the Proterozoic regions comprised a single east-facing passive margin in the late Neoproterozoic, attenuated by rifting, that was overthrust from the east in the Middle to Late Cambrian by the oceanic forearc rocks, now remaining only as small erosional and structural remnants. In support of the idea of limited relative transport of the Proterozoic terranes, Turner (1989, p. 6) noted that the Rocky Cape, Tyennan and Jubilee regions have somewhat similar primary lithologies and evolutionary histories.

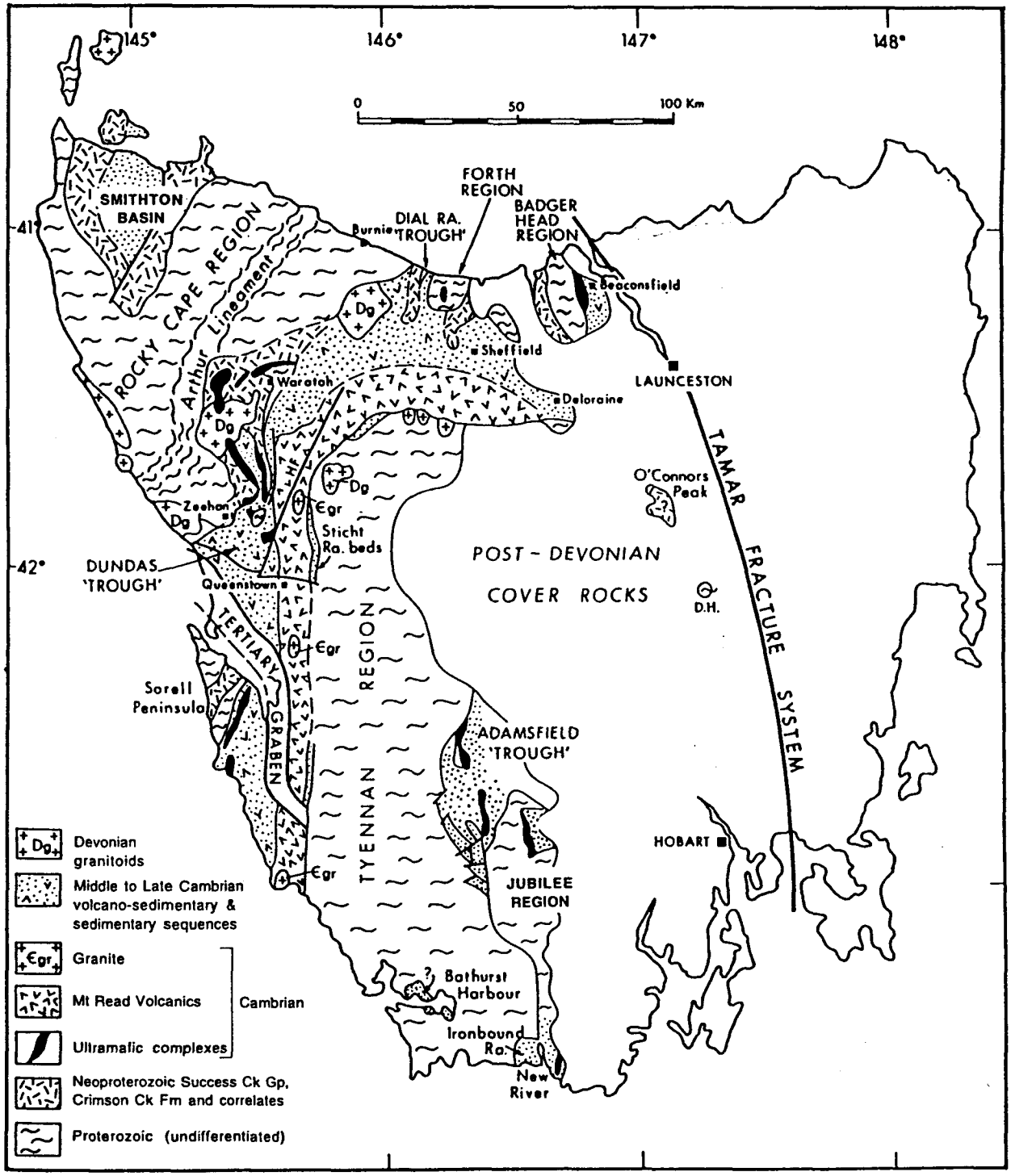

Fig. 5.1: Simplified geological map of Tasmania with post-Cambrian successions omitted, showing present distribution of major Proterozoic-Cambrian tectonic elements. Note position of Smithton Basin and Jubilee region in far north-west and central-south, respectively. Adapted from Corbett & Turner (1989).

5.3 Geological setting: Smithton Basin

The Rocky Cape region, which includes the Smithton Basin, is mostly gently deformed but is transected by a highly deformed and metamorphosed linear zone, the Arthur Lineament (Fig. 5.1). The oldest exposed succession is a thick (several km) sequence of cratonic orthoquartzite, siltstone and minor carbonate (the Rocky Cape Group) that forms basement to the Smithton Basin. No definite maximum age for the Rocky Cape Group is known, but lithologically similar successions in the Tyennan region have given Rb-Sr model ages of 1100 - 1150 Ma that probably correspond to the age of deposition (Raheim & Compston, 1977; Turner, 1989; Turner et al., 1992). A gently angular unconformity separates the Rocky Cape Group from the overlying Togari Group, which occupies a large synclinal structure, the Smithton Basin, in far NW Tasmania (Figs. 5.1; 5.2). The Togari Group (Everard et al., 1994) consists of basal siliciclastics (Forest Conglomerate), a carbonate-chert-shale unit (Black River Dolomite), rift tholeiites and associated volcaniclastics (Kanunnah Subgroup) and dolostone (Smithton Dolomite). The synclinal core of the Smithton Basin is occupied by a Middle to Late Cambrian siliciclastic unit, the Scopus Formation. Indirect radiometric evidence and stromatolite-palaeontological evidence, detailed below, suggests a late Neoproterozoic (< 725 Ma) age for the Togari Group, in agreement with the chemostratigraphy.

East of the Arthur Lineament, a thick Neoproterozoic quartzwacke succession, the Burnie Formation, contains a syndepositional dolerite intrusion dated by whole-rock K-Ar at 725 ± 35 Ma (Crook, 1979). A detrital muscovite mineral separate from the Oonah Formation (a probable correlate of the Burnie Formation) has been dated by K-Ar at 708 ± 6 Ma (Turner, 1993). Two current, alternative interpretations of the age of the Oonah and Burnie Formations relative to the Rocky Cape and Togari Groups both agree that the Oonah and Burnie Formations are older than the Black River Dolomite of the Togari Group. Turner (1991) and Turner et al. (1992) regard the Oonah and Burnie Formations as a distal, greatly thickened lateral equivalent of the Forest Conglomerate (basal Togari Group). On the other hand, Brown (1986) and E. Williams (1979) regard the Oonah Formation and a correlative of the Black River Dolomite in the southern Rocky Cape region as being separated by an unconformity associated with polyphase deformation in the Oonah Formation, implying a substantially greater age difference. These two dates provide a maximum age for the Black River Dolomite in either interpretation, bearing in mind the uncertainties inherent in the K-Ar method.

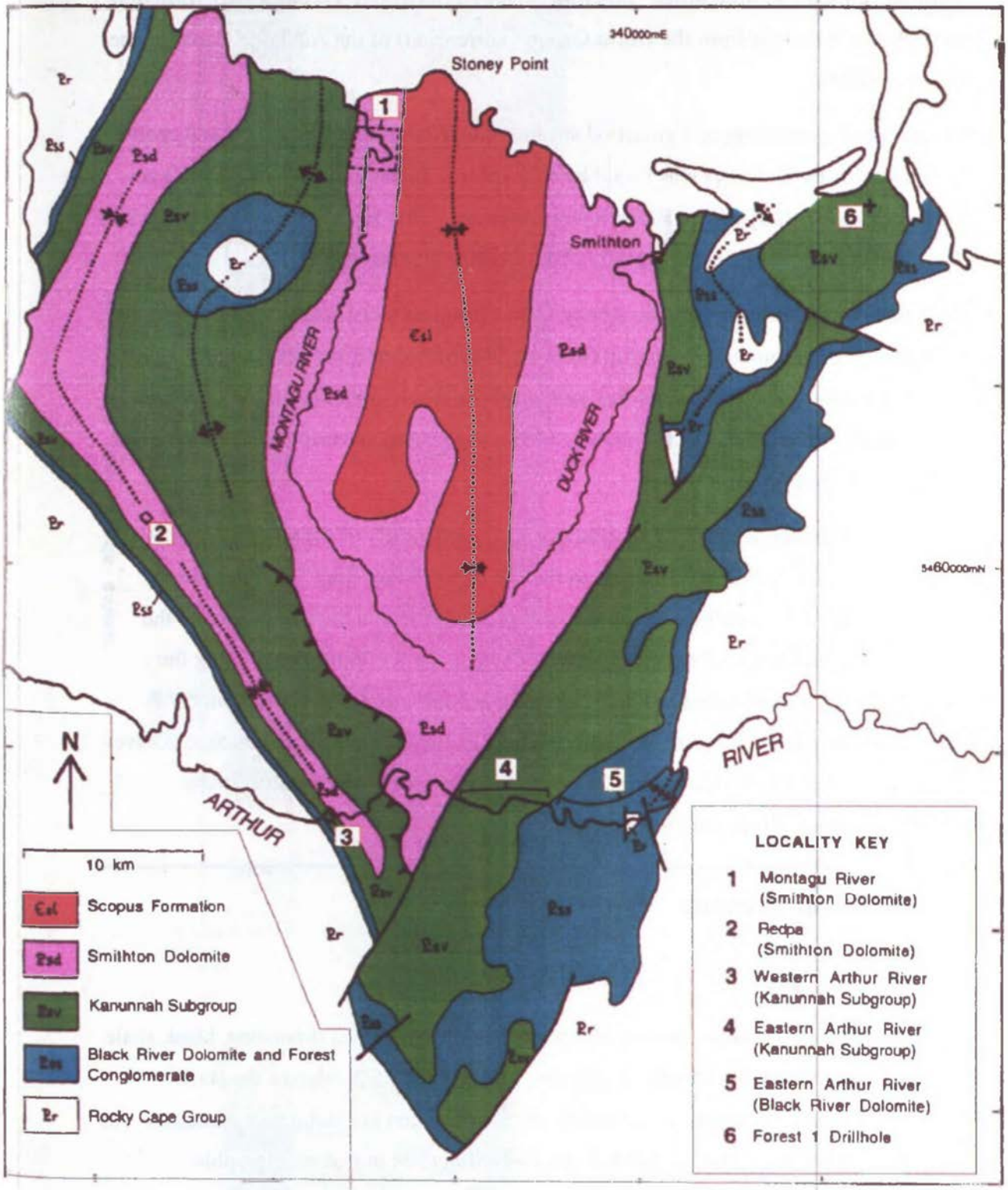

Fig. 5.2: Simplified geological map of Smithton Basin showing sections and localities mentioned in text. From Lennox et al. (1982), Seymour & Baillie (1992), Everard et al. (1994), Calver & Everard (in prep.) and Longman & Matthews (1962).

Diamictite occurs at or near the top of the Black River Dolomite. Clasts within the diamictite contain a stromatolite, *Baicalia* cf. *burra* (Griffin & Preiss, 1976). *Baicalia burra* Preiss is known from the Burra Group (Torrensian) of the Adelaide Geosyncline (Preiss, 1987d).

A loose block consisting of a silicified stromatolite, *Conophyton garganicum* Korolyuk (identification by K. Grey) was found by the writer at Julius River Quarry [AMG co-ordinates CQ 349423] within Black River Dolomite. This form is known from rocks of probable Willouran age in the Adelaide Geosyncline (Preiss, 1987d).

Some dolerite dykes intruding the Rocky Cape Group are chemically similar to the rift tholeiites of the Kanunnah Subgroup (Brown, 1989b) and may reflect the same extensional episode. Two such dykes yielded K-Ar whole-rock ages of 588 ± 8 and 600 ± 8 Ma (Adams et al., 1985; Brown, 1989), suggesting an early Ediacarian age for the Kanunnah Subgroup.

Outcrop is generally poor in the Smithton Basin, particularly of the carbonate units. A fully cored drillhole, Forest 1, located in the NE of the Basin (Fig. 5.2), provides a section through the lower half of the Kanunnah Subgroup and the upper third of the Black River Dolomite. An east-west traverse across the Smithton Basin along the Arthur River was undertaken to locate and sample further outcrop in these units. A detailed account and structural interpretation of this traverse is given elsewhere (Calver & Everard, in prep.). The Smithton Dolomite was sampled from outcrop in the northern Montagu River valley (Fig. 5.2).

5.4 Black River Dolomite

5.4a Stratigraphy

The Black River Dolomite consists of 600-800 m of interbedded dolostone, black shale and chert. The formation is thinner (approx. 280 m) at the SW edge of the Basin (Calver & Everard, in prep). Near the top of the formation is a dolomitic diamictite, the Julius River Member. The top third of the formation (208 m true stratigraphic thickness) was intersected in the Forest 1 drillhole in the NE of the Smithton Basin (Fig. 5.4), and further reconnaissance sampling was carried out along the Arthur River transect (Fig. 5.3).

Basal siliciclastics (the Forest Conglomerate) are absent at both ends of the Arthur River traverse, and an exposure of the unconformity in Lamprey Creek [CQ 404419] at

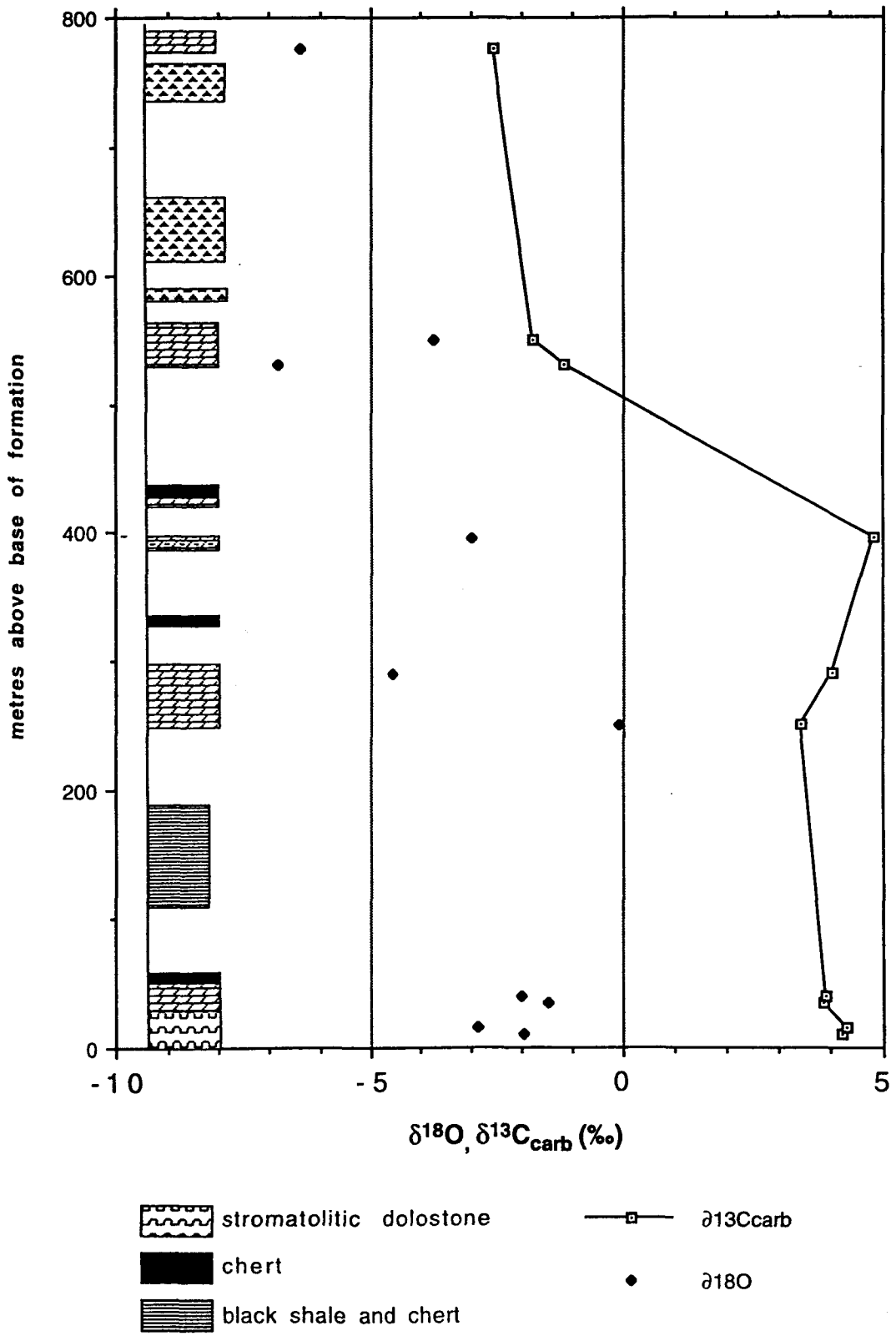

Fig. 5.3: Lithologic column of Black River Dolomite, eastern Arthur River section, and carbonate isotopic data.

the eastern margin of the basin shows dolostone resting directly on Rocky Cape Group. The lowest 50 - 100 m of the Black River Dolomite in the eastern Arthur River section (Fig. 5.3) consists of dolostone with domical stromatolites, coarse intraclastic breccia and oolitic grainstone. Stromatolite-derived intraclastic breccia fills interspaces between stromatolites. Stromatolites and intraclasts are characterised by a strongly banded microstructure similar to that of *Baicalia* (e.g. Griffin & Preiss, 1976) but the low domical shapes of the stromatolites are not characteristic of this genus (K. Grey, pers. comm.). The microstructure consists of rhythmically alternating dense micritic laminae spaced ½ - 1 mm apart separated by microsparry or sparry layers. Intraclasts are bound by a dark (in outcrop), isopachous cement, about 1 mm thick, and a later generation of clear coarse dolomite spar. This distinctive basal stromatolitic unit is structurally repeated several times along the river transect.

The basal unit is overlain by a thick (150 m) unit of interbedded black shale and black chert; then follows alternating poorly-exposed, creamy, fine-grained dolostone and black shale and chert. Many chert units are internally uniform but some contain well-preserved pisolitic, stromatolitic and oolitic fabrics suggesting replacement of carbonate, probably in early diagenesis. Dolostones, including the coarse cements of the basal unit, are non-ferroan. Ill-defined domical stromatolites are seen in a few dolostone outcrops, but they lack the banded microstucture characteristic of the basal unit.

The diamictite (Julius River Member) is about 200 m thick in the eastern Arthur River transect (Fig 5.3). It is a massive, open-framework diamictite consisting of sub-rounded clasts up to ½ m in size, apparently entirely of pale grey dolostone, in an abundant, dark grey, dolomitic silty mudstone matrix. There is no definitive sedimentological evidence for the mode of origin of the diamictite. At the top of this exposure, clasts containing the stromatolite *Baicalia* cf. *burra* were found and described by Griffin & Preiss (1976).

Downstream the river crosses the formation a second time and at CQ 253472, limestone, thickly interbedded with medium-crystalline ferroan dolostone, crops out below diamictite near the top of the formation. In thin section the limestone is an intraclast-peloid grainstone with scattered rhombs of ferroan dolomite.

Part of the Black River Dolomite (approximately the top third of the formation) was fully cored in Forest 1 (Fig. 5.4). Here the formation consists of, in upward succession:

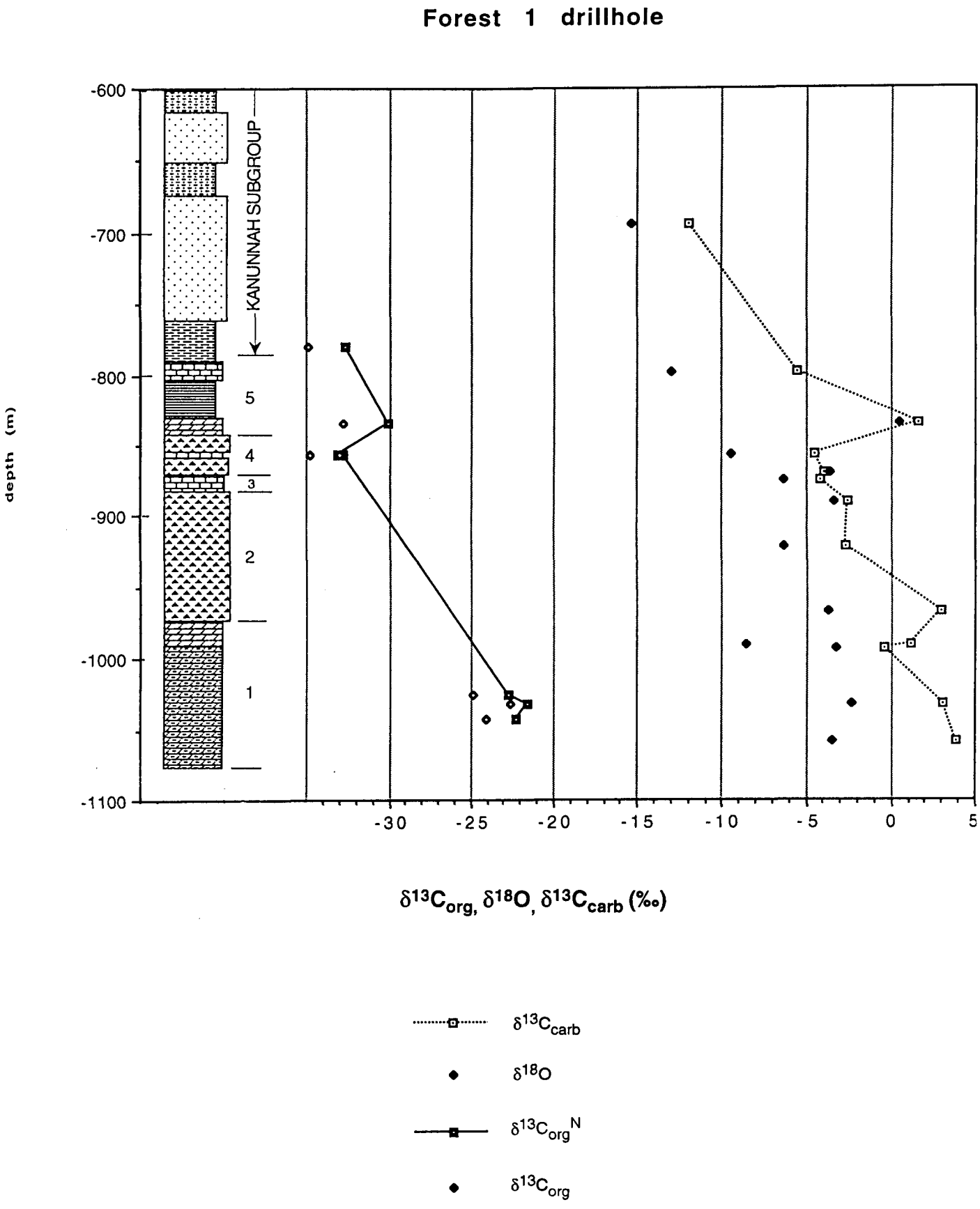

Fig. 5.4: Lithologic column of upper Black River Dolomite and lower Kanunnah Subgroup, Forest 1 drillhole; with organic carbon and carbonate isotopic data. Numbers in column refer to units described in text.

(1) 75 m (true stratigraphic thickness) of dolostone interbedded with black mudstone. The dolostone is a medium to dark grey, fine-grained, rather uniform rock, showing in thin sections micritic patches, of which some are rounded (apparently peloids and intraclasts ½ - 1 mm in size) but most are irregular to ragged, 'floating' in a cloudy microspar matrix. The microspar appears to be a replacement of an original micritic matrix. This is clearly the case in one sample, an ooid packstone (ABS 88) in which irregular areas of cloudy microspar partially replace ooids and dolomicrite matrix, leaving ragged unrecrystallised micritic remnants (Plate 5.1). Unaltered ooids are small (¼ mm) and display poorly preserved radial-fibrous fabric.

This lower unit includes about 10% black mudstone, as thin wavy laminae to units up to 3.5 m thick. The mudstone is not highly carbonaceous (two TOC determinations 2.6 and 4.2 mg/g) but oil stains are present on the core surface in a few places.

(2) 67 m of dolomitic diamictite. This consists of angular to subrounded dolostone and minor chert clasts in an abundant, dark grey to black, pyritic dolomitic mudstone matrix. Diamictite occurs as very thick beds up to ten metres thick, and there is minor interbedded black shale, siltstone and pebbly (dolomitic) mudstone. Many of the larger dolostone clasts carry well-preserved stromatolites identified by W. V. Preiss as *Baicalia* cf. *burra*. (Brown, 1985).

Dolostone clasts show a wide variety of textural types: uniform dolomicrite; dolostone with micrite/microspar stromatolitic lamination, replacive microspar with remnant micritic patches (as in unit 1); and intraclastic grainstone. In some grainstones, allochems consist only of micrite envelopes, with intra- and inter-particle porosity filled with at least two cement generations. In all cases, diagenesis was complete at the time of diamictite formation, as allochems and cements alike are cleanly transected by eroded surfaces of clasts (Plate 5.2).

(3) 8 m of fine-grained, grey, uniform microsparitic limestone with minor black shale interbeds.

(4) 23 m of predominantly limestone diamictite, texturally similar to the dolomitic diamictite but clasts are nearly all composed of limestone microspar; with minor beds of limestone and black mudstone.

(5) 41 m of black and grey mudstone; in places thinly bedded (banded black and grey); and minor fine-grained limestone and dolostone. Black, fine-grained, uniform dolostone overlies the diamictite; it does not resemble 'cap dolostones' such as the

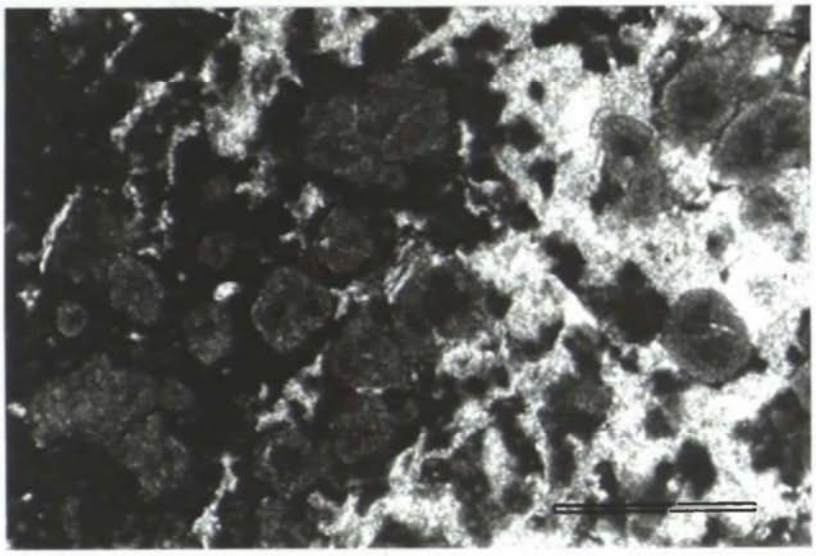

Plate 5.1: Thin section of clear dolomicrospar replacing dolomicrite matrix of oolitic dolostone, Black River Dolomite, Smithton Basin. Sample ABS88, 990 m depth, Forest 1 drillhole. Scale bar = 1mm.

Plate 5.2: Thin section of dolostone clast in diamictite within Black River Dolomite, showing truncation of cement phases at surface of clast. Sample ABS84, 890 m depth, Forest 1 drillhole. Scale bar = 1mm.

Nuccaleena Formation. Black shales are opaque to dark brown silty claystone in thin section, with bundled, faint, planar-parallel, silty microlaminae. The black shales are phosphatic in places. There is abundant pyrite and secondary calcite. Limestone is microspar, either black (organic-rich) (834 m depth), or pale grey with coarse poikilitic calcite cement (800 m). The top of the Black River Dolomite is transitional, and is taken as the point at which beds of volcaniclastic wacke become common (782 m depth).

5.4b Isotope Geochemistry

The relative position of outcrops on the Arthur River section through the Black River Dolomite (Fig. 5.3) is deduced from a structural profile constructed from 1:25 000 scale mapping along the river between CQ 426486 and CQ 343468 (see Calver & Everard, in prep). The topmost sample shown is from a locality further west [CQ 252469], and is placed at its correlative lithostratigraphic position immediately below the top of the formation.

The lower half of the Black River Dolomite is characterised by moderate ^{13}C enrichment (Fig. 5.3). Samples analysed - uniform, non-ferroan microsparitic dolostones and dolomicrites and one stromatolitic dolostone - all have $\delta^{13}C_{carb}$ between +3 and +5 ‰. Oxygen isotope compositions are relatively heavy, averaging about -2 ‰ with a maximum of 0 ‰. Stromatolitic dolostone with banded microstructure from the basal unit is 1 ‰ heavier in $\delta^{18}O$ than associated dolomicrite but essentially the same in $\delta^{13}C_{carb}$. There is a fall to negative $\delta^{13}C_{carb}$ (-1 to -2.5 ‰) in the upper part of the formation, in samples above and below the diamictite. $\delta^{18}O$ of these three samples is also somewhat lower.

The Forest 1 drillhole reached 100 m below the base of the diamictite, and samples low in this section are isotopically very similar to those of the lower half of the Arthur River section (Fig. 5.4). With one exception, all samples below the diamictite have positive $\delta^{13}C_{carb}$. A dolostone bed 5 m above the base of the diamictite is similar with $\delta^{13}C_{carb}$ at +3 ‰, $\delta^{18}O$ -3.7 ‰. However, three analyses of the limestone unit within the diamictite higher up have $\delta^{13}C_{carb}$ close to -4 ‰ and variable $\delta^{18}O$ (-4 to -9‰). A stromatolitic dolostone clast, and the fine-grained dolomitic matrix of the lower part of the diamictite have similarly depleted $\delta^{13}C_{carb}$ (ca. -3 ‰). There is a single sample of positive $\delta^{13}C_{carb}$ in the black dolostone overlying the diamictite, which also has unusually heavy $\delta^{18}O$ (-0.8 ‰). Two higher limestone horizons from the upward

transition to the Kanunnah Subgroup have strongly depleted, in part probably diagenetic isotopic compositions ($\delta^{13}C_{carb}$ -5 ‰ and -12 ‰).

Organic carbon isotopic compositions display a broadly parallel, but somewhat steeper fall from approximately -24 ‰ below the diamictite to approximately -34 ‰ around the top of the diamictite (Fig. 5.4). Also shown on Fig. 5.4 are organic carbon isotopic compositions with a correction factor applied ($\delta^{13}C_{org}{}^{N}$) to take account of an inherent observed TOC-$\delta^{13}C$ covariation, as described in Chapter 2. 'Corrected' and raw organic data show the same trend. Parallelism of $\delta^{13}C_{org}$ and $\delta^{13}C_{carb}$ signals is considered strong evidence for a primary origin (e.g. Knoll et al., 1986; Margaritz et al., 1992). $\delta^{13}C_{carb}$ of the dolostone above the diamictite seems to be an anomalously high. $\Delta\delta$ of this sample is very high (ca. 35 ‰) relative to $\Delta\delta$ in the lower part of the section (ca. 28 ‰).

Trace element analyses (Table 5.1) show that dolostones below the diamictite in both sections have low Sr (30 - 87 ppm) and low Mn contents (60 - 180 ppm). [Sr] is higher in the dolostone overlying the diamictite and in the dolostone just above the base of the diamictite (200 ppm).

The limestone unit within the diamictite contains 900 - 1200 ppm Sr. Initial $^{87}Sr/^{86}Sr$ ratios of this limestone are low (0.7063 - 0.7066, three determinations, Table 5.1). The sample with heaviest $\delta^{18}O$ has the lowest $^{87}Sr/^{86}Sr$ ratio. Four $^{87}Sr/^{86}Sr$ determinations from dolostones in Forest 1 are higher (up to 0.7093). With all samples plotted, strontium isotopic compositions covary with the Mn/Sr ratio with $^{87}Sr/^{86}Sr = 0.7060$ at the origin (Fig. 5.5). Thus, the lowest $^{87}Sr/^{86}Sr$ ratios are the least-altered, and primary $^{87}Sr/^{86}Sr$ values of 0.7060 - 0.7063 are implied (cf. Marshall, 1992).

5.4c INTERPRETATION

The $\delta^{13}C_{carb}$ compositions in the lower and middle parts of the formation (+3 to +5 ‰) are considered minimally altered because of low Mn/Sr, high $\delta^{18}O$ and locally excellent textural preservation. A drop in $\delta^{13}C_{carb}$ either below the diamictite (Arthur River) or within the lower part of the diamictite (Forest 1) probably also reflects a primary signal, being corroborated by a similar fall in $\delta^{13}C_{org}$, and because low and consistent $^{87}Sr/^{86}Sr$ values in the limestone unit in Forest 1 appear to be minimally altered, implying little-altered $\delta^{13}C_{carb}$ (cf. Banner & Hanson, 1990).

The abundance of the stromatolitic clasts in the diamictite in Forest 1 suggests local (intraformational) derivation. The stromatolitic clasts are similar to the basal

stromatolitic unit in the Arthur River section, but the slightly depleted carbon isotopic composition obtained from a stromatolitic clast within the diamictite in Forest 1 suggests that these clasts were probably derived from a unit high in the formation, not preserved in Forest 1, rather than from the (moderately ^{13}C-enriched) basal unit.

The carbon isotope profiles suggest that the base of the diamictite is younger at Arthur River than at Forest 1, in spite of the greater thickness of diamictite at the former locality. However, other interpretations are possible given the sparsity of data, for example that the base of the diamictite at Arthur River is equivalent in age to the minor negative excursion lower in the Forest 1 section.

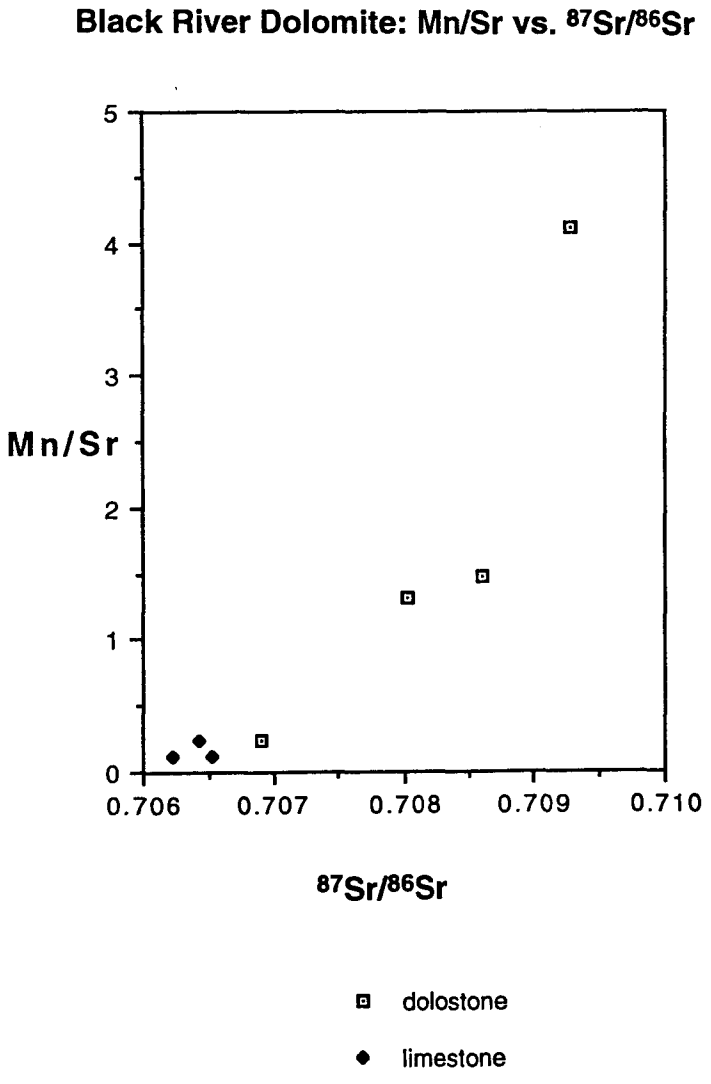

Fig. 5.5: Plot of $^{87}Sr/^{86}Sr$ vs. Mn/Sr, Black River Dolomite.

sample	rocktype	Sr(ppm)	Mn(ppm)	Mn/Sr	87Sr/86Sr	∂13C	∂18O	Rb(ppm)	87/86Srinit
Arthur River									
13.03	dolostone	58	104	1.79					
14.07	dolostone	30	64	2.13					
13.01a	dolostone	59	130	2.20					
Forest 1 drillhole									
21.01	dolostone	238	60	0.25	0.70691	3.01	-3.70		
21.02	dolostone	48	70	1.48	0.70861				
21.22	dolostone	56	322	5.75		-2.66	-6.03		
21.29	dolostone	178	199	1.12		1.64	-0.50		
21.03	dolostone	34	141	4.12	0.70926				
21.04	dolostone	53	70	1.32	0.70802				
21.05	limestone	1088	137	0.13	0.70656			0.061	0.70655
21.06	limestone	1196	161	0.13	0.70634			0.095	0.70633
21.07	limestone	937	227	0.24	0.70647	-4.11	-7.26	0.559	0.70646
21.09	dolostone	87	181	2.08		3.82	-8.56		

Table 5.1: Trace-element and strontium isotopic data, Black River Dolomite.

5.5 Kanunnah Subgroup

5.5a STRATIGRAPHY

The Kanunnah Subgroup consists predominantly of sedimentary rocks (shale, siltstone, volcaniclastic sandstone and conglomerate) known as the Keppel Creek Formation. A number of basalt flows are known collectively as the Spinks Creek Volcanics, and near the base there is an impersistent diamictite (the Croles Hill Formation) (Everard et al., 1994). The Kanunnah Subgroup is roughly 1200 m thick in the eastern and central Smithton Basin (Williams, 1989, Fig. 14.1), but is markedly thinner (ca. 500 m) at the western edge (Calver & Everard, in prep.).

In Forest 1 (Fig. 5.6) the sequence consists mainly of thick-bedded, fine- to coarse-grained volcaniclastic sandstone, with interbeds of siltstone and mudstone. The sandstone beds are usually graded, with sharp, often load-casted bases and sometimes laminated tops. The beds are considered to be turbidites (Brown, 1985). Sandstone is almost entirely of basaltic provenance. Basaltic breccia and conglomerate and three basalt flows were intersected in the hole.

About twenty-five percent of the drillhole section consists of fine-grained sedimentary units: thin-bedded, fine-grained sandstone, siltstone and mudstone. Turbidite structures are still present in the sandstone and siltstone: grading, climbing-ripple cross-lamination, plane-lamination. Mudstones are mostly grey-green to purplish but there are also distinct, sharply-bounded layers of black shale a few mm to a few cm in thickness. Some of these appear to be the sources of residual oil stains. The black shale has a distinctive appearance in thin section, consisting of thin (5-20μ), wavy anastamosing films of opaque organic matter in a matrix of claystone with scattered coarse silt grains and microscopic pods of diagenetic calcite (Plate 2.1). Almost identical fabrics have been described from the Belt Supergroup by Scheiber (1986, 1989) and ascribed an origin as benthic microbial mats (see Chapter 2). The grey-green mudstone associated with the black shale bands is slightly coarser, better sorted and is often faintly planar-laminated and gradational with underlying siltstone and sandstone. The grey-green mudstone layers are therefore probably of turbidite origin (Bouma Et division) while the black shale layers represent pelagic sedimentation (Ep division). As in the Belt Supergroup, thin, wispy intraclasts of black shale are abundant in some grey-green mudstone and siltstone layers (Plate 2.3).

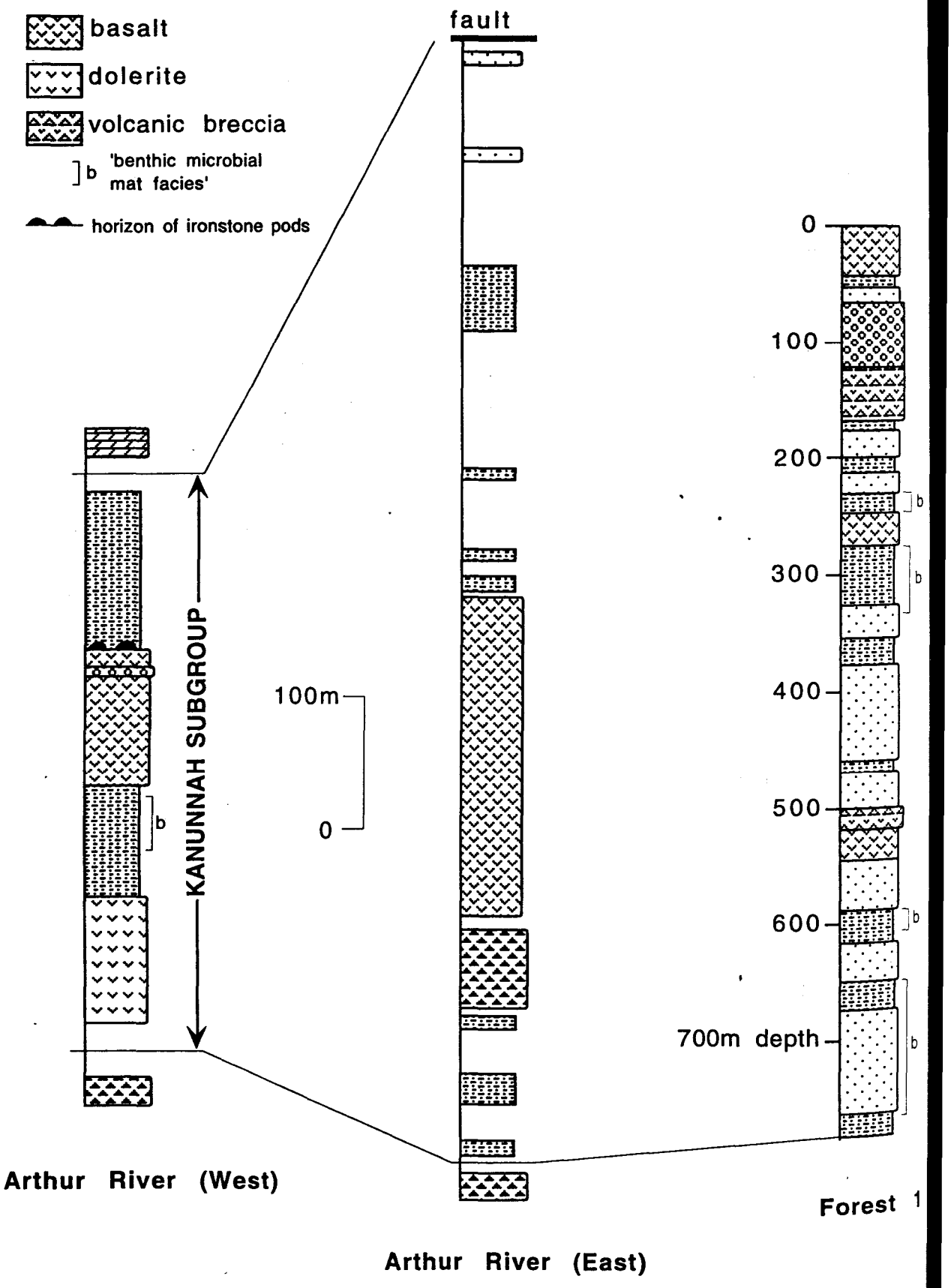

Fig. 5.6: Lithostratigraphy of the Kanunnah Subgroup at western Arthur River section, eastern Arthur River section and Forest 1 drillhole. Depths in Forest 1 corrected to true stratigraphic thickness.

A transect through the Kanunnah Subgroup along the Arthur River in the eastern part of the Basin (Fig. 5.6) consists of (from the base) roughly 120 m of grey-green and black, thin-bedded mudstone and siltstone; approximately 70 m of diamictite with predominantly basalt clasts (Croles Hill Diamictite); an uncertain thickness (probably around 250 m) of basalt; topped by an uncertain thickness (around 500 m) of grey to purplish siltstone, mudstone and fine-grained lithic sandstone. Outcrop of the sedimentary rocks is very poor.

On the western margin of the Basin, a relatively well-exposed outcrop section in the Arthur River is illustrated in Fig. 5.6. A dolerite sheet at the base of the section has a discordant, probably intrusive upper contact with 80 m of black to dark grey-green shale and siltstone. The upper part of this unit has the distinctively banded black-and-grey appearance of the 'benthic mat' facies described above. Then follows 80 m of basalt, 4 m of conglomerate containing well-rounded cobbles of basalt; then 15 m of basalt. This final basalt flow is overlain by a laterally spaced series of ironstone pods, 0.5 -1 m thick and 2 - 3 m wide. The central parts of the pods are composed of close-spaced columnar stromatolites composed of alternating cherty ironstone and minor carbonate laminae. The ironstone pods are onlapped and buried by 100 m or so of thinly interbedded grey-green siltstone, shale and sandstone, fining up to green and black, laminated shale and siltstone. The sandstone-siltstone layers are weakly graded, with sharp, undulose bases and occasional low-angle cross-lamination. These 'event beds' could be either turbidites or storm beds.

The Kanunnah Subgroup is therefore laterally variable across the Smithton Basin. Basalt flows are variable from place to place in stratigraphic position and number. The sedimentary succession is dominated by thick-bedded, basalt-derived volcaniclastic turbidites in the north-east (Forest 1), but is finer-grained, perhaps more distal, in the south and west. Fossil benthic microbial mats, if of photosynthetic origin (see Chapter 2 for discussion) may place constraints on depth of deposition.

The stromatolitic ironstone pods attest to exhalative activity associated with vulcanism and may be an example of microbially-mediated precipitation of hydrothermal iron and silica. Filamentous microbial forms are known from a number of ancient and modern hydrothermal iron-silica deposits, in some cases associated with volcanogenic massive sulphide occurrences (e.g. Duhig et al., 1992). Many of these are deep-water (e.g. Juniper & Fouquet 1988; Duhig et al., 1992), and the organisms are interpreted to be chemoautotrophs. The development of stromatolites and discrete bioherm-like pods in

the Arthur River occurrence suggests that the microbial mats were moulded by more or less persistent current action, and a relatively shallow environment is inferred.

5.5b Isotope Geochemistry

Only a few isotopic determinations were made from the Kanunnah Subgroup, all from the Forest 1 drillhole. Organic carbon from a black mudstone from the base of the unit is very low in ^{13}C (-35 ‰). Thin beds of impure limestone higher up are clearly of diagenetic origin to judge by one analysis at 694 m ($\delta^{13}C_{carb}$ = -11.9 ‰; Fig 5.4). A sample of the 'benthic microbial mat facies' and an adjacent shale were analysed from 321 m. As with nearly all other examples of this facies from Ediacarian successions from mainland Australia, organic carbon from the benthic microbial mat sample was distinctly more depleted in ^{13}C than the associated shale (Table 2.2 ; see Chapter 2 for a discussion).

5.6 Smithton Dolomite

5.6a Stratigraphy

In the northern Montagu River valley the Smithton Dolomite consists of two units (Fig. 5.7): a lower member, about 500 m thick, of dolomicrite and dolomite packstone and grainstone that have relatively well-preserved primary textures; and an upper member, about 1000 m thick, of massive crystalline dolostone with obscured primary textures. Limestone is a minor component of the upper member, but not of the lower. Dolostones throughout the formation appear pure, with little or no terrigenous component, and are grey to white in colour.

A brief reconnaissance suggests the two members can also be recognised in the Duck River valley, where dolomicrite crops out near the base of the formation at Scotchtown and in the Smithton Quarry, and massive crystalline dolostone occurs higher in the sequence in the Duck River at CQ 353616 and near Roger River West [CQ 310524-302536]. However, in the south, in the Arthur River, almost all outcrop is crystalline dolostone and the lower member appears to be absent (Calver & Everard, in prep).

Lower member

The lower member consists of pale grey micritic dolostone, often thinly bedded or laminated; with minor grainstone, and minor medium-crystalline dolostone similar to the upper member. Between 300 and 320 m above the base of the formation

dolomicrite contains abundant (up to 20% of rock volume) irregular quartz nodules. In thin section (sample 11.48) the quartz consists partly of bladed or lath-like crystals in radiating or felted aggregates, indicating an origin as anhydrite (see Chowns & Elkins, 1974).

Thin sections of some micritic dolostones reveal a wackestone or packstone texture, with small peloids and intraclasts in a cloudy microspar matrix that is probably recrystallised dolomicrite. There are also true dolomicrites (< 4μ grainsize), of which one example has abundant spar-filled fenestrae and an irregular eroded hardground (sample 11.41).

Intraclasts, peloids and ooids in grainstones are bound by a thin (20 μ) isopachous cement and later pore-filling xenotopic fine-grained dolospar cement. Ooids are small (0.1-0.5 mm) and have micritic, simple or weakly concentric cortices (Plate 5.3), and in many cases a large central pore space sometimes with internal geopetal sediment and occluded by coarse clear dolomite or calcite spar. In some instances, allochems have flattened, wispy shapes suggestive of compactive grain collapse following partial dissolution in early diagenesis. There are irregular, wavy, discontinuous dolomicrite layers, with a weak internal microlamination, possibly of microbial origin. One such layer (thin section 001662) contains small rectangular fenestrae, probably pseudomorphs of dolospar after anhydrite.

A small domical stromatolite overlain by grainstone is present under the Stuarts Road bridge [CQ 254829]. No limestones are kown in the lower member, and the dolostones are nearly all non-ferroan.

Upper member

The upper member consists predominantly of massive, grey to white, medium-crystalline (1/8-1/4 mm) dolostone. The dolostone in thin sections is pale brown, pseudopleochroic, and of idiotopic to xenotopic habit. Minor coarse-grained calcite spar is present in some samples (Plate 5.4). About half the thin sections show remnant poorly-preserved 'ghost' textures resembling coarse-grained (½-1 mm) ooid grainstone.

In the Montagu River section, limestone crops out at 750, 950 and 1100 m above the base of the formation (Fig 5.7). At 750 m black, impure (muddy) limestone is interbedded with black shale. At 950 m, dark grey micritic limestone is thinly interbedded with calcareous mudstone. One thin section (11.34) shows weakly cleaved calcite microspar partially replaced by ferroan dolospar; in another (11.36) microspar contains unusual tubular (0.5 × 2 mm) dolospar-filled fenestrae, possibly burrows. The

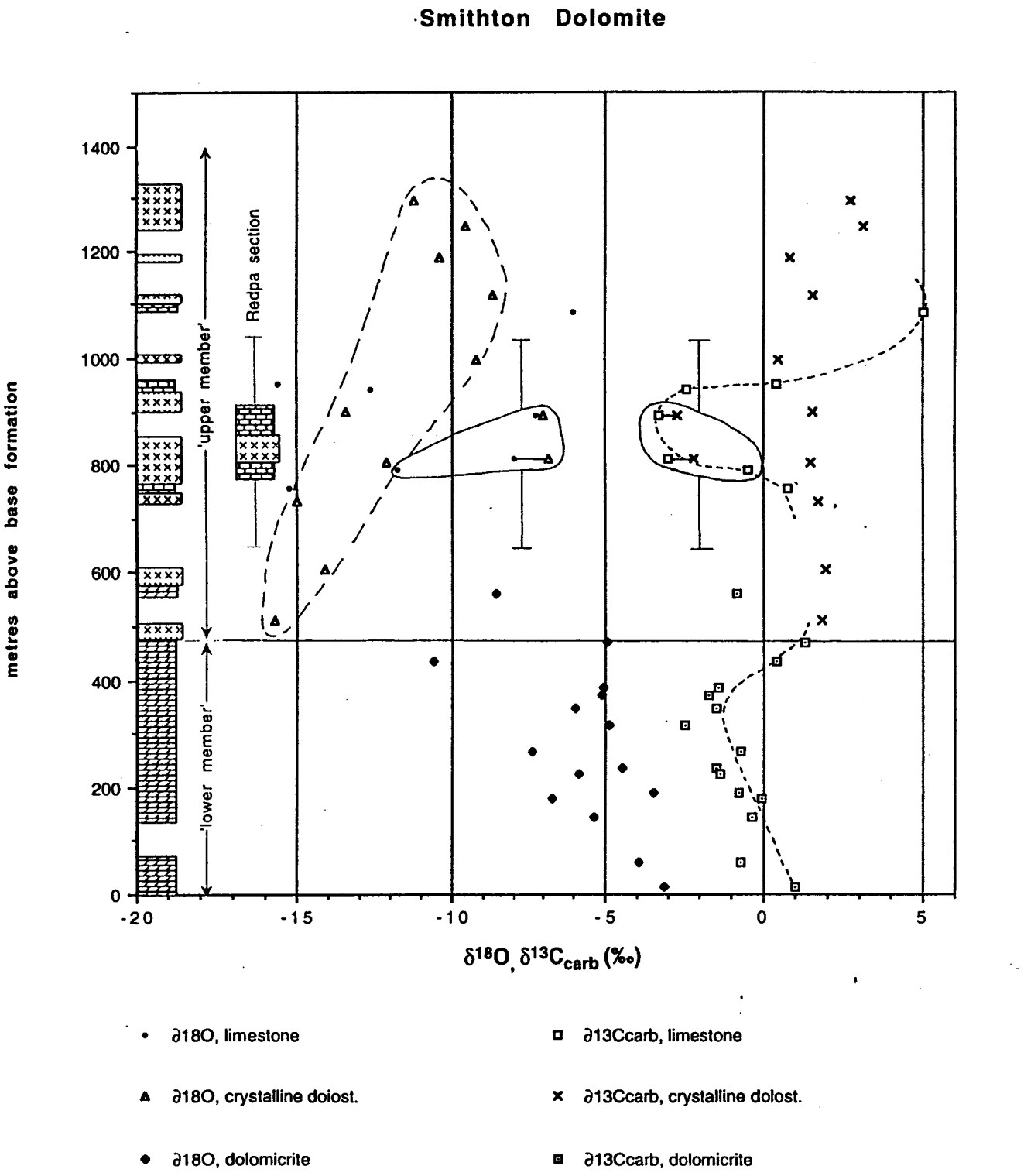

Fig. 5.7: Lithologic column and carbonate isotopic data, Smithton Dolomite, Montagu River and Redpa sections. Outlined groups of points (solid lines) are from the Redpa section; error bars indicate uncertainty in stratigraphic placement. Outlined $\delta^{18}O$ data (long-dashed line) are from crystalline dolostones at Montagu River section, highlighting upward-increasing stratigraphic trend. Short-dashed line through $\delta^{13}C_{carb}$ data represents inferred least-altered trend based on dolomicrite and limestone isotopic compositions.

limestone at 1100 m contains coarse quartz sand grains and small, well-rounded quartzite pebbles.

There is a large isolated outcrop of limestone near Redpa in the western part of the Smithton Basin (Fig. 5.2). This outcrop represents about 130 m (true stratigraphic thickness) of limestone and dolomitic limestone,and is 700-1000 m above the base of the formation (Fig 5.7), approximately at the same stratigraphic level as the limestone occurrences in the northern Montagu valley. The section begins with massive crystalline dolostone, and small isolated outcrops of massive dolostone occur in the paddocks to the west (i.e., at older stratigraphic levels). In the lower part of the limestone section and also near the top of the exposure there is interbedded oolitic grainstone, micritic limestone, and limestone with thin (5-10 mm) discontinuous layers ('stringers') of secondary dolostone. Herringbone crossbedding is present in the oolitic grainstone. A thin section of grainstone (Plate 5.5) shows well-preserved, dark brown radial-fibrous ooids 1 mm in diameter bound by a clear spar cement. Parts of the rock are replaced by granular ferroan dolomite.

5.6b Isotope Geochemistry

In the Montagu River section a broad, gentle negative excursion is seen in the lower member (Fig. 5.7). The lowermost sample has $\delta^{13}C_{carb}$ of +1 ‰; all higher samples in the lower member are slightly negative (0 to -2 ‰) except for the uppermost two, again around +1 ‰. $\delta^{18}O$ are mainly in the range -3 to -7 ‰. There is no consistent difference in isotopic composition between dolomicrites and dolospar - rich samples.

The crystalline dolostones comprising most of the upper member continue the trend of mild ^{13}C enrichment (+1 to +2 ‰) commenced in the uppermost lower member. Two limestone samples are a little lighter and one limestone notably so (-2.5 ‰, at 950 m). The uppermost limestone outcrop (1100m) is distinctly enriched at +5 ‰, but crystalline dolostones higher up are only +1 to +3 ‰.

The limestone section at Redpa begins with $\delta^{13}C_{carb}$ of -0.5 ‰ but is mostly quite strongly depleted (-3 ‰). Volumetrically minor crystalline dolostone in this section is enriched in ^{13}C by 0.7 to 1 ‰ (and in ^{18}O by 0.2 to 1.1 ‰) relative to co-existing limestone. The stratigraphic position of the Redpa section relative to the Montagu River section is uncertain, but it could be roughly equivalent to the single, similarly depleted limestone sample (Fig. 5.7).

sample	rocktype	member	Sr(ppm)	Mn(ppm)	Mn/Sr	87Sr/86Sr	∂13C	∂18O	Rb(ppm)	87/86Srinit
Montagu River section										
10.15	dolost.	upper	86	48	0.56		2.0	-13.8		
10.18	dolost.	upper	78	40	0.51		1.8	-15.4		
11.14	dolost.	upper	144	34	0.24		2.7	-10.9		
11.17	dolost.	upper	119	30	0.25		3.1	-9.3		
11.21	dolost.	upper	114	60	0.53		1.5	-8.4		
11.30	dolost.	upper	102	158	1.55		1.5	-13.3		
11.36	lst.	upper	236	127	0.54		0.4	-15.6		
11.39	lst.	upper	527	54	0.10	0.70850	5.0	-6.0	0.049	0.70850
10.14	dolost.	lower	84	122	1.45		-0.9	-8.3		
10.21	dolost.	lower	75	70	0.93		1.3	-4.7		
11.07	dolost.	lower	51	325	6.37		1.0	-2.8		
11.09	dolost.	lower	59	131	2.22		-1.5	-4.2		
11.41	dolost.	lower	87	104	1.20		-1.7	-4.8		
11.50	dolost.	lower	76	73	0.96		-0.7	-7.1		
11.53	dolost.	lower	57	50	0.88		-0.1	-6.5		
Montagu River area										
1661	dolost.	lower				0.70866				
1662	dolost.	lower				0.70891				
1663	dolost.	lower	95	55	0.58	0.70858				
1664	dolost.	lower	58	75	1.29	0.70914				
1665	dolost.	lower	79	102	1.29	0.70981				
Redpa section										
17.14	lst.	upper	127	37	0.29					
17.16	lst.	upper	141	18	0.13		-0.5	-11.8		
17.18	lst.	upper	199	23	0.12	0.70821	-3.3	-7.3	0.237	0.70817
2037d	dolost.	upper	209	19	0.09		-2.2	-6.6		
2037l	lst.	upper	274	21	0.08	0.70824	-3.0	-8.0	0.004	0.70823
2037		upper	274			0.70832			0.004	0.70831
Smithton Quarry										
S2	dolost.	lower	83	70	0.85	0.70840	0.1	-4.9		
S3	dolost.	lower	63	70	1.12	0.70991				
S4	dolost.	lower	47	70	1.51					

Table 5.2: Trace-element and strontium isotopic data, Smithton Dolomite.

The upper member is for the most part much more strongly depleted in $\delta^{18}O$ than the lower member: mostly -9 to -16 ‰. The heaviest $\delta^{18}O$ value, -6 ‰, corresponds to the most ^{13}C-enriched sample, this being the limestone with $\delta^{13}C_{carb}$ of +5 ‰. The crystalline dolostones display an upward-increasing trend in $\delta^{18}O$ from -16 ‰ at the base of the member to around -10 ‰ in the upper part (Fig. 5.7).

Trace-element compositions also differ systematically between lower and upper members. The lower member has 70 ± 15 ppm Sr and 101 ± 69 ppm Mn (n = 13); dolostones of the upper member are distinctly higher in Sr (122 ± 41 ppm) and lower in

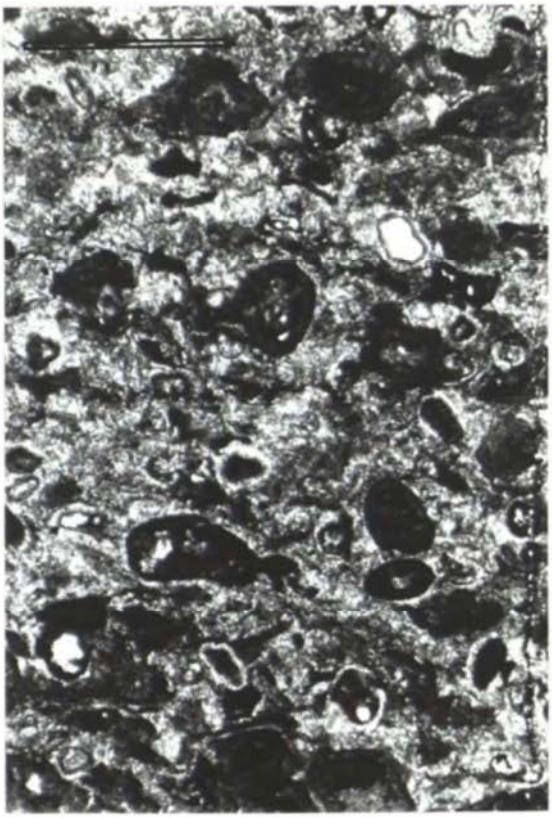

Plate 5.3: Thin section showing texturally well-preserved oolitic dolograinstone, lower member of Smithon Dolomite, Montagu River area. Sample 001661. Scale bar = 1mm.

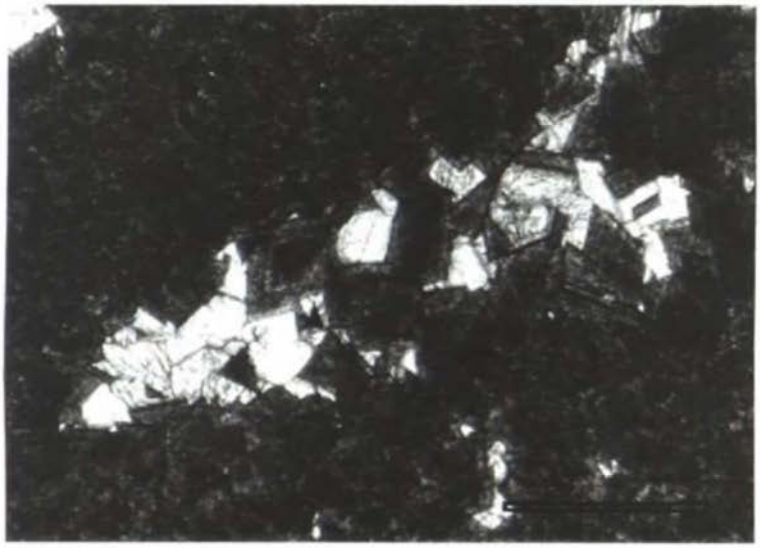

Plate 5.4: Thin section showing turbid, fabric-destructive coarse dolomitization characteristic of upper member of Smithton Dolomite; clear late calcite fills void. Sample 11.14, 1295 m, Montagu River section. Scale bar = 1mm.

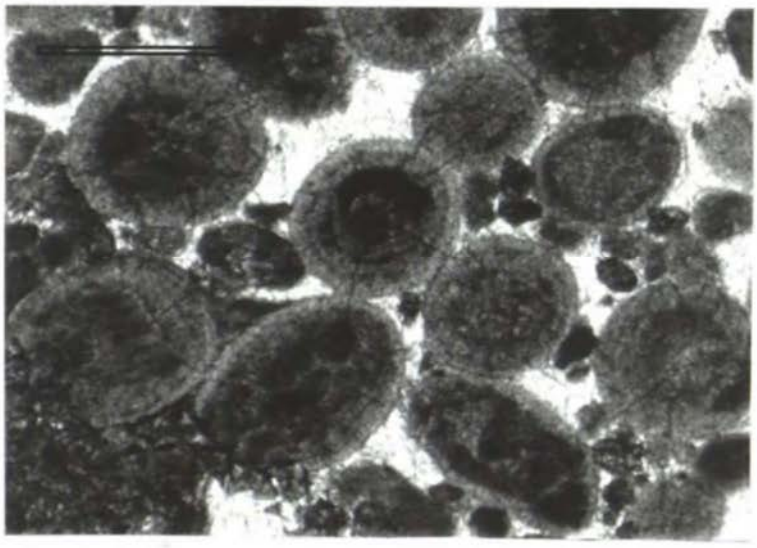

Plate 5.5: Thin section of oolitic limestone from the upper member of the Smithton Dolomite. Replacive granular ferroan dolomite at lower left. Sample 17.18, 890 m, Redpa section. Scale bar = 1mm.

Mn (56 ± 44 ppm; n = 7). Limestones (restricted to the upper member) have 251 ± 134 ppm Sr and 47 ± 38 ppm Mn (n = 6).

Seven $^{87}Sr/^{86}Sr$ determinations from dolostones of the lower member range from probably little-altered (0.7084) to considerably altered (0.7099) (Table 5.2). Two, probably little-altered determinations from the Redpa limestone section (upper member) are 0.70817 and 0.70824. Strontium contents of these samples (199, 274 ppm) are low compared to samples preserving inferred near-primary $^{87}Sr/^{86}Sr$ in other units in this investigation (ca. 1000 ppm; e.g. Black River Dolomite, see above). However, in other respects the limestones appear little altered ($\delta^{18}O$ > -8 ‰; good textural preservation; Mn/Sr only 0.1) and the succession as a whole appears very low in clays that are a major source of diagenetic ^{87}Sr. The relatively low Sr contents may be an indication of an original high-Mg calcite (rather than aragonite) mineralogy. A sample from the topmost limestone unit (with $\delta^{13}C_{carb}$ of +5 ‰) has $^{87}Sr/^{86}Sr$ of 0.70850. The strontium content is higher (527 ppm) and other criteria ($\delta^{18}O$, Mn/Sr) favour an interpretation as little-altered.

5.6c INTERPRETATION

The contrasting textures and geochemistry of the lower and upper members reflect early and late diagenetic dolomitization, respectively. Micritic grainsize and good textural preservation in the lower member is indicative of syndepositional or early diagenetic dolomitization (e.g. Tucker, 1983; Zempolitch et al., 1988). Very shallow-water, at times hypersaline conditions prevailed, allowing early dolomitization by a number of possible mechanisms (evaporative, seepage-reflux and mixing-zone models: Tucker & Wright, 1990). The cement-filled central pores of ooids indicate dissolution of a preexisting metastable phase (aragonite?), and the later occlusion of this secondary porosity by dolospar cement evidently post-dated compaction in some cases. With the possible exception of some grainstones, therefore, whole-rock $\delta^{13}C_{carb}$ is considered little-altered. The Mn/Sr index is low (Table 5.2).

On the other hand, the coarse, fabric-destructive dolomitization evident in the upper member is probably a burial-diagenetic phenomenon. The presence of remnant beds of oolitic limestone and 'ghost' ooids in the dolostone suggest that oolitic limestones may have originally comprised much of the upper member. Low [Sr] in the surviving limestones and the excellent textural preservation of limestone ooids suggest an original high-Mg calcite, rather than aragonite mineralogy (Sandberg, 1983; Brand & Veizer, 1980). Dolomitising fluids were probably oxidised since [Mn] is low. Very large

volumes of Mg-rich fluids must have been required to dolomitize the upper member, and seawater is an obvious possibility (e.g. Land, 1992). It is suggested that dolomitization of the upper member occurred by geothermal seawater convection sometime after the deposition of the Smithton Dolomite and before deposition of the Scopus Formation (in the middle Ediacarian to late Middle Cambrian interval; see below). The lower member was unaffected by this event, being already stabilised to dolostone. In this hypothesis, the upward-decreasing $\delta^{18}O$ profile in the upper member reflects the geothermal gradient at the time of dolomitization. The gradient in $\delta^{18}O$ (9 ‰ km^{-1}) implies a moderate geothermal gradient of approximately 35°C km^{-1}.

The high water-rock ratio required to bring about dolomitization means that carbon and strontium isotopic compositions of the crystalline dolostones of the upper member may have been shifted towards those of the circulating seawater, particularly in the upper part of the sediment pile. The primary $\delta^{13}C_{carb}$ and $^{87}Sr/^{86}Sr$ chemostratigraphic signal may therefore be preserved only in the limestones. The $\delta^{13}C_{carb}$ profile of upper member limestones displays a negative excursion to -3 ‰ followed by a steep rise to +5 ‰ (Fig. 5.7). The depleted limestones have probably-little-altered $^{87}Sr/^{86}Sr$ of 0.7082; this ratio increases to 0.7085 in the positive excursion.

A more detailed study of the isotope geochemistry of the upper member may constrain the timing of dolomitization, since in similar settings to that proposed, dolostones take on the C and Sr isotopic composition of the circulating seawater (cf. Saller, 1984).

5.7 Age and Correlation of the Togari Group

Black River Dolomite

The least-altered $^{87}Sr/^{86}Sr$ result of 0.7063 from the upper part of the Black River Dolomite provides a useful age constraint, given the configuration of the current 'global curve' of Neoproterozoic seawater $^{87}Sr/^{86}Sr$ variation (Fig. 1.13). The youngest known horizon that can be matched with this is in the lower Svanbergfjellet Formation (lower Akademikerbreen Group) in Spitzbergen (sample G19 of Derry et al., 1989) shown at 740 Ma in Fig. 1.13. This horizon is late Riphean, but its numerical age is poorly constrained (Derry et al., 1989). All younger known (published) Neoproterozoic $^{87}Sr/^{86}Sr$ ratios are distinctly higher (0.7066 or greater). Alternatively a match could be made with the more prolonged period of low $^{87}Sr/^{86}Sr$ between 775 and 825 Ma (Fig. 1.13). However, this part of the global curve is from the Shaler Group, which is known

to be older than 766 ± 24 Ma (Asmerom et al., 1991), distinctly greater than the maximum age constraint (708 Ma ?) for the Black River Dolomite.

A correlation of the Black River Dolomite with the lower Akademikerbreen Group is supported by a similarity of the $\delta^{13}C_{carb}$ profiles. In both, a plateau of moderately ^{13}C-enriched values (around +5 ‰ in the lower Akademikerbreen Group, between horizons 7 and 8 in Fig. 1.3) is succeeded by an excursion to negative values (-1 to -2 ‰ in the lower Svanbergfjellet Formation).

The negative $\delta^{13}C$ excursion in the lower Akademikerbreen Formation has been correlated on the basis of $\delta^{13}C$ stratigraphy with a probably-Sturtian glacigene unit in Namibia (Chuos Tillite: Kaufman et al., 1991; Kaufman & Knoll, 1995). Thus, correlation of the diamictite in the Black River Dolomite with the Sturtian glacials of the Adelaide Geosyncline is a possibility.

Stromatolite biostratigraphy is consistent with this correlation, since both *Baicalia burra* and *Conophyton garganicum* occur in the pre-Sturtian (Willouran - Torrensian) part of the Adelaide Geosyncline succession (Preiss, 1987d). However, a radiometric date of 802 ± 10 Ma on the Willouran Rook Tuff is older than the inferred maximum age of the Black River Dolomite.

A possible contradiction arises because the age of the Sturtian glacials is generally taken to be 750 - 800 Ma (e.g. Preiss, 1987c), greater than the supposed maximum age of the Black River Dolomite. However, the younger age limit for the Sturtian glacials is poorly constrained (Preiss, 1987c) and could be as much as 100 Ma younger (Walter et al., 1995). Also, the K-Ar dates constraining the maximum age of the Black River Dolomite may be in error (underestimates) because of argon loss.

Smithton Dolomite

The age of the Smithton Dolomite is constrained by radiometric dates of 580 - 600 Ma from dykes thought to be associated with the vulcanism of the Kanunnah Subgroup; and by late Middle Cambrian fossils in the overlying Scopus Formation. $^{87}Sr/^{86}Sr$ ratios thought to be little-altered are 0.7082 from limestone in the middle part of the formation, and 0.7085 from limestone higher up. Consistent with the known age constraints, these values indicate an Ediacarian age for the Smithton Dolomite (see Fig. 1.12). The carbon isotope profile of the Smithton Dolomite can also be matched in broad terms with the 'global' lower Ediacarian profile, which is probably best known from the Namibian sections (Fig. ; Kaufman et al., 1991; 1993). Limestone in the

middle of the Smithton Dolomite, with little-altered $^{87}Sr/^{86}Sr$ of 0.7082 and $\delta^{13}C_{carb}$ of -3 ‰, is a good chemostratigraphic match with carbonates in the Witvlei Group with $^{87}Sr/^{86}Sr$ of 0.7081 (Kaufman et al., 1993) and $\delta^{13}C_{carb}$ of -4 to -5 ‰ (Kaufman et al., 1991; see Fig. 1.4). Sparsity of data and unconformities within and at the base of the Witvlei Group preclude correlation of the lower part of the Smithton dolomite. The uppermost limestone horizon in the Smithton Dolomite - with $^{87}Sr/^{86}Sr$ of 0.7085 and $\delta^{13}C_{carb}$ of +5 ‰ - is a good match with the Zaris Formation of the lower Nama Group with least-altered $^{87}Sr/^{86}Sr$ of 0.7084 and $\delta^{13}C_{carb}$ around +5 ‰ (Kaufman et al., 1991; 1993).

One implication of the proposed correlation of the Smithton Dolomite is that the upper third of the formation lies within the range of Ediacara-type metazoan fossils and *Cloudina*.

5.8 King Island

On King Island, Proterozoic metasediments are intruded by granite dated at 760 Ma (Black, 1994) and overlain with inferred unconformity by an unmetamorphosed succession broadly similar to the Togari Group of the Smithton Basin (Waldron et al., in press). This succession begins with a thick shallow-water sandstone - siltstone sequence that forms most of the eastern half of the island. This is conformably overlain by diamictite (a thickness of 100 - 200 m can be inferred from Fig. 3 of Waldron et al., in press), laminated dolostone (20 - 50 m), siltstone with an upward-increasing volcaniclastic component (100 - 200 m) and then a thick succession of tholeiites, picrites and associated volcaniclastics. The basalts, like those of the Kanunnah Subgroup, have the chemical and geological characteristics of an intracontinental rift setting, but beyond this there is no closer geochemical similarity that would be persuasive evidence for a correlation (Waldron et al., in press). The diamictite, earlier considered glacigene (Carey, 1947), is now thought to be a debris flow (Waldron et al., in press). However, the overlying dolostone unit - laminated to thinly bedded, and grey to pink in colour - resembles base-Ediacarian 'cap dolostones' such as the Nuccaleena Formation of the Adelaide Geosyncline (see Chapter 3).

Three samples of the dolostone were analysed for stable isotopes. The samples (whose relative stratigraphic positions are unknown) show moderate depletion in ^{13}C ($\delta^{13}C_{carb}$ = -2.6 ± 0.2 ‰) and strong , non-uniform depletion in ^{18}O (-14.9 ± 2.5 ‰). These compositions are unlike that of the black dolostone overlying diamictite in the Forest 1

drillhole, which is slightly enriched in both ^{13}C and ^{18}O (see section 5.4b), but $\delta^{13}C_{carb}$ is similar to that of the Nuccaleena Formation and correlatives. Further work could readily determine whether the characteristic upward-decreasing $\delta^{13}C_{carb}$ profile of the Nuccaleena Formation is present in the King Island dolostone. With present data, little further can be said about the correlation of this unit.

5.9 The Jubilee Region

5.9a GEOLOGICAL SETTING

The Jubilee region adjoins the Tyennan region to the east, and the relationship of the two regions is poorly known. Jubilee successions may overlie rocks of the Tyennan region unconformably (e.g. Spry, 1962; E. Williams, 1979) or the regions may be broadly coeval. The latter alternative is suggested by a similar range of primary lithologies in both regions; and an overlap in tectonometamorphic rank with the (mostly higher-grade) Tyennan region (Calver, 1989b; 1990).

The oldest known succession in the Jubilee region consists of shallow-water orthoquartzite, siltstone, pelite and minor carbonate (the Clark Group and correlates, including the Mt Anne and Pandani Groups: Carey & Banks, 1954; Calver, 1989a, b; Calver et al., 1990). A gently angular unconformity separates this succession from the Weld River Group (Calver 1989c), a thick (few km) succession of dominantly dolostone with some diamictite and minor siliciclastics. Probably-glacigene units near the base and top of the Weld River Group (Calver, 1989c; unpubl.) suggest a broadly Cryogenian (850 - 600 Ma) age for this succession. A broad lithostratigraphic correlation of the Clark and Weld River Groups with the Rocky Cape and Togari Groups, respectively, of the Rocky Cape region has been proposed (Calver, 1989c). However there are no positively identified Proterozoic volcanics (Kanunnah Subgroup equivalents) in the Jubilee region.

In faulted juxtaposition with the Weld River Group and older units is an unfossiliferous lithicwacke-mudstone-chert-basalt-ultramafics association, the Ragged Basin Complex (Turner, 1989b). The ultramafics are chemically similar to those of the Dundas Trough, where an associated tonalite has been dated at 510 ± 6 Ma (latest Early Cambrian: Black, 1994).

The Proterozoic rocks and probably the Ragged Basin Complex are unconformably overlain by late Middle Cambrian siliciclastics (the Trial Ridge beds and correlates:

Turner, 1989b; Calver et al., 1990). Structural reorganisation into an imbricate stack of north- and east-facing thrust slices occurred around earliest Late Cambrian time, and further deformation occurred in the middle Devonian (Turner, 1989b; Calver, in prep.).

Thirty-five carbonates were analysed for stable isotopes in a reconnaissance chemostratigraphic survey of the Clark and Weld River Groups. Most of the samples were collected by the writer during geological mapping of the Pedder (Turner et al., 1985) and Styx (Calver, unpubl.) 1:50 000 mapsheets. Additionally, in the course of this project a traverse along the Huon River was undertaken in a search for more exposure; a detailed account of this traverse is given by Everard & Calver (in prep).

The Proterozoic successions are extensively disrupted by major faults, but lithostratigraphic correlation between fault blocks within the Jubilee Region is possible (Fig. 5.8). Only a brief outline of the lithostratigraphy is given here; for more detail see Calver (1989b) and Calver et al. (1990).

5.9b CLARK GROUP

The type area is at the Needles in the north of the region (Carey & Banks, 1954). The Needles Quartzite and correlates consist of 500 - 1000 m of supermature cross-bedded quartzarenite, and this unit is conformably overlain by several hundred metres of black, red and grey-green shales interbedded with dolostone and minor limestone. There are stromatolites, oolites and evaporite indicators (halite hopper casts, pseudomorphs of carbonate after gypsum, quartz nodules probably after anhydrite) in this carbonate-shale unit. 'Molar-tooth structures' (cement-filled, early diagenetic shrinkage cracks: Smith, 1968) are a feature of this unit, as they are of minor shaley carbonates in the Rocky Cape Group (Calver & Baillie, 1990).

This unit is succeeded by several hundred metres of shale and siltstone. At the top of the Clark Group correlative north of the Jubilee Range there is a second carbonate-bearing unit, which consists largely of intraclastic, stromatolitic and oolitic dolostone and minor limestone.

Isotope Geochemistry

A micritic limestone and an oolitic limestone from the first-mentioned carbonate-bearing unit have $\delta^{13}C_{carb}$ of 0.4 and 1.1 ‰ respectively. A single $^{87}Sr/^{86}Sr$ determination from this unit by Veizer & Compston (1976) is considerably elevated (0.71434) but their sample contained only 50 ppm Sr.

From the carbonate at the top of the Clark Group, single samples of micritic dolostone and micritic limestone are 1.6 and 1.2 ‰ in $\delta^{13}C_{carb}$, respectively. All samples from the Clark Group are rather low in ^{18}O (-10 to -14 ‰; Fig. 5.9).

5.9c Weld River Group

The Weld River Group overlies with gently angular unconformity or paraconformity, correlatives of the Clark Group (Calver, 1989c). A basal conglomerate and sandstone unit, the Annakananda Formation, is several hundred metres thick at Mt Bowes but is thin or absent in some places such as north of Jubilee Range. At two known localities, the Annakananda Formation is overlain by an apparently impersistent laminated shale-siltstone unit with pebble-sized lonestones (possibly glacial dropstones: Calver et al., 1990; Calver, unpubl).

The basal siliciclastics are overlain by 800 m of massive to laminated, fine-grained dolostone (the Gomorrah Dolomite). Stromatolites resembling *Conophyton* are known at one locality. Like the Smithton Dolomite, the Weld River Group dolostones have a characteristically 'clean', white to pale grey appearance with apparently very little in the way of terrigenous impurities. The Gomorrah Dolomite is succeeded by 1 - 2 km (thickness uncertain because of faulting) of alternating fine-grained (micritic or microsparitic) dolostone and oolitic dolograinstone, called the Devils Eye Dolomite. Petrography of the grainstones is described in detail in Calver et al. (1990). Ooids, intraclasts and catagraphs (irregular grains of possible microbial origin: Hofmann, 1987) are usually texturally well-preserved except that most ooids and catagraphs have a central pore space filled with clear dolospar. Cementation occurred early (prior to compaction) as shown by the prevalence of tangential contacts and the rarity of compactive deformation of grains. Quartz is common as a late-stage cement. Massive sucrosic crystalline dolostones (like the upper member of the Smithton Dolomite) are locally present.

The Devils Eye Dolomite is conformably succeeded by another unit of predominantly fine-grained dolostone (the Styx Dolomite). In faulted contact with the Styx Dolomite and the older units is the Cotcase Creek Formation, which is included in the Weld River Group on the grounds of lithologic similarity. Faulting, poor outcrop and rarity of facing indicators make this the most poorly-known part of the Weld River Group. There may be overlap in age between the Cotcase Creek and Styx Formations. The Cotcase Creek Formation consists of dolostone (predominantly fine-grained and massive, with minor grainstone), diamictite, shale and sandstone. Dolostones are

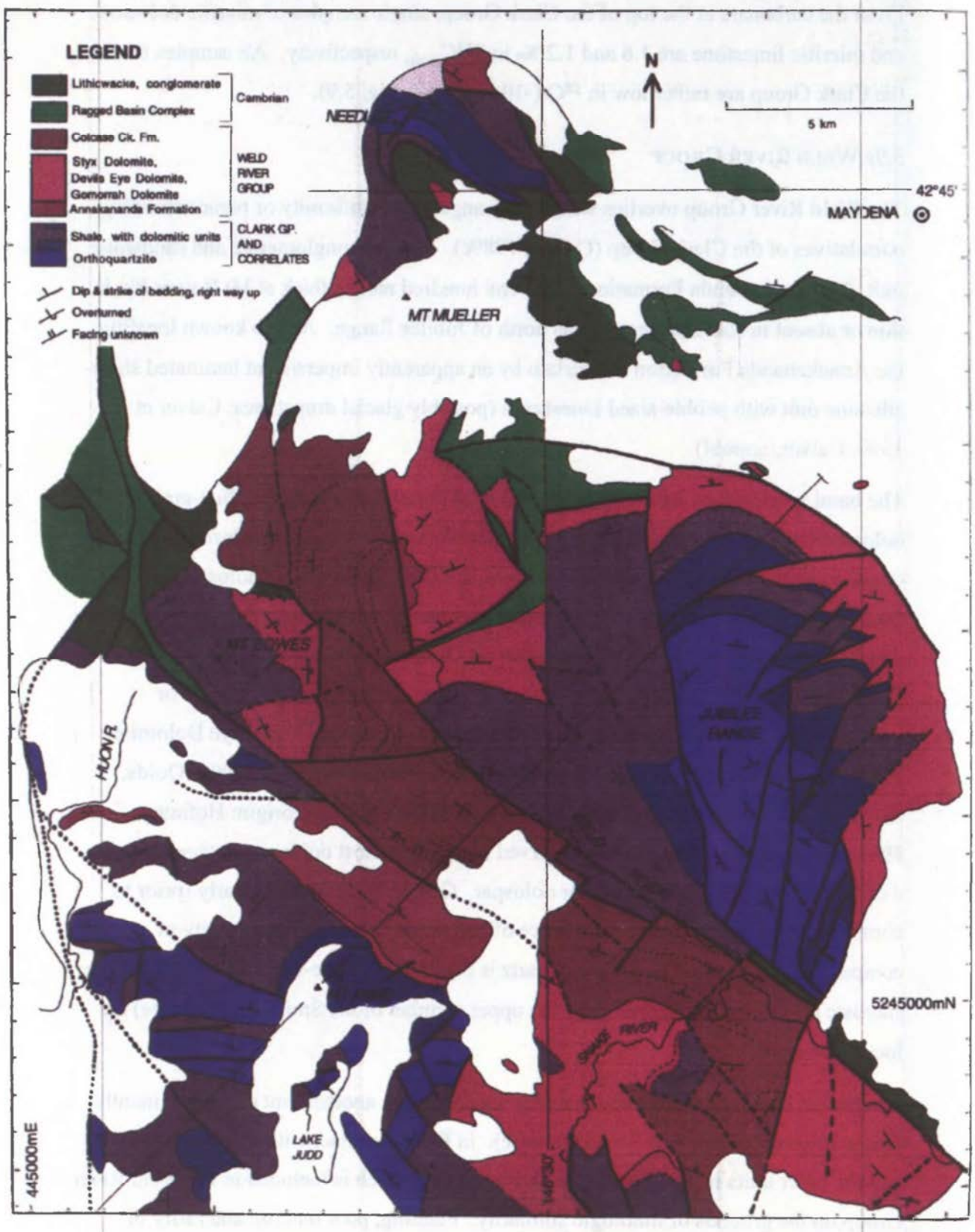

Fig. 5.8: Simplified geological map of the northern part of the Jubilee region. Adapted from Turner et al. (1985), Everard & Calver (in prep) and Calver (unpubl.).

mostly lithologically identical to the other fine-grained units (Gomorrah and Styx Formations).

The many diamictite occurrences may be structural repetitions of a smaller number of stratigraphic units. Diamictites are typically wholly massive, consisting of angular to subrounded clasts of pebble to (rarely) boulder size in a dark grey, dolomitic mudstone matrix. Clasts are predominantly dolostone identical to the enclosing sequence, but orthoquartzite, mudstone and chert are also present. 'Flatiron' and pentagonal shapes of probable glacial origin are seen in quartzite clasts in one extensive outcrop on the Huon River (Everard & Calver, in prep).

At four known localities there is a unit of interlaminated dolomitic shale and siltstone with sparse, granule and pebble-sized lonestones of dolostone and orthoquartzite. Sparse facing evidence suggests that at least three of these occurrences are at or near the top of the Cotcase Creek Formation. Probably all four belong to the same stratigraphic unit, and (as with the similar unit near the base of the Weld River Group) the lonestones are considered evidence for ice-rafting.

No limestones are known from the Weld River Group.

Isotope Geochemistry

In spite of the relatively small number of samples analysed and the great thickness of the succession, a twofold $\delta^{13}C$ chemostratigraphic subdivision of the Weld River Group is apparent (Figs. 5.9, 5.10). Samples from the Gomorrah and Devils Eye Formations all have $\delta^{13}C_{carb}$ below +1 ‰ and most are below 0 ‰. The most ^{13}C-depleted sample (-5.4 ‰) is a crystalline quartz-dolomite rock that is likely to have been isotopically altered.

No attempt is made to place the Cotcase Creek samples in stratigraphic order, except for two lonestone-bearing dolomitic laminites that are shown at the top of the formation (Fig.5.10). Carbon isotopic compositions are nearly all *above* +1 ‰. A single analysis from the Styx Dolomite at +5 ‰ suggests a grouping of this unit with the Cotcase Creek Formation, and possibly overlap in age.

Oxygen isotopic compositions of the Weld River Group are moderately heavy, with most samples above -6 ‰ and several above -2 ‰. There is a similar range in $\delta^{18}O$ in the Cotcase Creek as in the earlier dolostones (Fig. 5.9). The $\delta^{18}O$ compositions lend support to an interpretation of generally little-altered $\delta^{13}C_{carb}$.

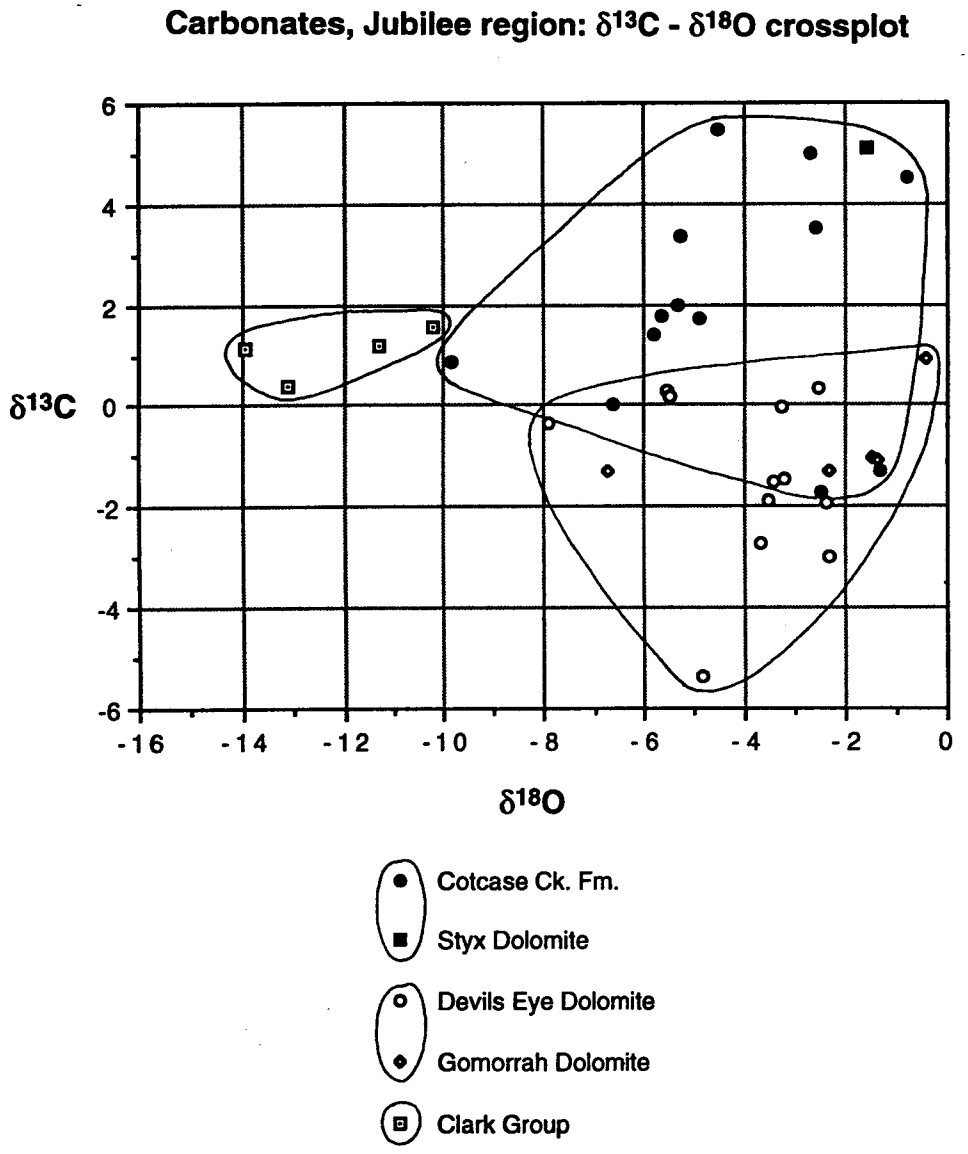

Fig. 5.9: $\delta^{13}C$-$\delta^{18}O$ crossplot of carbonates from the Jubilee region.

5.9d Correlation between Jubilee Region and Smithton Basin

Correlation of the Jubilee Region successions on the basis of the $\delta^{13}C$ data set presented here is severely hindered by the lack of corroborative data. There is clearly a broad lithologic similarity at group level between the Clark and Rocky Cape Groups, and between the Weld River and Togari Groups except that there is no known equivalent of the volcanic Kanunnah Subgroup in the Jubilee Region; and cherts such as those common in the Black River Dolomite are rare or absent in the Weld River Group.

However, the carbon isotope data would seem to preclude correlation of the lower part of the Weld River Group (Gomorrah and Devils Eye Dolomites) with the lower part of

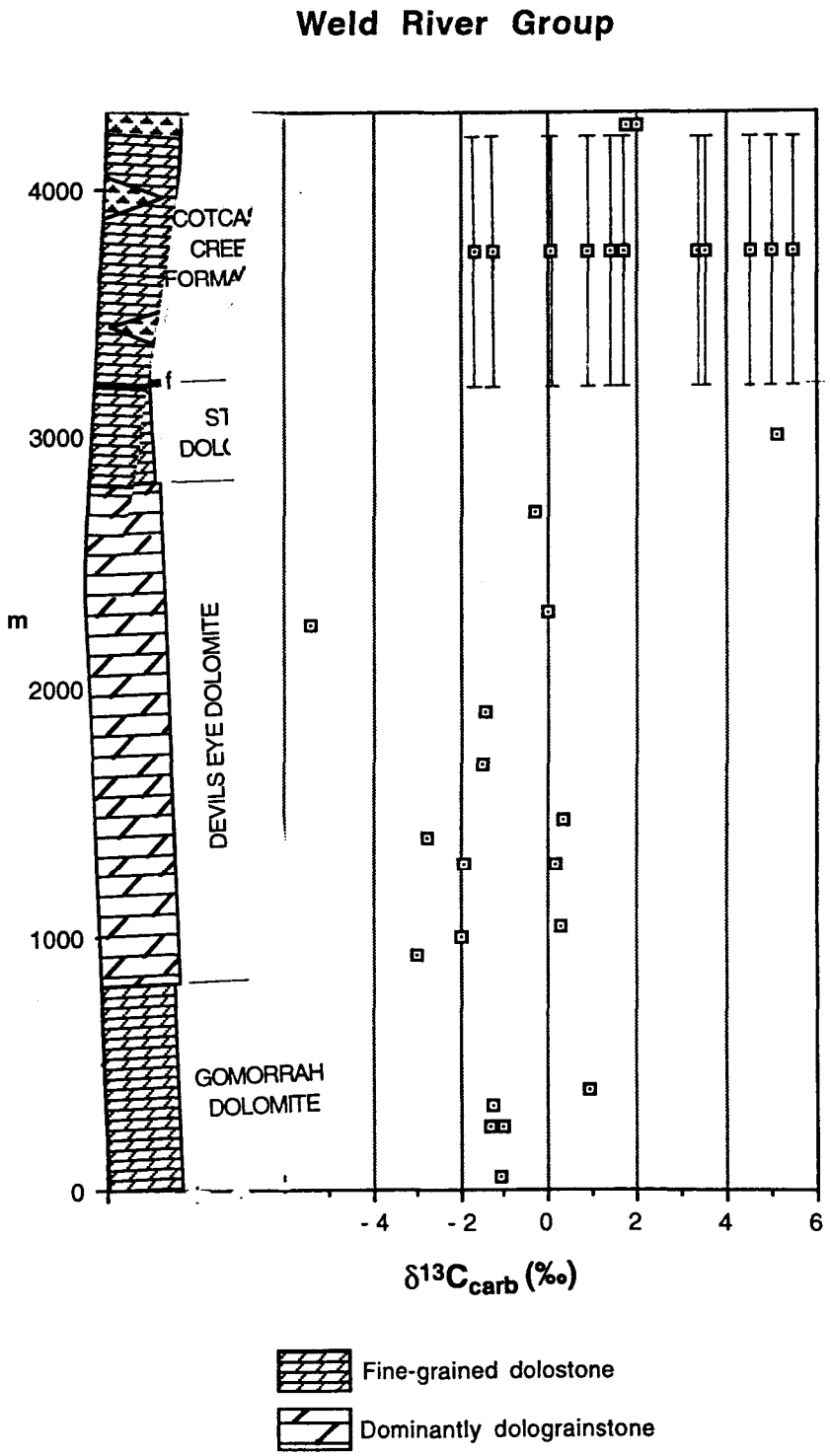

Fig. 5.10: Generalised lithologic column and stratigraphic plot of $\delta^{13}C_{carb}$ for the Weld River Group. Vertical error bars indicate uncertainty of stratigraphic placement.

the Togari Group (the moderately ^{13}C-enriched Black River Dolomite). Rather, there is a quite close stable-isotopic and lithologic resemblance of the Gomorrah and Devils Eye Formations with the Smithton Dolomite. The ^{13}C-enriched (up to +5 ‰) carbonates of the Styx and Cotcase Creek Formations may be lateral equivalents of similarly enriched limestone in the upper part of the Smithton Dolomite. No diamictites are known from the upper part of the Smithton Dolomite, but in Namibia the glacigene Vingerbreek Diamictite is thought to be of about this age on C- and Sr-isotope chemostratigraphic evidence (Kaufman et al., 1991; and see above). This correlation implies that the Black River Dolomite and the Kanunnah Subgroup are not represented in the Jubilee Region, and that the Weld River Group is mostly or entirely Ediacarian in age.

Alternatively, the Styx and Cotcase Creek Formations may be broadly equivalent to the Black River Dolomite and the older, relatively ^{13}C-depleted part of the Weld River Group may be unrepresented in the Smithton Basin. This alternative results in a better match of the diamictites.

Testing of these alternatives, with a Sr isotope survey of the Weld River Group or a search for acritarchs or other fossils, is required.

Poorly-preserved structures resembling the Ediacarian shelly fossil *Cloudina* are present in the Devils Eye Dolomite (S. Grant, pers. comm.). If substantiated, such an identification would strongly support the first alternative.

6

The Australian Ediacarian isotope-chemostratigraphic record and its correlation

6.1 Introduction

This chapter collates results from previous chapters to arrive at generalised Australian Ediacarian signals of secular variation in carbon, strontium, and sulphur isotopes, with the aim of correlation with previously published records on other continents. The discussion centres on carbon isotopes for which much the largest number of analyses have been obtained. For two reasons, it is not a straightforward matter to compare the Australian Ediacarian $\delta^{13}C$ record with similar-aged records elsewhere. Firstly, the published records on other continents are based almost wholly on $\delta^{13}C$ of shallow-water carbonates that are poorly represented in the Australian successions. In this study, a systematic and detailed approach using $\delta^{13}C$ of total organic carbon has been found useful in correlation within mainland Australia, but the organic $\delta^{13}C$ signal may in part reflect palaeoenvironmental and post-depositional factors as well as secular change in $\delta^{13}C_{DIC}$ (Hayes et al., 1983; Dean et al., 1986; Popp et al., 1989; and see section 2.3a). Secondly, some Australian Ediacarian carbonates such as the Wonoka Formation are anomalously ^{13}C-depleted and are here hypothesised to have formed in equilibrium with the lower layer of a stratified water column, a depositional setting not previously documented in Neoproterozoic carbonates (e.g. Kaufman & Knoll, 1995). Observed $\delta^{13}C_{org}$ records and simple modelling (section 3.6c) suggest that surface waters may be perturbed towards ^{13}C enrichment at the same time as bottom waters are perturbed towards strong ^{13}C depletion. Thus, a prerequisite in deriving an Australian Ediacarian $\delta^{13}C$ signal comparable with those of other continents (including Tasmania) is to assess the effects of basin stratification on the Australian $\delta^{13}C$ record, and accordingly the first part of this chapter is devoted to delineating the timing and extent of this phenomenon.

6.2 Ediacarian marine stratification - timing and extent

The preceding chapters have documented circumstantial evidence for stratification of basin waters at several widespread horizons in the Australian Ediacarian. The

interbasinal correlation scheme of Fig. 4. 37 allows the timing and extent of this phenomenon to be delineated.

The existence of basin stratification has important general implications for carbon isotope stratigraphy, and for Ediacarian palaeoceanography, sedimentology and palaeogeography. There is a prevailing assumption, implicit or explicit (e.g. Kaufman & Knoll, 1995) that carbon isotopic composition of little-altered Neoproterozoic carbonates reflect mixed or surface-layer seawater composition and therefore can be used to derive a global stratigraphic signal. Strong compositional divergence in $\delta^{13}C_{DIC}$ of upper and lower layers in limited parts of the ocean, and preservation in the geological record of carbonates equilibrated with the lower layer, have not been previously documented in the Neoproterozoic despite much circumstantial evidence for periods of stratification (e.g. Donnelly et al., 1990). Basin stratification with a hypersaline lower water mass suggests an arid palaeogeographic setting and a basin semi-isolated from the global ocean. The hypothesis therefore complements the 'Messinian-type' basin desiccation hypothesis for formation of deep canyons at one, and possibly two horizons in the Ediacarian of the Adelaide Geosyncline (von der Borch et al., 1989; Christie-Blick et al., 1990).

Three phenomena are considered to offer circumstantial evidence for basin stratification:

(i) Occurrence of evaporite minerals in marine palaeoenvironments of relatively deep-water aspect - that is, not of perilittoral setting. Hypersalinity of bottom waters is the clear implication.

(ii) Strongly ^{13}C-depleted carbonates ($\delta^{13}C_{carb} < -3$ ‰) of relatively deep-water (sublittoral) facies, with good evidence for preservation of depositional $\delta^{13}C_{carb}$. It is suggested that carbonates were precipitated within the lower layer as a result of increased alkalinity due to Fe^{3+} reduction or sulphate reduction; or, if precipitated from surface water, the carbonate later reequilibrated with bottom water, probably as a result of diagenetic stabilization to low-Mg calcite or dolomite. In all cases (upper Nuccaleena Formation and correlative cap dolostones in the Amadeus Basin; Wonoka Formation; limestone immediately below 'F' unconformity in Rodda beds) coexisting $\delta^{13}C_{org}$ is not depleted in parallel with $\delta^{13}C_{carb}$ but is enriched relative to underlying and overlying successions (typically -23 to -26 ‰), and is considered to reflect a relative enrichment of the isotopic composition of the surface layer where most fixation of carbon by pelagic organisms occurred. Thus, the $\delta^{13}C_{carb}$ signal in these intervals may

be considered a bottom-water proxy while the $\delta^{13}C_{org}{}^{N}$ signal might be considered to reflect changes in surface-water carbon isotopic composition.

(iii) Fossil benthic microbial mats with organic carbon isotopic compositions strongly depleted relative to coexisting organic carbon that is inferred to be of pelagic origin ($\Delta_{p\text{-}b} >> 0$). As indicated in section 2.3b, this phenomenon seems best explained by microbial mats fixing carbon from ^{13}C-depleted CO_2 at the sediment-water interface, with pelagic rainout being relatively ^{13}C-enriched through fixation in the surface layer.

Conversely, 'normal' $\delta^{13}C_{carb}$ (> -3 ‰) may be taken as evidence for sedimentation beneath a mixed water column or surface layer; and likewise benthic mat occurrences with $\delta^{13}C_{org}$ similar to that of associated carbon of pelagic origin ($\Delta_{p\text{-}b} \approx 0$). Also, evidence for high-energy, shallow-water deposition - oolitic carbonates such as the Julie Formation or uppermost Wonoka Formation; or texturally mature, cross-bedded quartzarenites such as the ABC Range Formation - may be taken as an indicator of upper-layer conditions at the sediment-water interface.

The phenomena suggestive of stratified conditions occur in a loose stratigraphic association (Fig. 6.1), reinforcing the idea that they have a common cause. Two broad stratigraphic zones are delineated, each delimited above and below by the converse association of features suggestive of shallow, well-ventilated or surface-water conditions. The upper zone contains the 'canyon' horizons at which Messinian-type desiccation events are proposed: two in the Adelaide Geosyncline (Christie-Blick et al., 1990) and one in the Officer Basin.

Individual occurrences of the features pertinent to basin stratification are briefly reiterated below.

Moderately depleted dolostones (-1.5 ‰) at the base of the Nuccaleena Formation and low in the cap dolostone at Mt Capitor conceivably reflect mixed-layer conditions but the trend to more depleted carbonate higher up (and the pattern of lateral variation in the Nuccaleena Formation: see section 3.3c) is consistent with sedimentation under a stratified water body that was becoming deeper, or increasingly stratified, or both.

In the Adelaide Geosyncline, rare evaporite is present in the upper Nuccaleena Formation (section 3.3). Strongly depleted benthic microbial mats occur in the lower Brachina Formation (section 3.4). Evaporite indicators are locally present in the upper Brachina Formation but these are associated with subaerial exposure (Dyson & von der Borch, 1983) and therefore cannot be construed as evidence for salinity stratification.

Minor evaporites are found in subtidal carbonates in Units 1, 4 and 5 of the lower to middle Wonoka Formation, and strongly-depleted carbonates (ca. -8 ‰) are characteristic of Units 3 - 7, in contrast to Units 9 and 11 at the top of the formation which have normal marine $\delta^{13}C_{carb}$ (0 to 2.5 ‰) (section 3.6).

In the Officer Basin, depleted benthic microbial mats were found at a single horizon in the 'Giles Mudstone' and minor anhydrite nodules are found higher up (section 3.8). Normal marine $\delta^{13}C_{carb}$ is characteristic of the Rodda beds except for ^{13}C-depleted limestone immediately below the canyon unconformity (section 3.10). Benthic microbial mats with similar isotopic composition to 'background' organic carbon in enclosing horizons occur within the interval of enriched $\delta^{13}C_{carb}$; while relatively ^{13}C-depleted benthic microbial mats occur stratigraphically higher, not far below the depleted carbonate.

In the Amadeus Basin, barite-filled microfenestrae in the upper part of the cap dolostone at Mt Capitor may be after sulphate evaporites (section 4.4). ^{13}C-depleted carbonates (-3.5 ‰) are present in the upper parts of the cap dolostones at Wallara 1 and Mt Capitor, and in the lower part of the Pertatataka Formation (-6 to -8 ‰: 'Halfway Dam Formation') (sections 4.4, 4.5). The strong *increase* in $\delta^{13}C_{org}$ through the cap dolostone (seen in Wallara 1, Amadeus Basin) is suggested to directly reflect the divergence in C isotopic composition between the surface and lower water masses, with the onset of stratification. Depleted benthic microbial mats are locally present in the lower Pertatataka Formation (sections 2.3b, 4.5b). The upper stratigraphic limit of this phase of basin stratification is not well constrained. ^{13}C-enriched carbonates are characteristic of the upper Pertatataka and Julie Formations.

Horizons marked by the incision of deep incised valleys or canyons in the Adelaide Geosyncline and Officer Basin (ca. 1 km deep in the case of the lower of two horizons in the Wonoka Formation) are also indicated in Fig. 6.1. Consistent with the link between salinity stratification and 'Messinian-type' basin isolation and desiccation, these horizons fall within or at the end of periods of basin stratification.

Stratification is a convenient hypothesis to account for this conjunction of phenomena, but as discussed previously in the case of the Wonoka Formation (section 3.6c), stratification appears to be contra-indicated by some features of the successions. Evidence for storm wave action at the sediment-water interface, and low TOC in what must almost certainly have been anoxic sedimentary environments beneath stratified water columns, are perhaps the two most outstanding such features. However, studies

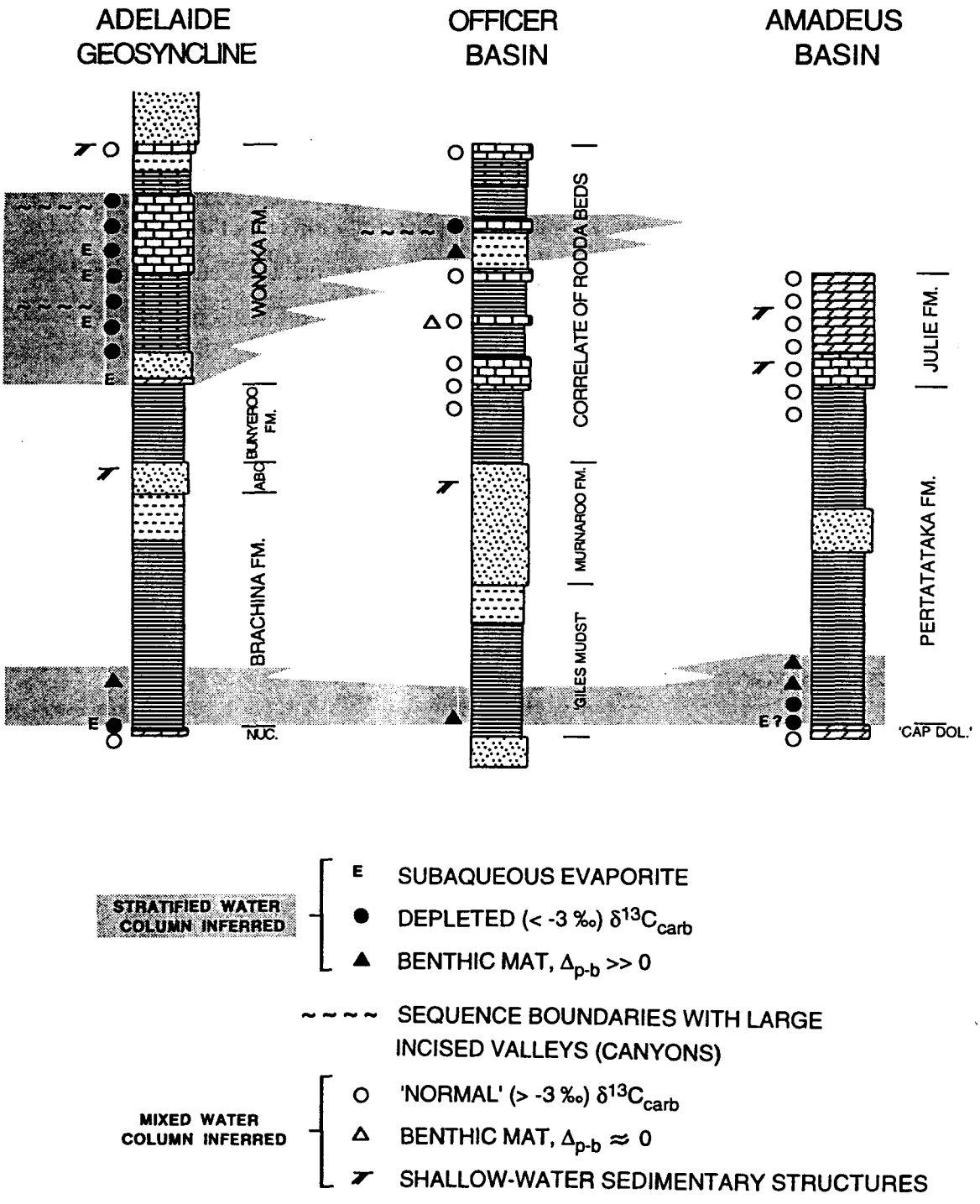

Fig. 6.1: Generalised stratigraphic columns (not to scale, but with timelines roughly horizontal) from the Adelaide Geosyncline, Officer Basin and Amadeus Basin showing distribution of features relating to stratification of the water column. See text for discussion.

of stratified lakes show that intermittent storm wave motion can be transmitted to the lower layer by internal seiching without breakdown of the pycnocline (Fisher et al., 1979; Heaps & Ramsbottom, 1966; Thorpe, 1974). Low TOC may be explained by low productivity (Pedersen & Calvert, 1990), and the distinctly Precambrian phenomena of an absence of refractory, terrestrial-derived organic matter, and absence of fecal-pellet packaging leading to highly efficient recycling of organic matter within the water column (Logan et al., in press).

Sulphur isotopes and basin stratification

Stratification of the water column appears to have had little effect on the isotopic composition of marine sulphate, with four samples showing no significant difference in $\delta^{34}S_{sulphate}$ between periods of inferred stratification or non-stratification. Two $\delta^{34}S_{sulphate}$ analyses fom the Nuccaleena Formation in SCYW1a and the 'Giles Mudstone' are, at 20 and 23 ‰ respectively, slightly less than younger horizons not associated with stratification (24 to 25 ‰: middle Rodda beds, Elkera Formation). This may simply reflect a general Neoproterozoic increase in world-ocean $\delta^{34}S$ (see next section). A single relatively depleted $\delta^{34}S_{sulphate}$ analysis of disseminated gypsum from the middle Wonoka Formation (9 ‰) is thought to be partly diagenetic in origin (section 3.6c). Pyrite $\delta^{34}S$ compositions are considered to predominantly reflect variations in the degree of closure during early diagenesis (section 4.5c).

Dissolved sulphate in restricted or isolated basins tends to be perturbed towards ^{34}S enrichment because of sequestering of ^{32}S into pyrite. Examples are the pre-Recent Black Sea basin (Vinogradov et al., 1962) and the Palaeozoic Selwyn Basin (Goodfellow, 1987), both characterised by highly enriched (+16 to +30 ‰) sulphides. However, it is likely that the trend towards ^{34}S enrichment in a *hypersaline* restricted basin (such as that proposed above for the Ediacarian) will be considerably muted or much slower than that in a normal-salinity or hyposaline basin such as the Black Sea. This is because evaporative concentration of sulphate (to levels up to five times normal salinity if gypsum saturation is attained) means that sulphate reduction will take much longer to approach completion and maximal ^{34}S enrichment, and may never be significant if some degree of reflux is involved (as is proposed for the Wonoka Formation basin: section 3.6c). Holser (1977) suggests some tens of millions of years are required to enrich $\delta^{34}S$ in hypothetical large hypersaline basins.

Because the molar concentration of sulphur in the ocean is much greater than that of carbon (presently about ten times higher), and because in bacterial sulphate reduction

two moles of carbon are oxidised for every mole of sulphur reduced (Goldhaber & Kaplan, 1974), bulk $\delta^{13}C_{DIC}$ in a restricted basin with negligible input of terrestrial organic matter (such as is proposed for the Ediacarian) could be considerably perturbed through processes involving sulphate reduction without significant effect on either $[SO_4^{2-}]$ or $\delta^{34}S_{sulphate}$.

6.3 The Isotope-Chemostratigraphic Record of the Australian Ediacarian

6.3a Carbon Isotopes

Carbon isotope chemostratigraphy in the Australian Ediacarian is hampered by a general dearth of carbonates, and by anomalous C isotopic compositions thought to be due to significant episodes of basin stratification. For example, in the entire 3500 m thickness of the type section of the Wilpena Group (the type Ediacarian at Bunyeroo Gorge) only about 15 m (units 9 and 11 of the upper Wonoka Formation) consists of shallow-water carbonates of the kind that have formed the basis of most previous studies in Neoproterozoic - Cambrian $\delta^{13}C$ chemostratigraphy (e.g. Kaufman et al., 1991; Narbonne et al., 1994; Brasier et al., 1990, 1994). Thus, derivation of an Australian Ediacarian $\delta^{13}C$ curve must largely be concerned with interpretation of the organic carbon isotopic record. In this study, an attempt has been made to take account of post-depositional change in $\delta^{13}C_{org}$ using correction factors based on TOC and maturation indices (sections 2.3c, 2.3d). However, the $\delta^{13}C_{org}$ signal can also be expected to reflect particular palaeoenvironmental factors such as temperature, degree of heterotrophic reworking and physiological differences between C-fixing communities (e.g. Popp et al., 1989; Hayes et al., 1989; and see section 2.3a). Such factors may well induce basinwide signal features but not necessarily global ones. Below, an attempt is made to derive from the Australian data an Ediacarian $\delta^{13}C$ signal in terms of carbonate in equilibrium with surface or mixed layer of the water column, excluding the effects of basin stratification, in order to allow comparison with published records from other continents.

Maximum depositional $\delta^{13}C_{carb}$ from the lowermost parts of cap dolostones are -1.6 ‰ in the Amadeus Basin (Mt Capitor) and -1.3 ‰ in the Adelaide Geosyncline (BMW1a-1, UB17: see Fig. 3.4). (Locally, more ^{13}C-enriched horizons are present (Mt Capitor, Ellery Creek) but carbonate in these samples is recrystallised or largely detrital). These values (-1.6 ‰, -1.3 ‰) conceivably precede the onset of basin stratification (sections 3.3c; 6.2). Relatively depleted $\delta^{13}C_{org}{}^{N}$ in the lowermost part of the cap dolostone in

Wallara 1 (the only cap dolostone section for which a full organic $\delta^{13}C$ profile was obtained) are consistent with surface waters being in equilibrium with moderately depleted carbonate (ca. -3 ‰, Fig. 4.36). Thus, at the very commencement of the Ediacarian, data are consistent with surface waters (or the whole water column, if well-ventilated) being in equilibrium with slightly depleted carbonate (-1 to -3 ‰).

After this, in the Nuccaleena Formation and correlatives, $\delta^{13}C_{org}{}^{N}$ rises steeply while $\delta^{13}C_{carb}$ falls, due, it is suggested here, to the proposed onset of basin stratification. Mean composition of basin waters (more closely approximating the global $\delta^{13}C$ signal, if the oceans as a whole were well-ventilated and connected to the Australian basins) presumably evolved along an intermediate path. After the deposition of the cap dolostones, in early Brachina/Pertatataka time, there is evidence that bottom-water $\delta^{13}C_{DIC}$ continued to fall, with strongly depleted carbonates (-6 to -8 ‰) in the 'Halfway Dam Formation' (= lower Pertatataka Formation) (Jenkins, 1993b; and see section 4.5c); and with the appearance of strongly depleted benthic microbial mats in the Adelaide Geosyncline and the Officer and Amadeus Basins ($\Delta_{p\text{-}b}$, the depletion of the benthic mats relative to carbon of inferred pelagic origin corrected for post depositional change ($\delta^{13}C_{org}{}^{N}$) is 9 ‰ in the Officer and Amadeus Basins and 10 to 14 ‰ in the Adelaide Geosyncline: Table 2.2). At the fall in $\delta^{13}C_{org}{}^{N}$ defining the top of Cycle I, benthic microbial mat isotopic compositions *rise* in Wallara 1 (Fig. 4.37). (In other sections, benthic microbial mat occurrences are not sufficiently long-ranging stratigraphically for any significant trend to be apparent). Thus, in at least the Amadeus Basin, the Cycle I positive excursion in $\delta^{13}C_{org}{}^{N}$ appears to be mirrored by a negative excursion in indicators of bottom-water isotopic composition. This period of apparent, strong divergence in $\delta^{13}C_{DIC}$ of surface and deep water layers is considered to reflect a particularly intense period of water column stratification, that became less intense at the end of Cycle I. The magnitude of the Cycle I positive excursion in $\delta^{13}C_{org}{}^{N}$ - variable from basin to basin - may have been enhanced by palaeoenvironmental factors such as warming in the surface layer resulting in lowering of $[CO_2(aq)]$ and thus lowering of the fractionation associated with the photosynthetic fixation of carbon (ε_P).

Thus, Cycle I and the corresponding inferred negative excursion in bottom-water $\delta^{13}C_{DIC}$ may simply reflect an episode of enhanced water-column stratification. In early Cycle II time, however, there is good evidence for an increase in mean composition of $\delta^{13}C_{DIC}$ of basin waters. A gentle increase in $\delta^{13}C_{org}{}^{N}$ is seen in many localities, and this is paralleled in Wallara 1 by the isotopic composition of benthic microbial mat carbon ($\delta^{13}C_{bmm}$) (Fig.4.37). In Wallara 1, the $\delta^{13}C_{bmm}$ signal records a total increase

of about 4 ‰ from mid-Cycle I to mid-Cycle II, and the lower part of Cycle II sees a parallel rise of about 3 ‰ in $\delta^{13}C_{org}{}^{N}$. The broad maximum in $\delta^{13}C_{org}{}^{N}$ of Cycle II is consistent with equilibrium carbonate with $\delta^{13}C_{carb}$ of approximately +3 ‰ in most sections (Wallara 1, Ellery Creek, DDC1, DDC2, SCYW1a) but somewhat higher in a couple of sections (+5 to +6 ‰ in Giles 1 and Bunyeroo Gorge).

Cycle III is an abrupt positive excursion seen only at Ellery Creek and perhaps incompletely at SCYW1a. At Ellery Creek, within Cycle III, $\delta^{13}C_{org}$ is directly proportional to TOC (the inverse of the usual relationship - see section 2.3c). By analogy with documented examples of phytoplankton blooms (e.g. Hollander & McKenzie, 1991; Simoneit et al., 1993), an increase in productivity may have raised TOC at the same time causing a drawdown in $[CO_2(aq)]$, resulting in a decrease in ε_P (the fractionation effect associated with photosynthesic carbon fixation; see section 2.3a) and hence deposition of more ^{13}C-enriched organic matter. However, maximum TOC is still very low (less than 1.5 mg/g) and there is no evidence (such as phosphate) for an excess of nutrients to the extent that $[CO_2(aq)]$ became a limiting factor. In any case, the apparently local nature of Cycle III suggests that its broader chronostratigraphic significance is dubious.

The ensuing negative excursion is, however, widespread and well defined in all basins except the Georgina Basin where there may be a correlative lacuna (Fig 4.36). Interbasinal correlation of the negative excursion is confirmed by the Acraman Impact Ejecta Layer, which slightly precedes it, and the first appearance of the large spiny acritarch association (Grey, in prep.) which roughly coincides with it. $\delta^{13}C_{org}{}^{N}$ at the minimum is consistent with carbonate of about +2 ‰, and the organic signal is supported by consistent $\delta^{13}C_{carb}$ of isolated beds of limestone (2.6 ‰ and 2.0 ‰ in the Amadeus and Officer Basins respectively). In Brachina Gorge the organic data suggest a distinctly more pronounced negative excursion, for reasons perhaps partly palaeoenvironmental (section 3.4c).

In the Cycle IV peak the signal is derived largely from the $\delta^{13}C_{carb}$ record. The peak is +5 to +6 ‰ in the Officer, Amadeus and Georgins Basins, but in the Adelaide Geosyncline the signal in the Cycle IV - V interval is thought to be masked by the effects of basin stratification, leading to strongly depleted $\delta^{13}C_{carb}$ and perhaps some enrichment in $\delta^{13}C_{org}$.

In the Officer Basin, $\delta^{13}C_{carb}$ is seen to fall to +3 ‰ above the Cycle IV peak. Slightly higher stratigraphically, $\delta^{13}C_{org}{}^{N}$ rises strongly at the beginning of a proposed period of

basin stratification associated with the canyon unconformity. This positive excursion (Cycle V) - of considerably greater stratigraphic extent in the Adelaide Geosyncline (Wonoka Formation) - may, like Cycle I, be simply the result of an episode of water column stratification. Possibly during this time surface-water $\delta^{13}C_{carb}$ underwent a negative excursion to around 0 ‰ as seen in shallow-water carbonates in the Elkera Formation, Georgina Basin. Above Cycle V, $\delta^{13}C_{carb}$ attained a composition of around +2.5 ‰ in the upper Rodda beds, the uppermost Wonoka Formation, the uppermost Elkera Formation and the uppermost Julie Formation (Phillipson Pound area), and all available evidence is consistent with these horizons being correlative (Fig. 4.37).

At younger levels, evidence of this study is restricted to Ungoolya 1 in the Officer Basin where a rising trend in $\delta^{13}C_{org}{}^{N}$ is apparent. A rise in $\delta^{13}C_{carb}$ is also apparent in the Adelaide Geosyncline where values as high as +6 ‰ are seen in the uppermost Wonoka Formation where the uppermost unit thickens northwards (Urlwin et al., 1993; Pell et al., 1993). Similarly enriched carbonate (+7 ‰) is seen at still younger horizons in the Billy Springs Formation (Pell et al., 1993). A negative excursion (to -0.7 ‰) shown by Pell et al. in the Billy Springs Formation appears to be based on a single sample for which no other data are given, and therefore must be regarded as not well established.

Thus, the mainland Australian Ediacarian carbon isotope signal, in terms of inferred shallow-water $\delta^{13}C_{carb}$ and excluding the effects of water-column stratification, may be conservatively described as follows (Fig. 6.2). The rising post-glacial seas were initially in equilibrium with slightly depleted (-1 to -3 ‰) $\delta^{13}C_{carb}$. Based on organic carbon, the signal then rises relatively rapidly to an inferred maximum of +3 ‰ or more (Cycle II) before falling to +2 ‰ at the time of the appearance of the large acanthomorphic acritarchs. Then, on direct $\delta^{13}C_{carb}$ evidence, the signal rises to a +6 ‰ maximum (Cycle IV: Julie Formation, 'Karlaya Limestone'). The signal then falls and the large acanthomorphs disappear. Shallow-water $\delta^{13}C_{carb}$ goes perhaps as low as 0 ‰ (Elkera Formation) before climbing again to +6 to +7 ‰ (uppermost Wonoka Formation, Billy Springs Formation: Pell et al., 1993). A thickness corresponding approximately to the upper third of the type Ediacarian (the Pound Subgroup) was not sampled for chemostratigraphy in any Australian basin. Diverse assemblages of soft-bodied metazoans (Ediacara fauna) are restricted to this unsampled interval (Cloud & Glaessner, 1982; Jenkins, 1984).

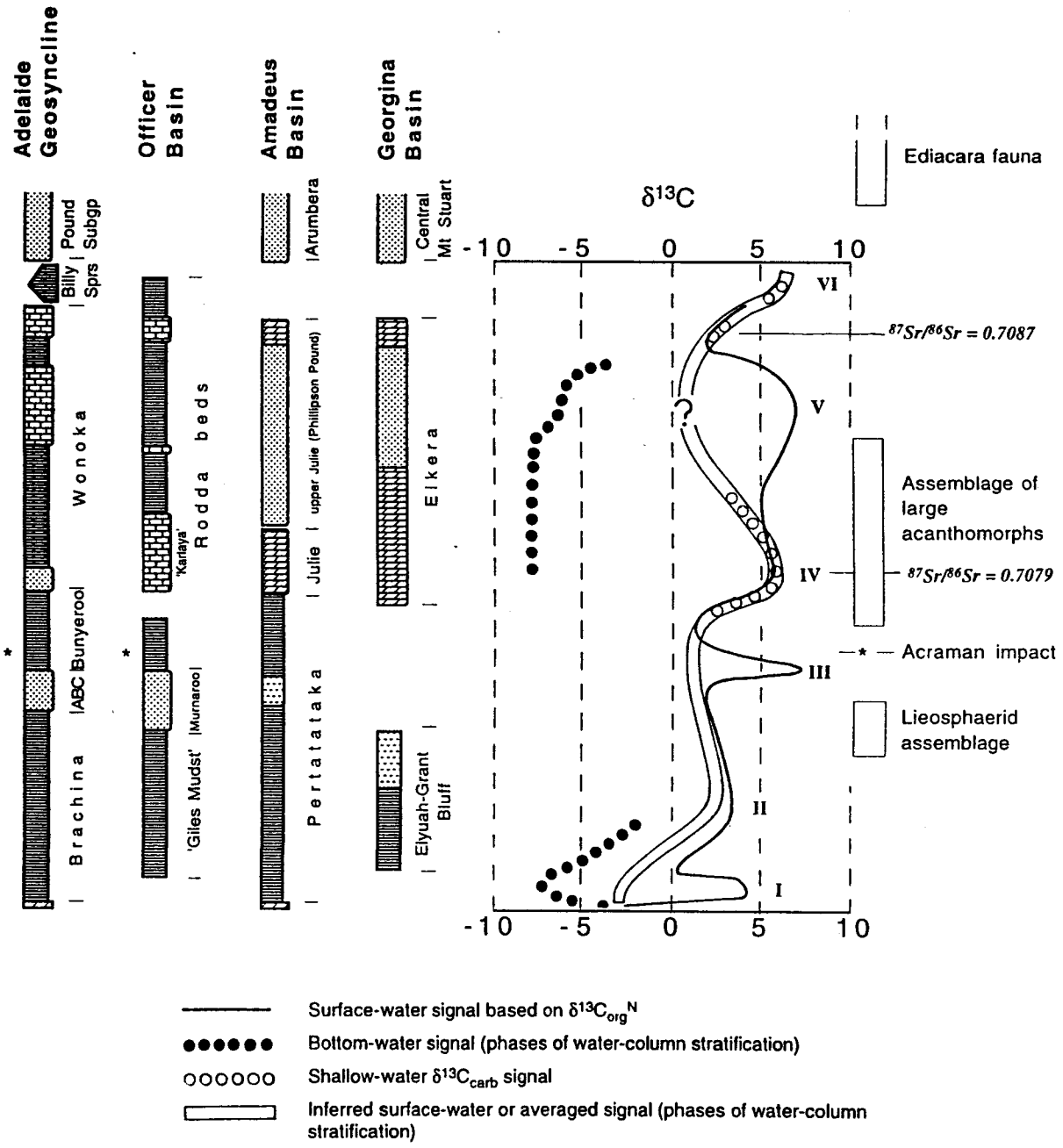

Fig. 6.2: Generalised $\delta^{13}C$ signals, Australian Ediacarian basins. At left, generalised stratigraphic columns for four major basins of this study. At right, $\delta^{13}C$ signals: generalised surface-water signal in terms of equilibrium $\delta^{13}C_{carb}$, based on $\delta^{13}C_{org}{}^{N}$ (see figs. 3.26; 4.36, 4.37); bottom-water signal during phases of enhanced water-column stratification, lower data based on isotopic compositions of benthic microbial mats in Wallara 1 (see Fig. 4.36) and of carbonates in lower Pertatataka Formation; upper data based on $\delta^{13}C_{carb}$ of Units 3 to 7 of the Wonoka Formation (this phase is of much smaller stratigraphic extent outside the Adelaide Geosyncline: see Fig. 6.1); $\delta^{13}C_{carb}$ signal of shallow-water carbonates (question-marked negative excursion is based only on a few results from the Elkera Formation, Georgina Basin); and inferred averaged signal during phases of water-column stratification or surface-water signal outside such phases. At far right, supplementary chronostratigraphic data. See text for full explanation.

6.3b Strontium Isotopes

The longer oceanic residence time of strontium, and its lack of direct interaction with the biosphere, mean that the oceans have a stronger tendency towards instantaneous spatial uniformity in $^{87}Sr/^{86}Sr$ than in $\delta^{13}C_{DIC}$. Also because of the apparent monotonic increase in marine $^{87}Sr/^{86}Sr$ through the Ediacarian (Kaufman et al., 1993), strontium isotopes can be expected to be useful in interbasinal and global correlation and have proved so in this study, in spite of the fact that only a small number of samples yielded chronostratigraphically useful results.

The potential resolution of the Sr isotope record is important in evaluating results, and this issue is critically linked to the selection criteria used to determine least-altered samples. In a recent discussion of the Vendian Sr isotope signal, Kaufman et al. (1993) compiled Vendian $^{87}Sr/^{86}Sr$ results and considered that limestones with Mn/Sr < 1.5, $^{87}Rb/^{86}Sr < 0.001$ and $\delta^{18}O > -11$ ‰ record near-primary Sr isotopic compositions. In this study, a more rigorous set of criteria excludes all but the lowest (least-altered) $^{87}Sr/^{86}Sr$ results and the closeness (within ca. 0.0001) of results thus selected within the same stratigraphic unit (Table 6.1) is good evidence that near-primary values are preserved. The selection criteria used are two or more of: [Sr] > 1000 ppm, Mn/Sr < 0.4, $\delta^{18}O > -8$ ‰. Eight of a total of 73 $^{87}Sr/^{86}Sr$ analyses satisfy these criteria. $^{87}Rb/^{86}Sr$ is less than 0.001 in six samples for which [Rb] was determined (Table 6.1).

If these criteria are applied to the larger data set of Kaufman et al. (1993), points thus selected display a spread of 0.0002 in $^{87}Sr/^{86}Sr$ in the densely-sampled 560 - 580 Ma interval. Thus, the resolution of the Ediacarian/Vendian Sr isotope signal may be limited to 0.0002 with present data. A similar resolution is seen through most of the Phanerozoic (Burke et al., 1982; Veizer, 1989).

A dolostone sample from the (pre-Ediacarian) Pioneer Formation yielded a ratio of 0.7078. This sample is likely to be altered in $^{87}Sr/^{86}Sr$ (section 4.3e). Nevertheless, this ratio is lower than that obtained from any Ediacarian unit sampled in this study.

The lowest $^{87}Sr/^{86}Sr$ ratio from basal Ediacarian cap dolostone (0.7092) is altered and well above likely contemporaneous marine compositions (see next section). The first consistent, low $^{87}Sr/^{86}Sr$ values from samples answering the selection criteria proposed above come from the first thick limestone unit ('Karlaya Limestone' of Lindsay & Reine, 1995) in the Rodda beds correlative (0.70791, 0.70795). The Julie Formation, a probable correlative of the 'Karlaya Limestone' in the Amadeus Basin, has a minimum (least-altered) $^{87}Sr/^{86}Sr$ of 0.70835, but this ratio is probably somewhat altered since

[Sr] is only 246 ppm. The next-youngest group of selected results are from the upper part of the Wonoka Formation in the Adelaide Geosyncline. Unit 7 yielded values (two from different localities at 0.70876) indistinguishable from Unit 11 (0.70874). The results from the topmost Rodda beds limestone in Munta 1 (two at 0.70885, one at 0.70898) may not be significantly different from the upper Wonoka Formation since (as established above) the resolution of the $^{87}Sr/^{86}Sr$ signal is unlikely to be better than 0.0002 given the vagaries of diagenetic alteration.

The $^{87}Sr/^{86}Sr$ results are thus consistent with previous work showing a monotonic rise in the ratio through the Ediacarian. The sparsity of little-altered data from the Australian sections means that a more complex pattern of variation cannot yet be ruled out. Nevertheless, the data are here taken as evidence that the Julie Formation is significantly older than the upper part of the Wonoka Formation (in contrast to previous suggestions of equivalence or a younger age for the Julie Formation, e.g. Jenkins, 1993b); and that the upper part of the Wonoka Formation may be similar in age to the upper part of the Rodda beds correlative (in contrast to some previous interpretations, e.g. Sukanta et al., 1991; Pell et al., 1993). Also, the $^{87}Sr/^{86}Sr$ data are good evidence that the ^{13}C-enriched carbonates of the Julie and 'Karlaya' Formations are significantly older than similarly-^{13}C enriched Ediacarian-aged carbonates in some overseas sections (see below).

Stratigraphic unit	Sample	Sr(ppm)	Mn/Sr	87Rb/86Sr	87Sr/86Sr	87Sr/86Srinit
Unit C, Rodda beds	15.02	1540	0.16	0.0004	0.70886	0.70885
Unit C, Rodda beds	15.04	1112	0.2	0.0005	0.70886	0.70885
Unit C, Rodda beds	15.05	1026	0.27	0.0008	0.70899	0.70898
Unit 11, Wonoka Fm	7.19	847	0.18	0.0002	0.70874	0.70874
Unit 7, Wonoka Fm	8.35	1161	0.39	n.d.	0.70876	n.d.
Unit 7, Wonoka Fm	5.52	1420	0.24	n.d.	0.70876	n.d.
Unit B, Rodda beds ('Karlaya Lst')	15.83	1638	0.06	0.0003	0.70791	0.70791
Unit B, Rodda beds ('Karlaya Lst')	14.11	1120	0.3	0.0006	0.70795	0.70795

Table 6.1: Strontium isotopic and associated analytical data for mainland Australian Ediacarian samples with two or more of {[Sr] > 1000 ppm; Mn/Sr < 0.4; $\delta^{18}O$ > -8 ‰}.

6.3c SULPHUR ISOTOPES

Sulphate sulphur isotopic compositions were analysed at five horizons in this study, and the results are consistent with a slight increase (from 20 ‰ to 25 ‰) in marine $\delta^{34}S_{sulphate}$ during the early to middle Ediacarian. Isolated anhydrite nodules from the Nuccaleena Formation and upper 'Giles Mudstone' are 20.4 ‰ and 23.1 ‰ respectively. A number of analyses from the lower Elkera Formation, Georgina Basin (Julie Formation correlative?) lie close to 25 ‰. A similar-aged or possibly slightly younger horizon in the middle Rodda beds (section 3.10e) has an anhydrite nodule with $\delta^{34}S_{sulphate}$ of 24.3 ‰. Disseminated gypsum in a sample from the middle Wonoka Formation (Unit 5) has $\delta^{34}S$ of 9 ‰, but the sulphate is volumetrically minor and its isotopic composition suggests it is not wholly of marine origin.

Sparse Neoproterozoic $\delta^{34}S_{sulphate}$ data of Claypool et al. (1980) and earlier compilations left open the possibility of a rapid rise (from about 17 ‰ to 30 ‰) in the Ediacarian sulphur isotope age curve (see also Ross et al., 1995). Holser (1977) suggested that this rise (and two later, Phanerozoic steep rises) may require catastrophic mixing of ^{34}S-enriched basinal brines with the world ocean. If the values obtained here for the Australian Ediacarian are representative of the world ocean, a gentler rise may characterise this part of the age curve, and Holser's proposed catastrophic terminal Proterozoic mixing event (the 'Yudomski event') may be unnecessary.

Twenty sulphide sulphur isotopic compositions are widespread and variable (-31 to +4 ‰), reflecting varying degrees of partial closure in early diagenetic environments. The sulphide $\delta^{34}S$ signal is unlikely to contain a useful chronostratigraphic component given the evidently slight increase in seawater sulphate ^{34}S.

6.4 Correlation with overseas sections

Outside Australia, carbon isotope chemostratigraphic studies have been carried out on Ediacarian-age successions in Svalbard-east Greenland-Spitzbergen (Knoll et al., 1986, Fairchild & Spiro, 1987), Yangtze Gorge (Lambert et al., 1987), Namibia (Kaufman et al., 1991), Siberia (Knoll et al., 1995), and NW Canada (Narbonne et al., 1994). A carbon isotope record for the Huqf Group of Oman (Burns & Matter, 1993) is also partly Ediacarian in age but correlation of this record is in doubt (Kaufman & Knoll, 1995). Strontium isotope data have been obtained from the successions in Namibia, NW Canada, and Svalbard-east Greenland (Asmerom et al., 1991; Derry et al., 1992; Kaufman et al., 1993; Narbonne et al., 1994).

Very similar carbon isotope signals, almost entirely based on the carbonate $\delta^{13}C$ record, have been extracted from these successions (Knoll & Walter, 1992; Kaufman & Knoll, 1995). Sparser strontium data are also broadly consistent between sections (Kaufman et al., 1993). The main features are briefly reiterated below (and see section 1.3).

The late Cryogenian interval is characterised by enriched $\delta^{13}C_{carb}$ (+5 to +10 ‰; Knoll et al., 1986; Kaufman & Knoll, 1995); and low $^{87}Sr/^{86}Sr$ (ca. 0.707: Derry et al., 1992). In Spitzbergen, ^{13}C enrichment (+4 ‰) persists into intra-Varangian carbonates (members E3 and E4 of the Elbobreen Formation; Fairchild & Spiro, 1987) while in NW Canada there is a negative excursion to strongly depleted $\delta^{13}C_{carb}$ (-5 to -7 ‰) below the ?Varangian-correlative Ice Brook glacials. In Canada and Spitzbergen, 'cap dolostones' immediately overlying glacials have depleted carbonate carbon isotopic compositions (-2 to -5 ‰). There is a single, little-altered $^{87}Sr/^{86}Sr$ result of 0.7072 from cap dolostone in Canada. ^{13}C depletion persists into younger horizons in Spitzbergen and Namibia, where little-altered $^{87}Sr/^{86}Sr$ values of 0.7081 to 0.7082 are seen (Kaufman et al., 1993) but the C signal is poorly constrained until there is a discrete positive excursion to maximum $\delta^{13}C_{carb}$ values of +5.5 ‰ (Siberia) to +7 ‰ (Canada). This $\delta^{13}C$ peak (here called the 'Zaris maximum' after the Zaris Formation in Namibia) is characterised by little-altered $^{87}Sr/^{86}Sr$ of 0.7084 to 0.7085 in Namibia (Derry et al., 1992; Kaufman et al., 1993). The $\delta^{13}C$ peak is succeeded in several sections by an irregular plateau of moderate ^{13}C enrichment (0 to +3 ‰) that persists almost to the base of the Cambrian. Ediacara-type metazoan fossil assemblages occur within this $\delta^{13}C_{carb}$ plateau in China, Siberia, Canada and Namibia, and in the latter two localities, the metazoans first appear somewhat earlier (just before the Zaris maximum). During the plateau of moderate ^{13}C enrichment, $^{87}Sr/^{86}Sr$ values, mainly from Namibia, delineate a steady or gently rising trend and a least-altered ratio of 0.7085 is seen near the top of the Proterozoic part of the Nama Group (Derry et al., 1992; Kaufman et al., 1993). The ensuing rise to the middle Cambrian $^{87}Sr/^{86}Sr$ maximum (0.7090) is very poorly constrained. Younger details of the $\delta^{13}C$ 'global signal' lie beyond the range sampled in this study.

How well do the Australian isotopic data match the signals established on other continents, and do the data shed light on the critical question of intercontinental correlation of the glacigene units? Some corroborative chronostratigraphic information comes from biostratigraphy (Knoll & Walter, 1992). Simple putative metazoan fossils occur in pre-Ediacarian rocks in South Australia (Dyson, 1985; Lemon, in Jenkins et al., 1993) and, similarly, below the Ice Brook glacials in NW Canada (Hofmann et al., 1990). In the early part of the Australian Ediacarian, there are isolated occurrences of possible metazoan remains in the upper Wonoka Formation (Jenkins, 1984b; 1993a); and simple trace fossils in

the Grant Bluff and lower Elkera Formations of the Georgina Basin (Walter et al., 1989; Jenkins et al., 1992) and the upper Wonoka Formation (Jenkins, 1993a). However, diverse assemblages of soft-bodied metazoans (the 'Ediacara fauna') are known in the Adelaide Geosyncline only from the lower Rawnsley Quartzite, stratigraphically about four-fifths of the way up the type Ediacarian (Wade, 1970; Cloud & Glaessner, 1982). Assemblages broadly comparable in diversity and evolutionary grade to the 'type' Ediacara fauna first appear at a level just below the Zaris $\delta^{13}C$ maximum in Namibia and NW Canada (Narbonne et al., 1994; Kaufman et al., 1991). No widely-applicable zonal subdivision of the Ediacara fauna is yet practicable (Narbonne et al., 1994) because of endemism and palaeoenvironmental and preservational factors (Jenkins, 1992). The strong palaeoenvironmental and preservational constraints on the distribution of these forms argue against using first and last appearance as correlatable tie points (cf. Kaufman et al., 1993). The large acanthomorph acritarch assemblage comprises one or more zones below the Ediacara fauna but is not yet widely known (Zang & Walter, 1992; Grey, in prep.).

Low palaeolatitude of Marinoan glacials in South Australia (Embleton & Williams, 1986) and of the Varangian glacials in Europe (Harland & Herod, 1975) suggests near-global distribution and perhaps a synchronous Marinoan - Varangian glacial datum (Knoll & Walter, 1992). However, Eyles (1993) argues that Neoproterozoic glacigene rocks are a diachronous response to regional tectonic events, chiefly uplift associated with rifting. Thus the Sturtian and Rapitan glacials may be correlative units associated with the opening of a palaeo-Pacific Ocean at about 700 Ma, and the Varangian glacials of the North Atlantic region mark the rifting associated with the formation of the Iapetus Ocean at 600 Ma, but Marinoan, Varangian and Ice Brook glacials may not necessarily be correlative (Eyles, 1993; Young, 1995).

Isotope-stratigraphic data offer equivocal evidence regarding temporal correlation of Marinoan glacials with glacial units in NW Canada (Ice Brook Formation), Spitzbergen (the Varangian Wilsonbreen Formation) and Namibia (Numees Tillite). A sounder basis for (or against) correlation will be provided with systematic isotopic studies of pre-glacial units in Australia, work currently in progress by Dr. Stephen Grant at Macquarie University. On sparse published information, the Trezona Formation, a carbonate which underlies Marinoan glacials in the Adelaide Geosyncline, has negative $\delta^{13}C_{carb}$ (-7.4 to -7.7 ‰) and a minimum $^{87}Sr/^{86}Sr$ ratio of 0.7074 (Veizer & Hoefs, 1976, Veizer & Compston, 1976). The older Etina Formation is strongly enriched in ^{13}C (+ 9.4 ‰, +9.5 ‰) (Veizer & Hoefs, 1976, Veizer & Compston, 1976). A possibly-correlative, marked negative shift in $\delta^{13}C_{carb}$ occurs within the Keele Formation (underlying Ice Brook glacials) in NW Canada (Narbonne et al.,

1994) but ^{13}C-enriched carbonates persist right up to the base of Varangian-correlative glacials in Spitzbergen (Knoll et al., 1986; Fairchild & Spiro, 1987) and the Numees Tillite (Kaufman et al., 1991).

Base-Ediacarian 'cap dolostones' in Australia (Nuccaleena Formation and correlatives at Mt Capitor and Wallara 1 in the Amadeus Basin) are very similar in $\delta^{13}C_{carb}$ and $\delta^{18}O$ to cap dolostones in NW Canada ('Tepee Dolostone': Narbonne et al., 1994) and Spitzbergen (member D1, Dracoisen Formation: Fairchild & Spiro, 1987). The upward-decreasing $\delta^{13}C_{carb}$ trend characteristic of the Australian cap dolostone is not evident in the few samples analysed by these workers; in contrast member D1 appears to have an upward-increasing trend (Fig. 1 of Fairchild & Spiro, 1987). The Numees Tillite of Namibia is overlain by a pinkish, banded cap dolostone (Kröner, 1977) but no isotopic analyses have been published. Since the Nuccaleena $\delta^{13}C_{carb}$ signal may at least in part be determined by basin stratification, intercontinental correlation of cap dolostones on the basis of $\delta^{13}C_{carb}$ may be spurious. Strontium isotopic ratios would provide valuable evidence on the relative timing of these units since marine $^{87}Sr/^{86}Sr$ appears to rise steeply at about this time (Kaufman et al., 1993). Only from the 'Tepee dolostone', however, has a little-altered ratio (0.7072) been obtained (Narbonne et al., 1994).

^{13}C-enriched carbonates of the Doushantuo Formation directly overlie tillite of the Nantou Formation (Lambert et al., 1987) suggesting either that the Nantou is younger than the Marinoan, Ice Brook or Varangian glacials or that there is a lacuna at the base of the Doushantuo. Similarly, on the Siberian Platform, ^{13}C-enriched carbonates correlated with the Zaris maximum unconformably overlie Riphean rocks (Knoll et al., 1995).

The C isotope signal is generally poorly constrained in the early post-glacial interval worldwide. Above 'cap dolostones' there are thick successions that are unsampled (NW Canada) or very sparsely sampled (Namibia, Spitzbergen) in part because of lack of carbonates. In Namibia there are unconformities within, an possibly at the top of the (?early Ediacarian) Witvlei Group and the relationship of the Gariep Group (which includes the Numees Tillite) to the Witvlei Group is contentious (Kaufman et al., 1993). Several hundred metres of section overlying 'cap dolostones' in Namibia, Spitzbergen and NW Canada are represented by a total of only a dozen or so $\delta^{13}C$ analyses (Fairchild & Spiro, 1987; Kaufman et al., 1991; Narbonne et al., 1994). On this sparse evidence, there is a long interval characterised by depleted $\delta^{13}C_{carb}$ (e.g. -2 to -4 ‰, Buschmansklippe and Mara Formations, Namibia: Kaufman et al., 1991; and see Fig. 1.4). The thick post-cap dolostone succession in Australia lacks carbonates (Brachina and Bunyeroo Formations and correlates)

but abundant organic carbon data throughout this interval suggest an apparently rapid increase in $\delta^{13}C_{DIC}$ to values in equilibrium with $\delta^{13}C_{carb}$ of +3 ‰ or higher (Cycle II), with no evidence for negative $\delta^{13}C$ in surface-water carbonate in any sections studied with the possible exception of Tasmania. The Tasmanian data from the Smithton Dolomite offer indirect support for a major negative excursion at this time. There is no known equivalent of the Marinoan glacials in the Smithton Basin, but least-altered C and Sr isotopic results are essentially congruent with the Witvlei-Zaris succession in Namibia (section 5.7). Three possibilities are suggested by the apparent lack of a major negative excursion, post-dating the cap dolostones in mainland Australia:

(i) The mainland Australian $\delta^{13}C$ record for this interval (Cycle II - III) is entirely derived from organic carbon, and its translation into terms of equilibrium carbonate $\delta^{13}C$ depends on $\Delta\delta$ derived from younger units (Cycle IV - VI). A substantially lower ε_P in Cycle II - III time (brought about, for example, by relatively low pCO_2) would have produced relatively enriched organic matter, disguising the negative excursion in carbonate carbon $\delta^{13}C$.

(ii) The Marinoan glacials are younger than glacials in Spitzbergen and Namibia, and the bulk of the post-Varangian negative excursion correlates with the pre-Ediacarian depleted carbonates of the Trezona Formation. The Marinoan glacials may still be synchronous with the Ice Brook Formation which is underlain by ^{13}C-depleted carbonates, and overlain by a large unsampled gap in the post-cap dolostone $\delta^{13}C$ profile (Narbonne et al., 1994; and see Fig. 1.5). However, Sr isotopes point to a significant difference in age between the Trezona Formation (0.7074) and the (post-Numees Tillite) Witvlei Group (0.7081).

(iii) The glacials may be correlative, but the mainland Australian Ediacarian successions were laid down in a basin or basins semi-isolated from the global ocean, which experienced some degree of separate evolution in $\delta^{13}C_{DIC}$. This seems a real possibility in the light of evidence for intervals of salinity-stratification in the Australian basins (see previous section) and possible episodes of Messinian-style basin desiccation during Wonoka Formation time (Christie-Blick et al., 1990; and see previous sections). Basin stratification would tend to enrich surface waters in ^{13}C because of sequestering of ^{12}C into bottom waters (section 3.6c). Relative enrichment of the organic record in Cycle II - III time may thus be coeval with the negative excursion seen on other continents and Tasmania.

Clearly, corroborative evidence for correlation of the glacials and enclosing successions is required. $^{87}Sr/^{86}Sr$ of semi-isolated marine basins is much less likely than $\delta^{13}C_{DIC}$ to deviate strongly from global marine compositions because of the longer residence time of strontium and the low Sr content of meteoric waters (Veizer, 1989). Rare carbonates in the Pertatataka

Formation and the Brachina Formation (Dyson, 1992, p.9) might be amenable to detailed further Sr isotope work.

Two $\delta^{13}C$ maxima with similar peak $\delta^{13}C_{carb}$ values to each other (+6 ‰) and to the Zaris Formation maximum are evident in the Australian data (Cycle IV, VI: Fig. 6.2). The little-altered $^{87}Sr/^{86}Sr$ ratio of 0.7079 for the earlier peak (= 'Karlaya Limestone', Julie Formation and correlatives) is significantly lower than little altered $^{87}Sr/^{86}Sr$ values (0.7084 to 0.7085) associated with the Zaris maximum. Thus a distinctly earlier $\delta^{13}C$ peak is established that is not recognised in current 'global curves' (e.g. Kaufman et al., 1993). In support of this interpretation, there is no evidence for diverse Ediacara-grade metazoan assemblages at the level of Cycle IV, as there is with the Zaris Formation and correlatives (Kaufman et al., 1991; Narbonne et al., 1994).

An assemblage of large acanthomorphic acritarchs defines one or more biostratigraphic zones embracing this $\delta^{13}C$ peak (Grey, in prep.). Perhaps significantly, this assemblage is presently unknown outside Australia with the possible exception of the Doushantuo Formation in China (Zang & Walter, 1992). The Doushantuo Formation is characterised , like Cycle IV, by ^{13}C-enriched (up to +7 ‰) carbonates (Lambert et al., 1987). No $^{87}Sr/^{86}Sr$ analyses are available except for an elevated ratio (0.7129) from the basal bed which is clearly altered or of non-marine origin (Lambert et al., 1987). On the basis of the Australian record, a little-altered $^{87}Sr/^{86}Sr$ composition close to 0.7079 might be expected.

The Cycle IV peak may be present, but unrecognised, in sections such as those of Namibia and NW Canada because of gaps in sampling, or it may be absent because of unconformities or hiatuses. The latter possibility is suggested where processing for acritarchs has been carried out without revealing the acanthomorphic assemblage (e.g. NW Canada: Narbonne et al., 1994). It is also possible that the Cycle IV $\delta^{13}C$ maximum was geographically restricted to the mainland Australian depositional basins. The second major phase of water-column stratification had already commenced in the Adelaide Geosyncline (^{13}C-depleted lower Wonoka Formation, Fig. 6.1) at the time the Julie and 'Karlaya' Formations were being laid down in shallower, surface waters on the craton. Thus, the Cycle IV maximum may be a result of basin stratification as suggested above for earlier maxima. It is noteworthy that the least-altered $^{87}Sr/^{86}Sr$ ratio at the +6 ‰ Cycle IV maximum (0.7079) may not be significantly different from the Witvlei Group (0.7081; $\delta^{13}C_{carb}$ = -2 to -4 ‰) or the middle part of the Smithton Dolomite, also with slightly depleted $\delta^{13}C_{carb}$.

The second major Australian $\delta^{13}C_{carb}$ excursion, commencing in the uppermost Wonoka Formation (Cycle VI, Fig. 6.2), is most simply correlated with the Zaris maximum. Least-

altered $^{87}Sr/^{86}Sr$ ratios are similar (0.70875 in the uppermost Wonoka Formation versus 0.7084 at the equivalent level just below the Zaris maximum: Kaufman et al., 1993) but not so close as to unequivocally support the correlation. Possible metazoan fossils - simple discs and a frond-like form - occur with trace fossils including *Palaeopascichnus* in the upper Wonoka Formation (Jenkins, 1984b; 1993a; Haines, 1990) but diverse Ediacara-grade assemblages are unknown from this level. Shallow-water carbonates in the upper Wonoka Formation (Units 9 and 11) should lie within the range of *Cloudina* if this correlation is valid, but this shelly fossil is not known from these units despite careful searches(S. Grant, pers. comm.).

If Cycle VI should prove to be not coeval with the Zaris maximum, it may represent a second $\delta^{13}C$ excursion, probably pre-Zaris in age on the above tenuous biostratigraphic evidence, hitherto unrecognised in overseas sections. This alternative would suggest a slight positive excursion in $^{87}Sr/^{86}Sr$, to around 0.70875, prior to the 'plateau' of 0.7084 - 0.7085 characteristic of the Zaris Formation and younger Neoproterozoic units.

6.5 Conclusion

This study has demonstrated that isotope chemostratigraphy can contribute significantly to precise (formation level or finer) correlation within the originally-continuous mainland Australian basins (Fig. 4.37). The data are significantly more ambiguous, however, with respect to correlation with other continents and Tasmania. This can be attributed to the very real possibility that the oceans were spatially significantly non-uniform in $\delta^{13}C_{DIC}$, and to a lack of data - particularly $^{87}Sr/^{86}Sr$ data - in critical sections, both here and overseas.

Isotopic composition of total organic carbon, neglected in most previous chemostratigraphic studies, has proved useful in correlating within and between the Amadeus, Officer, and Georgina Basins and the Adelaide Geosyncline, even in sections with low (< 0.5 mg/g) or variable TOC. The utility of the organic record is enhanced by the systematic application of 'correction factors' based on TOC, kerogen H/C and $\Delta\delta$, developed or extended in this study, to take account of post-depositional alteration including thermal maturation. Multiple overlapping sections within basins show lateral changes in $\delta^{13}C$ profiles that accord, in at least some cases, with patterns of diachrony expected from sequence-stratigraphic interpretations (sections 3.4c, 4.5d). A distinct benthic organic facies has been recognised that appears to record a discrete, bottom-water carbon isotopic record.

Strontium isotopes have provided important constraints in correlation, particularly in regard to the relative ages of the Julie Formation, Wonoka Formation and the Rodda beds, despite widespread diagenetic alteration of $^{87}Sr/^{86}Sr$.

Circumstantial evidence for salinity stratification of basin waters - involving strong ^{13}C depletion of bottom waters relative to the surface layer - is seen through much of the mainland Australian successions, and this evidence, suggestive of a semi-isolated basin of at least Meditteranean dimensions, is consonant with previous proposals of Messinian-type desiccation events in the Australian Ediacarian (von der Borch et al., 1989; Christie-Blick et al., 1990). In such a palaeogeographic setting it is likely that $\delta^{13}C_{DIC}$ of both surface and deep waters evolved separately from that of the global ocean. In general, ^{13}C-enrichment of surface waters in such a basin would be expected because of sequestering of ^{12}C into bottom waters. This is the explanation favoured here for the apparent absence, in mainland Australia, of the major negative excursion of presumed early Ediacarian age seen on other continents and Tasmania. Strontium isotopic composition of marine waters is more likely to have remained globally uniform, and corroborative $^{87}Sr/^{86}Sr$ data therefore need to be sought.

A strong positive excursion in shallow-water $\delta^{13}C_{carb}$, coinciding in time approximately with the occurrence of large acanthomorphic acritarchs, may likewise be geographically restricted to mainland Australia, being older than the first Ediacarian-age positive excursion of similar amplitude on other continents (Zaris maximum) on good $^{87}Sr/^{86}Sr$ evidence and tenuous biostratigraphic evidence. A later $\delta^{13}C$ maximum, encompassing the uppermost Wonoka and Billy Springs Formations and uppermost Rodda beds correlative, is perhaps most simply correlated with the Zaris maximum, although $^{87}Sr/^{86}Sr$ data and biostratigraphy are equivocal on this point.

This work reinforces the desirability, in future work, of obtaining multiple, widespread chemostratigraphic sections within each major basin (Figs. 3.26, 4.36) to gain as complete as possible a picture of secular variation in the isotopic record. Systematic organic carbon isotope chemostratigraphy should be part of Proterozoic chemostratigraphic studies, metamorphic grade permitting, as this will considerably extend the carbon isotope signal in carbonate-poor successions and provide critical information on the integrity of the carbonate $\delta^{13}C$ record.

Strong spatial non-uniformity in Neoproterozoic $\delta^{13}C_{DIC}$, both vertical (through stratification) and horizontal (through periodic semi-isolation of large basins) is strongly suggested here, and this has obvious practical implications for global-scale

$\delta^{13}C$ chemostratigraphy and for modelling of biogeochemical elemental cycles, which relies on global records of $\delta^{13}C$ secular variation. That some sublittoral carbonates, and black shales of benthic microbial mat origin, may record isotopic signals strongly dissimilar to surface water signals, must now be regarded as a real (but testable) possibility. Testing of horizontal spatial non-uniformity in $\delta^{13}C_{DIC}$ must rely on the continued integration of $\delta^{13}C$ isotope chemostratigraphy with $^{87}Sr/^{86}Sr$ data and other tools - such as biostratigraphy, sequence stratigraphy and lithostratigraphy - in interbasinal correlation studies.

References

Adams, C.J., Black, L.P., Corbett, K.D. & Green, G.R., 1985: Reconnaissance isotopic studies bearing on the tectonothermal history of Early Palaeozoic and Late Proterozoic sequences in western Tasmania. *Australian Journal of Earth Science,* 32:7-36.

Adams, J.M., Faure, H., Faure-Denard, L., McGlade, J.M. & Woodward, F.I., 1990: Increases in terrrestrial carbon storage from the Last Glacial Maximum to the present. *Nature*, 348:711-714.

Ager, D.V., 1973: *The nature of the stratigraphic record.* Wiley & Sons, New York, 114pp.

Aharon, P. & Liew, T.C., 1992: An assessment of the Precambrian-Cambrian transition events on the basis of carbon isotope records. In: Schidlowski, M., Golubic, S., Kimberley, M.M., McKirdy, D.M. & Trudinger, P.A., (editors): *Early Organic Evolution*, pp:212-223. Springer.

Aharon, P., Schidlowski, M. & Singh, I.B., 1987: Chronostratigraphic markers in the end-Precambrian carbon isotope record of the lesser Himalaya. *Nature*, 327:699-702.

Algeo, T.J., Wilkinson, B.H. & Lohmann, K.C., 1992: Meteoric-burial diagenesis of Middle Pennsylvanian limestones in the Orogrande Basin, New Mexico: water/rock interactions and basin geothermics. *Journal of Sedimentary Petrology*, 62:652-670.

Allan, J.R. & Matthews, R.K., 1982: Isotopic signatures associated with early meteoric diagenesis. *Sedimentology*, 29:797-817.

Anderson, T.F., 1969: Self-diffusion of carbon and oxygen in calcite by isotope exchange with carbon dioxide. *Journal of Geophysical Research*, 74:3918-3932.

Anderson, T.F. & Arthur, M.A., 1983: Stable isotopes of oxygen and carbon and their application to sedimentologic and paleoenvironmental problems. In: *Stable Isotopes in Sedimentary Geology, 1.1-1.151.* Society of Economic Paleontologists and Mineralogists Short Course 10.

Arntz, W.E., Tarazona, J., Gallardo, V.A., Flores, L.A., & Salzwedel, H., 1991: Benthos communities in oxygen-deficient shelf and upper slope areas of the Peruvian and Chilean Pacific coast and changes caused by El Niño. In: Tyson, R.V. & Pearson, T.H. (editors): Modern and Ancient Continental Shelf Anoxia. *Geological Society Special Publication,* 58:131-154.

Arthur, M.A. & Natland, J.H., 1979: Carbonaceous sediments in the North and South Atlantic: the role of stable stratification of Early Cretaceous Basins. In: Talwani, M., Hay, W. & Ryan, W.B.F., (editors): Deep Drilling Results in the Atlantic Ocean: Continental Margins and Palaeoenvironment. Maurice Ewing Series 3, *American Geophysical Union*, Washington D.C., pp:375-401.

Asmerom, Y., Jacobsen, S.B., Knoll, A.H., Butterfield, N.J. & Swett, K., 1991: Strontium isotopic variations of Neoproterozoic seawater: implications for crustal evolution. *Geochimica et Cosmochimica Acta,* 55:2883-2894.

Assereto, R.L.M. & Kendall, C.G.St.C., 1977: Nature, origin and classification of peritidal teepee structures and related breccias. *Sedimentology*, 24:153-210.

Bain, R.J., 1990: Diagenetic, nonevaporative origin for gypsum. *Geology*, 18:447-450.

Baker, P.A. & Burns, S.J., 1985: Occurrence and Formation of Dolomite in Organic-rich Continental Margin Sediments. *American Association of Petroleum Geologists Bulletin*, 69:1917-1930.

Banner, J.L. & Hanson, G.N., 1990: Calculation of simultaneous isotopic and trace-element variations during water-rock interaction and with applications to carbonate diagenesis. *Geochimica et Cosmochimica Acta*, 54:3123-3137.

Bathurst, R.G.C., 1971: Carbonate sediments and their diagenesis. *Developments in Sedimentology*, 12:620p. Elsevier.

Baud, A., Margaritz, M. & Holser, W.T., 1989: Permian-Triassic of the Tethys: carbon isotope studies. *Geologische Rundschau*, 78:642-677.

Baum, G.R. & Vail, P.R., 1988: Sequence stratigraphic concepts applied to Paleogene outcrops, Gulf and Atlantic basins. *in* Wilgus, C.K. et al. (eds.): *Sealevel changes: an integrated approach.* Society of Economic Paleontologists and Mineralogists. Special Publication 42: 309-328.

Beeunas, M.A. & Knauth, L.P., 1985: Preserved stable isotopic signature of subaerial diagenesis in the 1.2 b.y. Mescal Limestone, central Arizona: implications for the timing and development of a terrestrial plant cover. *Geological Society of America Bulletin*, 96:737-745.

Benus, A.P., 1988: Sedimentologic context of a deep-water Ediacarian fauna (Mistaken Point Formation, Avalon Zone, eastern Newfoundland). In: Landing, E., Narbonne, G.M. & Myrow, P., (editors): *Trace Fossils, Small Shelly Fossils, and the Precambrian-Cambrian Boundary*. New York State Museum Bulletin, 463:8-9.

Berger, W.H. & Vincent, E., 1986: Deep-sea carbonates: reading the carbon-isotope signal. *Geologische Rundschau*, 75:249-269.

Berner, R.A., 1970: Sedimentary pyrite formation. *American Journal of Science*, 268:1-23.

Berner, R.A., 1984: Sedimentary pyrite formation: an update. *Geochimica et Cosmochimica Acta*, 48:605-615.

Berner, R.A., 1987: Models for carbon and sulfur cycles and atmospheric oxygen: application to Paleozoic and geologic history. *American Journal of Science*, 287:177-96.

Berner, R.A. & Raiswell, R., 1983: Burial of organic carbon and pyrite sulfur in sediments over Phanerozoic time: a new theory. *Geochimica et Cosmochimica Acta*, 47:855-862.

Berry, R.F. & Crawford, A.J., 1988: The tectonic significance of Cambrian allochthonous mafic-ultramafic complexes in Tasmania. *Australian Journal of Earth Science*, 35:523-534.

Beukes, N.J., Klein, D., Kaufman, A.J. & Hayes, J.M., 1990: Carbonate petrography, kerogen distribution, and carbon and oxygen isotope variation in an early Proterozoic transition from limestone to iron-formation deposition, Transvaal Supergroup, South Africa. *Economic Geology,* 85:663-690.

Black, L.P., 1994: The significance of current and proposed SHRIMP dating. *Tasmania Development & Resources Report*, 1994/16.

Bottomley, D.J., Veizer, J., Nielsen, H. & Moczydlowska, M., 1990: Isotopic compositions of disseminated sulfur in Precambrian sedimentary rocks. *Geochimica et Cosmochimica Acta*, 56:3311-3322.

Bowring, S.A., Grotzinger, J.P., Isachsen, C.E., Knoll, A.H., Pelechaty, S. & Kolosov, P., 1993: Calibrating rates of Early Cambrian evolution. *Science*, 261:1293-1298.

Bradshaw, J., 1988: The Namatjira Formation, a mixed carbonate and clastic, Late Proterozoic - Early Cambrian sequence, Amadeus Basin, central Australia. *Australian Journal of Earth Sciences,* 35:15-27.

Bralower, T.J. & Thierstein, H.R., 1987: Organic carbon and metal accumulation rates in Holocene and mid-Cretaceous sediments: palaeoceanographic significance. In: Brooks, J. & Fleet, A.J. (editors): *Marine Petroleum Source Rocks*. Geological Society Special Publication, 26:345-370. Blackwell, Oxford.

Brand, U. & Veizer, J., 1980: Chemical diagenesis of a multicomponent carbonate system - 1: trace elements. *Journal of Sedimentary Petrology*, 50:1219-1236.

Brand, U. & Veizer, J., 1981: Chemical diagenesis of a multicomponent carbonate system - 2: stable isotopes. *Journal of Sedimentary Petrology*, 51:987-998.

Brasier, M.D., 1992: Global ocean-atmosphere change across the Precambrian-Cambrian transition. *Geological Magazine*, 129:161-168.

Brasier, M.D., Anderson, M.M. & Corfield, R.M., 1992: Oxygen and carbon isotope stratigraphy of early Cambrian carbonates in southeastern Newfoundland and England. *Geological Magazine,* 129:265-279.

Brasier, M.D., Margaritz, M., Corfield, R., Luo Huilin, Wu Ziche, Ouyang Lin, Jiang Zhi Wen, Hamdi, B., He Tingguie & Fraser, A.G., 1990: The carbon- and oxygen-isotope record of the Precambrian-Cambrian boundary interval in China and Iran and their correlation. *Geological Magazine*, 127:319-332.

Brasier, M.D., Rozanov, A.Y., Zhuravlev, A.Y., Corfield, R.M., & Derry, L.A., 1994: A carbon isotope reference scale for the Lower Cambrian succession in Siberia: report of IGCP Project 303. *Geological Magazine*, 131:767-783.

Bray, N.A., 1988: Thermohaline circulation in the Gulf of California. *Journal of Geophysical Research,* 93:4993-5020.

Brewer, A.M., Dunster, J.N., Gatehouse, C.G., Henry, R.L. & Weste, G., 1987: A revision of the stratigraphy of the eastern Officer Basin. *South Australian Geological Survey, Quarterly Geological Notes*, 102:2-15.

Broecker, W.S., 1970: A boundary condition on the evolution of atmospheric oxygen. *Journal of Geophysical Research*, 75(18):3553-3557.

Broecker, W.S. & Peng, T.H., 1982: Tracers in the Sea. *Lamont-Doherty Geological Observatory: Palisades, N.Y.*, 690 pp.

Brookfield, M.E., 1993: Neoproterozoic Laurentia - Australia fit. *Geology*, 21:683-686.

Brown, A.V., 1985: Preliminary report on the Forest No. 1 diamond-drill hole and chemical analyses of associated tholeiitic basalts in the Smithton and Woolnorth Quandrangles. *Tasmanian Department of Mines.* Unpublished report, 1985/62.

Brown, A.V., 1986: Geology of the Dundas-Mt. Lindsay-Mt. Youngbuck region. *Bulletin of the Geological Survey of Tasmania*, 62.

Brown, A.V., 1989(a): Chapter 3: Eo-Cambrian-Cambrian. In: Burrett, C.F. & Martin, E., (editors): *Geology and Mineral Resources of Tasmania.* Geological Society of Australia, Special Publication 15:47-83.

Brown, A.V. (compiler), 1989(b): *Smithton, Tasmania.* Geological Survey Explanatory Report, Tasmanian Department of Mines Geological Atlas 1:50,000 series. Sheet 21 (79165).

Brown, A.V. & Jenner, G.A., 1988: Tectonic implications of the reinterpretation of Eocambrian-Cambrian mafic volcanics and associated ultramafic rocks in western Tasmania. In: Turner, N.J., (editor): *The Geology and Evolution of the Latest Precambrian and Cambrian rocks in the Western Tasmania Terrane.* Abstracts Volume, Geological Society of Australia (Tasmania Division).p. 23-25.

Burdett, J.W., Grotzinger, J.P. & Arthur, M.A., 1990: Did major changes in the stable-isotope composition of Proterozoic seawater occur? *Geology*, 18:227-230.

Burek, P.J., Walter, M.R. & Wells, A.T., 1979: Magnetostratigraphic tests of lithostratigraphic correlations between latest Proterozoic sequences in the Ngalia, Georgina and Amadeus Basins, central Australia. *BMR Journal of Australian Geology and Geophysics*, 4:47-55.

Burke, W.M., Denison, R.E., Hetherington, E.A., Koepnick, R.B. & Nelson, H.F., 1982: Variations of seawater $^{87}Sr/^{86}Sr$ throughout Phanerozoic time. *Geology*, 10:516-519.

Burns, S.J. & Matter, A., 1993: Carbon isotopic record from the latest Proterozoic from Oman. *Eclogae Geol. Helv.*, 86: 595-607.

Calver, C.R., 1989(a): Needles area. In: Brown, A. V., McClenaghan, M.P., Baillie, P.W., McClenaghan, J., & Calver, C. R. *Huntley, Tasmania.*Geological Survey Explanatory Report, Geological Atlas 1:50 000 series. Tasmanian Department of Mines. pp:39-40.

Calver, C.R., 1989(b): The Jubilee Region. In: Burrett, C.F. & Martin, E., (editors): *Geology and Mineral Resources of Tasmania*, Geological Society of Australia, Special Publication 15:53-54.

Calver, C.R., 1989(c): The Weld River Group: A major Upper Precambrian dolomite sequence in southern Tasmania. *Papers and Proceedings of the Royal Society of Tasmania*, 123:43-53.

Calver, C.R., 1993: Wallara 1. In: Jenkins, R.J.F., Lindsay, J.F. & Walter, M.R.: Field Guide to the Adelaide Geosyncline and Amadeus Basin, Australia. *AGSO Record* 1993/35:48-49.

Calver, C.R. & Baillie, P.W., 1990: Early diagenetic concretions associated with intrastratal shrinkage cracks in an upper Proterozoic dolomite, Tasmania, Australia. *Journal of Sedimentary Petrology*, 60:293-305.

Calver, C.R. & Everard, J.L., (in prep): A geological traverse across the Smithton Basin along the Arthur River. *Tasmania Development and Resources Report.*

Calver, C.R., Turner, N.J., McClenaghan, J. & Brown, A.V., 1990: *Pedder, Tasmania.* Tasmanian Department of Mines, Geological Atlas 1:50,000 series. Explanatory Report, Sheet 8112S.

Calvert, S.E., Karlin, R.E., Toolin, L.J., Donahue, D.J. & Southon, J.R., 1991: Low organic carbon accummulation rates in Black Sea sediments. *Nature*, 350:692-694.

Calvert, S.E., and Pedersen, T.F., 1992: Organic Carbon Accumulation and Preservation in Marine Sediments: how important is anoxia? In: Whelan, J.K., and Farrington, J.W., eds, *Organic Matter: Productivity, Accumulation and Preservation in Recent and Ancient sediments.* Columbia University Press, New York. p.231-263.

Carey, S.W. & Banks, M.R., 1954: Lower Palaeozoic unconformities in Tasmania. *Papers and Proceedings of the Royal Society of Tasmania*, 88:245-269.

Carey, S.W., 1947: Occurrence of tillite on King Island. *Rep. Aust. Assoc. Adv. Sci.* 25:349.

Carozzi, A.V., 1963: Half-moon Oolites. *Journal of Sedimentary Petrology,* 33:633-646.

Carpenter, S.J., Lohmann, K.C., Holden, P., Walter, L.M., Huston, T.J. & Halliday, A.N., 1991: $\delta^{18}O$ values, $^{87}Sr/^{86}Sr$ and Sr/Mg ratios of Late Devonian abiotic marine calcite: implications for the composition of ancient seawater. *Geochimica et Cosmochimica Acta*, 55:1991-2010.

Chafetz, H.S., 1986: Marine peloids: a product of bacterially induced precipitation of calcite. *Journal of Sedimentary Petrology*, 56:812-817.

Chaudhuri, S. & Clauer, N., 1993: Strontium isotopic compositions and potassium and rubidium contents of formation waters in sedimentary basins: clues to the origin of the solutes. *Geochimica et Cosmochimica Acta*, 57:429-437.

Choquette, P.W. & James, N.P., 1990: Limestones - the burial diagenetic environment. In: McIlreath, I.A. & Morrow, D.W., (editors): *Diagenesis. Geoscience Canada Reprint Series.* 4:75-112.

Choquette, P.W. & James, N.P., 1987: Diagenesis in limestones - 3: the deep burial environment. *Geoscience Canada*, 14:3-35.

Chowns, T.M. & Elkins, J.E., 1974: The origin of quartz geodes and cauliflower cherts through the silicification of anhydrite nodules. *Journal of Sedimentary Petrology*, 44:884-1003.

Christie-Blick, N., 1991: Onlap, offlap and the origin of unconformity-bounded depositional sequences. *Marine Geology*, 97:35-56.

Christie-Blick, N., 1993: Wonoka Canyons, Umberatana Syncline. In: Jenkins, R.J.F., Lindsay, J.F. & Walter, M.R.: *Field Guide to the Adelaide Geosyncline and Amadeus Basin, Australia*. AGSO Record 1993/35:29-31.

Christie-Blick, N., Dyson, I. A., & von der Borch, C. C., 1995: Sequence stratigraphy and the interpretation of Neoproterozoic Earth history. *Precambrian Research*, 73:3-26.

Christie-Blick, N. & Levy, M., 1989: Concepts of sequence stratigraphy, with examples from strata of Late Proterozoic and Cambrian age in the western United States. In: Christie-Blick, N. & Levy, M. (editors): Late Proterozoic and Cambrian Tectonics, Sedimentation and Record of Metazoan Radiation in the western United States. *28th International Geological Congress, Field Trip Guidebook T331*. American Geophysical Union, Washington D.C. pp23-38.

Christie-Blick, N., Grotzinger, J.P. & von der Borch, C.C., 1988: Sequence stratigraphy in Proterozoic successions. *Geology*, 16:100-104.

Christie-Blick, N., von der Borch, C.C. & Dibona, P.A., 1990: Working hypotheses for the origin of the Wonoka Canyons (Neoproterozoic), South Australia. *American Journal of Science*. 290A:295-323.

Claypool, G.E., Holser, W.T., Kaplan, I.R., Sakai, H. & Zak, I., 1980: The age curves of sulfur and oxygen isotopes in marine sulfate and their mutual interpretation. *Chemical Geology*, 28:199-260.

Cloud, P.E. & Glaessner, M.F., 1982: The Ediacarian Period and System: Metazoa inherit the earth. *Science*, 217:783-792.

Cloud, P.E. & Semikhatov, M.A., 1969: Proterozoic stromatolite zonation. *American Journal of Science*, 267:1017-1061.

Coats, R.P. & Blissett, A.H., 1971: Regional and economic geology of the Mount Painter Province. *Geological Survey of South Australia*, Bulletin 43.

Coleman, M.L., 1983: Geochemistry of diagenetic non-silicate minerals: kinetic considerations. *Philosophical Transactions of the Royal Society of London*, 315A:39-56.

Coleman, M.L. & Raiswell, R., 1981: Carbon, oxygen and sulphur isotope variations in concretion from upper Lias of N.E. England. *Geochimica et Cosmochimica Acta*, 45:329-340.

Colley, S., Thomson, J., Wilson, T.R.S. & Higgs, N.C., 1984: Post-depositional migration of elements during diagenesis in brown clay and turbidite sequences in the northeast Atlantic. *Geochimica et Cosmochimica Acta,* 48:1223-1235.

Compston, W. & Arriens, P.A., 1968: The Precambrian geochronology of Australia: *Canberra Journal of Earth Science,* 5:561-583.

Corbett, K.D. & Lees, T.C., 1987: Stratigraphic and structural relationships and evidence for Cambrian deformation at the western margin of the Mount Read Volcanics, Tasmania. *Australian Journal of Earth Science,* 34:45-67.

Corbett, K.D. & Solomon, M., 1989: Mount Read Volcanics and associated deposits. In: Burrett, C.F. & Martin, E.L., (editors): *Geology and Mineral Resources of Tasmania.* Geological Society of Australia, Special Publication 15:84-153.

Corbett, K.D. & Turner, N.J., 1989: Early Palaeozoic deformation and tectonics. In: Burrett, C.F. & Martin, E.L., (editors): *Geology and Mineral Resources of Tasmania.* Geological Society of Australia, Special Publication 15. p.154-181.

Corsetti, F.A. & Kaufman, A.J., (1994): Chemostratigraphy of Neoproterozoic-Cambrian units, White-Inyo Region, Eastern California and Western Nevada: Implications for Global Correlation and Faunal Distribution.*Palaios,* 9:211-219.

Cowan, C.A. & James, N.P., 1992: Diastasis cracks: mechanically generated synaeresis-like cracks in Upper Cambrian shallow-water oolite and ribbon carbonates. *Sedimentology,* 39:1101-1118.

Cowie, J.W., 1989: Introduction. In: J.W. Cowie & M.D. Brasier, (editors):*The Precambrian-Cambrian Boundary*, Oxford monographs on Geology and Geophysics, 12:3-6. Oxford University Press.

Craig, H., 1965: The measurement of oxygen isotope paleotemperatures. In: *Stable isotopes in Ocenographic studies and Paleotemperatures, Spoleto, 26-27 July 1965*, Consiglio Nazionale delle Richerche, Lab. di Geologia Nucleare, Pisa.

Crawford, A.J. & Berry, R.F., 1992: Tectonic implications of Late Proterozoic - Early Palaeozoic igneous rock associations in western Tasmania. *Tectonophysics*, .214:37-56.

Crook, K.A.W., 1979: Tectonic implications of some field relationships of the Adelaidean Cooee Dolerite, Tasmania. *Journal of the Geological Society of Australia,* 26:353-361.

Cruse, T., Harris, L.B. & Rasmussen, B., 1993: Geological Note: The discovery of Ediacaran trace and body fossils in the Stirling Range Formation, Western Australia: implications for sedimentation and deformation during the 'Pan-African' orogenic cycle. *Australian Journal of Earth Science,* 40:293-296.

Curtis, C.D., 1977: Sedimentary geochemistry: environments and processes dominated by involvement of an aqueous phase. *Philosophical Transactions of the Royal Society of London,* 286A:353-372.

Daily, B., 1972: The base of the Cambrian and the first Cambrian fauna. *University of Adelaide, Centre for Precambrian Research, Special Paper*, 1:13-41.

Damassa, S.P. & Knoll, A.H., 1986: Micropalaeontology of the late Proterozoic Arcoona Quartzite Member of the Tent Hill Formation, Stuart Shelf, South Australia. *Alcheringa*, 10:417-430.

Dean, W.E., Arthur, M.A. & Claypool, G.E., 1986: Depletion of ^{13}C in Cretaceous marine organic matter: source, diagenetic, or environmental signal? *Marine Geology*, 70:119-157.

Degens, E.T. & Epstein, S., 1964: Oxygen and carbon isotope ratios in coexisting calcites and dolomites from recent and ancient sediments. *Geochimica et Cosmochimica Acta*, 28:23-44.

Degens, E.T., Guilliard, R.L., Sackett, W.M., & Hellebust, J.A., 1968: Metabolic fractionation of carbon isotopes in marine plankton - I. Temperature and respiration experiments: *Deep - Sea Research*, 15:1-9.

Demaison, G.J. & Moore, G.T., 1980: Anoxic environments and oil source bed genesis. *American Association of Petroleum Geologists Bulletin*, 64:1179-1209.

Derry, L.A., Kaufman, A.J. & Jacobsen, S.B., 1992: Sedimentary cycling and environmental change in the Late Proterozoic: evidence from stable and radiogenic isotopes. *Geochimica et Cosmochimica Acta*, 56:1317-1329.

Derry, L.A., Keto, L.S., Jacobsen, S.B., Knoll, A.H. & Swett, K., 1989: Sr isotopic variations in Upper Proterozoic carbonates from Svalbard and east Greenland. *Geochimica et Cosmochimica Acta*, 53:2331-2339.

Des Marais, D.J., Strauss, H., Summons, R.E. & Hayes, J.M., 1992: Carbon isotope evidence for the stepwise oxidation of the Proterozoic environment. *Nature*, 359:605-609.

Deuser, W.G., 1970: ^{13}C in Black Sea waters and implications for the origin of hydrogen sulfide. *Science*, 168:1575-1577.

Dibona, P.A., 1989: Geologic history and sequence stratigraphy of the Late Proterozoic Wonoka Formation, Northern Flinders Ranges, South Australia. PhD thesis, Flinders University of South Australia.

Dibona, P.A., 1991: A previously unrecognised Late Proterozoic succession: Upper Wilpena Group, northern Flinders Ranges, South Australia. *Quarterly Geological Notes, Geological Survey of South Australia*, 117:2-9.

Dibona, P.A., von der Borch, C.C. & Christie-Blick, N., 1990: Sequence stratigraphy and evolution of a basin-slope succession: the Late Proterozoic Wonoka Formation, Flinders Ranges, South Australia. *Australian Journal of Earth Science*, 37:135-145.

Dickson, J.A.D., 1966: Carbonate identification and genesis as revealed by staining. *Journal of Sedimentary Petrology*, 36:491-505.

Donnelly, T.H., Shergold, J.H. & Southgate, P.N., 1988: Anomalous geochemical signals from phosphatic Middle Cambrian rocks in the southern Georgina Basin, Australia. *Sedimentology*, 35:549-570.

Donnelly, T.H., Shergold, J.H., Southgate, P.N. & Barnes, C.J., 1990: Events leading to global phosphogenesis around the Proterozoic/Cambrian boundary. In: Northolt, A.J.G. & Jarvis, I., (editors): *Phosphorite Research and Development,* Geological Society Special Publication 52:273-287.

Duhig, N.C., Davidson, G.J. & Stolz, A.J., 1992: Microbial involvement in the formation of Cambrian sea-floor silica-iron oxide deposits, Australia. *Geology*, 20:511-514.

Dunn, P.R., Plumb, K.A. & Roberts, H.G., 1966: A proposal for time-stratigraphic subdivision of the Australian Precambrian. *Journal of the Geological Society of Australia,* 13:593-608.

Dyson, I.A., 1985: Frond-like fossils from the base of the late Precambrian Wilpena Group, South Australia.
Nature, 318:283-285.

Dyson, I.A., 1992: Stratigraphic nomenclature and sequence stratigraphy of the Lower Wilpena Group, Adelaide Geosyncline: the Sandison Subgroup. *Geological Survey of South Australia, Quarterly Geological Notes*, 122:2-13.

Dyson, I.A. & von der Borch, C.C., 1983: Evidence of evaporite minerals in the late Precambrian Brachina Subgroup, Hallett Cove, South Australia. *Geological Society of Australia Abstracts,* 10:68-69.

Dyson, I.A. & von der Borch, C.C., 1986: A field guide to the geology of the late Precambrian Wilpena Group, Hallett Cove, South Australia. In: Parker, A.J., (compiler): *One day geological excursions of the Adelaide region.* Geological Society of Australia (South Australia Division). Adelaide. pp:17-40.

Eickhoff, K.H., von der Borch, C.C. & Grady, A.E., 1988. Proterozoic canyons of the Flinders Ranges, South Australia: submarine canyons or drowned river valleys? *Sedimentary Geology*, 58:217-235.

Embleton, B.J.J. & Williams, G.E. 1986: Low palaeolatitude of deposition for Late Precambrian periglacial varvites from South Australia: implications for palaeoclimatology. *Earth & Planetary Science Letters,* 79:419-430.

Emerson, S., 1985: Organic Carbon Preservations in Marine Sediments. In: Sundquist, E.T. & Broecker, W.S., (editors): *The Carbon Cycle and Atmospheric CO_2: Natural Variations Archaean to Present.* Geophysical Monograph 32:78-87.

Emerson, S. & Hedges, J.I., 1988: Processes controlling the organic carbon content of open ocean sediments. *Palaeoceanography*, 3:621-634.

Emiliani, C., 1955: Pleistocene temperatures. *Journal of Geology*, 63:538-578.

Epstein, S., Buchsbaum, R., Lowenstam, H.A., & Urey, H.C., 1953: Revised carbonate-water isotopic temperature scale. *Bulletin of the Geological Society of America,* 64: 1809-1814.

Everard, J.L. & Calver, C.R., (in prep): A geological traverse along the Huon River in the Blakes Opening area. *Tasmania Development & Resources Report.*

Everard, J.L., Seymour, D.B., Brown, A.V. & Calver, C.R., (in press): *Trowutta, Tasmania.* Geological Atlas 1:50,000 series, Sheet 27(7915N). Mineral Resources Tasmania.

Eyles, N., 1993: Earth's glacial record and its tectonic setting. *Earth Science Reviews,*35: 1-248.

Fairchild, I.J., 1991: Origins of carbonate in Neoproterozoic stromatolites and the identification of modern analogues. *Precambrian Research,* 53:281-299.

Fairchild, I.J., Hambrey, M.J., Spiro, B. & Jefferson, T.H., 1989: Late Proterozoic glacial carbonates in northeast Spitsbergen: new insights into the carbonate-tillite association. *Geological Magazine,* 126:469-490.

Fairchild, I.J., Marshall, J.D. & Bertrand-Sarfati, J., 1990: Stratigraphic shifts in carbon isotopes from Proterozoic stromatolitic carbonates (Mauritania): influences of primary mineralogy and diagenesis. *American Journal of Science.,* 290A:46-79.

Fairchild, I.J. & Spiro, B., 1987: Petrological and isotopic implications of some contrasting Late Precambrian carbonates, NE Spitsbergen. *Sedimentology,* 34:973-989.

Fallick, A.E. & Hamilton, P.J., 1989: Isotopic geochemistry of ocean waters through time. *Transactions of the Royal Society of Edinburgh: Earth Science,* 80: CHECK

Fanning, C.M., Ludwig, K.R., Forbes, B.G. and Preiss, W.V., 1986: Single and multiple grain U-Pb zircon analyses for the early Adelaidean Rook Tuff, Willouran Ranges, South Australia. In: *8th Australian Geological Convention, Adelaide, 1986. Abstracts,* Geological Society of Australia, 15:71-72.

Faure, G., 1986: *Principles of Isotope Geology.* J. Wiley & Sons, Chichester, 589 pp.

Field, B.D., 1991: Paralic and periglacial facies and contemporaneous deformation of the Late Proterozoic Olympic Formation, Pioneer Sandstone and Gaylad Sandstone, Amadeus Basin, central Australia. In: Korsch, R.J. & Kennard, J.M. (editors): *Geological and geophysical studies in the Amadeus Basin, central Australia.* Australian Bureau of Mineral Resources, Bulletin. 236:127-136.

Fischer, H.B., List, E.J., Koh, R.C.Y., Imburger, J. & Brooks. N.H., 1979: *Mixing in Inland and Coastal Waters.* New York Academic Press. 483 pp.

Forbes, B.G. & Preiss, W.V., 1978: Stratigraphy of the Wilpena Group. In: Preiss, W.V., (compiler): *The Adelaide Geosyncline. Late Proterozoic Stratigraphy, Sedimentation, Palaeontology and Tectonics.* Bulletin of the Geological Survey of South Australia, 53:211-248.

Freeman, K.H. & Hayes, J.M., 1992: Fractionation of Carbon Isotopes by Phytoplankton and Estimates of Ancient CO_2 levels. *Global Biogeochemical Cycles*, 6:185-198.

Freeman, K.H., Hayes, J.M., Trendel, J.M. & Albrecht, P., 1990: Evidence from carbon isotope measurements for diverse origins of sedimentary hydrocarbons. *Nature*, 343:254-256.

Freeman, M.J., Oaks, R.Q. (Jr.) & Shaw, R.D., 1991: Stratigraphy of the Late Proterozoic Gaylad Sandstone, northeastern Amadeus Basin, and recognition of an underlying regional unconformity. In: Korsch, R.J. & Kennard, J.M., (editors): *Geological and geophysical studies in the Amadeus Basin, central Australia.* Australian Bureau of Mineral Resources, Bulletin. 236: 137-154.

Freeman, M.J., Shergold, J.H., Morris, D.G. & Walter, M.R., 1990: Late Proterozoic and Palaeozoic Basins of Central and Northern Australia- regional geology and mineralisation. In: Hughes, F.E., (editor): *Mineral Deposits of Australia.* Australian Institute of Mineralogy and Metallurgy, 1125-1133.

Friedman, G.M., 1972: Significance of the Red Sea in the problem of evaporites and basinal limestones. *American Association of Petroleum Geologists Bulletin,* 56:1072-1086.

Friedman, G.M. & Sanders, J.E., 1978: Principles of Sedimentology. John Wiley & Sons, New York. 792 pp.

Galloway, W.E., 1989: Genetic stratigraphic sequences in basin analysis I: architecture and genesis of flooding - surface bounded depositional units. *American Association of Petroleum Geologists Bulletin,* 73:125-142.

Gao, G. & Land, L.S., 1991: Early Ordovician Cool Creek Dolomite, Middle Arbuckle Group, Slick Hills, SW Oklahoma, USA: origin and modification. *Journal of Sedimentary Petrology,* 61:161-173.

Garrels, R.M. & Lerman, A., 1984: Coupling of the sedimentary sulfur and carbon cycles - an improved model. *American Journal of Science.* 284:989-1007.

Gieskes, J.M., Elderfield, H. & Palmer, M.R., 1986: Strontium and its isotopic composition in interstitial waters of marine carbonate sediments. *Earth & Planetary Science Letters*, 77:229-235.

Glaessner, M.F., 1969: Trace fossils from the Precambrian and basal Cambrian. *Lethaia*, 2:369-393.

Glaessner, M.F. & Walter, M.R., 1975: New Precambrian fossils from the Arumbera Sandstone, Northern Territory, Australia. *Alcheringa*, 1:59-69.

Goldhaber, M.B., & Kaplan, I.R., 1974: The sulfur cycle, Chapter 17, in Goldberg, E.D. (editor), The Sea, Vol. 5, Marine Chemistry. New York, John Wiley & Sons, p. 569-655.

Goldstein, S.J. & Jacobsen, S.B., 1987: The Nd and Sr isotope systematics of river water dissolved material: Implications for the source of Nd and Sr in seawater. *Chemical Geology (Isotope Geoscience Section)*,66:245-272.

Goodfellow, W.D., 1986: Anoxic oceans and short-term carbon isotope trends. *Nature*, 322:116-117.

Goodfellow, W.D., 1987: Anoxic stratified oceans as a source of sulphur in sediment-hosted stratiform Zn - Pb deposits (Selwyn Basin, Yukon, Canada). *Chemical Geology (Isotope Geoscience section)*, 65: 359-382.

Gostin, V.A., Haines, P.W., Jenkins, R.J.F., Compston, W. & Williams, I.S., 1986: Impact ejecta horizon within late Precambrian shales, Adelaide Geosyncline, South Australia. *Science*, 233:198-200.

Gostin, V.A. & Jenkins, R.J.F., 1983: Sedimentation of the early Ediacaran, Flinders Ranges, South Asutralia. *Geological Society of Australia, Abstracts*, 9:196-197.

Gostin, V.A. & Williams, G.E., 1986: Giant impact structure and widely dispersed ejecta in the Precambrian of South Australia. In: *8th Australian Geological Convention, Adelaide, 1986. Geological Society of Australia, Abstracts*, 15:84.

Grant, S.W.F., 1990: Shell structure and distribution of *Cloudina*, a potential index fossil for the terminal Proterozoic. *American Journal of Science.*, 290A:261-294.

Grant, S.W.F., 1992: Carbon isotopic vital effect and organic diagenesis, Lower Cambrian Forteau Formation, northwest Newfoundland: implications for $\delta^{13}C$ chemostratigraphy. *Geology*, 20:243-246.

Gregory, R.T., 1990: Time scales for boundary event changes in the $^{18}O/^{16}O$ of seawater (abstract). *Geological Society of Australia, Abstracts*, 27 (ICOG 7). p41.

Grey, K., (in prep.): *Ediacarian acritarch biostratigraphy of Australia.* Unpublished PhD thesis, Macquarie University.

Griffin, B.J. & Preiss, W.V., 1976: The significance and provenance of stromatolitic clasts in a probable late Precambrian diamictite in north-western Tasmania. *Royal Society of Tasmania, Papers & Proceedings*, 110: 111-127.

Grotzinger, J.P., 1989: Facies and evolution of Precambrian carbonate depositional systems: emergence of the modern platform archetype, In: Crevello, P.D., Wilson, J.L., Sarg, J.F. & Read, J.F., (editors): *Controls on Carbonate Platform and Basin Development, Society of Economic Paleontologists and Mineralogists, Special Publication*, 44: 79-106.

Gruszczynski, M., Hoffman, A., Malkowski, K, & Veizer, J., 1992: Seawater strontium isotopic perturbation at the Permian-Triassic boundary, West Spitzbergen, and its implications for the interpretation of strontium isotopic data. *Geology*, 20:779-782.

Haines, P.W., 1987: Carbonate shelf and basin sedimentation, late Proterozoic Wonoka Formation, South Australia. PhD thesis, University of Adelaide (unpublished).

Haines, P.W., 1988. Storm-dominated mixed carbonate/siliciclastic shelf sequence displaying cycles of hummocky cross-stratification, Late Proterozoic Wonoka Formation, South Australia. *Sedimentary Geology*, 58:237-254.

Haines, P.W., 1990. A late Proterozoic storm-dominated carbonate shelf sequence: the Wonoka Formation in the central and southern Flinders Ranges, South Australia. In: Jago, J.B. & Moore, P.S., (eds): *The evolution of a Late Precambrian-Early Palaeozoic rift complex, Adelaide Geosyncline.* Geological Society of Australia, Special Publication 16:177-198.

Hardie, L.A., 1987: Dolomitization: a critical view of some current views. *Journal of Sedimentary Petrology*, 57:166-183.

Hargrave, B.T., 1972: Oxidation-reduction potentials, oxygen concentration and oxygen uptake of profundal sediment in a eutrophic lake. *Oikos*, 23:166-177.

Harland, W.B. & Herod, K.N., 1975: Glaciations through time. In: Wright, A.E. & Moseley, F., (editors): *Ice Ages: ancient and modern.* Geology Journal, Special Issue, 6:189-216.

Harland, W.B., Armstrong, R.L., Cox, A.V., Craig, L.E., Smith, A.G. & Smith, D.G., 1990: *A Geological Time Scale 1989.* Cambridge Univ. Press, Cambridge, 263pp.

Harte, J., 1988: *Consider a spherical cow: a course in environmental problem solving.* University Science Books, Mill Valley, CA. 283pp.

Harvey, M.R., Fallon, R.D. & Patton, J.S., 1986: The effect of organic matter and oxygen on the degradation of bacterial membrane lipids in marine sediments. *Geochimica et Cosmochimica Acta,* 50:795-804.

Hayes, J.M., 1993: Factors controlling ^{13}C contents of sedimentary organic compounds: Principles and evidence. *Marine Geology*, 113:111-125.

Hayes, J.M., Kaplan, I.R. & Wedeking, K.W., 1983. Chapter 5. Precambrian organic geochemistry, preservation of the record. In: Schopf, J.W., (editor): *Earth's Earliest Biosphere: its Origin and Evolution.* Princeton University Press, Princeton, pp. 93-134.

Hayes, J.M., Lambert, I.B. & Strauss, H., 1992: The sulfur-isotopic record. In: Schopf, J.W. & Klein, C., (eds): *The Proterozoic Biosphere: a Multidisciplinary Study.* Cambridge Uni. Press. pp:129-132.

Hayes, J.M., Popp, B.N., Takigiku, R. & Johnson, M.W., 1989: An isotopic study of biogeochemical relationships between carbonates and organic carbon in the Greenhorn Formation. *Geochimica et Cosmochimica Acta,* 53:2961-2972.

Hayes, J.M., Takigiku, R., Ocampo, R., Calloth, H.J. & Albrecht, P., 1987: Isotopic compositions and probable origins of organic molecules in the Eocene Messel Shale. *Nature*, 329:48-51.

Hays, P.D. & Grossman, E.L., 1991: Oxygen isotopes in meteoric calcite cements as indicators of continental palaeoclimate. *Geology*, 19:441-444.

Heaps, N.S. & Ramsbottom, A.E., 1966: Wind effects on the water in a narrow two-layered lake. *Phil. Trans. Roy. Soc. Lond. A.* 259:391-430.

Hird, K., & Tucker, M.E., 1988: Contrasting diagenesis of two Carboniferous oolites from south Wales: a tale of climatic influence. *Sedimentology*, 35:587-602.

Hird, K., Tucker, M.E., & Waters, R.A., 1987: Petrography, geochemistry and origin of Dinantian dolomites from south-east Wales. In: Miller, J., Adams, A.E., & Wright, V.P. (eds): *European Dinantian Environments*. John Wiley, Chichester. pp. 359-373.

Hodell, D.A., Mead, G.A. & Mueller, P.A., 1990: Variation in the strontium isotopic composition of seawater (8 Ma to present): implications for chemical weathering rates and dissolved fluxes to the oceans. *Chemical Geology*, 80:291-307.

Hoefs, J. 1987. *Stable Isotope Geochemistry*, 3rd ed., Springer-Verlag, Berlin, 241 pp.

Hoffman, A., Gruszczynski, M. & Malkowski, K., 1991: On the interrelationship between temporal trends in $\delta^{13}C$, $\delta^{18}O$ and $\delta^{34}S$ in the world ocean. *Journal of Geology*, 99:355-370.

Hofmann, H.J., 1987. Precambrian biostratigraphy. *Geoscience Canada*, 14:135-154.

Hofmann, H.J., Narbonne, G.M., & Aitken, J.D., 1990: Ediacaran remains from intertillite beds in northwestern Canada. *Geology*, 18:1199-1202.

Hollander, D.J. & McKenzie, J.A., 1991: CO_2 control on carbon isotope fractionation during aqueous photosynthesis: a paleo - pCO_2 barometer. *Geology*, 19:929-932.

Holser, W.T., 1977: Catastrophic chemical events in the history of the ocean. *Nature*, 267:403-408.

Holser, W.T. & Kaplan, I.R., 1966: Isotope geochemistry of sedimentary sulfates. *Chemical Geology*, 1:93-135.

Holser, W.T., Schidlowski, M., MacKenzie, F.T. & Maynard, J.B., 1988: Biogeochemical cycles of carbon and sulfur. In: Gregor, C.B., Garrels, R.M., MacKenzie, F.T. & Maynard, J.B., (editors): *Chemical Cycles in the Evolution of the Earth*. John Wiley & Sons. New York, pp: 105-174.

Holt, B.D. & Engelkemeir, A.G., 1970: The thermal decomposition of barium sulphate to sulfur dioxide for mass spectrometric analysis. *Analytical Chemistry*, 42:1451-3.

Horvath, Z. & Jackson, K.S., 1981: *Procedure for the Isolation of Kerogen from Sedimentary Rocks. Report 1981/82*, Bureau of Mineral Resources, Canberra, 6 pp.

Hovland, M., Talbot, M.R., Quale, H., Olaussen, S. & Aasberg, L., 1987: Methane-related carbonate cements in pockmarks of the North Sea. *Journal of Sedimentary Petrology*, 57:881-892.

Hsü, K.J., Oberhansli, H., Gao, J.Y., Jhu, S., Haihang, C. & Krahenbuhl, V., 1985: 'Strangelove Ocean' before the Cambrian explosion. *Nature*, 316:809-811.

Hsü, K.J., Ryan, W.B.F., & Cita, M.B., 1973: Late Miocene desiccation of the Mediterranean. *Nature*, 242: 240 - 244.

Hudson, J.D. & Anderson, T.F., 1989: Ocean temperatures and isotopic compositions through time. *Transactions of the Royal Society of Edinburgh. Earth Sciences*, 80:183-192.

Hudson, J.D., 1977: Stable isotopes and limestone lithification. *Journal of the Geological Society of London*, 133:637-660.

Irwin, H., Curtis, C. & Coleman, M., 1977: Isotopic evidence for source of diagenetic carbonates formed during burial of organic-rich sediments. *Nature*, 269:209-213.

Jackson, K.S., McKirdy, D.M. & Deckelman, Z., 1984: Hydrocarbon generation in the Amadeus Basin. *Australian Petroleum Exploration Association Journal*, 24:42-65.

Jenkins, R.J.F., 1981: The concept of an "Ediacaran Period" and its stratigraphic significance in Australia. *Transactions of the Royal Society of South Australia*, 105(4):179-194.

Jenkins, R.J.F., 1984: Ediacaran events: boundary relationships and correlation of key sections, especially in 'Armorica'. *Geological Magazine*, 121:635-643.

Jenkins, R.J.F., 1984b: Interpreting the oldest fossil cnidarians. *Palaeontographica Americana*, 54:95-104.

Jenkins, R.J.F., 1992: Functional and ecological aspects of Ediacaran assemblages. In: Lipps, J.H., & Signor, P.W. (eds): *Origin and early evolution of the metazoa.* New York and London, Plenum Press, p.131-176.

Jenkins, R.J.F., 1993a: Conceptsof Ediacarian and Ediacaran Systems. In: Jenkins, R.J.F., Lindsay, J.F. & Walter, M.R.: Field Guide to the Adelaide Geosyncline and Amadeus Basin, Australia. *AGSO Record* 1993/35:7-14.

Jenkins, R.J.F., 1993b: Ringwood area. [incorrectly attributed to M.R.Walter] In: Jenkins, R.J.F., Lindsay, J.F. & Walter, M.R.: Field Guide to the Adelaide Geosyncline and Amadeus Basin, Australia. *AGSO Record* 1993/35:54-57.

Jenkins, R.J.F. & Gehling, J.G., 1978: A review of the frond-like fossils of the Ediacara assemblage. *Records of the South Australian Museum*, 17(23):347-359.

Jenkins, R.J.F., Lindsay, J.F. & Walter, M.R., 1993: Field Guide to the Adelaide Geosyncline and Amadeus Basin, Australia. *AGSO Record* 1993/35

Jenkins, R.J.F., McKirdy, D.M., Foster, C.B., O'Leary, T. & Pell, S.D., 1992: The record and stratigraphic implications of organic-walled microfossils from the Ediacaran (terminal Proterozoic) of South Australia. *Geological Magazine*, 129:401-410.

Jewell, P.W., 1993: Water-column stability, residence times, and anoxia in the Cretaceous North American seaway. *Geology*, 21:579-582.

Jorgensen, B.B., Nelson, D.C., & Ward, D.M., 1992: Chemotrophy and decomposition in modern microbial mats. In: Schopf, J.W. & Klein, C., (eds): *The Proterozoic Biosphere: A Multidisciplinary Study.* Cambridge University Press. pp:287-293.

Juniper, S.K. & Fouquet, Y., 1988: Filamentous iron-silica deposits from modern and ancient hydrothermal sites. *Canadian Mineralogist*, 26:859-869.

Karhu, J. & Epstein, S., 1986: The implication of the oxygen isotope records in coexisting cherts and phosphates. *Geochimica et Cosmochimica Acta,* 50:1745-1756.

Kaufman, A.J. & Knoll, A.H., 1995: Neoproterozoic variations in the carbon-isotopic composition of seawater: stratigraphic and biogeochemical implications. *Precambrian Research*, 73: 27-50.

Kaufman, A.J., Hayes, J.M., Knoll, A.H. & Germs, G.J.B., 1991: Isotopic compositions of carbonates and organic carbon from upper Proterozoic successions in Namibia: stratigraphic variation and the effects of diagenesis and metamorphism. *Precambrian Research*, 49:301-327.

Kaufman, A.J., Jacobson, Stein B. & Knoll, A.H., 1993: The Vendian record of Sr and C isotopic variations in seawater: implications for tectonics and palaeoclimate. *Earth & Planetary Science Letters*, 120:409-430.

Kaufman, A.J., Knoll, A.H. & Awramik, S.M., 1992: Biostratigraphic and chemostratigraphic correlation of Neoproterozoic sedimentary successions: Upper Tindir Group, northwestern Canada, as a test case. *Geology*, 20:181-185.

Kaye, C.A. & Zartman, R.F., 1985: A late Proterozoic Z to Cambrian age for the stratified rocks of the Boston Basin, Massachusetts, U.S.A. In: Wones, D.R., (editor): *The Caledonides of the U.S.A. Dept. Geol. Sci. Virginia Polytech. Inst., State Univ. Mem.*, 2:257-261.

Keays, R.R., Wallace, M.W. & Gostin, V.A., 1992: Mobilization of the Platinum Group Elements by low temperature fluids: Implications for mineralization in red bed environments. *Geological Society of Australia Abstracts,* 32:64-65.

Keith, M.L. & Weber, J.N., 1964: Carbon and oxygen isotopic compositions of selected limestones and fossils. *Geochimica et Cosmochimica Acta,* 28:1789-1816.

Kennard, J.M., 1991: Lower Cambrian archaeocyathan buildups, Todd River Dolomite, northeast Amadeus Basin, central Australia: sedimentology and diagenesis. In: Korsch, R.J. & Kennard, J.M., (editors): *Geological and geophysical studies in the Amadeus Basin, central Australia*, Bureau of Mineral Resources, Australia, Bulletin 236, p. 195-225.

Kennard, J.M. & Lindsay, J.F., 1991: Sequence stratigraphy of the latest Proterozoic. Cambrian Pertaoorrta Group, northern Amadeus Basin, central Australia. In: Korsch, R.J. & Kennard, J.M., (editors): *Geological and geophysical studies in the Amadeus Basin, central Australia*, Bureau of Mineral Resources, Australia, Bulletin 236, p. 171-194.

Kennedy, M., 1993: The Undoolya Sequence: Late Proterozoic salt influenced deposition, Amadeus Basin, central Australia. *Australian Journal of Earth Science,* 40:217-228.

Kennedy, M.J. & Wallace, M.W., 1993: The stratigraphy and significance of post-glacial carbonate horizons in the Amadeus Basin. In: Alexander, E.M. & Gravestock, D.I., (editors): *Central Australian Basins Workshop*, Programme & Abstracts, p. 75-76.

Kinsman, D.J.J., Boardman, M. & Boresik, M., 1974: An experimental determination of the solubility of oxygen in marine brines. In: Coogan, A.H., (editor):*4th Symposium on salt: Cleveland, Ohio, Northern Ohio Geological Society*,p. 325-327.

Kirschvink, J.L., Margaritz, M., Ripperdan, R.L., Zhuravlev, A.Y. & Rozanov, A.Y., 1991: The Precambrian-Cambrian boundary: magnetostratigraphy and carbon isotopes resolve correlation problems between Siberia, Morocco, and South China. *GSA Today*, 1:69-71, 87-91.

Knoll, A.H., Grotzinger, J.P., Kaufman, A.J. & Kolosov, O., (1995): Integrated approaches to Terminal Proterozoic Stratigraphy: an example from the Olenek Uplift, Northeast Siberia. *Precambrian Research,* 73:251-270.

Knoll, A.H., Hayes, J.M., Kaufman, A.J., Swett, K. & Lambert, I.B., 1986: Secular variation in carbon isotope ratios from Upper Proterozoic successions of Svalbad and East Greenland. *Nature*, 321:832-838.

Knoll, A.H. & Swett, K., 1990: Carbonate deposition during the Late Proterozoic era: an example from Spitsbergen. *American Journal of Science*, 290A:104-132.

Knoll, A.H. & Walter, M.R., 1992: Latest Proterozoic stratigraphy and earth history. *Nature*, 356:673-678.

Korsch, R.J., 1986: Pertatataka Formation. In: Kennard, J.M., Nicoll, R.S. & Owen, M., (editors): *Field Excursion 25B, 12th International Sedimentological Congress*, BMR Canberra, Australia. pp:103-107.

Kroopnick, P.M., 1985: The distribution of ^{13}C of total CO_2 in the world oceans. *Deep Sea Research*, 32:57-84.

Kröner, A., 1977: Non-synchroniety of late Precambrian glaciations in Africa. *Journal of Geology*, 85:289-300.

Krough, T.E., Strong, D.F., O'Brien, S.J. & Papezik. V., 1988: Precise U-Pb zircon dates from the Avalon Terrain in Newfoundland. *Canadian Journal of Earth Science*, 25:442-453.

Kump, L.R., 1991: Interpreting carbon-isotope excursions: "Strangelove oceans". *Geology*, 19:299-302.

Kvenvolden, K.A., 1993: Gas hydrates - geological perspective and global change. *Reviews of Geophysics*, 31:173-187.

Lambert, I.B. & Donnelly, T.H., 1990: Atmospheric oxygen levels in the Precambrian: a review of isotopic and geological evidence. In: *Atmospheric Oxygen Variation through Geologic Time.* Penn State.

Lambert, I.B. & Donnelly, T.H., 1992: Global oxidation and a supercontinent in the Proterozoic: evidence from stable isotopic trends. In: Schidlowski, M., (editor): *Early Organic Evolution: implications for mineral and energy resources*. Springer-Verlag.

Lambert, I.B., Walter, M.R., Zang, W., Lu, S. & Ma, G., 1987: Paleoenvironment and carbon isotope stratigraphy of Upper Proterozoic carbonates of the Yangtze Platform. *Nature*, 325:140-142.

Land, L.S., 1980: The isotopic and trace element geochemistry of dolomite: the state of the art. In: Zenger, D.H., Durham, J.B. & Ethington, R.L., (editors): *Concepts and Models of Dolomitization*. SEPM Special Publication, 28:87-110.

Land, L.S., 1992: The dolomite problem: stable and radiogenic isotope clues. In: Clauer, N. & Chaudhuri, S., (editors): *Isotopic signatures and sedimentary records*. Lectures notes in Earth Sciences, 43. N.Y., Springer.p.49-68.

Landing, E., 1994: Precambrian-Cambrian boundary stratotype ratified and a new perspective on Cambrian time. *Geology*, 22:179-182.

Lasemi, Z. & Sandberg, P.A., 1984: Transformation or aragonite-dominated lime muds to microcrystalline limestones. *Geology*, 12:420-423.

Lasemi, Z., Sandberg, P.A. & Boardman, M.R., 1990: New microtextural criterion for differentiation of compaction and early cementation in fine-grained limestone. *Geology*, 18:370-373.

Lazar, B. & Erez, J., 1990: Extreme ^{13}C depletions in seawater-derived brines and their implications for the past geochemical carbon cycle. *Geology*, 18:1191-1194.

Lazar, B. & Erez, J., 1992: Carbon geochemistry of marine-derived brines: 1. ^{13}C depletions due to intense photosynthesis. *Geochimica et Cosmochimica Acta,* 56:335-346.

Leaman, D.E., Baillie, P.W. & Powell, C.McA., 1994: Precambrian Tasmania: a Thin-Skinned Devil. *Exploration Geophysics*, 25:19-23.

Lemon, N.M., 1985: Physical modelling of sedimentation of sedimentation adjacent to diapirs and comparison with late Precambrian Oratunga breccia body in central Flinders Ranges, South Australia. *American Association of Petroleum Geologists Bulletin,* 69:1327-1338.

Lemon, N.M. & Gostin, V.A., 1990: Glacigenic sediments of the late Proterozoic Elatina Formation and equivalents, Adelaide Geosyncline, South Australia. In: Jago, J.B. & Moore, P.S., (editors): *The Evolution of a Late Precambrian-early Palaeozoic Rift Complex: the Adelaide Geosyncline.* Geological Society of Australia, Special Publication 16:149-163.

Lemon, N.M., Cooper, A.M. & McKirdy, D.M., 1992: Late Proterozoic source rocks associated with Diapirs in the Central Flinders Ranges, South Australia (abstract). In: *1992 A.A.P.G. International Conference and Exhibition, Sydney, Australia.* p:61.

Lennox, P.G., Corbett, K.D., Baillie, P.W., Corbett, E.B. & Brown, A.V., 1982: *Smithton, Tasmania.* Tasmanian Department of Mines Geologicasl Atlas 1:50,000 series. Sheet 21 (7916S).

Lindsay, J.F., 1987: Sequence stratigraphy and depositional controls in Late Proterozoic-early Cambrian sediments f the Amadeus Basin, central Australia. *American Association of Petroleum Geologists Bulletin,* 71:1387-1403.

Lindsay, J.F., 1989: Depositional controls on glacial facies associations in a basinal setting, Late Proterozoic, Amadeus Basin, Central Australia. *Palaeogeography, Palaeoclimatology, Palaeoecology*, 73:205-232.

Lindsay, J.F. & Korsch, R.J., 1991: The evolution of the Amadeus Basin, central Australia. In: Korsch, R.J. & Kennard, J.M., (editors): *Geological and geophysical studies in the Amadeus Basin, central Australia.* Australian Bureau of Mineral Resources, Bulletin 236:7-32.

Lindsay, J.F., Korsch, R.J. & Wilford, J., 1987: Timing the breakup of a Proterozoic supercontinent: evidence from Australian intracratonic basins. *Geology*, 15:1061-1064.

Lindsay, J.F., Leven, J., Krieg, G. & Cockshell, D., 1992: The Petroleum Potential of the Officer Basin (abstract). In: *1992 American Association of Petroleum Geologists International Conference and Exhibition, Sydney.* p. 62.

Lindsay, J.F. & Reine, K., 1995: Well-log Data, Officer Basin, South Australia. *Australian Geological Survey Organisation, Record* 1995/2. 13pp.

Logan, G.A., Hayes, J.M., Hieshima, G.B., & Summons, R.E., in press: Terminal Proterozoic Reorganisation of Biogeochemical Cycles. *Nature*.

Lohmann, K.C., 1982: "Inverted J" carbon and oxygen isotopic trends: a criterion for shallow meteroic phreatic diagenesis (abstract). *Geological Society of America. Abstracts with programs.* p. 548.

Longman, M.J. & Matthews, W.L., 1961: *Geology of the Bluff Point and Trowutta quadrangles*. Tasmanian Department of Mines Technical Report 6:48-54.

Maliva, R.G., Knoll, A.H. & Siever, R., 1990: Secular change in chert distribution: A reflection of evolving biological participation in the silica cycle. *Palaios*, 4: 519-532.

Malone, M.J., Baker, P.A., & Burns, S.J., 1994: Recrystallization of dolomite: evidence from the Monterey Formation (Miocene), California. *Sedimentology*, 41:1223-1240.

Margaritz, M., 1989: ^{13}C minima follow extinction events: a clue to faunal radiation. *Geology*, 17:337-340.

Margaritz, M., Holser, W.T. & Kirschvink, J.L., 1986: Carbon-isotope events across the Precambrian/Cambrian boundary in the Siberian Platform. *Nature*, 320:258-259.

Margaritz, M., Kirschvink, J.L., Latham, A.J., Zhuravlev, A.Y. & Rozanov, A.Y., 1991: Precambrian/Cambrian boundary problem: carbon isotope correlations for Vendian and Tommotion time between Siberia and Morocco. *Geology*, 847-850.

Margaritz, M., Krishnamurphy, R.V. & Holser, W.T., 1992: Parallel trends in organic and inorganic carbon isotopes across the Permian-Triassic boundary. *American Journal of Science*, 292:727-739.

Marshall, D.J., 1988: *Cathodoluminescence of Geological Materials*. Unwin Hyman Ltd. 146 pp.

Marshall, J. D., 1992: Climatic and oceanographic isotopic signals from the carbonate rock record and their preservation. *Geological Magazine*, 129:143-160.

Marshall, J.E.A., 1990: Determination of thermal maturity. In: Briggs, D.E.G. & Crowther, P.R., (editors): *Palaeobiology: a synthesis*. Blackwell. pp:511-515.

McConnaughy, T. & McRoy, C.P., 1979: Food web structure and the fractionation of carbon isotopes in the Bering Sea. *Marine Biology*, 53:257-262.

McCrea, J.M., 1950: On the isotopic chemistry of carbonates and a paleotemperature scale. *Journal of Chemical Physics*, 18:849 857.

McKenzie, J.A., 1981: Holocene dolomitization of calcium carbonate sediments from the coastal sabkhas of Abu Dhabi, UAE: a stable isotope study. *Journal of Geology*, 89:155-198.

McKenzie, J.A., Jenkyns, H.C. & Bennet, G.G., 1979: Stable isotope study of the cyclic diatomite-claystones from the Tripoli Formation, Sicily: a prelude to the Messinian salinity crisis. *Palaeogeography, Palaeoclimatology, Palaeoecology*, 29:125-141.

McKirdy, D.M., 1976: Biochemical markers in stromatolites. In: Walter, M.R., (editor): *Stromatolites - developments in sedimentology*, 20:163-191. Elsevier, Amsterdam.

McKirdy, D.M., Pell, S.D. & Smyth, M., 1992: Rodda beds, eastern Officer Basin: anatomy of a lean Neoproterozoic petroleum source rock (abstract). *Geological Society of Australia Abstracts* No. 32. p. 128.

McKirdy, D.M. & Powell, T.G., 1974: Metamorphic alteration of carbon isotopic composition in ancient sedimentary organic matter: new evidence from Australia and South Africa. *Geology*, 2:591-595.

McKirdy, D.M., Sumartojo, J., Tucker, D.H. & Gostin, V., 1975: Organic, mineralogic and magnetic indicators of metamorphism in the Tapley Hill Formation, Adelaide Geosyncline. *Precambrian Research*, 2:345-373.

Miall, A.D., 1992: Exxon global cycle chart: an event for every occasion? *Geology*, 20:787-790.

Mizutani, H. & Wada, E., 1982: Effect of high atmospheric CO_2 concentration on ^{13}C of algae. *Origins of Life*, 12:377-387.

Mook, W.G., Bommerson, J.C. & Staverman, W.H., 1974: Carbon isotope fractionation between dissolved bicarbonate and gaseous carbon dioxide. *Earth & Planetary Science Letters*, 22:169-176.

Moores, E.M., 1991: Southwest U.S.- East Antarctic (SWEAT) connection: a hypothesis. *Geology*, 19:425-428.

Mozley, P.S., & Burns, S.J., 1993: Oxygen and carbon isotopic compositions of marine carbonate concretions: an overview. *Journal of Sedimentary Petrology*, 63:73-83.

Muelenbachs, K. & Clayton, R.N., 1976: Oxygen isotope composition of the oceanic crust and its bearing on seawater. *Journal of Geophysical Research,* 81:4365-4369.

Mullins, H.T., Dix, G.R., Gardulski, A.F. & Land, L.S., 1988: Neogene deep-water dolomite from the Florida-Bahamas Platform. In: Shukla, V. & Baker, P.A., (editors): *Sedimentology and Geochemistry of Dolostones,* SEPM Special Publication No. 43:235-243.

Narbonne, G.M., Kaufman, A.J. & Knoll, A.H., 1994: Integrated chemostratigraphy and biostratigraphy of the Windermere Supergroup, northwestern Canada: implications for Neoproterozoic correlations and the early evolution of animals. *Geological Society of America Bulletin,* 106:1281-1292.

Oaks, R.Q. (Jr.), Deckelman, J.A., Conrad, K.T., Hamp, L.T., Phillips, J.O. & Stewart, A.J, 1991: Sedimentation and tectonics in the northeastern and central Amadeus Basin, central Australia. In: Korsch, R.J. & Kennard, J.M., (editors): *Geological and geophysical studies in the Amadeus Basin, central Australia.* Australian Bureau of Mineral Resources, Bulletin 236:73-90.

Oaks, R.Q. (Jr.), Stewart, A.J., Deckelman, J.A. & Conrad, K.T., 1990: *Geology of the Northeastern Amadeus Basin* (1:100,000 scale map). Bureau of Mineral Resources, Canberra.

Palmer, M.R. & Elderfield, J.M., 1989: The Sr isotope budget of the modern ocean. *Earth & Planetary Science Letters*, 92:11-26.

Pederson, T.F. & Calvert, S.E., 1990: Anoxia vs. Productivity: what controls the formation of organic-carbon-rich sediments and sedimentary rocks? *American Association of Petroleum Geologists Bulletin,* 74:454-466.

Pell, S.D., McKirdy, D.M., Jansyn, J. & Jenkins, R.J.F., 1993: Ediacaran carbon isotope stratigraphy of South Australia - an initial study. *Transactions of the Royal Society of South Australia*, 117:153-161.

Peterman, Z.E., Hedge, C.E. & Tourtelot, H.A., 1970: Isotopic composition of stontium in sea water throughout Phenerozoic time. *Geochimica et Cosmochimica Acta*, 34:105-120.

Plumb, K.A., 1991: New Precambrian time scale. *Episodes*, 14:139-140.

Plummer, P.S. & Gostin, V.A., 1981: Shrinkage cracks: Desiccation or Synaeresis? *Journal of Sedimentary Petrology*, 51:1147-1156.

Plummer, P.S., 1978. Stratigraphy of the lower Wilpena Group (late Precambrian), Flinders Ranges, South Australia. *Transactions of the Royal Society of South Australia*, 102:25-38.

Plummer, P.S., 1979: Note on the Palaeoenvironmental Significance of the Nuccaleena Formation (Upper Precambrian), Central Flinders Ranges, South Australia. *Journal of the Geological Society of Australia,* 25:395-402.

Popp, B.N., Anderson, T.F. & Sandberg, P.A., 1986: Brachiopods as indicators of original isotopic compositions in some Paleozoic limestones. *Geological Society of America Bulletin*, 97:1262-1269.

Popp, B.N., Takigiku, R., Hayes, J.M., Louda, J.W. & Baker, E.W., 1989. The post-Paleozoic chronology and mechanism of $\delta^{13}C$ depletion in primary marine organic matter. *American Journal of Science*, 289:436-454.

Posamentier, H.W., & Vail, P.R., 1988: Eustatic controls on clastic deposition II: Sequence and systems tract models. *in* Wilgus, C.K. et al. (eds.): *Sealevel changes: an integrated approach.* Society of Economic Paleontologists and Mineralogists. Special Publication 42: 125-154.

Powell, C.McA., 1992: New perspectives in Tasmanian Geology. in *Tasmania: an island of potential. Bulletin of the Geological Survey of Tasmania*, 70:177-187.

Preiss, W.V., 1984: Correlation of the uppermost late Precambrian succession across the Torrens Hinge Zone in the Port Augusta region of South Australia: a discussion. *Transactions of the Royal Society of South Australia*, 108:223-224.

Preiss, W.V., (compiler), 1987a: The Adelaide Geosyncline - late Proterozoic stratigraphy, sedimentation, palaeontology and tectonics. *Geological Survey of South Australia, Bulletin*, 53:438p.

Preiss, W.V., 1987b: Stratigraphic nomenclature and classification. in Preiss, W.V., (compiler): The Adelaide Geosyncline - late Proterozoic stratigraphy, sedimentation, palaeontology and tectonics. *Geological Survey of South Australia, Bulletin*, 53: p. 29-34.

Preiss, W.V., 1987c: A review of available geochronology for the Adelaidean. in Preiss, W.V., (compiler): The Adelaide Geosyncline - late Proterozoic stratigraphy, sedimentation, palaeontology and tectonics. *Geological Survey of South Australia, Bulletin*, 53: p. 249-254.

Preiss, W.V., 1987d: Precambrian Palaeontology of the Adelaide Geosyncline. in Preiss, W.V., (compiler): The Adelaide Geosyncline - late Proterozoic stratigraphy, sedimentation, palaeontology and tectonics. *Geological Survey of South Australia, Bulletin*, 53: p. 283-313.

Preiss, W.V., 1993: Neoproterozoic. In: Drexel, J.F., Preiss, W.V. & Parker, A.J., (editors): *The geology of South Australia. Volume 1: The Precambrian.* Bulletin of the Geological Survey of South Australia, 54:171-203.

Preiss, W. & Forbes, B.G., 1981: Stratigraphy, correlation and sedimentary history of Adelaidean (Late Proterozoic) basins in Australia. *Precambrian Research*, 15:255-304.

Preiss, W.V., & Forbes, B.G., 1987: Stratigraphy of the Wilpena Group. in Preiss, W.V., (compiler): The Adelaide Geosyncline - late Proterozoic stratigraphy, sedimentation, palaeontology and tectonics. *Geological Survey of South Australia, Bulletin*, 53: p. 211-248.

Preiss, W.V. & Kreig, G.W., 1992: Stratigraphic drilling in the northeastern Officer Basin: Rodda 2 Well. *Mines and Energy Review, South Australia*, 158:48-51.

Preiss, W.V., Walter, M.R., Coates, R.P. & Wells, A.T., 1978: Lithological correlations of Adelaidean glaciogenic rocks in parts of the Amadeus, Ngalia, and Georgina Basins. *BMR Journal of Australian Geology & Geophysics*, 3:45-53.

Prichard, C.E. & Quinlan, T., 1962: *The geology of the southern half of the Hermannsburg* 1:250,000 sheet. Bureau of Mineral Resources Report 61.

Quay, P.D., Broecker, W.S., Hesslein, R.H. & Schindler, D.W., 1980: Vertical diffusion rates determined by tritium tracer experiments in the thermocline and hypolimnion of two lakes. *Limnology and Oceanography*, 25:201-218.

Radke, B.H. & Mathis, R.l.L., 1980: On the formation and occurrence of saddle dolomite. *Journal of Sedimentary Petrology,* 50:1149-1168.

Raheim, A. & Compston, W., 1977: Correlations between metamorphic events and Rb-Sr ages in metasediments and eclogite from Western Tasmania. *Lithos*, 10:271-290.

Raiswell, R., 1971: The growth of Cambrian and Liassic concretions. *Sedimentology*, 17:147-171.

Raiswell, R., 1982: Pyrite texture, isotopic composition and the availability of iron. *American Journal of Science.*, 282:1244-1236.

Rao, C.P., 1990: Petrography, trace elements and oxygen and carbon isotopes of Gordon Group carbonates (Ordovician), Florentine Valley, Tasmania, Australia. *Sedimentary Geology,* 66:83-98.

Rau, G.H., Froelich, P.A., Takahashi, T. & Des Marais, D.J., 1991: Does sedimentary organic $\delta^{13}C$ record variation in Quaternary ocean [CO_2(aq)]? *Palaeoceanography*, 6:335-347.

Rau, G.H., Takahashi, T. & Des Marais, D.J., 1989: Latitudinal variations in plankton $\delta^{13}C$: implications for CO_2 and productivity in past oceans. *Nature*, 341:516-518.

Reineck, H.E. & Singh, I.B., 1973: *Depositional sedimentary environments.* Springer-Verlag, New York-Heidelberg-Berlin, 439p.

Roeske, C.A. & O'Leary, M., 1984. Carbon isotope effects on the enzyme-catalyzed carboxylation of ribulose bisphosphate. *Biochemistry*, 1984:6275-6284.

Romanek, C.S., Grossman, E.L., & Morse, J.W., 1992: Carbon isotopic fractionation in synthetic aragonite and calcite: effects of temperature and precipitation rate. *Geochimica et Cosmochimica Acta*, 56:419-430.

Rosenbaum, J. & Sheppard, S.M.F., 1986. An isotopic study of siderites, dolomites and ankerites at high temperatures. *Geochimica et Cosmochimica Acta,* 50:1147-1150.

Ross, G.M., 1991: Meltdown of the second Windermere glaciation: a working hypothesis. *Geological Association of Canada, Programs with Abstracts*, 14A:99.

Ross, G.M., Block, J.D. & Krause, H.R., 1991: Sulphur isotope geochemistry of authigenic pyrite, late Proterozoic Windermere Supergroup, Cariboo Mountains, British Columbia. *Geological Association of Canada, Programs with Abstracts*, 16:108.

Ross, G.M., Block, J.D. & Krause, H.R., 1995: Neoproterozoic strata of the southern Canadian Cordillera and the isotopic evolution of seawater sulfate. *Precambrian Research*, 73:71-100.

Salter, A.H., 1984: Petrologic and geochemical constraints on the origin of subsurface dolomite, Enewetak Atoll: an example of dolomitization by normal seawater. *Geology*, 12:217-220.

Sandberg, P.A., 1983: Evaluation of Ancient Aragonite Cements and their Temporal Distribution. (abstract) *American Association of Petroleum Geologists Bulletin*, 67:544.

Sarmiento, J.L., Freely, W.H., Moose, W.S., Bainbridge, A.E. & Broecker, W.S., 1976: The relationship between vertical eddy diffusion and bouyancy gradient in the deep sea. *Earth & Planetary Science Letters*, 32:357-370.

Savin, S.M., & Yeh, H.W., 1981: Stable isotopes in ocean sediments. In: Emiliani, C. (ed): *The Sea*, Vol. 7: The Oceanic Lithosphere. Wiley-Interscience, New York, pp. 1521-1554.

Schidlowski, M., 1988. A 3,800-million-year old isotopic record of life from carbon in sedimentary rocks. *Nature*, 333:313-317.

Schidlowski, M., Eichmann, R. & Junge, C., 1975: Precambrian sedimentary carbonates: carbon and oxygen isotope geochemistry and implications for the terrestrial oxygen budget. *Precambrian Research*, 2:1-69.

Schidlowski, M, Gorzawski, H., & Dor, I., 1992: Experimental hypersaline ponds as Model Environments for Stromatolite Formation 2. Isotopic biogeochemistry. In: Schidlowski, M., Golubic, S., Kimberley, M.M., McKirdy, D.M. & Trudinger, P.A., (editors): *Early Organic Evolutions*, pp:494-508. Springer.

Schidlowski, M., Hayes, J.M. & Kaplan, I.R., 1983. Isotopic inferences of ancient biochemistries: carbon, sulfur, hydrogen, and nitrogen. In: Schopf, J.W., (editor), *Earth's Earliest Biosphere: Its Origin and Evolution.* (Princeton University Press: Princeton), pp:149-187.

Schieber, J., 1986: The possible role of benthic microbial mats during the formation of carbonaceous shales in shallow mid-Proterozoic basins. *Sedimentology*, 33:521-536.

Schieber, J., 1989: Facies and origin of shales from the mid-Proterozoic Newland Formation, Belt Basin, Montana, USA. *Sedimentology*, 36:203-219.

Schieber, J., 1990: Significance of styles of epicontinental shale sedimentation in the Belt Basin, mid-Proterozoic of Montana, USA. *Sedimentary Geology*, 69:297-312.

Scholle, P. A. & Arthur, M. A., 1980: Carbon Isotope Fluctuations in Cretaceous Pelagic Limestones: Potential Stratigraphic and Petroleum Exploration Tool. *American Association of Petroleum Geologists Bulletin,* 64:67-87.

Scruton, P.C., 1953: Deposition of Evaporites. *American Association of Petroleum Geologists Bulletin,* 37:2498-2512.

Semikhatov, M.A., 1979: New stratigraphic scale of the Precambrian in the USSR: an analysis and its implications. *International Geology Review*, 23:139-154.

Seymour, D.B. & Baillie, P.W., 1992: *Woolnorth, Tasmania.* Tasmanian Department of Mines Geological Atlas 1:50,000 series, Sheet 20(7816S).

Shackleton, N.J., 1968: Depth of pelagic foraminifera and isotopic changes in Pleistocene oceans. *Nature,* 218:79-80.

Shackleton, N.J., 1977: Tropical rainforest history and the equatorial Pacific carbonate dissolution cycles. In: Anderson, N.R. & Malahoff, A., (editors): *The fate of fossil fuel* CO_2 *in the oceans.* Plenum Press, N.Y. p:401-428.

Shaw, R.D., Etheridge, M.E. & Lambeck, K., 1991: Development of the Late Proterozoic to mid-Palaeozoic, intracratonic Amadeus Basin in Central Australia: a key to understanding tectonic forces in plate interiors. *Tectonics*, 10: 688-721.

Sheppard, S.M.F. & Schwarcz, H.P., 1970: Fractionation of carbon and oxygen isotopes and magnesium between co-existing metamorphic calcite and dolomite. *Contributions to Mineral Petrology*, 26:161-198.

Sibley, D.F., 1991: Secular changes in the amount and texture of dolomite. *Geology*, 19:151-154.

Simoneit, B.R.T., Schoell, M., Dias, R.F. & Aquino Neto, F.R., 1993: Unusual carbon isotopic compositions of biomarker hydrocarbons in a Permian tasmanite. *Geochimica et Cosmochimica Acta,* 57:4205-4211.

Sippel, R.F. & Glover, E.D., 1965: Structures in carbonate rocks made visible by luminescence petrography. *Science*, 150:1283-1287.

Smith, A.G., 1968: The origin and deformation of some "molar-tooth" structures in the Precambrian Belt - Purcell Supergroup. *Journal of Geology,* 76:426-443.

Smith, L.H., Kaufman, A.J. & Knoll, A.H., (in press): Chemostratigraphy of predominantly siliciclastic Neoproterozoic successions: a case study of the Pocatello Formation and Lower Brigham Group. Idaho, USA.

Solomon, M. & Griffiths, F.J., 1972: Tectonic evolution of the Tasman Orogenic Zone, eastern Australia. *Nature*, 237:3-6.

Spry, A., 1962: The Precambrian Rocks. In: Spry, A. & Banks, M.R., (editors): *The Geology of Tasmania.* Journal of the Geological Society of Australia, 107-126.

Stainton, P.W., Weste, G. & Cucuzza, G., 1988: *Exploration of PEL23 and PEL30, eastern Officer Basin, South Australia (1983-1988).* South Australia Department of Mines and Energy, open file envelope 5073:1243-1321.

Steiger, R.M. & Jäger, E., 1977: Subcommission on Geochronology: convention on the use of decay constants in geochronology and cosmochronology. In: Cohee, G.V., Glaessner, M.F. & Hedburg, H.D., (editors): *Contributions to the Geological Time Scale. American Association of Petroleum Geologists Studies in Geology*, 6:67-71.

Stewart, A.J., Oaks, R.Q. (Jr)., Deckelman, J.A. & Shaw, R.D., 1991: 'Mesothrust' versus 'megathrust' interpretations of the structure of the northeastern Amadeus Basin, central Australia. In: Korsch, R.J. & Kennard, J.M., (editors): *Geological and geophysical studies in the Amadeus Basin, central Australia.* Australian Bureau of Mineral Resources, Bulletin 236:361-384.

Strauss, H. & Schieber, J., 1990: A sulfur isotope study of pyrite genesis: the mid-Proterozoic Newland Formation, Belt Supergroup, Montana. *Geochimica et Cosmochimica Acta*, 54:197-204.

Strauss, H., Bengtson, S., Myrow, P.M. & Vidal, G., 1992(a): Stable isotope geochemistry and palynology of the late Precambrian to Early Cambrian sequence in Newfoundland. *Canadian Journal of Earth Science*, 29:1662-1673.

Strauss, H., Des Marais, D.J., Hayes, J.M., Lambert, I.B. & Summons, R.E., 1992(b): Procedures of whole rock and kerogen analysis. In: Schopf, J.W. & Klein, C., (eds): *The Proterozoic Biosphere: A Multidisciplinary Study.* Cambridge University Press. pp:699-708.

Strauss, H., Des Marais, D.J., Hayes, J.M., & Summons, R.E., 1992(c): Proterozoic Organic Carbon - Its Preservation and Isotopic Record. In: Schidlowski, M., Golubic, S., Kimberley, M.M., McKirdy, D.M. & Trudinger, P.A., (editors): *Early Organic Evolution*, pp:203-211. Springer.

Strauss, H., Des Marais, D.J., Summons, R.E. & Hayes, J.M., 1992(d): The carbon-isotopic record. In: Schopf, J.W. & Klein, C., (editors): *The Proterozoic Biosphere: A Multidisciplinary Study.* Cambridge University Press. pp:117-128.

Sukanta, U., Thomas, B., von der Borch, C.C. & Gatehouse, C.G., 1991: Sequence stratigraphic studies and canyon formation, South Australia. *P.E.S.A. Journal, September, 1991.* 68-73.

Summons, R.E. & Hayes, J.M., 1992: Principles of molecular and isotopic biogeochemistry. In: Schopf, J.W. & Klein, C., (editors): *The Proterozoic Biosphere: A Multidisciplinary Study.* Cambridge University Press. pp: 83-94.

Summons, R.E. & Powell, T.G., 1986: Chlorobiaceae in Palaeozoic seas revealed by biological markers, isotopes and geology. *Nature*, 319:763-765.

Sweeney, R.E., & Kaplan, I.R., 1973: Pyrite framboid formation: laboratory synthesis and marine sediments. *Economic Geology*, 68:618-634.

Swift, D.J.P., Hudelson, P.M., Brenner, R.L. & Thompson, P., 1987: Shelf construction in a foreland basin: storm beds, shelf sandbodies, and shelf-slope depositional sequences in the Upper Cretaceous Mesaverde Group, Book Cliffs, Utah. *Sedimentology*, 34: 423-457.

Takahashi, T., Broecker, W. S., Li, Y. H. & Thurber, D., 1968: Chemical and isotopic balances for a meromictic lake. *Limnology and Oceanography*, 13:272-292.

Tappan, H., 1986: Phytoplankton: below the salt at the global table. *Journal of Paleontology*, 60:545-554.

Thomson, B.P., 1969: Precambrian basement cover: the Adelaide System. In: Parkin, L.W., (editor): *Handbook of South Australian Geology.* Geological Survey of South Australia. pp:49-83.

Thorpe, S.A., 1974: Near-resonant forcing in a shallow two-layer fluid: a model for the internal surge in Loch Ness? *Journal of Fluid Mechanics*, 63:509-527.

Traverse, A., 1988: *Paleopalynology.* Unwin Hyman, London, 600 pp.

Tucker, M.E. & Wright, V.P., 1990: *Carbonate sedimentology.* Blackwell Scientific Publications, 482pp.

Tucker, M.E., 1982: Precambrian dolomites: petrographic and isotopic evidence that they differ from Phanerozoic dolomites. *Geology*, 10:7-12.

Tucker, M.E., 1983: Diagenesis, geochemistry, and origin of a Precambrian dolomite: The Beck Spring Dolomite of eastern California. *Journal of Sedimentary Petrology*, 53:1097-1119.

Tucker, M.E., 1986a: Carbon isotope excursions in Precambrian/Cambrian boundary beds, Morocco. *Nature*, 319:48-50.

Tucker, M.E., 1986b: Formerly aragonitic limestones associated with tillites in the late Proterozoic of Death Valley, California. *Journal of Sedimentary Petrology*, 56:818-830.

Turner, N.J., 1989a: Chapter 2: Precambrian. In: Burrett, C.F. & Martin, E.L., (editors): *Geology and Mineral Resources of Tasmania.* Geological Society of Australia, Special Publication 15:5-46.

Turner, N.J., 1989b: The Adamsfield District. In: Burrett, C.F. & Martin, E.L., (editors): *Geology and Mineral Resources of Tasmania.* Geological Society of Australia, Special Publication 15:168-174.

Turner, N.J., 1991: Western margin of the Dundas-Fossey terrane, Tasmania - new mapping, new dates, new interpretation. *Eigth International Symposium on Gondwana. Abstracts volume*: 84-85.

Turner, N.J., 1993: K-Ar geochronology in the Arthur Metamorphic Complex, Ahrberg Group and Oonah Formation, Corinna district. *Mineral Resources Tasmania Report* 1993/27.

Turner, N.J., Bottrill, R.S., Crawford, A.J. & Villa, I., 1992: Geology and prospectivity of the Arthur Mobile Belt. *Bulletin of the Geological Survey of Tasmania*, 70:227-233.

Turner, N.J., Calver, C.R., McClenaghan, M.P., McClenaghan, J., Brown, A.V. & Lennox, P.G., 1985: *Pedder*. Geological Atlas 1:50,000 series. Sheet 81125S.

Tyson, R.V. & Pearson, T.H.: 1991: Modern and Ancient Continental Shelf Anoxia: an overview. In Tyson, R.V. & Pearson, T.H., (editors), 1991: *Modern and Ancient Continental Shelf Anoxia*. Geological Society Special Publication. 58:1-24.

Urlwin, B., Ayliffe, D.J., Jansyn, J., McKirdy, D.M., Jenkins, R.J.F. & Gostin, V.A., 1993: A $\delta^{13}C$ survey of carbonate in the early Ediacaran Wonoka Formation. In: Jenkins, R.J.F., Lindsay, J.F. & Walter, M.R.: *Field Guide to the Adelaide Geosyncline and Amadeus Basin, Australia.* AGSO Record 1993/35:92-96.

Vahrenkamp, V.C. & Rossinsky, V., 1987: Discussion of "Preserved stable isotopic signature of subaerial diagenesis in the Mescal Limestone, central Arizona: implication for the timing of a terrestrial plant cover." *Geological Society America Bulletin*, 99:595-596.

Vahrenkamp, V.C. & Swart, P.K., 1990: New distribution coefficient for the incorporation of strontium into dolomite and its implications for the formation of ancient dolomites. *Geology*, 18:387-391.

Vail, P.R., Mitchum, R.M. (Jr.), Todd, R.G., Widmier, J.M., Thompson, S. (III), Sangree, J.B., Bubb, J.N. & Hatlelid, W.G., 1977: Seismic stratigraphy and global changes of sea-level. In: Payton, C.E., (editor): *Seismic Stratigraphy - Applications to Hydrocarbon Explorations*: American Association of Petroleum Geologists Memoir 26:49-212.

van Wagoner, J.C., Posamentier, H.W., Mitchum, R.M., Jr., Vail, P.R., Sarg, J.F., Loutit, T.S. & Hardenbol, J., 1988: An overview of the fundamentals of sequence stratigraphy and key definitions. In: Wilgus, C.K., Hastings, B.S., Kendall, C.G.St.C., Posamentier, H.W., Ross C.A. & Van Wagoner J.C., (editors): *Sea-Level changes: an integrated approach*. Society Econ. Paleontol. Mineral. Special Publication, 42:39-45.

Veevers, J.J., (editor), 1984: *Phanerozoic Earth History of Australia.* Clarendon Press, Oxford, 418 p.

Veizer, J., 1983: Chemical diagenesis of carbonates: theory and application of trace element technique. In: Arthur, M.A. (organizer): *Stable Isotopes in Sedimentary Geology.* Society of Economic Paleontologists and Mineralogists Short Course Notes, 10..p. (3)1 -(3)100.

Veizer, J., 1989: Strontium isotopes in seawater through time: *Annual Review of Earth and Planetary Science*, 17:141-167.

Veizer, J., 1992: Depositional and Diagenetic History of Limestones: Stable and Radiogenic Isotopes. In: Clauer, N. & Chaudhuri, S., (editors): *Isotopic signatures and sedimentary records.* Lecture notes in Earth Sciences, 43:13-48. New York, Springer.

Veizer, J. & Compston, W., 1974: $^{87}Sr/^{86}Sr$ composition of seawater during the Phanerozoic. *Geochimica et Cosmochimica Acta,* 38:1461-1484.

Veizer, J. & Compston, W., 1976: $^{87}Sr/^{86}Sr$ in Precambrian carbonates as an index of crustal evolution. *Geochim. et Cosmochim. Acta,* 40:905-914.

Veizer, J., Compston, W., Clauer, N. & Schidlowski, M., 1983: $^{87}Sr/^{86}Sr$ in late Proterozoic carbonates: evidence for a "mantle" event at ca. 900 Ma ago. *Geochimica et Cosmochimica Acta*, 47:295-302.

Veizer, J., Fritz, P. & Jones, B., 1986: Geochemistry of brachiopods: oxygen and carbon isotopic records of Paleozoic oceans. *Geochimica et Cosmochimica Acta*, 50:1679-1696.

Veizer, J. & Hoefs, J., 1976: The nature of O^{18}/O^{16} and C^{13}/C^{12} secular trends in sedimentary carbonate rocks. *Geochimica et Cosmochimica Acta*, 40:1387-1397.

Veizer, J., Holser, W.T. & Wilgus, C.K., 1980: Correlation of $^{13}C/^{12}C$ and $^{34}S/^{32}S$ secular variations. *Geochimica et Cosmochimica Acta*, 44:579-587.

Vidal, G., 1979: Acritarchs and the correlation of the Upper Proterozoic. *Publications of the Institutes of Mineralogy, Palaeontology and Quaternary Geology*. University of Lund, Sweden. No. 219, 22p.

Vidal, G., 1979: Acritarchs from the Upper Proterozoic and Lower Cambrian of East Greenland. *Gronlands Geologiske Undersogelse Bulletin,* No.134:55.

Vinogradov, A.P., Grinenko, V.A., & Ustinov, V.I., 1962: Isotopic composition of sulphur compounds in the Black Sea. *Geochemistry (USSR)*, 10, 973-997.

von der Borch, C.C., 1993: "Wall plaster" carbonate veneer. In: Jenkins, R.J.F., Lindsay J.F. & Walter, M.R.: *Field Guide to the Adelaide Geosyncline and Amadeus Basin, Australia.* AGSO Record 1993/35:27-28.

von der Borch, C.C., Christie-Blick, N. & Grady, A.E., 1988: Depositional sequence analysis applied to Late Proterozoic Wilpena Group, Adelaide Geosyncline, South Australia. *Australian Journal of Earth Sciences*, 35:59-72.

von der Borch, C.C., Grady, A.E., Aldam, A.E., Miller, D., Newmann, R., Rovira, A. & Eickhoff, K., 1985: A large-scale meandering submarine canyon: outcrop example from the late Proterozoic Adelaide Geoshyncline, South Australia. *Sedimentology*, 32:507-518.

von der Borch, C.C., Grady, A.E., Eickhoff, K., Dibona, P. & Christie-Blick, N., 1989: Late Proterozoic Pasty Springs Canyon, Adelaide Geosyncline: submarine or subaerial origin? *Sedimentology*, 36:777-792.

von der Borch, C.C., Smith, R. & Grady, A.L., 1982: Late Proterozoic submarine canyons of Adelaide Geosyncline, South Australia. *American Association of Petroleum Geologists Bulletin*, 66:332-347.

Wachter, E.A. & Hayes, J.M., 1985. Exchange of oxygen isotopes in carbon dioxide phosphoric acid systems. *Chemical Geology (Isotope Geoscience Section)*, 52:365-374.

Wade, M., 1970: The stratigraphic distribution of the Ediacara fauna in Australia. *Transactions of the Royal Society of South Australia*, 94:87-104.

Wadleigh, M.A. & Veizer, J., 1992: $^{18}O/^{16}O$ and $^{13}C/^{12}C$ in lower Palaeozoic articulate brachiopods: implications for the isotopic composition of seawater. *Geochimica et Cosmochimica Acta*, 56:431-443.

Waldron, H.M., Brown, A.V. & Keays, R.R., (in press): Geological setting and petrochemistry of Eocambrian-Cambrian volcano-sedimentary rock sequences from southeast King Island. *Australian Journal of Earth Science.*

Walker, J.C.G., 1986: Global geochemical cycles of carbon, sulfur and oxgyen. *Marine Geology*, 70:159-174.

Wallace, M.W., Gostin, V.A. & Keays, R.R., 1989: Discovery of the Acraman impact ejecta blanket in the Officer Basin and its stratigraphic significance. *Australian Journal of Earth Science*, 36:585-587.

Walter, M.R., 1972: Stromatolites and the biostratigraphy of the Australian Precambrian and Cambrian. *Special Papers in Palaeontology, 11, Palaeontological Association London*, 190 pp.

Walter, M.R., 1980: Adelaidean and Early Cambrian stratigraphy of the southwestern Georgina Basin: correlation chart and explanatory notes. *Bureau of Mineral Resources Report* 214, BMR Microform MF92.

Walter, M.R., & Bauld, J., 1983: The association of sulphate evaporites, stromatolitic carbonates and glacial sediments, examples from the Proterozoic of Australia and the Cainozoic of Antarctica: *Precambrian Research*, 21:129-148.

Walter, M.R., Elphinstone, R. & Heys, G.R., 1989: Proterozoic and Early Cambrian trace fossils from the Amadeus and Georgina Basins, central Australia. *Alcheringa*, 13:209-256.

Walter, M.R., Grey, K., Williams, I.R., & Calver, C., 1994: Stratigraphy of the Neoproterozoic to ealy Palaeozoic Savory Basin, Western Australia, and correlation with the Amadeus and Officer Basins. *Australian Journal of Earth Science*, 41:533-546.

Walter, M.R., Krylov, I.N. & Preiss, W.V., 1979: Stromatolites from Adelaidean (Late Proterozoic) sequences in central and South Australia: *Alcheringa*, 3:287-305.

Walter, M.R., Shergold, J.H., Muir, M.D. & Kruse, P.D., 1979: Early Cambrian and latest Proterozoic stratigraphy, Desert Syncline, southern Georgina Basin. *Journal of the Geological Society of Australia*, 26:305-312.

Walter, M.R., Veevers, J.J., Calver, C.R. & Grey, K., (1995): Neoproterozoic Stratigraphy of the Centralian Superbasin, Australia. *Precambrian Research*, 73: 173-196.

Wells, A.T., Foreman, D.J., Ranford, L.C. & Cook, P.J., 1970: Geology of the Amadeus Basin, Australia. *Bureau of Mineral Resources Bulletin*, 100:222p.

Wells, A.T., Ranford, L.C., Stewart, A.J., Cook, P.J. & Shaw, R.D., 1967: The geology of the northeastern part of the Amadeus Basin, Northern Territory. *Bureau of Mineral Resources Bulletin*, 113:97p.

Wickham, S.M. & Peters, M.T., 1993: High $\delta^{13}C$ Neoproterozoic carbonate rocks in western North America. *Geology*, 21:165-168.

Williams, E., 1979: *Tasman Fold Belt system in Tasmania.* Revised edition. Tasmanian Department of Mines. 29pp.

Williams, G.E., 1979: Sedimentology, stable-isotope geochemistry and palaeoenvironment of dolostones capping late Precambrian glacial sequences in Australia. *Journal of the Geological Society of Australia,* 26:377-386.

Williams, G.E., 1981: Reply: Sedimentology, stable-isotope geochemistry and palaeoenvironment of dolostones capping late Precambrian glacial sequences in Australia *Journal of the Geological Society of Australia,* 28:102-105.

Williams, G.E., 1989: Late Precambrian tidal rhythmites in South Australia and the history of the Earth's rotation. *Journal of the Geological Society of London*, 146:97-111.

Williams, L.A. & Reimers, C., 1983: Role of bacterial mats in oxygen-deficient marine basins and coastal upwelling regimes: preliminary report. *Geology*, 11:267-269.

Wilson, J.A., 1975: Carbonate Facies in Geologic History. New York, Springer-Verlag, 471p.

Young, G.M., 1992: Late Proterozoic stratigraphy and the Canada-Australia connection. *Geology*, 20:215-218.

Young, G.M., 1995: Are Neoproterozoic glacial deposits preserved on the margins of Laurentia related to the fragmentation of two supercontinents? *Geology*, 23:153-156.

Zachos, J.C. & Arthur, M.A., 1986: Paleoceanography of the Cretaceous/Tertiary Boundary Event: inferences from stable isotopic and other data. *Paleoceanography*, 1:5-26.

Zang, W.L. & Walter, M.R., 1989: Latest Proterozoic plankton from the Amadeus Basin in central Australia. *Nature*, 337:6208, 642-645.

Zang, W.L. & Walter, M.R., 1992: Late Proterozoic and Cambrian microfossils and biostratigraphy, Amadeus Basin, central Australia. *Association of Australasian Palaeontologists, Memoir 12*, 132 pp.

Zang, W.L., 1988: Preliminary study of the well Ungoolya-1 from the Officer Basin, South Australia. In: Stainton, P.W., Weste, G. & Cucuzza, G.: *Exploration of PEL 23 and PEL 30, eastern Officer Basin, South Australia, 1983-1988.* South Australia Department of Mines and Energy, open file envelope, 5073:1243-1321 (unpublished).

Zempolitch, W.G., Wilkinson, B.H. & Lohmann, K.C., 1988: Diagenesis of Late Proterozoic carbonates: the Beck Spring Dolomite of eastern California. *Journal of Sedimentary Petrology*, 58:656-672.

	Basin Stratigraphic Units	Locality/*drillhole*(units sampled)
CHAPTER 3	**Adelaide Geosyncline** Bonney Fm Wonoka Fm Bunyeroo Fm ABC Range Quartzite Brachina Fm Nuccaleena Fm	Brachina Gorge (Bu, W, Bo) Bunyeroo Gorge (N, Br, Bu, W) *BWM1A-1* (N, Br) First Hill (W) Hallett Cove (N) Near Angepena (W) *SCYW1A* (N, Br, A, Bu, W) *UB-17* (N) Umberatana (N) Umberatana (Old Station Ck) (W)
	Officer Basin Rodda Beds Murnaroo Fm 'Giles Mudstone'	*Giles-1* (G) *Munta-1* (M, R) *Observatory Hill-1* (R) *Ungoolya-1* (R)
CHAPTER 4	**Amadeus Basin** Todd River Dolomite Namatjira Fm Julie Fm Pertatataka Fm Olympic/Pioneer Fm Aralka Fm Boord Fm	Acacia Well (P) *Alice Springs-27* (P) Ellery Creek (O, P, J) Fenn Gap (O) Gardiner Range (N) Glen Helen (J) 'Hidden Valley' (O, P) Hijinx Syncline (O) Katapata Gap (J) Mt Capitor (O, P) Mt Conner (O) Mt Greene (B) Phillipson Pound (J) *Rodinga-4* (P) Ross River (P, J, T) *Wallara-1*(A, O, P)
	Georgina Basin Elkera Fm Grant Bluff Fm Elyuah Fm	*DDC (Mt Skinner)-1* (Ely, G, Elk) *DDC (Mt Skinner)-2* (Ely, G) *Huckitta-7* (Elk)
APPENDIX 2	**Savory Basin** Boondawari Fm	Boondawari Creek
CHAPTER 5	**Smithton Basin (Tas)** Smithton Dolomite Keppel Ck Fm Black River Dolomite Dolostone (King I.)	Arthur River (B) *Forest-1* (B, K) King I. (D) Montagu R. (S) Redpa (S)
	Jubilee Region (Tas) Weld River Gp Clark Gp	Jubilee Region (W, C)

Appendix 1.1

Sample locations, descriptions, stable-isotopic analyses and TOC

EXPLANATORY NOTES

Results are tabulated according to locality in the order shown in Table 0.1 (reproduced opposite). Full sample numbers are formatted according to a year-month-day date code followed by number. Suffixes *a*, *b* etc are analytical repeats. Two samples were used as internal standards for $\delta^{13}C_{org}$ analysis (910306.18 Amadeus Basin, Rodinga 4 and 910528.138 Amadeus Basin, Wallara 1). Suffixes */1*, */2* etc. are subsamples.

Sample locations are given as depths in metres below drillhole collar or as stratigraphic heights above the datum given, in the case of outcrop sections (all sections are figured graphically in the text). Locations of drillholes and outcrop sections are given in Fig. 3.1 (Officer Basin); Fig. 3.2 (Adelaide Geosyncline); Fig. 4.4 (Amadeus Basin); Section 4.8 (Georgina Basin); and Fig. 5.2 (Smithton Basin). Drillcore from the Adelaide Geosyncline and Officer Basin is stored at the South Australian Department of Mines and Energy Core Library at Glenside, Adelaide, South Australia. Drillcore from the Amadeus and Georgina Basins is stored at the Northern Territory Geological Survey core store in Alice Springs, N. T., except for Rodinga 4 and AS 27, stored at the Australian Geological Survey corestore at Fishwyck, Canberra, A.C.T. Drillcore from the Smithton Basin is stored at the Mineral Resources Tasmania corestore at Mornington, Hobart, Tasmania.

"% insol" is the acid-insoluble fraction in percent. "TOC" is the total organic carbon content in mg/g. "$\delta^{13}C_{org}{}^{N}$" is the quantity, $\delta^{13}C_{org} + [3.5 \times \log_{10}(TOC_{insol})]$ (see section 2.3c). See section 2.4 for analytical methods. $\delta^{18}O$ values are corrected for reaction at 50°C using fractionation factors of 1.00925 for calcite and 1.01066 for dolomite (see section 2.4).

Adelaide Geosyncline: Brachina Gorge: sample prefix 920507.**								
sample	height(m)	description	% insol	TOC	∂13Corg	∂13CorgN	∂13Carb	∂18O
Bunyeroo Formation			*(datum = base fm.)*					
7.01	64	gy-gn mudst		0.29	-22.12	-24.00		
7.03	133	gy-gn mudst	82	0.18	-27.22	-29.52		
7.02	80	dk gy-gn mudst		0.26	-23.71	-25.76		
7.05	147	bl sh		17.05	-33.81	-29.50		
7.06	183	bl sh		4.37	-31.79	-29.55		
7.07	187	bl sh		7.85	-33.14	-30.01		
7.08	210	bl sh		3.87	-32.35	-30.29		
7.09	254	gy-gn mudst	82	0.49	-27.23	-28.01		
7.10	268	impure lst (conc'n)	58	0.52	-29.87	-30.05		
7.11	298	impure lst (conc'n)	52	0.76	-31.82	-31.26		
7.12	298	gy-gn mudst	82	0.45	-27.25	-28.16		
7.13	329	gy-gn mudst	81	0.21	-23.52	-25.57		
Wonoka Formation			*(datum = base fm.)*					
7.18	688	lst					2.05	-8.82
7.17	690	lst					0.6	-8.35
7.19	694	lst					2.72	-5.89
7.20	698.5	lst					1.42	-5.49
7.21	705.5	lst					2.32	-6.95
Bonney Formation			*(datum = base Wonoka)*					
7.23	746.3	dolost					0.85	-3.5

Adelaide Geosyncline: Bunyeroo Gorge: sample prefix 92040*.**										
sample	height(m)	description	%insol	TOC(mg/g)	∂13Corg	∂13CorgN	∂13Ccarb	∂18O	∂34Spy	∂34Sgyp
sample	height(m)	description	%insol	TOC(mg/g)	∂13Corg	∂13CorgN	∂13Ccarb	∂18O	∂34Spy	∂34Sgyp
Nuccaleena Formation			*(datum = base fm.)*							
3.01	0.50						-1.97	-7.84		
3.02	1.50						-2.25	-8.23		
3.03	3.50						-2.44	-8.37		
3.04	5.50						-2.76	-7.76		
3.05	7.20						-3.07	-8.28		
3.06	8.40						-3.49	-8.24		
Brachina Formation			*(datum= base Nuccaleena Fm.)*							
3.08	49	gy-gn sh		0.56	-23.35	-24.23				
3.11	73	br-gy mudst		0.61	-23.27	-24.02				
3.14	194	gy silty mudst		0.59	-23.19	-23.99				
3.19a	318	gy silty mudst		0.36						
3.19b	318	gy silty mudst		0.35	-23.65	-25.34				
3.19c	318	gy silty mudst		0.31						
4.05a	453	gy mudst		0.65	-23.99	-24.64				
4.05b	453	gy mudst		0.72	-23.75	-24.25				
4.07	541	gy-gn silty mudst		0.45	-23.22	-24.43				
4.09	631	red-br mudst		0.45	-23.17	-24.38				
4.10	716	red-br mudst		0.37	-23.00	-24.51				
4.13	842	gy-gn mudst		0.32	-23.89	-25.62				
4.16a	996	gy-gn silty mudst		0.26						
4.16b	996	gy-gn silty mudst		0.19	-23.27	-25.79				
4.16c	996	gy-gn silty mudst		0.25	-23.57	-25.68				
4.16d	996	gy-gn silty mudst		0.25	-23.70	-25.81				
4.20	1086	gy-gn silty mudst		0.29						
4.23	1189	gy-gn silty mudst		0.41	-23.05	-24.41				
4.25	1265	gy-gn silty mudst		0.42	-24.33	-25.65				
4.28	1411	gy silty mudst		0.52	-24.72	-25.71				
Bunyeroo Formation			*(datum = base Nuccaleena Fm)*							
4.29	1502	gn silty mudst		0.24						
4.30	1556	red mudst		0.16	-22.98	-25.77				
5.01	1567	gy muddy siltst		0.17	-23.20	-25.89				
5.04/1	1606	gn mudst		0.19						
5.04/2	1606	red mudst		0.14	-23.47	-26.46				
5.05	1640	gy-gn muddy siltst		0.19	-24.07	-26.59				
5.07a	1703	gy siltst		0.34	-24.55	-26.19				
5.07b	1703	gy siltst		0.36	-25.12	-26.67				
5.08	1730	gy siltst		0.48	-25.87	-26.99				
5.10	1750	impure lst (con	65	0.28	-24.52	-25.80	-6.79	-14.87		
5.11	1750	gy siltst		0.37						
5.12	1763	gy siltst	73	0.29	-24.05	-25.44				
5.13	1788	gy-gn silty mud	82	0.23	-23.82	-25.75				
5.14a	1836	gy-gn silty mudst		0.22	-23.38	-25.68				
5.14b	1836	gy-gn silty mudst		0.22	-23.78	-26.08				
Wonoka Formation			*(datum=base fm., 1876m. above base Nuccaleena)*							
5.15/1	0	gy dol'tic muds	79	0.19	-23.84	-26.01				
5.15/2	0	dolomic					-0.72	-6.72		
5.16/1	0.6	impure dolost	24	0.09						

Adelaide Geosyncline: Bunyeroo Gorge: sample prefix 92040*.**										
sample	height(m)	description	%insol	TOC(mg/g)	∂13Corg	∂13CorgN	∂13Ccarb	∂18O	∂34Spy	∂34Sgyp
5.16/2	0.6	dolomicspar					-1.40	-6.18		
5.17	1.6	dolomicspar					-3.46	-7.90		
5.19	37	gy siltst		0.63	-23.47	-24.17				
5.21	90	micritic lst					-11.19	-14.98		
5.23	106	micritic lst					-10.07	-14.62		
5.24	120	micritic lst					-9.47	-14.52		
5.26	132	micritic lst					-9.13	-14.21		
5.27a	134	gn siltst & sh	54	0.13						
5.27b	134	gn siltst & sh	52	0.12	-22.80	-25.03				
5.29	159	micritic lst					-8.56	-13.89		
5.31	176	micritic lst					-8.26	-13.85		
5.32	178	gn dol'tic siltst	51	0.39	-22.72	-23.14				
5.33/1	189	micritic lst					-8.10	-13.70		
5.33/2	189	micritic lst					-8.00	-13.53		
5.33/3	189	micritic lst					-7.98	-13.54		
5.35	214	micritic lst					-8.00	-13.19		
5.37	247	gy sh	45	0.34	-22.75	-23.17				
5.36	247.5	micritic lst					-7.51	-13.12		
5.38	280	micritic lst					-7.62	-12.71		
5.39	314	gy fine-g'd lst	28	0.11	-22.30	-23.73	-7.49	-12.68		
5.41	333	micritic lst					-7.45	-12.68		
5.43a	377	gy fine-g'd lst	43	0.3	-22.70	-23.24			-24.0	
5.43b	377	gy fine-g'd lst	46	0.37	-22.68	-23.00				
5.43	377	micritic lst					-7.72	-12.53		
5.44	413	micritic lst					-7.67	-12.57		
5.45	433	gy fine-g'd lst	30	0.27	-22.86	-23.04	-7.48	-12.97	-19.6	9.0
5.46	453	micritic lst					-7.77	-13.69	-20.7	
5.47	489	gy fine-g'd lst	37	0.21	-22.20	-23.05	-7.74	-12.87		
5.50	518	impure fine lst	41	0.26	-23.30	-23.98	-7.08	-12.22		
5.51	528	fine g'd lst	15	0.09	-22.85	-23.58	-6.82	-11.12		
5.52	542	stylonod. lst	15	0.15	-25.80	-25.80	-6.36	-10.16		
5.54	565	fine g'd lst	23	0.14	-23.48	-24.26	-6.27	-10.29		
5.56/1	592	impure lst	52	0.26	-22.20	-23.25				
5.56/2	592	fine-g'd lst					-6.03	-9.93	-14.5	
5.57	617	fine g'd lst	8	0.04			-4.00	-10.97		
5.59	625	gy dol'tic muds	70	0.49	-22.56	-23.10				
6.01/1	629	lst					-2.87	-11.39		
6.01/2	629	lst					-2.93	-11.68		
5.60	636	lst					-1.81	-11.23		
5.61a	638	gy-gn mudst	71	0.55						
5.61b	638	gy-gn mudst	72	0.54	-23.08	-23.52				
5.62	656	dk gy lst	23	0.42	-24.77	-23.87				
6.02	656	lst					-2.82	-11.80		
6.03	662	lst	19	0.27	-25.80	-25.27	-0.63	-12.50		
6.04	690	lst					-1.09	-12.28		
6.05/1	691.3	lst					0.20	-11.20		
6.05/2	692	lst	15	0.22	-28.52	-27.92				
6.09	695	oolitic lst	3	0.2	-30.22	-27.26	0.93	-9.73	-24.0	
6.18	696	stromatolitic lst	2	0.13						

Adelaide Geosyncline: Bunyeroo Gorge: sample prefix 92040*.**										
sample	height(m)	description	%insol	TOC(mg/g)	∂13Corg	∂13CorgN	∂13Ccarb	∂18O	∂34Spy	∂34Sgyp
6.13	703	lst					-2.04	-4.39		
6.12	706	lst					2.36	-4.73		
6.11	706.5	lst					0.66	-4.47		
6.10	707.5	dolost					-1.95	-8.34		
6.12	709	gy fine g'd lst	2	0.5	-29.55	-24.75				

Adelaide Geosyncline: BWM1A-1: sample prefix 920520.**									
sample	depth(m)	description	%insol	TOC(mg/g)	∂13Corg	∂13corgN	∂13Ccarb	∂18O	∂34Spy
Brachina Fm.									
20.01	-146.5	bl sh (bmm)		2.50	-32.19				
20.03/1	-157.5	gy-gn sh	78	0.91	-26.68	-26.45			-31.1
20.03/2	-157.5	bl sh (bmm)		2.21	-32.28				-28.9
20.05/1	-169.4	bl sh (bmm)		2.34	-32.72				
20.05/2	-169.4	gy-gn silty sh		0.66	-26.00	-26.63			
20.07	-183.3	bl sh		1.38	-28.35	-27.86			
20.08	-191.2	gy-gn sh	88	0.68	-24.55	-24.95			
20.09	-198.3	gy-gn sh		0.60	-24.54	-25.32			
Nuccaleena Fm.									
20.11/1	-215.1	dolost:centre nod.					-2.85	-8.04	
20.11/2	-215.1	dolost: edge nod.					-2.51	-8.45	
20.12/1	-222.7	dolomicr.					-1.92	-8.14	
20.12/2	-222.7	pale gy-gn sh		0.42	-24.39	-25.71			
20.13	-226.8	dolomicr					-1.43	-8.13	
20.14	-230.5	dolomicr					-1.27	-7.61	

Adelaide Geosyncline: First Hill: sample prefix 920508.**								
sample	height(m)	description	%insol	TOC(mg/g)	∂13Corg	∂13CorgN	∂13Ccarb	∂18O
Wonoka Formation			*(datum : base fm.)*					
8.02	0.1	dolomicr					-2.90	-6.50
8.04/1	63	fine-g'd lst					-10.93	-13.91
8.04/2	63	fine-g'd lst					-11.33	-14.27
8.05/1	82	fine-g'd lst					-10.46	-14.25
8.05/2	82	fine-g'd lst					-9.77	-13.35
8.09	128	fine-g'd lst					-8.85	-13.83
8.10	186	fine-g'd lst					-7.95	-12.88
8.14	227	fine-g'd lst					-7.71	-13.24
8.18	301	fine-g'd lst					-7.48	-12.70
8.20	332	fine-g'd lst	22	0.14	-22.54	-23.27		
8.24	393	fine-g'd lst	14	0.12	-22.20	-22.41	-7.64	-13.29
8.25	456	fine-g'd lst					-8.17	-13.49
8.28	526	fine-g'd lst	29	0.16	-22.72	-23.60	-7.32	-11.98
8.30	550	fine-g'd lst	25	0.18	-24.07	-24.55		
8.31	572	fine-g'd lst	15	0.12	-25.69	-25.99	-6.29	-10.95
8.34	611	fine-g'd lst	13	0.14	-25.15	-25.06	-6.39	-10.78
8.35	624	fine-g'd lst					-6.46	-10.42
8.37	649	fine-g'd lst	26	0.28	-26.96	-26.86		
8.38	674	fine-g'd lst	26	0.28	-25.98	-25.89	-5.35	-10.07
8.40	708	fine-g'd lst	14	0.12	-25.63	-25.88		
8.41	723	fine-g'd lst	14	0.14	-25.89	-25.95	-4.68	-10.75
8.42	745	fine-g'd lst	12	0.07	-26.05	-26.85	-4.18	-11.54
8.43	765	fine-g'd lst	25	0.1	-24.30	-25.69	-3.04	-12.05
8.44	809	dolost					1.83	-7.43

Adelaide Geosyncline: Hallett Cove: sample prefix 920518.**				
sample	height(m)	description	∂13Ccarb	∂18O
Seacliff Sst/Nuccaleena Fm.		*(datum = base Seacliff Sst.)*		
18.01	12.6	impure fine g'd dolost	-2.66	-6.62
18.02	13.25	impure fine g'd dolost	-2.52	-4.28
18.03	13.9	impure fine g'd dolost	-3.41	-4.83
18.04	39.75	impure fine g'd dolost	-1.78	-10.65
18.06	70	impure fine g'd dolost	-2.5	-8.24

Adelaide Geosyncline: near Angepena			
sample	description	∂13Ccarb	∂18O
'Burr Well Member' (Wonoka Fm.)			
930514.01	fine g'd dolost	-7.78	-10.42

Adelaide Geosyncline: SCYW1A: sample prefix 920522.**									
sample	depth(m)	description	%insol	TOC(mg/g)	∂13Corg	∂13CorgN	∂13Ccarb	∂18O	∂34Sanh
Wonoka Formation									
22.01	-208.3	silty gn sh		0.73	-24.48	-24.96			
22.05	-247.7	silty gn sh		0.63	-25.13	-25.83			
22.08	-283.2	silty gn sh		0.51	-24.55	-25.57			
22.10	-308.7	gy mudst		0.44	-23.09	-24.34			
22.11/1	-310.0	dolomicr intraclast					-1.95	-7.60	
22.11/2	-310.0	dolomicr					-1.93	-7.93	
Bunyeroo Formation									
22.12	-324.3	gy-gn mudst	76	0.13					
22.13	-332.2	gy-gn mudst	76	0.16	-24.22	-26.59			
22.14	-343.4	gy dol'tic mudst	55	0.06	-25.50	-28.86			
22.16	-365.3	gy dol'tic mudst	56	0.05	-24.10	-27.76			
22.17	-384.2	gy mudst		0.13	-24.47	-27.57			
ABC Range Formation									
22.18	-399.2	dk gy sh	80	1.54	-28.04	-27.04			
22.19	-411.6	dk gy silty mudst		0.63	-26.00	-26.70			
22.20	-422.8	dk gy sh	83	0.97	-28.19	-27.95			
22.21	-444.9	dk gy mudst		1.69	-28.84	-28.04			
22.23/1	-467.1	dk gy sh		1.02	-27.34	-27.31			
22.23/2	-467.1	dk gy sh		0.59	-26.97	-27.77			
22.24	-473.9	dk gy silty mudst		0.99	-28.28	-28.30			
22.26	-498.7	gy sh		1.7	-28.90	-28.09			
22.27	-523.0	dk gy mudst		0.78	-26.60	-26.98			
22.27/1	-523.0	dk gy sh		0.86	-26.79	-27.02			
22.27/2	-523.0	dk gy sh		0.5	-25.49	-26.54			
22.30	-586.2	dk gy mudst		0.65	-25.87	-26.52			
22.31	-666.0	dk gy silty mudst		0.8	-26.19	-26.53			
22.33	-711.0	gy sh		1.33	-26.16	-25.73			
Brachina Formation									
22.34	-734.0	dk purple sh		0.82	-26.67	-26.97			
22.36	-768.3	dk gy sh		1.07	-26.54	-26.44			
22.38	-794.2	dk gy sh		1.5	-26.90	-26.28			
22.41	-835.6	dk gy sh		1.34	-27.05	-26.61			
22.43/1	-866.5	dk gy sh(bmm)		1.16	-29.35				
22.43/2	-866.5	gy sh		1.3	-27.69	-27.29			
22.45	-887.8	gy sh		0.87	-25.97	-26.18			
22.47/1	-917.6	dk gy sh		0.76	-25.96	-26.38			
22.47/2	-917.6	gy sh(bmm)		1.1	-29.61				
22.48a	-929.1	gy-gn sh		0.75	-25.62	-26.06			
22.48b	-929.1	gy-gn sh		0.72	-24.93	-25.43			
22.49	-939.5	dk gy sh (bmm)		1.19	-29.23				
22.51	-965.4	dk gy sh (bmm)		0.91	-25.89				
22.53	-987.3	dk gy sh (bmm)		0.88	-26.55				
22.54	-1000.1	gy sh		0.89	-24.89	-25.07			
22.55	-1010.7	gy sh		0.64	-24.56	-25.24			
Nuccaleena Formation									
22.56	-1031.5	anhydrite nod.							20.4
22.57/1	-1031.6	edge of dolost nod.					-3.06	-7.60	
22.57/2	-1031.6	centre of nod.					-3.06	-7.53	
22.58/1	-1033.6	dolomicr					-2.26	-7.91	
22.58/2	-1033.6	pale gy sh+dol	45	0.1	-24.53	-26.83			

Adelaide Geosyncline: UB 17: sample prefix 920521.**				
sample	depth(m)	description	∂13Ccarb	∂18O
Nuccaleena Formation				
21.09	-171.7	pale dolomicrite	-2.78	-8.62
21.11	-179.2	pale dolomicrite	-1.28	-8.18

Adelaide Geosyncline: Umberatana (Nuccaleena Fm)				
sample	height(m)	description	∂13Ccarb	∂18O
Nuccaleena Formation		*(datum: base fm.)*		
920512.04	1	dolomicrite	-2.24	-12.68
920512.05	5	dolomicrite	-2.59	-12.23
920512.06	11	dolomicrite	-3.75	-10.9

Adelaide Geosyncline: Umberatana (Wonoka Fm.): sample prefix 920510.**				
sample	height(m)	description	∂13Carb	∂18O
Wonoka Formation		*(datum: base of measured section)*		
(Old Station Creek section)				
10.36	3	fine g'd lst	-7.18	-14.89
10.35	53	fine g'd lst	-7.33	-14.98
10.33	109	fine g'd lst	-7.32	-13.68
10.30	180	fine g'd lst (intraclast)	-1.99	-4.06
10.37	263	fine g'd muddy lst	-7.52	-14.82
10.28/1	360	fine g'd lst	-7.05	-15.00
10.28/2	360	calcareous siltst	-6.77	-14.46
10.01/1	435	fine g'd lst (intraclast)	-7.85	-15.10
10.01/2	435	fine g'd lst	-7.43	-15.00
10.07	480	fine g'd lst	-8.18	-15.12
10.11	543	fine g'd silty lst	-7.85	-14.67
10.15	603	fine g'd silty lst	-6.80	-15.71
10.17	688	fine g'd silty lst	-9.00	-14.07
10.22	860	fine g'd lst	1.33	-14.85
(First limestone within canyon fill: see text)				
930515.01		fine-g'd lst	-6.74	-13.07

Officer Basin: Giles 1: sample prefix 930510.**							
sample	depth(m)	description	%insol	TOC(mg/g)	∂13Corg	∂13CorgN	∂34Sanh
'Giles Mudstone'							
10.11a	-881.8	gy-gn sh		0.79	-26.24	-26.60	
10.11b	-881.8	gy-gn sh		0.77	-26.21	-26.61	
10.13	-907.1	gy-gn sh		0.84	-26.20	-26.47	
10.32	-919.6	anhydrite nodule					23.1
10.15	-930.9	gy-gn sh		0.82	-27.41	-27.71	
10.17	-947.4	gy-gn sh	83	0.74	-26.37	-26.55	
10.19	-970.0	dk red-gy sh	82	0.80	-26.56	-26.61	
10.21	-990.7	red sh		0.64	-26.62	-27.30	
10.23	-1015.1	gy-gn sh	87	0.39	-26.49	-27.70	
10.24	-1028.85	bl sh lamina (bmm)		1.11	-30.38		
10.27	-1044.8	red sh		0.55	-26.75	-27.66	
10.29	-1056.5	gy-gn sh		0.72	-27.23	-27.73	
10.31	-1063.2	gy-gn sh		0.38	-25.90	-27.37	

Officer Basin: Munta 1: sample prefix 920515.**										
sample	depth(m)	description	%insol	TOC(mg/g	∂13Corg	∂13CorgN	∂13Ccarb	∂18O	%carb	∂34S
Rodda beds correlate										
15.02	-909.2	gy micrite	10	0.35	-31.49	-29.62	2.37	-5.02	77	
15.04/1	-929.9	gy micrite	18	0.64	-31.91	-29.98	2.19	-4.69	73	
15.04/2	-929.9	dk gy calc sh	40	1.91	-32.27	-29.88				
15.05	-938.7	gy micrite					2.00	-4.51	71	
15.08/1	-960.5	gy micrite	30	0.87	-32.41	-30.81	2.13	-9.63	60	
15.08/2	-960.5	dk gy sh	52	1.75	-32.86	-31.00				(py)4.1
15.11	-990.3	gy micrite	31	0.61	-30.14	-29.09	2.90	-9.33	60	
15.13a	-1007.7	gy-gn silty sh	71	1.01	-28.12	-27.58				
15.13b	-1007.7	gy-gn silty sh	72	0.99	-27.95	-27.46				
15.15	-1024.9	gy-gn calc mudst	66	0.49	-25.95	-26.41	-2.73	-4.98	19	
15.18	-1058.4	gy-gn calc sh	62	0.47	-25.61	-26.03	-1.84	-5.37	21	
15.21/1a	-1079.3	gy-gn calc mudst	68	0.51	-26.20	-26.64				
15.21/1b	-1079.3	gy-gn calc mudst	67	0.50	-26.14	-26.58				
15.21/2	-1079.3	calc mudst					-2.00	-5.55	16	
15.24/1	-1106.1	dk gy mudst	69	1.60	-28.64	-27.37				
15.24/2	-1106.1	gy-gn mudst	68	0.85	-26.40	-26.06				
15.24/3	-1106.1	gy-gn calc mudst	69	0.60	-25.80	-26.01	0.83	-7.22	17	
15.27	-1136.6	calc mudst					-0.18	-6.84	30	
15.28	-1145.5	dk gy sh		0.67	-24.85	-25.46				
15.29	-1156.1	micrite					-6.03	-7.30	79	
15.3	-1164.8	micrite					-7.76	-7.99	78	
15.31	-1167.0	micrite					-8.13	-8.04	77	
15.32	-1177.0	gy-gn sh	76	0.71	-26.07	-26.18				
15.33	-1186.6	gy gn silty sh	82	0.37	-24.28	-25.49				
15.34	-1198.6	gy-gn silst (bmm)		0.78	-28.83					
15.37	-1224.6	dk gy sh		0.82	-25.81	-26.11				
15.39/1	-1243.6	bl. silty sh(bmm)		1.32	-29.96					
15.39/2	-1243.6	gy-gn silty sh		0.51	-26.49	-27.51				
15.41	-1265.1	gy sh		0.72	-28.23	-28.73				
15.42	-1270.6	dk gy calc sh	73	0.65	-27.38	-27.56	1.02	-10.10	22	
15.44	-1292.1	gy-gn sh		0.65	-23.82	-24.47				
15.45	-1302.5	gy sh	73	0.55	-26.39	-26.83				
15.47/1	-1313.2	grainstone(lst)	7	0.52	-28.90	-25.94				
15.47/2	-1313.2	dk gy micrite	12	0.39	-29.28	-27.47				
15.47/3	-1313.2	pale gy micrite	7	0.14						
15.47/4	-1313.2	dk gy micrite	10	0.31	-29.08	-27.39	1.27	-6.66	71	
15.48	-1318.5	micrite					2.83	-5.71	73	
15.49	-1326.5	gy-gn silty sh	70	1.01	-28.41	-27.85				
15.51/1	-1347.4	dk gy gn silty mst	69	0.86	-27.13	-26.79				
15.51/2	-1347.4	calc mudst					4.00	-8.53	39	
15.54	-1376.1	dk gy-gn calc sh	73	0.69	-26.87	-26.96	-1.82	-7.69	10	
15.56	-1395.7	dk gy mudst		0.48	-25.84	-26.96				
15.46	-1406.6	calc mudst					2.00	-9.62	64	
15.58	-1414.7	gy micrite	24	0.33	-27.49	-27.01	4.22	-6.41	58	
15.60/1	-1438.3	bl sh (bmm)	78	2.38	-27.30					
15.60/2	-1438.3	gy micrite	27	0.62	-27.44	-26.19	2.39	-9.22	73	
15.66/1	-1441.3	micrite					5.95	-9.83	85	
15.66/2	-1441.3	anhydrite nodule								(anh)24.4
15.61/1	-1443.6	bl sh (bmm)	70	3.56	-27.47					
15.61/2	-1443.6	gy lst	14	0.39	-27.59	-26.02				

Officer Basin: Munta 1: sample prefix 920515.**										
sample	depth(m)	description	%insol	TOC(mg/g	∂13Corg	∂13CorgN	∂13Ccarb	∂18O	%carb	∂34Ş
15.62/1	-1453.6	dk gy calc sh	75	0.82	-26.75	-26.61				
15.62/2	-1453.6	impure micrite					4.98	-7.06	46	
15.65/1	-1485.3	dk gy silty sh	73	0.67	-26.20	-26.33				
15.65/2	-1485.3	calc mudst					2.63	-8.14	35	
15.68	-1512.0	dk gy silty mudst		0.48	-26.37	-27.49				
15.7	-1532.1	gy gn silty sh		0.55	-27.02	-27.93				
15.73	-1561.9	dk gy silty mudst		0.80	-27.90	-28.24				
15.75	-1581.3	gy micrite	25	0.46	-28.19	-27.27	4.69	-6.39	63	
15.77	-1596.2	dk gy micrite	20	0.47	-28.77	-27.48	5.35	-6.31	71	
15.79	-1612.5	gy micrite					4.77	-5.16	80	
15.81/1	-1636.8	dk gy sh	63	1.09	-28.11	-27.27				
15.81/2	-1636.8	gy micrite	9	0.21	-28.48	-27.25	5.53	-4.57	83	
15.83/1	-1656.3	dk gy calc mudst	65	1.75	-28.91	-27.41				
15.83/2	-1656.3	gy micrite					5.35	-2.59	87	
15.85	-1670.0	gy micrite	7	0.34	-28.38	-26.06	5.97	-4.01	85	
15.85/2	-1670.0	bl mudst	68	1.97	-28.59	-26.98				
15.87	-1681.3	gy gn silty sh		2.66	-30.18	-28.69				
15.89	-1702.9	dk gy sh	84	1.42	-29.72	-28.91				
15.91	-1728.4	gy gn silty sh		0.93	-29.03	-29.14				(py)-20.8
15.93	-1745.5	dk gy lst	30	0.18	-26.67	-27.45	1.96	-10.60	56	
15.94	-1760.4	gn+red mudst								(py)-21.2
15.95	-1770.1	dk gy silty sh		0.46	-27.51	-28.69				
15.97/1	-1789.2	dk gy lst	36	0.41	-29.38	-29.18	-17.22	-6.70	48	
15.97/2	-1789.2	dk gy mudst		0.58	-28.51	-29.34				
15.99	-1810.5	dk gy sh		6.56	-32.19	-29.33				(py)-31.1
15.101	-1834.1	gy gn silty sh		0.51	-26.43	-27.45				
15.103	-1852.0	dk gy sh		0.48	-25.94	-27.06				
15.107	-1884.2	gy-gn udst		0.39	-25.44	-26.87				
15.110a	-1915.3	dk gy sh		0.53	-25.24	-26.21				
15.110b	-1915.3	dk gy sh		0.00						
15.114/1	-1951.5	pale gn sh		0.19	-23.70	-26.22				
15.114/2	-1951.5	red sh		0.16	-23.37	-26.16				
Murnaroo Formation										
15.118	-1987.6	gy sh		1.02	-26.14	-26.11				
15.121	-2031.8	gy-gn siltst		0.27	-24.00	-25.99				

Officer Basin: Observatory Hill 1: sample prefix 920514.**								
sample	depth(m)	description	%insol	TOC(mg/g)	∂13Corg	∂13CorgN	∂13Ccarb	∂18O
Rodda beds correlate								
14.02	-188.9	dolost					5.38	-7.09
14.04	-206.6	dolost					5.98	-7.83
14.06	-223.8	dolost					6.22	-7.93
14.08		dk gy calc sh	74	8.59				
14.09/1	-240.1	dk gy calc sh	39	3.53	-30.22	-26.86		
14.09/2	-240.1	micrite					4.27	-8.64
14.10	-246.7	micrite					6.24	-8.50
14.11	-253.7	micrite					5.78	-5.28
14.12	-258.0	micrite	10	0.86	-29.86	-26.66	5.81	-4.96
14.13	-264.3	gy sh	84	2.42	-30.22	-28.62		
14.14	-273.0	rd+gn silty sh		0.23	-27.29	-29.52		
14.15/1	-279.3	dk gy-gn sh		2.36	-31.44	-30.13		
14.15/2	-279.3	gy-gn sh		0.79	-29.24	-29.60		
14.16	-291.2	gy-gn sh		0.23	-26.01	-28.24		
14.17a	-300.8	gy-gn sh	82	0.74	-29.07	-29.23		
14.17b	-300.8	gy-gn sh	83	0.75	-29.24	-29.40		
14.18	-314.2	pale gy-gn sh		0.33	-26.02	-27.71		
14.19/1	-325.8	pale gy-gn sh		0.26	-24.81	-26.86		
14.19/2	-325.8	red sh		0.26	-25.20	-27.25		
14.21	-344.6	pale gy-gn sh		0.25	-24.18	-26.29		

Officer Basin: Ungoolya 1: sample prefix 920526.**									
sample	depth(m)	description	%insol	TOC(mg/g)	∂13Corg	∂13CorgN	%carb	∂13Ccarb	∂18O
Correlate of Rodda beds									
26.02	-1300.0	gy calc mudst	66	0.81	-26.74	-26.43			
26.02a	-1300.0	gy calc siltst					11	-3.09	-4.41
26.02b	-1300.0	gy calc siltst					13	-2.75	-4.37
26.04a	-1328.7	gy calc silty mudst	73	0.75	-26.87	-26.83			
26.04b	-1328.7	gy calc silty mudst	72	0.73	-26.48	-26.45			
26.06	-1353.4	gy calc silty mudst	69	1.20	-30.44	-29.60			
26.08	-1369.9	gy calc siltst					60	2.77	-6.24
26.09	-1380.5	gy calc siltst	58	2.32	-31.35	-29.25	22	1.39	-5.31
26.11	-1407.5	gy calc silty mudst	71	0.65	-27.50	-27.64			
26.13a	-1441.9	gy calc silty mudst	69	1.06	-29.25	-28.60	9	0.25	-0.96
26.13b	-1441.9	gy calc siltst					11	0.27	-1.14
26.15	-1468.0	gy calc silty mudst	74	1.07	-29.14	-28.58			
26.18	-1497.8	micritic gy lst	12	0.68	-32.00	-29.33	76	0.91	-4.07
26.20	-1524.2	micritic gy lst	15	0.82	-32.78	-30.19	80	1.45	-3.39
26.22	-1554.7	gy calc silty mudst	70	0.67	-27.71	-27.77			
26.24/1	-1584.5	calc mudst					10	2.44	-7.43
26.24/2	-1584.5	silty lst					47	5.29	-7.84
26.26	-1615.4	gy calc silty mudst	67	2.00	-30.64	-28.97			
26.28	-1644.1	gy calc silty mudst	65	0.85	-27.86	-27.46	11	0.14	-5.43
26.30	-1676.1	gy calc silty mudst	66	1.52	-29.51	-28.25			
26.32	-1705.8	silty calc mudst	70	0.96	-27.92	-27.43	8	0.57	-6.28
26.36	-1734.2	gy calc mudst	67	2.08	-28.96	-27.23			
26.38/1	-1763.6	gy calc mudst	63	1.48	-27.68	-26.39			
26.38/2	-1763.6	calc siltst					36	3.48	-5.97
26.41	-1783.7	calc sandstone					23	3.05	-9.24
26.42	-1795.0	silty calc mudst	71	0.84	-27.47	-27.22			
26.42/2	-1795.0	dk gy mudst	74	1.88	-28.26	-26.85			
26.44	-1826.6	gy calc silty mudst	69	1.20	-27.62	-26.78			
26.46/1	-1855.5	gy calc silty mudst	66	1.53	-25.61	-24.34			
26.46/2	-1855.5	calc siltst					13	1.87	-6.82
26.49	-1884.8	dk gy mudst	82	1.48	-26.11	-25.21			
26.51	-1905.4	calc sandstone					14	1.55	-9.26
26.52	-1916.1	gy calc mudst	77	1.37	-26.76	-25.89			
26.55	-1945.5	gy calc mudst	77	1.24	-24.90	-24.17			
26.59	-1975.5	gy calc mudst	73	0.90	-25.19	-24.86			
26.62/1	-2005.9	gy calc mudst	71	1.48	-28.56	-27.45			
26.62/2	-2005.9	silty lst					49	-3.95	-7.85
26.66/1	-2049.2	gy calc mudst	72	1.41	-28.30	-27.27			
26.66/2	-2049.2	muddy lst					28	-3.51	-8.16
26.69/1	-2096.5	dk gy mudst	72	1.15	-27.41	-26.70			
26.69/2	-2096.5	dk gy calc siltst	32	0.49	-28.10	-27.43			
26.69	-2096.5	silty lst					55	-4.01	-8.53
26.71/1	-2129.0	gy calc mudst	63	1.23	-27.93	-26.91			
26.71/2	-2129.0	muddy lst					26	-3.76	-10.01
26.74/1	-2162.0	gy calc mudst	65	1.61	-29.68	-28.31			
26.74/2	-2162.0	silty lst					43	-7.04	-8.81
26.76	-2191.9	gy calc mudst	69	1.37	-29.83	-28.79			
26.76	-2191.9	muddy lst					22	-6.04	-10.60

Amadeus Basin: Acacia Well								
sample	height(m)	description	%insol	TOC(mg/g)	∂13Corg	∂13CorgN	∂13Ccarb	∂18O
Pertatataka Formation			*(datum: base Julie Fm.)*					
910601.52	-80	fine g'd silty lst	33	0.71	-28.07	-26.94	2.57	-8.83

Amadeus basin: Alice Springs 27: sample prefix 930527.**					
sample	depth(m)	description	TOC(mg/g)	∂13Corg	∂13CorgN
Pertatataka Formation					
27.01	-15	pale gn sh	0.12	-24.45	-27.67
27.02	-25	pale gn sh	0.18	-23.76	-26.37
27.03	-35	pale gn sh	0.26	-24.12	-26.17
27.04	-45.1	pale gn sh	0.12	-23.31	-26.53
27.05a	-53	pale gn sh	0.11	-23.78	-27.14
27.05b	-53	pale gn sh	0.1	-23.68	-27.18
27.06	-59.4	pale gn sh	0.11	-23.63	-26.99

Amadeus Basin: Ellery Creek: sample prefix 910606.**								
sample	height(m)	description	%insol	TOC(mg/g)	∂13Corg	∂13CorgN	∂13Ccarb	∂18O
Julie Fm. Datum base Julie								
6.46a	63	dolomicrite					1.59	-8.17
6.46	63	dolomicrite	3	0.08	-26.33	-24.68	1.57	-8.32
6.43	54.7	dolomicrite					5.8	-5.29
6.41	46.3	microsparite (lst)	3	0.48	-26.66	-22.30	3.98	-15.74
6.40	44.7	dolomicrite					5.79	-9.45
6.37	0.7	dolomicrite	21	0.35	-25.78	-24.84	4.06	-8.28
Pertatataka Fm. Datum base Pertatataka								
6.36	283.5	pale gy-gn sh		0.39	-22.38	-23.81		
6.35a	275	pale gy-gn sh		0.60	-24.91	-25.68		
6.35b	275	pale gy-gn sh		0.63	-25.17	-25.87		
6.34	265.5	pale gy-gn sh		0.78	-25.48	-25.86		
6.33	245.5	pale gy-gn sh		0.31				
6.33	245.5	pale gy-gn sh		0.26	-24.85	-26.93		
6.32	236	pale gy sh		0.22	-24.93	-27.23		
6.31	229	pale gy sh		0.22	-24.51	-26.81		
6.30	221	pale gy-gn sh		0.50				
6.30	221	pale gy-gn sh		0.44	-25.75	-27.00		
6.29	211	pale gy-gn sh		0.21				
6.29	211	pale gy-gn sh		0.25	-23.84	-25.97		
6.28	203	pale gy-gn sh		0.47	-23.40	-24.55		
6.27	197	gy-gn sh		0.76	-24.02	-24.44		
6.26	190.5	gy-gn sh		1.28	-21.93	-21.55		
6.25a	184	gy-gn sh		1.47	-21.68	-21.09		
6.25b	184	gy-gn sh		1.45	-21.75	-21.19		
6.24	174.5	pale gy-gn sh		1.34	-23.50	-23.06		
6.23	167	pale gy-gn sh		0.98	-24.74	-24.77		
6.22	159	pale gy-gn sh		0.57	-24.00	-24.85		
6.20	129	pale gy sh		0.43	-24.02	-25.30		
6.19	123	pale gy sh		0.48	-24.07	-25.19		
6.18	112	pale gy-gn sh		0.39	-23.37	-24.80		
6.17	104.5	pale gy-gn sh		0.48	-23.78	-24.90		
6.16	98	pale gy-gn sh		0.42	-23.39	-24.71		
6.15	93	pale gy-gn sh		0.35	-23.90	-25.50		
6.14	70	red sh		0.15	-23.21	-26.09		
6.13a	30	pale gy-gn sh		0.38	-26.17	-27.64		
6.13b	30	pale gy-gn sh		0.39	-26.20	-27.63		
6.12	25.5	pale gy-gn sh		0.59				
6.11	20	pale gy-gn sh		0.53	-27.13	-28.10		
6.09	15.5	pale gy-gn sh		1.04	-28.25	-28.19		
'Cap dolostone': datum: base cap dolostone								
6.03	1	dolomicrosparite					0.42	-12.22
6.02	0.5	dolomicrosparite					-0.73	-13.12
6.01	0	dolomicrosparite					0.77	-12.74

Amadeus Basin: Fenn Gap				
sample	height(m)	description	∂13Ccarb	∂18O
Correlate of Pioneer Fm.		*(datum: base measured section)*		
910606.58	4.0	dolomicrite	-1.80	-2.98
910606.59	14.0	dolomicrite	-1.91	-1.83
910606.61	20.5	dolomicrite	-0.03	-2.16
910606.62	29.0	dolomicrite	1.56	-2.80
910606.64	38.0	dolomicrite	2.22	-1.83

Amadeus Basin: Gardiner Range				
sample	height (m)	description	∂13Ccarb	∂18O
Namatjira Formation		*(datum: base fm.)*		
910521.08	30.5	fine g'd dolost	-0.40	-5.51
910521.09	33.0	fine g'd sandy dolost	-0.41	-6.50
910521.10	35.5	micritic dolost	-0.52	-6.18

Amadeus Basin: Glen Helen				
sample	height(m)	description	∂13Ccarb	∂18O
Julie Formation		*(datum: base Julie Fm.)*		
930521.01	0.5	fine g'd dolost	5.49	-5.39

Amadeus Basin: 'Hidden Valley'								
sample	height(m)	description	%insol	TOC(mg/g)	∂13Corg	∂13CorgN	∂13Ccarb	∂18O
Pertatataka Fm		*(datum: base Pertatataka Fm.)*						
910605.16a	462	gy-gn silty sh	84	0.21	-24.28	-26.65		
910605.16b	462	gy-gn silty sh	83	0.2	-23.82	-26.27		
910605.15	448	gy shaly sltst		0.26	-26.29	-28.34		
910605.14	426	pale gy-gn sh		0.17	-23.56	-26.25		
910605.30	402	gy-gn sh		0.21	-24.97	-27.34		
910605.28	323	gy-gn silty sh		0.14	-22.71	-25.70		
910605.29	302	gy-gn silty sh		0.14	-23.04	-26.03		
910605.25	161	sltst		0.09	-25.24	-28.90		
910605.20	135	gy shaly sltst		0.29	-26.77	-28.65		
910605.19	118	pale gy-gn sh		0.37	-28.76	-30.27		
910605.21	105	pale gy-gn sh		0.2	-24.51	-26.96		
910605.09	57	pale gy-gn sh		0.21	-24.18	-26.55		
910605.07	38	gn+red sh		0.17	-23.9	-26.59		
'Cap dolostone' correlate								
910522.03	-0.05	sandy Xine dol					-2.27	-4.25
Pioneer Fm correlate								
950522.04	-0.8	sandy Xine dol					0.18	-9.35
930519.02	-5.1	silty dolost					-2.08	-5.38

Amadeus Basin: Hijinx Syncline				
sample	height(m)	description	∂13Ccarb	∂18O
Dolost. in Olympic Fm.		*(datum: base dolost. unit)*		
910523.10	0.6	sandy dolostone	-1.04	-4.15
910523.14	3.0	dolomicrite	3.10	-0.62
910523.15	5.3	silty dolostone	1.54	-2.10

Amadeus Basin: Katapata Gap: sample prefix 910521.**				
sample	height(m)	description	∂13Ccarb	∂18O
Julie Fm.	*(datum: base fm.)*			
21.15	7.3	dolomicrite	5.23	-5.42
21.18	15.1	dolomicrite	4.94	-5.70
21.21	26.7	dolomicrite	5.95	-5.78
21.22	34.2	dolomicrite	4.03	-6.92
21.23	39.6	dolomicrite	5.39	-6.67
21.24a	44.6	dolomicrite	1.00	-6.68
21.24b	44.6	dolomicrite	1.03	-6.65

Amadeus Basin: Mt Capitor: sample prefix 930522.**							
sample	height(m)	description	∂13Ccarb	∂18O	TOC(mg/g)	∂13Corg	∂13CorgN
Pertatataka Fm.('Halfway Dam Fm.')		*(datum: base fm.)*					
22.16a	22	fine g'd lst	-7.89	-11.46			
22.17	9.1	fine g'd lst	-5.75	-10.28			
22.15	7.8	fine g'd lst	-6.19	-12.25			
22.14	7.4	fine g'd lst	-6.18	-12.91			
22.13	5.9	gy sh			0.36	-25	-26.6
'Cap dolostone'		*(datum: base cap dol.)*					
22.12	35.4	dolomicrite	-4.08	-7.37			
22.11	25.1	dolomicrite	-2.75	-6.69			
22.09	17.4	dolomicrite	-2.35	-7.24			
22.07	12.2	dolomicrite	-1.99	-7.12			
22.05	7.7	dolomicrite	-1.61	-6.63			
22.04	3.5	dolomitic siltst	0.83	-5.83			
22.03	0.5	dolomitic siltst	0.99	-5.16			
Dolostone unit in Olympic Fm.							
22.01	-180.0	dolomicrite	3.23	0.14			

Amadeus Basin: Mt Conner			
sample	description	∂13Ccarb	∂18O
Pioneer Fm. correlate?			
910607.01	fine g'd dolost	-1.10	-1.50
910607.06	fine g'd dolost	-1.56	-1.10

Amadeus Basin: Mt Greene			
sample	description	∂13Ccarb	∂18O
Boord Formation			
CPC19002	stromatolitic lst	4.00	-5.94
CPC19003	stromatolitic micrite	4.08	-5.93
CPC19004	stromatolitic micrite	3.17	-7.38
CPC19005	stromatolitic micrite	3.66	-6.15

Amadeus Basin: Phillipson Pound: sample prefix 910524.**									
sample	locality	ht(m)	description	∂13Ccarb	∂18O	%insol	TOC(mg/g)	∂13Corg	∂13CorgN
24.24	Twin Bore	491.5	dologrst	1.79	-1.64				
24.21	Twin Bore	470.5	dologrst	2.30	-2.39				
24.15	N of Rodinga 4 drillsite	247.0	dolomicrite	4.64	-4.34				
24.17	N of Rodinga 4 drillsite	214.0	dolomicrite	5.70	-3.11	14	0.40	-25.75	-24.17
24.18	N of Rodinga 4 drillsite	197.0	dol'tic micspar	5.12	-8.39				
24.19	N of Rodinga 4 drillsite	192.9	dol'tic micspar	4.15	-5.30				
24.12	N of Rodinga 4 drillsite	97.1	dolomicrite	3.80	-4.91				
24.11	N of Rodinga 4 drillsite	87.5	dolomicrite	5.03	-7.60				
24.09	N of Rodinga 4 drillsite	58.5	sandy micspar	5.66	-7.86				
24.07	N of Rodinga 4 drillsite	45.5	sandy micspar	4.88	-8.83				
24.04	N of Rodinga 4 drillsite	22.5	dolomicrite	4.08	-5.97				
24.01	N of Rodinga 4 drillsite	10.5	sandy micspar	4.99	-7.12	31	0.30	-26.25	-26.28

Amadeus Basin: Rodinga 4: sample prefix 910306.**						
sample	depth (m)	description	TOC(mg/g)	∂13Corg	∂13CorgN	∂34Spy
Pertatataka Formation						
6.46a	-15.54	weathered sh	0.31	-26.26	-28.04	
6.46b	-15.54	weathered sh	0.29	-25.83	-27.71	
6.45	-20.60	weathered sh	0.18	-26.87	-29.48	
6.44a	-24.62	gy sh	0.68	-27.78	-28.37	
6.44b	-24.62	gy sh	0.68	-28.17	-28.76	
6.41	-30.40	dk gy sh	0.56	-27.91	-28.79	
6.37	-40.35	gy sh	0.75	-28.01	-28.45	
6.34	-49.50	gy sh	0.84	-29.18	-29.45	
6.27	-67.95	dk gy silty sh	0.69	-28.27	-28.83	
6.26	-70.49	gy sh	1.25	-29.89	-29.55	-6.6
6.25	-74.82	gy sh	1.02	-28.76	-28.73	
6.57	-76.48	dk gy silty sh	0.78	-28.75	-29.13	
6.56	-79.09	gy sh	0.68	-28.75	-29.34	
6.55	-82.04	dk gy sh	1.10	-29.67	-29.53	
6.51	-92.90	dk gy sh				-10.3
6.50	-93.65	dk gy sh	0.96	-29.51	-29.57	
6.48	-99.40	dk gy sh	1.27	-30.14	-29.78	
6.49	-97.22	dk gy sh				-3.7
6.23/1	-106.10	dk gy sh	1.45	-30.1	-29.54	
6.23/3	-106.10	dk gy sh	1.42	-29.79	-29.26	
6.23/4	-106.10	dk gy sh	1.30	-29.6	-29.20	
6.23/5	-106.10	dk gy sh	1.19	-29.39	-29.13	
6.24/1	-114.22	gy sh	1.15	-29.39	-29.18	
6.24/2	-114.22	gy silty sh	1.73	-30.41	-29.58	
6.24/3	-114.22	dk gy silty sh	1.92	-30.43	-29.44	
6.24/4	-114.22	dk gy silty sh	1.93	-30.56	-29.56	
6.24/5	-114.22	dk gy silty sh	1.62	-30.11	-29.38	
6.24/6	-114.22	dk gy silty sh	1.20	-29.81	-29.53	
6.24/7	-114.22	dk gy silty sh	1.89	-30.46	-29.49	
6.24/8	-114.22	dk gy silty sh	2.00	-30.27	-29.22	
6.24/9	-114.22	dk gy silty sh	1.58	-29.83	-29.13	
6.18a	-119.23	gy sh	1.73	-30.62	-29.79	
6.18b	-119.23	gy sh	1.76	-30.58	-29.72	
6.18c	-119.23	gy sh	1.98	-30.71	-29.67	
6.18d	-119.23	gy sh	1.84	-30.72	-29.79	
6.18e	-119.23	gy sh	1.83	-30.69	-29.77	
6.18f	-119.23	gy sh	1.89	-30.74	-29.77	
6.18g	-119.23	gy sh	1.87	-30.67	-29.72	
6.18h	-119.23	gy sh	1.81	-30.66	-29.76	
6.18i	-119.23	gy sh	1.84	-30.70	-29.77	
6.18j	-119.23	gy sh	1.83	-30.65	-29.73	
6.18k	-119.23	gy sh	1.85	-30.58	-29.64	
6.18l	-119.23	gy sh	1.85	-30.52	-29.58	
6.18m	-119.23	gy sh	1.83	-30.74	-29.82	
6.18n	-119.23	gy sh	1.87	-30.69	-29.74	
6.18o	-119.23	gy sh	1.84	-30.54	-29.61	
6.18p	-119.23	gy sh	1.81	-30.67	-29.77	
6.17	-122.25	gy sh	1.04	-29.64	-29.58	

Amadeus Basin: Rodinga 4: sample prefix 910306.**						
sample	depth (m)	description	TOC(mg/g)	∂13Corg	∂13CorgN	∂34Spy
6.16	-125.00	gy silty sh	1.12	-29.69	-29.52	
6.14a	-131.19	dk gy sh	1.69	-30.88	-30.08	
6.14b	-131.19	dk gy sh	1.69	-30.51	-29.71	
6.11	-140.14	dk gy sh	1.96	-30.64	-29.62	
6.08	-149.13	dk gy sh	1.70	-30.56	-29.75	
6.07	-152.29	dk gy sh	0.91	-28.92	-29.06	
6.04	-161.22	dk gy sh	1.81	-30.37	-29.47	
6.02	-167.21	dk gy sh	1.92	-30.24	-29.25	

Amadeus Basin: Ross River								
sample	height(m)	description	∂13Ccarb	∂18O	%insol	TOC	∂13Corg	∂13CorgN
Todd River Dolomite		*(datum: base Todd R. Dol.)*						
910611.08	50.0	fine g'd dolost	0.23	-6.75				
910611.16	68.5	fine g'd dolost	0.61	-6.05				
910611.22	128.0	fine g'd dolost	0.54	-6.15				
Julie Formation		*(datum: base Julie Fm.)*						
910601.51	115.1	fine g'd dolost.	4.36	-8.29	8	0.11	-26.95	-26.51
910601.49	107.6	fine g'd dolost.	4.62	-9.38				
910601.45	101.4	fine g'd dolost.	2.01	-7.34				
910601.44	100.3	fine g'd dolost.	4.13	-9.44				
910601.42	95.1	fine g'd dolost.	4.15	-8.45				
910601.38	81.9	fine g'd dolost.	4.99	-8.78				
910601.37	77.1	fine g'd dolost.	4.90	-8.87				
910601.34	70.2	fine g'd dolost.	3.38	-8.49				
910601.31	60.7	fine g'd dolost.	0.30	-7.90				
930519.05	58.5	fine g'd dolost.	4.47	-9.31				
910601.30/1	57.5	fine g'd dolost.	-5.82	-6.24	17	0.19	-21.96	-21.81
910601.30/2	57.5	fine g'd dolost.	-5.48	-5.53				
910601.29	56.5	fine g'd dolost.	4.90	-9.04	9	0.16	-27.24	-26.29
910601.28	54.2	fine g'd dolost.	5.23	-8.94				
910601.27a	52.7	fine g'd dolost.	5.83	-8.57				
910601.27b	52.7	fine g'd dolost.	5.82	-8.54				
910601.24	48.2	fine g'd dolost.	4.98	-9.30				
910601.16	41.1	fine g'd dolost.	4.14	-9.24				
910601.13	38.8	fine g'd dolost.	4.45	-10.10	8	0.33	-27.63	-25.45
910601.11	29.7	fine g'd dolost.	1.99	-6.79				
910601.10	24.3	fine g'd dolost.	4.25	-8.86				
910601.09	21.6	fine g'd dolost.	3.51	-8.80				
910601.07	11.2	silty lst	5.20	-9.55				
910601.06	9.9	silty lst	4.98	-10.11				
910601.03	4.2	silty lst	5.37	-10.95				
910601.02	3.8	silty lst	5.19	-9.55	13	0.55	-27.59	-25.43
910601.01	0.5	silty lst	3.75	-9.98	7	0.34	-28.42	-25.97

Amadeus Basin: Wallara 1: sample prefix 910528.**									
sample	depth(m)	description	%insol	TOC(mg/g)	∂13Corg	∂13CorgN	∂13Ccarb	∂18O	∂34Spy
Pertatataka Formation									
02	-724.60	gy sh		1.14	-28.27	-28.07			
04	-731.50	gy sh		1.16	-28.90	-28.67			
06	-739.50	gy sh		1.41	-28.96	-28.44			
10	-742.20	gy sh		1.24	-28.04	-27.71			
11	-742.20	gy sh		0.89	-28.00	-28.18			
8	-749.00	gy sh		0.79	-26.99	-27.35			
14	-758.40	gy sh		1.06	-28.03	-27.94			
16	-771.70	gy sh		1.10	-28.58	-28.44			
18a	-780.00	gy sh		1.22	-28.98	-28.68			
18b	-780.00	gy sh		1.41	-28.86	-28.34			
20	-788.20	gy sh		1.00	-28.49	-28.49			
22	-793.50	gy sh		1.06	-27.67	-27.58			
24	-802.70	gy sh		1.06	-28.26	-28.17			
26	-812.30	gy sh		0.95	-27.11	-27.19			
30	-827.60	gy sh		1.03	-27.88	-27.84			
32/1a	-837.30	silty gy sh		0.85	-26.82	-27.07			
32/1b	-837.30	silty gy sh		0.90	-27.00	-27.16			
32/2	-837.30	gy-gn sh		0.94	-27.81	-27.90			
34	-845.30	gy sh		1.30	-28.82	-28.42			
36	-856.50	gy sh		1.06	-27.75	-27.66			
38	-863.70	gy sh		0.82	-26.99	-27.29			
39	-869.70	gy sh		0.70	-26.31	-26.85			
42	-886.00	gy sh		0.65	-27.33	-27.98			
44a	-892.20	gy sh		1.08	-27.35	-27.23			
44b	-892.20	gy sh		1.10	-26.92	-26.78			
46	-902.10	gy sh		0.56	-26.46	-27.34			
48	-914.50	gy sh		0.82	-27.59	-27.89			
50	-921.40	gy sh		0.76	-27.58	-28.00			
52a	-930.70	gy sh		0.74	-27.18	-27.64			
52b	-930.70	gy sh		0.68	-27.14	-27.73			
54	-941.50	gy sh		0.75	-26.58	-27.02			
56	-953.00	gy sh		0.71	-27.17	-27.69			
58	-961.70	gy sh		0.56	-26.69	-27.57			
60	-971.40	gy sh		0.75	-26.90	-27.34			
62	-980.20	gy sh		0.78	-27.35	-27.73			
64a	-991.40	gy sh		0.86	-27.45	-27.68			
64b	-991.40	gy sh		0.86	-27.56	-27.79			
66	-996.80	gy sh		0.58	-27.20	-28.03			
66	-999.80	calc siltst					-16.10	-10.46	
68/1	-1008.80	bl sh (bmm)		2.30	-30.52				
68/2	-1008.80	gy sh		0.50	-26.96	-28.01			
68/3	-1008.80	gy sh		0.80	-27.35	-27.69			
70	-1016.20	gy sh		0.92	-28.23	-28.36			
72	-1026.80	gy sh		0.75	-27.01	-27.45			
74	-1038.70	gy sh		1.04	-28.41	-28.35			
76	-1045.20	gy sh		0.74	-26.94	-27.40			
78	-1055.90	dk gy sh (bmm)		2.32	-30.64				
80	-1066.80	dk gy sh (bmm)		1.87	-30.64				

Amadeus Basin: Wallara 1: sample prefix 910528.**									
sample	depth(m)	description	%insol	TOC(mg/g)	∂13Corg	∂13CorgN	∂13Ccarb	∂18O	∂34Spy
82	-1077.00	gy sh		1.05	-28.50	-28.43			-0.1
84	-1080.60	gy sh		0.39	-27.21	-28.64			
86/2	-1083.70	gy sh		0.92	-28.01	-28.14			
86/1	-1083.70	bl sh (bmm)		2.04	-30.93				
147	-1086.00	calc siltst					-17.75	-11.02	
88	-1095.30	gy sh		1.09	-27.66	-27.53			
90	-1103.20	gy sh		0.85	-27.45	-27.70			
92/1	-1115.20	bl sh (bmm)		2.99	-31.95				
92/2	-1115.20	gy sh		0.69	-27.35	-27.91			
94a	-1125.60	bl sh (bmm)		3.63	-32.37				
94b	-1125.60	bl sh (bmm)		3.59	-32.35				
95/2a	-1127.30	gy sh		1.51	-27.53	-26.90			
95/1	-1127.30	bl sh (bmm)		4.00	-31.77				
96	-1132.80	bl sh (bmm)		4.49	-32.23				-8.8
98	-1142.60	gy sh		1.84	-31.37	-30.44			
100	-1152.60	bl sh (bmm)		3.14	-32.86				
102/1	-1156.00	bl sh (bmm)		3.23	-32.42				
102/.2	-1156.00	gy sh		2.25	-29.72	-28.49			
102/4	-1156.00	gy sh		0.81	-28.10	-28.42			
101	-1161.60	bl sh (bmm)							-28.1
104	-1173.00	bl sh (bmm)		2.55	-32.30				-17.3
105/4	-1177.80	bl sh (bmm)		6.81	-33.37				
105/1	-1177.80	gy sh		1.93	-30.09	-29.09			
106	-1181.70	bl sh (bmm)		5.18	-33.95				
108	-1184.40	bl sh (bmm)		3.73	-33.69				
109/2	-1190.00	dk gy sh		1.71	-31.05	-30.23			
109/1	-1190.00	bl sh (bmm)		5.85	-33.27				
110	-1193.40	gy-gn sh		1.17	-30.56	-30.32			
112/1	-1206.50	bl sh (bmm)		4.35	-34.41				
112/2	-1206.50	gy sh		1.32	-30.36	-29.94			
114	-1216.00	bl sh (bmm)		3.62	-33.34				
115	-1221.50	bl sh (bmm)							-24.0
18.02	-1224.40	gy sh	80	1.11	-27.31	-26.81			
116	-1225.50	bl sh (bmm)		3.41	-33.38				
118	-1232.50	bl sh (bmm)		3.31	-33.10				-12.6
18.03	-1234.00	gy sh	83	1.20	-27.49	-26.93			
120	-1243.90	bl sh (bmm)		1.53	-32.94				
18.04	-1245.10	gy sh	76	0.77	-26.33	-26.31			
122	-1251.80	gn sh		1.04	-26.92	-26.86			
124	-1264.00	red sh		0.24	-25.71	-27.88			
125a	-1267.00	gy-gn sh		0.57	-25.10	-25.95			
125b	-1267.00	gy-gn sh		0.57	-25.19	-26.04			
'Cap dolostone'									
126/1	-1272.40	gy sh	76	0.25	-26.61	-28.30			
126/2	-1272.40	dolomicrite					-3.40	-7.23	
126/3	-1272.40	dolomicrite					-3.55	-7.47	
128	-1273.40	dolomicrite					-3.59	-7.85	
129	-1274.10	dolomicrite					-3.50	-7.98	
130/2	-1274.80	gy sh		1.17	-31.08	-30.84			

Amadeus Basin: Wallara 1: sample prefix 910528.**									
sample	depth(m)	description	%insol	TOC(mg/g)	∂13Corg	∂13CorgN	∂13Ccarb	∂18O	∂34Spy
130/1	-1274.80	dolomic	18	0.12	-29.74	-30.39			
132/1	-1276.70	gy sh		0.69	-31.71	-32.27			
132/2	-1276.70	dolomicrite					-3.32	-7.95	
134a	-1278.70	dk gy sh		1.50	-33.77	-33.15			
134b	-1278.70	dk gy sh		1.63	-33.53	-32.79			
Aralka Formation									
137/1	-1281.50	carb nodule	31	1.65	-30.95	-30.19			
137/2	-1281.50	sh matrix		4.90	-31.59	-29.17			
138a	-1282.10	dk gy sh		5.72	-31.08	-28.43			
138b	-1282.10	dk gy sh		5.55	-31.06	-28.45			
138c	-1282.10	dk gy sh		5.82	-30.96	-28.28			
138d	-1282.10	dk gy sh		5.51	-30.94	-28.35			
138e	-1282.10	dk gy sh		5.81	-31.03	-28.36			
138f	-1282.10	dk gy sh		5.80	-31.05	-28.38			
138g	-1282.10	dk gy sh		5.92	-31.10	-28.40			
138h	-1282.10	dk gy sh		5.72	-31.06	-28.41			
138i	-1282.10	dk gy sh		5.77	-31.04	-28.38			
140	-1292.90	dk gy sh		8.13	-32.54	-29.35			
142	-1302.80	dk gy sh		8.46	-34.60	-31.35			

Georgina Basin: DDC (Mt Skinner) 1: sample prefix 910531.**									
sample	depth(m)	description	%insol	TOC(mg/g)	∂13Corg	∂13CorgN	∂13Ccarb	∂18O	∂34Sanh
Central Mt Stuart Fm									
31.11	-379.5	dk gy sh		1.56	-30.08	-29.40			
Elkera Fm									
31.12	-381.3	dologrst					2.06	-7.35	
31.13	-382.8	dolomic					2.54	-3.47	
31.15	-419.1	dolomic+anh					-0.10	-4.69	25.7
31.17	-432.8	saddle dol					-0.42	-10.92	
31.18	-439.8	saddle dol					-0.81	-11.34	
31.19	450.8	anh							29.2
31.20a	-455.4	dk gy sh		0.38	-27.29	-28.76			
31.20b	-455.4	dk gy sh		0.37					
31.21	-458.1	dolomic	27	0.18	-29.66	-30.29	0.77	-3.50	
31.22	-458.4	dolomic + sh	52	0.36	-29.47	-30.03	0.75	-4.16	
31.23	-464.2	dk gy sh	61	1.33	-31.3	-30.12			
31.24	-463.3	dolomitic sh	72	0.78	-29.11	-28.98			
31.25	-468.2	dolomic					1.50	-6.93	
31.26	-468.8	dolomic+anh					1.38	-5.15	
31.27	469.7	anh							27.7
31.28	-474.3	gy sh + anh					0.26	-10.94	26.9
31.29	-487.7	gy sh + dolomic	49	0.36	-27.26	-27.74	0.32	-4.08	
31.30	488.3	anh							25.8
31.31	-493.5	dolomic+anh					0.64	-4.74	25.9
31.31a	-493.5	dolomic+anh	49	0.34	-28.96	-29.52			
31.31b	-493.5	dolomic+anh	49	0					
31.32	-505.4	dolomic+gy sh	39	0.8	-28.95	-27.85	1.67	-4.18	
31.33	-504.4	dolomic+anh	25	0.24	-19.83	-19.91	1.57	-6.00	25.3
31.34	-509.3	dolomic					1.64	-3.32	
31.34a	-509.3	gy sh	48	2.09	-34.38	-32.16			
31.34b	-509.3	gy sh	48	2.07	-34.38	-32.14			
31.35	-512.4	dolomic+anh	25	0.94	-33.12	-31.11	1.86	-3.28	25.8
31.36	-523.3	silty dst +anh	63	0.51			2.84	-3.41	25.5
31.37	-518.5	dolomic					2.12	-3.43	
31.38	-524.0	dol'tic silty sh	31	0.75	-29.87	-28.52	3.29	-5.09	
31.39	-528.2	dst+anh					4.48	-5.72	
31.40	533.7	anh							25.4
31.41	-540.7	dolomic					4.61	-3.03	
31.42	-542.9	dolomic+anh					5.19	-4.36	26.4
31.43	-543.8	dk gy sh		0.49	-26.31	-27.39			
31.44	-525.2	dst		0.51	-20.68	-21.70	3.30	-4.50	
31.45	558.4	anh							25.4
31.46	-560.2	dst		0.26			2.66	-3.82	
31.48	-568.5	dst					2.38	-3.47	
Grant Bluff/Elyuah Fms									
31.49	-576.4	dk gy sh		1.11					
31.50	-583.4	dk gy sh		0.3					
31.51	-590.7	dk gy sh		1.2	-24.82	-24.54			
31.52	-602.0	dk gy sh		0.31					
31.53	-609.0	dk gy sh		1.43	-29.25	-28.71			
31.53	-609.0	dk gy sh		1.4	-29.27	-28.76			

Georgina Basin: DDC (Mt Skinner) 1: sample prefix 910531.**									
sample	depth(m)	description	%insol	TOC(mg/g)	∂13Corg	∂13CorgN	∂13Ccarb	∂18O	∂34Sanh
31.54	-615.1	dk gy sh		0.63	-26.05	-26.75			
31.55	-626.7	dk gy sh		1.41	-28.84	-28.32			
31.56	-634.0	dk gy sh		1.32	-28.55	-28.13			
31.57	-644.4	dk gy sh		2.67	-28.84	-27.35			
31.58	-651.1	dk gy sh		2.54	-29.31	-27.89			
31.58	-651.1	dk gy sh		2.31	-29.27	-28.00			
31.59	-660.2	dk gy sh		1.86	-29.4	-28.46			
31.60a	-670.0	dk gy sh		1.54	-29.06	-28.40			
31.60b	-670.0	dk gy sh		1.56	-29.06	-28.38			
31.61	-676.4	dk gy sh		1.46	-29.12	-28.54			
31.62	-685.8	dk gy sh		1.54	-29.56	-28.90			
31.63	-695.3	dk gy sh		2.02	-29.63	-28.56			
31.64	-703.8	dk gy sh		3.07	-30.09	-28.39			
31.65	-714.5	dk gy sh		2.25	-29.47	-28.24			
31.66	-719.6	dk gy sh		3.2	-30.17	-28.40			
31.67	-728.8	dk gy sh		3.51	-30.3	-28.39			
31.68	-734.9	dk gy sh		3.47	-30.1	-28.21			
31.69	-744.0	dk gy sh		2.96	-30.04	-28.39			
31.70	-755.3	dk gy sh		6.33	-30.85	-28.05			
31.71	-760.2	dk gy sh		6.19	-30.61	-27.84			

Georgina Basin: DDC (Mt Skinner) 2: sample prefix 910604.**					
sample	depth(m)	description	TOC(mg/g)	∂13Corg	∂13CorgN
Grant Bluff+ Elyuah Fms					
4.01	-528.83	gy sh	1.08	-32.74	-32.62
4.02	-521.21	bl sh	3.89	-32.42	-30.36
4.03	-511.76	bl sh	3.97	-30.64	-28.54
4.05	-505.36	bl sh	4.72	-30.24	-27.88
4.06	-497.43	bl sh	5.02	-30.3	-27.85
4.07	-489.81	bl sh	1.97	-29.13	-28.10
4.09	-484.94	bl sh	2.53	-29.55	-28.14
4.11	-476.4	bl sh	4.08	-29.75	-27.61
4.13	-467.56	bl sh	2.62	-30.01	-28.55
4.15	-457.2	bl sh	3.18	-29.31	-27.55
4.17	-450.8	bl sh	3.3	-29.78	-27.97
4.19a	-443.18	bl sh	2.04	-29.57	-28.49
4.19b	-443.18	bl sh	2.02	-29.57	-28.50
4.21	-431.9	bl silty sh	3.69	-30.04	-28.06
4.23	-426.11	bl sh	4.87	-29.97	-27.56
4.25	-418.19	bl silty sh	3.45	-29.25	-27.37
4.27	-409.65	bl silty sh	2.24	-29.13	-27.90
4.29	-401.42	bl silty sh	3.07	-29.33	-27.63
4.31	-392.89	bl silty sh	2.88	-29.31	-27.70
4.33	-384.35	bl silty sh	1.97	-29.37	-28.34
4.35	-375.82	bl silty sh	2.35	-29.36	-28.06
4.37	-362.1	shaly siltst	0.69	-27.46	-28.02
4.39	-355.4	gy sh	1.32	-29.54	-29.12

Georgina Basin: Huckitta 7: sample prefix 910612.**				
sample	depth(m)	description	∂13Ccarb	∂18O
Elkera Formation				
12.05	-127.60	dolomicrite	1.66	-5.41
12.09	-142.00	dolomicrite	1.73	-4.33
12.10	-150.25	dolomicrite	3.09	-3.64
12.12	-162.30	dolomicrite	4.59	-3.45
12.13	-171.80	dolomicrite	3.92	-4.70
12.14	-182.80	dolomicrite	3.74	-5.08
12.15	-191.60	dolomicrite	4.52	-6.78

Savory Basin: Boondawari Ck.			
sample	description	∂13Ccarb	∂18O
Boondawari Formation			
13.08	pink ooid grst	7.99	-1.99
13.04	red silty dolost	7.20	-3.15
13.03	ooid dologrst	7.95	-3.95
13.01	ooid dologrst	7.34	-4.68
12.10	oolitic dologrst	7.82	-4.69
12.07	stromatolitic lst	6.79	-12.66
9.03	lst with 5mm. ooids	7.36	-11.90
11.08	red micritic dolost	-2.94	-4.66

Smithton Basin: Arthur River: sample prefix 9203**.**				
sample	height(m)	description	∂13Ccarb	∂18O
Black River Dolomite		*(datum: base fm.)*		
16.07	775	dolomicrite	-2.55	-6.41
14.14	550	microsparitic dol.	-1.78	-3.74
14.12	530	microsparitic dol.	-1.19	-6.83
14.10	395	dolomicrite	4.82	-2.99
14.07	290	stromatolitic dol.	4.03	-4.58
14.09	250	dolomicrite	3.43	-0.10
13.13	40	dolomicrite	3.90	-2.00
14.03	35	pale microsparitic dol.	3.89	-1.46
13.01	15	dolomicrite	4.32	-2.88
13.03	10	stromatolitic dol.	4.23	-1.96

Smithton Basin: Forest 1								
sample	depth(m)	description	%insol	TOC(mg/g)	∂13Corg	∂13CorgN	∂13Ccarb	∂18O
Kanunnah Subgroup								
21.38	-694.3	fine g'd lst					-11.94	-15.40
21.34	-779.1	fine g'd lst	78	3.57	-34.96	-32.65		
Black River Dolomite								
21.33	-798.0	lst					-5.48	-13.02
21.29	-834.0	black fine dol	100	5.97	-32.82	-30.11	1.64	0.50
21.05	-856.3	fine g'd lst	8	0.24	-34.77	-33.15	-4.50	-9.47
21.27	-857.1	black mudst	88	1.01	-32.99	-32.78		
21.06	-869.4	fine g'd lst					-3.94	-3.59
21.07	-874.7	fine g'd lst					-4.11	-6.26
ABS 84	-890.0	matrix of diamictite					-2.62	-3.33
21.22	-921.0	strom. dol clast					-2.66	-6.33
21.01	-967.5	dol					3.01	-3.73
ABS 88	-990.0	dolomicrite					1.19	-8.60
21.17	-993.4	dol					-0.39	-3.30
21.14	-1025.8	black mudst	100	4.18	-24.84	-22.66		
21.13	-1032.7	dol	5	0.10	-22.55	-21.56	3.11	-2.32
21.12	-1043.0	black mudst	78	2.62	-24.12	-22.27		
21.09	-1057.8	dol					3.82	-3.54

King Island			
sample	description	∂13Ccarb	∂18O
Dolostone overlying diamictite (Cottons Breccia)			
7786/135	red, siliceous lam dolomicrite	-2.62	-17.79
7786/139	pale pinkish-gy. lam fine-g'd dolost	-2.7	-13.18
7786/146	pale gy, fine g'd, lam. dolost.	-2.4	-13.74

Smithton Basin: Montagu River: sample prefix 9203**.**				
sample	height	description	∂13Ccarb	∂18O
Kanunnah Subgroup				
11.04	-10	v.f.g'd impure dolost	-1.75	-1.33
Smithton Dolomite		*(datum: base Smithton Dolomite)*		
11.07	15	v.f.g'd dolost	1.00	-3.11
11.05	60	micritic dolost	-0.70	-3.99
11.11	145	micritic dolost	-0.34	-5.38
11.10	190	micritic dolost	-0.78	-3.49
11.09	235	micritic dolost	-1.51	-4.51
11.53	180	v.f.g'd dolost	-0.06	-6.76
11.51	225	micritic dolost	-1.38	-5.86
11.50	265	med Xine dolost	-0.74	-7.38
11.47	315	micritic dolost	-2.49	-4.89
11.45	345	micritic dolost	-1.46	-5.94
11.41	370	micritic dolost	-1.70	-5.13
10.25	385	micritic dolost	-1.44	-5.10
10.23	435	micritic dolost	0.42	-10.55
10.21	470	v.f.g'd dolost	1.26	-4.97
10.18	510	med. Xine dolost	1.81	-15.68
10.14	560	micritic dolost	-0.85	-8.58
10.15	605	finely Xine dolost	1.95	-14.09
11.34	730	finely Xine dolost	1.72	-15.01
11.32	755	f.g'd lst	0.75	-15.22
11.30	805	med Xine dolost	1.46	-12.12
11.27	900	finely Xine dolost	1.50	-13.45
11.23	940	f.g'd lst	-2.43	-12.62
11.22	995	finely Xine dolost	0.45	-9.21
11.21	1115	med. Xine dolost	1.54	-8.67
11.19	1185	med. Xine dolost	0.79	-10.37
11.17	1245	med. Xine dolost	3.11	-9.59
11.14	1295	med. Xine dolost	2.67	-11.24
11.36	950	v.f.g'd lst	0.40	-15.60
11.39	1085	v.f.g'd lst	5.02	-6.03

Smithton Basin: Redpa				
sample	height	description	∂13Ccarb	∂18O
Smithton Dolomite		*(datum: base Smithton Dolomite)*		
920317.16	790	v.f.g'd lst	-0.46	-11.77
920317.18(L)	890	Oolitic lst; ooids selected	-3.33	-7.26
920317.18(D)	890	Xine dolomite	-2.73	-7.02
002037(L)	810	v.f.g'd lst	-3.01	-7.95
002037(D)	810	med Xine dolomite	-2.19	-6.87

Jubilee Region					
sample	height(m)	AMG grid co-ords	description	∂13Ccarb	∂18O
Clark Group					
P129		DN 534 451	oolitic lst	1.12	-13.98
K67		DN 591 671	micritic lst	0.39	-13.11
S107		DN 669 540	micritic lst	1.21	-11.33
S108		DN 669 540	dolomicrite	1.58	-10.25
Weld River Group (Gomorrah Dolomite)				*(datum base W.R.G.)*	
P132	50	DN 544 464	dolomicrosaprite	-1.06	-1.35
J21	250	DN 5355 4720	dolomicrosaprite	-1.03	-1.48
S102	250	DN 673 544	dolomicrite	-1.32	-6.73
J19	330	DN 532 477	dolomicrite	-1.29	-2.3
J37	400	DN 561 457	dolomicrite	0.94	-0.42
Weld River Group (Devils Eye Dolomite)					
W14	930	DN 558 546	dolomicrite	-2.97	-2.3
W6	1000	DN 5725 5490	dolomicrite	-1.95	-2.36
W7	1050	DN 580 549	dolomicrite	0.29	-5.52
S92	1300	DN 682 563	dolomicrite	-1.9	-3.5
W13	1300	DN 554 551	dolomicrosparite	0.17	-5.48
W68	1400	DN 526 494	dolomicrosparite	-2.73	-3.69
W69	1470	DN 527 494	finely Xine dolost	0.32	-2.5
J44	1700	DN 562 471	dolomicrosparite	-1.5	-3.4
W11	1900	DN 557 556	dolomicrite	-1.44	-3.19
W9	2250	DN 557 561	med Xine dolost	-5.39	-4.81
W113	2300	DN 554 569	dolomicrite	-0.05	-3.23
W104	2700	DN 557 578	dolomicrite	-0.33	-7.91
Weld River Group (Styx Dolomite)					
W109	3000	DN 553 580	dolomicrite	5.1	-1.55
Weld River Group (Cotcase Creek Dolomite)					
W59	3750±500	DN 562 504	fine-g'd dolost	-1.7	-2.45
S328	3750±500	DN 666 436	dolomicrite	-1.29	-1.3
W29	3750±500	DN 554 515	dolomicrosparite	0.05	-6.61
W19	3750±500	DN 535 545	matrix of diamict.	0.87	-9.87
S382	3750±500	DN 623 454	dolomicrite	1.42	-5.75
S388	3750±500	DN 610 463	matrix of diamict.	3.37	-5.27
BO4	3750±500	DN 669 287	dolomicrite	3.54	-2.55
S306	3750±500	DN 643 438	dolomicrite	4.5	-0.8
W116	3750±500	DN 545 573	dolomicrosparite	4.97	-2.65
J47	3750±500	DN 547 496	dolomicrosparite	5.49	-4.5
Dropstone laminite of ?uppermost Cotcase Ck. Fm.					
J33	4250	DN 564 489	dolosiltite	1.75	-5.6
J35	4250	DN 564 489	dolosiltite	1.97	-5.32
S400	4250	DN 604 464	dolosiltite	1.7	-4.87

Appendix 1.2

Carbonate and sulphate trace-element (Mn, Sr, Rb) and $^{87}Sr/^{86}Sr$ analyses

Explanatory Notes

For full sample notation, descriptions and locational details, see Appendix 1.1. Abbreviations for sample mineralogy are D (= dolostone), L(= limestone), and A (= anhydrite). The atomic Ca/Mg ("atomCa/Mg") ratio is given. $\delta^{13}C_{carb}$ and $\delta^{18}O$ are repeated from Appendix 1.1. Initial $^{87}Sr/^{86}Sr$ ratios are calculated assuming an age of 580 Ma for all units except the Black River Dolomite (Smithton Basin) for which an age of 700 Ma is assumed.

See section 2.4 for analytical methods.

sample	min	atomCa/Mg	Sr(ppm)	Mn(ppm)	Mn/Sr	87Sr/86Sr	∂13C	∂18O	Rb(ppm)	87/86Srinit
Adelaide Geosyncline, Bunyeroo Gorge: Nuccaleena Fm.										
3.01	D	1.10	68	2104	30.94		-1.97	-7.54		
3.03	D	1.20	67	1930	28.81		-2.44	-8.07		
3.06	D		63	2846	45.17		-3.49	-7.94		
Adelaide Geosyncline, BWM1A-1: Nuccaleena Fm.										
20.13	D		174	1573	9.04		-1.43	-7.83		
20.14	D		98	1264	12.90		-1.27	-7.31		
20.11/1	D		87	3734	42.92		-1.95	-7.60		
Adelaide Geosyncline, SCYW1a: Nuccaleena Fm.										
22.56	A		744			0.713079			0.055	0.713077
Adelaide Geosyncline, Bunyeroo Gorge: Wonoka F										
5.16c	D	1.33	76	3506	46.13		-1.40	-5.88		
5.23	L	46.03	172	2200	12.79		-10.07	-14.62		
5.29	L		194	1744	8.99		-8.56	-13.89		
5.31	L	45.45	240	940	3.92		-8.26	-13.85		
5.35	L	47.94	295	884	3.00		-8.00	-13.19		
5.33b	L		246	691	2.81		-8.00	-13.53		
5.36	L	32.21	577	661	1.15	0.709100	-7.51	-13.12		
5.38	L		448	572	1.28		-7.62	-12.71		
5.39	L		494	418	0.85		-7.49	-12.68		
5.41	L	31.18	717	386	0.54	0.708876	-7.45	-12.68		
5.44	L	57.86	921	577	0.63	0.708683	-7.67	-12.57	0.091	0.708680
5.50	L	60.26	696	871	1.25		-7.08	-12.22		
5.52	L	47.62	1420	344	0.24	0.708757	-6.36	-10.16		
5.54	L	34.37	1064	449	0.42	0.708986	-6.27	-10.29		
5.55	L		799	681	0.85					
5.56	L		320	559	1.75		-6.03	-9.93		
5.60	L	41.94	520	1288	2.48		-1.81	-11.23		
6.02	L	39.84	234	1893	8.09		-2.82	-11.80		
6.05	L	14.42	259	891	3.44		0.20	-11.20		
6.11	L		96	845	8.80		0.66	-4.47		
6.12	L	42.42	429	269	0.63	0.709005	2.36	-4.73		
6.13	D	1.55	115	1609	13.99		-2.04	-4.39		
Adelaide Geosyncline, Brachina Gorge: Wonoka Fm.										
7.19	L	31.66	847	149	0.18	0.708744	2.72	-5.89	0.063	0.708742
7.20	L		373	357	0.96		1.42	-5.49		
7.21	L	35.31	664	612	0.92	0.708876	2.32	-6.95		
7.23	D	1.03	58	4402	75.90		0.85	-3.50		
Adelaide Geosyncline, First Hill: Wonoka Fm.										
8.05/2	L		135	2190	16.22		-9.77	-13.35		
8.10	L		208	694	3.34		-7.95	-12.88		
8.14	L		317	961	3.03		-7.71	-13.24		
8.18	L		325	518	1.59		-7.48	-12.70		
8.35	L	33.86	1161	451	0.39	0.708761	-6.46	-10.42		
8.36	L		763	759	0.99					
8.37	L		835	644	0.77					
8.38	L	41.64	1029	526	0.51	0.708832	-5.35	-10.07		
Adelaide Geosyncline, Umberatana: Wonoka Fm.										
10.07	L		968	1508	1.56		-8.18	-15.12		
10.15	L	22.36	1307	664	0.51	0.711028	-6.80	-15.71		

sample	min	atomCa/Mg	Sr(ppm)	Mn(ppm)	Mn/Sr	87Sr/86Sr	∂13C	∂18O	Rb(ppm)	87/86Srinit
10.22	L	22.90	1138	592	0.52	0.715715	1.33	-14.85		
10.30	L	33.18	381	411	1.08	0.711110	-1.99	-4.06		
10.35	L		608	959	1.58		-7.33	-14.98		
Officer Basin, Giles 1: 'Giles Mudstone'										
10.32	A					0.711708				
Officer Basin, Observatory Hill 1: Rodda beds correlate										
14.09	D	1.32	397	499	1.26		4.27	-8.64		
14.10	L	22.40	320	326	1.02		6.24	-8.50		
14.11	L	40.02	1120	340	0.30	0.707954	5.78	-5.28	0.244	0.707948
14.12	D	1.07	66	65	0.98		5.81	-4.96		
Officer Basin, Munta 1: Rodda beds correlate										
15.02	L	24.60	1540	243	0.16	0.708857	2.37	-5.02	0.219	0.708853
15.03	L	20.83	1199	176	0.15					
15.04	L	21.64	1112	219	0.20	0.708856	2.19	-4.69	0.187	0.708851
15.05	L	27.00	1026	274	0.27	0.708991	2.00	-4.51	0.294	0.708983
15.29	L	59.13	170	735	4.32		-6.03	-7.30		
15.30	L	54.37	164	697	4.25		-7.76	-7.99		
15.46	L	11.11	540	403	0.75	0.708657	2.00	9.62		
15.47	L		323	801	2.48		1.27	-6.66		
15.48	L	25.15	498	440	0.88	0.708515	2.83	-5.71	0.216	0.708503
15.58	L		228	855	3.75		4.22	-6.41		
15.61	L	41.94	443	528	1.19					
15.62	L		199	836	4.20		4.98	-7.06		
15.66	L	55.15	7699	682	0.09	0.712025	5.95	-9.83		
15.79	L	24.89	794	789	0.99		4.77	-5.16		
15.81	L	29.56	944	212	0.22	0.708055	5.53	-4.57	0.16	0.708050
15.83	L	39.22	1638	102	0.06	0.707914	5.35	-2.59	0.171	0.707911
15.84	L		373	195	0.52					
15.85	L	38.81	906	163	0.18	0.708123	5.97	-4.01	0.425	0.708110
Amadeus Basin, Wallara 1: Aralka Fm.										
6.06	D	1.22	278	1408	5.06	0.709372				
Amadeus Basin, Hijinx Syncline: Olympic Fm.										
23.14	D	0.99	75	704	9.43	0.708976	3.10	-0.32		
23.15	D	0.92	180	774	4.30	0.711570	1.54	-2.10		
Amadeus Basin, Fenn Gap: Correlate of Pioneer Fm.										
6.62	D	1.02	150	1689	11.25	0.707751	1.56	-2.50		
6.64	D		249	706	2.84		2.22	-1.53		
Amadeus Basin, Mt Conner: ?Correlate of Pioneer Fm.										
7.01	D	1.06	151	1408	9.30	0.710034	-1.10	-1.50		
7.06	D	1.15	219	2393	10.91	0.710319	-1.56	-1.20		
Amadeus Basin, Wallara 1: 'cap dolostone'										
28.128	D					0.709587				
28.129	D					0.709241	-3.50	-7.68		
28.132	D					0.708981	-3.32	-7.65		
Amadeus Basin, Acacia Well: Pertatataka F										
1.52	L	28.11	405	1285	3.17	0.710804	2.57	-8.83		
Amadeus Basin, Ross River: Julie Fm.										
1.01	L	4.56	136	549	4.04	0.710372	3.75	-9.98		
1.02	L	8.09	371	360	0.97	0.709045	5.19	-9.55		
1.03	L	24.94	182	336	1.85	0.709395	5.37	-10.95		

sample	min	atomCa/Mg	Sr(ppm)	Mn(ppm)	Mn/Sr	87Sr/86Sr	∂13C	∂18O	Rb(ppm)	87/86Srinit
1.06	L		118	336	2.85		4.98	-10.11		
1.09	D					0.711741	3.51	-8.80		
1.11	D	1.13	41	619	15.10		1.99	-6.79		
1.13	D	1.04	42	422	10.11	0.710315	4.45	-10.10		
1.24	D	1.02	33	422	12.78	0.709508	4.98	-9.30		
1.25	D	0.92	36	422	11.87	0.710298				
1.27	D	1.09	33	585	17.73		5.83	-8.87		
1.28	D	1.02	33	422	12.86	0.710211	5.23	-9.24		
1.30	D	1.18	137	56	0.41		-5.48	-5.83		
1.32	D	1.00	40	422	10.56	0.710529				
1.37	D	1.11	38	508	13.37	0.710050	4.90	-9.17		
1.38	D	1.00	32	493	15.48	0.710446	4.99	-9.08		
1.42	D	1.12	47	649	13.81	0.710960	4.15	-8.75		
1.45	D	1.14	67	392	5.85		2.01	-7.64		
Amadeus Basin, Ellery Creek: Julie Fm.										
6.40	D	1.18	55	563	10.21	0.712544	5.79	-9.15		
6.41	L		47	567	12.06		3.98	-15.74		
6.42	D	1.41	65	634	9.73	0.711201				
6.43	D	1.06	59	1408	23.70		5.80	-4.99		
6.46	D	1.19	48	4646	97.80	0.710353	1.57	-8.02		
Amadeus Basin, Katapata Gap: Julie Fm.										
21.18	D	0.87	54	1267	23.54	0.709552	4.98	-5.40		
21.21	D	0.91	43	774	18.18	0.709270	5.95	-5.48		
21.22	D	0.93	48	1267	26.39	0.709461	4.03	-6.62		
21.24	D	0.93	43	1267	29.40	0.709283	1.00	-6.38		
Amadeus Basin, Phillipson Pound: Julie Fm.										
24.09	L		221	164	0.74		5.66	-7.86		
24.14	D	0.93	61	352	5.78	0.709722				
24.17	D	0.94	61	282	4.64	0.708922	5.70	-2.81		
24.18	L	4.64	247	133	0.54	0.708431	5.12	-8.39	0.135	0.708416
24.19	L	3.90	246	110	0.45	0.708363	4.15	-6.30	0.092	0.708352
24.21	D	0.94	75	1619	21.61	0.709804	2.30	-2.09		
24.22	D	0.96	96	1126	11.77	0.711750				
24.24	D	0.94	73	1337	18.40	0.709710	1.79	-1.34		
Amadeus Basin, Mt Greene: Boord Fm.										
CPC19002	L		205	321	1.57		4.00	-5.94		
CPC19003	L		194	536	2.76		4.08	-5.93		
Amadeus Basin, Gardiner Range: Namatjira Fm.										
21.08	D	0.94	66	1126	16.98	0.713393				
21.09	D	0.96	65	915	14.09	0.710506				
21.10	D	0.88	120	704	5.88	0.713972				
Amadeus Basin, Ross River: Todd River Dolomite										
11.08	D	1.02	91	774	8.52	0.709139				
11.16	D	1.03	73	704	9.70	0.709729				
11.22	D	0.95	58	211	3.64	0.709289				
Georgina Basin, Huckitta 7: Elkera Fm.										
12.05	D	0.93	50	493	9.92	0.710038	1.66	-5.11		
12.10	D					0.710517	3.09	-3.64		
12.11	D	0.91	69	493	7.15	0.710579				
12.12	D					0.710853				

sample	min	atomCa/Mg	Sr(ppm)	Mn(ppm)	Mn/Sr	87Sr/86Sr	∂13C	∂18O	Rb(ppm)	87/86Srinit
12.15	D	0.93	69	563	8.22	0.710959	4.52	-6.48		
12.16	D	0.95	63	563	8.99	0.715387				
12.17	D	0.94	50	634	12.75	0.710497				
Georgina Basin, DDC(Mt Skinner) 1: Elkera Fm.										
31.13	D	0.98	65	2675	41.43	0.712811				
31.15	A		860			0.710995			0.091	0.710992
31.19	A					0.729506				
31.21	D					0.718568	0.77	-3.20		
31.27	A					0.727177				
31.28	A					0.722566				
31.30	A		1241			0.720403			0.769	0.720385
31.31	A					0.719325				
31.33	A		612			0.723585			0.106	0.723580
31.35	A		1017			0.713139			0.05	0.713138
31.39	A					0.714014				
31.39	D					0.714092	4.48	-5.42		
31.40	A		537			0.717925			0.474	0.717900
31.41	D					0.714471	4.61	-2.73		
31.45	A					0.717390				
31.48	D	1.20	297	2393	8.05	0.716573				
Savory basin, Boondawari Creek: Boondawari Fm.										
9.03	L	15.94	82	1686	20.56		7.36	-11.90		
12.07	L	60.60	88	947	10.76		6.79	-12.66		
12.10	D	0.98	47	226	4.81		7.82	-4.40		
13.01	D	1.19	34	2370	69.71		7.34	-4.39		
13.08	D	1.03	53	555	10.47		7.99	-1.70		
Smithton Basin, Arthur River: Black River Dolomite										
13.03	D	1.18	58	104	1.79					
14.07	D	1.02	30	64	2.13					
13.01a	D	1.09	59	130	2.20					
Smithton Basin, Forest 1: Black River Dolomite										
21.01	D	1.05	238	60	0.25	0.706907	3.01	-3.70		
21.02	D	0.98	48	70	1.48	0.708608				
21.22	D	1.10	56	322	5.75		-2.66	-6.03		
21.29	D	0.93	178	199	1.12		1.64	-0.50		
21.03	D	0.96	34	141	4.12	0.709262				
21.04	D	0.95	53	70	1.32	0.708016				
21.05	L	41.75	1088	137	0.13	0.706556			0.061	0.706554
21.06	L	56.46	1196	161	0.13	0.706337			0.095	0.706335
21.07	L	24.31	937	227	0.24	0.706472	-4.11	-7.26	0.559	0.706455
21.09	D	0.96	87	181	2.08		3.82	-8.56		
Smithton Basin, Montagu River: Smithton Dolomite										
10.14	D	1.04	84	122	1.45		-0.85	-8.28		
10.15	D	1.06	86	48	0.56		1.95	-13.79		
10.18	D	1.01	78	40	0.51		1.81	-15.38		
10.21	D	1.02	75	70	0.93		1.26	-4.67		
11.07	D	0.98	51	325	6.37		1.00	-2.81		
11.09	D	1.16	59	131	2.22		-1.51	-4.21		
11.14	D	1.26	144	34	0.24		2.67	-10.94		
11.17	D	1.23	119	30	0.25		3.11	-9.29		

sample	min	atomCa/Mg	Sr(ppm)	Mn(ppm)	Mn/Sr	87Sr/86Sr	∂13C	∂18O	Rb(ppm)	87/86Srinit
11.21	D	1.25	114	60	0.53		1.54	-8.37		
11.30	D	1.29	102	158	1.55		1.46	-13.34		
11.36	L	19.34	236	127	0.54		0.40	-15.60		
11.39	L	16.56	527	54	0.10	0.708498	5.02	-6.03	0.049	0.708495
11.41	D	1.02	87	104	1.20		-1.70	-4.83		
11.50	D	1.06	76	73	0.96		-0.74	-7.08		
11.53	D	1.01	57	50	0.88		-0.06	-6.46		
Smithton basin, Montagu River area: Smithton Dolomite, lower member										
1661	D					0.708661				
1662	D					0.708905				
1663	D	1.25	95	55	0.58	0.708579				
1664	D	1.18	58	75	1.29	0.709142				
1665	D	1.14	79	102	1.29	0.709814				
Smithton Basin, Redpa: Smithton Dolomite (upper member)										
17.14	L	27.61	127	37	0.29					
17.16	L	112.11	141	18	0.13		-0.46	-11.77		
17.18	L	7.48	199	23	0.12	0.708208	-3.33	-7.26	0.237	0.708174
2037d	D	1.60	209	19	0.09		-2.19	-6.57		
2037l	L	38.58	274	21	0.08	0.708235	-3.01	-7.95	0.004	0.708235
2037			274			0.708315			0.004	0.708315
Smithton Basin, Smithton Quarry: Smithton Dolomite										
S2	D	1.00	83	70	0.85	0.708401	0.10	-4.94		
S3	D	0.97	63	70	1.12	0.709906				
S4	D	0.95	47	70	1.51					

Appendix 1.3

Elemental analyses of kerogen

EXPLANATORY NOTES

For full sample notation, descriptions and locational details, see Appendix 1.1. TOC data are repeated from Appendix 1.1. See section 2.4 for analytical methods.

Appendix 1.3: Elemental analyses of kerogen										
sample	TOC(mg/g)	N(%)	C(%)	H(%)	S(%)	atomic N	atomic C	atomic H	**H/C**	N/C
Adelaide Geosyncline: BWM1A-1: Nuccaleena Fm.										
20.03/2	2.21	0.11	9.57	0.35	35.86	.008	0.80	0.35	**0.44**	.010
Adelaide Geosyncline: Brachina Gorge: Bunyeroo Fm.										
7.05	17.05	0.69	56.68	1.64	0.46	.049	4.72	1.63	**0.34**	.010
Adelaide Geosyncline: Bunyeroo Gorge: Wonoka I										
5.52	0.15	0.32	20.25	0.24	1.71	.023	1.69	0.24	**0.14**	.014
6.05/1		0.78	18.41	0.57	15.47	.056	1.53	0.57	**0.37**	.036
6.06		1.92	35.76	1.6	42.95	.137	2.98	1.59	**0.53**	.046
6.09	0.20	0.24	7.48	0.31	41.94	.017	0.62	0.31	**0.49**	.028
Officer Basin: Munta 1: Rodda beds correlate										
15.08/2	1.75	0.64	21.48	2.03	35.03	.046	1.79	2.01	**1.13**	.026
15.24/1	1.60	0.34	11.56	0.8	41.28	.024	0.96	0.79	**0.82**	.025
15.24/3	0.60	0.64	19.95	0.83	4.56	.046	1.66	0.82	**0.50**	.028
15.91	0.93	0.12	3.33	0.42	34.35	.009	0.28	0.42	**1.50**	.031
15.99	6.56	0.32	11.67	0.92	42.97	.023	0.97	0.91	**0.94**	.024
15.118	1.02	0.13	5.03	0.36	42.25	.009	0.42	0.36	**0.85**	.022
Amadeus Basin: Ellery Creek: Pertatataka Fm.										
6.09	1.04	0.89	54.13	1.79	2.06	.064	4.51	1.78	**0.39**	.014
6.09	1.04	1.25	61.81	1.9	2.11	.089	5.15	1.88	**0.37**	.017
6.23	0.98	0.17	21.68	0.31	0.22	.012	1.81	0.31	**0.17**	.007
6.26	1.28	0.44	36.99	0.92	0.84	.031	3.08	0.91	**0.30**	.010
6.26	1.28	0.94	58.68	1.32	1.18	.067	4.89	1.31	**0.27**	.014
6.35	0.62	0.18	16.3	0.36	0.32	.013	1.36	0.36	**0.26**	.009
Amadeus Basin: Rodinga 4: Pertatataka Fm.										
6.18	1.81	0.12	5.51	0.39	41.2	.009	0.46	0.39	**0.84**	.019
6.49		0.11	3.76	0.29	39.52	.008	0.31	0.29	**0.92**	.025
Amadeus Basin: Wallara 1: Pertatataka Fm.										
28.88	1.09	0.26	14.49	0.42	34.15	.019	1.21	0.42	**0.35**	.015
28.101		0.18	12.02	0.56	35.74	.013	1.00	0.56	**0.56**	.013
28.115		0.2	11.7	0.63	39.81	.014	0.97	0.63	**0.64**	.015
28.138	5.72	0.41	22.22	1.02	30.49	.029	1.85	1.01	**0.55**	.016

Appendix 2

Walter, M.R., Grey, K., Williams, I.R., & Calver, C., 1994: Stratigraphy of the Neoproterozoic to ealy Palaeozoic Savory Basin, Western Australia, and correlation with the Amadeus and Officer Basins. *Australian Journal of Earth Science,* 41:533-546.

Australian Journal of Earth Sciences (1994) **41**, 533–546

Stratigraphy of the Neoproterozoic to Early Palaeozoic Savory Basin, Western Australia, and correlation with the Amadeus and Officer Basins

M. R. WALTER,[1] K. GREY,[1] I. R. WILLIAMS[2] AND C. R. CALVER[1]

[1]*School of Earth Sciences, Macquarie University, Sydney, NSW 2109, Australia.*
[2]*Geological Survey of Western Australia, 100 Plain St, East Perth, WA 6004, Australia.*

The Savory Basin in central Western Australia was recognized in the mid-1980s during regional mapping of very poorly exposed Proterozoic rocks previously assigned to the Bangemall Basin. All of the sedimentary rock units in the Savory Basin have been included in the Savory Group, which unconformably overlies the Mesoproterozoic Yeneena and Bangemall Groups. Correlation with adjacent basins is impeded by poor outcrop and the lack of subsurface information. Possible correlations have been investigated with the much better known Amadeus Basin to the east, and with the Officer Basin. Two correlations now clarify the age and relationships of the Savory Group. First, the Skates Hills Formation contains distinctive stromatolites previously recorded from the Bitter Springs Formation of the Amadeus Basin. In addition, the Skates Hills and Bitter Springs Formations have many lithological features in common. This correlation is strengthened by comparison with surface and subsurface units in the northern Officer Basin. Second, the intergrading sandstone–diamictite of the Boondawari Formation is very similar to the intergrading Pioneer Sandstone–Olympic Formation of the Amadeus Basin, and the overlying siltstone closely resembles the Pertatataka Formation and its correlative the Winnall beds. The stromatolitic and oolitic carbonates at the top of the Boondawari Formation are broadly comparable with those of the Julie Formation (which grades down into the Pertatataka Formation). Support for this set of correlations comes from carbon isotope chemostratigraphy. The stromatolites include two new forms described herein, *Eleonora boondawarica* and *Acaciella savoryensis*, together with a third form too poorly preserved to be formally defined. The age of the upper sandstones is unknown. The McFadden Formation seems to have its provenance in the Paterson Orogen. The southeastern extension of this orogen is the Musgrave Block, where compression followed by uplift at about 560–530 Ma (Peterman Ranges Orogeny) led to the formation of large amounts of conglomerate (Mt Currie Conglomerate) and sandstone (Arumbera Sandstone). If tectonic events in the Paterson Orogen were contemporaneous with those in the Musgrave Block, the McFadden Formation would correlate with the Arumbera Sandstone.

Key words: **Proterozoic, Savory Basin, stratigraphic correlation, stromatolites.**

INTRODUCTION

The Savory Basin (Figure 1) occupies an area of about 53 000 km² southeast of Newman in central Western Australia (Williams 1992). It forms the western margin of the Centralian Superbasin (Walter *et al.* in press). The basin was recognized in the mid-1980s during regional mapping of the very poorly exposed Proterozoic rocks of this region (Williams 1987, 1990, 1992). All of the sedimentary rock units in the basin have been included in the Savory Group (Williams 1992; Figure 2); they are best exposed along the margins of the basin, particularly in the Robertson Range and southeast from Yanneri Creek. Away from the margins the rocks are poorly exposed and limited to scattered rocky hills, or to areas where incised drainage has exposed fresh bedrock beneath laterite-capped scarps, as in the Boondawari Creek area described here. The intervening areas are covered with desert sand. These Proterozoic rocks were previously assigned to the Calvie and McFadden Formations of the Bangemall Basin (Williams *et al.* 1976; Muhling & Brakel 1985). There is no well or seismic information.

Correlation with adjacent basins is difficult because of the paucity of outcrop and the lack of subsurface information. During 1991 three of the authors (KG, MRW, IRW) made a traverse across the western and southwestern parts of the basin, concentrating on the outcrops in the headwaters of Boondawari Creek, to investigate possible correlations with the much better known Amadeus Basin to the east (Figure 1). The correlations proposed in this paper are strengthened by comparison with surface and subsurface units in the northern Officer Basin, itself also very poorly known.

In the north and west the Savory Group lies unconformably on both the Yeneena and Bangemall Groups. Locally the unconformity divides a rock succession previously mapped as one unit, the Calvie Sandstone (Muhling & Brakel 1985b). Northeast of, and above, the unconformity, gently east-dipping medium- to coarse-grained sandstone and pebble to boulder conglomerate are now recognized as the basal units of the Savory Group. In the south the basal units of the Savory Basin lie unconformably on the Bangemall Group.

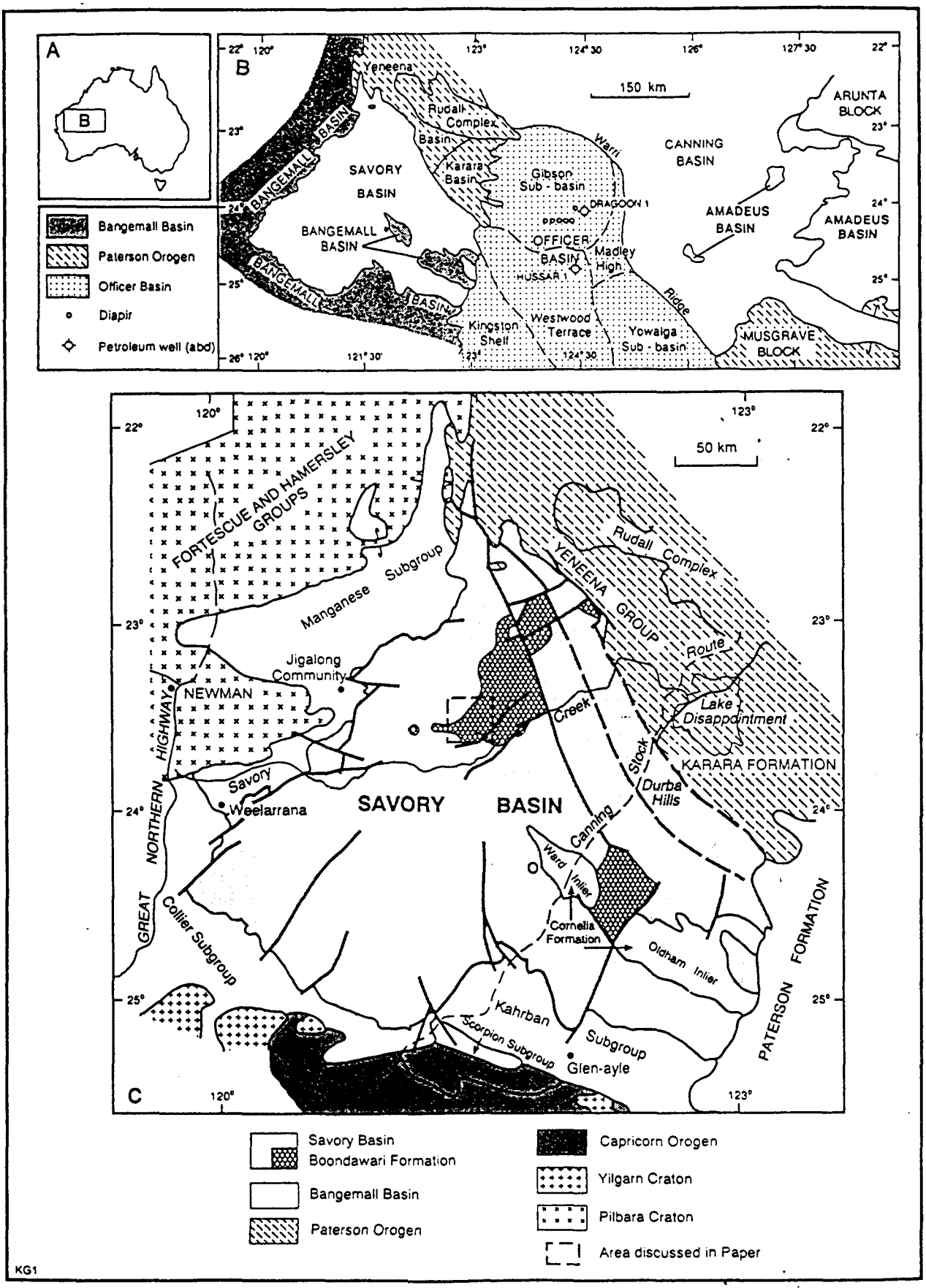

Figure 1 Location of the Savory Basin and adjacent structures (after Williams 1992).

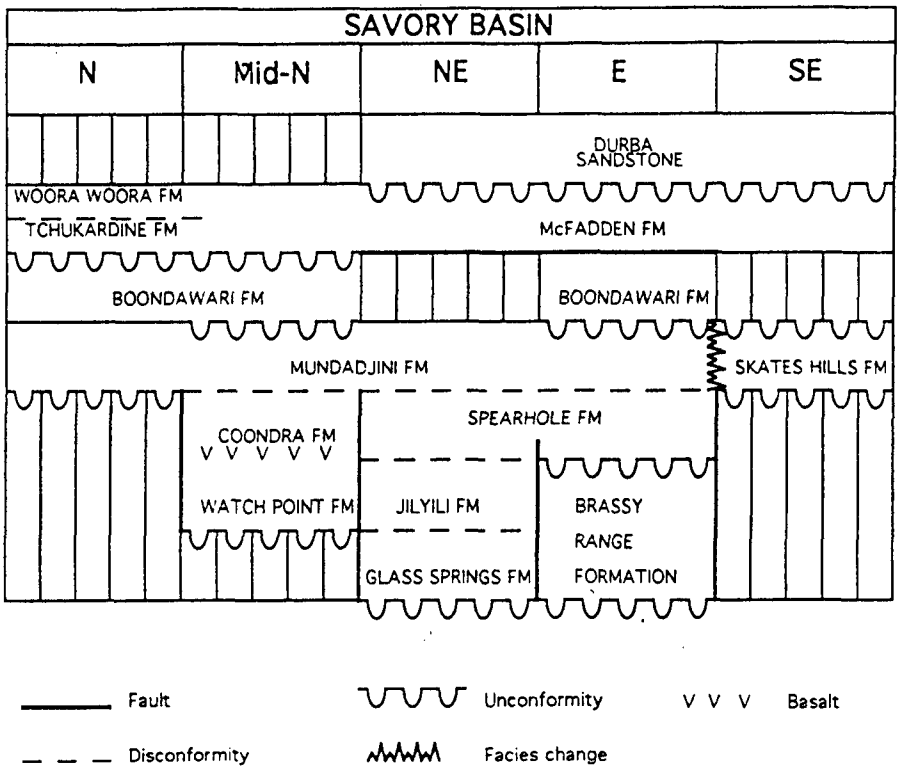

Figure 2 Stratigraphy of the Savory Basin (after Williams 1992).

STRATIGRAPHY

A stratigraphic summary of the Savory Group is given in Figure 2. This paper describes those formations examined during 1991 for which new information can be provided, and then several other units of particular importance are briefly described for correlation with the adjacent basins.

If the correlations proposed here (Figure 6) are correct, then there are several major time breaks within the Savory Group, and it would be appropriate to define new groups to encompass each supersequence. However, because the basin is very poorly known such action would be premature. Instead, the previously defined formations have been assigned to the supersequences described by Walter *et al.* (in press) for the Centralian Superbasin. Thus, in Figure 2, the Glass Springs to Mundadjini Formations and their correlatives belong to Supersequence 1; Supersequence 2 is not represented in the Savory Basin; the Boondawari Formation is part of Supersequence 3; and the uppermost units are (very tentatively) assigned to Supersequence 4.

Supersequence 1

WATCH POINT FORMATION

The basal Watch Point Formation (Williams & Tyler 1991; Williams 1992) occurs along the central part of the western edge of the Robertson Range. The formation unconformably overlies the Manganese Subgroup of the Bangemall Basin (although the unconformity is not exposed), and is conformably overlain by the Coondra Formation (Williams & Tyler 1991; Williams 1992). It consists of interbedded shale, siltstone, and thin-bedded fine-grained sandstone. East of the abandoned Robinson Range Homestead it consists of dark brown, thin bedded fine-grained micaceous sandstone with ripple marks (frequently flat-topped), desiccation cracks and intraclasts, passing up into medium to thick bedded arkosic and clayey sandstone. At Watch Point it is about 150–200 m thick, but has an estimated maximum thickness of about 400 m (Williams 1992). In general, the succession coarsens upwards, but locally there is a coarse basal facies. Load casts, graded bedding, symmetrical, asymmetrical ripples and climbing-ripples, trough and planar cross-bedding and small-scale scalloped cross-bedding structures, are abundant.

Vesicular and amygdaloidal fine-grained basalt occurs near the contact of the Watch Point and Coondra Formations, probably occurring as a series of small intrusive bodies (Williams 1992). In places the sandstone overlying the basalt is baked and has columnar jointing. This, together with the vesicularity, indicates that these bodies were emplaced at a shallow depth early in the history of the basin.

COONDRA FORMATION

The Coondra Formation (Williams & Tyler 1991; Williams 1992) is a medium to coarse-grained sandstone; pebbly to boulder-bearing sandstone; pebble to boulder

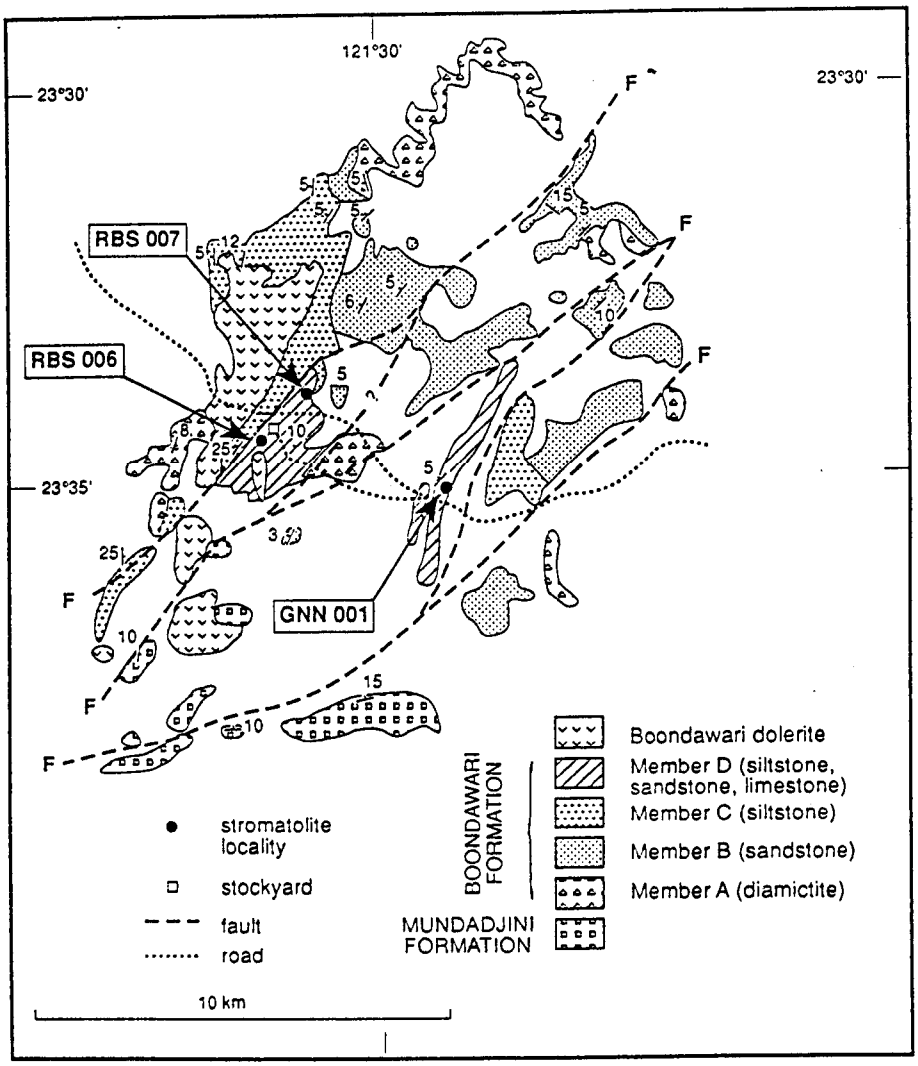

Figure 3 Map of the Boondawari Creek area. The numbers in rectangles are sample localities from which stromatolites are described herein (see Figure 1 for location).

conglomerate; and debris-flow, matrix-supported conglomerate, with a maximum estimated thickness of about 1000 m. Red to red-brown sandstone is the dominant rock, but the conglomerate component increases northwestwards towards the edge of the basin. The formation is poorly cemented and has matrix-supported quartz pebbles and boulders up to 50 cm wide. The pebbles are rounded and the boulders are sub-angular; both are concentrated in channel fills. Trough cross-beds and current striae are abundant in sandstone units interbedded with the conglomerate. Large cross-bed sets (up to 5 m) are dominant in the upper sandstone units. The basal conglomerates are poorly sorted, unstratified, and contain boulders up to 2.8 m in diameter. Thin-bedded conglomerates higher in the succession are better sorted and occupy channels in the sandstone. In the west, clasts of a greater range of compositions are present, and some are recognizable as having been sourced from the Bangemall Group.

This unit has been interpreted by Williams (1992) as the deposits of high-energy fluvial, deltaic to shallow-marine environments. The coarse-grained deposits may be best interpreted as fanglomerates. A probable fan lies northeast of Coondra Springs, where thick (up to 20 m) unstratified conglomerate beds are in faulted contact with the Bangemall Group. Current direction in this area is from the north. Overall current directions for the Coondra Formation are from the west and southwest.

Broadly equivalent units in other parts of the basin are the Glass Spring, Brassey Range, Jilyili and Spearhole Formations, all dominantly sandstone (Williams 1992).

MUNDADJINI FORMATION

The Mundadjini Formation (Williams & Tyler 1991; Williams 1992) occurs in the central part of the Savory Basin. It lies with angular unconformity on the Cornelia Formation of the Bangemall Basin, and elsewhere disconformably overlies the Coondra and Spearhole Formations of the Savory Group. It is overlain with apparent unconformity by the diamictites of the Boondawari Formation (Williams & Tyler 1991). In the northern and western parts of the basin it is successively overlain by units higher in the Savory Group, such as the Tchukardine and Woora Woora Formations, and in the central part of the basin is in faulted contact with the McFadden Formation. It has an estimated maximum

thickness of more than 1800 m and consists of a wide variety of rock types. Medium bedded, medium grained, well sorted, very clayey, light grey-brown sandstone, with abundant asymmetrical ripple marks is common. The basal part of the formation is better sorted, thinner bedded, and has an abundance of ripple marks. The proportion of shale, siltstone and dolomite increases upwards. Trough and planar cross-beds are abundant in the thicker sandstone units. In places these form cosets up to 6 m thick. Interbedded with the ripple-marked sandstone are beds containing hopper-structured halite casts and probable gypsum moulds. Halite pseudomorphs are up to 2.5 cm in diameter, and at least four former halite-bearing horizons have been recognized (Williams 1992). Gypsum casts have been found at two localities, but evaporite beds have not been found in outcrop. Carbonates, some with poorly preserved stromatolites, are also present. Patches of calcrete outside the main drainage basins possibly overlie Mundadjini carbonates. The Mundadjini Formation has a widespread distribution throughout the Savory Basin. It is interpreted as a near-shore, shallow-marine to tidal-flat and lagoonal succession.

SKATES HILLS FORMATION

On the eastern side of the Savory Basin the Skates Hills Formation (Brakel & Leech 1980) forms the base of the Savory Group. The formation consists of a patchily deposited basal conglomerate overlain by sandstone, siltstone, shale and dolomite. The formation is restricted to the northern margin of the Oldham Inlier, where it unconformably overlies steeply dipping shale and sandstone of the Cornelia Formation of the Bangemall Group (Williams 1990, 1992). Grey (1978, 1985) recorded the stromatolite *Acaciella* cf. *australica* (Howchin 1914) Walter 1972 from dolomite beds in the Skates Hills Formation. Further work by one of the authors (KG) has now confirmed the presence of *A. australica*, together with a second stromatolite, *Basisphaera irregularis* Walter 1972. Both *A. australica* and *B. irregularis* occur in the Bitter Springs Formation of the Amadeus Basin, and in other central Australian stratigraphic units underlying the Sturtian glacial successions.

Williams (1992) suggested that the Mundadjini Formation on the western side of the Savory Basin may be equivalent in part to the Skates Hills Formation, on the basis of stratigraphic position and the presence of carbonates and evaporite-bearing rocks.

Supersequence 3

BOONDAWARI FORMATION

The contact between the Mundadjini Formation and the overlying Boondawari Formation is not exposed, but the map relationships show the Mundadjini Formation in

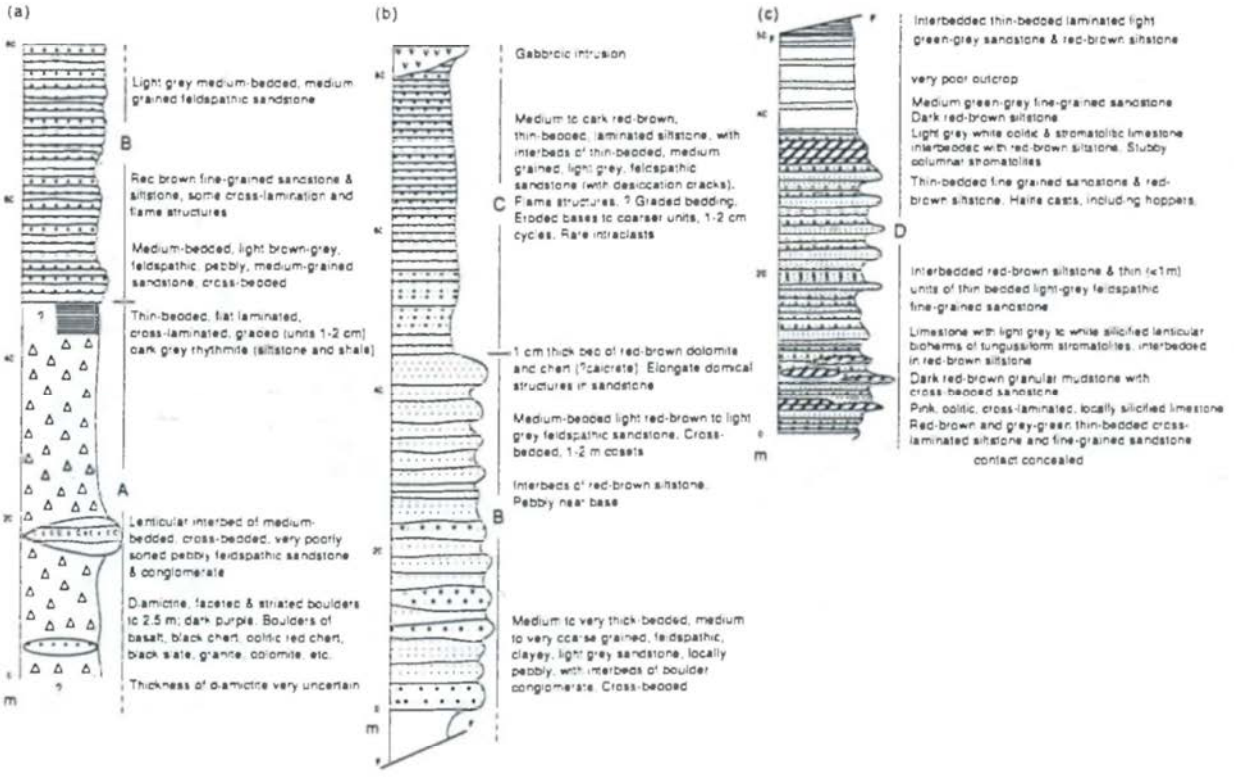

Figure 4 Stratigraphic sections of the Boondawari Formation in the Boondawari Creek area. (a) From near the stockyard to near locality RBS 007 (Figure 3). (b) From the area around 4 km north-northeast of the stockyard. (c) From the area around 6 km north-northeast of the stockyard, with observations 3 km southwest of the stockyard. Letter symbols beside columns refer to informal members described in the text.

close juxtaposition with the Boondawari Formation in many localities. The formation consists of diamictite, conglomerate, sandstone, siltstone and dolomite (Williams 1987, 1992). The main exposures lie in the headwaters of Boondawari Creek beneath laterite-capped erosion scarps. The total thickness of the formation in this area is about 200 m. The top of the section has been faulted out and intruded by coarse-grained dolerite (this is much coarser-grained than the basalt in the Watch Point Formation). This area has been partially re-mapped (Figure 3) in an attempt to clarify the internal stratigraphy of the Boondawari Formation (Figure 4). However, because of poor outcrop and the presence of numerous faults, many uncertainties remain. In particular, the nature of the contacts of the various rock types included in the Boondawari Formation are mostly obscure.

Three sections through the formation are shown in Figure 4; these have been compiled from observations in a number of areas. The upper part of the section can be characterized confidently because of fair exposure, although the thickness is uncertain because variable dips below 5° did not allow accurate measurement in the time available. In contrast, the lower part of the formation is known only from scattered outcrops; thicknesses have been estimated from the map, and by eye in the field, and the relationships between units have not been established. Four informal members, a–d, have been recognized from the base to the top of the formation.

Member 'a' is diamictite; dark grey to purple mudstone contains numerous randomly spaced, striated, faceted and polished pebbles, cobbles and boulders up to 3.5 m. A variety of sedimentary, volcanic, metamorphic and igneous clasts (including basalt, black slate, black chert, red chert, granite, gneiss and dolomite), indicates a distant, mixed provenance (detailed descriptions of the clasts are given in Williams 1992). There are lenticular interbeds of feldspathic sandstone and very poorly sorted conglomerate, up to 5 m thick. The maximum thickness of the diamictite is very uncertain, but may be about 40 m. At a locality 2 km west-southwest of the stockyard (Figure 3) the diamictite is overlain by 5 m of rhythmite; this is thin bedded, flat and cross laminated, graded shale and siltstone. Cyclic units range from 2–20 mm thick. There are some coarser interbeds up to 50 mm thick, with cross lamination and flame structures. The heterogeneous distribution of clasts within the diamictite and wide variety of clast compositions has led to the conclusion that the diamictite is a glaciogene marine deposit into which clasts have been dumped from melting icebergs (Williams 1987). However, the presence of sandstone and conglomerate interbeds may be more consistent with deposition at the margin of a retreating terrestrial glacier or ice sheet.

Map relationships and lithological similarities suggest that the diamictite intergrades laterally with the pebbly feldspathic sandstone and conglomerate of member 'b'. In addition, both this unit and the diamictite are overlain by feldspathic sandstone which is pebbly towards its base and which has interbeds of red-brown siltstone (also included in member 'b'). The maximum thickness of the two sandstones is about 50 m. Cross-bedding in the sandstones suggests that the dominant current was from the south and southeast. These can be interpreted as outwash sands associated with the waning glaciation.

The sandstone is overlain by 30–40 m of red-brown siltstone with interbeds of sandstone (member 'c'). Member 'd' is the youngest unit exposed and is about 50 m of thin bedded siltstone and sandstone, with thin interbeds of oolitic and stromatolitic limestone (Figure 4). Halite casts occur in the sandstone, and there are vertical cylindrical sandstone structures several millimetres in diameter which may be fluid escape structures. The lowermost siltstone and sandstone are considered to be the upper part of the siltstone unit described above. Low in member 'd' there are thick lenticular bioherms of tungussiform (markedly divergently branching) columnar stromatolites here described as *Eleonora boondawarica* new form (Figure 5a, b; these and other stromatolites are described in the appendix). Towards the top of this section there are several 5–20 cm thick beds of limestone interbedded with siltstone. There are low domical and small, erect columnar stromatolites, here referred to as Stromatolite form 1 (Figure 5c, d), and beds of ooids and pisoliths.

Five kilometres east of the stockyard there are very poor outcrops of limestone in and near Boondawari Creek. These outcrops are isolated and probably fault-bounded, and seem also to contain units repeated by faulting. Nonetheless, a number of lithological comparisons point to correlation with member 'd'. Outcrop is limited to beds of light grey and pink limestone and sandy limestone, but there is float of red-brown siltstone. There are beds of cross-laminated and cross-bedded coarse intraclast grainstone and ooid grainstone up to 3 m thick. Some contain chert nodules. Pisolitic limestone occurs in the float. Stromatolites occur as stratiform and low domical biostromes, here assigned to *Acaciella savoryensis* new form (Figure 5e, f). There are also beds of fissile silty pink dolomite with stratiform stromatolites which produce wrinkled bedding surfaces.

Seven samples from member 'd' were analysed for their carbon isotopic composition, and show marked enrichment in ^{13}C ($\delta^{13}C_{PDB}$ +6.8 to +8.0‰). That these values are close to primary compositions is indicated by their narrow range, and by good textural preservation of ooids and stromatolitic fabric in thin section. Late diagenetic cement was avoided in selecting material for analysis, and in most of the ooid grainstones cement is volumetrically insignificant due to strong compaction and consequent lack of interstitial space. Oxygen isotopic compositions of the five dolomites analysed are consonant with little diagenetic alteration ($\delta^{18}O_{PDB}$ −2.0 to −4.7‰). The two limestone samples have more depleted oxygen ($\delta^{18}O$ −11.9, −12.7‰) but $\delta^{13}C$ values nonetheless lie within the range quoted above.

The Mundadjini and Boondawari Formations are intruded by a stock of coarse-grained dolerite in the headwaters of Boondawari Creek. This has yielded a preliminary Rb/Sr isochron date of about 640 Ma (Williams, 1992), the details of which have not yet been published. The dolerite could be related to the widespread basalts of the Table Hill Volcanics of latest Proterozoic age (563 ± 40 Ma) in the adjacent Officer Basin; none of these units have well-established ages.

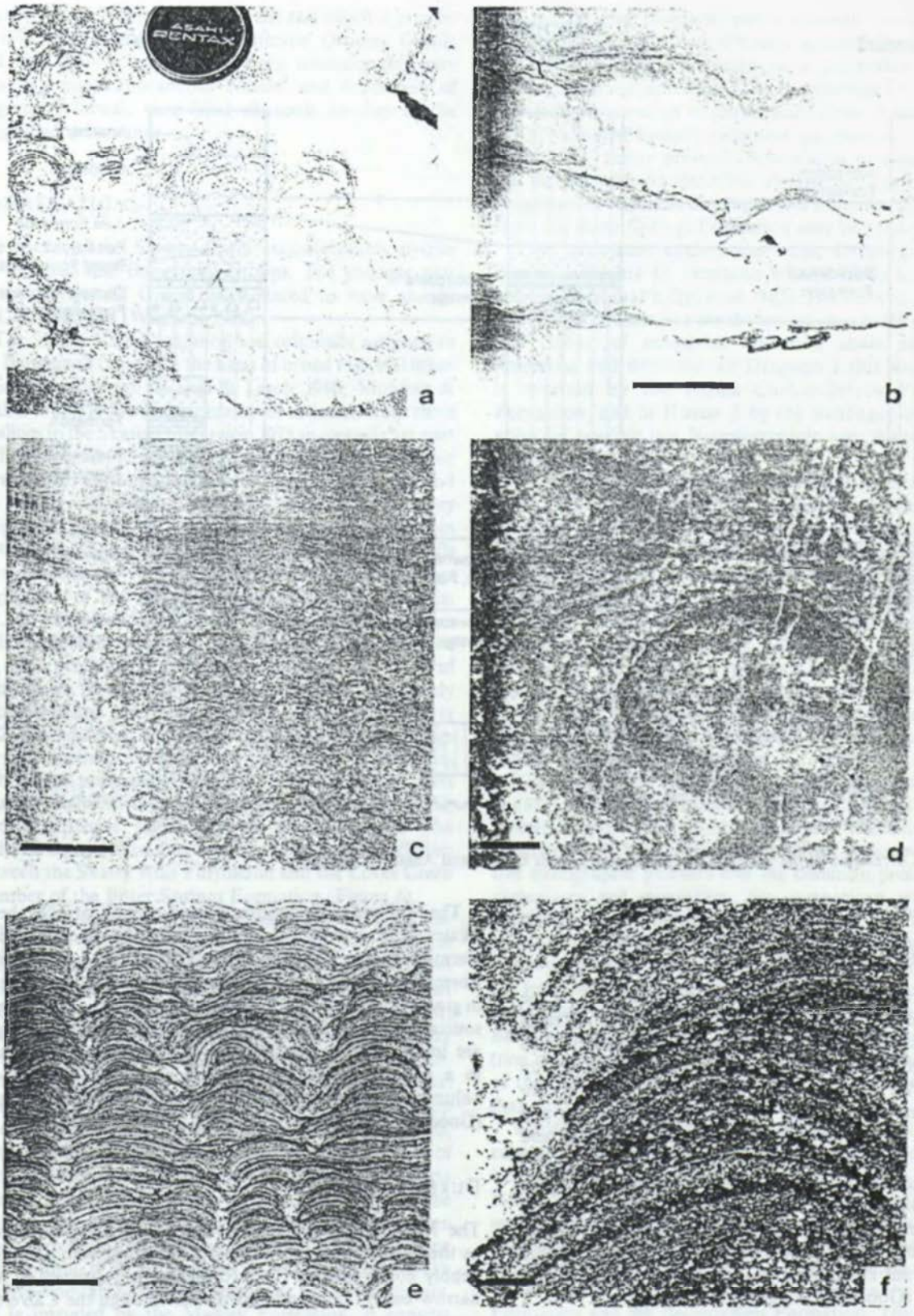

Figure 5 Stromatolites from the Boondawari Formation. (a, b) *Elcania boondawarica* from locality RBS 007: (a) field photograph showing plan view of radiating columns (after Williams 1992, figure 58); (b) thin section of sample GSWA F49028 showing columns in growth position. (c, d) Stromatolite form 1, thin section of poorly preserved stromatolite GSWA F47292 from locality RBS 006; (c) pseudocolumns showing rounded laminae and poorly preserved tussocks; (d) detail of microstructure showing alternating filmy dark laminae bounding thicker lensoid light laminae with faint traces of radiating filaments. (e, f) *Acaciella australica*, thin section of GSWA F49036, from locality GNN 001, (e) alternating columns and pseudocolumns, and laminae with a low degree of inheritance; (f) detail of microstructure. Bar scale in (b), (c) and (e), 1 cm; in (d) and (f), 1 mm.

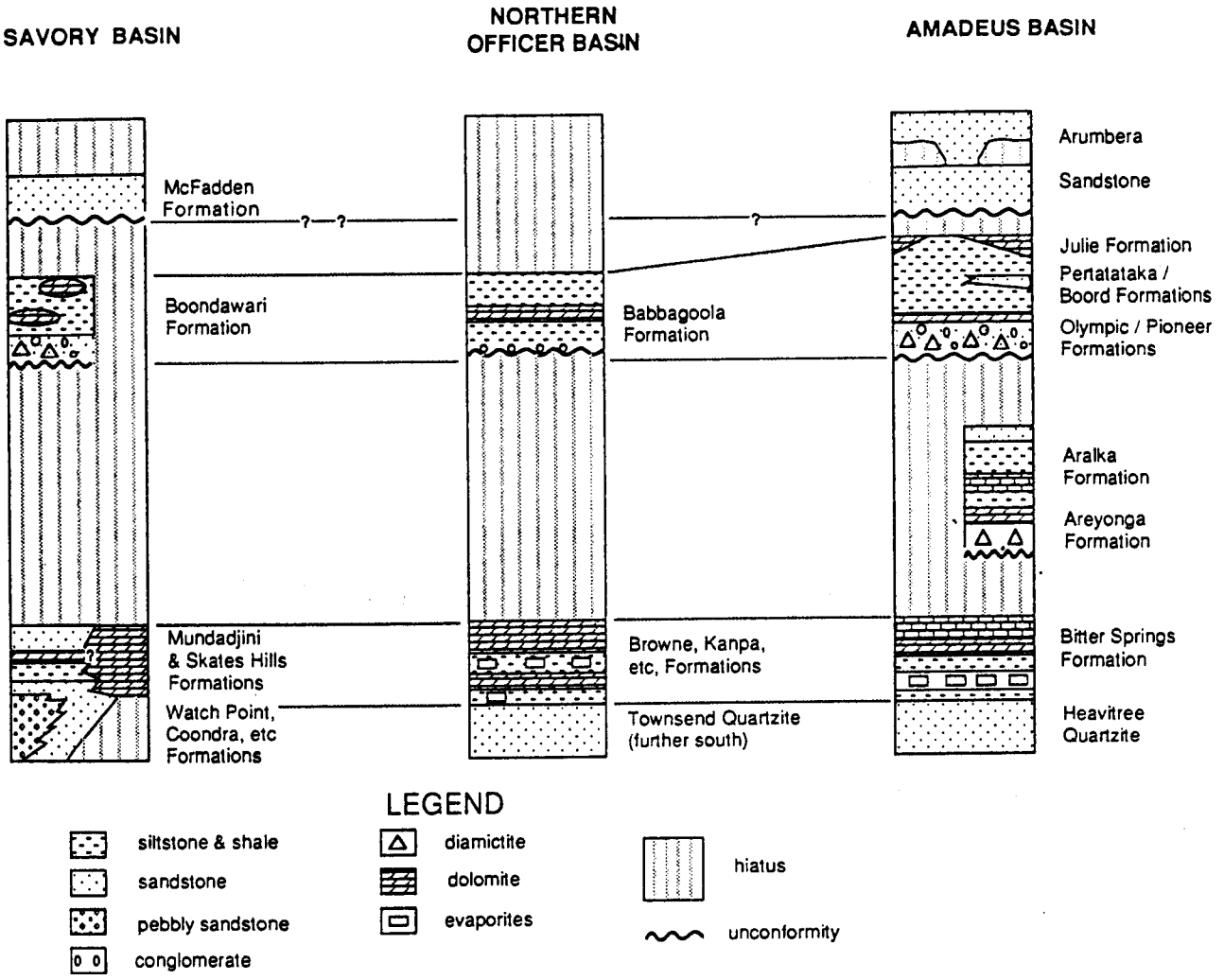

Figure 6 Correlation of the Savory Group with units in the Officer and Amadeus Basins.

Supersequence 4

McFADDEN FORMATION

The eastern half of the Savory Basin is occupied by the widespread McFadden Formation (Williams & Williams 1980) which rests disconformably on the Skates Hills Formation and unconformably on the Yeneena Group and Karara Formation. The McFadden Formation consists of laminated, flaggy to massive quartz wacke and sandstone with subordinate conglomerate, siltstone and shale. The rocks are not as well sorted as the sandstones of the Mundadjini and Coondra Formations, but like these formations they contain many trough cross-bed sets up to 10 m thick. The McFadden Formation has an argillaceous matrix, of possible volcanic origin, together with a small component of crystal tuff in the Durba Hills area (Goode & Hall 1981).

The McFadden Formation disconformably overlies the Skates Hills Formation in the south, the Boondawari Formation in the west and northwest and the Mundadjini Formation in the north. Current direction and increase in grain size point to the Paterson Orogen as the probable source of the sediments (Williams 1992). The cross-beds are interpreted as representing very large-scale foresets in a prograding succession such as a high-sediment-volume delta front advancing into a shallow-marine basin (Goode & Hall 1981).

DURBA SANDSTONE

The McFadden Formation is unconformably overlain by the Durba Sandstone, a quartz sandstone with a basal pebbly conglomerate. This formation is restricted to a narrow basin that trends northwest through the Calvert

Range, Durba Hills and Diebil Hills, and which is parallel to fold axes in the adjacent Paterson Orogen. Goode and Hall (1981) considered that the unconformity may represent contemporaneous erosion and deposition of migrating, fluvial, sand-filled channels on top of the prograded delta sands.

CORRELATIONS

The rocks of the Savory Basin unconformably overlie the Yeneena and Bangemall Groups. The younger part of the Bangemall Group is estimated to have an age of 1200–1400 Ma (Williams 1992).

The Skates Hills Formation was originally assigned to the Bangemall Group on the basis of broad regional lithological correlations (Brakel & Leech 1980; Muhling & Brakel 1985). However, stromatolites collected from three localities in the Skates Hills area in 1975 suggested that part of the succession might be younger than Mesoproterozoic (Grey 1978), although the material was fragmentary and the taxa could not be identified with certainty. Grey assigned the specimens to *Acaciella* cf. *australica* (Howchin 1914) Walter 1972, pointing out their similarity to *Acaciella australica* from the Neoproterozoic Bitter Springs Formation of the Amadeus Basin of central Australia.

Later extensive studies of stromatolites from the Skates Hills Formation by one of the authors (KG) confirmed the presence, not only of *A. australica*, but also of *Basisphaera irregularis* Walter 1972, both previously recorded from the Bitter Springs Formation (Walter 1972). In addition, the Skates Hills and Bitter Springs Formations have many lithological features in common, such as the presence of stromatolite bioherms as parts of upward shallowing thin units (Southgate 1989, 1991), ooid grainstones and evaporite pseudomorphs. The evidence compiled to date strongly suggests a correlation between the Skates Hills Formation and the Loves Creek Member of the Bitter Springs Formation (Figure 6).

The northernmost Officer Basin lies between the Savory and Amadeus Basins (Figure 1). The presence of a succession of stromatolitic carbonates and evaporites at depth in that region is revealed in a number of diapirs that reached the surface (Jackson & van de Graaff 1981; Iasky 1991; and earlier references therein). The Madley Formation comprises the evaporitic cores of the diapirs. It consists of gypsum, dolomite, anhydrite and halite. Blocks of dolomite and sandstone, which may be up to several tens of metres across and intensely brecciated, occur in the gypsum. The sandstone blocks consist of silicified, medium to coarse-grained, poorly sorted quartz arenite. Microfossils similar to those known from the Loves Creek Member of the Bitter Springs Formation are known from the Madley Formation (M. R. Walter, pers. comm. 1978, in Jackson & van de Graaff 1981). The Woolnough Formation forms the rim of the diapirs, and is intruded by the Madley Formation. It consists predominantly of a siliciclastic lower part with interbedded siltstone, dolomite and minor limestone, and an upper part of dolomite, silicified dolomite and minor limestone, in part oolitic. The carbonates occur as discrete lenticular bodies that grade laterally into siltstone, and are mainly grey to black, partly silicified, fine-grained limestone. The siltstone contains pseudomorphs after gypsum and halite. The sandstone is well-sorted, fine to medium-grained, and lithic. The Woolnough Formation contains stromatolites which require further study. Preiss (1976) identified a poorly preserved specimen as *Acaciella* form indet. Better preserved material is now available but has not yet been identified. Preliminary examination suggests that *Acaciella australica* and other forms known from the Bitter Springs Formation may be present.

Two petroleum exploration wells, Dragoon 1 and Hussar 1 (Figure 1), penetrate what is likely to be the same succession (Phillips *et al.* 1985). The Browne, Hussar and Kanpa Formations are the lowest units in these wells, and consist of anhydrite, claystone, shale, siltstone, sandstone and dolomite. In Dragoon 1 this succession is overlain by the Permo–Carboniferous Paterson Formation, and in Hussar 1 by the Babbagoola Formation (of possible late Neoproterozoic age: Walter *et al.* in press).

The Browne Formation in Yowalga 3 further to the south (Townson 1985) can be correlated with the Bitter Springs Formation based on lithology and the occurrence of the stromatolite *Acaciella australica* at a depth of 2390 m (Grey 1981). The stromatolite was originally identified as *A.* cf. *australica*, because it was only a fragmentary specimen. Further study of the range of variation in *A. australica*, particularly in the Skates Hills Formation, now allows the Yowalga 3 specimen to be unequivocally assigned to *A. australica*, supporting correlation with the Loves Creek Member of the Bitter Springs Formation. The underlying 1800 m is probably partially equivalent to the evaporitic Gillen Member.

The Mundadjini Formation is poorly exposed and it is difficult to determine its composition. Its relationship to the Skates Hill Formation is uncertain. Williams (1992) suggested that they could be correlatives, because of relative stratigraphic position and the common presence of carbonates and evaporites. By comparison with the Amadeus Basin, correlation with the lower (Gillen) member of the Bitter Springs Formation can be suggested.

It would follow from these correlations (Figure 6) that the basal sandstone units in the Savory Basin are likely to correlate with the Heavitree Quartzite of the Amadeus Basin and the Townsend Quartzite of the Officer Basin (one of the authors, IRW, considers that the sandstones of the Savory Basin probably have a greater age range than those of the adjacent basins).

The discovery of glaciogene rocks in the Savory Group suggested correlation with known glaciogene rocks of Neoproterozoic age in the nearby Officer Basin: the Turkey Hill beds at Miller Soak (Jackson & van de Graaff 1981), and the Lupton beds at Lupton Hills (Lowry *et al.* 1972); and possibly the Boord Formation at Boord Ridges (Wells *et al.* 1964) at the western edge of the Amadeus Basin.

There are a number of similarities between the Boord Formation and the Boondawari Formation. The Boord Formation seems from its lithology and stratigraphic position most likely to be a correlative of the Pioneer/Olympic/Pertatataka/Julie sequence of the eastern part of the Amadeus Basin. The intergrading sandstone–diamictite of the Boondawari Formation is very similar

to the intergrading Pioneer Sandstone–Olympic Formation, and the overlying siltstone closely resembles the Pertatataka Formation and its correlative the Winnall beds. The stromatolitic and oolitic carbonates in member 'd' of the Boondawari Formation are broadly comparable with those of the Julie Formation (which grades down into the Pertatataka Formation).

Support for this set of correlations comes from carbon isotope chemostratigraphy. Member 'd' has markedly enriched carbon isotopic compositions ($\delta^{13}C_{PDB}$ +6.8 to +8.0‰). In the Amadeus Basin, least-altered carbonates in the Julie Formation have $\delta^{13}C$ ranging from +4.0 to +6.0‰. These values are a maximum for the latest Proterozoic in the Amadeus Basin (including the Aralka, Pioneer, Olympic, Pertatataka and Julie Formations; Walter *et al.* in press). In the Officer Basin, a thick Proterozoic sequence probably younger than the Julie Formation, the upper Rodda Beds, contains carbonate carbon distinctly lighter isotopically than the Julie Formation (Jenkins *et al.* 1992; Walter *et al.* in press). Although slightly less enriched than member 'd', the Julie Formation therefore appears the most likely correlative in terms of isotopic composition as well as lithostratigraphy.

Lower in the succession, a thin bed of red, micritic dolomite overlying feldspathic sandstone and underlying red siltstone (Figure 4) is a possible lithostratigraphic correlative of the 'cap dolomite' that overlies Marinoan glacigene rocks and their correlatives in the Amadeus and other Neoproterozoic basins (Preiss *et al.* 1978; Preiss & Forbes 1981). An isotopic analysis of this rock ($\delta^{13}C$ −2.9‰, $\delta^{18}O$ −4.7‰) supports such a correlation, as the cap dolomites of the Amadeus Basin and Adelaide Geosyncline show similarly depleted carbon values (−3.5 to −2.0‰, Walter *et al.* in press; see also Williams 1979).

The age of the upper sandstones can only be speculated upon. The McFadden Formation seems to have its provenance in the Paterson Orogen. The southeastern extension of this orogen is the Musgrave-Mann Block, where compression followed by uplift at about 540 Ma (Maboko *et al.* 1989) led to the formation of large amounts of conglomerate (Mt Currie Conglomerate) and sandstone (Arumbera Sandstone). Myers (1990) considers that tectonic events in the Paterson Orogen may be contemporaneous with those in the Musgrave-Mann Block, and thus it is possible that the McFadden Formation is a product of this tectonism and thus a correlative of the Arumbera Sandstone. The presence of tuff in the McFadden Formation may broadly support this because it would be consistent with correlation with the Table Hill Volcanics of the Officer Basin, which can be related to the same tectonic event and have been dated by the Rb/Sr whole rock isochron method at 563 ± 40 Ma (recalculated from Compston 1974). There are few constraints on the age of the unconformably overlying Durba Sandstone, except that Goode and Hall (1981) interpreted their field observations to suggest that the two formations are parts of the one prograding delta system.

CONCLUSIONS

Two firmly established correlations now clarify the age and relationships of the Savory Group (Figure 6). First, the Skates Hills Formation contains distinctive stromatolites previously recorded from the Bitter Springs Formation of the Amadeus Basin. In addition, the Skates Hills and Bitter Springs Formations have many lithological features in common. This correlation is strengthened by comparison with surface and subsurface units in the northern Officer Basin. The Mundadjini Formation is poorly exposed and it is difficult to determine details of its lithology. By comparison with the Amadeus Basin, correlation with the lower (Gillen) member of the Bitter Springs Formation can be suggested. It would follow from these correlations that the basal sandstone units in the Savory Basin are likely to correlate with the Heavitree Quartzite of the Amadeus Basin and the Townsend Sandstone of the Officer Basin.

Second, the intergrading sandstone–diamictite of the Boondawari Formation is very similar to the intergrading Pioneer Sandstone–Olympic Formation of the Amadeus Basin, and the overlying siltstone closely resembles the Pertatataka Formation and its correlative the Winnall beds. The stromatolitic and oolitic carbonates at the top of Boondawari Formation are broadly comparable with those of the Julie Formation (which grades down into the Pertatataka Formation). Support for this set of correlations comes from carbon isotope chemostratigraphy.

The age of the upper sandstones can only be speculated upon. The McFadden Formation seems to have its provenance in the Paterson Orogen. The southeastern extension of this orogen is the Musgrave-Mann Block, where compression followed by uplift at about 540 Ma led to the formation of large amounts of conglomerate (Mt Currie Conglomerate) and sandstone (Arumbera Sandstone). Tectonic events in the Paterson Orogen are likely to be contemporaneous with those in the Musgrave-Mann Block, and thus it is possible that the McFadden Formation is a product of this tectonism and a correlative of the Arumbera Sandstone.

ACKNOWLEDGEMENTS

The Director of the Geological Survey of Western Australia is thanked for providing a vehicle and equipment to enable MRW and KG to accompany IRW in the field. John Veevers, Peter Southgate and Wolfgang Preiss are thanked for commenting on the manuscript. Ian Percival is responsible for much of the drafting. KG and IRW publish with the permission of the Director of the Geological Survey of Western Australia. This is a contribution to IGCP 261 and 320, and to the Ediacarian history project supported by an ARC grant to John Veevers and Malcolm Walter.

REFERENCES

BERTRAND-SARFATI J. 1976. An attempt to classify Late Precambrian stromatolite microstructures. *In* Walter M.R. ed. *Stromatolites, Developments in Sedimentology*, Vol. 20, pp. 251–259. Elsevier, Amsterdam.

BERTRAND-SARFATI J. & CABY R. 1976. Carbonates et stromatolites du sommet du Groupe d'Eleonore-Bay (Precambrien

terminal) au Canning Land (Groenland oriental). *Gronlands Geologiske Undersogelse, Bulletin* **119**.

BRAKEL A. T. & LEECH R. E. J. 1980. Trainor, WA: *Western Australia Geological Survey. 1:250 000 Geological Series Explanatory Notes.*

COMPSTON W. 1974. The Table Hill Volcanics of the Officer Basin: Precambrian or Palaeozoic? *Journal of the Geological Society of Australia* **21**, 403–411.

GOODE A. D. T. & HALL W. D. M. 1981. The Middle Proterozoic eastern Bangemall basin, Western Australia. *Precambrian Research*, **16**, 11–29.

GREY K. 1978. *Acaciella* cf. *australica* from the Skates Hills Formation, eastern Bangemall Basin, Western Australia. *Western Australia Geological Survey Annual Report* **1977**, 71–73.

GREY K. 1981. *Acaciella* cf. *australica* and organic-walled microfossils from the Proterozoic Browne beds, Shell Yowalga 3, Officer Basin. *Western Australia Geological Survey, Palaeontology Report* **44/1981** (unpubl.).

GREY K. 1985. Stromatolites and other organic remains in the Bangemall Basin. *In* Muhling P. C. and Brakel A. T. eds. Geology of the Bangemall Group: The evolution of an intracratonic basin. *Western Australia Geological Survey, Bulletin* **128**, 221–256.

HOFMANN H. J. 1978. New stromatolites from the Aphebian Mistassini Group, Quebec. *Canadian Journal of Earth Sciences*, **15**, 571–585.

IASKY R. P. 1990. Officer Basin. *In* Geology and Mineral Resources of Western Australia. *Western Australia Geological Survey, Memoir* **3**, 362–380.

JACKSON M. J. & VAN DE GRAAFF W. J. E. 1981. Geology of the Officer Basin, Western Australia. *Bureau of Mineral Resources, Australia, Bulletin* **206**.

JENKINS R. J. F., MCKIRDY D. M., FOSTER C. B., O'LEARY T. & PELL S. D. 1992. The record and stratigraphic implications of organic-walled microfossils form the Ediacaran (terminal Proterozoic) of South Australia. *Geological Magazine*, **129**, 401–410.

LOWRY D. C., JACKSON M. J., VAN DE GRAAFF W. J. E. & KENNEWELL P. J. 1972. Preliminary results of geological mapping in the Officer Basin, Western Australia, 1971. *Western Australia Geological Survey, Annual Report* **1971**, 50–56.

MABOKO M. A. H., MCDOUGALL I., ZEITLER P. K. & WILLIAMS I. S. 1992. Geochronological evidence for the ~530–550 Ma juxtaposition of two Proterozoic metamorphic terranes in the Musgrave Ranges, Central Australia. *Australian Journal of Earth Sciences* **39**, 457–571.

MUHLING P. C. & BRAKEL A. T. 1985. Geology of the Bangemall Group: The evolution of an intracratonic Proterozoic Basin. *Western Australia Geological Survey, Bulletin* **128**.

MYERS J. S. 1990. Precambrian tectonic evolution of part of Gondwana, southwestern Australia, *Geology*, **18**, 537–540

PHILLIPS B. J., JAMES A. W. & PHILIP G. M. 1985. The geology and hydrocarbon potential of the north-western Officer Basin. *The APEA Journal* **25(1)**, 52–61.

PREISS W. V. 1972. The systematics of South Australian Precambrian and Cambrian stromatolites, Part 1. *Transactions of the Royal Society of South Australia* **96**, 67–100.

PREISS W. V. 1976. Proterozoic stromatolites from the Nabberu and Officer Basins, Western Australia, and their stratigraphic significance. *South Australia Geological Survey, Report Investigations* **47**.

PREISS W. V. & FORBES B. G. 1981. Stratigraphy, correlation and sedimentary history of Adelaidean (late Proterozoic) basins in Australia. *Precambrian Research* **15**, 255–304.

PREISS W. V., WALTER M. R., COATS R. P. & WELLS A. T. 1978. Lithological correlations of Adelaidean glaciogenic rocks in parts of the Amadeus, Ngalia, and Georgina Basins. *BMR Journal of Australian Geology & Geophysics* **3**, 45–53.

SOUTHGATE P. N. 1989. Relationship between cyclicity and stromatolite form in the Late Proterozoic Bitter Springs Formation, Australia. *Sedimentology* **36**, 323–339.

SOUTHGATE P. N. 1991. A sedimentological model for the Loves Creek Member of the Bitter Springs Formation, northern Amadeus Basin. *In* Korsch R. J. and Kennard J. M. eds. Geological and geophysical studies in the Amadeus Basin, central Australia. *Bureau of Mineral Resources, Bulletin* **236**, 113–126.

TOWNSON W. G. 1985. The subsurface geology of the western Officer Basin: Results of Shell's 1980–1984 petroleum exploration campaign. *The APEA Journal* **25(1)**, 34–51.

WALTER M. R. 1972. Stromatolites and the biostratigraphy of the Australian Precambrian and Cambrian. *Special Papers in Palaeontology* **11**, Palaeontological Association of London, London.

WALTER M. R., VEEVERS J. J., CALVER C. R. & GREY K. Neoproterozoic Stratigraphy of the Centralian Superbasin, Australia. *Precambrian Research* (in press).

WELLS A. T., FORMAN D. J. & RANFORD L. C. 1964. Geological reconnaissance of the Rawlinson and MacDonald 1:250 000 sheet areas, Western Australia. *Bureau of Mineral Resources Report* **65**.

WILLIAMS G. E. 1979. Sedimentology, stable-isotope geochemistry and palaeoenvironment of dolostones capping late Precambrian glacial sequences in Australia. *Journal of the Geological Society of Australia* **26**, 377–386.

WILLIAMS I. R. 1987. Geological Note. Late Proterozoic glaciogene deposits in the Little Sandy Desert, Western Australia. *Australian Journal of Earth Sciences* **34**, 153–155.

WILLIAMS I. R. 1990. Savory Basin. *In* Geology and Mineral Resources of Western Australia. *Western Australia Geological Survey Memoir* **3**, 329–335.

WILLIAMS I. R. 1992. Geology of the Savory Basin, Western Australia. *Western Australia Geological Survey, Bulletin* **141**.

WILLIAMS I. R., BRAKEL A. T., CHIN R. J. & WILLIAMS S. J. 1976. The stratigraphy of the eastern Bangemall Basin and the Paterson Province. *Western Australia Geological Survey, Annual Report* **1975**, 79–82.

WILLIAMS I. R. & TYLER I. M. 1991. Robertson, WA 2nd edn. *Western Australia Geological Survey, 1:250 000 Geological Series Explanatory Notes.*

WILLIAMS I. R. & WILLIAMS S. J. 1980. Gunanya, WA. *Western Australia Geological Survey, 1:250 000 Geological Series Explanatory Notes.*

(Received 20 July 1993; accepted 28 March 1994)

APPENDIX: STROMATOLITE DESCRIPTIONS
(by K. Grey and M. R. Walter)

At least three forms of stromatolite are present in the Boondawari Formation, but only two are sufficiently well-preserved to allow formal description.

Group *Eleonora* Bertrand-Sarfati and Caby 1976

Type form *Eleonora ramosa* Bertrand Sarfati and Caby 1976.

Diagnosis 'Columns flaring outwards, vertical or oblique, with branching in very small lateral outgrowths and often different from the central columns. The microstructure displays a carpet of dark fibres. Supergroup Tungussides.' (Translated from Bertrand-Sarfati and Caby 1976).

Content *Eleonora ramosa* Bertrand-Sarfati and Caby, 1976, *Eleonora boondawarica* new form.

Age and distribution Unit 12, pre-glacial part of the Neoproterozoic of the Eleonore Bay Group, East Greenland (Bertrand-Sarfati & Caby 1976); Ediacarian, Boondawari Formation, Savory Basin, Western Australia.

Eleonora boondawarica Grey and Walter new form
(Figure 5a, b)

1992 Stromatolite, unassigned of Williams, Figure 58

Material Holotype: GSWA F49028; Paratypes: GSWA F49024, F49025, F49026, F49027, F49029, F49030, F49031, F49032 (poorly preserved). All from locality RBS 007, Lat. 23°34'S, Long. 121°29'E.

Derivation of name After Boondawari Creek, the type locality.

Description

Outcrop details Stromatolites outcrop as a series of domes in an area about 300 m long by about 50 m wide, on a gently dipping hillside. The outcrop is pink and white carbonate, partially silicified, is rubbly, and the tops of the domes are eroded. The bases of the domes are not exposed, but they overlie a pink oolitic limestone. The stromatolitic horizon has a maximum thickness of 2 m.

Mode of occurrence The stromatolites occur in tabular, possibly lensoid, stacked bioherms mostly about 1 m in diameter, occasionally up to 2 m. Commonly several bioherms are crowded together, and are separated from the next group by several metres. Areas between bioherms are pooly exposed, but probably consist of fine-grained white and pink carbonate. The nature of the contact between the bioherms and encompassing sediments could not be determined because of poor exposure.

Material is too fragmented to permit three-dimensional reconstruction, but each bioherm apparently consists of a single fascicle characterized by a distinctive growth pattern. Growth is initially as a discoidal dome about 5–10 cm in diameter, which develops into a central column. Branches initially grow as lobes around the main column, producing an erratic, petaliform pattern. They then form true branches that radiate outwards, mainly in the horizontal plane, and are characterized by lobes and globular areas. Branching is infrequent except near the base, and branches in the centre of the bioherm are short and stubby, although this may partly result from erosion of the top of the bioherm. Lateral branches are much longer and are commonly horizontal or are sometimes decumbent. Horizontal lengths may be up to 20 cm before the branches turn upwards.

Branches widen rapidly from the point of division until they are up to about 1 cm in diameter. Diameters then remain more or less uniform. Branches are closely spaced, separated by only about 2 mm, and are commonly subparallel. Short lateral lobes, often with tapering ends, develop on the undersurface of branches.

Column shape Columns are subcylindrical in their upper parts, and are slightly constringed. In plan view the upper parts of the columns are round to lobate. There is no obvious surface ornament or lateral linkage of columns.

Lamina shape Laminae are closely spaced, smooth, steeply to moderately convex and with a moderate degree of inheritance. Lateral continuity is consistent. Laminae form walls of very variable nature. Short stretches of the column margin may be naked, with laminae terminating abruptly, but this is rare. More commonly several laminae downturn at the column margin to form an inconsistent wall. In narrow sections of the columns the margins are often overgrown by a subsequent and independent set of laminae in a manner resembling overgrowths in *Mistassinia* Hofmann 1978. From the Aphebian Mistassini Group of Quebec (Hofmann 1978).

Microstructure and fabric Laminae are distinctly banded with alternating light and dark laminae. The light laminae are variable in width, tapering towards the margins in a regular manner. Dark laminae also taper slightly towards the margins, but tend to be more constant in width. Light laminae are micritic. Dark laminae are slightly coarser and have small irregular patches of clear quartz, possibly infilling fenestrae. A radial fabric, pseudomorphing needle-like crystals, cross-cuts the laminae in many sections of the column.

Interspace filling Interspaces are often crowded with faintly preserved laminae and are micritic in texture.

Secondary alteration The stromatolites have been completely replaced by very fine-grained silica.

Comparisons The form has many features in common with *Eleonora ramosa*, most notably in the development of a central column, widely divergent branches, globular areas and lateral lobes. However, *E. boondawarica* has less frequently developed lateral lobes, the lobes develop on the underside of branches, and a patchy wall is present. The spreading habit is similar to that occurring in bioherm series constructed by *Linella ukka* Krylov 1967 and *Tungussia bassa* Krylov 1967, but *E. boondawarica* is more regular in its branching habit and the columns are smoother, and the laminae are also smoother and finer.

Group *Acaciella* Walter 1972 in Preiss 1972

1972 *Acaciella* Walter in Preiss 1972, p. 72.
1972 *Acaciella* Walter, 1972, p. 115.

Type form *Acaciella australica* (Howchin 1914) Walter 1972.

Diagnosis As given by Walter in Preiss 1972.

Content *Acaciella australica* (Howchin 1914) Walter 1972; ?*A. angepena* Preiss 1972; *A. augusta* Preiss 1972; *A. emmerugga* Walter, Krylov and Muir 1988; *A. gouhouensis* Cao, Zhao and Xia 1985; *A. multia* Cao, Zhao and Xia 1985; *A. savoryensis* new form.

Remarks Both Walter (1972) and Preiss (1972) published an identical diagnosis for this group. However, the publication by Preiss (in which the diagnosis was attributed to Walter) appeared in May and therefore has priority over the publication by Walter, which appeared in December.

Age and distribution Neoproterozoic of the Amadeus, Georgina, Officer and Savory Basins; Cambrian of the Adelaide Geosyncline; Palaeoproterozoic of the McArthur Basin; all in Australia; Jinshanzhai Formation of the Neoproterozoic Huaibei Group of north Anhui Province, China.

Acaciella savoryensis Grey and Walter new form
(Figure 5e, f).

Material Holotype: F49036; Paratypes: F49034, F49035, F49036, F49037, F49038, F49039, F49040, F49041, F49043, F49044, F49045, F49046, F49047, F49048, F49049, ?F49051; from locality GNN 001, Lat. 23°35'S, Long. 121°31'E.

Derivation of name After the Savory Basin.

Description

Outcrop details Stromatolites are exposed in a reddish dolomite in the bed and banks of a small creek. Stromatolitic bands are separated by areas of non-exposure, and consequently could either consist of several stromatolitic horizons, or be repeated by faulting. Commonly they occur as flat to gently undulating biostromes about 50 cm to 1 cm high and of uncertain length, and each biostrome consists of contiguous bioherms. Isolated bioherms, up to 2 m in diameter, are also present. These are circular in plan view and are separated by interspace areas of fine-grained, white dolomite with slight mottling. The contact areas between the bioherm margins and surrounding sediment are well-defined.

The tops of the biostromes are commonly erosional, and at least one was overlain by a cross-bedded grainstone. Tops are generally elongate and ripple-like in plan view. Ripples are oriented east–west, are about 1 cm wide, and over 20 cm long. Adjacent bioherms may lack rippled tops and be more or less concentric. Bioherms are interspersed with each other in such a way that the bases of new bioherms may be level with the top of adjacent ones.

Mode of occurrence Columns arise directly from the underlying surface, usually developing on small mounds of sediment. Some bioherms have patchy areas of flat laminae and broader columns, particularly near the base. Mostly bioherms consist of superimposed layers of short columns. Some bioherms are surrounded by a continuous wall about 10 cm thick in plan view. The wall is composed only of laminae and lacks columns.

Column shape Bioherms consist mainly of closely spaced columns or pseudocolumns. Columns are generally about 1 cm wide, and consist of short alternating stretches of laterally linked and separate columns, both extending for heights of about 50 cm. Columns are more or less parallel, and closely spaced, separated by about 2 mm. Two or more columns frequently anastomose, and the overgrown areas continue as a single column or pseudocolumn. The column margins are slightly irregular, constringed and stubby.

Lamina shape Laminae are flat to gently convex and lack walls. The degree of inheritance is variable; laminae can be regularly stacked for short stretches and then become offset at a micro-unconformity. Most laminae terminate abruptly at the column margins, although bridging involving several laminae is common; infrequently some overlap of laminae occurs. Laminae are usually smooth.

Microstructure and fabric Microstructure is of the micritic mat type of Bertrand-Sarfati (1976), and consists of alternating light and dark laminae in which the light laminae are considerably thicker than the dark ones. The upper boundary between a light and dark lamina pair appears gradational while the upper boundary of the dark laminae is sharp. Both types of laminae are fine-grained, mainly micritic, although dark laminae contain coarse grains. The grains may be irregular and clear or rounded and dark brown; platy intraclasts are also present.

Interspace filling Interspaces are filled with coarse rounded clasts of clear grains. Patches or grains are

frequently overgrown by bridges. Platy clasts occur in patches in the interspaces.

Secondary alteration Stylolites parallel to the laminae are present infrequently, and small patches of dendritic manganese are abundant.

Comparisons The microstructure is typical of forms assigned to *Acaciella*, but it differs from all other described forms in the consistent development of alternating stretches of columns and pseudocolumns.

Stromatolite form 1
(Figure 5c, d)

Material F47292, F49042, F49052: All from locality RBS 006, Lat. 23°34′55″S, Long. 121°28′26″ E.

Description Three poorly preserved specimens are characterized by a distinctive microstructure and occur in small weathered bioherms (15–25 cm in diameter) protruding through rubble. Bioherms consist of small, short, stubby, closely spaced columns about 0.5 cm in diameter. Columns are subcylindrical, straight, erect, have irregular margins, lack walls, and are overgrown by pseudocolumnar and stratiform laminae. Laminae are moderately to steeply convex, smooth, with moderate to low inheritance. Microstructure is tussocky, consisting of a filmy dark lamina overlying a lensoid, thick, light lamina characterized by radiating fabric. Interspaces are infilled by ooids. The stromatolites are recrystallized and many features are difficult to determine. No immediate comparisons with published forms are possible.

Appendix 3

Walter, M.R., Veevers, J.J., Calver, C.R. & Grey, K., (1995): Neoproterozoic Stratigraphy of the Centralian Superbasin, Australia. *Precambrian Research,* 73: 173-196.

Note: This paper contains a preliminary synthesis of Ediacarian isotope stratigraphy of mainland Australian basins, now superseded by work fully described in this thesis.

ELSEVIER

Precambrian Research 73 (1995) 173–195

Precambrian Research

Neoproterozoic stratigraphy of the Centralian Superbasin, Australia

M.R. Walter*, J.J. Veevers, C.R. Calver, K. Grey

School of Earth Sciences, Macquarie University, Sydney, N.S.W. 2109, Australia

Received 23 May 1993; revised version accepted 17 January 1994

Abstract

The basement of central Australia includes the Arunta Block and the 1200–1100 Ma Musgrave Block succeeded by 1075–1000 Ma bimodal volcanic rifts and dolerite dykes. A regional hiatus at 1000–800 Ma, interpreted as reflecting a central post-volcanic (underplated) upland, was followed at 800 Ma by a second swarm of dykes in the Musgrave Block, Gawler Craton and Stuart Shelf, associated with the crustal sagging that initiated the Centralian Superbasin.

The Centralian Superbasin is defined here to encompass the Neoproterozoic fill of the Amadeus, Georgina, Ngalia, Officer and Savory Basins. The intra-cratonic superbasin was disrupted internally 540–600 Ma ago ("Petermann Ranges Orogeny") by a central uplift and associated thrusts, and by mid-Carboniferous (320 Ma) tectonism ("Alice Springs Orogeny") to form the structural basins listed above. The stratigraphy and sedimentology of the relatively well known areas can be used as a basis for predicting those of the poorly known regions. New results from acritarch biostratigraphy and isotope chemostratigraphy, in conjunction with conventional lithostratigraphy and sequence analysis, allow better stratigraphic resolution than previously possible. Field observations in the recently discovered Savory Basin in Western Australia provide a basis for correlations with the adjacent basins.

1. Introduction

In Neoproterozoic times 2 million km^2 of Australia was occupied by a single depositional system, the Centralian Superbasin (Fig. 1; Walter et al., 1992; Gorter, 1992; Walter and Gorter, 1993). A plate margin in the east (between Australia and, perhaps, North America) developed through extension culminating in Early Cambrian seafloor spreading; part of this margin is exposed in the Adelaide Geosyncline (Preiss, 1987). The intra-cratonic superbasin was disrupted internally 540–600 Ma ago ("Petermann Ranges Orogeny") by a central uplift and associated thrusts, and by mid-Carboniferous (320 Ma) tectonism ("Alice Springs Orogeny") to form numerous structural basins, including the Amadeus, Georgina, Ngalia, Officer and Savory (Fig. 1). Recognition of the integrity of the original depositional system allows the stratigraphy of relatively well known areas to be extrapolated to predict that of those that are poorly known. Acritarch biostratigraphy and isotope chemostratigraphy, in conjunction with conventional lithostratigraphy and sequence analysis, allow a new synthesis of the stratigraphy (Figs. 2, 3). This is supplemented with observations in the recently discovered Savory Basin in Western Australia (Williams, 1992; Walter et al., 1994).

* Correspondence to: M.R. Walter, Rix and Walter Pty Ltd., Brush Island Farm, Murramarang Road, Bawley Point, N.S.W. 2359, Australia. Fax: +61 44 571566; Tel.: +61 44 571565; e-mail: gc-walter@hope.ocs.mq.edu.au

SSDI 0301-9268(94)00077-8

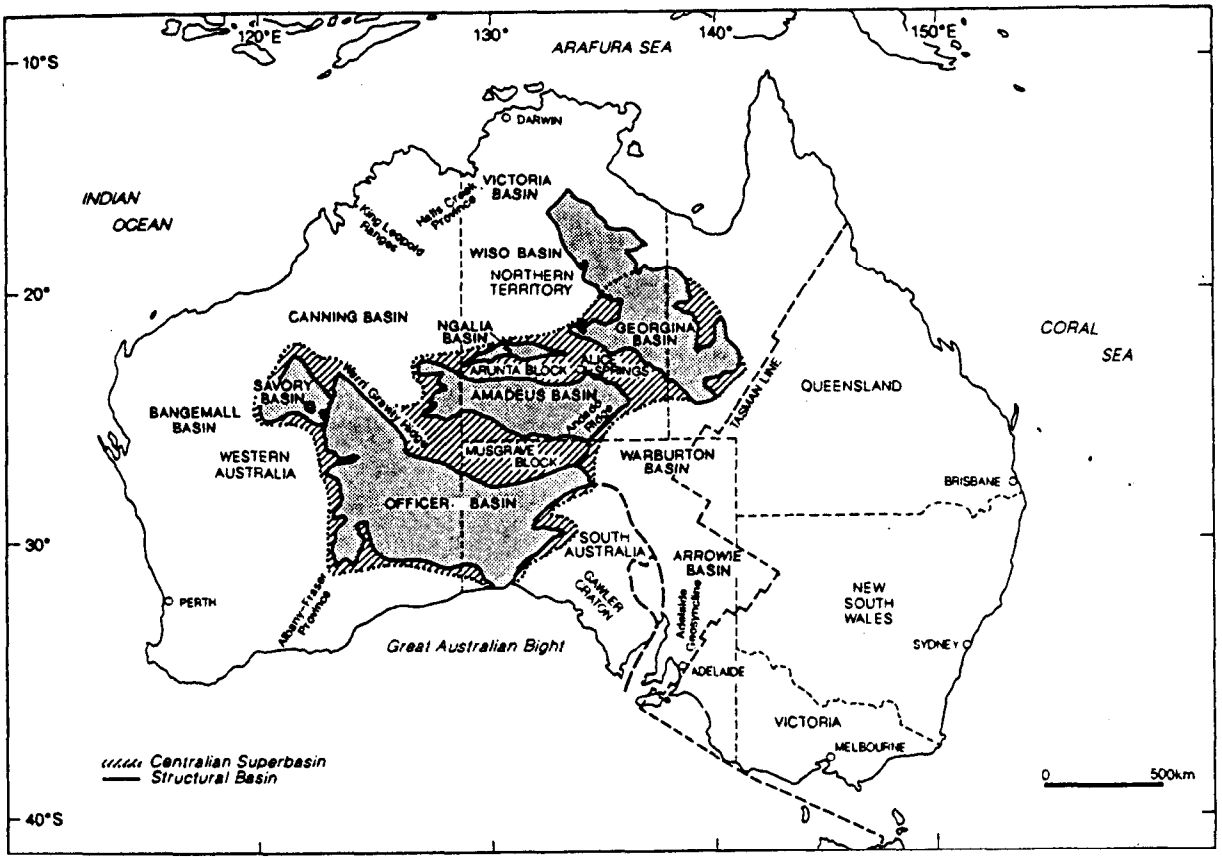

Fig. 1. The Centralian Superbasin and its constituent basins.

The basement of central Australia includes the Arunta Block and the 1200–1100 Ma Musgrave Block succeeded by 1075–1000 Ma bimodal volcanic rifts and dolerite dyke swarms. A regional hiatus at 1000–800 Ma, interpreted as reflecting a central post-volcanic (underplated) upland, was followed at 800 Ma by a second swarm of dykes in the Musgrave Block and Stuart Shelf. Basin initiation probably resulted from crustal thinning over a large mantle plume, at about 800 Ma (Zhao et al., 1994).

Crustal sagging around 800 Ma initiated the superbasin with deposition of hundreds of metres of marine and fluvial sands. These form a uniform sheet over much of the superbasin, wedging out against granitic basement in the northeast (Georgina Basin) and apparently thickening greatly in the west (Savory Basin). An overlying kilometre of marine and lacustrine carbonates, evaporites and fine siliciclastics completes the first depositional supersequence (1). Faulting during and after deposition of Supersequence 1 localized subsequent Sturtian glacigene sediments and overlying marine shales and carbonates (Supersequence 2).

Supersequence 3 begins with renewed glacial sedimentation (Marinoan), perhaps ~600–610 Ma ago. This glaciation may have been global, and post-glacial transgression was extensive, depositing turbiditic sands and pelagic shales over most of the superbasin. A carbonate–evaporite unit caps the supersequence. In the latest Proterozoic, marine sands and silts (Supersequence 4) were widespread, and continental flood basalts were erupted, following compression in the Officer Basin and southern Amadeus Basin. The culmination of this tectonic event is the Petermann Ranges Orogeny, which ended about 540 Ma ago (Maboko et al., 1992). The orogeny fragmented the Centralian Superbasin area into several smaller basins. The younger part of

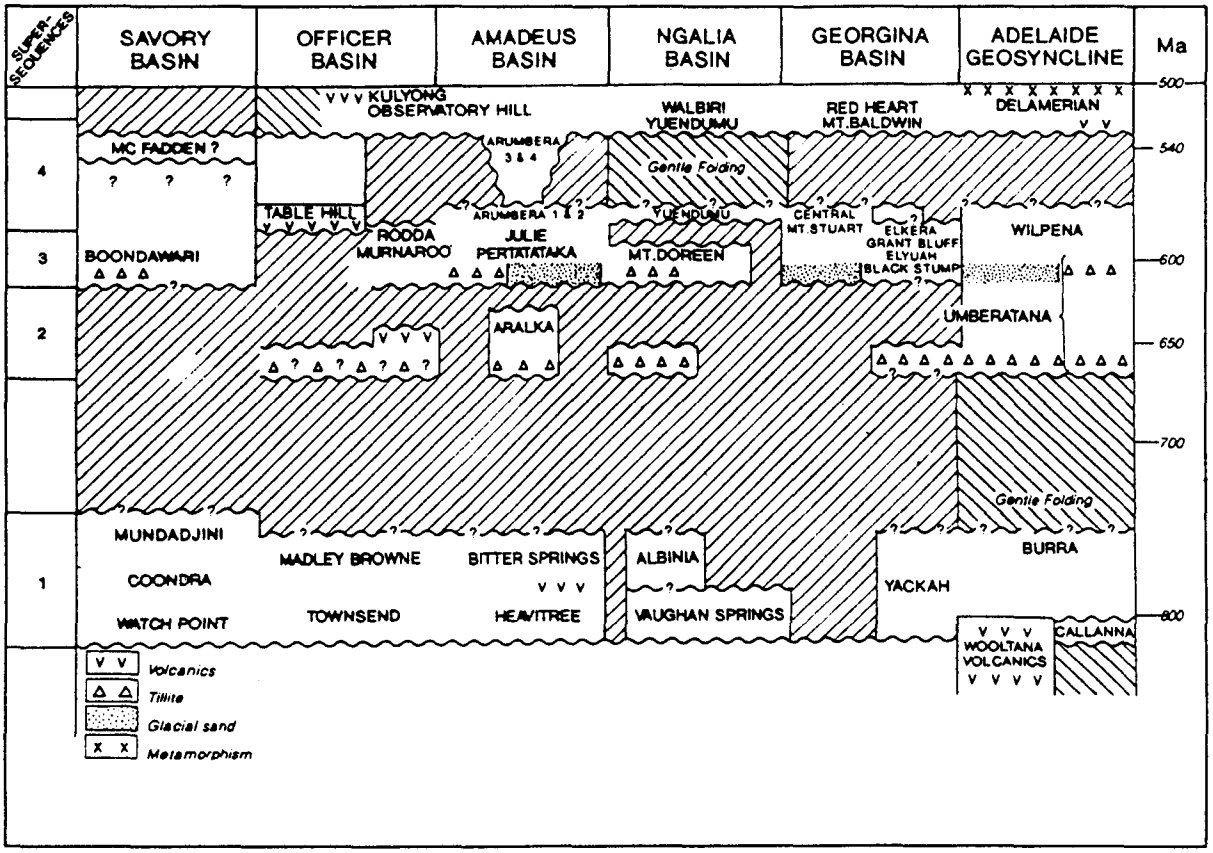

Fig. 2. Ages and constituent formations of the Neoproterozoic supersequences of the Centralian Superbasin.

Supersequence 4 (Cambrian) commences with more deposition of marine sands and silts, followed by carbonates and evaporites.

The Neoproterozoic fill of the superbasin is not well dated. A U/Pb zircon date of 802 ± 10 Ma from volcanics near the base of the Adelaide Geosyncline is the only reliable precise isotopic date from the entire Australian Neoproterozoic succession; correlation with the Centralian Superbasin suggests that this date can be used as the approximate maximum age of Supersequence 1. Abundant basic dykes in the basement have been dated by Sm/Nd techniques at about 800 Ma (790–867 Ma with errors of up to 49 Ma; Zhao et al., 1994). They are not in direct contact with older units of the fill of the superbasin, but on the basis of their detailed geochemistry they are considered co-magmatic with volcanics low in the fill of the Adelaide Geosyncline; they are also similar to volcanics in the Bitter Springs Formation (Supersequence 1) of the Amadeus Basin. The extensive Table Hill Volcanics (Officer Basin, $?563 \pm 40$ Ma), and ?correlative Antrim Plateau Volcanics (northern Australia) are a second important datum. The base of the Cambrian is now dated elsewhere at <544 Ma (Bowring et al., 1993), consistent with earlier estimates (Jenkins, 1984).

Preliminary results of studies by M.R. Walter (stratigraphy), J.J. Veevers (tectonics), C.R. Calver (sedimentology, isotope chemostratigraphy) and K. Grey (acritarch biostratigraphy) are presented here in outline.

2. Basement

In central Australia, the basement of the 1200–1100 Ma Musgrave orogen (Arriens and Lambert, 1969; U/

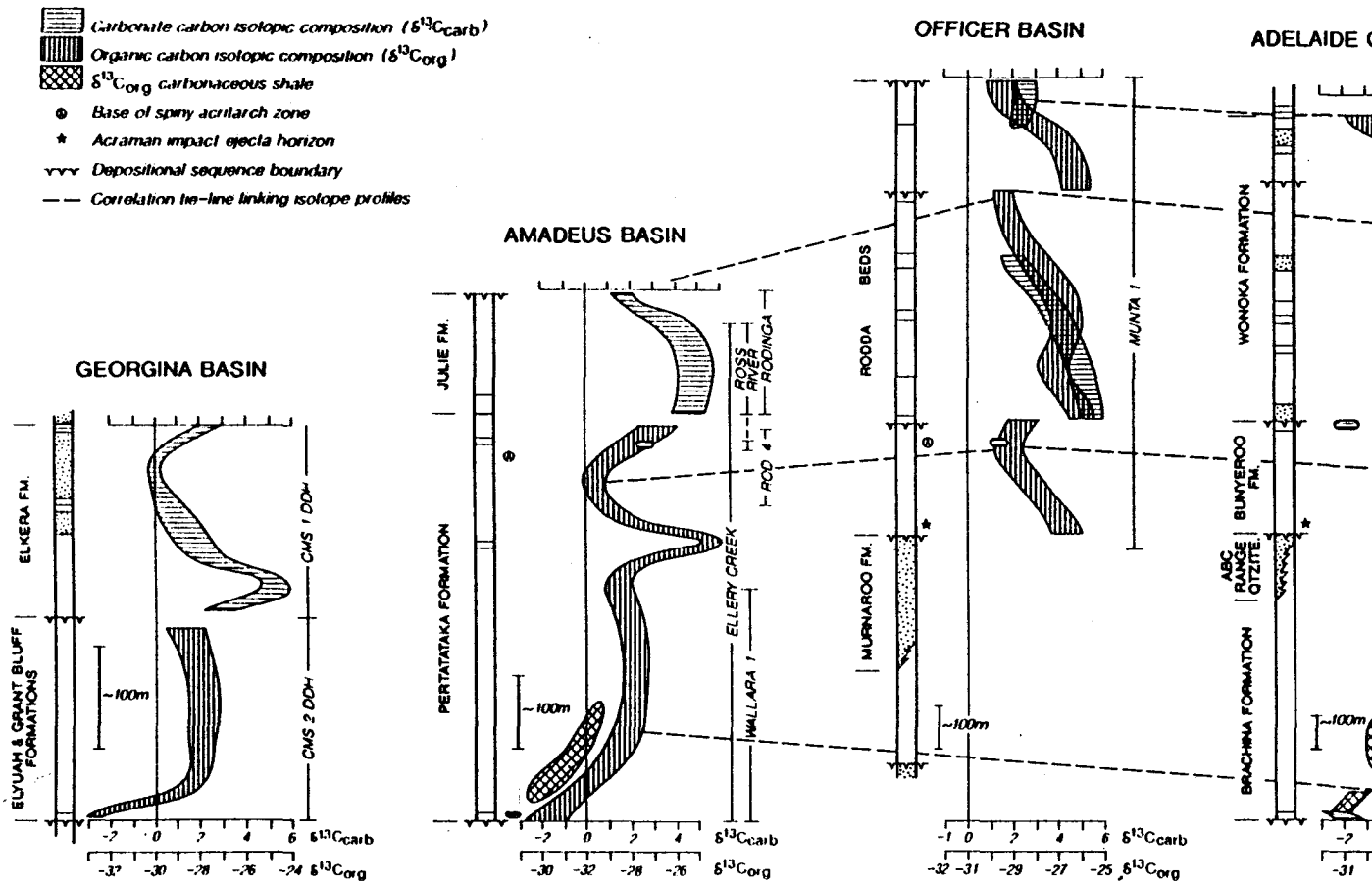

Fig. 3. Generalised isotopic record and acritarch occurrences in major regions of the Centralian Superbasin. Details of these results will be published elsew isotopic analyses (of which there are about 1000) lie within the plotted envelopes.

Pb SHRIMP dates by Maboko et al., 1991; Camacho and Fanning, 1992; Sun and Sheraton, 1992) and older consolidated blocks (e.g., Arunta Inlier, Collins, 1992) is covered by rocks of the 1075–1000 Ma Bentley Volcanic Province, comprising:

(a) The volcanic rifts and cauldrons filled with the 5 km thick Bentley Supergroup of bimodal volcanics near the NT–SA–WA border (GSWA, 1990), including the Tollu Volcanics with SHRIMP U/Pb dates of ~1060 Ma (Sun and Sheraton, 1992);

(b) The Stuart Dyke Swarm beneath the northern margin of the Amadeus Basin (Sm–Nd mineral isochron dates of 1049±94 and 1061±36 Ma, superseding the Rb/Sr date of 897±9 Ma of Black et al., 1980) and the Kulgera Dyke Swarm beneath the southern (Musgrave) margins of the Amadeus Basin (1054±14 and 1076±49 Ma, Zhao et al., 1992c; Camacho and Fanning, 1992) and the Lakeview Dolerite (1116±12 Ma; Page, 1983) near Mt Isa to the northeast.

The development of the Bentley Volcanic Province was followed by a regional hiatus at 1000–800 Ma, interpreted as reflecting a central post-volcanic (underplated) upland in central Australia. At about 800 Ma, the Musgrave Block was intruded by a second swarm of dykes in the Amata area (Sm–Nd: 790±40, 797±48 Ma, Zhao et al., 1992b) and Tomkinson Ranges (SHRIMP U/Pb ~800 Ma, Sun and Sheraton, 1992). The Gairdner Dyke Swarm in the Gawler Craton and Stuart Shelf on the southeastern margin of the superbasin is the same age (Sm–Nd: 867±47, 802±35 Ma, Zhao et al., 1994). Other magmatism at about this time included pipes in the Kimberleys (conventional U/Pb zircon dates ~800 Ma, Pidgeon et al., 1989) and an alkaline ultrabasic dyke near Norseman (Rb/Sr 849±9 Ma, Robey et al., 1989) in Western Australia, the Rook Tuff in South Australia (SHRIMP and conventional U/Pb on zircon 802±10 Ma, Fanning et al., 1986; Preiss, 1987; see also Zhao et al., 1994) and the basalt flows in the Loves Creek Member of the Bitter Springs Formation near Alice Springs in central Australia. Soon afterwards, central Australia subsided by collapse of the post-Bentley Upland.

3. Supersequence 1

Sedimentation in the Centralian Superbasin commenced with the deposition of a thick sheet of sand that covered much of the present continent of Australia west of the "Tasman Line" (a line marking the easternmost known occurrences of Archaean and Proterozoic rocks). In every basin this sand is overlain by dolomites, limestones, evaporites and fine siliciclastics (Fig. 2).

This supersequence reaches a thickness of more than 3000 m in the Yowalga Sub-basin (Fig. 4A), and similar thicknesses can be expected elsewhere in the central and eastern areas of the superbasin (for instance on the Bedourie Block in the southern Georgina Basin; Lodwick and Lindsay, 1990). It wedges out against basement highs in the southern Georgina Basin (Walter, 1980). The carbonate component is thin in the Ngalia Basin, and probably is replaced westwards by sandstones and conglomerates in the western Savory Basin.

The Burra Group of the Adelaide Geosyncline is considered to be the correlative on the developing plate margin; this correlation is tenuous and is based on lithological similarities and the possible common presence of a distinctive form of stromatolite (see below). Correlation with the older Callanna Group cannot be excluded as a possibility.

3.1. Amadeus Basin

The Heavitree Quartzite and its southwestern equivalent, the Dean Quartzite, unconformably overlie highly deformed basement consisting of the Arunta Orogen and Musgrave–Mann (Wingelina) Complex. The correlation of the two sandstones is established by lithology, superposition, and surface and subsurface distribution. Lindsay and Korsch (1991) consider that they overlie a rift succession (Bloods Range beds and Dixon Range beds and a slightly metamorphosed sequence in the Kintore Range), but there is no geochronological information available to support this interpretation. The basal sands are in turn overlain by the widespread carbonates and evaporites of the Bitter Springs Formation and its lateral equivalent, the Pinyinna beds. The supersequence consists of initial intertidal and fluvial deposits, deepening upwards to a maximum depth in the Gillen Member (the lower member of the Bitter Springs Formation) and then shallowing upwards in the Loves Creek Member in the upper Bitter Springs Formation to a lacustrine association at the top of the supersequence (Southgate, 1986, 1989, 1991). The Gillen Member is characterized by

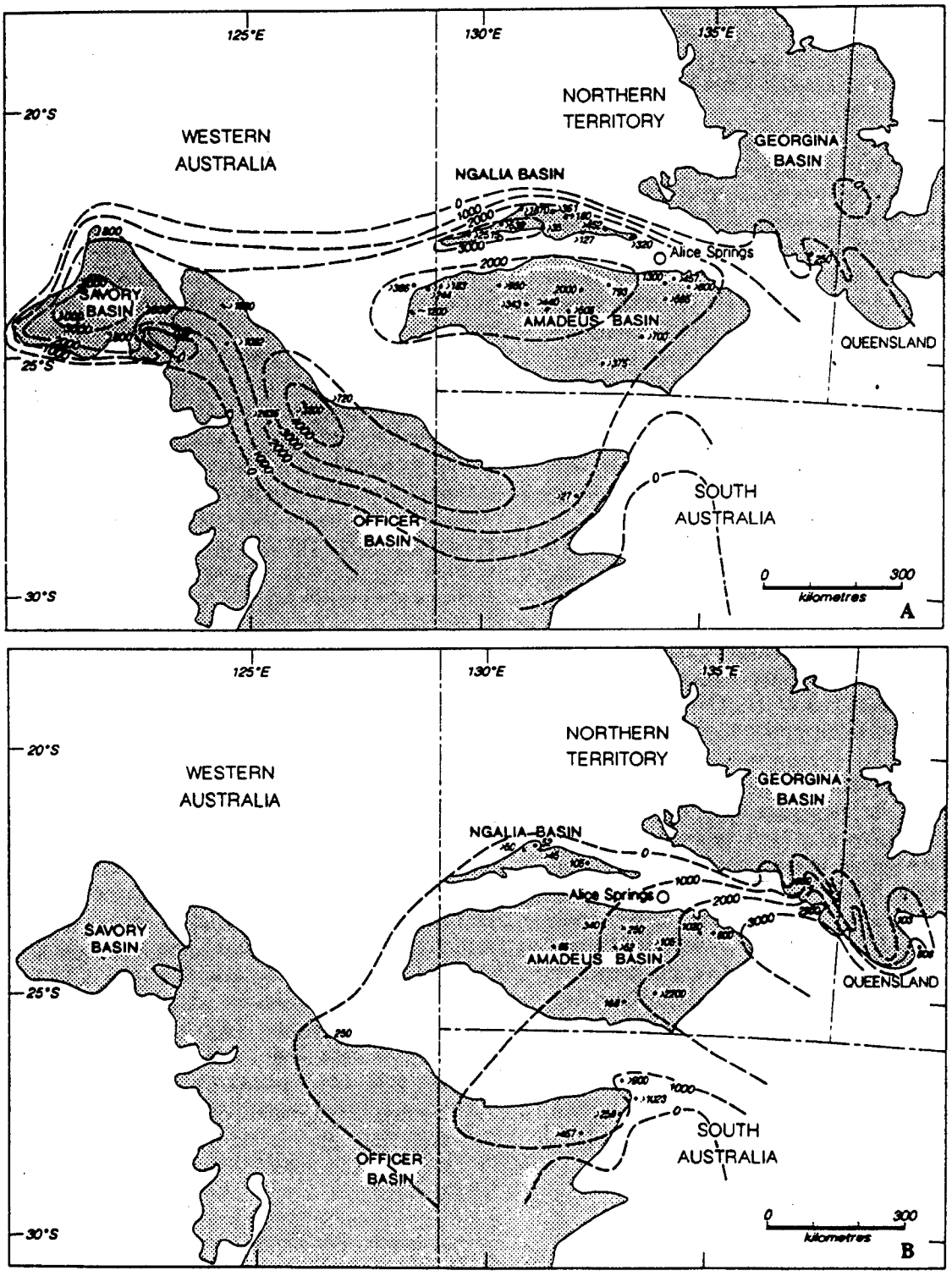
125°E
130°E
135°E
20°S
25°S
30°S
WESTERN AUSTRALIA
NORTHERN TERRITORY
GEORGINA BASIN
NGALIA BASIN
Alice Springs
SAVORY BASIN
AMADEUS BASIN
QUEENSLAND
OFFICER BASIN
SOUTH AUSTRALIA
0
300
kilometres
A
B

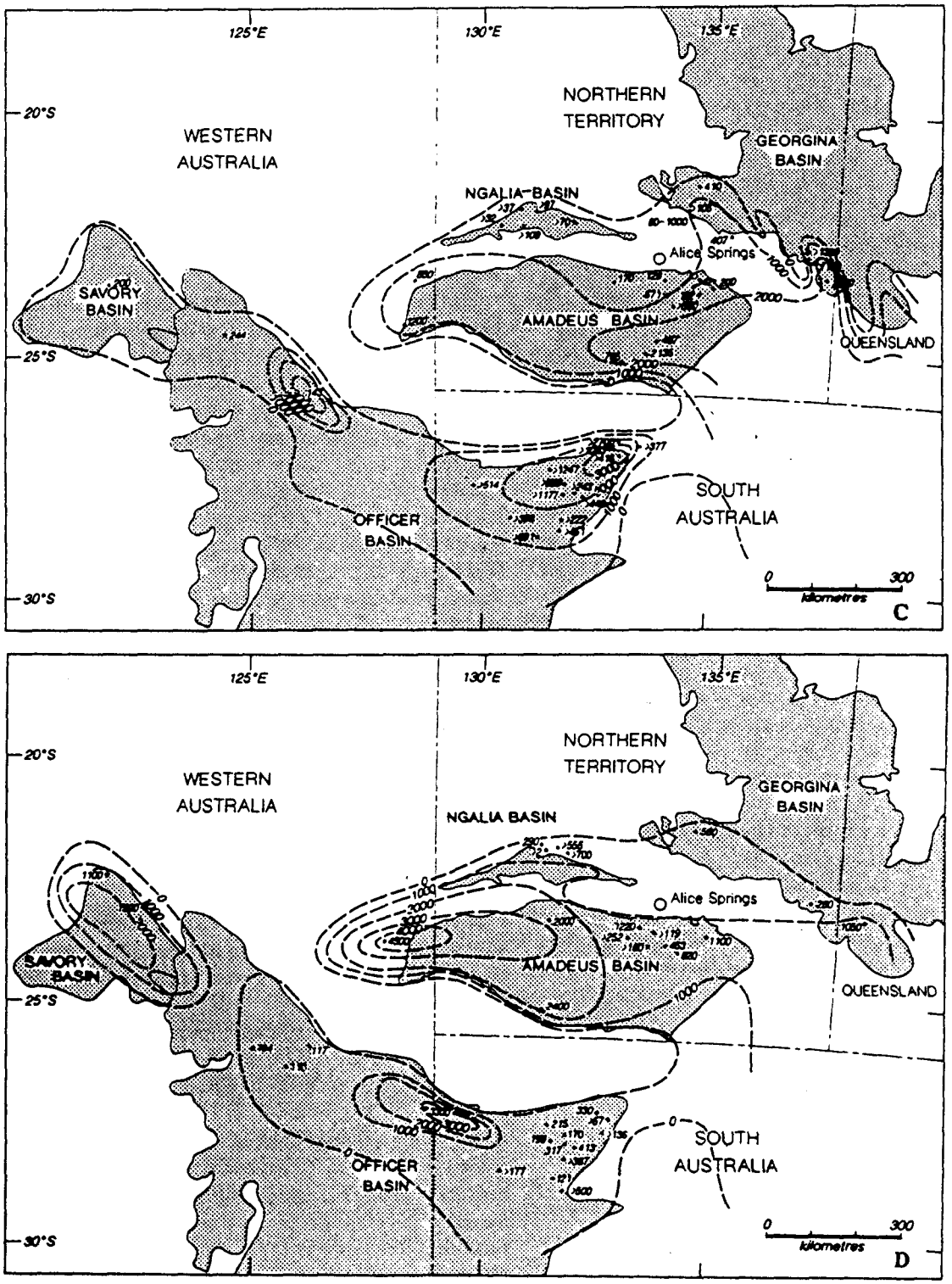

Fig. 4. Palaeo-isopachs for the supersequences; contour intervals are 1000 m. Data are sparse, as indicated by the plotted datapoints. The directions of facies changes have been used to assist with interpreting the patterns of thickness variation. Maximum preserved thicknesses have been used to approximate original thicknesses. (A) Supersequence 1. (B) Supersequence 2. (C) Supersequence 3. (D) Supersequence 4.

evaporites that show significant variations in thickness and considerable evidence of salt tectonics (Lindsay, 1987b). Highly altered basalts occur locally in the Loves Creek Member (Wells et al., 1967; Zhao et al., 1994).

The Bitter Springs Formation has a diverse assemblage of distinctive columnar branching stromatolites (Walter, 1972; Walter et al., 1979a). These have proven to be very useful in facilitating correlations with other basins in the superbasin. It also has microfossils preserved in chert (Schopf, 1968; Schopf and Blacic, 1971; Knoll and Golubic, 1979) and acritarchs (Zang and Walter, 1992).

3.2. Georgina Basin

Exposure of the Yackah beds is very limited, but they have also been tentatively recognised in seismic records; they seem to reach a thickness of 250 m in the Adam Trough (Walter, 1980). They consist of interbedded fine to very coarse feldspathic grey sandstone and laminated shale, apparently overlain by grey siliceous dolomite. Correlation with the Heavitree Quartzite and Bitter Springs Formation is established by lithology, superposition and the presence of the distinctive stromatolite *Acaciella australica* (Howchin) Walter 1972. Exposure of the unit is very poor, but it can be expected to have the same range of lithologies as the Bitter Springs Formation. The very thick (> 8 km) apparently Proterozoic succession recognised in the subsurface Bedourie Block by Lodwick and Lindsay (1990) is likely to include a correlative of this unit.

The Yackah beds thin out against basement highs in the southern part of the basin; they are the basal part of the fill in the Keepera Trough, Adam Trough and probably the Toko Syncline (Walter, 1980).

3.3. Ngalia Basin

The Vaughan Springs Quartzite is very similar to the Heavitree Quartzite of the Amadeus Basin and the nearest outcrops are only 20 km apart. The overlying Albinia Formation is a succession of siltstone, shale and dolomite comparable with the Bitter Springs Formation but thinner where exposed (up to 150 m); they contain similar assemblages of microfossils in chert (M.R. Walter and K. Cloud, in Wells and Moss, 1983). Exposure of this latter unit is very poor, but it can be expected to have the same range of lithologies as the Bitter Springs Formation.

3.4. Officer Basin

The Townsend Quartzite is the basal unit of the western Officer Basin. It contains more conglomerate than the Heavitree Quartzite. Its equivalent to the east is the Pindyin beds.

Carbonates and evaporites overlying the Townsend Quartzite are known from most of the petroleum exploration wells in the western Officer Basin, and from outcrop (Jackson and van de Graaff, 1981). They are known as the Ilma, Neale, Browne, Madley, Woolnough, Hussar, Steptoe and Kanpa Formations. There is a proliferation of names because outcrop is very poor and many of the units are known from only one or two intersections by petroleum exploration wells. These units are exposed at the surface in the Madley and Woolnough diapirs in the northwestern part of the basin. Correlation with the Bitter Springs Formation is established by lithology, superposition and the presence of the distinctive stromatolite *Acaciella australica* both in core (K. Grey, unpubl. observ.) and surface samples. Microfossils comparable with those in the Bitter Springs Formation are known from the Madley diapirs (M.R. Walter, pers. commun., 1978, in Jackson and van de Graaff, 1981), and there are sphaeromorph acritarchs (K. Grey, unpubl. observ.). The Neale Formation contains the stromatolite *Baicalia* cf. *burra* (Preiss, 1976), suggesting correlation with the Burra Group in the Adelaide Geosyncline.

In drill hole Lungkarta 1 the Steptoe Formation has an assemblage of large leiosphaerid acritachs including probable *Chuaria circularis* Walcott (K. Grey, unpubl. observ.).

Although seismic and depth-to-basement information for the eastern Officer Basin can be used to infer the probable presence of Supersequence 1, the only possible well penetration is in Giles 1. There, sandstones with overlying dolomitic anhydritic sandstones, dolomitic anhydritic siltstones and sandy anhydrite beds are probably of this age, although correlation with the older Callanna Group of the nearby Adelaide Geosyncline is also possible (W.V. Preiss, pers. commun., 1993). Resolution of this uncertainty is particularly important, as this unit is the source of salt for the diapirs

of the eastern Officer Basin, and could well be a significant petroleum source and seal as well.

3.5. Savory Basin

The presence of Supersequence 1 in this basin is established by the close comparisons that can be made between the Skates Hill and Bitter Springs Formations (Williams, 1992; Grey, 1995; Walter et al., 1994). Not only are the lithologies essentially identical, but they also share the common presence of distinctive stromatolites (*Acaciella australica* and *Basisphaera irregularis* Walter). On the structural high where the Skates Hill Formation occurs, the basal siliciclastics are represented by only a thin conglomerate, but elsewhere there are sandstones and conglomerates reaching a thickness of perhaps 4000 m (the Glass Spring, Brassey Range, Jilyili, Watch Point, Coondra and Spearhole Formations). These are locally sourced (Williams, 1992) and can be interpreted to indicate a tectonically active area of high ground marking the western margin of the superbasin.

The Mundadjini Formation is considered by Williams (1992) to be the western lateral equivalent of the Skates Hill Formation, although it is predominantly siliciclastic. Evaporite pseudomorphs are abundant. Its presence on the tectonically active western margin of the superbasin is consistent with the interpretation of a facies change westwards from carbonates to sandstones. One of us (KG) prefers to correlate the Mundadjini Formation with the lower (Gillen) member of the Bitter Springs Formation.

3.6. Comments

None of the basal sandstones has been studied in detail, except for the largely unpublished work by Clarke (1976) on the Heavitree and Vaughan Springs Quartzites (these units are generally not metamorphosed—the term "quartzite" is used in Australia for clean quartz arenites that, at least at the surface, are well cemented by silica). All appear to be marginal marine to fluvial and lacustrine deposits.

Of all the carbonate–evaporite units only the Bitter Springs Formation has been thoroughly studied, and then only in its upper, stromatolitic carbonate part, the Loves Creek Member (Walter, 1972; Southgate, 1986, 1989, 1991; Lindsay, 1987b). This was deposited on an epicontinental platform of very low relief. Its lower part is shallow marine, with water depths generally less than 10 m; this is demonstrated by facies analyses and by carbon isotopic studies (unpubl. work of P. Southgate and D. DesMarais). This is overlain by an upper section that has interbedded lacustrine carbonates and alluvial flood plain deposits (red silty carbonates, with some sands). A brief period of volcanism is recorded by the presence of basaltic lavas in the northeastern part of the Amadeus Basin (Zhao et al., 1994).

The thick evaporites of the lower Bitter Springs Formation of the Amadeus Basin were interpreted as lagoonal by Stewart (1979) but are known from well intersections and seismic interpretation (Lindsay, 1987b) to be very extensive. Evaporites are known from this level in the western Officer Basin (and probably also the eastern part of the basin; see above), and can be expected in the other basins as well. They have produced diapirs in both the Amadeus and Officer Basins. The evaporites (halite and anhydrite) are interbedded with stromatolitic dolomites and fine siliciclastics, and their sheer mass as well as their bulk chemistry argue for a marine source. Consideration of the palaeogeography of the underlying sands and the overlying carbonates suggests deposition on a platform with low relief expressed as a mosaic of carbonate banks with intervening evaporite lagoons, with distant rivers providing sources of silt. However, Lindsay (1987b) favoured formation in poorly circulated anoxic subbasins of the 'saline giant' type, with carbonates and sulphates developed around basin margins, and halite and possibly potassium salts deposited in the sub-basin centres. Small, tectonically controlled intra-platformal basins such as the Yowalga Sub-basin of the Officer Basin and the various half-grabens of the southern Georgina Basin can be expected to have the thickest accumulations of evaporites.

4. Supersequence 2

The Sturtian glaciation and the subsequent widespread flooding of the Australian plate left a distinctive sedimentary record. This is used to define Supersequence 2, the base of which is marked by glacial deposits. These are overlain by widespread silts and shales with interbedded carbonates and sandstones (Figs. 2, 4B).

The unconformably overlying Marinoan glacial deposits form the base of Supersequence 3.

4.1. Amadeus Basin

The tillitic Areyonga Formation and the siltstones and shales of the overlying Aralka Formation are the only representatives of this supersequence in the northern Amadeus Basin (Preiss et al., 1978). They are largely confined to the northeastern part of the basin, where by analogy with the nearby Georgina Basin (Walter, 1980) we postulate that they occupy one or more penecontemporaneous fault-bounded troughs. It could be suggested that the troughs are a result of salt withdrawal from the underlying Bitter Springs Formation (cf. Kennedy, 1993), but their apparently large size makes this less likely. Complex structure has so far prevented the elucidation of this situation. The units reach a total thickness of 1600 m in the northeastern Amadeus Basin. The Aralka Formation has a stromatolitic carbonate member (Ringwood Member) with columnar stromatolites (*Tungussia inna* Walter, 1972) and a sandstone member (Limbla Member). At its base is the distinctive "lower marker cap dolomite" which is a very useful marker in correlating this horizon Australia-wide (Preiss et al., 1978).

Thin occurrences of the same formations occur as erosional remnants further west (e.g., at Ellery Creek and Areyonga). The Inindia beds in the southern part of the basin are probably correlative, and include about 2100 m of diamictite, sandstone and siltstone.

The Boord and Carnegie Formations of the western Amadeus Basin are usually correlated with the units of this supersequence, but here they are considered to be components of Supersequence 3.

4.2. Georgina Basin

Thick development of this supersequence in the Georgina Basin is confined to the Keepera Trough, the Adam Trough, and possibly the adjacent Toko Syncline and Bedourie Block, where thicknesses of up to 2900 m have been measured. The only named units in these areas are the Yardida Tillite and Mt Cornish Formation (Walter, 1980). These consist of blue-green and green-grey diamictite and laminated siltstone with infrequent fine- to very coarse-grained brown to grey sandstone and arkose. Clasts up to 12 m in diameter have been reported. A thin diamictite at the base of the Central Mount Stuart Formation further west may be correlative (Walter, 1980). The upper Yardida Tillite is a siltstone and shale with the distinctive "lower marker cap dolomite" at its base (there is likely to be a major sequence boundary at this position).

4.3. Ngalia Basin

The Nabarula Formation is a thin unit consisting of basal diamictite, shale and "cap dolomite". It is overlain by green or dark grey siltstone and shale, the Rinkabeena Shale. The two units reach a maximum thickness of about 100 m.

4.4. Officer Basin

On the basis of lithology and superposition the 600 m thick Chambers Bluff Tillite of the eastern part of the basin is considered to be Sturtian (Preiss, 1987). There is only one level of tillite known in this basin. No distinctive marker beds have been recognised.

The Wantapella Volcanics overlie the Chambers Bluff Tillite in the northeastern part of the basin (Preiss, 1987). They are 290 m of grey-green to pale grey, amygdaloidal, low-silica basalts. They are interpreted as flood basalts extruded into a shallow-marine to subaerial environment. Their stratigraphic position is not clear; regional relationships suggest that it is possible that they are part of Supersequence 3 (W.V. Preiss, pers. commun., 1993).

The Lupton Formation and Turkey Hill Formation of the western part of the basin could be Sturtian or Marinoan. The former is diamictite, cross-bedded sandstone, minor siltstone, conglomerate, sandstone and siltstone. The Turkey Hill Formation comprises sandstone, siltstone, claystone and minor diamictite (Jackson and van de Graaff, 1981).

4.5. Savory Basin

No representatives of Supersequence 2 are known from this basin, though because of paucity of outcrop and total lack of subsurface information, this is of little significance.

4.6. Comments

The glacial origin of the diamictites at the base of this supersequence is established by the diversity of erratics, the fact that many of them are faceted and striated, and the presence of lonestones in laminated siltstone. Correlation of these diamictites continent-wide is well established (Preiss and Forbes, 1981).

Lindsay (1989) interprets the lower part of the Areyonga Formation as a massive basal till, probably a lodgement till, associated with subglacial or marginal channels cut by high-pressure water flow. Overlying diamictites are thinner and probably represent subglacial and ice-margin deposits. Subtle changes in ice conditions gave rise to boulder concentrations and sheets of sandstone and conglomerate deposited subglacially. The final phase of sedimentation consisted of shallow-marine ice-proximal deposits indicated by poorly bedded diamictites and sandstone bodies with abundant soft-sediment deformation. Anoxic dark shales and carbonates were deposited between the ice lobes and the proto-Central Ridge of the Amadeus Basin to the south which acted as a barrier. Fluvial sedimentation occurred between the ice lobes, further north.

This seems to have been a severe glaciation that may well have representatives on other continents (Hambrey and Harland, 1981). Thus the thick shales that overlie the tillites very likely resulted from a eustatic rise of sea level following deglaciation. Isostatic rebound following deglaciation can explain the observation that the supersequence shallows up to have shallow-water stromatolitic carbonates (e.g., Ringwood Member) and cross-laminated sandstones (e.g., Limbla Member) in its middle to upper parts.

5. Supersequence 3

Glacial deposits mark the base of this supersequence (Figs. 2, 4C). They are readily correlated continent-wide (Preiss and Forbes, 1981), and there is increasingly convincing evidence that they are coeval with the Varangian tillites of Europe (Knoll and Walter, 1992). If this is so, the Varangian–Marinoan glaciation would seem to have been the most severe that the Earth has experienced.

The supersequence is characterised palaeontologically by the presence of the "Pertatataka microbiota", two or more assemblages of very large sphaeromorph and acanthomorph acritarchs described first from the Pertatataka Formation of the Amadeus Basin (Zang and Walter, 1989, 1992) and subsequently found in the Rodda beds of the Officer Basin (Jenkins et al., 1992; K. Grey, unpubl. observ.). Comparable assemblages are known from the Sinian of China (Yin, 1985), the latest Proterozoic of Svalbard (Knoll, 1992) and the Vendian of Siberia (Moczydłowska et al., 1993).

Large variations in the carbon isotopic composition of carbonates and kerogen occur up through the supersequence in patterns that are proving useful for correlation within the superbasin (C.R. Calver, unpubl. observ.; Fig. 3). Similar patterns have been recognised on other continents (e.g., Kaufman et al., 1991, 1992; see also Kaufman and Knoll,.1995) and seem to reflect secular variations in the composition of seawater, and thus to be useful for global correlation (Knoll and Walter, 1992). Jenkins (1995) reports results on carbonates only from the Wonoka Formation of the Adelaide Geosyncline; many of these carbonates are extremely enriched in ^{12}C, whereas the associated kerogen (analysed by C.R. Calver) is within the normal compositional range, indicating that these particular carbonates are not reflecting the isotopic composition of the global ocean.

The distinctive "upper marker cap dolomite" overlies the glacial deposits in the Amadeus and Ngalia Basins. The most remarkable marker unit though is the Acraman impact ejecta blanket first recognised in the Adelaide Geosyncline and then later discovered in the Rodda beds of the Officer Basin (Wallace et al., 1991). However, this bed is only 1–10 mm thick in the Officer Basin, so the chances of finding it in more distant basins must be remote. Nonetheless, its presence confirms previous correlations of the Rodda beds with the Bunyeroo Formation, Wonoka Formation and probably, at least in part, the Billy Springs Formation, of the Adelaide Geosyncline. In turn, the Rodda beds can now be widely correlated using acritarchs and patterns of carbon isotopes, as well as more conventional techniques. Thus compelling links can be made to the classic sections in the Flinders Ranges proposed as the type Ediacarian of Cloud and Glaessner (1982) and Ediacaran of Jenkins (1981).

5.1. Amadeus Basin

The diamictites of the Olympic Formation are restricted to the northeastern part of the basin and pass westwards into conglomerates and then arkosic sandstones of the Pioneer Sandstone (Preiss et al., 1978). This correlation has been questioned (Lindsay, 1989; Field, 1991), but has been confirmed by recent mapping (Jenkins and Walter, in prep.). The Olympic Formation includes a reddish diamictite containing striated and faceted clasts and dropstones, but mostly consists of red and green mudstone and siltstone, with intercalated sandstone (Field, 1991; see also table 1 in Preiss et al., 1978). The "upper marker cap dolomite" contains the distinctive stromatolite *Anabaria* [*Kotuikania*] *juvensis* Cloud and Semikhatov (1969) = *Elleria minuta* Walter et al. (1979a) on an erosional surface in the upper Pioneer Sandstone at Ellery Creek, and the same form has now been recognised in this marker bed in a large area of the northeastern part of the basin (Jenkins and Walter, in prep.). The least altered of the "cap dolomites" in drill hole Wallara 1 (Fig. 4) has depleted carbon isotopic compositions (-3 to -4° $\delta^{13}C$) similar to those of the Nuccaleena Formation capping the Marinoan glacials in the Adelaide Geosyncline (C.R. Calver, unpubl. observ.). Locally, the Pioneer Sandstone grades down into a talus breccia, and where this overlies carbonates of the Bitter Springs Formation, a thin fossil pedogenic calcrete often is present (Jenkins and Walter, in prep.). At present there is debate about the relationships of these various units, and the associated Gaylad Sandstone, and important details of the local stratigraphy are not yet understood.

The overlying Pertatataka Formation is up to 1400 m of siltstone and shale with a prominent unit of thin-bedded sandstone (the Cyclops Member) in the middle. At Wallara 1 in the centre of the basin, the unit is dominated by grey-green, red and black shale, with common (20%) sandstone turbidite beds occurring in the middle of the formation and again at the top. The upper sandy interval becomes more sandy upwards, and thin-bedded, cross-laminated sandstones suggest shallowing to within wave base (C.R. Calver, unpubl.). These two sandy intervals may be distal equivalents of the two sandstone units (Wells et al., 1970) in the correlative Winnall beds further south. In seismic sections the formation is distinguished by weak, discontinuous, parallel reflectors, but in places there are large, north-prograding clinoforms (e.g., Kennard and Lindsay, 1991, their fig. 10). Distinctive but as yet undescribed stromatolites occur at the base of the Pertatataka Formation at Fenn Gap west of Alice Springs and at the base of the Winnall beds at Mt Connor in the southern part of the basin.

Organic carbon $\delta^{13}C$ profiles (Fig. 3) show an initial rise and plateau that may be equivalent to the profile from the Elyuah Formation of the Georgina Basin. The "Pertatataka microbiota" first appears within the topmost rising $\delta^{13}C$ trend.

The Pertatataka Formation grades up into the Julie Formation, a dolomite with abundant oolite and sparse stromatolites (*Tungussia julia* Walter) comparable with a form in the probably correlative Wonoka Formation of the Adelaide Geosyncline (Walter et al., 1979a; Preiss, 1987). The high values of $\delta^{13}C$ ($+4$ to $+6$‰) in the formation match those of the lower carbonate of the Rodda beds of the Officer Basin and the lower Elkera Formation of the Georgina Basin (Fig. 3; C.R. Calver, unpubl.)

The Pertatataka Formation becomes sandier to the south, grading into the sandstones and siltstones of the Winnall beds, over 2000 m thick. The Boord Formation and Carnegie Formation in the westernmost part of the basin are here considered to belong to Supersequence 3. The Boord Formation is a succession of calcilutite, calcarenite, dolomitic limestone, sandstone and siltstone, with boulder beds of possible glacial origin (Wells et al., 1964). The Carnegie Formation consists mainly of purple-brown sandstone and siltstone; a conglomeratic bed with boulders and rounded cobbles derived from the Bitter Springs Formation and possibly the Heavitree Quartzite is present in some areas. Previous authors have correlated these units, at least in part, with the older Inindia beds of Supersequence 2 (Wells et al., 1970; Preiss and Forbes, 1981). All these correlations are tenuous, but it seems to us that broad lithologic comparisons support our interpretation. The base of the Boord Formation is described as a breccia unconformably overlying the Bitter Springs Formation, reminiscent of the relationship between the Pioneer Sandstone and the Bitter Springs Formation. Overlying diamictite can be correlated with the Olympic Formation. No equivalent of the "upper marker cap dolomite" is known. There are thin beds of dolomite higher in the formation; these contain the distinctive but

endemic stromatolite *Tesca stewartii* Walter et al. (1979a), and an unnamed form comparable with one found in the Boondawari Formation of the Savory Basin. Four samples of stromatolitic limestone from the formation have yielded $\delta^{13}C$ analyses of +3 to +4° (C.R. Calver, unpubl. observ.). These values are similar to those from the Julie Formation, and quite different from those of the "cap dolomite" at the top of the Pioneer Formation.

5.2. Georgina Basin

No diamictites of this age are known with confidence, though that of the Mount Birnie beds is probably Marinoan, to judge from its position beneath red shales like those of the Pertatataka Formation (De Keyser and Cook, 1972; Preiss and Forbes, 1981). The coarse-grained arkoses (Black Stump Arkose, Sun Hill Arkose, Oorabra Arkose) that are prominent in the half-grabens in the southern part of the basin, and up to 1000 m thick, are considered to be glacial outwash deposits, comparable to the Pioneer Sandstone of the Amadeus Basin (Walter, 1980). The overlying Wannadinna Dolomite of the Adam Trough occupies the position of the "upper marker cap dolomite", but is very different, with a fenestral fabric like that of some of the clasts in the regolith at the base of the Pioneer Formation. The formation was deposited largely during periods of normal polarity, although there were two brief periods of magnetic reversal (Burek et al., 1979).

The Mopunga Group (Walter, 1980) forms the upper part of the supersequence in much of the southern part of the basin. Fine-grained siliciclastics at the base (Elyuah Formation) and top (Elkera Formation) are separated by thin-bedded sandstone (Grant Bluff Sandstone) very similar to that of the correlative Cyclops Member. In the Adam Trough the base is marked by the Gnallan-a-gea Arkose, up to 1450 m of pebbly arkose, cross-bedded sandstone, siltstone and shale. To the west this is represented by a few metres of pebbly sandstone at the base of the Elyuah Formation (this is similar to the Gaylad Sandstone of the Amadeus Basin). The oldest metazoan trace fossils known in Australia occur in the Mopunga Group: Walter et al. (1989) report the simple burrow *Planolites ballandus* Webby from the Elkera Formation, and Jenkins et al. (1992) report *Planolites montanus* Richter and *Palaeophycus tubularis* Hall from the Grant Bluff Formation. The group is over 2600 m thick in the Adam Trough.

Near the top of the Elkera Formation there is a dolomite with the distinctive but endemic stromatolite *Georginia howchini* Walter. On the basis of stratigraphic position this dolomite is correlated with the Julie Formation of the Amadeus Basin. Carbon isotopic compositions are interpreted by C.R. Calver (unpubl.) to suggest that the upper part of the Elkera Formation is younger than the Julie Formation (Fig. 3).

5.3. Ngalia Basin

Three members have been recognized in the Mount Doreen Formation as redefined by A.T. Wells (in Preiss et al., 1978): the Mount Davenport Diamictite Member, the Wanapi Dolomite Member and the Newhaven Shale Member. The Mount Doreen Formation is about 100 m thick (Wells and Moss, 1983).

The Mount Davenport Diamictite Member was defined by Wells and Moss (1983) as diamictite at the base of the Mount Doreen Formation. The Wanapi Dolomite Member is fine-grained, pink, laminated dolomite. Walter and Bauld (1983) reported dolomite and barite pseudomorphs after gypsum and anhydrite. Stromatolites are common. The Newhaven Shale Member is red shale, and a few thin interbeds of pink dolomite near the base.

5.4. Officer Basin

The presence of the "Pertatataka microbiota" in the Rodda beds (Jenkins et al., 1992; K. Grey, unpubl. observ.) establishes a correlation with the upper Pertatataka Formation, in agreement with previous lithostratigraphic correlations. Carbonate-rich units in the middle Rodda beds are likely to be equivalents of the Julie Formation of the Amadeus Basin; carbon isotopic compositions are consistent with this: the lower limestone unit in drill hole Munta 1 has enriched $\delta^{13}C$ values of about +5, similar to the Julie Formation (see also Jenkins et al., 1992). Higher up, $\delta^{13}C$ falls, rising again to +2 to +3 in the topmost limestone (Fig. 3). The Rodda beds are more than 3700 m thick in the Munyarai Trough (Preiss and Krieg, 1992); thinner equivalents (150–200 m) are present on the southern platform area (Sukanta et al., 1991). The Rodda beds comprise grey-green siltstone, frequently calcareous and dolomitic.

They include grey and minor pink, brown and purple limestone and dolomite beds, feldspathic and calcareous sandstone, and pebble–cobble conglomerate beds. The upper part of the succession consists of grey-green siltstone with thin beds of very fine sandstone. Several sequence boundaries, one related to a "canyon-forming" event, have been identified in the Rodda beds (Sukanta et al., 1991; Jenkins et al., 1992). However, recognition of active syndepositional tectonism, some apparently related to salt movement (Sukanta et al., 1991), casts doubt on the widespread significance of these boundaries. The Rodda beds become conglomeratic northwards, towards the Musgrave Block (Preiss and Krieg, 1992).

The underlying sandstones of the Murnaroo Formation occupy the same stratigraphic position as the ABC Quartzite of the Adelaide Geosyncline (and probably the Cyclops Member of the Pertatataka Formation). Unnamed siltstones and shales under the Murnaroo Formation in the drill hole Giles 1 can be correlated with the Brachina Formation of the Adelaide Geosyncline (W.V. Preiss, pers. commun., 1993), and probably with the lower Pertatataka Formation.

Whether Supersequence 3 is represented in the western Officer Basin relies on the interpretation of the age of the Babbagoola Formation, a contentious matter. The Babbagoola Formation consists of shale, siltstone, sandstone, anhydrite, gypsum and conglomerate, up to 1200 m thick (Jackson and van de Graaff, 1981; Townson, 1985; Phillips et al., 1985). It is broadly comparable with the Rodda beds, and also with the shales in Supersequence 2. Correlation of the two formations is supported by well log interpretations (M.R. Walter, unpubl. rep.). The Babbagoola Formation was interpreted as Early Cambrian by Jackson and Muir (1981) because of the occurrence of poorly preserved simple acritarchs somewhat comparable with those of the Cambrian of Europe. However, it is now known that the unit contains an assemblage of large sphaeromorph acritarchs more like those typical of the Neoproterozoic (K. Grey, unpubl. observ.). A Neoproterozoic age would be consistent with the tentative dating of the overlying Table Hill Volcanics at 563 ± 40 Ma (recalculated from Compston, 1974), now that the base of the Cambrian is considered to be < 544 Ma old (Bowring et al., 1993). However, this is not straightforward, as the dating of the volcanics is also tenuous. Nonetheless, on balance, placement in Supersequence 3 seems the simplest interpretation.

5.5. Savory Basin

The intergrading sandstone–diamictite of the Boondawari Formation is very similar to the intergrading Pioneer Sandstone–Olympic Formation of the Amadeus Basin, and the overlying siltstone closely resembles the Pertatataka Formation and its correlative, the Winnall beds. Stromatolitic and oolitic carbonates in the upper Boondawari Formation are broadly comparable with those of the Julie Formation. Support for this set of correlations comes from carbon isotope chemostratigraphy. The reasons for interpreting the Boondawari Formation as belonging to Supersequence 3 are discussed in detail by Walter et al. (1994).

5.6. Comments

As with Supersequence 2, the deposits of a glaciation are overlain by the sedimentary products of an extensive marine transgression resulting from a eustatic rise in sea level following deglaciation. Once again the supersequence shallows up to finish in shallow-water carbonate deposits. Lindsay's (1989) arguments for a mass flow, non-glacial origin for the Olympic Formation are countered by extensive evidence of glaciation elsewhere in the continent, including patterned ground on the Stuart Shelf (Williams, 1986; Preiss, 1987) and striated pavements in northern Australia (Dow and Gemuts, 1969; Preiss and Forbes, 1981; Edgoose, 1986). The severity of this glaciation is attested by palaeomagnetic results indicating a near-equatorial location (5°N for the Elatina Formation in South Australia; Embleton and Williams, 1986).

The Pertatataka Formation was deposited in a relatively deep basin, as it includes pelagic shales and turbidites from a prodelta environment (R.J. Korsch, in Kennard et al., 1986; C.R. Calver and K. Grey, unpubl.). It becomes sandier southwards, indicating a source of sediments in the Musgrave Block. In the Officer Basin, salt was moving at this time, and there was synsedimentary faulting, resulting in the complex depositional geometry expressed in the Rodda beds. The Rodda beds were deposited in a deep-water slope and basin environment by mass flow, and turbidity currents and hemipelagic processes (Brewer et al.,

1987) in the northern part of the basin, but probably on a shelf environment in the southern (platform) area. Conglomerates and slumping in the northern occurrences of the Rodda beds demonstrate that the Musgrave Block was emergent (Preiss and Krieg, 1992). Faulting in the western Officer Basin pre-dated extrusion of the Table Hill Volcanics (Townson, 1985) and could well be the same age as the low-angle thrust faulting that produced nappes in the northern Musgrave–Mann Block (Wells et al., 1970). The last phase of movement on the Woodruffe Thrust is dated at 550–530 Ma (Maboko et al., 1991, 1992).

6. Supersequence 4

The lower part of this unit records the "Ediacara fauna" of soft-bodied metazoans. In Australia, carbonates are rare at this level, and the supersequence everywhere is dominated by sandstone. In the Adelaide Geosyncline the equivalent units and their fossil fauna have been studied in great detail for 40 years or more (see summaries by Glaessner, 1984; Preiss, 1987; more recent work includes that of Mount, 1989; Jenkins, 1991, 1992; Gehling, 1991). Within the Centralian Superbasin the Ediacara fauna is poorly represented; only a few taxa are known, most of which are not found in the Adelaide Geosyncline (e.g., *Hallidaya brewer*i Wade and *Skinnera brooksi* Wade); some of the reported occurrences are dubious (e.g., the Punkerri beds, see Preiss, 1987). The upper part of the supersequence is Early Cambrian and is not described here.

6.1. Amadeus Basin

The Arumbera Sandstone consists of red-brown and white sandstone and minor siltstone, shale, conglomerate and carbonate (Wells et al., 1970). It was deposited in the Ooraminna and Carmichael Sub-basins, and in the central zone between the two sub-basins, the Missionary Plains Trough, where it is considerably thinner. In the Carmichael Sub-basin the Arumbera Sandstone is about 2000 m thick (Kennard et al., 1986). To the south it is very thin. The basal contact has been studied both in outcrop and from seismic data (Lindsay, 1987a). In the two northern sub-basins it appears to conformably overlie the Julie Formation; however, this contact is now regarded as a disconformity and a sequence boundary (Kennard and Lindsay, 1991). The contact is unconformable on the Central Ridge of the Amadeus Basin, where the Arumbera Sandstone overlies older Proterozoic units. Bradshaw (1988) reported that the lower Arumbera Sandstone grades laterally into the dolomites of the Namatjira Formation, in the Gardiner Range, but the contact between the two formations is abrupt and likely to be a disconformity with erosional relief of 10 m or so (M.R. Walter, unpubl. observ.).

Four lithological units can be recognised, in ascending order (Wells et al., 1967): 1, predominantly red-brown micaceous siltstone and shale; 2, red-brown and purple-brown medium- and coarse-grained cross-bedded and slump-folded sandstone; clay pellets are common in some beds and lenses of conglomerate occur at some localities; 3, siltstone and shale with minor sandstone and dolomite; the siliciclastics are mainly dark red-brown and in places are glauconitic and calcareous, tracks and trails are common, dolomite occurs as lenses, and the unit is capped by sandstone; 4, brown and buff medium-grained sandstone.

The Arumbera Sandstone is generally considered to straddle the Proterozoic/Cambrian boundary. Most authors have considered the boundary to coincide with a disconformity, although Lindsay (1987a) and Walter et al. (1989) argued for continuous deposition in the deep sub-basins. A recent detailed study of the sequence boundary has shown that on the northern margin of the basin it is a disconformity with very gentle topography and only about 10 m of relief. In places the disconformity coincides with the contact between units 2 and 3, whereas elsewhere it lies within unit 3 (R.J.F. Jenkins and M.R. Walter, unpubl. observ.). In the Ooraminna Sub-basin no disconformity or lithological break was detected in this latter study, consistent with the interpretation that sedimentation was not significantly interrupted.

Both trace fossils (tracks, trails and burrows), and body fossils of the Ediacara fauna have been recorded from the Arumbera Sandstone (Wells et al., 1967, 1970; Glaessner, 1969; Young, 1972; Daily, 1972; Glaessner and Walter, 1975; Kruse and West, 1980; Walter et al., 1989; R. Elphinstone and M.R. Walter, in Shergold et al., 1991). Arumbera 2 contains *Charniodiscus* and other metazoan body fossils of the latest Proterozoic Ediacara fauna, but no definite trace fossils have been found (Walter et al., 1989; R. Elphinstone

and M.R. Walter, in Shergold et al., 1991). Units 3 and 4 contain trace fossil assemblage 3 of Walter et al. (1989), indicating an Early Cambrian age.

The Mount Currie Conglomerate in the southern part of the basin is a presumed correlative of the Arumbera Sandstone, though whether the lower Neoproterozoic part, or the upper Cambrian part, or both, is unknown. The same applies to the Sir Frederick Conglomerate and its correlative the Ellis Sandstone, in the western part of the basin (Wells et al., 1964). The Sir Frederick Conglomerate is at least 1200 m thick. The Ellis Sandstone is kaolinitic and pebbly sandstone, and subordinate calcareous sandstone and siltstone. Comparable units in the nearby Officer Basin are Cambrian.

6.2. Georgina Basin

The upper part of the Central Mount Stuart Formation of the western part of the basin consists of red and white quartz sandstone and siltstone, with some feldspathic sandstone (Shaw and Warren, 1975). It contains a soft-bodied metazoan fauna (Wade, 1970) and a few trace fossils (Walter et al., 1989) consistent with correlation with the lower Arumbera Sandstone. The trace fossil *Hormosiroidea arumbera* Walter et al. 1989 occurs near the top of the formation (Walter et al., 1989), along with the medusoids *Hallidaya brueri* Wade 1969 and *Skinnera brooksi* Wade 1969 which are regarded as members of the Ediacara fauna. The Central Mount Stuart Formation also contains a dubiofossil (Walter et al. 1989) showing some similarities to *Bergaueria*.

Sandstones in the uppermost Elkera Formation further east may also be of this age.

6.3. Ngalia Basin

The lower Yuendumu Sandstone is likely to be a correlative of the lower Arumbera Sandstone (Burek et al., 1979).

6.4. Officer Basin

The Punkerri Formation of the northern Officer Basin consists of pink sandstone and feldspathic sandstone, siltstone and minor conglomerate, with minor carbonate. A possible *Charniodiscus* characteristic of the Ediacara fauna is recorded from the sandstone (Glaessner, 1984) though it is very poorly preserved and unconvincing (Jenkins and Gehling, 1978; Preiss, 1987). The age of this unit is poorly constrained, and the apparent absence of the Rodda beds below it suggests that it might be equivalent to the Murnaroo Sandstone (W.V. Preiss, pers. commun., 1993).

The Table Hill Volcanics are amygdaloidal and vesicular tholeiitic basalt (Jackson and van de Graaff, 1981) and occur in the west and central zone of the western Officer Basin. They are (tenuously) dated by Rb/Sr whole-rock analysis at 563 ± 40 Ma (recalculated from Compston, 1974), about the same age inferred for the Ediacara fauna (Jenkins, 1984; Knoll and Walter, 1992). Otherwise their age is very poorly constrained. We consider that they can be related to extension that occurred during uplift of the Musgrave Block, and thus could be about the same age as the sandstones also resulting from this uplift (Fig. 2).

6.5. Savory Basin

Some of the upper sandstones of this basin may belong to this supersequence. For instance, the MacFadden Sandstone and its correlatives, the Woora Woora and Tchuckardine Formations, had their source in the Paterson Province (Williams, 1992). The Paterson Province is a western continuation of the Musgrave Block ("Wingelina Complex") and seems to have been emergent at the same time (about 540–600 Ma), and so it can be inferred that these sandstones could be correlatives of the Arumbera Sandstone which was sourced in the Musgrave Block.

6.6. Comments

A central ridge was prominent in the superbasin at this time (Paterson Province–Musgrave Block), providing the main source of sandy sediment for deltas building out into the northern basins. Only the northernmost areas were marine. Much of the southern region of the superbasin may have been emergent.

The Arumbera Sandstone was deposited in a shallow-marine and deltaic or coastal-plain setting (Lindsay, 1987a), with a sediment supply derived from the southwest and carried by heavily laden, braided streams. Toward the end of the Proterozoic, the shape of the Amadeus Basin was modified as a result of the Petermann Ranges Orogeny to form a shallow, east–

west-trending basin along the northern margin, separated from a shallower-shelf area by a broad Central Ridge. The subsequent nature of sedimentation was controlled by varying rates of subsidence in each of the major tectonic subdivisions. Four lithologic units have been recognised and form two large-scale shallowing-upward cycles that have been described in detail by Lindsay (1987a). Each cycle comprises storm deposits passing into prodelta sediments and finally into thick sandstones of a channelised delta or coastal plain.

The first cycle commences with an abrupt deposition of poorly sorted sandstones or shales above the shallow-water carbonates of the Julie Formation, probably as small-scale deltas that prograded across the carbonate platform sediments. Relative sea level then fell rapidly, at about the time of the Neoproterozoic–Cambrian boundary, exposing large areas of sediment, and restricting deposition to the two rapidly subsiding sub-basins. Deposition was largely progradational, as major deltaic complexes developed on the southern and southwestern margins of the sub-basins, while most of the Missionary Plain Trough remained exposed. The upper prograding sequence occurs only in the two sub-basins, which subsided rapidly at this time.

7. Age of supersequences

The nature of the contact with basal Cambrian sediments within Supersequence 4 is the subject of many studies (e.g., Wells et al., 1970; Daily, 1972, 1973; Burek et al., 1979; Walter, 1980; Walter et al., 1989; Mount, 1989) and is not examined in detail here. A regionally extensive disconformity underlies the Early Cambrian sandstones of all the northern basins, except that there is no clear evidence of this break in the depocentres in the northern Amadeus Basin.

A rich trace fossil record in the sandstones of upper Supersequence 4 in the Amadeus and Georgina Basins confirms an Early Cambrian age for those sandstones and also confirms lithostratigraphic correlations with the Adelaide Geosyncline (Glaessner, 1969; Walter et al., 1989). The overlying carbonates contain shelly fossils of Tommotian–Atdabanian age. Thus the age of the middle of Supersequence 4 is the age of the basal Cambrian, 540–545 Ma, and that of the top is the age of the Atdabanian, < 525–530 Ma.

The Table Hill Volcanics are (tenuously) dated at 563 ± 40 Ma (recalculated from Compston, 1974). The Ediacara fauna is inferred to be about 560–580 Ma old (Jenkins, 1984; Knoll and Walter, 1992; Jenkins, 1995).

Thus the age range of Supersequence 4 seems to be about 580–530 Ma.

The acritarch flora and carbon isotopic composition of Supersequence 3 point to correlation with the Sinian of China, the Vendian of Europe and equivalent units elsewhere. If these correlations can be substantiated by the detailed studies in progress at present, and the dating of the Varanger glacials at 600–610 Ma (Knoll and Walter, 1992) can be confirmed, this will fix the age of Supersequence 3 as ~ 610–580 Ma.

There are numerous Rb/Sr whole-rock shale dates for Neoproterozoic units in Australia (e.g., see Compston and Arriens, 1968 and the review by Preiss, 1987), including prominent units that can be attributed to Supersequence 2, but none are convincing or have narrow error limits. Compston et al. (1991) reinterpret some of the dates from the Adelaide Geosyncline, concluding that units attributed here to Supersequence 3 are 593 ± 32 Ma old, and others attributed to Supersequence 2 are 713 ± 38 Ma old.

The most powerful constraint on the maximum age of the base of Supersequence 1 comes through correlation with the Burra Group of the Adelaide Geosyncline. This is based on superposition, comparable lithologies, and the common presence of the stromatolite *Baicalia burra* Preiss in the Neale Formation (western Officer Basin) and the Burra Group. The Rook Tuff in the Callanna Group underlying the Burra Group is reliably dated by U/Pb on zircons as 802 ± 10 Ma old (Preiss, 1987). This is the only reliable absolute date in the whole of the Neoproterozoic sedimentary succession of Australia. As outlined above, this is consistent with dates on dyke swarms probably associated with the initiation of the superbasin (Zhao et al., 1994).

8. Pangean supercycle

The supersequences recognised here can be placed in the context of the tectonic cycles described by Veevers (1990). Following the ~ 1100 Ma Musgravian orogeny (possibly recording a Grenville-age collision), Pangean Supercycle C comprises the 1100–1000 Ma Bentley Volcanic Province, a 1000–800 Ma hiatus, the 800–750 Ma Supersequence 1 of the Centralian Superbasin (Heavitree and Bitter Springs), terminated

by the ~750–700 Ma shortening events in Tasmania (Penguin) and Western Australia (Pinjarra, Paterson) and the mild folding in the Adelaide area and the Arltunga Movement (Wells et al., 1970) in the Amadeus Basin, that reflect collision along the Mozambique Belt of East Africa, dated at 750–650 Ma by Stern et al. (1992). Supercycle B follows with a 700–650 Ma hiatus and then widespread deposition of the very poorly dated but possibly 650 Ma old Areyonga glacials and equivalents during the Sturtian ice age, and later (?600 Ma) the Marinoan glacials during the Varanger Ice Age. Glacials at the base of Supercycle B are matched by the ~300 Ma Gondwana glacials at the base of Supercycle A. Supercycle B continues past the Antrim Plateau and Table Hill flood basalts and the Boyagin Dyke Swarm (GSWA, 1990), 550–530 Ma shortening (Petermann Ranges Nappe, Woodroffe Thrust; Maboko et al., 1992) and uplift of the Musgrave Block (cf. the 230 Ma Gondwanides of the Panthalassan margin of Gondwanaland), and the Palaeozoic Uluru Sequence (Veevers, 1984), terminated by the Alice Springs shortening at the ~320 Ma Variscan collision of Gondwanaland and Laurussia.

The three collisional events 320 Ma Variscan, 700 (750–650) Ma Mozambiquean, and 1100 Ma Grenville, define a supercycle length of 400 Ma. Australian events in Supercycle C directly comparable with North America are:

North America	Australia
1100–1000 *Ma, widespread sediment*	
Flinton, Jacobsville	Halls Creek Mobile Zone and Victoria River Basin
1100 *Ma, start of volcanic rifts and dykes*	
Keweenawan	Bentley, Kulgera, Stuart
SW USA	
1100–1200 *Ma, orogenesis*	
Grenville	Musgrave, Albany–Fraser, Pinjarra

Supercycle C in North America/Australia is further compared with the modern Supercycle A in Australia/Europe:

N America/Australia	E Australia + Europe
Widespread marine sediment	
< 800 Ma Burra? = Bitter Springs	115 Ma Aptian–Albian
Heavitree	
200 m.y. HIATUS	115 m.y. HIATUS
Widespread non-marine sediment	
1100–1000 Ma Flinton	290–230 Ma Gondwana Series, Rotliegende (base only)
Volcanic extension	
1100 Ma Keweenawan/Bentley	290 Ma E Aust., Europe (Oslo Rift)
Terminal (collisional) orogeny	
1100 Ma Grenville/Musgrave	320 Ma Variscan/Alice Springs

The postulated 200 Ma hiatus between the Bentley Volcanic Province and the Heavitree Quartzite–Bitter Springs Formation would be analogous to the observed 115 Ma hiatus between the widespread basal Permian non-marine glacials (e.g., Paterson Formation of the Officer Basin, Veevers, 1984) and the overlying Aptian/Albian marine sediment (e.g., Bejah Formation), each representing a Pangean stage with extensive platform deposition.

9. Summary

The basement of central Australia consists of the Arunta Block and the 1200–1100 Ma Musgrave Block succeeded by the 1075–1000 Ma Bentley Volcanic Province of bimodal volcanic rifts, dolerite dyke swarms and sills. A regional hiatus at 1000–800 Ma, interpreted as reflecting a central post-volcanic (underplated) upland, was followed at 800 Ma by a second

swarm of dykes which probably led to the crustal sagging that initiated the Centralian Superbasin.

The Centralian Superbasin is defined here to encompass the Neoproterozoic fill of the Amadeus, Georgina, Ngalia, Officer and Savory Basins. Recognition of the integrity of the original depositional system allows the stratigraphy of relatively well known areas to be extrapolated to predict that of those that are poorly known. Within the Neoproterozoic to Early Cambrian fill, four depositional supersequences are recognised. Crustal sagging around 800 Ma initiated the superbasin with deposition of hundreds of metres of marine and fluvial sands. These form a uniform sheet over much of the superbasin. An overlying kilometre of marine and lacustrine carbonates, evaporites and fine siliciclastics completes the first depositional supersequence (1). Faulting during and after deposition of Supersequence 1 localized subsequent Sturtian glacigene sediments and overlying marine shales and carbonates (Supersequence 2). Supersequence 3 begins with renewed glacial sedimentation (Marinoan), perhaps about 600–610 Ma ago. This refrigeration may have been global, and post-glacial transgression was extensive, depositing turbiditic sands and pelagic shales over most of the superbasin. A carbonate–evaporite unit caps the supersequence. In the latest Proterozoic, marine sands and silts (Supersequence 4) were widespread, and continental flood basalts were erupted, following compression in the Officer Basin and southern Amadeus Basin. The culmination of this tectonic event is the Petermann Ranges Orogeny, which ended about 540 Ma ago (Maboko et al., 1992). The orogeny fragmented the Centralian Superbasin area into several smaller basins. The younger part of Supersequence 4 (Cambrian) commences with more deposition of marine sands and silts, followed by carbonates and evaporites.

Deposition continued through the early Palaeozoic in parts of the superbasin, but ended with the Alice Springs Orogeny in the mid-Carboniferous which completed the dismembering of the superbasin into its present constituent structural basins.

Acknowledgements

This research was supported by ARC grants to the two senior authors, and subsequently a Special Investigator Award to JJV, and APRA grants to CRC and KG. Dr. Wolfgang Preiss and Prof. Gonzalo Vidal are thanked for their detailed comments on an earlier version of the paper.

References

Aitken, J.D., 1991. Two Late Proterozoic glaciations, Mackenzie Mountains, northwestern Canada. Geology, 19: 445–448.

Arriens, P.A. and Lambert, I.B., 1969. On the age and strontium isotopic geochemistry of granulite-facies rocks from the Fraser Range, Western Australia, and the Musgrave Ranges, central Australia. Geol. Soc. Aust. Spec. Publ., 2: 377–388.

Black, L.P. and Shaw, R.D., 1992. U/Pb zircon chronology of prograde Proterozoic events in the Central and Southern Provinces of the Arunta Block, central Australia. Aust. J. Earth Sci., 39: 153–171.

Black, L.P., Shaw, R.D. and Offe, L.A., 1980. The age of the Stuart Dyke Swarm and its bearing on the initiation of sedimentation in the Birrindudu Basin. Geol. Soc. Aust., J., 27: 151–155.

Bowring, S., Grotzinger, J., Isaacson, G., Knoll, A.H., Pelechaty, S. and Kolosov, P., 1993. Calibrating rates of Early Cambrian evolution. Science, 261: 1293–1298.

Bradshaw, J., 1988. The Namatjira Formation, a mixed carbonate and clastic, Late Proterozoic–Early Cambrian sequence, Amadeus Basin, central Australia. Aust. J. Earth Sci., 35: 15–27.

Braun, J., McQueen, H. and Etheridge, M., 1991. A fresh look at the later Palaeozoic tectonic history of western-central Australia. Geol. Soc. Aust., Abstr., 30: 112–113.

Brewer, A.M., Dunster, J.N., Gatehouse, C.G., Henry, R.L. and Weste, G., 1987. A revision of the stratigraphy of the eastern Officer Basin. South Aust. Geol. Surv., Q. Geol. Notes, 102: 2–15.

Burek, P.J., Walter, M.R. and Wells, A.T., 1979. Magnetostratigraphic tests of lithostratigraphic correlations between latest Proterozoic sequences in the Ngalia, Georgina and Amadeus Basins, central Australia. BMR J. Aust. Geol. Geophys., 4: 47–55.

Camacho, A. and Fanning, C.M., 1992. Some isotopic constraints on the evolution of the granulite and upper amphibolite grade terranes in the Musgrave Block, central Australia. In: W.J. Collins (Editor), The Application of Geochronology to Field-Related Geological Problems. Geological Society of Australia SGGMP (Specialist Group in Geochemistry, Mineralogy and Petrology), University of Newcastle, Newcastle, Australia, 2 unnumbered pages.

Chumakov, N.M., 1991. Middle Siberian glacial horizon—traces of the earliest Late Precambrian glaciation? In: M. Deynoux (Editor) Earth's Glacial Record. Rep. Int. Geol. Correlation Progr., Proj. 260. Annu. Mtg., 7–17 Jan., p. 9.

Clarke, D., 1976. Heavitree Quartzite. In: A.T. Wells (Editor), Geology of the Late Proterozoic–Palaeozoic Amadeus Basin. 25th Int. Geol. Congr., Excursion Guide 48A, pp. 26–28.

Cloud, P. and Glaessner, M.F., 1982. The Ediacarian period and system. Metazoa inherit the Earth. Science, 217: 4562: 783–792.

Cloud, P.E. and Semikhatov, M.A., 1969. Proterozoic stromatolite zonation. Am. J. Sci., 267: 1017–1061.

Collins, W.J., 1992. Geochronological constraints on orogenic events in the Arunta Inlier: a review. Geological Society of Australia Specialist Group in Petrology and Dating (SGPD) Meeting, Alice Springs, pp. 1–31.

Compston, W., 1974. The Table Hill Volcanics of the Officer Basin: Precambrian or Palaeozoic? Geol. Soc. Aust., J., 21: 403–412.

Compston, W. and Arriens, P.A., 1968. The Precambrian geochronology of Australia. Canberra J. Earth Sci., 5: 561–583.

Compston, W., Cooper, J.A., Jenkins, R.J.F., Kirschvink, J., Ma Guogan, Williams, I.S. and Zhang Zichao, 1990. Numerical age of the Early Cambrian. Aust. Ntl. Univ., Res. School Earth Sci., Annu. Rep., 1990: 26–27.

Daily, B., 1972. The base of the Cambrian and the first Cambrian faunas. Univ. Adelaide, Cent. Precambrian Res., Spec. Pap., 1: 13–37.

Daily, B., 1973. Discovery and significance of basal Cambrian Uratanna Formation, Mt Scott Range, Flinders Ranges, South Australia. Search, 4: 202–205.

Dalziel, I.W.D., 1991. Pacific margins of Laurentia and East Antarctica–Australia as a conjugate rift pair: evidence and implications for an Eocambrian supercontinent. Geology, 19: 598–601.

De Keyser, F. and Cook, P.J., 1972. Geology of the Middle Cambrian phosphorites and associated sediments of northwestern Queensland. Aust., Bur. Miner. Resour., Geol. Geophys., Bull., 138: 79.

Dow, D.B. and Gemuts, I., 1969. Geology of the Kimberley Region, West Australia, The East Kimberley. West. Aust. Geol. Surv., Bull. 120.

Dunlap, W.J., Teyssier, C. and McDougall, I., 1990. Tectonic evolution of the Altunga Nappe Complex, central Australia: an integrated structural and isotopic dating study. EOS, 71: 1596.

Edgoose, C.J., 1986. First report of Late Proterozoic glacigene sediments and striated pavements, Litchfield Province, Northern Territory, Australia. 12th Int. Sedimentol. Congr., Canberra, pp. 90–91.

Embleton, B.J.J. and Williams, G.E., 1986. Low paleolatitude of deposition for Late Precambrian periglacial varvites in South Australia: implications for palaeoclimatology. Earth Planet. Sci. Lett., 79: 419–430.

Fanning, C.M., Ludwig, K.R., Forbes, B.G. and Preiss, W.V., 1986. Single and multiple grain U–Pb zircon analyses for the early Adelaidean Rook Tuff, Willouran Ranges, South Australia. Geol. Soc. Aust. Abstr., 15: 71–72.

Field, B.D., 1991. Paralic and periglacial facies and contemporaneous deformation of the Late Proterozoic Olympic Formation, Pioneer Sandstone and Gaylad Sandstone, Amadeus Basin, central Australia. In: R.J. Korsch and J.M. Kennard (Editors), Geological and Geophysical Studies in the Amadeus Basin, Central Australia. Aust., Bur. Miner. Resour., Bull., 236: 127–136.

Gehling, J.G., 1991. The case for Ediacaran fossil roots to the metazoan tree. In: B.P. Radhakrishna (Editor), The World of Martin F. Glaessner. Geol. Soc. India Mem., 20: 181–223.

Geological Survey of Western Australia, 1990. Geology and Mineral Resources of Western Australia. West. Aust. Geol. Surv., Mem., 3: 827.

Glaessner, M.F., 1969. Trace fossils from the Precambrian and basal Cambrian. Lethaia, 2: 369–393.

Glaessner, M.F., 1984. The Dawn of Animal Life: A Biohistorical Study. Cambridge University Press, Cambridge, 244 pp.

Glaessner, M.F. and Walter, M.R., 1975. New Precambrian fossils from the Arumbera Sandstone, Northern Territory, Australia. Alcheringa, 1: 59–69.

Goellnicht, N.M., Groves, D.I. and McNaughton, N.J., 1991. Late Proterozoic fractionated granites of the mineralized Telfer area, Paterson Province, Western Australia. Precambrian Res., 51: 375–391.

Gorter, J.D., 1992. Cambro–Ordovician petroleum in the Centralian Superbasin: relationships with sea-level changes. Am. Assoc. Pet. Geol., 76(7): 1103.

Grey, K., 1995. Neoproterozoic stromatolites from the Skates Hill Formation, Stavory Basin, Western Australia, and a review of the distribution of *Acaciella australica*. Aust. J. Earth Sci., 42, in press.

Hambrey, M.J. and Harland, W.B. (Editors), 1981. Earth's Pre-Pleistocene Glacial Record. Cambridge University Press, Cambridge, 1004 pp.

Hoffman, P.F., 1991. Did the breakout of Laurentia turn Gondwanaland inside-out? Science, 252: 1409–1412.

Jackson, M.J. and Muir, M.D., 1981. The Babbagoola Beds, Officer Basin, Western Australia: correlations, micropaleontology and implications for petroleum prospectivity. Aust., Bur. Miner. Resour., J. Aust. Geol. Geophys., 6: 81–93.

Jackson, M.J. and van de Graaff, W.J.E., 1981. Geology of the Officer Basin, Western Australia. Aust., Bur. Miner. Resour., Geol. Geophys., 206: 102.

Jago, J.B. and Moore, P.S. (Editors), 1990. The evolution of a Late Precambrian–Early Palaeozoic rift complex: the Adelaide Geosyncline. Geol. Soc. Aust., Spec. Publ. 16, 495 pp.

Jenkins, R.J.F., 1981. The concept of an "Ediacaran Period" and its stratigraphic significance in Australia. Trans. R. Soc. South Aust., 105(4): 179–194.

Jenkins, R.J.F., 1984. Ediacaran events: boundary relationships and correlation of key sections, especially in 'Armorica'. Geol. Mag., 121: 635–643.

Jenkins, R.J.F., 1991. The early environment. In: C. Bryant (Editor), Animal Life Without Oxygen. Chapman and Hall, London, pp. 38–64.

Jenkins, R.J.F., 1992. Functional and ecological aspects of Ediacaran assemblages. In: J.H. Lipps and P.W. Signor (Editors), Origin and Early Evolution of the Metazoa. Plenum Press, New York, N.Y., pp. 131–176.

Jenkins, R.J.F., 1995. The problems and potential of using animal fossils and trace fossils in terminal Proterozoic biostratigraphy. In: A.H. Knoll and M. Walter (Editors), Neoproterozoic Stratigraphy and Earth History. Precambrian Res., 73: 51–70 (this volume).

Jenkins, R.J.F. and Gehling, J.G., 1978. A review of the frond-like fossils of the Ediacara assemblage. Rec. South Aust. Mus., 17: 347–359.

Jenkins, R.J.F., McKirdy, D.M., Foster, C.B., O'Leary, T. and Pell, S.D., 1992. The record and stratigraphic implications of organic-

walled microfossils form the Ediacaran (terminal Proterozoic) of South Australia. Geol. Mag., 129: 401–410.

Kaufman, A.J. and Knoll, A.H., 1995. Neoproterozoic variations in the C-isotopic composition of seawater: stratigraphic and biogeochemical implications. In: A.H. Knoll and M. Walter (Editors), Neoproterozoic Stratigraphy and Earth History. Precambrian Res., 73: 27–49 (this volume).

Kaufman, A.J., Hayes, J.M., Knoll, A.H. and Germs, G.J.B., 1991. Isotopic compositions of carbonates and organic carbon from upper Proterozoic successions in Namibia: stratigraphic variation and the effects of diagenesis and metamorphism. Precambrian Res., 49: 301–327.

Kaufman, A.J., Knoll, A.H. and Awramik, S.M., 1992. Biostratigraphic and chemostratigraphic correlation of Neoproterozoic sedimentary successions: Upper Tindir Group, Northwestern Canada, as a test case. Geology, 20: 181–185.

Kennard, J.M. and Lindsay, J.F., 1991. Sequence stratigraphy of the latest Proterozoic. Cambrian Pertaoorrta Group, northern Amadeus Basin, central Australia. In: R.J. Korsch and J.M. Kennard (Editors), Geological and Geophysical Studies in the Amadeus Basin, Central Australia. Bur. Miner. Resour., Aust., Bull., 236: 171–194.

Kennard, J.M., Nicoll, R.S. and Owen, M. (Editors), 1986. Late Proterozoic and Early Palaeozoic Depositional Facies of the Northern Amadeus Basin, Central Australia. 12th Int. Sedimentol. Congr., Field Excursion 25B. Bureau of Mineral Resources, Canberra, 125 pp.

Kennedy, M., 1993. The Undoolya Sequence: Late Proterozoic salt influenced deposition, Amadeus Basin, central Australia. Aust. J. Earth Sci., 40: 217–228.

Knoll, A.H., 1992. Vendian microfossils in metasedimentary cherts of the Scotia Group, Prins Karls Forland, Svalbard. Palaeontology, 35: 751–774.

Knoll, A.H. and Golubic, S., 1979. Anatomy and taphonomy of a Precambrian algal stromatolite. Precambrian Res., 10: 115–151.

Knoll, A.H. and Walter, M.R., 1992. Latest Proterozoic stratigraphy and earth history. Nature, 356: 673–678.

Kruse, P.D. and West, P.W., 1980. Archaeocyatha of the Amadeus and Georgina Basins. BMR J. Aust. Geol. Geophys., 5: 165–181.

Kukla, P.A. and Stanistreet, I.G., 1991. Record of the Damaran Khomas Hochland accretionary prism in central Namibia: refutation of an "ensialic" origin of a Late Proterozoic orogenic belt. Geology, 19: 473–476.

Lindsay, J.F., 1987a. Sequence stratigraphy and depositional controls in Late Proterozoic–Early Cambrian Sediments of Amadeus Basin, central Australia. Am. Assoc. Pet. Geol. Bull., 71: 1387–1403.

Lindsay, J.F., 1987b. Upper Proterozoic evaporites in the Amadeus basin, central Australia, and their role in basin tectonics. Geol. Soc. Am. Bull., 99: 852–865.

Lindsay, J.F., 1989. Depositional controls on glacial facies associations in a basinal setting, Late Proterozoic, Amadeus Basin, central Australia. Palaeogeogr., Palaeoclimatol., Palaeoecol., 73: 205–232.

Lindsay, J.F. and Korsch, R.J., 1991. The evolution of the Amadeus Basin, central Australia. In: R.J. Korsch and J.M. Kennard (Editors), Geological and Geophysical Studies in the Amadeus Basin, Central Australia. Aust. Bur. Miner. Resour., Bull., 236: 7–32.

Lodwick, W.R. and Lindsay, J.F., 1990. Southern Georgina Basin: a new perspective. APEA J., 30(1): 137–148.

Maboko, M.A.H. and McDougall, I., 1988. Chronology of pressure–temperature history of high grade metamorphic terranes in the Musgrave Ranges, central Australia. Aust. Ntl. Univ., Res. School Earth Sci., Annu. Rep., 1988: 80–85.

Maboko, M.A.H., Williams, I.S. and Compston, W., 1991. Zircon U/Pb chronometry of the pressure and temperature history of granulites in the Musgrave Ranges, central Australia. J. Geol., 99: 675–697.

Maboko, M.A.H., McDougall, I., Zeitler, P.K. and Williams, I.S., 1992. Geochronological evidence for ≈530–550 Ma juxtaposition of two Proterozoic metamorphic terranes in the Musgrave Ranges, central Australia. Aust. J. Earth Sci., 39: 457–471.

Moczydłowska, M., Vidal, G. and Rudavskaya, V.A., 1993. Neoproterozoic (Vendian) phytoplankton from the Siberian Platform, Yakutia. Palaeontology, 36: 495–521.

Moores, E.M., 1991. Southwest U.S.–East Antarctic (SWEAT) connection: a hypothesis. Geology, 19: 425–428.

Mount, J.F., 1989. Re-evaluation of unconformities separating the "Ediacaran" and Cambrian systems, South Australia. PALAIOS, 4: 366–373.

Murphy, J.B. and Nance, R.D., 1991. Supercontinent model for the contrasting character of Late Proterozoic orogenic belts. Geology, 19: 469–472.

Myers, J.S., 1990. Precambrian tectonic evolution of part of Gondwana, southwestern Australia. Geology, 18: 537–540.

Page, R.W., 1983. Chronology of magmatism, skarn formation, and uranium mineralization, Mary Kathleen, Queensland, Australia. Econ. Geol., 78: 838–853.

Parker, A.J., 1992. Mafic dyke swarms as a guide to Precambrian tectonics. Geol. Soc. Aust., Abstr., 32: 3–4.

Phillips, B.J., James, A.W. and Philip, G.M., 1985. The geology and hydrocarbon potential of the north-western Officer Basin. APEA J., 25(1): 52–61.

Pidgeon, R.T., Smith, C.B. and Fanning, C.M., 1989. Kimberlite and lamproite emplacement ages in Western Australia. Geol. Soc. Aust. Spec. Publ., 14: 369–381.

Preiss, W.V., 1976. Proterozoic stromatolites from the Nabberu and Officer Basins, Western Australia, and their biostratigraphic significance. South Aust. Geol. Surv. Rep. Invest., 47: 1–51.

Preiss, W.V. (Compiler), 1987. The Adelaide Geosyncline—late Proterozoic stratigraphy, sedimentation, palaeontology, and tectonics. Geol. Surv. South Aust. Bull., 53, 438 pp.

Preiss, W.V. and Forbes, B.G., 1981. Stratigraphy, correlation and sedimentary history of Adelaidean (late Proterozoic) basins in Australia. Precambrian Res., 15: 255–304.

Preiss, W.V. and Krieg, G.W., 1992. Stratigraphic drilling in the northeastern Officer Basin: Rodda 2 Well. Min. Energ. Rev., South Aust., 158: 48–51.

Preiss, W.V., Walter, M.R., Coats, R.P. and Wells, A.T., 1978. Lithological correlations of Adelaidean glaciogenic rocks in parts of the Amadeus, Ngalia, and Georgina Basins. BMR J. Aust. Geol. Geophys., 3: 45–53.

Robey, J.V.A., Bristow, J.W., Marx, M.R., Joyce, J., Danchin, R.V. and Arnott, F., 1989. Alkaline ultrabasic dikes near Norseman,

Western Australia. Geol. Soc. Aust. Spec. Publ., 14: 382–391.
Ross, G.M., 1991. Tectonic setting of the Windermere Supergroup revisited. Geology, 19: 1125–1128.
Schopf, J.W., 1968. Microflora of the Bitter Springs Formation, Late Precambrian, central Australia. J. Paleontol., 42: 651–688.
Schopf, J.W. and Blacic, J.M., 1971. New microorganisms from the Bitter Springs Formation (Late Precambrian) of the north-central Amadeus Basin, Australia. J. Paleontol., 45: 925–959.
Shaw, R.D. and Black, L.P., 1991. The history and tectonic implications of the Redbank Thrust Zone, central Australia, based on structural, metamorphic and Rb–Sr isotopic evidence. Aust. J. Earth Sci., 38: 307–332.
Shaw, R.D. and Warren, R.G., 1975. Alcoota, NT, 1:250,000 Geological Series. Bureau of Mineral Resources, Canberra, Explanatory Notes SF53/10.
Shaw, R.D., Tyler, I.M., Griffin, T.J. and Webb, A., 1992. New K–Ar constraints on the onset of subsidence in the Canning Basin, Western Australia. BMR J. Aust. Geol. Geophys., 13: 31–35.
Shergold, J.H., Elphinstone, R., Laurie, J.R., Nicoll, R.S., Walter, M.R., Young, G.C. and Zang, W., 1991. Late Proterozoic and early Palaeozoic palaeontology and biostratigraphy of the Amadeus Basin. In: R.J. Korsch and J.M. Kennard (Editors), Geological and Geophysical Studies in the Amadeus Basin, Central Australia. Bur. Miner. Resour., Bull., 236: 97–111.
Southgate, P.N., 1986. Depositional environment and mechanism of preservation of microfossils, upper Proterozoic Bitter Springs Formation, Australia. Geology, 14: 683–686.
Southgate, P.N., 1989. Relationships between cyclicity and stromatolite form in Late Proterozoic Bitter Springs Formation, Australia. Sedimentology, 36: 323–339.
Southgate, P.N., 1991. A sedimentological model for the Loves Creek Member of the Bitter Springs Formation, northern Amadeus Basin. In: R.J. Korsch and J.M. Kennard (Editors), Geological and Geophysical Studies in the Amadeus Basin, Central Australia. Aust. Bur. Miner. Resour., Bull., 236: 113–126.
Stern, R.J., Sultan, M. and Abdel-Salam, M.G., 1992. Comment on "Pacific margins of Laurentia and East Antarctica–Australia as a conjugate rift pair: evidence and implications for an Eocambrian supercontinent". Geology, 20: 190.
Stewart, A.J., 1979. A barred basin marine evaporite in the Upper Proterozoic of the Amadeus Basin, central Australia. Sedimentology, 26: 33–62.
Sukanta, U., Thomas, B., Von Der Borch and Gatehouse, C.G., 1991. Sequence stratigraphic studies and canyon formation, South Australia. PESA J., 19 (September): 68–73.
Sun, S. and Sheraton, J., 1992. Zircon U/Pb chronology, tectonothermal and crust-forming events in the Tomkinson Ranges, Musgrave Block, central Australia. Aust. Geol. Surv. Organ. Res. Newslett., 17: 9–11.
Teyssier, C.P., 1990. The role of deformation–recrystallization on oxygen and argon isotopes, Arltunga Nappe Complex, central Australia. EOS, 71: 1596.
Townson, W.G., 1985. The subsurface geology of the western Officer Basin—results of Shell's 1980–1984 petroleum exploration campaign. APEA J., 25: 34–51.
Veevers, J.J. (Editor), 1984. Phanerozoic Earth History of Australia. Oxford Geological Science Series 2, Clarendon Press, Oxford, 418 pp.
Veevers, J.J., 1990. Tectonic–climatic supercycle in the billion-year plate-tectonic eon: Permian Pangean icehouse alternates with Cretaceous dispersed-continents greenhouse. Sediment. Geol., 68: 1–16.
Wade, M., 1970. The stratigraphic distribution of the Ediacara fauna in Australia. Trans. R. Soc. South Aust., 94: 87–104.
Wallace, M.W., Keays, R.R. and Gostin, V.A., 1991. Stromatolitic iron oxides: evidence that sea-level changes can cause sedimentary iridium anomalies. Geology, 19: 551–554.
Walter, M.R., 1972. Stromatolites and the biostratigraphy of the Australian Precambrian and Cambrian. Special Papers in Palaeontology, 11, Palaeontological Association, London, 190 pp.
Walter, M.R., 1978. Late Precambrian to early Cambrian stratigraphy of the S.W. Georgina Basin, Australia. Geol. Mag., 115(2): 137.
Walter, M.R., 1980. Adelaidean and Early Cambrian stratigraphy of the southwestern Georgina Basin: correlation chart and explanatory notes. Bur. Miner. Resour. Geol. Geophys. Aust. Rep. 214, BMR Microform MF92.
Walter, M.R. and Bauld, J., 1983. The association of sulphate evaporites, stromatolitic carbonates and glacial sediments, examples from the Proterozoic of Australia and the Cainozoic of Antarctica. Precambrian Res., 21: 129–148.
Walter, M.R. and Gorter, J., 1993. Centralian Superbasin, Australia. Petroconsultants Australasia, Sydney (unpublished).
Walter, M.R., Krylov, I.N. and Preiss, W.V., 1979a. Stromatolites from Adelaidean (Late Proterozoic) sequences in central and South Australia. Alcheringa, 3: 287–305.
Walter, M.R., Shergold, J.H., Muir, M.D. and Kruse, P.D., 1979b. Early Cambrian and latest Proterozoic stratigraphy, Desert Syncline, southern Georgina Basin. Geol. Soc. Aust., J., 26: 305–312.
Walter, M.R., Elphinstone, R. and Heys, G.R., 1989. Proterozoic and Early Cambrian trace fossils from the Amadeus and Georgina Basins, central Australia. Alcheringa, 13: 209–256.
Walter, M.R., Veevers, J.J., Calver, C.R., Grey, K. and Hilyard, D., 1992. The Proterozoic Centralian Superbasin: a frontier petroleum province. 1992 AAPG Int. Conf. Exhib., p. 77.
Walter, M.R., Grey, K., Williams, I.R. and Calver, C.R., 1994. Stratigraphy of the Neoproterozoic to early Palaeozoic Savory Basin, Western Australia, and correlation with the Amadeus and Officer Basins. Aust. J. Earth Sci., 41: 533–546.
Wells, A.T. and Moss, J.F., 1983. The Ngalia Basin, Northern Territory: stratigraphy and structure. Bur. Miner. Resour., Aust., Bull., 212: 88.
Wells, A.T., Forman, D.J. and Ranford, L.C., 1964. Geological reconnaissance of the Rawlinson–MacDonald 1:250,000 sheet areas, Western Australia. Bur. Miner. Resour., Aust., Rep., 65: 35.
Wells, A.T., Ranford, L.C., Stewart, A.J., Cook, P.J. and Shaw, R.D., 1967. The geology of the northeastern part of the Amadeus Basin, Northern Territory. Aust. Bur. Miner. Resour., Bull., 113: 97.
Wells, A.T., Forman, D.J., Ranford, L.C. and Cook, P.J., 1970. Geology of the Amadeus Basin, central Australia. Aust. Bur. Miner. Resour., Bull., 100: 222.
Williams, G.E., 1986. Precambrian permafrost horizons as indicators of palaeoclimate. Precambrian Res., 32: 233–242.

Williams, I.R., 1992. Geology of the Savory Basin, Western Australia. West. Aust. Geol. Surv., Bull., 141: 115.

Yin, Leiming, 1985. Microfossils of the Doushantuo Formation in the Yangtze Gorge district, western Hebei, China. Palaeontologica Cathayana, 2: 229–249.

Young, F.G., 1972. Early Cambrian and older trace fossils from the Southern Cordillera of Canada. Can. J. Earth Sci., 9(1): 1–17.

Zang, W.L. and Walter, M.R., 1989. Latest Proterozoic plankton from the Amadeus Basin in central Australia. Nature, 337(6208): 642–645.

Zang, W. and Walter, M.R., 1992. Late Proterozoic and Cambrian microfossils and biostratigraphy, Amadeus Basin, central Australia. Assoc. Australas. Palaeontol., Mem., 12: 132.

Zhao, J.-X., McCulloch, M.T. and Bennett, V.C., 1992a. Sm–Nd and U/Pb zircon isotopic constraints on the provenance of sediments from the Amadeus Basin, central Australia: evidence for REE fractionation. Geochim. Cosmochim. Acta, 56: 921–940.

Zhao, J.-X., McCulloch, M.T., Warren, R.G., Rudnick, R., Camacho, A. and Ellis, D.J., 1992b. Geochemical and isotopic studies of Proterozoic mafic dyke swarms in central Australia. Aust. Ntl. Univ., Res. School Earth Sci., Annu. Rep., 1991: 103–105.

Zhao, J.-X., McCulloch, M.T. and Camacho, A., 1992c. Geochemical and isotopic studies of Proterozoic mafic dyke swarms in central Australia. Geol. Soc. Aust. Abstr., 32: 205–207.

Zhao, J.-X., McCulloch, M.T. and Korsch, R.J., 1994. Characterisation of a plume-related ~800 Ma magmatic event and its implications for basin formation in central-southern Australia. Earth Planet. Sci. Lett., 121: 349–367.